Biodiesel Synthesis, Optimization and Characterization from Novel Non-edible oil Seeds via High Performance Phyto-nano catalysts

BY

Rozina

Department of Plant Sciences Faculty of Biological Sciences
Quaid-i-Azam University, Islamabad, Pakistan
2023

Biodiesel Synthesis, Optimization and Characterization from Novel Non-edible oil Seeds via High Performance Phyto-nano catalysts

A dissertation submitted to the Department of Plant Sciences, Quaid-i-Azam University, Islamabad, in partial fulfillment of the requirements for the degree of

Doctor of Philosophy

In

Plant Sciences

By

Rozina

Department of Plant Sciences

Quaid-i-Azam University,
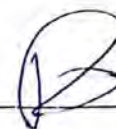
Islamabad, Pakistan

2023

Dedicated to
My Family

Certificate of Approval

This is to certify that research work presented in this thesis, entitled **"Biodiesel Synthesis, Optimization and Characterization from Novel Non-edible oil Seeds via High Performance Phyto-nano catalysts"** was conducted by **Ms. Rozina** under the supervision of **Prof. Dr. Mushtaq Ahmad**. No part of this thesis has been submitted anywhere else for any other degree. This thesis is submitted to the Department of Plant Sciences, Quaid-i-Azam University, Islamabad, Pakistan in partial fulfillment of the requirements for the degree of Doctor Philosophy in the field of **Plant Sciences (Plant Systematics and Biodiversity)**, Department of Plant Sciences, Quaid-i-Azam University, Islamabad, Pakistan.

Student name: **Ms. Rozina**   Signature: _____

Examination committee

External Examiner 1

Prof. Dr. Dr. Rahmatullah Qureshi   Signature: _____
Chairman Department of Botany
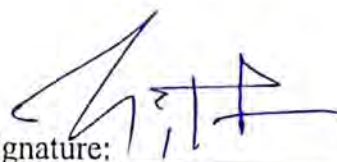Pir Mehr Ali Shah Arid Agriculture University,
Rawalpindi

External Examiner 2

Prof. Dr. Asif Mir   Signature: _____
Chairman Department of Biosciences
International Islamic University, Islamabad

Supervisor
Prof. Dr. Mushtaq Ahmad   Signature: _____
Department of Plant Sciences
Quaid-i-Azam University, Islamabad

Chairman
Prof. Dr. Mushtaq Ahmad   Signature: _____
Department of Plant Sciences
Quaid-i-Azam University, Islamabad

Dated: 05-12-2023

قائد اعظم یونیورسٹی

QUAID-I-AZAM UNIVERSITY

Department of Plant Sciences
Islamabad, Pakistan 45320

No. _____   **10 February, 2023**

Subject: <u>**Plagiarism Undertaking**</u>

I solemnly declare that the research work presented in the thesis titled "**Biodiesel Synthesis, Optimization and Characterization from Novel Non-edible oil Seeds via High Performance Phyto-nano catalysts**" is solely my research work with no significant contribution from any other person. Small contribution/help wherever taken has been duly acknowledged and that complete thesis has been written by me.

I understand the zero-tolerance policy of the HEC and Quaid-i-Azam University towards plagiarism. Therefore, I as an author of the above-titled thesis declare that no portion of my thesis has been plagiarized and any material used as reference is property referred/cited.

I undertake that if I am found faulty of any formal plagiarism in the above-titled thesis even after awarding of Ph.D. degree, the University reserves the right to withdraw/revoke my Ph.D. degree and that HEC and the University has the right to publish my mime on the HEC/University website on which name of students are placed who submitted plagiarized thesis
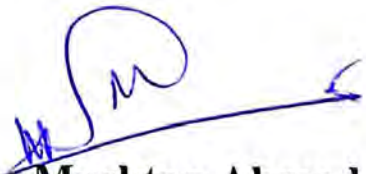
Student/Author Signature_____

Rozina

QUAID-I-AZAM UNIVERSITY

Department of Plant Sciences
Islamabad, Pakistan 45320

SIMILARITY INDEX CERTIFICATE

It is certified that Ms. Rozina has completed his Ph.D. research work and compilation of the thesis. The title of his thesis is "Biodiesel Synthesis, Optimization and Characterization from Novel Non-edible oil Seeds via High Performance Phyto-nano catalysts". His thesis has been checked on Turnitin for similarity index and found 9% that lies in the limits provided by HEC (20%).

Dr. Mushtaq Ahmad
Supervisor

QUAID-I-AZAM UNIVERSITY

Department of Plant Sciences
Islamabad, Pakistan 45320

Subject: <u>Author Declaration</u>

I Ms. Rozina hereby state that my Ph.D. thesis entitled **"Biodiesel Synthesis, Optimization and Characterization from Novel Non-edible oil Seeds via High Performance Phyto-nano catalysts"** is my work and has not been submitted previously by me for taking any degree from the Department of Plant Sciences, Quaid-i-Azam University or anywhere in the country/world.

At any time if my statement is found to be incorrect even after my Graduate, the university has the right to withdraw my Ph.D. degree.

Ms. Rozina

APPROVAL CERTIFICATE

This thesis submitted by **Miss Rozina** is accepted for evaluation from foreign experts in its present form by the Department of Plant Sciences, Faculty of Biological Sciences, Quaid-i-Azam University, Islamabad.

Supervisor: _____

Prof. Dr. Mushtaq Ahmad

Prof. Dr. Mushtaq Ahmad
Chairman
Department of Plant Sciences
Quaid-i-Azam University
Islamabad-Pakistan

TABLE OF CONTENTS

LIST OF ABBREVATIONS

%	Percentage
°C	Degree Centigrade
μL	Mu Liter
ANOVA	Analysis of Variance
ASTM	American Society for Testing And Materials
B100	100% Biodiesel Blend
B20	20% Biodiesel and 80% Petro diesel
B80	80% Biodiesel and 20% Petro diesel
CCD	Central Composite Design
Cm	Centimeter
CO	Carbon Monoxide
CO_2	Carbon Dioxide
Cst	Centistokes (Unit of Kinematic Viscosity)
EDX	Energy Diffraction X-Ray
EN	European Norm (European committee for standardization)
FAMEs	Fatty Acid Methyl Esters
Fe_2O_3	Ferric Oxide
FFA	Free Fatty Acids
FID	Flame Ionization Detector
FTIR	Fourier-Transform Infrared Spectroscopy
F-value	Fisher Value
FWHM	Full Width Half Maximum
g	Gram
GC	Gas Chromatography
GCMS	Gas Chromatography-Mass Spectrometry
Kg	Kilogram
KOH	Potassium Hydroxide
M	Molar
Ml	Milli Liter
Nm	Nano meter

NMR	Nuclear Magnetic Resonance
PAH	Polycyclic Aromatic Hydrocarbons
PM	Particulate Matter
PMCC	Pensky-Martens Closed Cup Method
PPL	Pakistan Petroleum Limited
PSO	Pakistan State Oil
P-value	Probability Value
Rpm	Revolution per minute
RSM	Response Surface Methodology
SEM	Scanning Electron Microscopy
TAG	Triacylglycerol
TGA	Thermogravimetric Analysis
US	United States
XRD	X-Ray Diffraction

LIST OF PLATES

	of seeds and sculpturing	
3.1.14	*Nannorrhops ritchieana* (Griff.) Aitch. **(a)** entire plant, **(b)** seeds, **(c, d)** SEM micrograph of seeds and sculpturing	**80**
3.1.15	*Cupresssus sempervirens* **(a)** entire plant, **(b)** seeds, **(c, d)** SEM micrograph of seeds and sculpturing	**82**

LIST OF FIGURES

LIST OF TABLES

Acknowledgements

Countless praises and thanks to Almighty Allah, the Omnipotent, the most Beneficent and the most Merciful, who showered His umpteen blessings on mankind and the ability to learn, knowledge is one of them. This particular blessing distinct human from all other worldly creatures. He has given me strength and courage to undertake this uphill task. Countless salutations upon our Holy Prophet Hazrat Muhammad (S.A.W) the savior of Mankind who brought the message of Allah and enlightened the life of downtrodden and ignorant people.

The completion of this research-based work is not a one man's show. I really feel indebted in expressing my heartfelt gratitude to my honorable supervisor Dr. Mushtaq Ahmad, Professor and Chairperson of Department of Plant Sciences, Faculty of Biological sciences, Quaid-i-Azam University, Islamabad for his guidance, patronage, rationale advice, supervision consultation and precious time. He has always been a source of inspiration for me. He inculcated in me the ability to be patient and consistent in achieving research goals.

I am extremely thankful to Prof. Dr. Sarwat Jahan, Dean Faculty of Biological Sciences for her implausible support throughout my Ph. D, without his help it would have been not possible. All my colleagues deserve huge applause for their support.

I extend my deep gratitude and regards to Dr. Muhammad Zafar, Assistant Professor, Department of Plant Sciences and Dr. Shazia Sultana for consistent encouragement and moral support.

Thanks are extended to Higher Education Commission (HEC) of Pakistan for IRSIP regarding my six months visit to The Ohio State University (OSU) United States of America. I owe a lot to Prof. Dr. Thaddeus Ezeji, Ph.D., OSU for his motivation and support in my hard times. I am also obliged to Okezie Emmanuel (Graduate Fellow) Bioenergy Lab, The Ohio State University, for unconditional support and guidance.

I am grateful to my friends, lab fellows and colleagues for their help especially I extend my regards to Dr. Maria ameen, Dr. Salman, Dr. Nabila, Mr. Jamil Raza Bhatti and MS. Shaista Jabeen, for their commendable help in this work. Their consistent support made this uphill task appear easier.

My parents, and my family deserve to be acknowledged and thanked for an unconditional love

and support. Though, it is difficult to mention the name of each individual whose contribution brought this research project to its logical culmination. But I would like to emphatically state that their contribution is highly revered and appreciated.

Rozina

\

Turnitin Originality Report

Biodiesel Synthesis, Optimization and Characterization from Novel Non-edible oil Seeds via High Performance Phyto-nano catalysts   by Rozina .

From PhD (PhD DRSML)

- Processed on 08-Feb-2023 11:43 PKT
- ID: 2009167699
- Word Count: 77936

Similarity Index
15%
Similarity by Source

Internet Sources:
     11%
Publications:
     10%
Student Papers:
     3%

---

sources:

1   1% match (Internet from 13-Dec-2022)
https://www.frontiersin.org/articles/10.3389/fenrg.2022.830845/full

---

2   1% match (Maryam Tanveer Akhtar, Mushtaq Ahmad, Mohamed Fawzy Ramadan, Trobjon Makhkamov et al. "Sustainable Production of Biodiesel from Novel Non-Edible Oil Seeds (Descurainia sophia L.) via Green Nano CeO2 Catalyst", Energies, 2023)
Maryam Tanveer Akhtar, Mushtaq Ahmad, Mohamed Fawzy Ramadan, Trobjon Makhkamov et al. "Sustainable Production of Biodiesel from Novel Non-Edible Oil Seeds (Descurainia sophia L.) via Green Nano CeO2 Catalyst", Energies, 2023

---

3   1% match (Internet from 05-Jan-2023)

http://prr.hec.gov.pk/jspui/bitstream/123456789/18861/1/Anam%20Fatima%20botany%202021%20QAU%20isb.pdf

---

4   1% match (Maryam Tanveer Akhtar, Mushtaq Ahmad, Maliha Asma, Mamoona Munir et al. "Efficient Production of Wild and Non-Edible Brassica juncea (L.) Czern. Seed Oil into High-Quality Biodiesel via Novel, Green and Recyclable NiSO4 Nano-Catalyst", Sustainability, 2022)
Maryam Tanveer Akhtar, Mushtaq Ahmad, Maliha Asma, Mamoona Munir et al. "Efficient Production of Wild and Non-Edible Brassica juncea (L.) Czern. Seed Oil into High-Quality Biodiesel via Novel, Green and Recyclable NiSO4 Nano-Catalyst", Sustainability, 2022

---

5   1% match (Mamoona Munir, Mushtaq Ahmad, Muhammad Saeed, Amir Waseem et al. "Biodiesel production from novel non-edible caper (Capparis spinosa L.) seeds oil employing Cu–Ni doped ZrO2 catalyst", Renewable and Sustainable Energy Reviews, 2020)
Mamoona Munir, Mushtaq Ahmad, Muhammad Saeed, Amir Waseem et al. "Biodiesel production from novel non-edible caper (Capparis spinosa L.) seeds oil employing Cu–Ni doped ZrO2 catalyst", Renewable and Sustainable Energy Reviews, 2020

---

6   < 1% match (Internet from 29-Jan-2023)

https://www.researchgate.net/publication/327371585_Synthesis_of_biomass_as_heterogeneous_catalyst_for_application_in_biodiesel_pr

---

7   < 1% match (Internet from 14-Jul-2022)

https://www.researchgate.net/publication/285042763_Recent_trends_in_acetone_butanol_and_ethanol_ABE_production

---

8   < 1% match (Internet from 07-Aug-2022)

https://www.researchgate.net/publication/272121729_Transesterification_for_Biodiesel_Production_Using_Thespesia_Populnea_Seed_Oi

---

9   < 1% match (Internet from 20-Oct-2022)

https://www.researchgate.net/publication/297745704_Biodiesel_production_using_heterogeneous_catalysts_including_wood_ash_and_th

---

10   < 1% match (Internet from 07-Aug-2022)

https://www.researchgate.net/publication/362462685_Cleaner_production_of_biodiesel_from_novel_and_non-edible_seed_oil_of_Chamaerops_humilis_using_recyclable_cobalt_oxide_nanoparticles_A_contribution_to_resilient_and_sustainable_wo

---

11   < 1% match (Internet from 07-Feb-2023)

https://www.researchgate.net/publication/305827886_Sustainable_biodiesel_production_via_transesterification_of_waste_cooking_oil_by

Abstract

Cleaner and sustainable production of biodiesel from non-edible seed oils offers distinctive opportunity to cater with energy crises associated with depleting fossil fuel. Large scale production of biodiesel could lead to positive outcomes in terms of environmental quality by reducing greenhouse gasses emission and Societal-Economic development. This research engrossed on biodiesel production from fifteen (15) novel, highly potential of non-edible, novel and biodegradable feedstocks such as *Cestrum nocturnum* L, *Cichorium intybus* L, *Zanthoxylum armatum* DC, *Citrus medica* L, *Citrus paradisi* Macfad and *Citrus aurantium* L., *Cupressus sempervirens*, *Trachyspermum ammi* (L.), *Cupressus macrocarpa, Nannorrhops ritchieana* (Griff.) Aitch., *Cordia myxa* L., *Cordia dichotoma* G.Forst., *Chamaerops humilis* L., *Monotheca buxifolia*, and *Grewia asiatica* (L.) using a variety of green nanocatalysts.

These non-edible oil seeds have been studied systematically including their collection, morphological identification, Scanning Electron Microscopy (SEM) of seeds, oil content determination, oil extraction, biodiesel synthesis, optimization, characterization and analysis of fuel properties in relation to the international standards.

Fifteen different green nanocatalysts were synthesized with aqueous leaves extract of *Silybum marianum*, *Boerhavia diffusa*, *Anagallis arvensis*, *Alternanthera pungens*, *Salvia moocroftiana*, *Portulaca oleracea*, *Boerhavia procumbens*, *Galium boreale*, *Alternanthera pungens*, *Parthenium hysterophorus*, *Colchicum aitchisoni*, *Chenopodium album*, *Nasturtium officinale*, *Calendula arvensis* and *Fumaria indica*. It is stated that these green nano catalysts are found to be recyclable in nature with easy recovery and reusability. Synthesized nanoparticles were characterized *via* X-Ray Diffraction (XRD), scanning electron microscopy (SEM), and Energy, spectroscopy (GC/MS), Fourier-transform infrared spectroscopy (FTIR) and Nuclear magnetic resonance (NMR).

Response Surface Methodology was used to compose central composite design for optimization reactions. The maximum yield of methyl ester (95%) was recorded for *Monotheca buxifolia* at optimum reaction conditions of oil to methanol molar ratio 1:7, CaO loading 0.5 (wt.%), temperature 90 °C and time 2 h. Whereas, lowest yield of 90% biodiesel was recorded for *Grewia asiatica* at a catalyst loading (Nb_2O_5)of 0.32 (wt.%), a Met:Oil ratio of 9:1, 180 min, and a temperature of 60 °C. Fuel properties of all synthesized methyl esters were found comparable to international standards of fuels. The current analysis came to the conclusion that

such plant species that produce non-edible seed oil are highly promising and less expensive biomass feedstock for sustainable production of biodiesel that could have favorable environmental and socioeconomic implications at many levels. This study also recommends that such non-edible feedstock be grown in large quantities on waste, marginal, saline, and wet soil to increase the quality and production of biodiesel for industrial usage and the worldwide market. This study also suggests emission analysis of synthetic biodiesel as well as the commercial synthesis of alternative catalysts, such as nano-sized hybrids of metal oxide.

Introduction

1.1 Present Energy Scenario: Global prospective

Rapid urbanization and population growth have led to issues including high energy demand, greenhouse gas (GHG) emissions, and environmental pollution as a result of the heavy use of fossil fuels like gas, oil, and coal. All of these primary energy sources contribute to the production of organic and inorganic air pollutants, such as soot, ashes, tar droplets, and gases like CO_x, SO_x, NO_x, and CH_x (Hydrocarbons). Significant environmental challenges like the greenhouse effect and global warming are frequently caused by these contaminants (Lawan et al., 2019). Over the past 20 years, there has been a sharp rise in the global demand for fossil fuels. Global warming and the degradation of natural resources are the end results of this overuse of fossil fuels. Fossil fuels are non-renewable energy sources that are being used up exponentially faster than they can be replenished. It takes a very long time to replenish these natural resources (Rozina et al., 2017). Fuel costs are therefore skyrocketing, which is rising the worldwide inflation rate (Tang et al., 2018).

About 90% of the energy used in industrial production comes from non-renewable sources such fossil fuels including crude oil, coal, and gas. The energy crises of the 1970s were a driving force in the search for alternative energy sources since countries were becoming more dependent on fossil fuels. The search for a dependable alternative to energy was prompted by price volatility and environmental concerns surrounding CO_2 gas emissions from fossil fuels, such as smog, global warming, and decline in biodiversity (Demirbas et al., 2008). In order to assure low-cost and resource-efficient economic management, the European Commission has offered the concepts of the circular economy and the bioeconomy as system models. To produce renewable energy and protect the environment from careless waste biomass disposal, the circular economy can be combined with biofuel technology (Maina et al., 2017). Recycling and reusing materials are important tenets of the circular economy, which help to harmonize the bioeconomy and are intended to hasten the integrated application of sustainable biomass resources. According to Székács (2017), the bioeconomy relies on the conversion of recyclable carbon reservoirs from organic resources into a range of products like bioenergy, fuel, bio-based chemicals, and polymers that contribute to the circular economy. The circular economy places a strong emphasis on minimizing reliance on non-renewable energy sources, such as fossil fuels, and on the

sustainable use of natural resources. A step in the right direction towards a circular economy is the advancement of the use of renewable energy sources like bioethanol and biodiesel as alternatives to traditional fossil fuels. Therefore, the policy of the European Commission has encouraged the use of renewable energy resources for the production of bioenergy in order to improve environmental and social sustainability (Alaswad et al., 2015).

1.2 Biodiesel as a Renewable Energy source

A non-toxic, biodegradable, environmentally friendly, and sustainable form of fuel is called biofuel (Lamba et al., 2017). One of the effective ways to combat climate change and ensure a sufficient supply of energy is to employ renewable energy fuel in the transportation industry. Many countries are producing biofuels including biodiesel, bioethanol, biomethanol, and biogas to meet the world's growing energy demand and offer a renewable alternative to fossil fuels. Reusing agricultural waste and investigating plants that produce non-edible seed oils for biofuel generation are two alternatives.

Biofuel is ranked as the fourth-largest source of energy and supplies 9.5% of the world's primary energy (I.E.A 2021). Additionally, biofuel is regarded as the most advantageous fossil fuel substitute because it has the power to reduce greenhouse gas (GHG) emissions, a factor that contributes to the phenomena of global warming. A recent study found that by 2050, the world's biomass resource potential would be between 100-600 EJ. This amount of energy corresponds to 15-65% of the fundamental energy requirement, according to the International Energy Agency (I.E.A 2021).

Although biofuel help to reduce dependency on fossil fuels, the production of biodiesel from edible oils creates a conflict between the need for food and the need for fuel. If non-edible seed oil is used in place of edible oil as the second generation feedstock for biodiesel production, these difficulties can be resolved. *Thevetia peruviana*, *Azadirachta indica*, *Eruca sativa*, *Pistacia chinensis*, and other plants that produce non-edible seed oils for methyl ester synthesis are listed in the prior literature (Rozina et al., 2017a).

The Sustainable Development Goals (SDGs), which aim to improve human well-being and the sustainable use of natural resources, were signed by 193 nations in September 2015, marking the first time that this has ever happened. Goal 12 focuses on preserving the ecosystem, recycling biomass for environmentally friendly biofuels, halting global warming, and promoting the green

economy. Sir Rudolf Diesel discovered biodiesel in the 1900s. Nearly 95% of commercial biodiesel produced worldwide is made from vegetable oils (Gui et al., 2008). Many nations throughout the world are using their own resources to produce biodiesel. Indonesia and Malaysia, two of the top Asian nations, have a variety of possible biodiesel feedstocks but still do not produce a significant amount of bioethanol due to limited industrial use (Ingle et al ., 2020).

Unique characteristics of biodiesel include its non-toxicity, reduced SOx gas emissions, and biodegradability. Triglycerides and methanol are transesterified in the presence of an appropriate catalyst. The usage of biodiesel reduces greenhouse gas emissions by 41% (Silitonga et al., 2020). The most prevalent process for producing biodiesel is transesterification. It requires a reaction between crude oil and an alcohol, which is usually methanol, selected because of its short carbon chain, lower cost, and physical characteristics (Shaah et al., 2021). The use of biodiesel in fuel engines has no impact on engine performance, but due to its self-lubricating qualities, it minimizes hazardous engine emissions and increases the efficiency of the mechanical parts of the engine.

1.3 Resources used for Production of Biodiesel

There are numerous feed stocks that can be used to produce biodiesel, including different kinds of vegetable oils, microbial oils, animal fats, and waste oils (Rozina et al., 2019). Many nations around the world are using their own resources to produce biodiesel. Indonesia and Malaysia, two of the top Asian nations, offer a variety of possible biodiesel feedstocks but still do not produce a significant amount of bioethanol due to limited industrial use (Mba et al., 2015). Malaysia is one of the world's top producers of methyl esters and the third-largest producer of oil, contributing around 42% of the world's palm oil (Helmi et al., 2021). Currently, China, India, Indonesia, Philippines, and Thailand use their non-edible oil feedstocks, such as cottonseed, rubber seed, and Jatropha, to produce biodiesel. Around 60% of the world's castor oil is extracted in India (Ayoub et al., 2021). The use of edible oil for biodiesel production eventually gave rise to a dispute between food and fuel, though. This problem has raised the biodiesel cost to twice the price of petro diesel.

Non-edible oils, however, are a suitable and attractive choice for the production of biodiesel. Non-edible seed oils' proximity is influenced by local topography, climate, native

plants, and soil (Ayetor et al., 2015). Nearly 95% of commercial biodiesel produced worldwide is derived from vegetable oils. Due to its low sulfur and aromatic content, biodiesel is an environmentally friendly and non-toxic fuel (Fedosov et al., 2011).

Tallow, or waste animal fat, has been considered fairly often as a potential feedstock for biodiesel synthesis. Animal waste fat can be used to make biodiesel at a lower cost and contribute to a cleaner environment. Additionally, the methyl esters produced from used animal fat have physical and chemical properties that are strikingly comparable to those of petroleum fuels (Fedosov et al., 2011).

In recent years, waste cooking oil (WCO) has been considered as a potential alternative source for the production of biodiesel. The use of used cooking oil has many advantages over the usage of traditional edible oils, including remedies for health problems and waste oil disposal (Kannimuthu et al., 2021). It is estimated that, the world produces 4.1 kg of waste cooking oil per person per year, or over 29 Mt of waste cooking oil annually (Elkelawy et al., 2019). Cooking oil waste is five times more affordable than cooking oil itself. Due to the waste cooking oil's high free fatty acid (FFA) content and low oxidation stability from prolonged heating, pretreatment measures are required before the oil can be used to make biodiesel.

1.4 Plant based resources for biodiesel production

Several edible and non-edible seed oil sources have been examined for their potential for biodiesel production.

1.4.1 Edible Seed Oils

The choice of food is an important phase in the production of biodiesel and has a direct impact on a number of variables, including yield, prices, purity, and the composition of synthesized biodiesel. It is possible to choose between edible, waste, and non-edible feedstocks due to their availability and source types (Yang et al., 2004). The region influences the choice of raw materials used in the production of biodiesel. palm and rapeseed oils are the primary sources of biodiesel in Europe and other developed nations, while soybean oil is a significant biodiesel feedstock in the United States (Rozina etal., 2021). While selecting a feedstock, various factors can be taken into consideration, including chemical composition, oil content, suitable qualities, and physical characteristics (Ambat et al., 2018). Worldwide, a variety of feedstocks have been

used to produce biodiesel. Oils from plants are part of the basic materials (corn, palm, rapesecx1 and soybean).

Different edible seed oils, like rope oil, soybean, and sunflower oil, used as the raw material for the production of biodiesel (Anantharaman et al., 2016). However, a significant variance in food intake has an impact on the use of edible seed oil for biodiesel synthesis. This disparity has caused food and fuel prices to compete, which raises the price of biodiesel. Finally, because there is such a huge demand for biodiesel made from edible oil, it promotes awareness of non-edible oils like jatropha, beaver oil, and neem oil (Nguyen et al., 2021).

1.4.2 Non-Edible Seed Oils

Biodiesel is produced from a variety of sources, including edible and non - edible vegetable oils, animal fats, algae, fungi, and used cooking oil from both commercial and residential settings (Rozina et al., 2022). Due to their renewability and minimal impact on the environment, non-edible seed oils are the most productive and preferred feedstock among all others. Large production capacity of non-edible oil seeds and their ability to resolve the food versus fuel paradox, they are cost-effective. Certain plant species' seed oils and their compounds have demonstrated toxicity that can be employed to combat a variety of insect species (Torabi et al., 2020). There are numerous toxic and environmental hazardous plant seeds available, which are considered non-edible. These non-edible toxic oils include *Calophyllum inophyllum* (Arumugam et al., 2019), *Cerbera odollam* (Kansedo et al., 2009), *Brucea javanica* (Hasni 2017), *Saussurea heteromalla* (Rozina et al., 2019), *Reutealis trisperma* (Riayatsyah et al., 2017), *Linum usitatissimum* (Niazi et al., 2022), *Sisymbrium sophia* (Sahafi et al., 2018), *Croton megalocarpus* (Kafukuet al., 2010), *Schleichera oleosa* (Silitonga, et al., 2015) and *Silybum marianum* (Takase et al., 2014). These non-edible seeds contain a significant amount of oil, which can be converted into fatty acid methyl esters (FAMEs) via transesterification reaction using different solvents, such as methanol for reactivity, and inexpensive catalysts, such as homogeneous, heterogeneous, and enzymatic catalysts (Moreira et al., 2020).

Ultimate availability and lack of competition between food and fuel, non-edible feedstocks are preferred over edible feedstock. On barren land, plant species that produce non-edible seed oil can thrive with no assistance from humans. As a result, non-edible plant seed oil is a potential growth opportunity for the biodiesel industry since it is abundant, unpalatable, and

only needs a small amount of moisture to grow and develop into a product that can be produced in large quantities. In order to upsurge the production of biodiesel on a large scale, it is necessary to explore more non-edible seed oils as a raw material.

Non-edible oil offers an important source for the production of biodiesel is (Pandit et al., 2017). There are various benefits to making biodiesel from non-edible oil, including cheaper raw material costs and a reduction in food price rivalry (Rahimi et al., 2021). Biodiesel can be an effective answer to the energy dilemma if non-edible seed oil crops are produced on barren soil (Shaheen et al., 2018).

Regardless of the climate or the health of the soil, non-eating oil feedstocks have been produced on a large scale for an affordable price and high profit. Currently, a lot of researchers have discussed the usage of seeds that produce biodiesel. According to Bokhari et al. (2016), non-edible oil production sources such as rubber seed, kapok, pongamia, jatropha, and kapok oil have a higher potential for biodiesel synthesis than edible oils (Rozina et al., 2017). Non-edible oil-producing plants do not require specific environmental conditions because they have ideal adaptations and can grow in salty, infertile, and sodium-rich soils. Waste cooking oil (WCO) was also considered as a potential source for the generation of biodiesel. The synthesis of biodiesel from used cooking oil reduces the amount of food oils used in big quantities while also solving the disposal and health issues associated with used cooking oil (Saman et al., 2021). Brown or yellow waste cooking oil are the two different kinds. The yellow grate has a lower fatty acid content (around 15%) and could provide for a potentially inexpensive biodiesel feedstock. More than 15% of the fatty acids in brown grade have an adverse effect on the synthesis of biodiesel (Adewale et al., 2015).

Another source of biodiesel is the waste material produced when meat is processed and cooked. Animal fats include lard, meat, mouthwash, yellow grease, omega-3 fatty acid byproducts from fish oil, and yellow grease. Waste animal fats are inexpensive feedstocks that produce biodiesel, which contributes to a cleaner environment. Animal fats low in saturated fatty acids provide various benefits, such as a quick ignition time, a high heat value, and superior oxidative stability (Li et al., 2020).

In addition to edible or inedible seed oils, cooking oil waste, and animal byproduct fats, microalgae are another source of biodiesel synthesis. Microalgae has emerged as a very effective

environmentally friendly replacement due to the rising cost of petroleum and the growing concern about the greenhouse effect, which is mostly caused by the burning of fossil fuels (Ajith et al., 2020). A separate class of organisms known as microalgae photosynthesize can convert CO_2 into bioactive compounds in the presence of sunshine. Some algae species, notably *Pavlova lutheri* and *Chaetoceros muelleri,* have lipid contents of 35.5% and 33.6%, respectively (Mata et al., 2010). The highest barrier to algal fuels is the greater capital expense required to effectively convert microalgae into biofuels. Other issues include the production of algal oil, processing of fuel, managing waste, and extracting oil from a single or mixture of algae species (Adeniyi et al., 2018).

1.5 Preference of Non-Edible Oil Seeds for Biodiesel Production

Research and recommendations on various green oil sources, such as non-edible seed oil for biodiesel synthesis, have been made to overcome and minimize the energy related issues. Owing to their widespread availability in different regions of the world, numerous publications on the synthesis of biodiesel from different feedstocks, such as non-edible plant seed oil, have been published in the previous few decades (Foroutan et al., 2021). In various parts of the world, inedible seed oils such as *Jatropha curcas* and *Croton megalocarpus* have been declared competent for biodiesel synthesis (Rozina et al., 2017). According to previous studies, non-edible feedstock is an efficient source for alternative fuel that is sustainable. However, there are other elements that affect the choice of feedstock. These elements include: (1) a thorough examination of the feedstock's life cycle; (2) its accessibility; (3) land usage and growing techniques; and (4) its contribution to biodiversity and ecosystem losses. Impact on the environment, logistic costs (distribution and storage), economic worth of the feedstock considering byproducts, water requirements for the feedstock, and yield per acre of oil are among the factors to consider (Adepoju et al., 2020). Plants that produce non-edible seed oils can flourish in versatile environments; they can be utilized as fertilizers to improve soil after the oil has been extracted (Rozina et al., 2021). Another socioeconomic benefit of indigenous non-edible oil based biodiesel production might be a program to reduce poverty for the local poor population by creating jobs in addition to supplying the locals with sustainable energy. All of these opportunities significantly improve and raise the living standards of rural residents. These seeds grow naturally in a variety of ecological settings and are easily adapted to any environment.

1.6 Exploration of the Novel Non-edible oil seeds for the current Project

A key step in the development of sustainable biodiesel production is the choice of non-edible oil. This is the primary variable affecting the process clearance and production costs. There are many different non-edible feedstocks that have been reported by previous literature, however the majority of them are not sustainable solutions in terms of feasibility and yield. Topography, climate, and terrain of Pakistan have endowed the country with a rich variety of flora. Pakistan has a great deal of potential and a promising future for renewable energy. In the current study project, some prospective novel feedstocks have been sought out from throughout the nation keeping in mind all of these factors. None of this feedstock has been documented for use in the synthesis of biodiesel in earlier research. According to our review of the literature, no thorough research has been done on these possible candidates for nonedible products. Additionally, there were no comparative data on the oil profile and use of these potential species for the synthesis and optimization of biodiesel. Our paper is the first in-depth analysis of the morphology, total oil characterization (qualitative and quantitative), synthesis of novel green nano-particles and their characterization via innovative techniques, biodiesel synthesis, parametric optimization by response surface methodology (RSM), biodiesel characterization, and ASTM standardization.

1.7 Technologies used for biodiesel production

A number of technologies, including pyrolysis, micro-emulsification, dilution, and transesterification, have been employed to produce biodiesel from non-edible feedstock (Ansori et al., 2021). Catalysts are not consumed during chemical reactions; they play a significant role in accelerating the rate of reaction. catalysts are used up during the first stage of a chemical reaction and then regenerate during the second stage. As a result, this process keeps happening without threatening to modify the catalyst permanently. Thermodynamic calculations can be used to change the reaction rate. Without a catalyst, the transesterification reaction requires somewhat more time (Ma et al., 2021).

Various methods of synthesis are used for biodiesel production. The main issue barring vegetable oils from being used in diesel engines is viscosity. Low combustion and knocking may also be caused by other issues, such as low cetane number and high oil flash point. Different approaches can be used to tackle these issues, including (1) pyrolysis (2) dilution/blending (3)

micro-emulsion (4) transesterification, which is the most widely used technique for producing biodiesel.

1.7.1 Transesterification

Transesterification is the utmost practical technology for producing biodiesel from oil and fat feedstocks. Vegetable oils and fats (triglycerides) undergo transesterification to become their alkyl esters with reduced viscosity, practically identical to petroleum fuel. In this reaction, 3 moles of alcohol (methanol or ethanol) and 1 mole of fatty acid combine (Avhad et al., 2015). Transesterification, in general, is a type of reversible reaction that considerably moves forward under heat or pressure. However, the inclusion of a catalyst speeds up the reaction rate. In order to obtain the best concentration of fatty acid methyl esters, numerous oils to alcohol molar ratios have been reported by various studies. The amount and kind of catalyst, the type of alcohol, the reaction time and temperature, the FFA content, and the water content in oils are the main variables affecting the rate of the transesterification reaction (Fatah et al., 2012).

There are two types of transesterification reactions: non-catalytic and catalytic methods. Catalysts that are heterogeneous or homogeneous can be used to catalyze the catalytic transesterification (acid or base). Owing to their viability, effective catalyst recovery, and high product yield, transesterification reactions are used for the synthesis of biodiesel in the current research study.

1.7.1.1 Homogenous Alkali Catalyzed Transesterification Reaction

Homogeneous alkali catalyzed transesterification process is the technique used to produce biodiesel most frequently (Mofijur et al., 2021). Base catalysts are very active and economical, and they quickly produce biodiesel of excellent quality. KOH and NaOH are the two alkali catalysts that are most frequently utilized in transesterification reactions.

As compared to acid catalyst, homogenous base catalyst has numerous advantages, including (a) quick turnaround for higher biodiesel yield, (b) simple accessibility at minimum cost, and (c) somewhat favorable reaction conditions. Alkali-based homogeneous transesterification accelerates the reaction 4000 times more quickly than an acid catalyst (Behera et al., 2020). Alkali catalyzed transesterification, however, have certain drawbacks, such as the fact that it is quite sensitive to the FFA level of vegetable oils and fats. High FFA level (>11

w/w) will eventually cause soap to form, which limits catalyst effectiveness, causes higher viscosity and gel formation, and complicates the glycerol separation process (Rozina et al., 2019). Application of several pretreatment phases before beginning the alkali catalyzed transesterification reaction can alleviate this issue.

1.7.1.2 Homogenous Acid-Catalyzed Transesterification

The practical and economically viable approach for biodiesel production from vegetable oil containing high FFA content is acid catalyzed transesterification. Two acids which are most frequently employed for homogeneous transesterification are sulfuric acid and hydrochloric acid. The process starts by mixing acidified methanol or ethanol directly with the feedstock oil, completing the transesterification and separation in one step (Hammouda et al., 2017). This process has many advantages over base catalysts, including the fact that (a) it is influenced by the FFA and water contents in the feedstock, (b) the esterification and transesterification processes happen at the same time, and (c) only mild reaction conditions are needed to carry out the reaction. Consequently, a major benefit of acid catalyst is that it may produce biodiesel straight from inexpensive feedstock with a high FFA level (Takase et al., 2018). However, compared to base catalyst, this approach has several drawbacks, such as high temperature and longer reaction times (Rozina et al., 2022). The main downsides of this method include the high equipment costs and the acid effluents' lack of catalyst reusability.

1.7.1.3 Heterogeneous Catalyzed Transesterification

Heterogeneous catalysts are solid by nature and have the advantages of being reused after use. They are easy to recover and separate from the reaction medium. Consequently, heterogeneous catalysis is perceived as a green process (Roy et al., 2019). Synthesis of biodiesel requires a number of solid base catalysts including hydrotalcites, alkali earth metal oxides, and some zeolites (Abd et al., 2019). The advantages of heterogeneous catalysts over homogeneous catalysts include the following (i) longer lifespan and recyclable nature (ii) easy product separation and no soap formation (iii) lack of washing requirement, preventing water pollution (iv) environmentally friendly and non-corrosive. Owing to their great selectivity and reusability, heterogeneous catalysts offer a wide spectrum for catalyst selection (Obi et al., 2020). Molaei Dehkordi and Dehkordi and Ghasemi (2012) employed a mixed oxide of Zr and Ca as a heterogeneous catalyst for transesterification and produced 92.7% of methyl esters. Calcium

oxide was identified as the preferable heterogeneous catalyst owing to its better performance, ready availability, low cost, and favorable reaction conditions (Amesho et al., 2022). The primary issue with heterogeneous catalysts is the catalyst's deactivation after repeated applications, which causes leaching, coking, and poisoning.

1.7.1.4 Nano-Catalyst Derived Transesterification

Nano-catalysts improve the reaction process of transesterification by allowing low temperature requirements, energy consumption recovery, high recycling rates, and decreasing side reactions (Bano et al., 2020). The advantages of utilizing nano-catalysts for biodiesel synthesis over traditional alkali/acid catalysts are significant. The term "nano-catalysis" refers to the use of various nanomaterials as catalysts in various heterogeneous catalytic processes. High surface energy, high surface to volume area, and high catalytic efficiency are all characteristics of nano-catalyst.

Since they have a specific surface area with high catalytic efficiency and lessen the issue of material exchange resistance associated with conventional catalysts, nano-catalysts are potential replacements for conventional catalysts in the efficient biodiesel synthesis from fats and vegetable oils. Hashmi et al., (2016) studied the transesterification of jatropha oil into biodiesel, a $CaO-Al_2O_3$ nano-catalyst has been developed. KF/CaO nano-catalyst for biodiesel synthesis with a yield of about 96% was studied by Hu et al. (2011). The abovementioned catalyst can be effectively employed to produce biodiesel from vegetable oils with a high acid value. Gupta et al., (2016) investigate the potential of CaO nanocatalysts for converting soybean oil into biodiesel.

The calcination temperature used to prepare the catalyst often affects the catalytic effectiveness of nano-catalysts. High calcination temperatures are advantageous for the interaction and support of active substances, which results in the creation of new active sites in the catalyst (Bohlouli and Mahdavian 2019). Metal nanoparticles are often created using a variety of chemical and physical processes. However, these methods are frequently pricy, time-consuming, and perhaps hazardous to the environment and living organisms. Finding an alternative, eco-friendly, and cost-effective technology for nanoparticle synthesis is therefore important (Ambat et al., 2022).

1.7.2 Pyrolysis

Pyrolysis is the term for the heat breakdown of an organic material in the presence of a suitable catalyst. Once different kinds of organic material are subjected to higher temperatures, triglycerides eventually turn into biodiesel, which is naturally renewable. Owing to its low viscosity and flash point, the pyrolyzed product can be used in conventional diesel engines. The presence of different carboxylic acids, alkanes, aromatics, and alkadienes was discovered through the pyrolysis of triglycerides (Pourkarimi et al., 2019).

1.7.3 Dilution/Blending

Vegetable oil is used directly during the dilution process, although with a few modifications. Several successful tests have been carried out with this technique. Petro gasoline was also added in it at different ratios. Many experts hypothesized that petro-diesel could not be replaced with 100% pure vegetable oil (Yaqoob et al., 2020). Vegetable oils cannot be used promptly in both indirect and direct diesel engines without producing unsatisfactory results. The obvious difficulties with pure vegetable oil are its FFA level, acid value, high viscosity, gum production, and polymerization as a result of oxidation and combustion (Ganitha et al., 2020). Therefore, dilution or blending causes vegetable oils density and viscosity to decrease. According to Hoang et al. (2021), adding 4% ethanol to petro-diesel would increase the effectiveness of braking thermal torque and power while simultaneously reducing fuel consumption (Hoang et al., 2021).

1.7.4 Micro-emulsification

A micro-emulsion is an optical dispersion made up of oil, water, and surfactants that is stable thermodynamically and isotropic with a dispersed domain range of 1-100 nm, typically 10-50 nm (Kumar et al., 2020). Vegetable oil is typically treated with this process to reduce its viscosity by mixing it with different solvents (ethanol, butanol, methyl esters and methanol). Vegetable oil, diesel, surfactant, alcohol, and cetane enhancer are all components of a biodiesel micro-emulsion in the proper ratios (Shenavaei et al., 2020). As a result of micro-emulsion, biodiesel has improved cetane number, decreased viscosity, and good spray characteristics (Charoensaeng et al., 2018).

1.7.5 Supercritical Transesterification

One of the potential processes is the transesterification reaction using supercritical conditions. With this method, the reaction rate is higher, the reaction time is shorter, the biodiesel purification and separation are straightforward because no soap or trash are produced, and the lack of a catalyst makes it simpler to recover the glycerol (Singh et al.. 2021). The primary disadvantages of a supercritical reaction are the expensive cost of the equipment, especially at high temperatures, and the breakdown of produced esters. Furthermore, this approach has drawbacks due to its use of high pressure, temperature, and volume of alcohol (Nguyen et al., 2020).

1.8 Emerging Technologies for Production of Biodiesel

As previously mentioned, mechanical impact of stirring   and the mass transfer of fatty acids from the oil state toward the oil-methanol interface ultimately regulate the rate of ethanol oxidation. The rate of mechanical stirring is influenced by a number of variables, including reaction duration. A number of technologies, such as super critical conditions, microwave, ultrasonic, hydrodynamic cavitation, and spinning disks, have been preferred by many researchers over the traditional method to address the issues in a noticeably shorter amount of time with less energy consumption. Ultrasonication technique and microwave assisted trans-esterification reaction are two examples of the new technologies for biodiesel synthesis using trans-esterification reaction.

1.9 Catalysts used in biodiesel production

Numerous catalysts, including homogeneous, heterogeneous, and enzymatic catalysts, are used to catalyze the transesterification. Use of homogeneous catalyst, however, raises a number of environmental issues, such as the production of enormous quantities of chemical waste, whereas heterogeneous and enzyme-based catalysts confront a number of difficulties, such as catalyst reusability and mass transfer resistance (Bokhari et al., 2016). Homogenous catalysts are more affordable and accessible. They do, however, have several drawbacks, including toxicity, corrosiveness, sensitivity to feedstock free fatty acid (FFA) level, non-recyclability, and difficulty in separating from reaction mixture. heterogeneous catalysts are solid multiphasic. They are made up of complexes of metal oxides. Due to their higher reactivity at optimal

reaction conditions, heterogeneous catalysts have an advantage over homogeneous catalysts (Sharma et al., 2018).

1.9.1 Homogeneous catalyst

Alkoxides as well as potassium, sodium, and other hydroxides make up homogeneous catalysts. Soap formation, washing to remove impurities, and catalyst recovery are problems with the homogeneously manufactured catalysts used to make biodiesel. Since homogenous catalysts are hygroscopic, efforts to bridge the synthesis and purification stages with heterogeneous catalysts have been focused (Sahani et al., 2020). These catalysts speed up the transesterification of oil and fats under ideal conditions of moderate temperature and pressure. However, the drawback is that the catalyst cannot be retrieved after the process.

1.9.1.1 Homogeneous Alkaline Catalysts

These catalysts are suited for oils with FFA content of <2% for transesterification reactions, while oils that have an FFA level of more than two percent should be pre-treated. Animal fat has an FFA content of 5–30% while cooking oil has an FFA content of 2–7% (Ayoub et al., 2021). $NaOC_4H_9$, KOH, $KOCH_3$, $NaOC_2H_5$, NaOH, Na_2O_2, and $NaOCH_3$ are notable homogeneous alkaline catalysts used for transesterification. The choice of catalysts is important in determining the performance of the fuel. The production of water from potassium hydroxide and sodium hydroxide limits the effectiveness of biodiesel.

1.9.1.2 Homogeneous Acid Catalysts

These catalysts can withstand higher moisture in the reaction mixture. The homogenous acid catalysts reduce the FFA amount in oils and fats. These catalysts are unfavorable compared to alkali catalysts because the reactions they catalyze need a high temperature. The most popular examples are hydrochloric acid (HCl), sulfonic acid (HSO_3R), and sulfuric acid. They need exclusive processing equipment in order to remove the high FFA concentration of cooking oil and animal fat (Allami et al., 2020). The production of soap and then an emulsion prevents proper separation when the FFA concentration is above 5%.

1.9.2 Heterogeneous catalyst

Calcium oxide has been shown to be one of the most effective heterogeneous nano-catalysts in catalyzing transesterification. Previous studies have found that calcium oxide may be

used economically and effectively, which is supported by its unique qualities such strong basicity, a simple technique of production, and other relevant economic advantages (Navajas et al., 2020). Natural resources like eggshell, chicken bone, oyster shell, and snail shell are rich sources of calcium oxide. Several CaO-based catalysts, including CaO/C, Li/CaO, and CaO/TiO2, have previously been created for the production of biodiesel (Kumar et al., 20121).

The employment of metal oxides during transesterification causes large oil particles, such as triglycerides, to quickly disperse into the pores of the catalyst for effective reactivity, as has been discovered through prior research investigations (Kafuku et al., 2010; Olutoye et al., 2011). Leaching, active site swelling, difficulties in catalyst production, and expensive pre-treatment are some of the drawbacks of heterogeneous catalysis (Mkhize et al., 2015).

1.9.2.1 Heterogeneous Catalyst with alkaline nature

Heterogeneous base catalysts get around problems with homogeneous base catalysts, like the difficulty in separating glycerol from the biodiesel layer because of saponification. The best heterogeneous base catalysts are metal oxides which have demonstrated good catalytic activity in transesterification reactions. These catalysts have a low solubility compared to homogeneous catalysts, and because their active sites are removed during reactions, they are simple to separate and reuse. On the other hand, they can also be easily restored. Heterogeneous catalysts only have one drawback: they store well and absorb water. Numerous metallic oxides, including transition metals, alkalis, and alkaline earth, have emerged as possible candidates for oils transesterification. Due to the fact that metal oxides contain both bronsted base and bronsted acid characteristics (anions). Composites can occasionally be created for use as catalysts (Lu et al., 2016).

1.9.2.2 Heterogeneous Catalysts with Acidic nature

These catalysts include zeolite, oxides of silica, alumina, molybdenum, and zirconium, as well as heteropoly acids. Compared to their homogeneous equivalents, such catalysts are more environmentally benign and stable. To reduce the problems with diffusion, such catalysts ought to contain a lot of active sites, being water-resistant, have a mild acidity, and be porous (Calgaroto et al., 2013). By eliminating separation procedures and allowing for reuse, their use will enable a decline in corrosion phenomena (Mkhize et al., 2015; Peng et al., 2008).

Additionally, solid acid catalysts are preferred over liquid acid catalysts since they have more sites with a range of Lewis or Bronsted acidity strengths (Muthu et al., 2010).

1.9.3 Biomass-based Catalysts

Heterogeneous nano-catalysts derived from plants and animals. Shells are greatly preferred for the production of heterogeneous base catalysts since they can be used to produce CaO-based catalysts of animal origin. Throughout the process, the byproduct CO_2 must be eliminated. When the temperature rises and the surface of the carbonate moves from the outer to the inner surface, the carbonate dissociates. During this conversion, the surface porosity rises, and a CaO catalyst (active) is created. Solid catalysts have been employed successfully for biodiesel production (Changmai et al., 2020). Due to the high concentration of potassium, phosphorus, calcium, and magnesium ions found in tucuma palm peels, they demonstrated high catalytic activity (Mendonça et al., 2019). Bombax ceiba seed extract was used by Hebbar et al. (2018) to synthesize CaO nanoparticles from *Bombax ceiba* seed oil, yielding 96.2 % biodiesel. The green nanocatalysts could be recycled up to five times (Hebbar et al., 2018). The techniques for producing phytonanocatalyst using sodium and potassium oxides found in banana peels are shown in Figure 10.

Waste pine apple leaves were effectively employed to produce solid base catalysts, and this phytonanocatalyst was used to synthesize biodiesel from soybean oil with a 98.92% yield (de Barros et al., 2020). However, *Sargassum horneri* carbon (10 wt.%) sulfonated to produce 96.4 % biodiesel when utilized as a phytonanocatalyst (acid solid catalyst) for oleic acid esterification in the presence of a 1:15 M oleic acid/methanol ratio. The production of 91.2 % FAME from mixed non-edible oil was accomplished using rubber deoiled (Malani et al., 2018). According to prior investigations, the same process (calcination at 900 °C for 4 hours) is utilized to manufacture an affordable solid base catalyst using chicken bones. The transesterification of soybean seed oil resulted in yield of 89.3 %. This catalyst helped to increase process efficiency four times (Farooq et al., 2015). Nisar et al., 2021 treated animal bones with potassium hydroxide in order to test its effectiveness on transesterification of Jatropha under ideal circumstances. High conversion yield (96.1%) was achieved with a 9:1 methanol to oil ratio, 6 percent weight per weight of oil used, and a 3h reaction period at 70°C (Nisar et al., 2021). In study of Ali et al (2018) goat bones were employed to transesterify old

cooking oil. They increased the bone's catalytic properties by calcining it with CaO at a 1:9 Oil:Met ratio at 65 °C for 5 hours, and they reached an 84 percent yield after three cycles of reusability (Ali et al., 2018).   CaO was produced from egg shell with 3% catalyst loading, and 96 percent conversion efficiency, vegetable oil was transformed to biodiesel. As a result, affordable and environmentally friendly biodiesel was created (Kara et al., 2019). Although, there is long list of investigated homogenous and heterogonous (both basic and acidic) catalysts synthesized using the method of chemical synthesis still there is need to explore more reliable, eco-friendly and bio-mediated to avoid its harmful consequences on environment and living societies.

1.9.4 Biocatalysts

The application of biological systems or their elements to accelerate chemical reactions and their rate is getting attention now days as they are non-hazardous and environmentally friendly. Owing to their reusability and natural nature, biocatalysts have become a vital alternative to chemical catalysts. They are used to conduct diverse reactions and have proven successful in resolving a wide range of difficulties relating to human and environmental concerns (Dhake et al., 2011). Since these factors directly affect the overall cost of the process, a biocatalyst that meets these criteria is one that is easily accessible, highly selective, affordable, and reusable. Research on enzymatic biodiesel utilized lipases in powdered or liquid form. The majority of preferred biocatalysts are proteins considered to be enzymes (Bhatia et al., 2021). These free-form enzymes are far less expensive such as single-useability (they become inactive after one use) and lower operational stability, which makes them less efficient. Aggregates are created through powdered preparation, which reduces the amount of active sites that are available (Ganesan et al., 2009). Additionally, using powder raises health risks because it might trigger allergies when inhaled. Commercial immobilized lipases are currently being targeted due to issues with using free lipases (Jacoby et al., 2013; (Kumar and Pal 2021). However, the high cost of these preparations is what prevents their use in the manufacturing of vast quantities of goods, such biodiesel (Sundaramahalingam et al., 2021; (Freitas et al., 2019).

1.9.5 Green nanocatalyst

Phytonano-catalysts are plant-mediated nanoparticles that enhance the rate of reaction and reduce the dependency on hazardous solvents and reagents. Phytonano-catalysts improve the energy efficacy of chemical processes and enhanced the design of various non-toxic products. The implication of such principles in nano-science will assist the synthesis and processing of fundamentally harmless nanoparticles and devices with nano-based structures. Various parts of the plant can be used to reduce nanoparticles, which are an eco-friendly, biodegradable, hazardous free and non-toxic method compared to chemical and physical methods. Plant leaf extracts have the benefit of acting as stabilising and reducing agents, which makes the production of nanoparticles easier. Reducing agents used in biomedicine are present at varying amounts in different types of leaf extracts; hence the leaf extract composition does have effect on the nanoparticle formation. The key phytochemicals used in the manufacture of nanoparticles are terpenoids, flavones, ketones, amides, aldehydes, and carboxylic acids.

Nano-catalysts also play a significant role in the production of biodiesel due to their great stability, reusability, and effective catalytic activity (Nayebzadeh et al., 2020). The production of nanoparticles using non-toxic aqueous plant extracts has captured the interest of researchers since it is a straightforward, environmentally acceptable technique. These nano-catalysts can be used in various organic transformation activities. In comparison to other heterogenous catalysts, nano-catalysts have a higher catalytic activity and a larger surface area (Dawood et al., 2021). Nano-catalysts are important in the manufacture of biodiesel because of their effective catalytic activity and stability. Recently, nano-catalysts have drawn a lot of interest in a range of applications, such as the delivery of medication, optoelectronics, and wastewater cleanup (Ameen et al., 2022). The use of green nano synthesis is now preferred over chemical nanoparticle production. Due to the existence of stabilizers, surfactants, metabolites, and enzymes that can function as reducing and stabilizing agents as well as stabilizers and natural reducing agents, plant exudates and herbal extracts are the primary substrates utilized for green nanoparticle synthesis (Banerjee et al., 2019).

Plant extracts produced under diverse conditions and commonly utilized as reducing reagents in various physical and chemical processes have helped to advance the field of phyto-

nano synthesis in recent years. Green synthesis is a secure and environmentally responsible procedure. Stabilizing agents are employed in the previously discussed procedures to prevent accretion, however in green synthesis, biomolecules like amino acids from plant extract and enzymes can function as a reducing and stabilizing agent (Davoodbasha et al., 2021). Phytonano-catalysts are nanoparticles produced by plants that speed up reactions and lessen reliance on potentially harmful solvents and chemicals. Phytonano-catalysts boost the design of several non-toxic goods and increase the energy efficacy of chemical processes. The application of similar concepts to nanoscience will facilitate the production of essentially innocuous nanoparticles and nano-based gadgets. Different plant parts can be utilized to reduce nanoparticles, which is an alternative to chemical and physical approaches that is eco-friendly, biodegradable, risk-free, and non-toxic (Mittal et al., 2022). Nanoparticle synthesis has also been shown to be advantageous compared to microbial processes.

They contain a range of biological chemical substances, including phenols, terpenoids, alkaloids, vitamins, and flavonoids which play a significant role in reducing metal oxides. Their useful qualities, such as antioxidant, anti-inflammatory, antispasmodic, diuretic, laxative, stomachic, expectorant, purgative, and rejuvenates, led to their selection. Additionally, the use of naturally occurring, less expensive biomass materials like *Boerhavia procumbens* could produce metal oxide in an aqueous media, avoiding the need for hazardous chemical solvents.

Metals are regarded as models since they have been employed frequently in the creation of nanoparticles (NPs). Aqueous extracts from *Trigonella foenum-graecum* seed were used to create the silver NPs (Karpagam et al., 2020). *Salocornia brachiata* was utilized as a catalyst in the photosynthetic synthesis of the gold nanoparticles. For catalysis, the bark of *Eucommia ulmoides* was utilized to synthesize palladium nanoparticles in an aqueous extract and the bran of sorghum was used to synthesize iron nanoparticles (Velusamy et al., 2021). Abbasi et al. (2021) synthesized CoO NPs with *Rhamnus virgata* leaf extract and studied it for antibacterial activity, revealing promising biological potential. According to Bibi et al. (2017), *Punica granatum* could be used to synthesize cobalt-oxide NPs for photo-catalytic applications. The majority of researchers are drawn to silver-based nanoparticles because they are effective in oxidative catalysis, biosensing, and photo-induced visual effects. In numerous industrial processes such isomerization, transesterification, and alkylation, silver oxide has been employed consistently. The use of plant extracts to synthesis nanoparticles has been shown to be advantageous

compared to the microbiological procedure. The mass production of nanoparticles is mediated by the use of plant extracts (Kumari, et al., 2022).

1.10 Background Justification of Present Project

High energy costs, increasing energy imports, concerns about the supply of petroleum, and a growing understanding of the harmful environmental effects of fossil fuels have all contributed to an increase in interest in the development of renewable plant-based biofuels (Mahlia et al., 2020). In order to address energy shortages and environmental concerns, a sizable number of diverse oil-yielding crops (more than 350) have been identified and designated as strong candidates for the future biodiesel sector. However, due to the application of intensified technologies regarding exploration of novel non-edible feedstock and their subsequent processing for biodiesel production via accessible, accessible, and stable catalysts, the majority of these non-edible oil resources have not been thoroughly explored, and there is a significant gap (Tabatabaei et al., 2019). Edible oils have previously been employed as a feedstock to address energy shortages. This approach has sparked a heated debate over the merits of food and fuel, which ultimately results in deforestation and the depletion of quality soil, rendering the area infertile. Due to aberrant rainfall patterns, extensive agronomic practices, and deforestation for industrialization and community development, Pakistan, an agricultural nation, is today experiencing the same problems as other agricultural nations with regard to arid land (Gebremariam et al., 2018). The negative effects of these actions on our motherland include salinity, drought, and ultimately unproductive soil. In Pakistan, there are over 28 million hectares of marginal land that cannot be farmed because of a lack of water, exposure to radiation, salinity, and soil erosion. They might replace edible crops while having a long-term good influence on the ecology, non-edible crops, also known as second-generation feedstock, have become more important to the biodiesel sector (Mathew et al., 2021).

The main benefits of using non-edible oil-producing crops as fuel are their ready availability, liquid nature, biodegradability, and environmentally beneficial qualities. These plants can be grown on waste or marginal areas with little moisture requirement because they are drought tolerant and have the ability to improve soil quality by fixing nitrogen. In addition, these plants were not consumed by people due to the toxins they contained, which are dangerous to

health. In this regard, non-edible plants as pongame and jatropha show promising results in their ability to withstand extreme salinity, hard climatic conditions, and greatest oil yield. Therefore, the focus of the current study is on the investigation, identification, and application of fifteen novel, non-edible feedstock for the biodiesel sector. These feedstocks include *Cestrum nocturnum* L, *Cichorium intybus* L, *Zanthoxylum armatum* DC, *Citrus medica* L, *Citrus paradisi* Macfad and *Citrus aurantium* L., *Cupressesu sempervirens*, *Trachyspermum ammi* (L.), *Cupressus macrocarpa, Nannorrhops ritchieana* (Griff.) Aitch., *Cordia myxa* L., *Cordia dichotoma* G.Forst., *Chamaerops humilis* L., *Monotheca buxifolia*, and *Grewia asiatica* (L.). These non-edible seed oil yielding plants were selected due to high oil content and little free fatty acids that are unfit for human consumption. They grow wildly and require less or no human efforts for cultivation. Seeds of these plants are wasted and not utilized for human food. These plants can be grown on waste marginal lands hence, have potential to be used as renewable alternative to fossil fuel.

Transesterification reaction is catalyzed by a variety of catalysts, including enzymatic, heterogeneous, and homogeneous catalysts. However, the use of homogeneous catalyst presents a number of environmental concerns, including the generation of vast amounts of chemical waste, whereas heterogeneous and enzyme-based catalysts face a number of challenges, including catalyst reusability and mass transfer resistance (Ramos et al., 2019). Heterogeneous catalysts offer an advantage over homogeneous catalysts due to higher reactivity under ideal reaction conditions. Nano-catalysts are more catalytically active and have a bigger surface area than other heterogenous catalysts. Due to their efficient catalytic activity and stability. Recently, a variety of applications, including drug production, optoelectronics, and wastewater treatment, have spawned a lot of interest in nano-catalysts (Zhong et al., 2020). The toxic materials utilized in the chemical synthesis of nanoparticles restrict their application. The production of green nanoparticles is currently preferred over chemical nanoparticles. Plant exudates and herbal extracts are the main substrates employed for green nanoparticle synthesis due to the presence of stabilizers, surfactants, metabolites, and enzymes that can function as reducing and stabilizing agents (Karpagam et al., 2020). Therefore, in this research project green mediated synthesis method was applied to prepare nanoparticles using plant parts of various species including *Anagallis arvensis* L., *Boerhavia diffusa*, *Parthenium hysterophorus*, *Alternanthera pungens*, *Portulaca oleracea*, *Galium boreale*, *Salvia moocroftiana*, *Silybum marianum*. Selection of these

plants was made on their rich phytochemical constituents. They have high concentration of alkaloid, flavonoids, phenol, vitamins, terpenoids and carboxylic acids which are essential phytochemicals used in nanoparticle synthesis.

These factors, such as the use of waste resources and pollution-free emissions, would make biodiesel a more affordable source of energy while also improving the economy and nature. The commercialization of this technique would then open the door for extraordinary industrial opportunities, which might be a significant step towards the development of clean, green transportation fuels. This study confirms that biodiesel is a cost-effective source of energy by highlighting the effects of biofuel production from non-edible feedstocks using green nanocatalysts.

1.11 Objectives of the study

Considering the worldwide threat posed by the depletion of fossil fuels and the resulting climatic changes has compelled us to pursue effective study for a solution to this grave issue. The current dissertation will aid in introducing fresh renewable possibilities for the sustainable production of biodiesel which will ultimately lessen the burden of environmental deterioration. The principal objectives of the current investigation are

- The study might concentrate on finding new, inedible oil seeds with high oil concentrations for biodiesel synthesis and determination of seed oil contents (%) to declare non-edible oil seed as cost-effective biodiesel feedstock

- Synthesis and application of different green nano catalysts (synthesized using various plants extracts) as cheap, economically feasible and non-toxic catalysts for biodiesel production

- Characterization of Green Nano-catalysts using innovative techniques such as XRD, SEM, EDX, TGA and FT-IR.

- Use of in situ and operando techniques, such as FT-IR, 1H NMR, 13C NMR, and GC-MS, to characterize synthesized biodiesel and learn more about the functional groups and methyl esters contained in biodiesel samples.

- Determination of fuel properties of prepared biodiesel, their comparison with International Standards of China GB/T 20828 (2007), American (ASTM-951, 6751) and European Union (EU-14214), to assess whether it may be implemented for being used as alternative to petro-diesel.

- Using statistical tools like Response Surface Methodology (RSM) and ANOVA to optimize synthesized biodiesel.

Materials and Methods
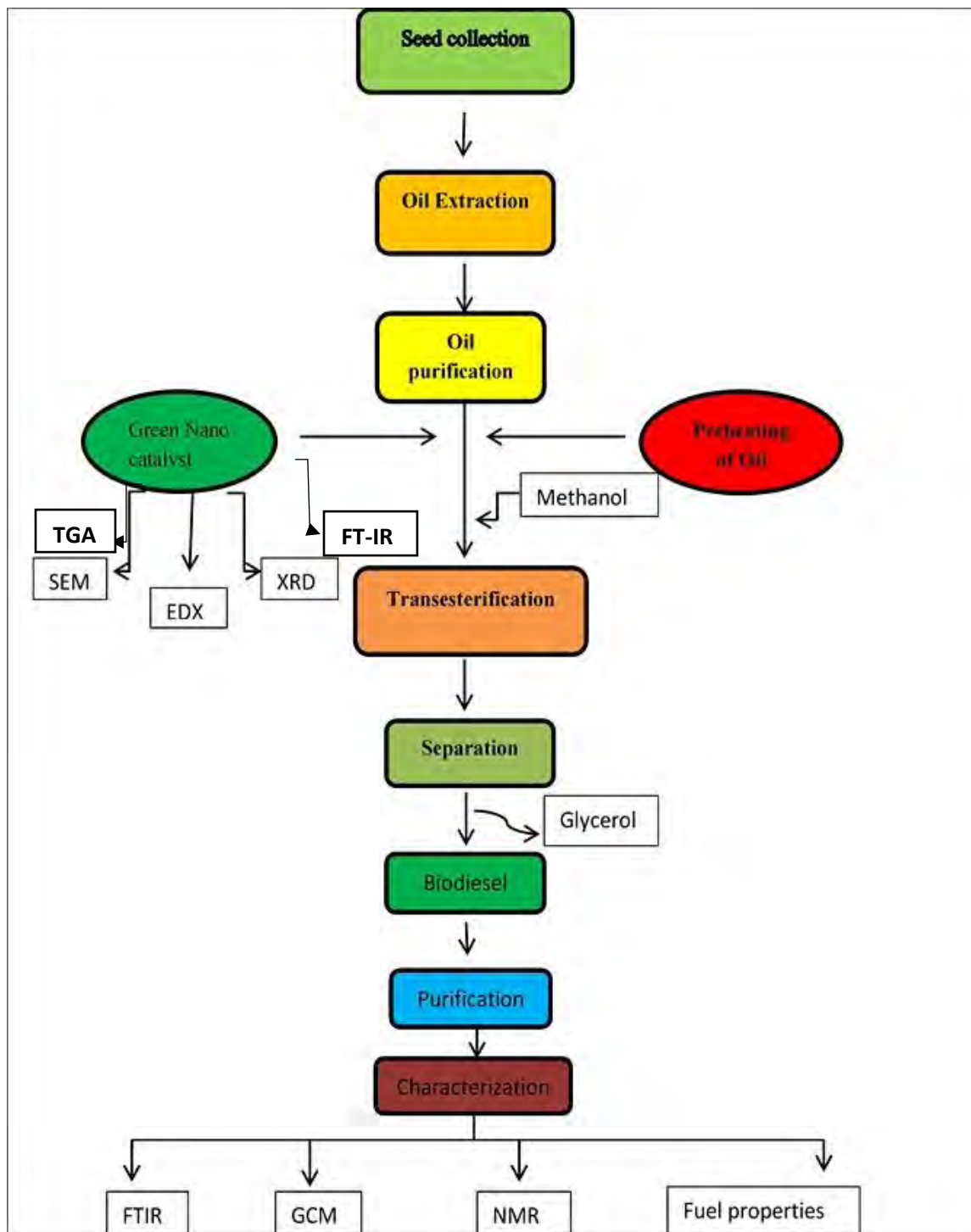
Flow chart 2.1. Flowsheet diagram of Research Methodology

2.1 Seeds collection

Seeds of selected plant species were collected from various areas of Pakistan in different seasons of the year for systematic study and investigation of their potential for biodiesel synthesis. Collected seeds were dried in the shed to eliminate moisture content and then kept in the oven at 60 ºC. Fifteen novel, non-edible seed oil producing plants species belonging to different families were targeted in the current investigation for micro morphological variations in the surface of their seeds. These plant species include *Cestrum nocturnum* L, *Cichorium intybus* L, *Zanthoxylum armatum* DC, *Citrus medica* L, *Citrus paradisi* Macfad and *Citrus aurantium* L., *Cupressesu sempervirens*, *Trachyspermum ammi* (L.), *Cupressus macrocarpa, Nannorrhops ritchieana* (Griff.) Aitch., *Cordia myxa* L., *Cordia dichotoma* G.Forst., *Chamaerops humilis* L., *Monotheca buxifolia*, and *Grewia asiatica* (L.).

2.2 Identification and Morphological description

Morphological representation of selected novel, non-edible oil yielding seeds was investigated with binocular Light microscope (Bosch and Lomb model W, New York). Sample seeds were observed at various magnification powers *i.e.* of 10X, 20X, 30X, and 40X. All measurements were recurrently taken for three to five times and mean values were recorded. Length and width of sample seeds were measured using a ruler. Macromorphological characters were further authenticated from flora of Pakistan. The selected samples were authenticated from expert Taxonomist. Further validation of the species name and author citation was done from International plant Name Index (www.ipni.org) and The Plant List (www.theplantlist.org) was referred**.**

2.3 Ornamentation of seed surface and scanning electron Microscopy (SEM)

SEM was employed for detailed micro morphological characteristics with scanning electron microscope (Model JEOL JSM- 5910) installed in Central Resource Laboratory, University of Peshawar, Pakistan. Ripened dried seeds of selected plant species were washed with 70% ethanol for 1 to 2 mins in order eliminate dust and other extra particles from seed surface. Seeds were dried after washing and mounted on stubs by using carbon sticky tape and were further passed to gold coating in a gold sputter machine for micro morphological study.

Various micro morphological characteristics of gold coated sampled seeds *i.e.* shape, surface texture, dimensions and structure were studied and SEM micrographs were taken.

2.4 Chemical Used

Seeds of were gathered and used for oil extraction. Chemicals used in the whole process included *n*-hexane, Methanol (99%), Anhydrous sodium sulphate, Chloroform, Phenolphthalein, Isopropyl alcohol, Zinc sulphate, Sodium hydroxide, Acetic acid, Diethyl ether, Indium (III) nitrate hydrate, $Ni(NO_3)$, zirconium nitrate, $FeSO_4$, $CuSO_4$, $CaSO_4$, cobalt acetate, silver nitrate ($AgNO_3$), $ZnSO_4$, $Mg(NO_3)_2$, $MnSO_4$, antimony sulfate ($Sb_2(SO_4)_3$), $PbSO_4$, Platinum (II) sulfate, tetrahydrate (H_8O_8PtS), Niobium(V) chloride, H_2SO_4, etc. All these chemicals were purchased from well-known companies like Merk (Germany), Schrlau (Spain) etc. Distilled water was used in the whole experimental work.

2.5 Seed oil Extraction

Organic solvent extraction method was conducted for determination of oil content in seeds of selected plant species. For this purpose, seeds were cleansed with water and dehydrated at 60 ℃ for 24 hours in the oven. A flask with round bottom calibrated 250 mL was loaded with n-hexane and 10 g of grounded powder of seed was placed in thimble and exposed to soxhlet apparatus fitted with reflex condenser. This process of extraction was carried out for 5 h at constant temperature of 60 ᵒC. Recovery of *n*-hexane was ensured at 55 using technique of rotatory evaporation. At the end of the process, wet sample was dried out in oven again for one day. Dried sample was weighted subsequently. The oil content of seeds was determined with the equation (1) given below (Arumugam and Ponnusami 2019).

$$Yield\% = \frac{Weight\ of\ seed\ oil\ produced}{Weight\ of\ seed\ sample\ used}\ x\ 100 \tag{1}$$

Plate 1 (a) Seed collection (b) Washing and rinsing of Seeds (c) Oil content determination (d) FFA content determination

2.6 Determination FFA content

FFA concentration of seed oil was calculated by acid base titration method. For this purpose, first a burette solution (0.025 M KOH) was prepared. In blank titration 10 mL of isopropanol along with few drops of indicator was taken in flask, followed by drop wise dripping of burette solution. In sample titration, a specific amount of seed oil was taken in the flask and titrated against burette solution (KOH). Initial and final readings were noted down. Finally, the formula (2) for estimating the FFA value of oil is given below (Yesilyurt and Cesur, 2020).

$$\text{Acid number} = \frac{(A-B) \; x \; C}{V} \tag{2}$$

where, A represents (sample), B for (Blank) KOH Volume, C: KOH Concentration, V: Oil Volume during titration.

2.7 Synthesis of Green Nano Catalyst

In the current study, fifteen novel, novel green nanocatalysts have been synthesized and successfully used to produce biodiesel during the transesterification process from non-edible seed oils. Schematic description of synthesis of green nano particles has been shown in Figure 2.1.

2.7.1 Synthesis of Indium oxide Nano catalyst

Leaves of *Boerhavia diffusa* were rinsed with water to remove the unwanted particles and cut into small pieces. For aqueous leaf extract preparation about 30 g of leaves was coupled with 500 mL distilled water and heated at 100 °C. Heating was continued until half of the water was evaporated, leaving the leaf extract fully saturated. Filter paper was used to remove plant residues from the extract, and the filtrate was stored in the refrigerator for future studies. To prepare a 400 mM indium nitrate solution, 48.13 g of Indium (III) nitrate hydrate was dissolved in 400 mL of H_2O and agitated for 30 min to ensure that all solute particles were completely dissolved. The Indium (III) nitrate hydrate solution was mixed with the filtrate and steamed at a steady temperature to make brown semi-liquid. This saturated solution was alienated into petri plates, desiccated in oven at 60 °C, and transferred into silica crucibles. Dried sample was calcined for 3 h in a muffled furnace at 500 °C (Chandra et al., 2020).

Figure 2.1. Schematic representation of synthesis of green nano particles

2.7.2 Synthesis of Nickel oxide Nanoparticles

Fresh and dry leaves of *Anagallis arvensis* were collected. In order to remove the unwanted particles, leaves were rinsed with distilled water and then sheared into small parts. About 20g of leaf powder was taken, mixed with 500 mL of distilled water and boiled at 100 ℃. This process continued until half of the water was evaporated, leaving the fully saturated leaf extract. Plant residues from the extract were removed using filter paper, and the filtrate was kept in the refrigerator for future experiments. To make 400 mM of nickel nitrate solution, 29.23 g of $Ni(NO_3)$ was solubilized in 400 mL of H_2O and the solution was stirred for 30 min for the complete dissolution of solute particles. For making brown semi-liquid, the $Ni(NO_3)$ solution was mixed with the filtrate (leaf extract) and steamed at a constant temperature. This solution was alienated into petri plates, dried in an oven at 60 ℃, and then scraped from the petri plates and alienated into silica pots using a scraper. After that, the sample was calcined for 3 h in a muffled reverb at 500 °C (Bindhu et al., 2020).

2.7.3 Synthesis of ZrO_2 Nanoparticles

Green nano-particles of ZrO_2 for transesterification reaction were synthesized using aqueous leaves extract of *Alternanthera pungens* collected from federal area of Pakistan. Collected leaves were rinsed with distilled water to confiscate impurities and hewn in to small pieces. 20 g of pieces of leaves were added to 500 ml of distilled water and boiled at 100 ℃ until 50% of water vaporized leaving saturated leave extract. Aqueous leaves extract was filtered through filter paper and kept in refrigerator. About 54.30 g of zirconium nitrate were dissolved in 400 mL of water by stirring it for 30 minutes to make 400 mM solution of zirconium nitrate. Prepared zirconium nitrate mM solution was added to leaf extract and boiled at constant temperature until dark colored semi liquid is obtained which was transferred to petri dishes and stored in oven 60 ℃ till it got fully dried. Dried mixture was scraped from petri dish with scraper and subjected to muffle furnace in silica crucibles for calcination. Sample was calcined for 3 h at 500 ℃.

2.7.4 Synthesis of Iron Oxide Nanoparticles

Fresh leaves of *Salvia moocroftiana* were collected from plants growing in Margalla hills Islamabad, Pakistan. Leaves of *Salvia moocroftiana* were washed with distilled water in order to eliminate unwanted dust particles and chopped into small pieces. 20 g of chopped leaves pieces were taken in a beaker and added 400 mL of distilled in it. It was boiled constantly until 50% of water was evaporated leaving saturated aqueous leaves extract. Saturated leaves extract was filtered via filter paper to remove plant residue and stored in refrigerator for future use. 200 mM solution of iron sul1phate was prepared by taking 6.027 g of $FeSO_4$ and dissolving in 200 mL of distilled water by stirring for 30 minutes. Saturated leave extract was added to molar solution and boiled at constant temperature until dark color semi liquid was obtained. After settling down, upper layer of water was discarded and down layer holding iron oxide was washed with distilled water and moved to petri dishes. They were kept in the oven and dried overnight at 60 ^{o}C. Dried sample was scraped and collected in silica crucibles for calcination in the muffle furnace. Calcination of the catalyst was carried out at 500 ^{o}C for 5 h.

2.7.5 Synthesis of Copper Oxide Nanoparticles

Green nanoparticles of CuO were synthesized with aqueous leaves extract of *Portulaca oleracea* collected from plants growing on roadsides of Quaid-i-Azam University Islamabad, Pakistan. Distilled water was used to wash plant leaves and eliminate contaminants. About 20 g of Portulaca oleracea leaves were cut into small pieces and added to 500 mL of distilled water. It was boiled at 100 $\circ$C until 50% of water evaporated leaving concentrated leaf extract. Resultant leaf extract was filtered using filter paper and stored in refrigerator for future use. About 25.537 g of $CuSO_4$ was taken and dissolved in 400 mL of distilled water by constant stirring for 30 min to prepare 400 mM solution of $CuSO_4$. Both aqueous leaf extract and $CuSO_4$ solution was mixed and boiled at constant temperature until dark colored semi liquid was obtained. It was poured into petri dishes and dried in the oven at 60 $\circ$C. Dried mixture was scraped from petri dishes and transferred to silica crucibles for calcination. Powdered sample was calcined in the muffle furnace at 500 $^{\circ}$C for 3 h.

2.7.6 Synthesis of Calcium Oxide Nanoparticles

Green nano-particles of calcium oxide were synthesized using fresh leaves of *Boerhavia procumbens* collected from plants growing in Federal areas of Pakistan. Leaves were first washed with distilled water in order to remove dust particles. They were dried and chopped into small pieces. Saturated aqueous leaf extract was prepared by taking 20 g of chopped leaf pieces in a beaker having 500 mL of distilled water and boiled constantly on hot plate until 50% of water was evaporated. Prepared leaf extract was filtered to remove plant residue and kept in refrigerator for future use. 5.4456 g of $CaSO_4$ was dissolved in 200 mL distilled water at constant stirring for 30 min to make 200 mM solution of calcium sulphate. Saturated leaf extract was added to the molar solution and heated at constant temperature until it appeared like dark color semi liquid.

Dark semi liquid was allowed to settle down for some time. Upper layer of water was discarded and lower layered containing calcium oxide was washed with distilled water and transferred to petri dishes. Petri dishes were kept in oven at 60 °C until they got fully dried. Dried catalyst sample was scraped with a scraper and collected in silica crucibles and calcined at 500 °C for 5 h.

2.7.7 Synthesis of Cobalt Oxide Nanoparticles

Fresh leaves of *Galium boreale* L. collected and rinsed with distilled water to eliminate unwanted particles from its surface. Around 20 g of chopped leaf fragments were added up to 400 mL distilled water in a beaker and stewed at 100 °C till concentrated leaf extract was formed. Leaf extract was percolated to eliminate leaves remainder. Molar solution of cobalt acetate was made by taking 28.32 g of cobalt acetate and dissolved in 400 mL water. Aqueous leaf extract was added to 400 mM solution of cobalt acetate and boiled at 100 °C until brown semi-liquid was obtained. After settling down for a while, upper liquid part was discarded leaving catalyst at the bottom and rinsed with distilled water repeatedly and desiccated in oven at 65 °C. Dehydrated particles were scraped from petri dishes and taken in crucibles to calcined in the furnace at 300 °C for 5 h (Ajith et al., 2020).

2.7.8 Synthesis of Silver Oxide Nanoparticles

Leaves of *Silybum marianum* were gathered from plants growing road sides of Quaid-i-Azam University Islamabad, Pakistan and undesirable particles were removed by washing it with distilled water. Leaves were then sliced into minor pieces. About 20 g of leaves powder was taken and boiled in 500 mL of distilled water and boiled it at 100 °C until 50% of water evaporated and leave extract was properly saturated. Extract obtained was filleted using filter paper in order to remove plant residue and stored in refrigerator for future use in experiments. About 27.17 g of silver nitrate ($AgNO_3$) was taken and dissolved in 400 mL water in order to make 400 mm solution of silver nitrate and stirred for 30 min to make it fully dissolved. Silver nitrate solution was added to aqueous leaf extract and boiled at unceasing temperature to get brown semi liquid. It was then transferred to petri dishes and stored in oven at 60 °C until it got fully dried. Scraper is used to scrape it from petri dished and transferred to silica crucibles. Sample was then calcined in muffle furnace at 500 °C for 3 h.

2.7.9 Synthesis of ZnO nanocatalyst

Collected fresh leaves of *Alternanthera pungens* were washed with distilled water and undesirable particles were eliminated. Clean dry leaves were sliced into small pieces. For making aqueous leaf extract about 30 g of leaves were boiled in 500 mL of distilled water on hotplate until it got reduced to 250 mL and saturated aqueous leaves extract was obtained. extract was cooled and purified using Whatman grade 2 filter paper to eliminate plant relics and stored at 4°C for use in future.

Zinc sulphate solution was prepared by dissolving 6.458 g of $ZnSO_4$ in 200 mL of distilled water and stirred for 15-20 min. Zinc sulphate solution was mixed with prepared leaf extract in a flask at continuous stirring at 65°C for 2 h. Mixture was let to settle down, upper layer of water was removed, and down layered containing zinc salt was washed with distilled water. The remaining solution was poured in the petri plates and left in oven for 24-48 h. The crystals formed were scratched with scraper and the powder was calcinated in silica crucible at 500°C for 3h.

2.7.10 Synthesis of MgO nanocatalyst

Leaves of *Parthenium hysterophorus* were collected and washed with distilled water to remove undesirable particles. After that, the leaves were sliced into small pieces. About 20 g of leaves pieces were taken and boiled in 500 mL of H_2O at 100 ^{o}C until half of water was vaporized leaving behind saturated leaf extract. In order to remove plant residue, the obtained leaf extract was filtered using filter paper and stored in the refrigerator for future use in experiments. About 5.93 g of $Mg(NO_3)_2$ was mixed in 200 mL water to form a 200 mM magnesium nitrate solution, which was then agitated for 30 minutes to dissolve completely. To make a dark brown semi-liquid, $Mg(NO_3)_2$ solution was added to leaf extract and boiled at a steady temperature. It was then poured in to petri dishes and kept in oven at 60 ^{o}C until it gets fully dried and scraped it with a scraper from petri dished and moved to silica crucibles for calcination. Catalyst sample was further calcined in muffle furnace at 500 ^{o}C for 5 h.

2.7. 11 Synthesis of Manganese oxide Nanoparticles

Colchicum aitchisoni., a weed that grows in Pakistan Federal Areas, was used to synthesize green nano-particles of manganese oxide using its fresh leaves. In order to clean off dust and other adherent debris, collected leaves were first rinsed with distilled water, and then were cut into little pieces with the use of scissors. The 500 mL of distilled water and 20 g of chopped leaf pieces were combined to prepare the saturated aqueous extract of the leaf, which was then continuously evaporated on a hot plate until half of the water was removed. Leaf extract was properly filtered to remove plant debris and stored in the fridge for later usage. A 200 mM solution of manganese sulfate was made by dissolving a known quantity of (6.04 g) $MnSO_4$ in 200 mL of pure distilled water for 30 min while stirring continuously. With the addition of saturated leaf extract and heating to a steady temperature, the molar solution took on the appearance of a dark color semi-liquid. Semi-liquid was finally made dark so that it could settle for ten minutes. The lower layer, which contained manganese oxide, was washed through distilled water and its crystal was transferred to Petri dishes while the semi-liquid upper layer was discarded. The Petri dishes were heated to 60 °C and fully dried in the oven. The catalyst sample was collected in silica crucibles after being scraped in dried form with a scraper and calcined for five hours at 500 °C.

2.7.12 Synthesis of Antimony oxide Nanoparticles

The Federal Areas of Pakistan are home to the weed *Chenopodium album* L., whose fresh leaves were utilized to prepare antimony oxide green nanoparticles. After being rinsed with distilled water and then chopped into little pieces with scissors, the gathered leaves were cleaned of dust and other clinging debris. In order to synthesize the saturated aqueous extract of the leaf, 500 mL of distilled water and 20 g of chopped leaf pieces were combined. This mixture was then constantly evaporated on a hot plate until half of the water was gone.

For subsequent use, leaf extract was adequately filtered to remove plant debris and kept in the refrigerator. A known quantity of 21.268 g of $Sb_2(SO_4)_3$ was dissolved in 200 mL of pure distilled water for 30 min while being constantly stirred to create a 200 mM solution of antimony sulfate. The molar solution assumed the appearance of a dark semi-liquid with the addition of saturated leaf extract and heating to a constant temperature. Finally, semi-liquid was turned black to allow it to settle for ten minutes. The semi-liquid upper layer was discarded while the lower layer, which contained antimony oxide, was washed through distilled water and its crystal was transferred to Petri dishes. Petri dishes were baked until completely dry at 60 °C. After being scraped in dried form with a scraper and calcined for five hours at 500 °C, the catalyst sample was collected in silica crucibles.

2.7.13 Synthesis of Lead oxide Nanoparticles

Nasturtium officinale R.Br. fresh leaves were collected, and unwanted particles were removed by washing with distilled water. Sliced into small pieces were clean, dry leaves. About 30 g of leaves were cooked in 500 mL of distilled water on a hotplate to make aqueous leaf extract; the mixture was then reduced to 250 mL and saturated aqueous leaf extract was obtained. To remove plant remnants, the extract was cooled, filtered using Whatman grade 2 filter paper, and then kept at 4 °C for later use. About 12.1304 g of $PbSO_4$ were dissolved in 200 mL of distilled water, 0.4 M solution of NaOH was added in it drop wise and agitated for 15 to 20 min to make lead sulphate solution. In a flask, produced leaf extract was combined with lead sulphate solution while being continuously stirred at 65 °C for two hours. After letting the mixture sit for a while, the top layer of water was removed, and the lower layer, which contained the lead salt,

was rinsed with distilled water. Petri plates were filled with the remaining solution, which was then placed in the oven for 24-48 h. The produced crystals were scraped using a scraper, and the powder was then calcined at 500 °C for three hours in a silica crucible.

2.7.14 Synthesis of Tellurium oxide Nanoparticles

Calendula arvensis L. leaves were gathered and cleaned with distilled water. The leaves were then cut into little bits. Approximately 20 g of leaf pieces were used, and 500 mL of water were heated with them at 100 ◦C until half of the water evaporated and left behind saturated leaf extract. The resulting leaf extract was filtered through filter paper to eliminate plant residue before being placed in the refrigerator for use in upcoming studies. About 200 mL of water and 8.86 g of Na_2TeO_3 were combined to create a 200 mM solution, which was then stirred for 30 min to completely dissolve. Na_2TeO_3 solution was added to leaf extract and heated at a constant temperature to produce a dark brown semi-liquid. It was then poured into petri dishes, dried in an oven at 60 ◦C, scraped out of the dishes with a scraper, and placed in silica crucibles for calcination. The catalyst sample was subsequently calcined at 500 ◦C for 5 h in a muffle furnace.

2.7.15 Synthesis of Niobium penta oxide Nanoparticles

Aqueous *Fumaria indica* (Hausskn.) Pugsley leaf extract was used to synthesize green nanoparticles of (Nb_2O_5). The plant was found growing along the roadsides of Quaid-i-Azam University in Islamabad, Pakistan. Plant leaves were washed with distilled water to remove impurities. About 500 mL of distilled water was combined with 20 g of small-grained *Fumaria indica* leaves. The leaf extract was concentrated after being heated at 100 ◦C until half of the water had evaporated. The final leaf extract was filtered using paper filters and kept in the refrigerator for later use. To create a 200 mM solution of Niobium(V) chloride 3 g of Niobium(V) chloride were taken and dissolved in 200 mL of ethanol (60%) for 30 minutes. Niobium(V) chloride solution and aqueous leaf extract were combined, then heated at a steady temperature until a black semi-liquid was formed. It was put on petri dishes and heated at 60 ◦C in the oven. The dried material was scraped from petri dishes and placed in silica crucibles for calcination. A powdered sample was calcined at 500 ◦C for three hours in a muffle furnace.

2.8 Characterization of Synthesized nano Catalyst

Techniques used in our current study to characterize green nano catalysts included XRD, SEM EDX, and FT-IR.

2.8.1 X-ray diffraction technique (XRD)

X-Ray Diffraction is a frequently used technique for investigating the elemental composition, size, and crystal structure of nanoparticles calcined at various temperatures and times. Crystalline structure of synthesized nano particles was determined by powder XRD analysis. Powder X-ray diffraction of samples was gathered using Cu-Kα radiations having 1.54 Å wavelength and the scanning rate of 2θ/min with 2θ=5-70°scale range. Debye–Scherer equation (5) at full width half maximum (FWHM) was used to calculate mean crystalline size of NPs utilizing XRD pattern of the most deep peaks at 2θ value.

$$D = \frac{0.9\lambda}{\beta \cos\theta} \tag{3}$$

Whereas, D = crystalline size of Ag_2O NPs, λ = wavelength of the X-Ray source used, β = full width at half maximum of the diffraction peak, and θ = Braggs diffraction angle.

2.8.2 Scanning Electron Microscopy (SEM)

Qualitative characterization such as surface topography of green nanoparticles was examined through SEM (SEM-Model-JSM5910). A suspension of copper oxide nanoparticles has been geared up and its drop is placed on aluminum coated SEM grid which is then analyzed. Electron microscopic field release was wielded to obtain SEM images at 20kV voltage.

2.8.3 Energy Diffraction X-ray analysis (EDX)

The Energy diffraction-X-ray analysis is carried out to specify the existence of diverse elements and metals in the green synthesized nanocatalyst. EDX was accomplished by efficiently utilizing the model (INCA200- Oxford instruments, UK) and the spectrum of EDX that examines chemical composition of copper oxide phyto-nanocatalyst falls in the range 0-1, 350eV.

2.8.4 Fourier Transform Infrared Spectroscopy (FTIR)

In order to pursue the structural composition of nanocatalysts, FTIR spectroscopic analysis was performed. Fourier Transform Infrared Spectroscopy (FTIR-Model-Bruker-Tensor 27) spectrum was obtained in the range of 400-4000 cm^{-1} to determine the organic and inorganic groups.

2.8.5 Thermogravimetric Analysis (TGA)

Thermo gravimetric analysis has been commanded in order to designate the thermal behavior of nanoparticles with respect to their temperature and weight along with determination of organic and inorganic proportion in the nanoparticles. In this approach, weight of sample nanoparticles is measured when it is heated and cooled. Sample is placed in furnace and temperature is increased gradually along with application of an inert gas. Weight of sample gets reduced owing to the decomposition and chemical activity happening to sample at elevated temperature. Thermal stability of phytonano-catalyst was detected through thermogravimetric analysis (TGA) using STARe SW 12.10 and performed in flowing air from room temperature to 1050 ^{o}C at heating rate 10 ^{o}C/ min.

2.9 Transesterification

Transesterification of seed oil was carried out at a specific temperature by adding specific volume of preheated seed oil, methanol (sonicated for 20 min) and green nano catalyst in flask (250 mL) having magnetic stirrer and a reflux condenser. The chemical reaction of Transesterification of seed oil has been shown in Figure 2.2 while Schematic representation of transesterification has been shown in Fig. 2.3. Synthesized biodiesel was separated from glycerol and catalyst via separating funnel and centrifuged at 4000 rpm for ten minutes (Figure 2.3). Moreover, a rotatory evaporator was employed to vaporize the excess methanol. Percentage yield of produced biodiesel was calculated by formula (3) (Yatish et al., 2020).

$$\%Yield = \frac{Biodiesel\ produced\ in\ grams}{Crude\ oil\ used\ in\ grams}\ x\ 100 \tag{4}$$
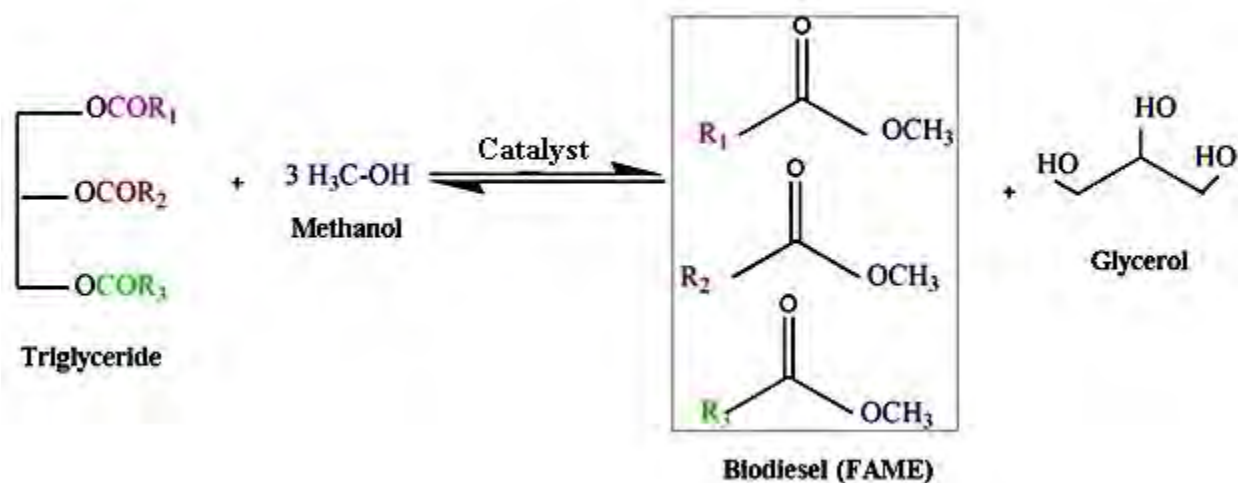
Figure 3.2 Chemical reaction of Transesterification of seed oil

2.10 Characterization of Synthesized Biodiesel

Following analytical techniques were used to characterize the synthetic biodiesel.:

2.10.1 Thin layer chromatography (TLC)

Thin layer chromatography technique was performed with solvent system which was composed of acetic acid-diethyl ether-n-hexane in fix ratio of 8:30:1. Identification of spots of seed oil triglycerides and fatty acid methyl esters was accomplished with Iodine vapor stain. TLC results were measured by using below equation (4) (Yadav et al., 2019).

$$Rf = \frac{Distance\ Traveled\ by\ Sample}{Distance\ traveled\ by\ Solvent\ Front} \tag{5}$$

R_f value was considered for confirmation of methyl esters formation as a result of transesterification.

2.10.2 Fourier Transform Infrared Spectroscopy (FT-IR)

Investigation of various functional groups and their structural arrangement found in FAMEs of biodiesel was accomplished with FTIR spectrum. FTIR spectrum of seed oil and methyl ester was executed on Perkin-Elmer Tensor 27 (Bruker) in the range 4000–400 cm^{-1} and resolution of 1 cm^{-1} and 15 cm^{-1} scan.

2.10.3 Nuclear Magnetic Resonance (NMR)

NMR analysis (^{1}H and ^{13}C) of methyl ester was collected at 300 MHz using spectrometer (Bruker) and (CDCl$_3$) solvent. Total conversion of seed oils into methyl ester was calculated using equation number 7 ('Doudin, 2021).

$$C = \frac{2AMe}{3ACH2} \text{ x } 100 \tag{6}$$

2.10.4 Gas Chromatography -Mass spectrometry (GC/MS)

Fatty acid composition of sample seed oils was identified by means of Gas chromatography and Mass spectrometry. The GC -6890N teamed with MS 5973 MSD fitted with duct column was used for recognition and characterization of biodiesel. Helium was used as a carrier gas with 1.5 mL/minute of flow rate and a programmed column temperature of 120-300 °C/min was employed. A 1.5 μL of prepared sample was placed in the column by means of split mode having the split ratio as 1:3.

2.10.5 Determination of Fuel Properties Biodiesel

The quality and efficiency of the biodiesel synthesized from non-edible seed oils was determined by measuring its fuel related properties which were then allied with American Society for Testing and Materials as ASTM D-6751 and further with Chinese standard GB/T (20828) and EN-14214 which is a European standard. These fuel properties take account of color, flash point °C, density, Kinematic viscosity, cloud point °C, pour point °C, sulphur wt. % and total acid number.

2.11 Experimental Design for optimization reactions

In order to obtain the highest possible yield of methyl esters, four different reaction parameters were evaluated using RSM. These parameters included catalyst loading (0.10-1.5 wt.%), time (60-180 min), temperature (55-110 °C), and methanol to oil (Met:oil) (3:1-12:1). Design Expert 13.4.0 was used to evaluate the regression analysis and statistical significance of the results. The Central Composite Design (CCD) with four separate and independent factors with distinct values one with the lowest value and the other with the highest was design to investigate their effect on the yield of FAMEs (response). Maximum of 30 experimental tests conducted. A significance test and an analysis of variance (ANOVA) were employed to evaluate the efficacy of the predicted model. Various criteria such as the correlation coefficient (R) and coefficient of determination were used to determine the feedback (R^2). The regression model was validated by the difference between actual and predicted values. The regression equation was used to find the best values for four individual variables (Aslan and Eryilmaz, 2020).

$$\mathbf{Y} = b0 + \sum_{i=1}^{k} biXi + \sum_{i=1}^{k} biiX2i + \sum_{i<j}^{k} bijXiXj + e \tag{7}$$

Whereas, y = biodiesel yield and b0 = intercept value (i= 1, 2, 3…k)

Results and Discussion

Nonedible Seed oil yielding Feedstock

Morphological Identification of Feedstock	Seed oil Extraction	Synthesis of Green Nanocatalyst
Light microscopy	Biodiesel Synthesis	Characterization of Green nanocatalysts
Scanning Electron Microscopy	Characterization of Biodiesel	Reusibility tests
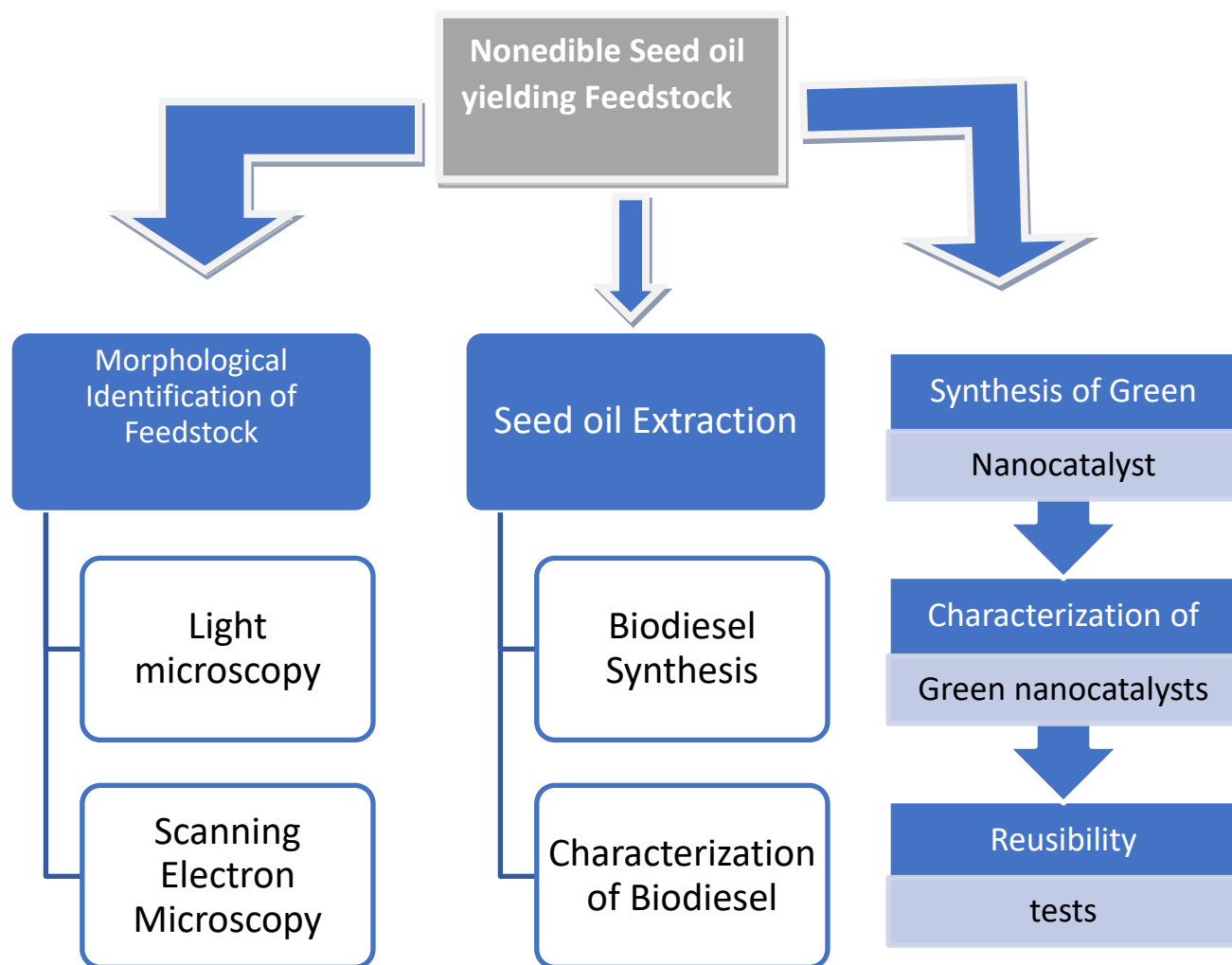
The flow sheet diagram of Results and Discussion.

Biodiesel Synthesis, Optimization and Characterization from Novel Non-edible oil Seeds via High Performance Phyto-nano catalysts

42

This chapter includes the results and discussions from the sixteen sections. These sections cover the morphological identification of non-edible feedstock, scanning electron microscopic examinations of seeds that produce oil, and the use of nine different catalysts to produce environmentally friendly biodiesel fuel using nine novel non-edible oil-producing seeds.

SECTION I: Morphological identification and Scanning Electron Microscopy of non-edible oil seeds

SECTION II: Biodiesel Production from *Zanthoxylum armatum* DC seed oil using Green nano Catalyst of Silver oxide

SECTION III: Biodiesel Production from *Citrus medica* L seed oil using Green nano Catalyst of Copper oxide

SECTION IV: Biodiesel Production from *Cichorium intybus* L seed oil using Green nano Catalyst of Magnesium oxide

SECTION V: Biodiesel Production from *Cestrum nocturnum* L. seed oil using Green nano Catalyst of Antimony oxide

SECTION VI: Biodiesel Production from *Citrus paradisi* Macfad seed oil using Green nano Catalyst of Lead oxide

SECTION VII: Biodiesel Production from *Citrus aurantium* L. seed oil using Green nano Catalyst of Zirconium oxide

SECTION VIII: Biodiesel Production from *Grewia asiatica* L. seed oil using Green nano Catalyst of Niobium oxide

SECTION IX: Biodiesel Production from *Monotheca buxifolia* seed oil using Green nano Catalyst of Calcium oxide

SECTION X: Biodiesel Production from *Cordia myxa* L. seed oil using Green nano Catalyst of Indium Oxide

SECTION XI: Biodiesel Production from *Cordia dichotoma* G.Forst. seed oil using Green nano Catalyst of Nickel Oxide

SECTION XII: Biodiesel Production from *Chamaerops humilis* L. seed oil using Green nano Catalyst of Cobalt oxide

SECTION XIII: Biodiesel Production from *Trachyspermum ammi* L. seed oil using Green nano Catalyst of Manganese oxide

SECTION XIV: Biodiesel Production from *Cupressus macrocarpa* seed oil using Green nano Catalyst of Iron oxide

SECTION XV: Biodiesel Production from *Nannorrhops ritchieana* (Griff.) Aitch. seed oil using Green nano Catalyst of Zinc oxide

SECTION XVI: Biodiesel Production from *Cupressus sempervirens* seed oil using Green nano Catalyst of Tellurium oxide

SECTION I

- Morphological identification and Scanning Electron Microscopy of non-edible oil seeds

3.1 Morphological identification and Scanning Electron Microscopy of non-edible oil seeds

This section describes the morphology of fifteen (15) novel non-edible oil producing plants using light microscopy along with a thorough examination of the micromorphological characteristics of seeds used as energy crops using scanning electron microscopy (SEM). It is essential to correctly identify and classify oil yielding seeds prior to use them as a promising feedstock for biodiesel production. This technique provides an open door for assessment of a few solid highlights for correct recognition and identification of closely related plant species and genera. For this purpose, scanning electron microscopy (SEM) was used by Dawood et al., (2020), to analyze the structure and micromorphological characteristics of non-edible oil seeds. SEM is the modern approach that enables us to identify and classify a variety of oil yielding seed species due to the stability of seed testa. Previous studies showed that use of SEM for the examination of morphological features of seeds provided useful information for their precise recognition. Using scanning electron microscope, Rashid et al., (2018) investigated the seed micromorphology of 12 *Vicieae* species. Kasem et al., (2011) reported 32 species of family Brassicaceae, while 51 seeds were investigated by (Murthy & Sanjappa, 2002). Similarly, Vural et al., (2008) investigated 48 *Astragalus* L. species in Turkey. Ahmad et al., (2020) reported 15 species of family Poaceae from Dera Ghazi Khan, Pakistan. Heiss et al., (2011) studies seed morphology of fifteen species of the genus *Nigella* for identification and diagnostic purpose. Luqman et al., (2019) described the seed morphology of 9 *Eucalyptus* species from Pakistan. The morphology of the seed coat provides a set of useful characters, knowledge and in the verification of plant seeds (Juan et al., 2000). Seed morphology, anatomical, and palynological characters are used to classify plants in various plant groups. Microscopic techniques are useful for the authentication of medicinal plant groups (Hadidchi et al., 2020).

In view of the importance of micromorphological characters for the taxonomic identification of species, we collected seeds of six novel plant species. This is the first detailed study on the seeds of selected fifteen novel oil yielding feedstocks. Table 1 paints wide range of micromophological characteristics of non-edible oil seeds such as surface sculpturing, cell arrangement, cell shape, periclinal wall shape, margins, protuberances and anticlinal wall shape. SEM micrographs and seed images of selected plant species are displayed in Figure 3.1.1(a-d) to Figure 3.1.15(a-d). This investigation revealed a great distinction and unambiguous variation in micromophological characters and seed size and shape of selected six novel, non-edible seed oil

feedstock which can be utilized as indicators for the identification of specific taxa. SEM is a very useful and reliable technique of the modern time which has solved numerous taxonomical issues related to plant identification and authentication by SEM micrographs of seeds (Alves, et al., 2009). Ultra-structural and micromophological study of seeds is a valid source of information as regard of evolution of angiosperm plants and their classification in the modern synthetic systems (Rashid, et al., 2018, Mokbli et al., 2018, Fatima et al., 2018). Likewise, our present study describes comprehensive evaluation of selected six oil seeds by SEM which assisted in their recognition as green and renewable source of biodiesel to tackle with issues raised by energy crises. Hexane has been used extensively for oil extraction and is a desirable chemical because it allows for fast oil recovery, has a narrow boiling point (63-69 °C), and has great solubilizing properties. Free fatty acid (FFA) content measurement is crucial for assessing the quality of raw materials, their deterioration during storage, and the shelf life of various vegetable oils. Free fatty acid (FFA) content measurement is crucial for assessing the quality of raw materials, their deterioration during storage, and the shelf life of various vegetable oils. The percentage of oil, FFA content, distribution, and micromorphological characteristics of selected seeds as determined by SEM are all included in Table 3.1.

3.1.1 *Zanthoxylum armatum* DC.

Zanthoxylum armatum (synonym; *Zanthoxylum alatum,*) commonly known as winged prickly ash or toothache tree, belongs to family Rutaceae is a non-edible oil yielding aromatic plant with mint and lime like flavor (Gupta et al., 2011). It is widely distributed in *East* Asia, Phillipines, Malaysia, North America, Korea and Japan. *Zanthoxylum armatum* is spiny xerophytic shrub or deciduous small tree having 3-7 folliate leaves and is pellucid-punctate with winged rachis and petiole. Ripened fruit follicles are typically rose-colored and 4-5 mm in diameter (Brijwal et al., 2013, Kalia et al., 1999). Seeds were 4.4 mm long and 9.4 mm wide (Table 3.1). Seeds of *Zanthoxylum armatum* are rounded or globose, solitary, shinning black in color and bitter in taste (Phuyal et al., 2019, Lawan et al., 2019). It has high oil content of 36% with FFA content of 0.680 mg KOH/g. In this regard *Zanthoxylum armatum* could be one of potential candidate and novel addition in pre-existing biodiesel feedstock record. SEM micrograph of *Zanthoxylum armatum* exhibited rugose to reticulate surface sculpturing with finer small pits, Elliptic to ovate cell outline, asymmetrical cell arrangement, convex ventral and

dorsal wall side, thick, deep anticlinal walls, thin and puzzled periclinal walls and with rounded basal point (Figure 3.1.1 c and d).
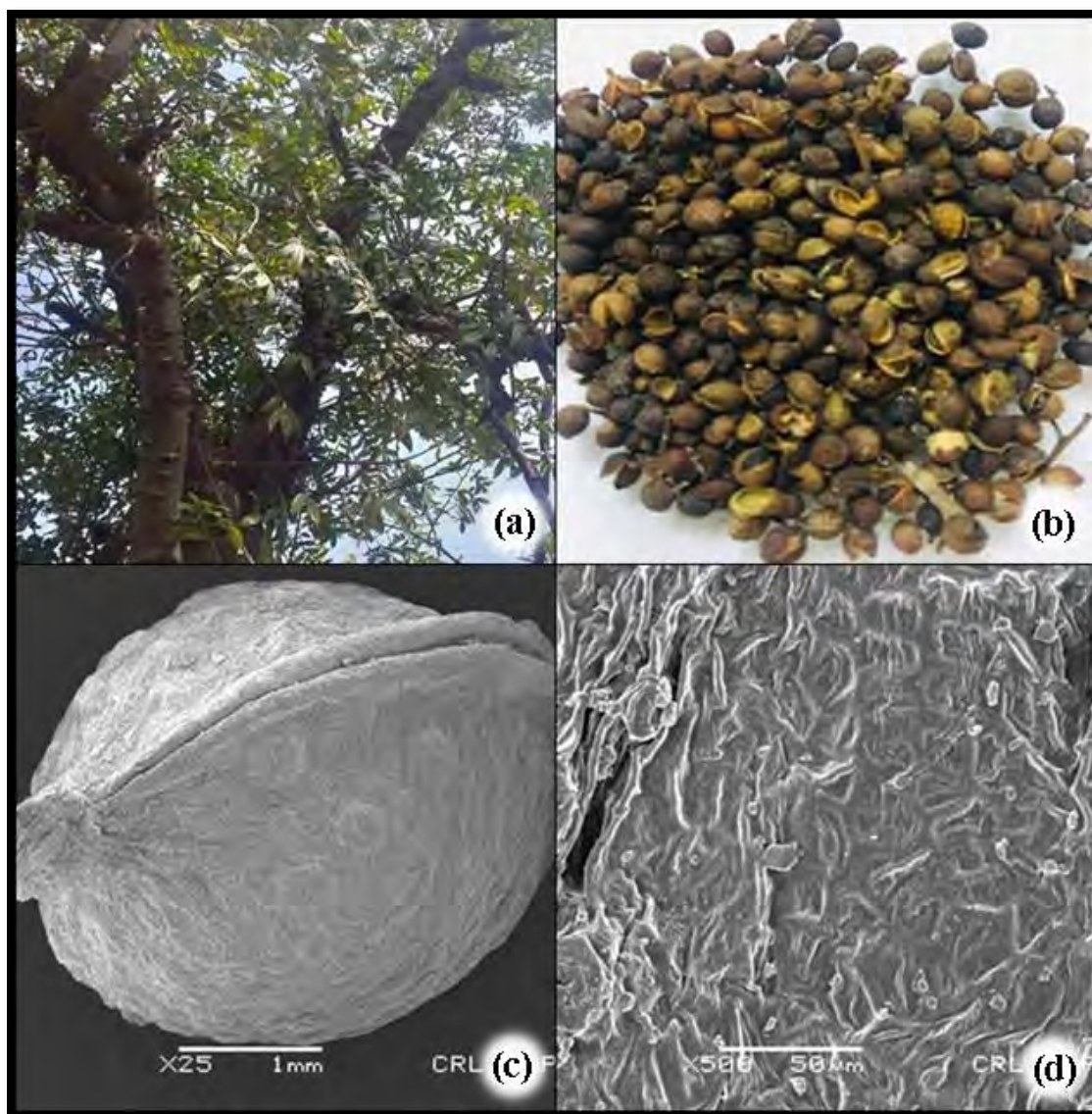
Plate 3.1.1. *Zanthoxylum armatum* DC **(a)** entire plant, **(b)** seeds, **(c,d)** SEM micrograph of seeds and sculpturing

3.1.2 *Citrus medica* **L.**

Citrus medica is an evergreen frequently spiny, small tree or shrub, commonly known as 'Citron'. It belongs to family Rutaceae and widely distributed in Eastern Himalaya, Persian Gulf, India, Pakistan and Italy. Fruit is plump hesperidium, globular, oblong to obovate. Rind contains oil glands and is constricted or slack. Ovary comprises 10-14 locule and ovules are biseriate. Seeds are small with smooth seed coat with solitary embryo and white cotyledons. They are semi deltoid in shape and greenish yellow in color (Figure 3.1.2b). Seeds were 9.1 mm long and 5.5 mm wide. Seeds have high oil content of 33% (w/w) with FFA content of 3.01 mg KOH/g. *Citrus medica* has high biodiesel potential of 93% (Table 3.1). SEM results of *Citrus medica* revealed reticulate surface sculpturing, cells are arranged in irregular fascicles and are chained in longitudinal lines in sulcate to ribbed pattern, thick, smooth anticlinal walls and deep and elevated periclinal wall was observed (Figure 3.1.2 c and d).

3.1.3 *Cichorium intybus* **L.**

Cichorium intybus is 4-110 cm tall, perennial herb, commonly known as 'Blue Dandelion'. It belongs to family Asteraceae and extensively distributed America, Australia, China, Europe, India and Pakistan. Achene was sub cylindric to obovoid in shape and brown in color. Seeds were yellow in color and cuneiform in shape. They have high oil content of 34% (w/). FFA content of seed oil was 0.56 mg KOH/g and biodiesel potential of 95% (Table 3.1). Seeds of *Cichorium intybus* were 15.8 mm long and 8.5 mm wide. SEM micrograph of *Cichorium intybus* has been shown in Figure 3.1.3 a-d. SEM results demonstrated Rugose, papillate surface sculpturing, narrow elliptic cell shape, layered and regular cell arrangement, raised, curved anticlinal wall and entire, depressed and glabrous periclinal wall. Seed powder of *Cichorium intybus* has anti-diabetic, anti-inflammatory, antiviral and antibacterial activity (Janda et al., 2021). Our current results are align with findings of Ayaz et al., (2019) who observed rugose papillate, verrucose papillate, and striated pattern in SEM micrograph of *Cichorium intybus*.
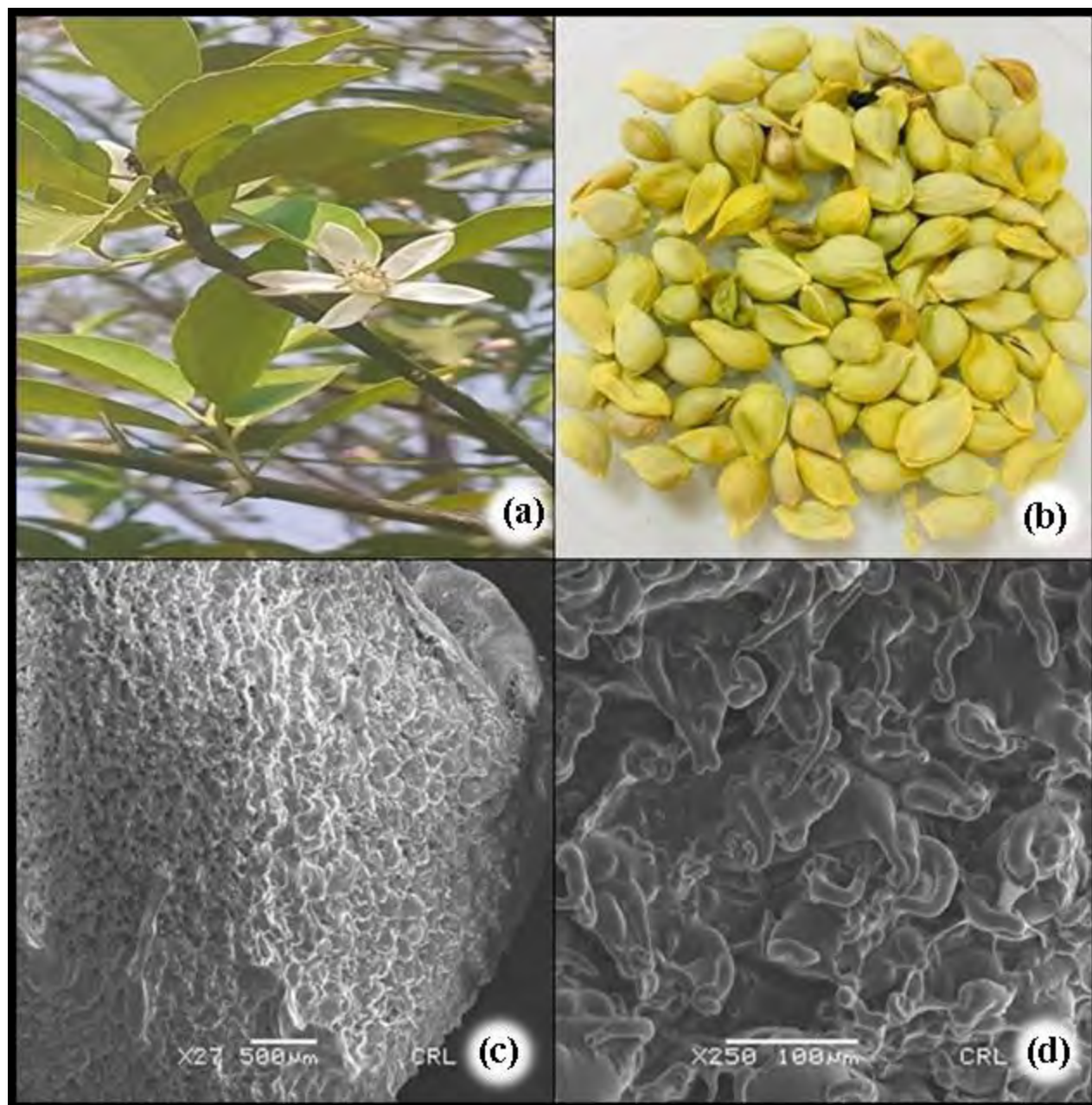
Plate 3.1.2. *Citrus medica* L. **(a)** entire plant, **(b)** seeds, **(c,d)** SEM micrograph of seeds and sculpturing
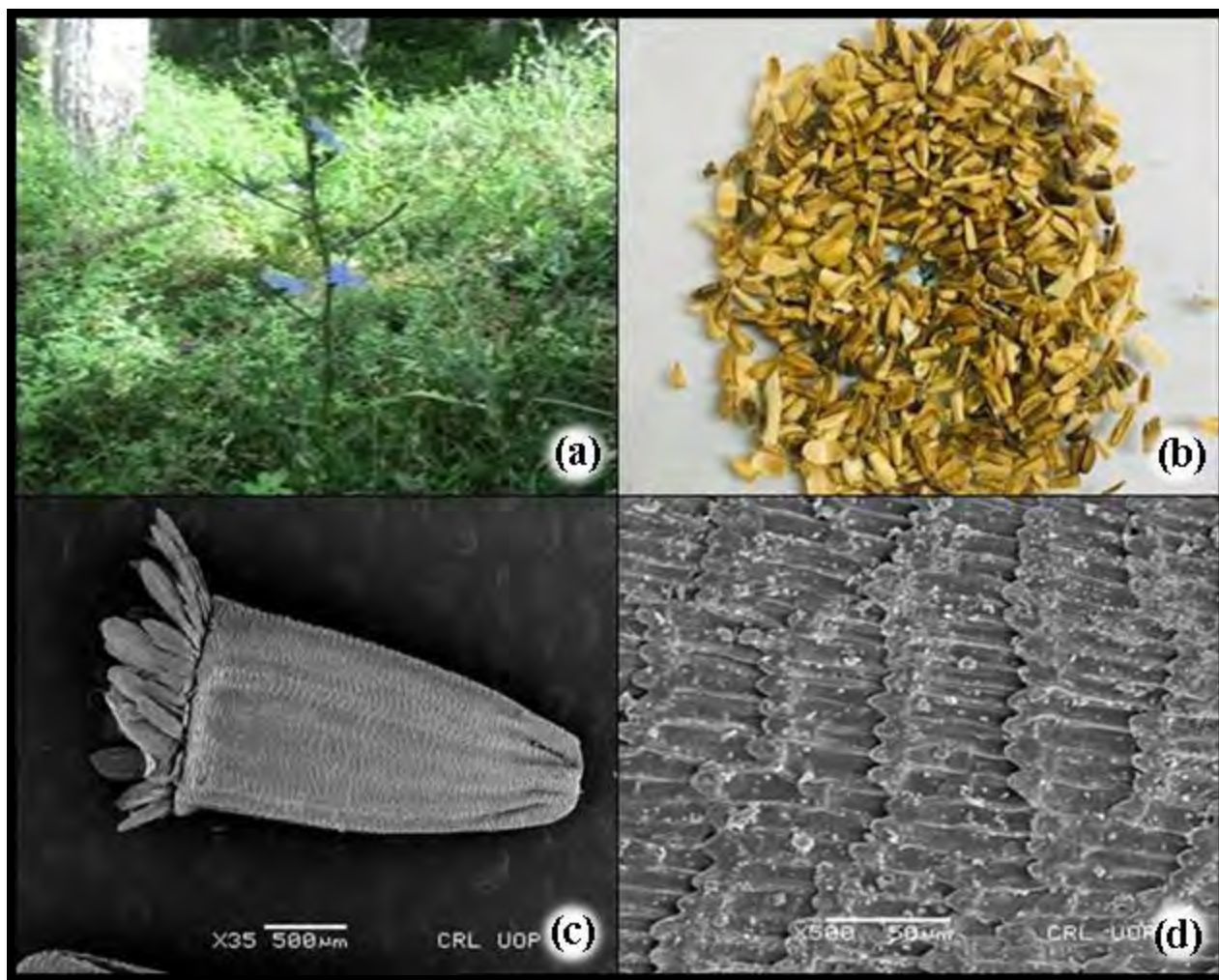
Plate 3.1.3. *Cichorium intybus* L. **(a)** entire plant, **(b)** seeds, **(c,d)** SEM micrograph of seeds and sculpturing

3.1.4 *Cestrum nocturnum* L.

Cestrum nocturnum is erect 1-3 m tall shrub with slandering branches. It belongs to family Solanaceae and is commonly known as 'Lady of the night' (Figure 3.1.4 a-d). It is distributed America, Australia, India and Pakistan. Fruit is ovoid, white, juicy berry. Seeds are black in color and triangular in shape. Seeds of *Cestrum nocturnum* were 1.8 mm long and 1.1 mm wide. They have high oil content of 28% (w/w). FFA content was found 1.5 mg KOH/g small enough to carry out single step transesterification. Biodiesel potential of non-edible seed oil of *Cestrum nocturnum* was 95% (Table 3.1). SEM micrograph illustrated striate, wrinkled surface pattern with rough cell outline, reticulate cell arrangement, wavy thick anticlinal wall and depressed, smooth and raised periclinal wall (Figure 3.1.4 c and d).

3.1.5 Citrus *paradisi* Macfad

Citrus paradisi is 6-13 m tall tree with a trunk of 15 cm in diameter and the top of tree is composed of spreading branches. It belongs to family Rutaceae and is commonly known as 'Grapefruit'. It is distributed in China, Pakistan, United States and Mexico. The fruit is bitter in taste, rounded to somewhat pear shaped with spotted peel and pale-lemon color. Seeds are yellowish in color and broad ovate in shape. Seeds were 15.8 mm long and 5 8.5 mm wide (Figure 3.1.5 a-d). Seeds of *Citrus paradisi* hold high oil content of 30% (w/w) and were found a potential feedstock for biodiesel production (Table 3.1). Free fatty acid (FFA) content of non-edible seed oil of *Citrus paradisi* was found 2.06 mg KOH/g. SEM micrograph of *Citrus paradisi* exposed reticulate surface sculpturing with granular bulging projections and fine small pits, irregular cell arrangement, thick and smooth anticlinal walls, elevated flat periclinal walls.
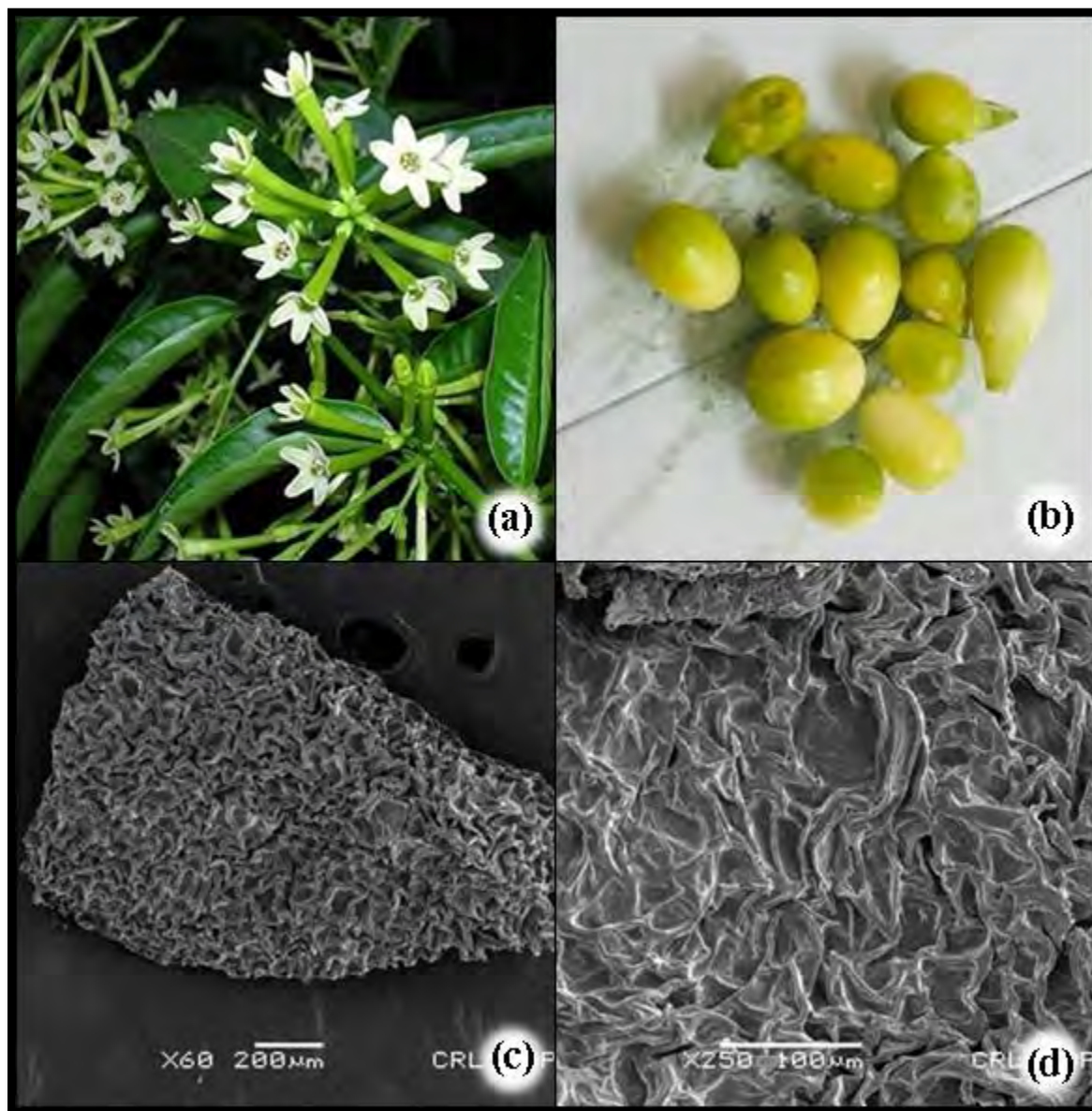
Plate 3.1.4. *Cestrum nocturnum* L **(a)** entire plant, **(b)** seeds, **(c,d)** SEM micrograph of seeds and sculpturing
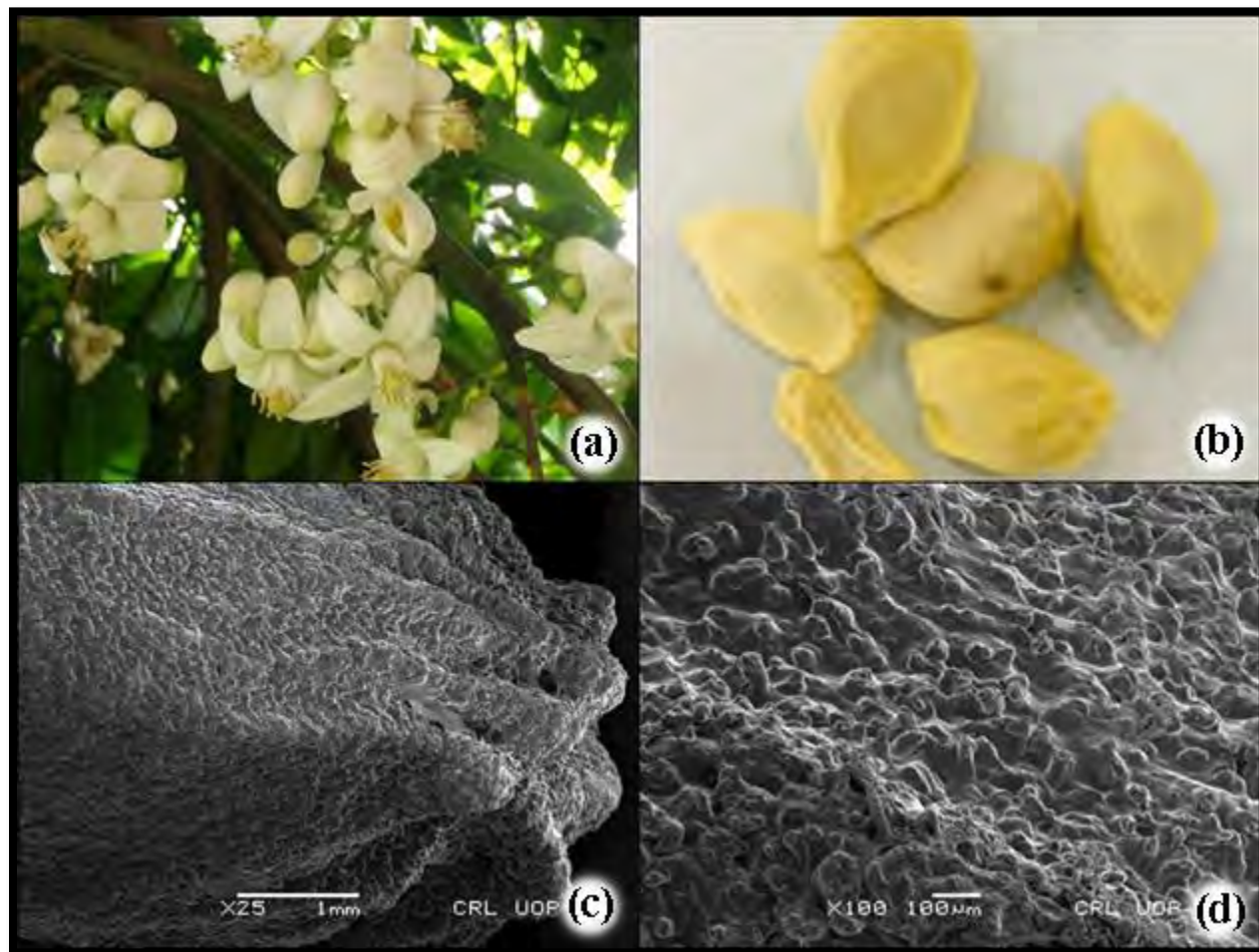
Plate 3.1.5. *Citrus paradisi* Macfad **(a)** entire plant, **(b)** seeds, **(c,d)** SEM micrograph of seeds and sculpturing

3.1.6 *Citrus aurantium* L.

Citrus aurantium is 7-8 m tall tree with sharp and spines axillary. It belongs to family Rutaceae and is widely distributed in Southeast Asia. Seeds were ovate in shape greenish yellow in color as shown in Figure 3. Seeds were 12.1 mm long and 6.2 mm wide (Table 1). Seeds of *Citrus aurantium* have high oil content of 38% (w/w). FFA content of non-edible seed oil was 0.14 mg KOH/g and high biodiesel potential of 94% (Table 3.1). Fruit flesh is bitter and acidic. On ripening, fruit rind is formed which is lumpy and glandular. SEM micrograph of *Citrus aurantium* has been illustrated in Figure 3.1.6 c and d. SEM micrograph of *Citrus aurantium* seeds showed perforate with semi tectate surface pattern, fitted with bulging protrusions, cells were found spherical to oval in shape, crooked cell arrangement, depressed, wavy anticlinal wall and thick periclinal walls elevation.

3.1.7 *Grewia asiatica* L.

Grewia asiatica is a small tree or large shrub belonging to family Malvaceae. It grows up to 8 m in height. Stem give rise to stellate tomentose young shoots. The bark of stem is greyish white in color. Leaves are calvate petiolate, mostly ovate to orbicular in shape with hairs on both surfaces, 5–15 cm in length. Abaxial surface of leaf lamina is greyish tomentose and adaxial surface is scabrous. Stipules are narrowly falcate or lanceolate. Inflorescence is cyme with 3 flowers (dischasial), 2–6 in axillary clusters. Peduncles are densely hairy and 2–3.5 cm long. Pedicels are 1– 1.3 cm long with thick hairs. Bracts linear– lanceolate in shape, up to 4mm long. Sepals broad, oblong, acute with inner glabrous surface and hairy outside. Petals are oblong, orange yellow in color having irregular lobes on the apex. The whitish gland of petals is surrounded by ring of hairs. Stamens are several with long filament, turn into purplish color. Anthers are oblong in shape. Ovary is globose with 4 mm long style. Stigma is indefinitely 4-lobed. Fruit is an edible drupe of dark purple color, globose shape, hairy, 5-12 mm diameter. Drupe contains fibrous mesocarp and is acidic in nature.

Seeds of *Grewia asiatica* were 10.3 mm long and 5.2 mm wide. They contain high seed oil content of 25% (w/w). FFA content of 0.72 mg KOH/g was detected in seed oil. A high yield of 95% of biodiesel was obtained with transesterification of seed oil. SEM micrographs exemplified webby surface sculpturing, asymmetrical cell arrangement, smooth, thick anticlinal

walls, thin, curved periclinal wall elevation (Figure 3.1.7 c and d). No record of SEM of *Grewia asiatica* seed was found in the previous literature. In general, SEM results disclosed that variation in the surface pattern of seed micromorphology would be helpful in differentiating various species of family Cupressaceae.
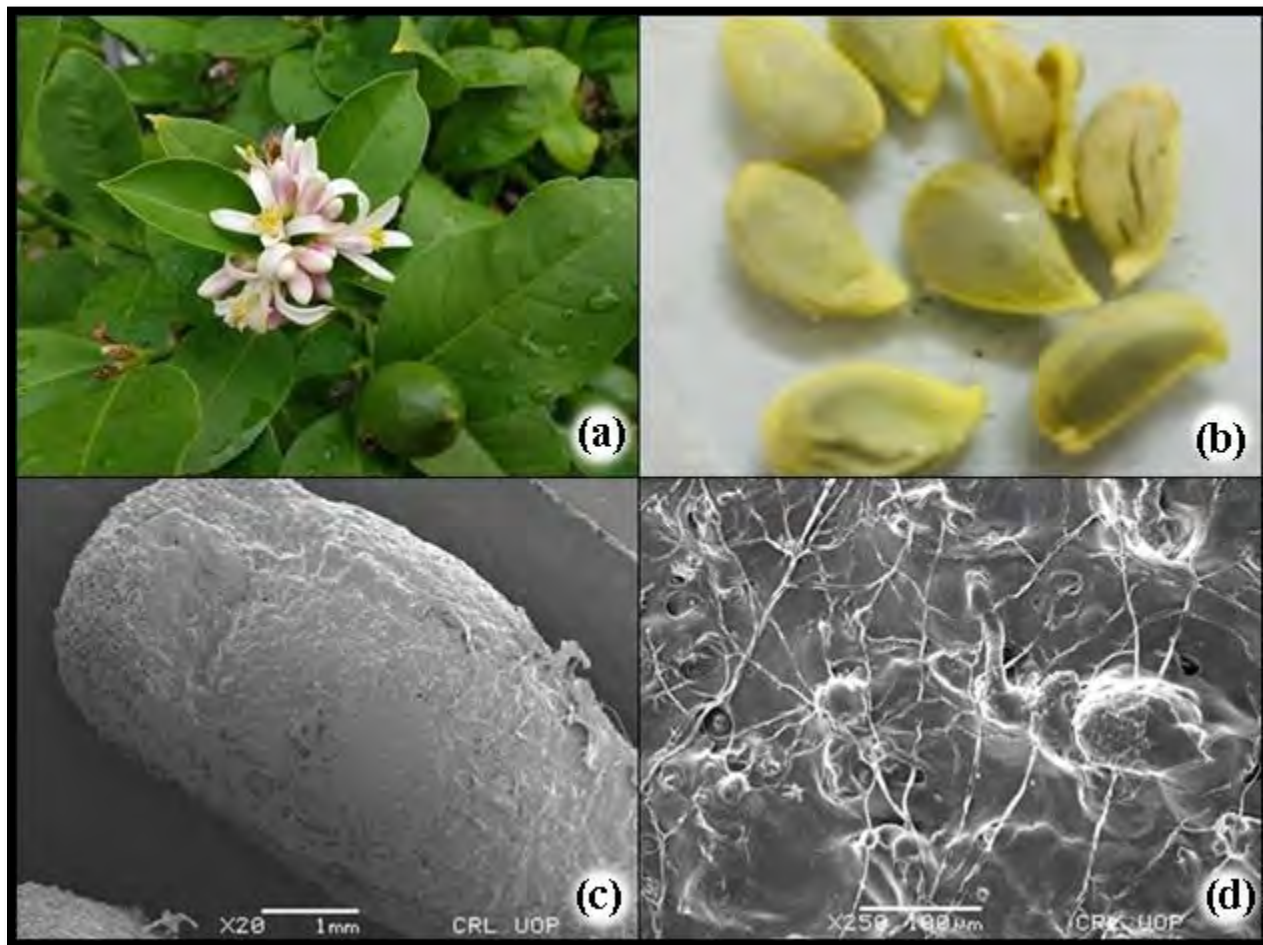
Plate 3.1.6. *Citrus aurantium* L. **(a)** entire plant, **(b)** seeds, **(c,d)** SEM micrograph of seeds and sculpturing
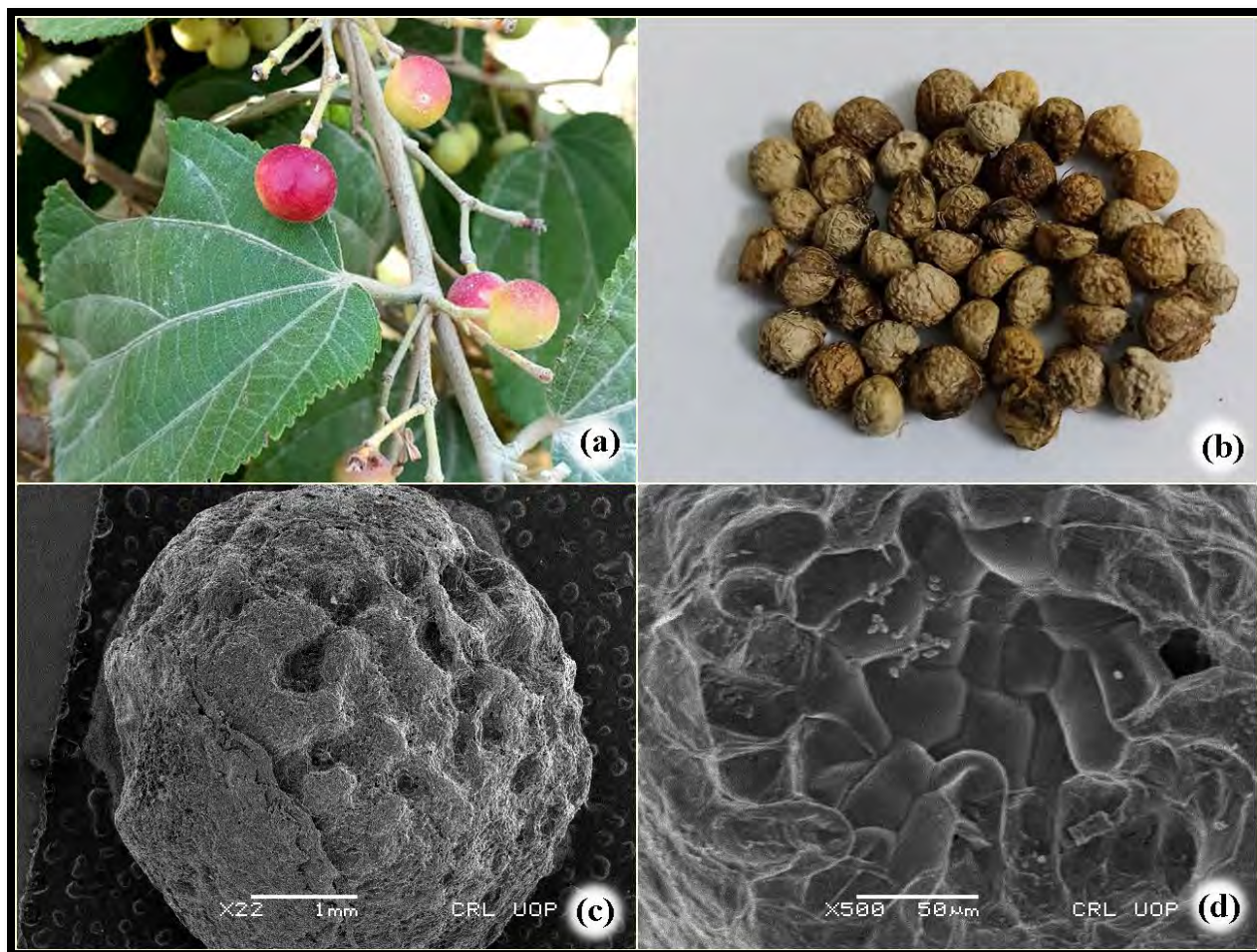
Plate 3.1.7. *Grewia asiatica L.* **(a)** entire plant, **(b)** seeds, **(c,d)** SEM micrograph of seeds and sculpturing

3.1.8 *Monotheca buxifolia*

Monotheca buxifolia is the large thorny shrub or small tree belonging to family Sapotaceae. It is widely distributed in Afghanistan, Ethiopia, Oman, Saudi Arabia, Yemen, and Pakistan. Thorns of this plant are usually short. Fruit is 1 seeded berry and 1 cm in diameter. Seeds are small, yellowish-brown with globose and circular shape. Seeds of *Monotheca buxifolia* were spherical in shape and dark brown in color (Figure 3.1.8 a-d). They were 6 mm long and 14 mm wide in size. Seeds have high oil content of 45% (w/w). The FFA content of seed oil was found to be 0.45 mg KOH/g and biodiesel potential was 95% as depicted in Table 1. No previous record of seed SEM of *Monotheca buxifolia* was found in the previous literature. Results of SEM micrograph of *Monotheca buxifolia* seed have been displayed in Figure 1c and d. SEM revealed perforate surface sculpturing with rough edges, uneven cell shape and irregular cell arrangement, smooth cell outline, thin anticlinal walls, deep and thick bulging periclinal walls.

3.1.9 *Cordia myxa* L.

Cordia myxa is a deciduous tree. It belongs to family Boraginaceae and is mostly cylindrical, straight up to 5 m in height. It is distributed in Afghanistan, Oman, Lebanon, Myanmar, Syria and Pakistan. Young branches and shoots with corroded pubescence. Stem is hairy in young stage and laterally become glabrous. Leaves dentate, petioate elliptic to oblong, sub orbicular and have size of 6-12.5 x 43-8.2 cm. The lower surface of leaves is glabrous to thick tomentose. Petiole extended about 43 cm long. Calyx lobed with campanulate condition. Corolla elliptic with white color. Fruit is fleshy drupe, 1 seeded, apiculate, brownish yellow in color, ovoid in shape and 20 mm long. The enlarged copular calyx surrounds base of drupe. Seeds were cordial in shape and brown in color (Figure 3.1.9 a-d). They were 16 mm long and 18.4 mm wide in size. Results of oil determination of seeds showed a high oil content of 37% (w/w). FFA content of seed oil was found to be 0.62 mg KOH/g while biodiesel potential was 94 (Table 3.1). Micromorphological examination of seed illustrated reticulate surface ornamentation, asymmetrical cell arrangement, pentagonal shape cells with puzzled cell outline,

thick, wavy, raised, and deep anticlinal walls, thick, rough periclinal walls. Seeds of *Cordia myxa* were not previously explored for micromorphological characteristics *via* SEM
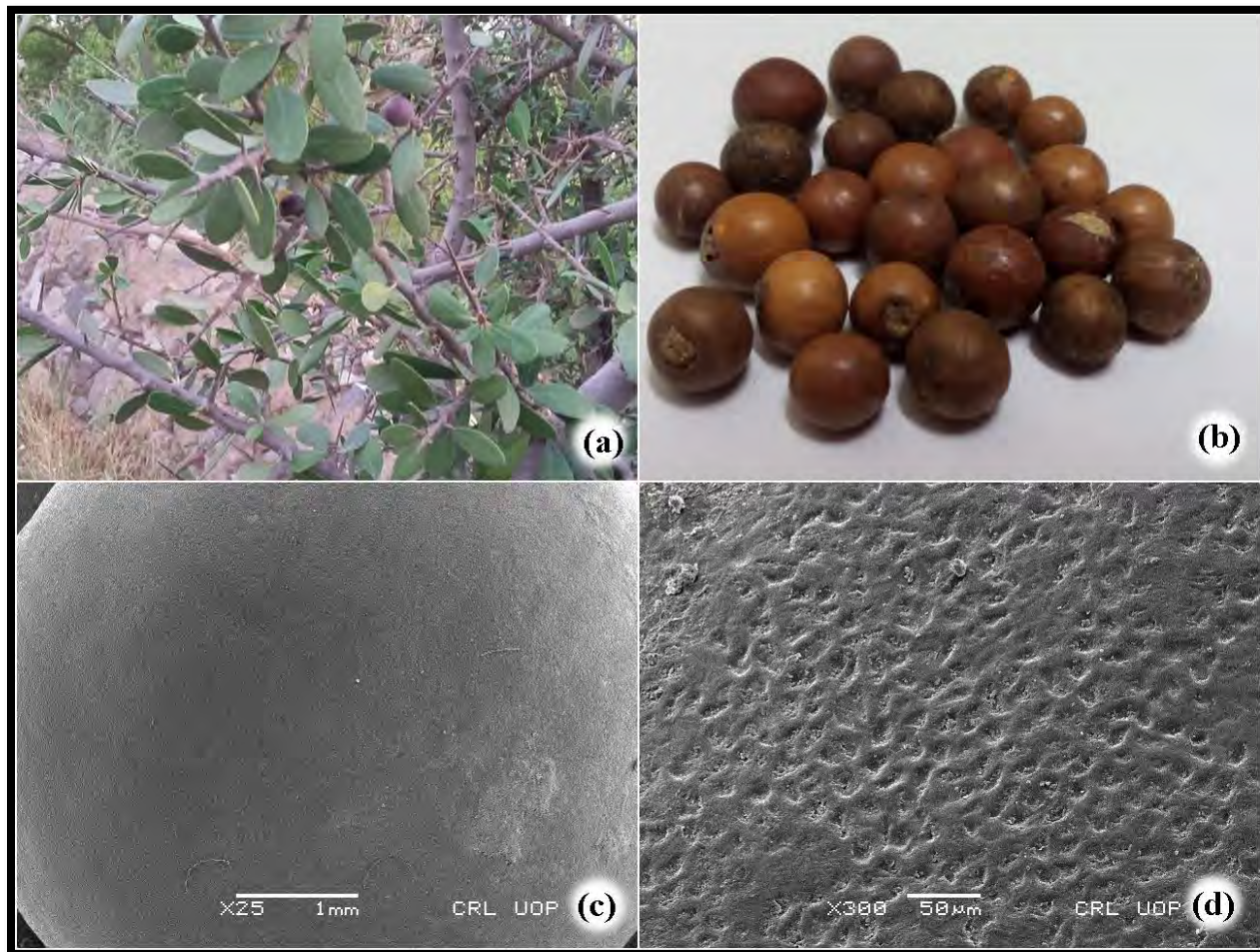
Plate 3.1.8. *Monotheca buxifolia* **(a)** entire plant, **(b)** seeds, **(c,d)** SEM micrograph of seeds and sculpturing
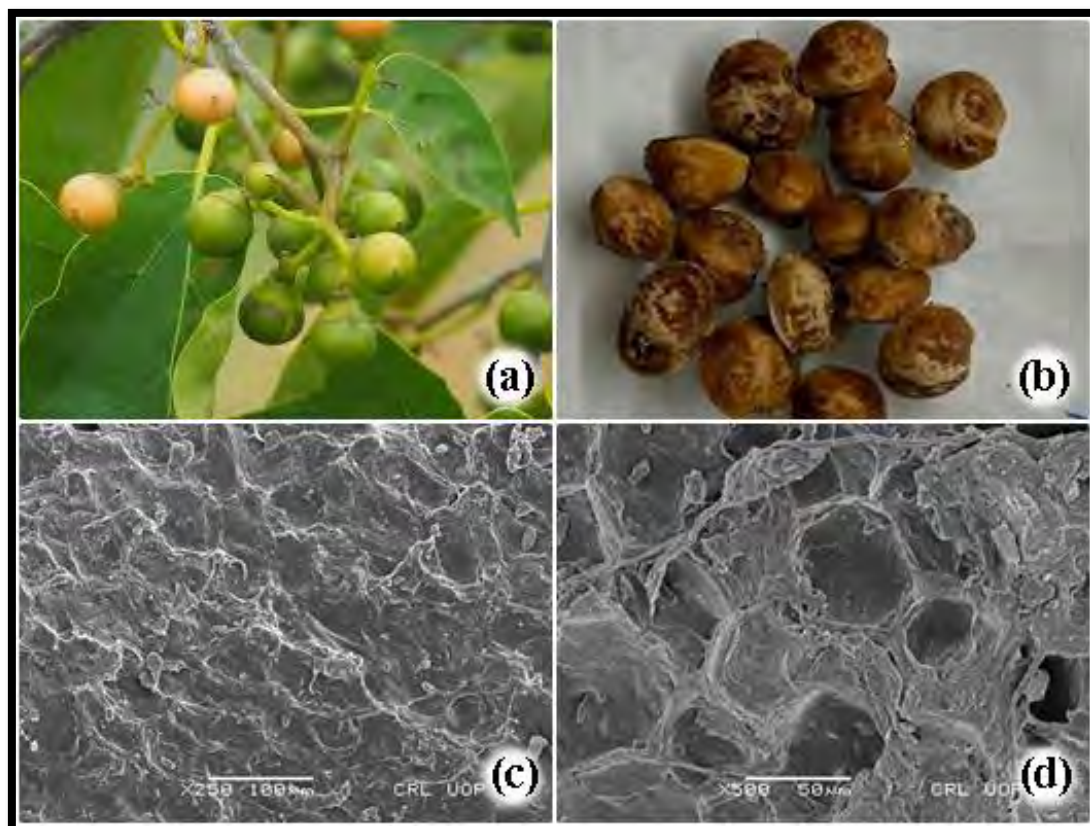
Plate 3.1.9. *Cordia myxa* L. **(a)** entire plant, **(b)** seeds, **(c,d)** SEM micrograph of seeds and sculpturing

3.1.10 *Cordia dichotoma* G.Forst.

Cordia dichotma belonging to family Boraginaceae is about 15 m tall dioecious tree with pubescent branches. It is distributed in Asia, Australia, Japan, India and Pakistan. Leaf lamina is ovate to broadly elliptic, glabrous or pubescent with usually undulate margin. The apex of leaf obtuse to mucronate and the base cuneate to rounded. Leaf size is about 5-8 x 1.5-3.0 cm. Petiole is 3 cm long. Inflorescence corymbose cyme with terminating horizontal branches. Flower is dimorphic, sessile and ebracteate. Calyx campanulate with lobes of unequal sizes and dense hairs inside. Lobes are shorter, mostly recurved due to oblenceolate form. Filaments adnate to tube with hairy lower portion up to 4.5 mm long. Female flowers are larger than male flower. Drupe subglobose with sticky mesocarp, yellowish red up to 15 mm long. Fruit is surrounded by persistent calyx. Seeds of *Cordia dichotma* were cordial in shape and brown in color. Seeds were 12 mm long and 10 mm wide in size. Oil content of 35% (w/w) with FFA content of 0.41 mg KOH/g was calculated in results. Biodiesel potential of seed oil was found to be 92% (Table 3.1). SEM of *Cordia dichotma* seed was carried out for the first time in the current study. SEM micrographs demonstrated reticulate surface sculpturing, irregular cell layout, wavy cell outline, raised, rough anticlinal wall, ridged, deep and thick periclinal wall (Figure 3.1.10 c and d).
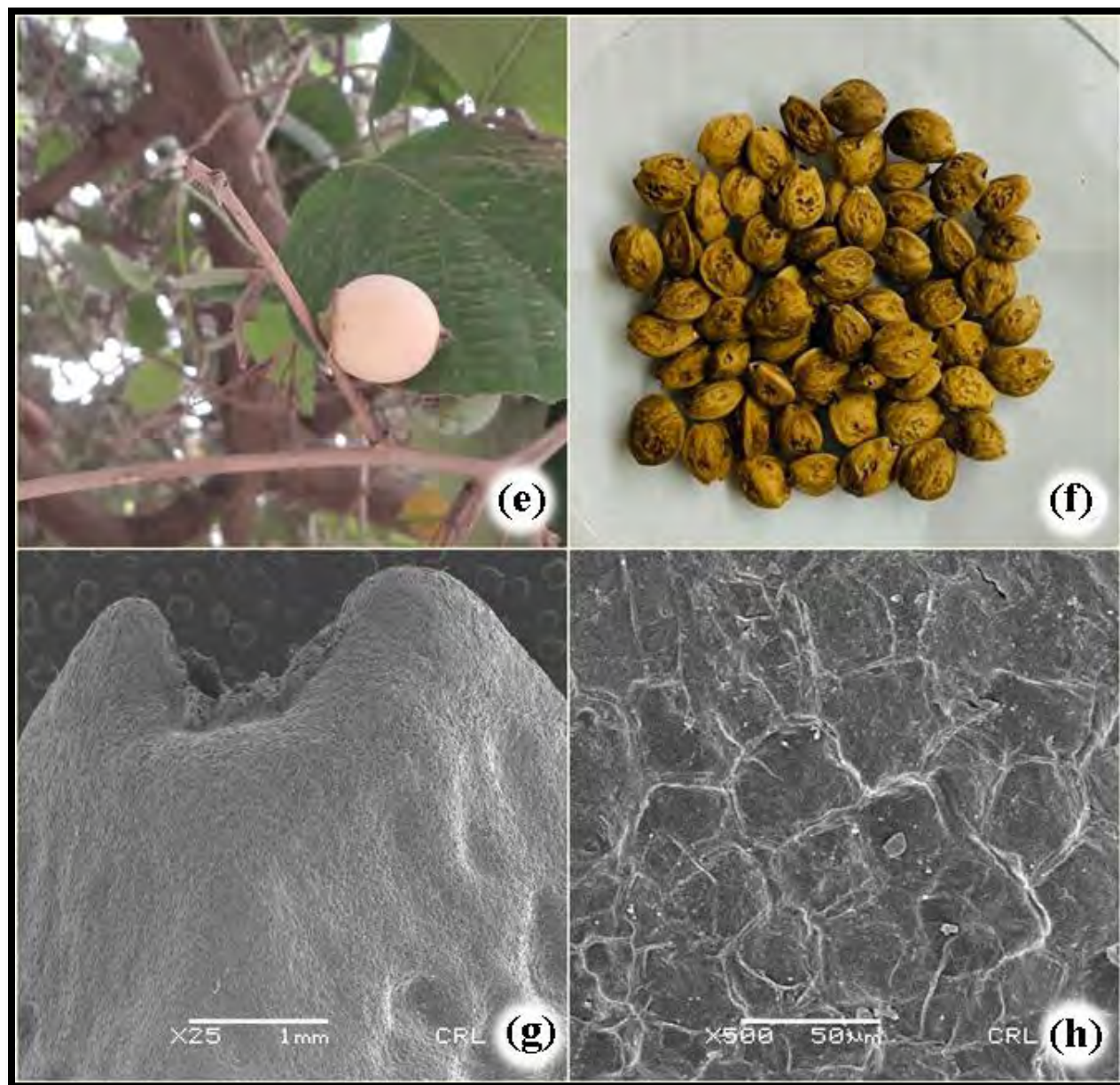
Plate 3.1.10. *Cordia dichotoma* **(a)** entire plant, **(b)** seeds, **(c,d)** SEM micrograph of seeds and sculpturing

3.1.11 *Chamaerops humilis* **L.**

Chamaerops humilis is a fetching palm belonging to family Arecaceae. It grows up to 6 m in height. It is distributed in Europe, France, Italy, Monaco, Spain, Portugal, India and Pakistan. Stem is bulbiferous and short tufted covered by bases of petiole. Trunk is uniformly thick, erect, less branched. Leaves are pinnate, sub-glaucous with scattered and numerous pinnae, interruptedly fascicled. Inflorescence axillary branched. Flowers are small, sessile attached to peduncle. Calyx ovate, Petals oblong and valvate. Fruit 1- seeded, 1.25 cm long with oblong shape and thin pericarp. Seeds straight and grooves at ventral side.

Seeds were narrow elliptic in shape and brown in color. Seeds were 10.14 mm long and 6.5 mm wide. Seeds have high oil content of 30%. (w/w). FFA content of 2.42 mg KOH/g was observed in seed oil. High yield of 98% of methyl ester was obtained using *Chamaerops humilis* seed oil. SEM micrograph exposed Striate surface ornamentation, layered, regular cell arrangement, square shaped cell with smooth cell outline, deep, raised and smooth anticlinal walls, thick, curved and slightly depressed periclinal walls (Figure 3.1.11 c and d). No previous record of seed SEM of *Chamaerops humilis* was found in the previous literature.
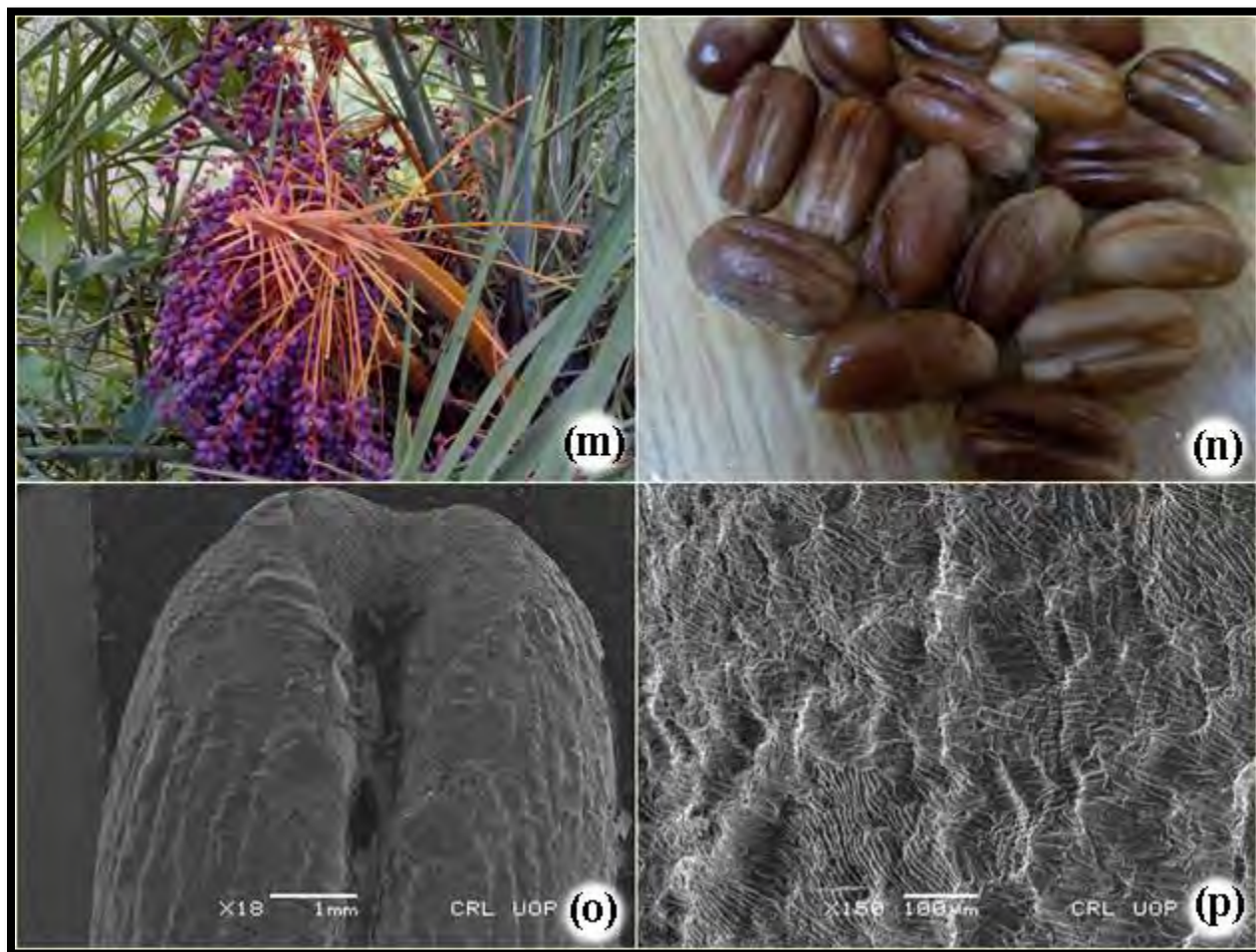
Plate 3.1.11. *Chamaerops humilis* L. **(a)** entire plant, **(b)** seeds, **(c,d)** SEM micrograph of seeds and sculpturing

3.1.12 *Trachyspermum ammi* (L.) Sprague

Trachyspermum ammi is an annual herb which is 15-20 cm tall with many branches, commonly known as Ajowan caraway. It belongs to family Apiaceae. It is distributed in Afghanistan, Iran, Pakistan and India. Fruit of *Trachyspermum ammi* is 2 mm long, ovoid, spinous with temporary ridges. Seed were oval in shape and light brown in color (Figure 3.1.12 a-d). They were 3.6 mm long and 1.9 mm wide. They have high oil content of 34% (w/w). FFA content of seed oil was found to be 2.5 mg KOH/g and biodiesel potential of 94% (Table 3.1). SEM micrograph of *Trachyspermum ammi* has been shown in Figure 1c and d. results of SEM demonstrated rugged surface sculpturing with rough edges, irregular cell shape and arrangement, profuse undulating anticlinal walls, deep and bulging periclinal walls. Seeds of *Trachyspermum ammi* are highly medicinal and contain antispasmodic and carminative properties. Essential oil of seeds poses germicidal and fungicidal properties (Chahal et al., 2017).
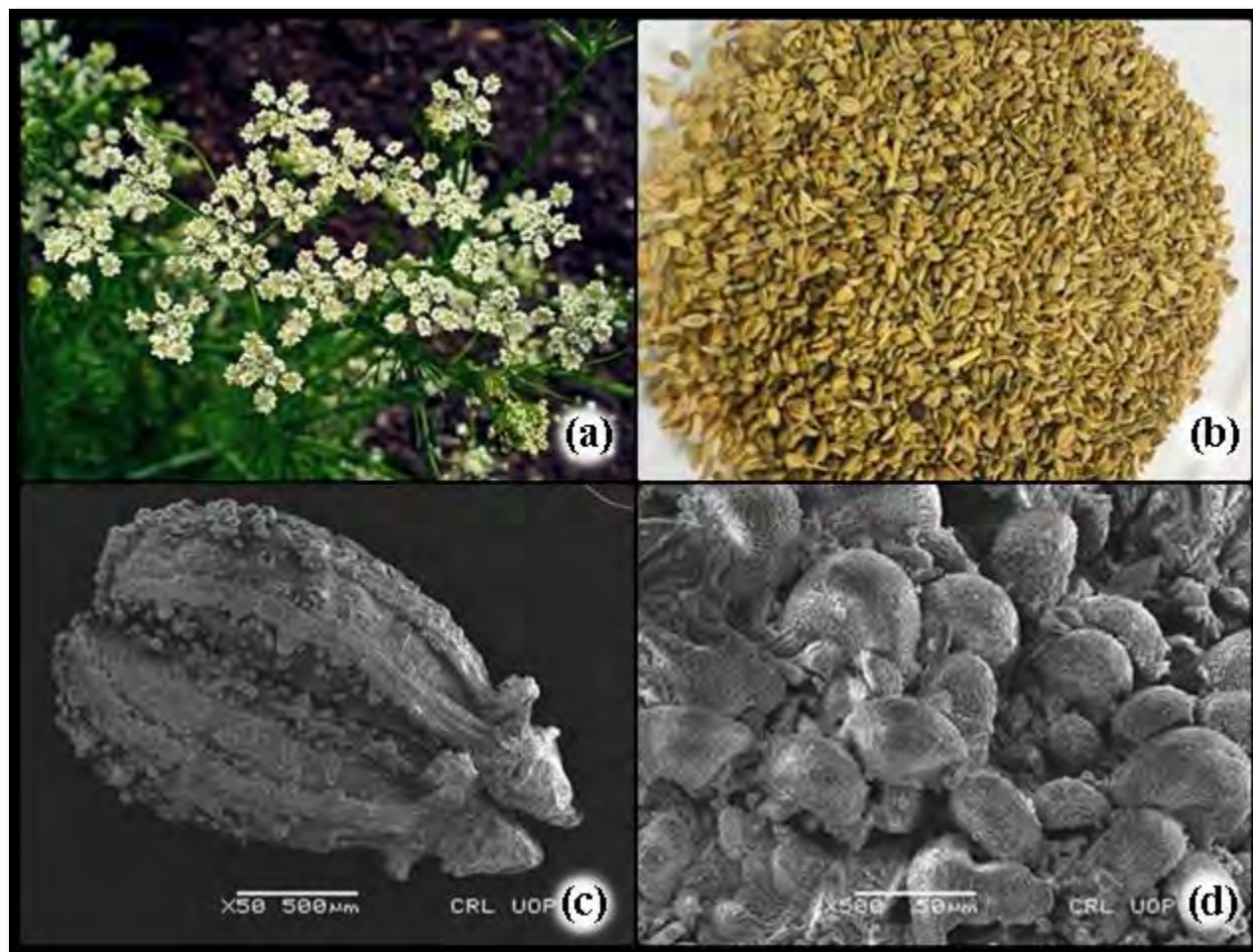
Plate 3.1.12. *Trachyspermum ammi* (L.) Sprague **(a)** entire plant, **(b)** seeds, **(c, d)** SEM micrograph of seeds and sculpturing

3.1.13 *Cupressus macrocarpa* **Hartw.**

Cupressus macrocarpa is an average size coniferous tree which grows up to a height of 40m in suitable environmental conditions. It belongs to family Cupressaceae. Seed cones are initially green in color but laterally converted into brown in the duration of 20-24 months after pollination. The pollen cones which are 3-5mm long release their pollen in early arrival of spring or in late winter. Seeds are triangular in shape and maroon in color. Seeds were 5.3 mm long and 4.7 mm wide. They have high oil content of 26% (w/w). FFA content of 0.53 mg KOH/g was observed in seed oil. Maximum yield of 93% of methyl ester was obtained with transesterification of seed oil. SEM micrographs illustrated striate surface sculpturing; linear cells with regular, layered arrangement, anticlinal walls are smooth and thin, thick and deep periclinal wall elevation (Figure 3.1.13 a-d). No previous record of SEM *Cupressus macrocarpa* was found in the previous literature. In general, SEM results disclosed that variation in the surface pattern of seed micromorphology would be helpful in differentiating various species of family Cupressaceae.
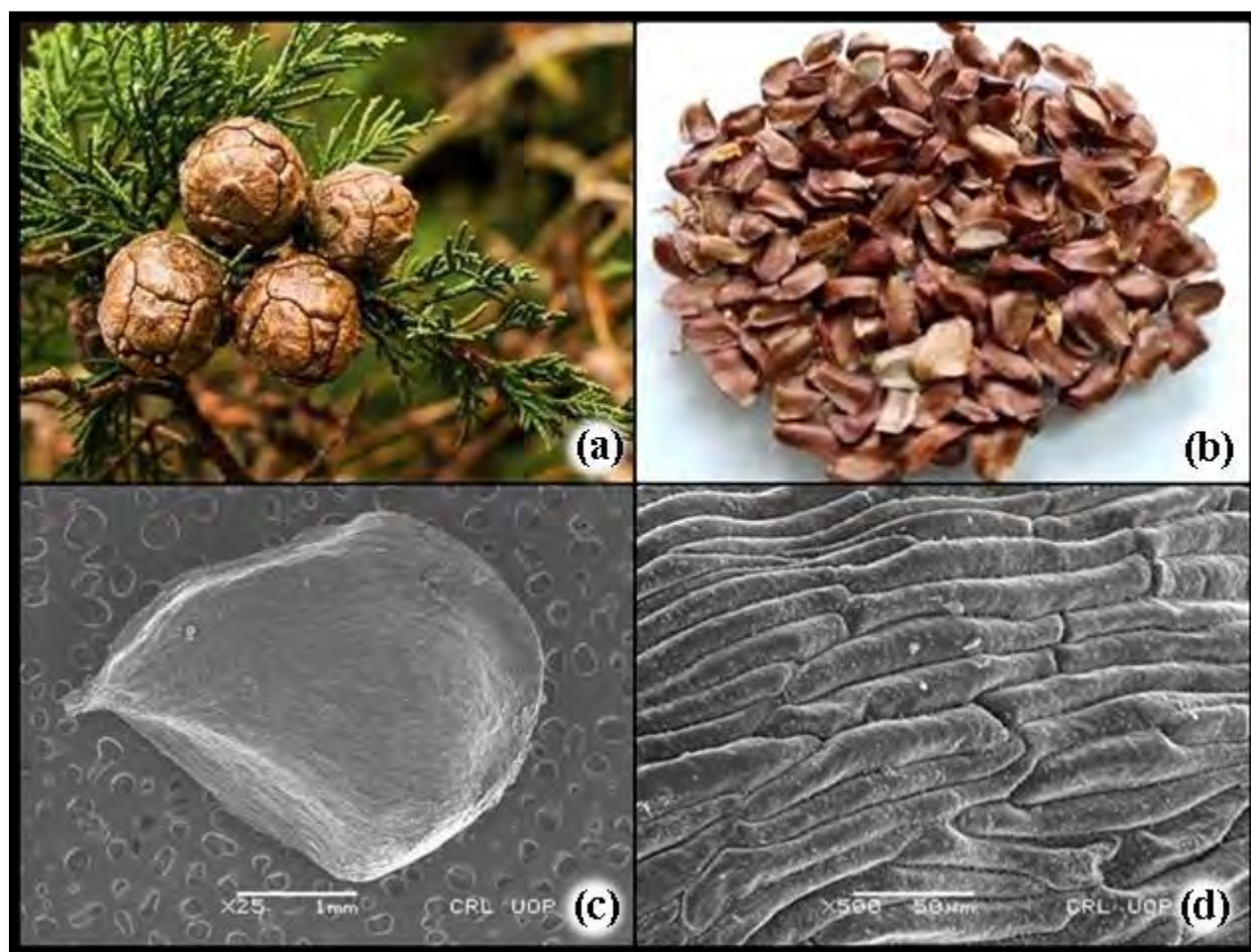
Plate 3.1.13. *Cupressus macrocarpa* **(a)** entire plant, **(b)** seeds, **(c, d)** SEM micrograph of seeds and sculpturing

3.1.14 *Nannorrhops ritchieana* **(Griff.) Aitch.**

   Nannorrhops ritchiana is the small, cordial bunched shrub having branched rhizome with erect stem up to 7-8 m in length. It belongs to family Arecaceae and commonly known as Mazari Palm. It is distributed in Afghanistan, Oman, Saudi Arabia, Iran and Pakistan. Fruit of *Nannorrhops ritchiana* is ovoid berry of various sizes (Mahmood et al., 2017). Seeds were found round in shape and brown in color (Figure 3.1.14 a-d). They were 16.3 mm long and 12.4 mm wide. Oil estimation of seeds revealed high oil content of 25% (w/w). Whereas, FFA content of seed oil was found to be 0.32 mg KOH/g and biodiesel potential of 94% as depicted in Table 1. Micromorphological investigation via SEM illustrated Reticulate surface sculpturing, regular cell arrangement, cells are ovate in shape with smooth ,thick and deep anticlinal walls, periclinal walls were depressed and elevated. Seeds of *Nannorrhops ritchiana* remain viable for three to four years if they are stored properly after drying (Ali et al., 2020).
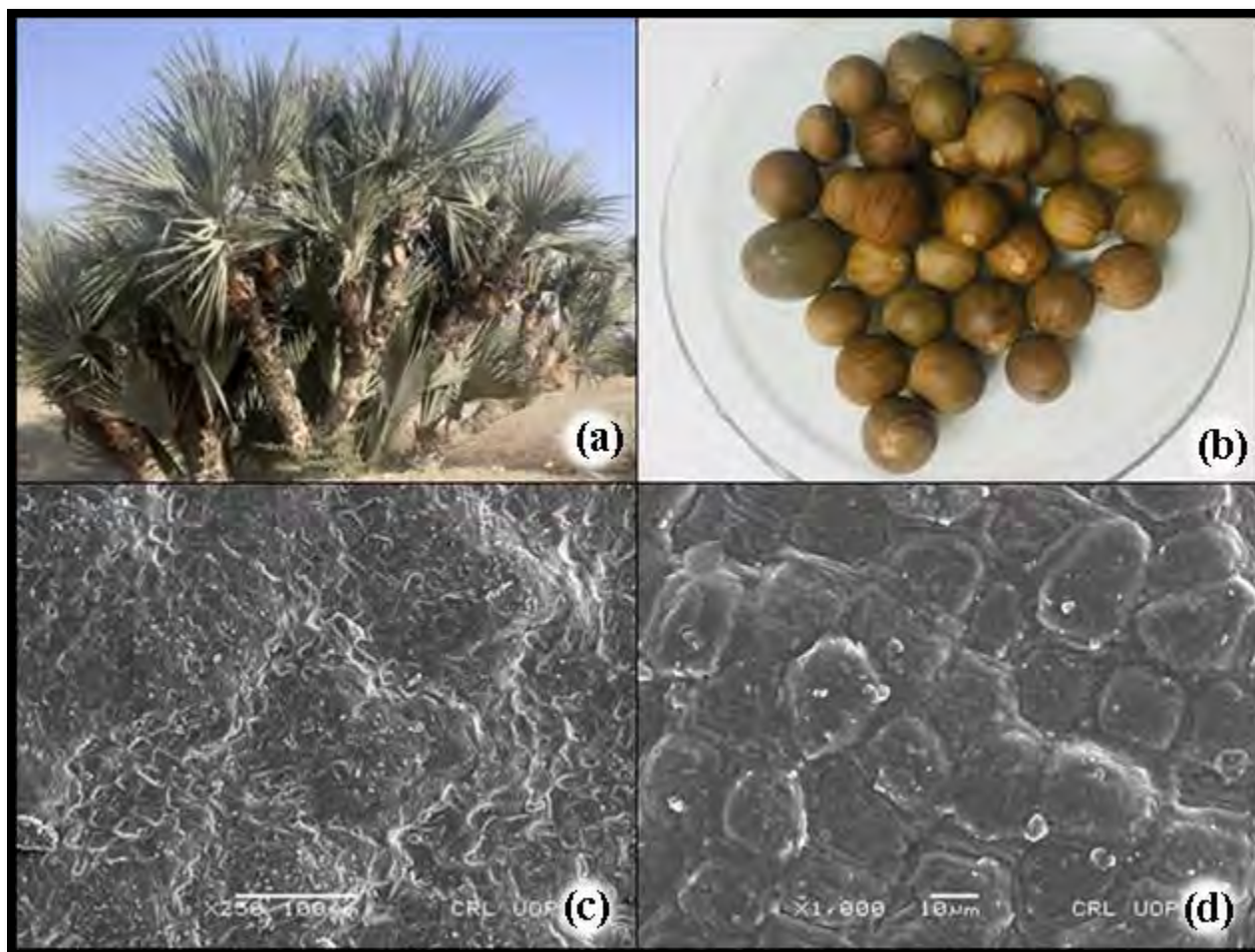
Plate 3.1.14. *Nannorrhops ritchieana* (Griff.) Aitch. **(a)** entire plant, **(b)** seeds, **(c, d)** SEM micrograph of seeds and sculpturing

3.1.15   *Cupressesus sempervirens* **L.**

Cupressesus sempervirens is evergreen 30 m tall tree with grayish brown bark, superficially fissured. It belongs to family Cupressaceae. It is drought tolerant plant species (Roque, et al., 1999). Seed cones are spheroidal or sub globose and become yellowish gray when ripened. Cone scales are 8-14 in which each fertile scale contains 8-20 seeds. Seed were brown and winged and ovoid. Seeds were 5.1 mm long and 4.5 mm wide. FFA content of 0.42 mg KOH/g was observed in seed oil. Maximum oil content of dried seed was found 29% (w/w). High yield of 98% of methyl ester was obtained by transesterification of *Cupressesus sempervirens* seed oil. SEM of *Cupressesus sempervirens* seed was done for the first time in the current research. Results of SEM showed Striate surface sculpturing, regular, symmetrical cell arrangement, even, smooth cell outline, raised and depressed anticlinal walls, thin, rough and wavy periclinal walls (Figure 3.1.15 c and d).
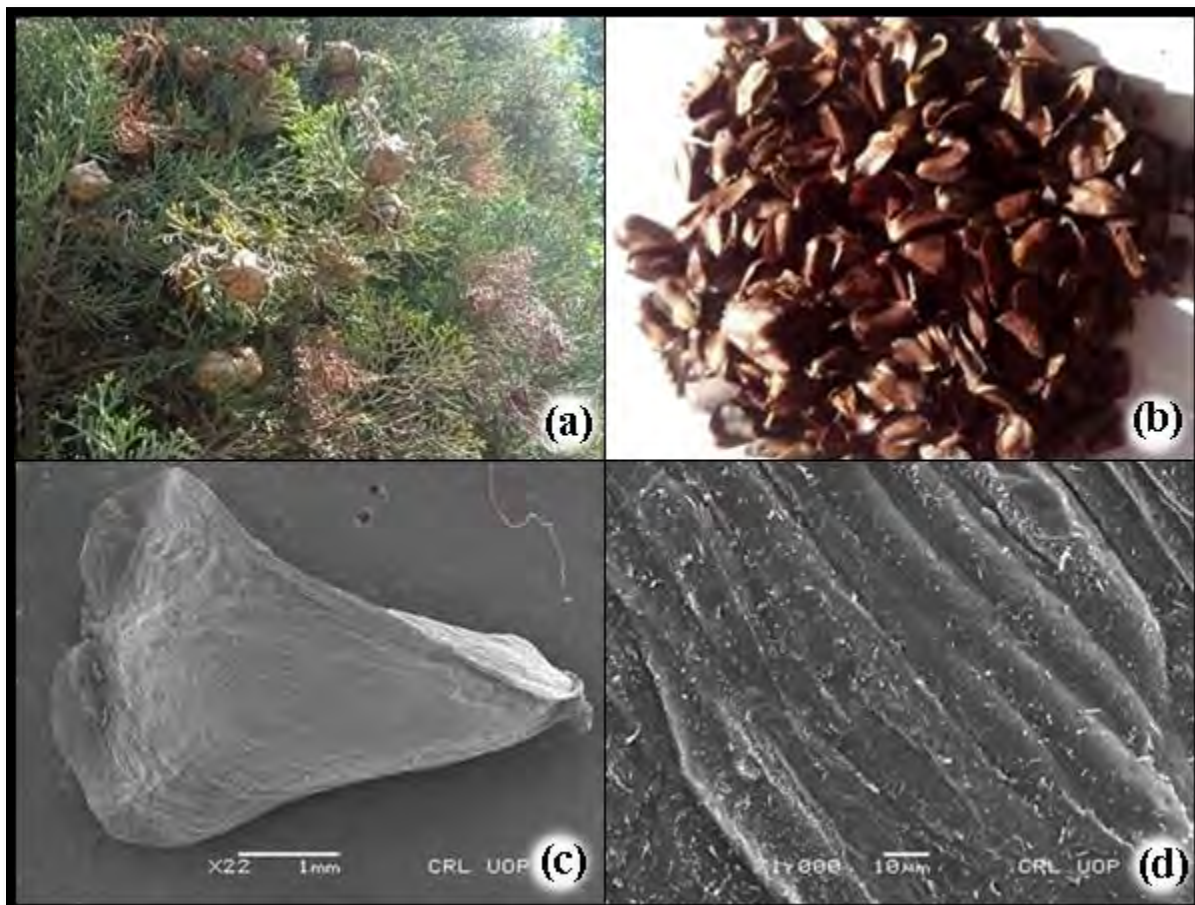
Plate 3.1.15. *Cupressus sempervirens* **(a)** entire plant, **(b)** seeds, **(c, d)** SEM micrograph of seeds and sculpturing

Table 3.1 Characteristics of novel nonedible oil seeds and their micro morphological features via SEM

Plant name	Synonym	Family	Distribution in Pakistan	Worldwide Distribution	Seed size (L×W) mm	Shape	Color	Oil content (%)	FFA (mg KOH/g)	Biodiesel potential (%)	Micromorphological Feature determined from SEM
Citrus paradisi Macfad.	-	Rutaceae	Swabi	China, United states, Mexico	15.8 mm × 8.5 mm	Broad ovate	Yellow	30	2.06	92	Reticulate surface sculpturing with granular bulging projections and fine small pits, irregular cell arrangement, thick and smooth anticlinal walls, elevated flat periclinal walls
Zanthoxylum armatum DC.	*Zanthoxylum alatum* Roxb.	Rutaceae	Swat to Bhutan	East Asia, Phillipines, Malaysia, North America, Korea , Japan	4.4 mm × 9.4 mm	Rounded	Black	36	0.680	95	Rugose to reticulate surface sculpturing with finner small pits, Elliptic to ovate cell outline, asymmetrical cell arrangement, convex ventral and dorsal wall side, thick, deep anticlinal walls, thin and puzzled periclinal walls, rounded basal point
Citrus aurantium L.	*Aurantium acre* Mill.	Rutaceae	Sahiwal, Multan, Faisal Abad	Southeast Asia	12.1 mm × 6.2 mm	Ovate	Greenish/Yellow	38	0.14	94	Perforate with semitectate surface pattern, fitted with bulging protrusions, cells are spherical to oval in shape, crooked cell arrangement, depressed, wavy anticlinal wall, thick periclinal walls elevation
Citrus medica	*Citrus alata*	Rutaceae	Northern	Eastern	9.1 mm	Semi	Greenis	33	2.01	93	Reticulate surface sculpturing, cells are
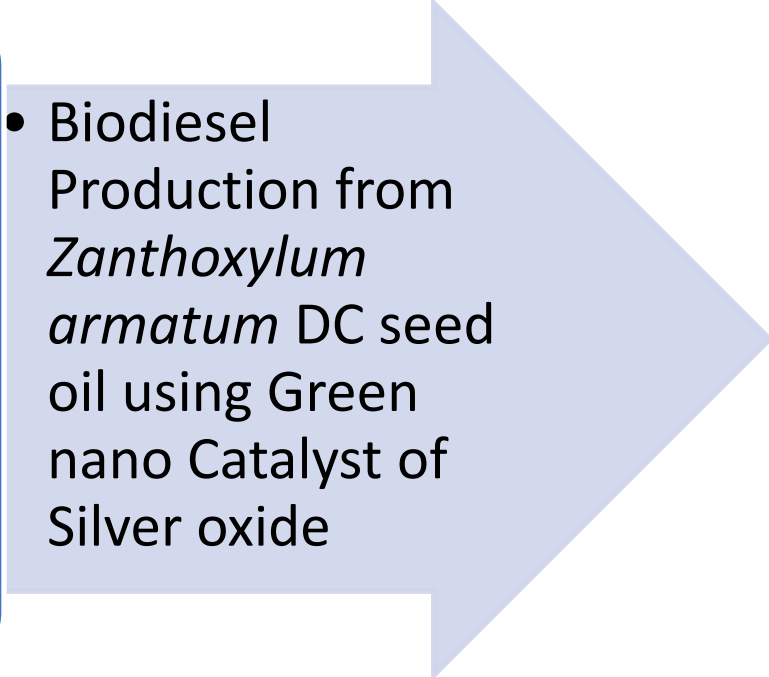
L.	(Tanaka) Tanaka		Punjab, Baluchistan	Himalaya, Persian Gulf, India, Italy	× 5.5 mm	deltoid	h				arranged in irregular fascicles and are chained in longitudinal lines in sulcate to ribbed pattern, thick, smooth anticlinal walls, deep and elevated periclinal wall
Cestrum nocturnum L.	*Cestrum graciliflorum* Dunal	Solanaceae	Kotli, Kohat, Islamabad, Rawalpindi, Lahore	America, Australia, Pakistan	1.8 mm × 1.1 mm	Triangular	Black	28	1.5	95	Striate, wrinkled surface pattern with rough cell outline, reticulate cell arrangement, wavy thick anticlinal wall and depressed, smooth and raised periclinal wall
Cichorium intybus L.	*Cichorium balearicum* Porta	Asteraceae	Lahore, Mansehra, Swabi	America, Australia, China, Europe	2.7 mm × 1.16 mm	Cuneiform	Yellow	34	0.56	95	Rugose, papillate surface sculpturing, narrow elliptic cell shape, layered and regular cell arrangement, raised, curved anticlinal wall and entire, depressed, glabrous periclinal wall
Trachyspermu mammi (L.) Sprague	*Ammi copticum* L.	Apiaceae	Gilgit, Skardu, Jhelum, Rawalpindi, Swabi, Hassan abdal, Kashmir, Pishin, Loralai	Afghanistan, Iran, India	3.6 mm × 1.9 mm	Oval	Light brown	27	2.5	94	Rugged surface sculpturing with rough edges, irregular cell shape and arrangement, profuse undulating anticlinal walls, deep, bulging periclinal walls
Nannorrhops ritchieana (Griff.) Aitch.	*Nannorrhops arabica* Burret	Arecaceae	Sheikh Baddin National	Afghanistan, Oman, Saudi	16.3 mm × 12.4 mm	Round	Brown	25	0.32	95	Reticulate surface sculpturing, regular cell arrangement, cells are ovate in shape with smooth ,thick and deep

74

			Park, Dera Ismail Khan, Malakand, Hangu, ,	Arabia, Iran							anticlinal walls, periclinal walls are depressed and elevated
Cupressus macrocarpa Hartw.	*Callitropsis macrocarpa* (Hartw.)	Cupressacea e	Abbottabad, Balochistan, Murre, Gilgit Baltistan, Kaghan	California, New Zealand, South Africa, China, India and Pakistan	5.3 mm × 4.7 mm	Triangular	Maroon	26	0.53	93	Striate surface sculpturing, linear cells with regular, layered arrangement, anticlinal walls are smooth and thin, thick and deep periclinal wall elevation
Cupressesus sempervirens L.	*Chamaecyparis thujiformis* R.Sm. ex Gordon	Cupressacea e	Islamabad, Murre, Kaghan, Gilgit Baltistan,	E. Mediterran ean, W. Asia, Lebanon, Israel, Malta, Italy, Turkey, Cyprus	5.1 mm × 4.5 mm	Ovoid	brown	29	0.42	95	Striate surface sculpturing, regular, symmetrical cell arrangement, even, smooth cell outline, raised and depressed anticlinal walls, thin, rough and wavy periclinal walls
Trachyspermu mammi (L.) Sprague	*Ammi copticum* L.	Apiaceae	Gilgit, Skardu, Jhelum, Rawalpindi, Swabi, Hassan abdal,	Afghanista n, Iran, India	3.6 mm × 1.9 mm	Oval	Light brown	27	2.5	94	Rugged surface sculpturing with rough edges, irregular cell shape and arrangement, profuse undulating anticlinal walls, deep, bulging periclinal walls

			Kashmir, Pishin, Loralai								
Sideroxylon mascatense (A.DC.) T.D.Penn.	*Monotheca buxifolia*	Sapotaceae	Chitral, Jandola, Miran Shah, Waziristan, Peshawar valley	Afghanistan, Ethiopia, Oman, Saudi Arabia, Yemen	6.2 mm × 14 mm	Spherical	Dark brown	45	0.45	95	Perforate surface sculpturing with rough edges, uneven cell shape and irregular cell arrangement, smooth cell outline, thin anticlinal walls, deep, thick bulging periclinal walls
Cordia myxa L.	*Cordia latifolia*	Boraginaceae	Dera Ismail Khan, Layyah	Afghanistan, Oman, Lebanon, Myanmar, Syria	16 mm × 18.4 mm	Cordial	Brown	37	0.62	94	Reticulate surface ornamentation, asymmetrical cell arrangement, pentagonal shape cells with puzzled cell outline, thick, wavy, raised and deep anticlinal walls, thick, rough periclinal walls
Cordia dichotoma	*Cordia griffithii*	Boraginaceae	Chanab, Skardu, Rawalpindi,	Asia, Australia, Japan, India	12 mm × 10 mm	Cordial	Dark brown	35	0.41	92	Reticulate surface sculpturing, irregular cell layout, wavy cell outline, raised, rough anticlinal wall, ridged, deep and thick periclinal wall
Chamaerops humilis L.	*Phoenix humilis*	Arecaceae	Islamabad, Peshawar Swat, Hazara, Rawalpindi, Murree	Europe, France, Italy, Monaco, India	10.14 mm × 6.5 mm	Narrow elliptic	Brown	30	1.43	98	Striate surface ornamentation, layered, regular cell arrangement, square shaped cell with smooth cell outline, deep, raised and smooth anticlinal walls, thick, curved and slightly depressed periclinal walls

SECTION II

- Biodiesel Production from *Zanthoxylum armatum* DC seed oil using Green nano Catalyst of Silver oxide

Ag_2O is utilized as the catalyst in the current investigation because of its special properties. Silver-based nanoparticles attract most researchers and are efficiently used in oxidative catalysis, bio-sensing and photo-induced optical effects. Silver oxide has been systematically utilized in several industrial applications such as alkylation, transesterification, and isomerisation. Hence, we made an attempt to determine its efficacy in the process of transesterification.

3.2.1 Catalyst characterization

In order to understand the performance of synthesized catalyst, several methodologies were used in this discussion.

3.2.1.1 X-Ray Diffraction (XRD) of Ag_2O

X-Ray Diffraction is a frequently used technique for investigating the elemental composition, size, and crystal structure of nanoparticles calcined at various temperatures and times. XRD pattern of green NPs of Ag_2O is given in Figure 3.2.1. Energy peaks at 2θ values of 38.7º, 46.3º, 64.32º and 77.22º corresponded to 111, and 200, 220, 311 *hkl* were determined. Debye–Scherer Equation (5) at full width half maximum (FWHM) was castoff to determine the crystalline size of Ag_2O NPs by using XRD pattern of most deep peaks at 2θ value of 77.2º (highest peak 111).

Face centered cubic lettuce structure has been identified from the reflection peaks. In the present study, average size of Ag_2O NPs was around 32 nm which significantly illustrated that Ag_2O particles synthesized from the green method are nanoparticles in nature. The comparison of the XRD pattern with the standard JCPDS data (Card No. 04-0783) has confirmed the formation of green NPs of Ag_2O. The results of X-Ray Diffraction of Ag_2O were found in accordance with SEM.

3.2.1.2 Scanning Electron Microscopy (SEM) of Ag_2O

The surface morphology of green nanoparticles of Ag_2O was studied with SEM. A typical view of the Nano catalyst was observed with homogenous cubical morphology. A micrograph of SEM is depicted in Figure 3.2.2, showing cubical and relatively uniform particle structure. Larger nanoparticles are also observed due to the aggregation of small nanoparticles in SEM measurement.

3.2.1.3 Energy Diffraction X-ray (EDX) of Ag₂O

Energy diffraction (EDX) was used for the recognition of the chemical composition of synthesized nanoparticles. The formation of Ag_2O nanoparticles was confirmed by peaks of Ag and O illustrated in the spectrum (Figure 3.2.3). The overall percentage of Ag and O was found 56.22% and 43.88%. The absence of other irrelevant peaks in the EDX spectrum revealed that green nanoparticles are pure and have no other element.

3.2.1.4 Thermogravimetric analysis (TGA) of Ag₂O

Thermogravimetric analysis (TGA) is used for testing the thermal stability of Ag_2O nano-particles. A Thermogram of Silver-based nano-particles has been depicted in Figure 5a with a corresponding derivative thermogram (Figure 3.2.4). Both thermograms showed thermal degradation in three stages. In the initial stage, 0.164% loss in the mass of Ag_2O nanoparticles was observed at the temperature range of 50 ℃ to 200 ℃, which is attributed to evaporation and water removal from the surface of molecules. In the second stage, thermal deterioration (0.690%) was noticed at the temperature range of 500 ℃ to 600 ℃, which exposed relatively higher thermal stability of Ag_2O nanoparticles and greater catalytic activity. In the third stage, at the temperature range of 600 ℃-700 ℃, further transformation (0.383%) of particles happened and gradually moved towards stability. The endothermic peaks revealed in the derivative curve (wt. %) in Figure 5a.

3.2.1.5 Fourier Transform Infrared Spectroscopy (FTIR)

The FTIR was used to detect the spectrum of Ag_2O nanoparticles in the absorbance mode. A wavelength range of 515-4000 cm⁻¹ was used to investigate the absorbance of Ag_2O nano-particles. FT-IR spectrum of Ag_2O nanoparticles is displayed in Figure 3.2.5. The distinctive characteristic absorption bands obtained at 1308.89 cm⁻¹ (OH stretch), which is attributed to the presence of physisorbed water molecules, an intense band at 1042.5 cm⁻¹ and 801.2 cm⁻¹ is assigned to Ag-O stretch. These all groups mediate the reduction process of Ag_2O nano-particles.
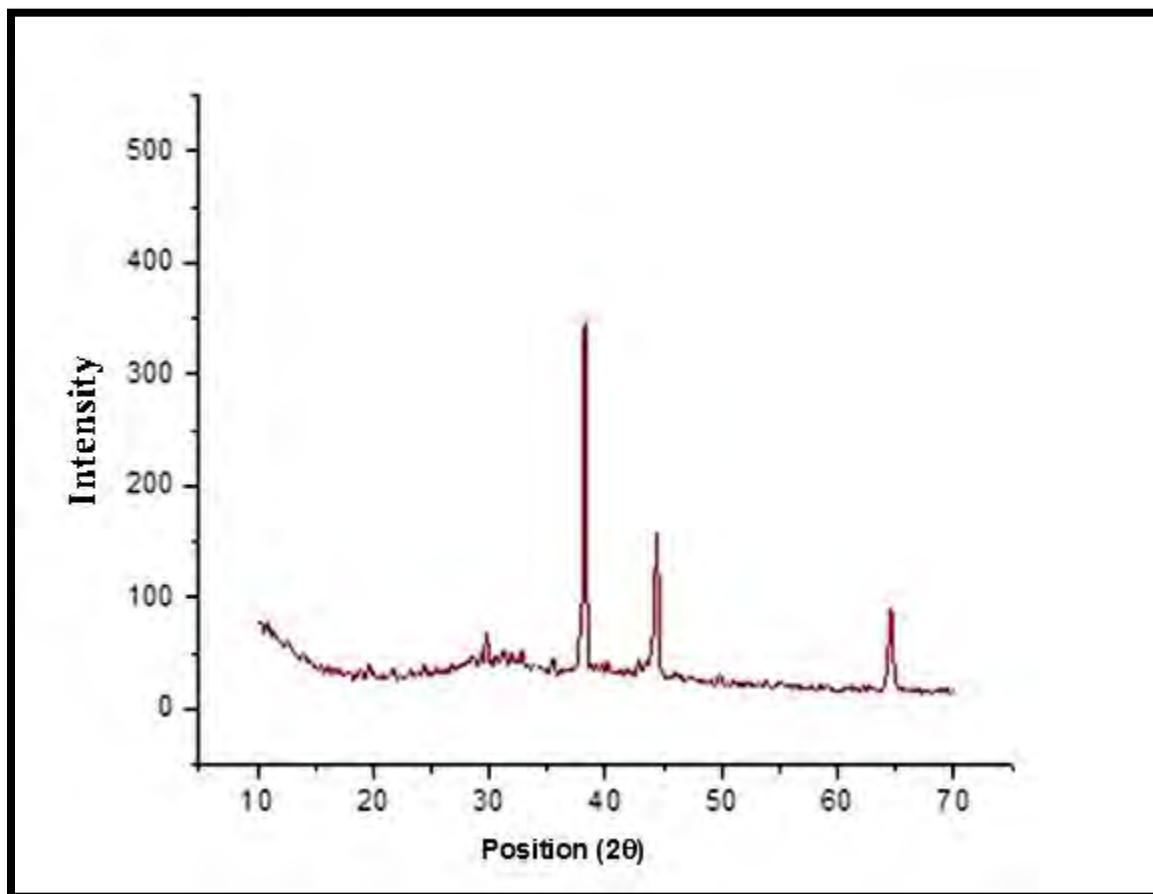
Figure 3.2.1. XRD Spectrum of calcined silver oxide green nanoparticles
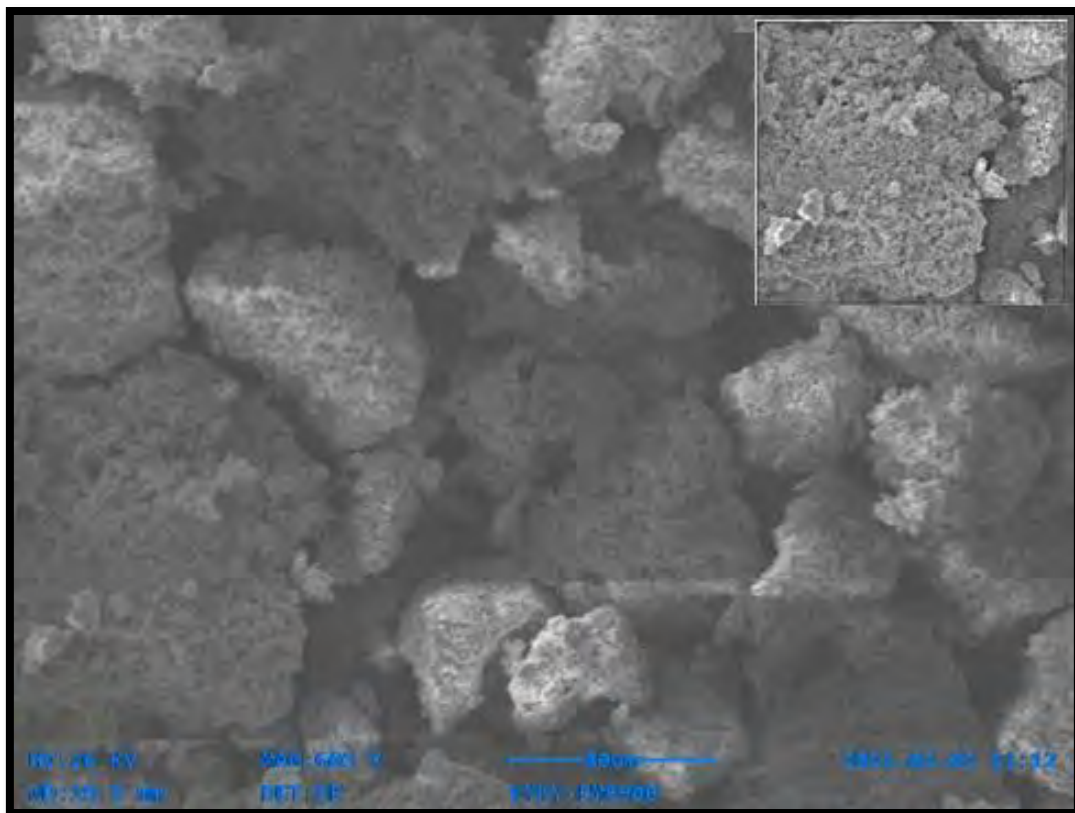
Figure 3.2.2. (a) Scanning electron microscopy (SEM) of calcined silver oxide (b) XRD pattern of silver oxide nanoparticles
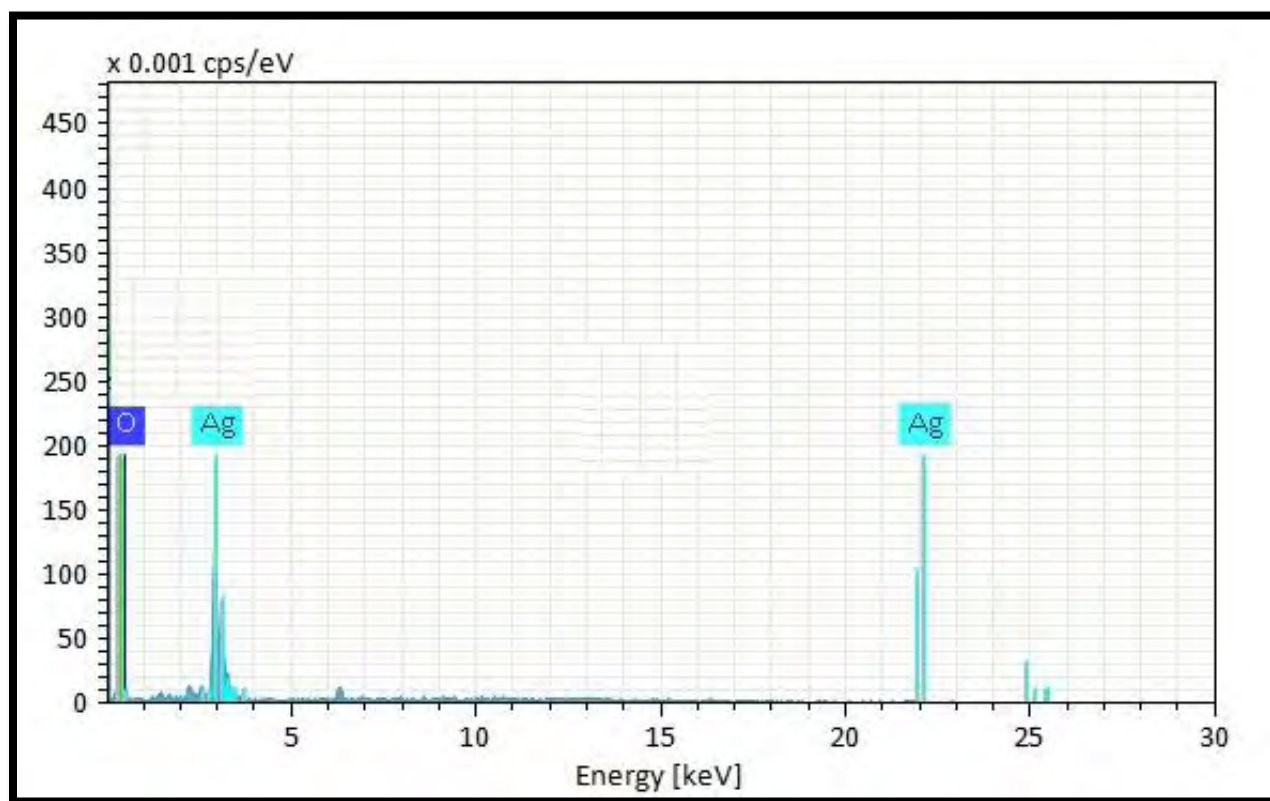
Figure 3.2.3. Energy diffraction X-Ray (EDX) of calcined silver oxide green nanoparticles
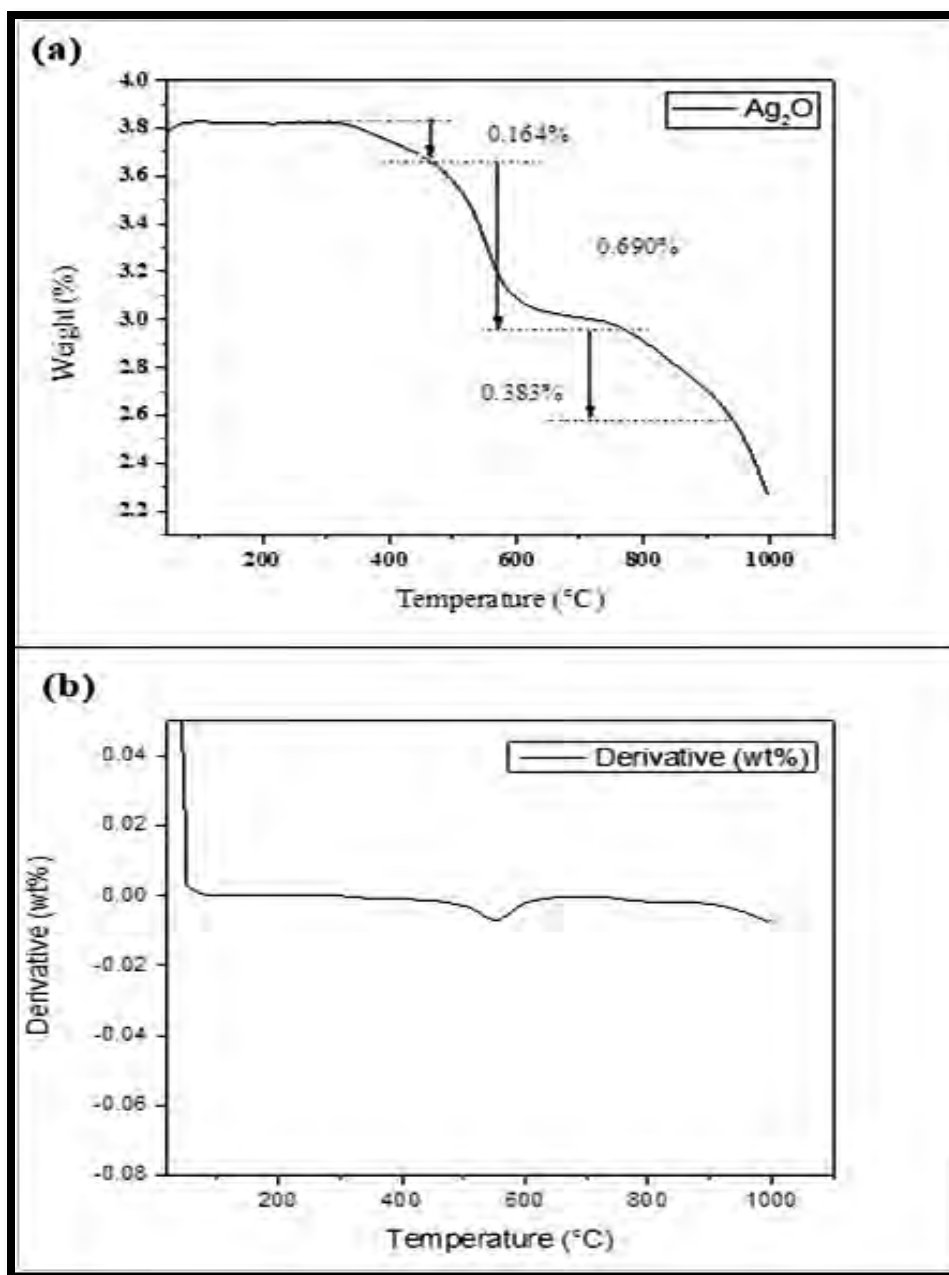
Figure 3.2.4. (a) TGA of silver oxide green nanoparticles (b) derivative thermogram of silver oxide nanoparticles
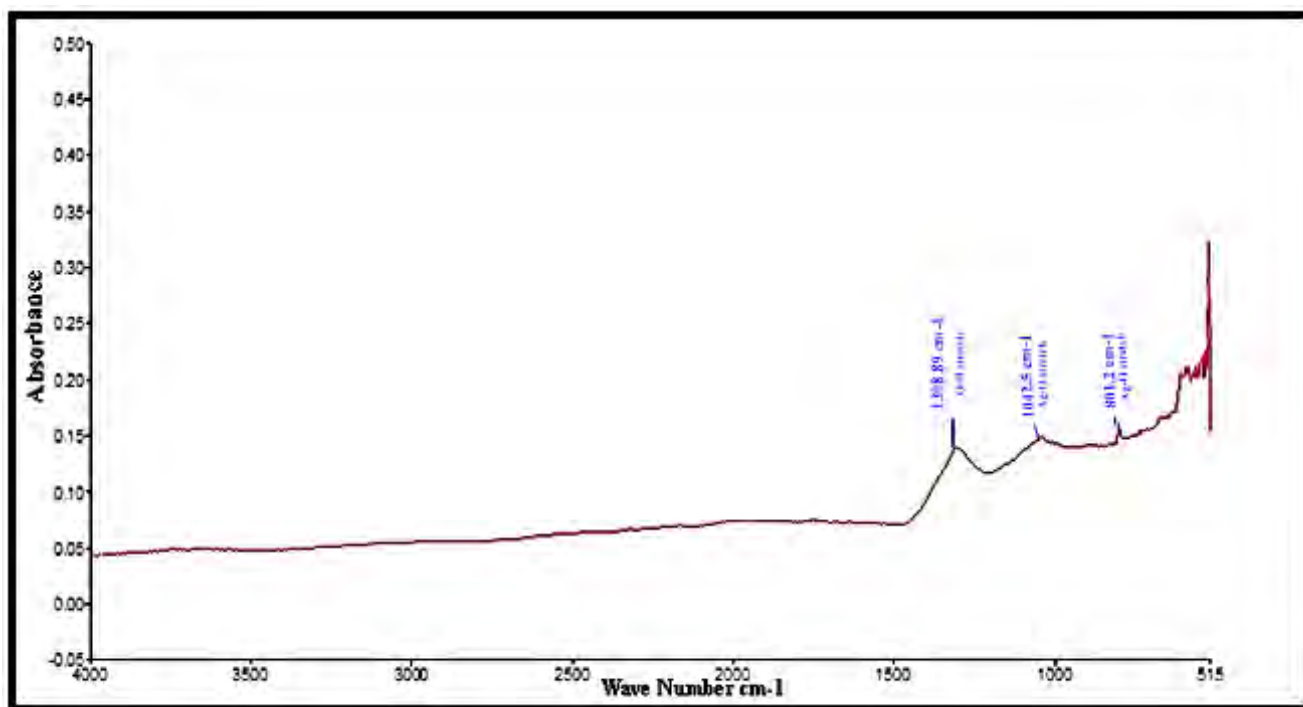
Figure 3.2.5. FTIR spectrum of silver oxide green nanoparticles

3.2.2 Biodiesel synthesis using transesterification

In the current study, novel, toxic and potential seed oil of *Zanthoxylum armatum* were used to produce green and sustainable biodiesel. It is essential to determine the FFA content of oil of a selected feedstock before biodiesel synthesis. It has been previously reported that those feedstocks which have oil content higher than 20% would only be considered for biodiesel production (Tang et al., 2018). The oil content was found to be 36%, which is significantly higher than the recommended percent value (Gopalakrishnan et al., 2015).

The *Zanthoxylum armatum* seed oil was found to be chocolate brown at 25 ℃. Since, the FFA content of ZASO in the present study was detected at a rate of 0.68 (wt. %), that is significantly lower and is reflected as impeccable for the operation of single-step base-catalyze transesterification reaction. The oil with the high FFAs content (more than 3%) is considered unfavorable as it needs an additional step of acid esterification (Dawood et al., 2021). The *Zanthoxylum armatum* seed oil can be utilized as a competent resource for methyl ester formation synthesis without using an additional step of acid esterification. Transesterification reaction of the *Zanthoxylum armatum* seed oil was carried out with green nanocatalyst of silver oxide synthesized from *Silybum marianum* aqueous leave extract.

Reaction parameters of the transesterification reaction have a substantial effect on the biodiesel yield. CCD was designed using DOE (Design of experiment) with the 4 autonomous variables having minimum and higher ranges of value, *i.e.* (A) catalyst concentration of 0.5-0.95 wt.%, (B) reaction time 50-120 min, (C) temperature 60-120 ℃ and (D) oil to methanol ratio 2:1-10:1 (Table 3.2.1). A comparison between the predicted versus actual yield has been shown in Figure 3.2.6. Optimal reaction conditions of transesterification were determined by carrying out 30 different experiments to get maximum yield of methyl ester (Table 3.2.2). Both predicted and actual values (obtained from experiments) are distributed near the straight line and representing that both predicted and actual values are align to each other. Results of ANOVA for the response surface quadric model are displayed in Table 3.2.3. The experimental model was found significant owning a *p*-value of 0.0002 (<0.05) illustrated by ANOVA results. The lack of fit (F-value) in the current model was not significant concerning pure error with an F-value of 2.14 and is considered suitable for the desired fit of the model. The chance of noise for lack of fit (F- value) was 20.76%. The Quadratic terms of the transesterification reaction like catalyst amount (A^2) and methanol to oil molar ratio (D^2) were exhibited the most significant p-value

lesser than 0.05, whereas quadric (C^2) temperature factor and reaction time (B^2) represented insignificant p-value greater than 0.05. The Predicted R^2 of 0.6074 is found near to the Adjusted R^2 value of 0.7030, and the variance is less than 0.2. In the current study, adequate precision of the model was 9.509. The experimental model can efficiently predict methyl ester yield (Lawan et al., 2019). The applied polynomial Equation 8 of the model is given below.

Biodiesel Yield (wt. %) = +81.98+0.0000 *A-2.00 *B+0.7778 *C-0.1667 *D+2.56 *AB+0.4375 *AC+2.06 *AD+1.06 BC+1.44 *BD+1.31 *CD-9.96 *A²+4.04 *B²+0.0351 *C²+8.54 *D²   (8)
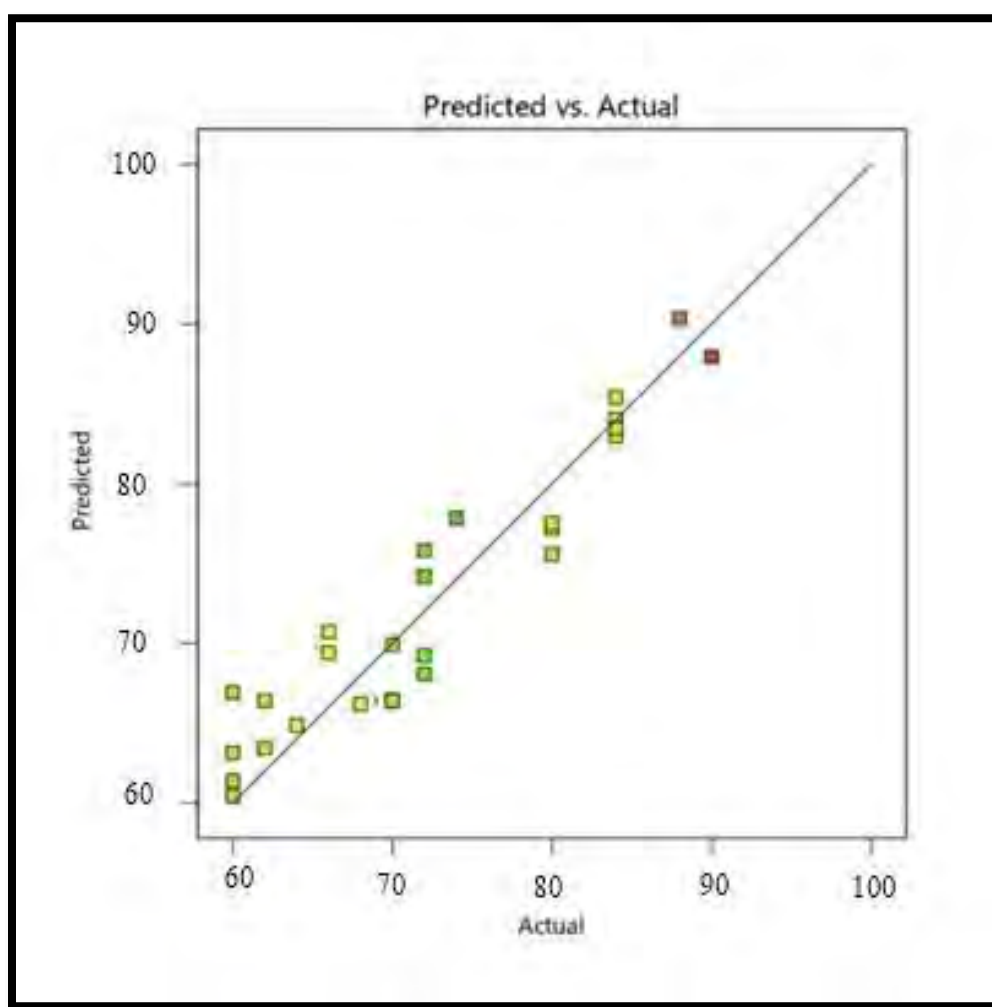
Figure 3.2.6. Comparison between the experimental biodiesel yield and the predicted yield of the model
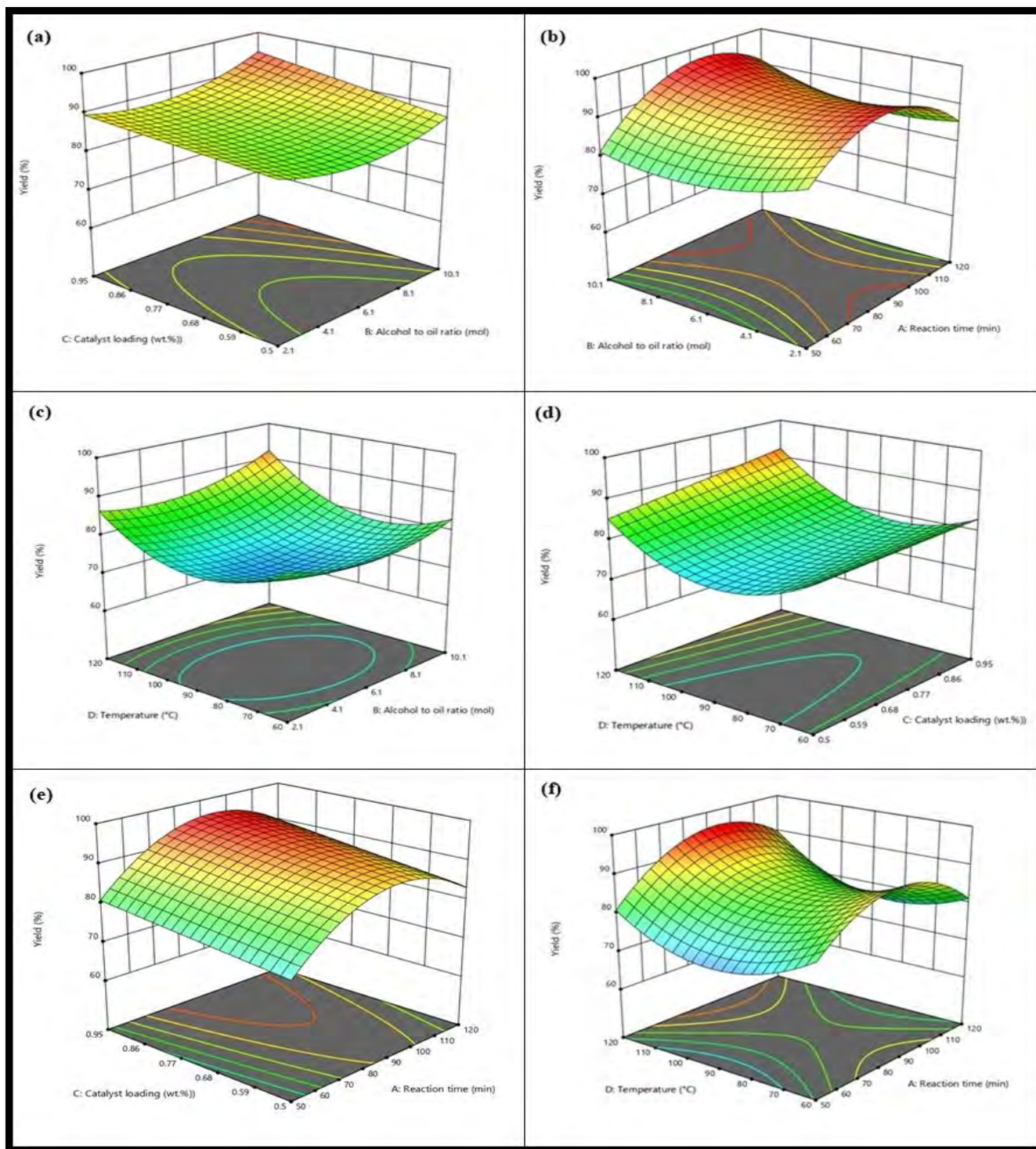
Figure 3.2.7. Influence of the reaction parameters of ZASO biodiesel.

Table 3.2.1- Experimental design by central composite design for transesterification reaction

Process parameters	−1	+1
Reaction time	50	120
Alcohol to oil ratio	2:1	10:1
Catalyst loading	0.5	0.95
Temperature	60	120

Table 3.2.2 - Detailed experimental result for transesterification reaction of ZASOD

Run	A:Catalyst loading (g)	B:Reaction Time (min)	C:Temperature (°C)	D: Oil to Methanol Ratio	Yield (wt%)
1	0.725	85	90	1:15	79
2	0.95	120	60	1:7	83
3	0.95	50	120	1:7	84
4	0.5	120	90	1:7	95
5	0.5	50	60	1:7	92
6	0.95	85	120	1:15	80
7	0.725	85	90	1:15	85
8	0.725	120	90	1:15	76
9	0.5	120	60	1:7	92
10	0.725	85	90	1:15	82
11	0.725	85	90	1:2	70
12	0.725	85	90	1:15	80
13	0.95	120	60	1:2	92
14	0.5	85	90	1:15	80
15	0.725	85	90	1:15	85
16	0.95	50	60	1:7	86
17	0.5	50	60	1:2	69
18	0.5	50	120	1:7	87

19	0.725	85	60	1:15	85
20	0.95	120	120	1:7	90
21	0.95	120	60	1:2	90
22	0.725	50	90	1:15	74
23	0.5	50	120	1:2	86
24	0.725	85	120	1:15	83
25	0.95	50	120	1:2	80
26	0.5	120	60	1:2	92
27	0.725	85	90	1:7	80
28	0.725	85	90	1:15	75
29	0.5	120	120	1:2	94
30	0.95	50	60	1:2	81

Table 3.2.3- ANOVA for Response Surface Quadratic model

Source	Sum of Squares	df	Mean Square	F-value	p-value	
Model	1.45	14	0.1034	7.31	0.0002	Significant
A-Catalyst Loading	0.3685	1	0.3685	26.07	0.0001	
B-Time	0.3961	1	0.3961	28.02	< 0.0001	
C-Temperature	0.0023	1	0.0023	0.1611	0.6938	
D-Oil to MetanolRatio	0.0106	1	0.0106	0.7489	0.2005	
AB	0.0011	1	0.0011	0.0788	0.5827	
AC	0.0065	1	0.0065	0.4598	0.5080	
AD	0.0105	1	0.0105	0.7432	0.4022	
BC	0.0853	1	0.0853	6.04	0.0267	
BD	0.1050	1	0.1050	7.43	0.0156	
CD	2.236E-06	1	2.236E-06	0.0002	0.9901	
A²	0.0640	1	0.0640	4.53	0.0503	
B²	0.0292	1	0.0292	2.07	0.1711	
C²	0.0295	1	0.0295	2.09	0.1693	
D²	0.0337	1	0.0337	2.38	0.1434	
Residual	0.2120	15	0.0141			
Lack of Fit	0.1719	10	0.0172	2.14	0.2076	not significant
Pure Error	0.0402	5	0.0080			
Cor Total	1.66	29				

R^2 = 0.6074, Std. Dev=0.1189, C.V. % = 1.28, Adeq Precision = 4

3.2.3 Effect of reaction variables on Transesterification

3.2.3.1 Combined effect of oil to methanol molar ratio and catalyst loading

The oil to methanol molar ratio and catalyst loading are significant reaction parameters, which is affecting the biodiesel yield during transesterification reaction. A sufficient amount of methanol is required to convert oil into methyl ester and push the reaction onward. Stoichiometric calculation exposed that 3 mol of the alcohol reacts with 1 mol of oil to produce biodiesel (3 mol) and glycerol (1 mol) (Ghanbariasad et al., 2019). The combined influence of molar ratio and catalyst loading on transesterification reaction of *Zanthoxylum armatum* seed oil has been displayed in three-dimensional plots grounded on central composite experimental design (Figure 3.2.7a). The highest yield (95%) of methyl ester was obtained at 0.5 wt. % catalyst loading, and molar ratio 1:7. A reduction in molar ratio from 1:7 to 1:2 with rise in a catalyst amount gives the 70% conversion of triglycerides to the methyl esters. At constant molar ratio of 1:7, increasing the catalyst amount up to 0.95 wt. % resulted in a reduction in yield to 80%. It is revealed that a rise in catalyst amount decreased the yield of biodiesel due to the formation of unwelcome reaction products (Sandhya et al., 2020). An excess amount of methanol (1:15) dropped the yield of biodiesel up to 74%. This decrease in yield is attributed to the reversible reaction of glycerolysis by mixing and solubilizing glycerol in FAMEs and facilitating recombination of glycerol with FAMEs, resulting in the reformation of monoglycerides in the reacting mixture (Abd et al., 2021). Dilution of the catalyst concentration happens due to excess methanol in the reacting mixture. It interferes with the separation of glycerol from FAMEs and adds to the low yield of biodiesel. The current results are in line with previous findings, where an excess volume of methanol results in the backward reaction of glycerolysis. It has been previously reported that a decrease in biodiesel yield happened with the rise in molar ratio from 15:1 to 20:1 at 80 ℃ and catalyst concentration of 1% (Elkelawy et al., 2019). The combined effect of molar ratio and catalyst loading was found insignificant in ANOVA with a p-value of 0.5827 (>0.05). The separate catalyst loading was significant by having a p-value of 0.0001and oil to methanol ratio insignificant with a p-value of 0.2005 (>0.05).

3.2.3.2 Combined influence of oil to methanol ratio and time

The oil to methanol molar ratio and reaction time is another critical reaction parameter that considerably affects biodiesel yield. Figure 3.2.7b depicts combined affect molar ratio (D) and reaction time (B), while other reaction variables like temperature (90 ℃) and catalyst loading (0.5 wt. %) was kept constant. A maximum yield of 95% was observed at molar ratio of 1:7 and time of 120 min. It credited to upsurge interaction of triglycerides with excess alcohol during the transesterification. In contrast, a shorter reaction time of 50 min of transesterification with lower molar ratio at run number 17 lead to a comparatively slighter yield of biodiesel (69%). It is most possibly due to insufficient time for the reactants to react properly, resulting in the incomplete conversion of reactants into products. Reduction in the biodiesel yield (76%) was observed at higher oil to methanol ratio of 1:15 with time 2 h at run number 8 due to excess amount of methanol, which shifted reaction towards unwanted reaction condition, facilitating reverse reaction and subsequent low yield of biodiesel. The comparable outcomes were testified by previous literature, where yield of 91% was reported at time of 50 min utilizing iron-doped zinc oxide catalyst to mediate the chemical reaction of transesterification (Fedosov et al., 2011). Higher conversion of triglycerides into methyl ester is possible even in a shorter reaction time with high catalyst loading (Ghosh et al., 2019). The ANOVA results illustrated a strong correlation between molar ratio and reaction time with a p-value lesser than 0.05 (0.0156) and were found significant.

3.2.3.3 Combined influence of oil to methanol molar ratio and temperature

The collective effect of molar ratio and the temperature is demonstrated in Figure 3.2.7c. Yield of methyl ester was increased up to 95% as the temperature of transesterification reached up to 90 ℃ at catalyst concentration 0.5 wt. % and oil to methanol ratio 1:7. Nevertheless, further increase in temperature above edge level (>90 ℃) significantly decreases biodiesel yield at run number 3 (84%). A lesser temperature of 60 ℃ caused a decrease in yield of methyl ester up to 69%. It is attributed to the reduced mass transfer rate of oil, methanol and catalyst as they all are immiscible at lower temperature and need sufficient kinetic energy to react appropriately and increase productivity in a shorter time period (Olutoye et al., 2016). It is determined from the current study that combines the effect of molar ratio and temperature is worthy of being considered during transesterification reaction. Outcomes of ANOVA showed this combined correlation insignificant by having a p-value > 0.05 (0.9901).

3.2.3.4 Combined influence of catalyst loading and reaction temperature

Collective influence of catalyst loading and temperature on the biodiesel yield % is presented in Figure 3.2.7d. Maximum yield of 95% was obtained at run number 4 at reaction temperature 90 °C, molar ratio 1:7 and time 2 h, which is attributed to maximum interaction of oil with methanol during transesterification. It is in line with the Arrhenius equation stating that an increase in reaction temperature steadily increases the chemical reaction and yield of methyl ester (Mendonça et al.,2019). A shorter reaction time (85 min) with lesser molar ratio (1:2) ensued a low yield of 70% in run number 11, which is more certainly due to incomplete conversion at a low time period reactant fails to reach an equilibrium state. In run number 8, high molar ratio of 1:15, at time 2 h and temperature 90 °C lead to a decrease in biodiesel yield (76%). The high amount of methanol favored unfavorable conditions and the consequent low yield of the biodiesel. Similar results were reported in previous literature (Rozina et al., 2019). ANOVA results revealed that the mutual influence of these variables is not significant by having a p-value (0.5) greater than 0.05.

3.2.3.5 Combined influence of time and catalyst loading

Figure 3.2.7e depicts the mutual effect of reaction time (B) and catalyst loading (A) of transesterification in the form of a 3D plot by keeping other reaction parameters like reaction temperature and molar ratio constant. Maximum yield of 95% was obtained at the optimal time (2 h) and catalyst loading 0.5 wt. % at run number 4 due to equilibrium in the transesterification reaction. The optimal level reaction time and catalyst loading decrease in biodiesel yield (83%) was notified at run number 2, which is similar to previously reported work (Ayetor et al., 2015). A shorter time renders the biodiesel yield (80%) even at a high catalyst loading of 0.95 wt. % (Run 6) due to the partial conversion of reactants into products. The prolonged reaction time (Run 8) favored a reversible transesterification reaction and minimized the yield (76%). The current study mutual influence of reaction time and catalyst loading was found not significant by having a *p*-value (0.5827) > 0.05 for methyl ester formation.

3.2.3.6 Combined influence of time and temperature

The combined influence of time and temperature of transesterification at constant oil to methanol molar ratio 1:7 and catalyst loading of 0.5 wt. % on biodiesel yield is illustrated in Figure 3.2.7f. It is manifested from Run 4 that 95% yield of methyl ester was achieved at

temperature 90 °C and reaction time 2 h. Any further increase in reaction temperature and time results in a decrease in methyl ester yield up to 76% (Run 8). The higher reaction time and temperature are considered to be expediting the chemical process of hydrolysis of alkyl esters into acids. The subsequent polar methanol in the reacting mixture is dropping the biodiesel yield (Anwar et al., 2019). The current investigation uncovered that increase in biodiesel yield with increase in temperature and time is up to the specified limit. Afterwards, a significant decrease in % yield happens, attributed to the endothermic nature of the transesterification. Outcomes of the ANOVA displayed the mutual influence of time and temperature on methyl ester yield as significant with a *p*-value (0.0267) <0.05.

3.2.4 Characterization of biodiesel

3.2.4.1 FTIR Study

Fourier-transform infrared spectroscopy (FTIR) is the most common technique used to determine various functional groups present in FAMEs from the mid-infrared region of 500-4,000 cm^{-1}. The presence of carbonyl and methyl group bands in the IR spectrum of biodiesel proves methyl ester production during transesterification. The IR region associated with the carbonyl group is considered as most chemically and molecularly changeable part in the biodiesel spectrum. FTIR spectroscopy is one of the defined laboratory techniques used to confirm biodiesel production next to transesterification reaction (Rashid et al., 2015). FTIR spectrum of the *Zanthoxylum armatum* seed oil and methyl ester has been presented in Figure 3.2.8a and 3.2.8b. The number of different stretches and bands representing the various functional groups were detected in the FTIR spectrum of ZASO and methyl ester. The deep and strong ester stretch at 1742.04 cm^{-1} represented carbonyl group (C=O), which was later confirmed by NMR results of biodiesel. Peak for carbonyl group at 1745.08 cm^{-1} in the IR spectrum of *Sylibum eberneum* biodesel (Shaheen et al., 2018) whereas it was found at 1740 cm^{-1} in the spectrum of *Celastrus paniculatus* biodiesel (Rana, and Das 2017), both are comparable to our current results. Biodiesel of *Zanthoxylum armatum* seed oil has sp^2 C-H stretching at 2922.66 cm-^{1}, sp^3 C-H at 2853.3 cm-^{1} and C-H bending (rocking) appeared at 1464.49 cm-^{1}. FTIR spectrum of the seed oil represented sp C-H stretch appeared at 3317.8 cm^{-1}, C-H (sp^2) stretching was detected at 2831.60 cm^{-1} and C-H (sp^3) 2929.97 cm^{-1}. Infra-Red region (1743.60 cm^{-1} and 1377.72 cm^{-1}) is a significant pointing signal demonstrating the considerable modification between the *Zanthoxylum armatum* seed oil and synthesized biodiesel.

The frequently identified variable IR region of seed oil and methyl ester lies within the ester control peak area of the spectrum existed at around 1100-1000 cm^{-1}. The C-H$_2$ wagging frequency stretch peak, which was observed at 1022.77 cm$^{-1,}$ disappeared in the IR spectrum of ZASO. Similarly, an intense peak detected at 1161.2 cm^{-1} (C-O) in the IR spectrum of ZASO was found to be absent in the spectrum of seed oil. A wide-ranging peak of 1403.95 cm^{-1} in ZASO was split into 1377.72 cm^{-1} and 1238.46 cm^{-1} in *Zanthoxylum armatum* seed oil biodiesel (ZASOD). Our results are in line with the previous findings (Tavizón-Pozos et al., 2021; Lamba et al., 2017). All these peaks of the IR spectrum confirmed the formation of biodiesel.

3.2.4.2 ^{1}HNMR spectroscopic analysis

^{1}HNMR and ^{13}CNMR spectrum of ZASOB is presented in Figure 3.2.9a and b. ^{1}HNMR technique was used to confirm the formation of methyl ester from triglycerides in the reacting mixture after transesterification reaction and find out the molecular composition of biodiesel. Characteristic peak of a methoxy group (– OCH$_3$) at 3.671 ppm indorsed the presence of methyl ester. A free methanol peak, which is usually observed at 3.45 ppm, was found absent in the ^{1}HNMR spectrum. Triplet of α methylene proton (α-CH$_2$) was detected at the 2.265 ppm, and β-CH$_2$ (β-methylene) protons were noticed at 1.260-1.67 ppm, which is indicating hydrogen atoms present on carbon number 3 in an aliphatic fatty chain.

Terminal methyl protons were observed at 0.896 and 0.9607 ppm and a peak of olefinic hydrogen (-CH=CH-) was found at 5.330-5.410 ppm, which is a sign for double bonds integrated for two hydrogen atoms per each double bond group. A peak at 2.758 ppm is allylic hydrogen (-CH$_2$-), which comprises two hydrogen atoms per non-conjugated group in the spectrum. Peaks of mono and di-glycerides at 4.15 and 4.3 ppm were not observed in the biodiesel ^{1}HNMR spectrum of biodiesel. A peak at 5.31 ppm represented the presence of a mono-unsaturated bond system. All these peaks in the ^{1}HNMR spectrum revealed the presence of methyl ester in ZASO biodiesel (Rozina et al., 2017).

Structural characteristics of the methyl ester of ZASOB were investigated with ^{13}CNMR (Figure 3.2.9b). ^{13}CNMR indicated the characteristic peak of methoxy carbon at 51.47 ppm and

signal carbonyl group (-COOH) at 174.35. Unsaturated position (-CH=CH-) in the methyl ester of ZASO was observed at 127.89 ppm for inner nun-conjugated carbon. Other chemical shifts at the δ (ppm) 129.95 (-CH=CH-) represented outer carbon of nun-conjugated carbon, 77.48 (-C-O) and the long chain of ethylene carbon at 29.35 (-CH$_2$-)$_n$ ppm were also observed in spectrum biodiesel. Signal for aliphatic methylene (-CH2-s) carbon was detected at the region of 34-27 ppm of the spectrum. Similar results of NMR spectroscopy are described in previous research (Lawan et al., 2019; Rashid et al., 2011).

3.2.4.3 GC-MS analysis of biodiesel

Deviation in the chemical composition of biodiesel is profoundly affecting various chemical and physical properties of biodiesel. The expansion of the carbon chain length results in a high cetane number and viscosity of biodiesel (Berman et al., 2011). Chemical composition and quantification of fatty acid methyl esters in ZASOB were executed with Gas chromatography and Mass spectrometry to ascertain the quality of synthesized biodiesel. GC-MS analysis is one of the critical factors to tell the biomass source suitability for biodiesel production. The higher degree of unsaturated fatty acids is considered undesirable (Ayetor et al., 2015) as it causes clogging in fuel engines (Rahimi etal., 2021). Various peaks of the FAMEs were detected in the GC-MS spectrum of ZASOB, which was further recognized by library match software NO. NIST02 presented in Figure 3.2.10. A Retention time of the various FAMEs was used to identify them and further confirm them by MS analysis (Helmi et al., 2021). The unsaturated fatty acids, 7- hexadecenoic acid methyl ester (C16:1), 9-Octadecenoic acid methyl ester (C18:1), 9, 12-Octadecadinoic acid methyl ester (C18:2), were observed in the spectrum. The Saturated fatty acids, eicosanoic acid methyl ester (C20:0) and 5, 8-octadecenoic acid methyl ester (C18:0), are detected too. 5, 8-octadecenoic acid was the major fatty acid methyl ester present in the ZASOB. The GC/MS analysis results indicated that the seed oil of *Zanthoxylum armatum* is suitable for biodiesel production at the industrial level.
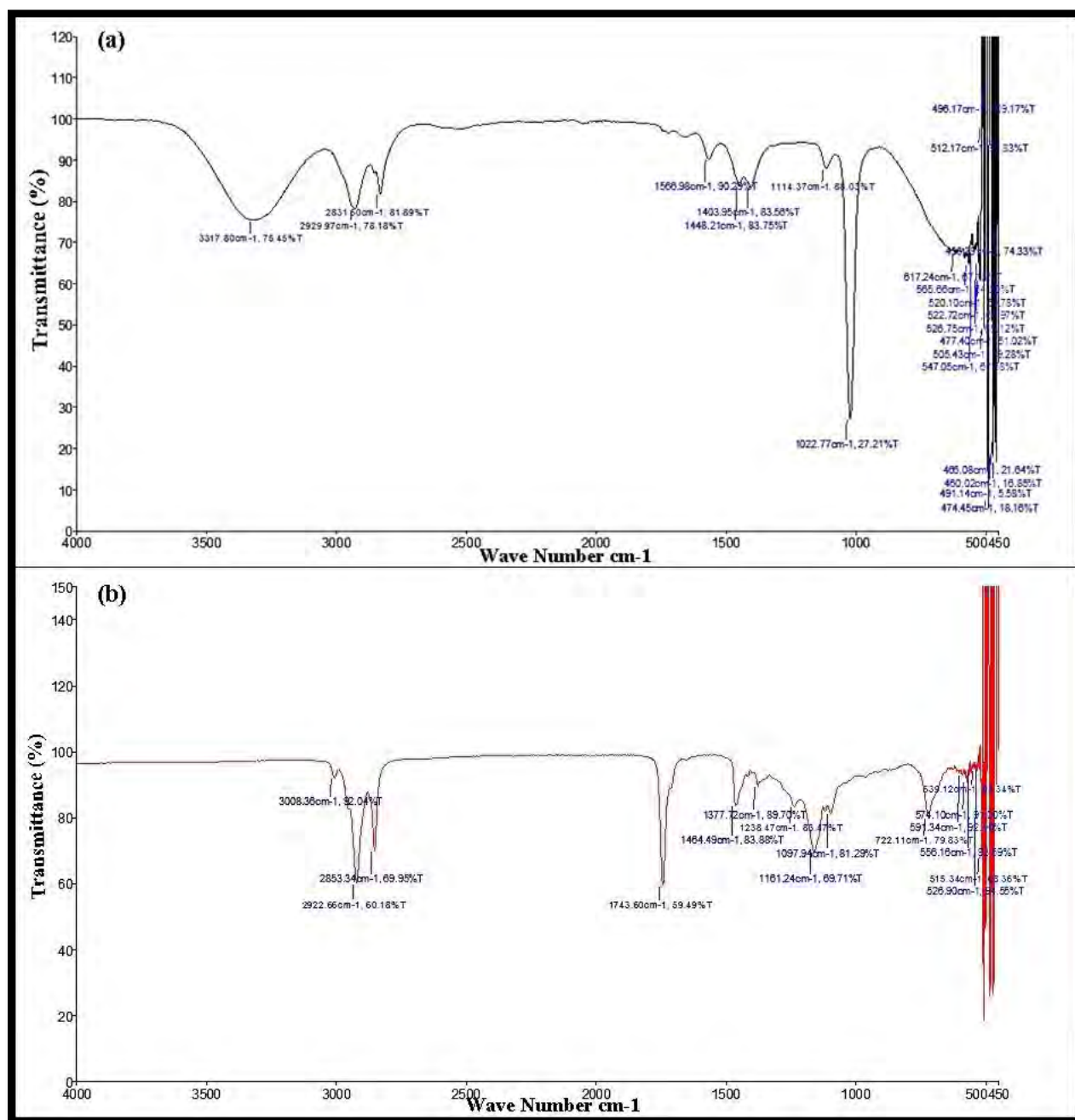
Figure 3.2.8. FTIR spectrum of **(a)** seed oil of *Zanthoxylum armatum* **(b)** *Zanthoxylum armatum* biodiesel
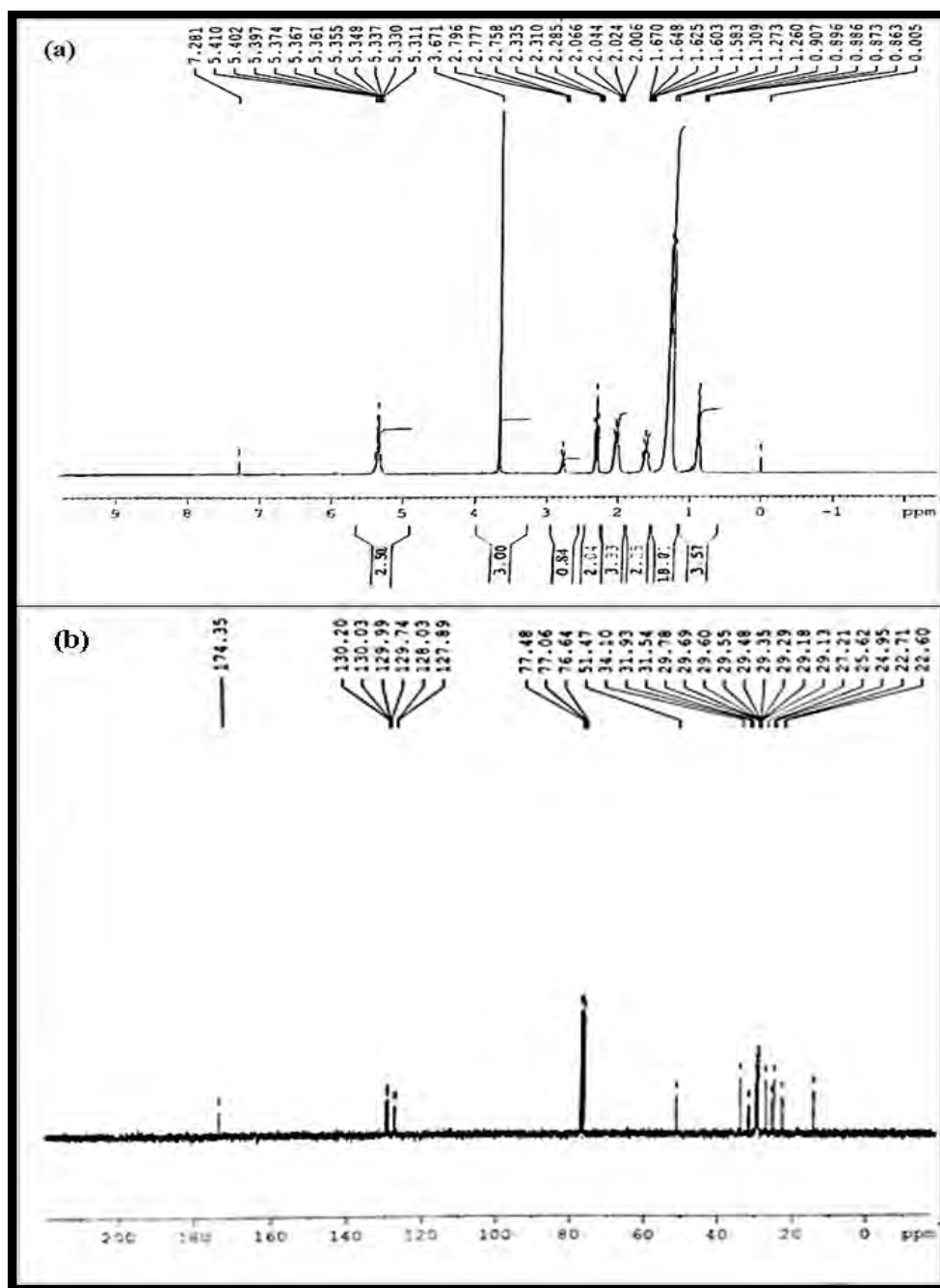
Figure 3.2.9. NMR spectrum of **(a)** ^{1}HNMR and **(b)** ^{13}CNMR of ZASOB
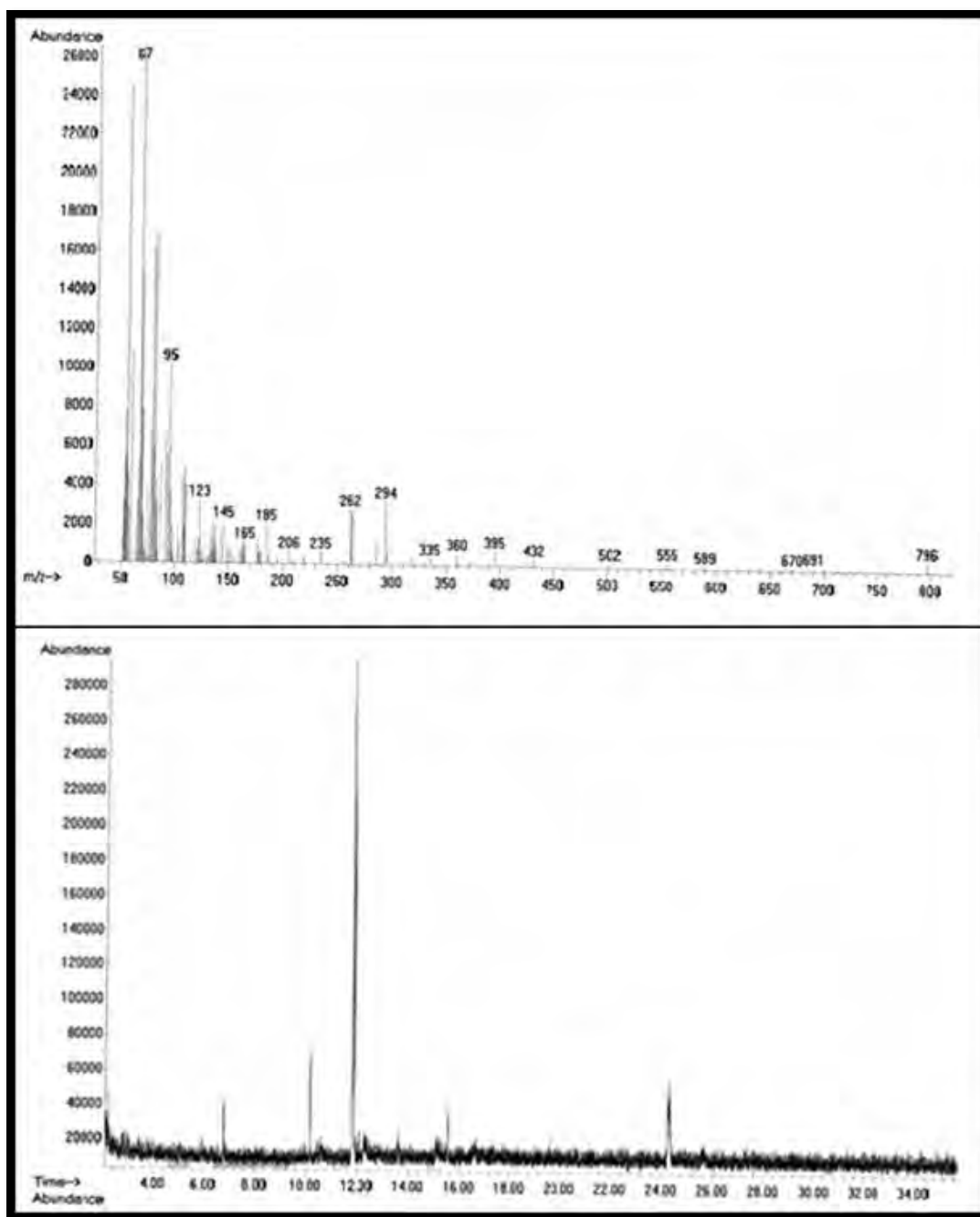
Figure 3.2.10. GC-MS spectrum of *Zanthoxylum armatum* biodiesel

3.2.5 Fuel properties of *Zanthoxylum armatum* biodiesel

Fuel properties of the ZASOB were investigated and compared with ASTM D-6751 and European Union EN 14214 to predict its quality and efficiency for fuel engines before its practical implication. Fuel properties of the ZASOB and its comparison with previously reported feedstock is shown in Table 5. Comparison of the fuel properties with previous studies displayed consistency in their properties with some slight variation.

The acid value of biodiesel is a significant fuel property that depends upon the free fatty acids contents of the fuel. The higher value of acid value is not appreciable and affects fuel engine performance by damaging its parts by causing corrosion in the fuel supply line, particularly in injectors. The acid value of ZASOB in the current study was 0.177 (mg KOH/gm) and well-matched with international standards (Table 3.2.4). The purity and quality of biodiesel are described in terms of density. It has been reported that long-chain and high saturation level increases the density of biodiesel (Singh et al., 2021). Biodiesel with high fuel density affects the efficiency of the engine. According to the international standards, (ASTM, EN) density of biofuels should lie under the range of 860 and 900 kg/m^3, which is slightly above that of petro-diesel, *i.e.* 827.2 kg/m^3 (Foroutan et al., 2021). The density of ZASOB in the current study was found 0.910 (mm^2/s), which lies within limits of fuel density given in international standards and revealing its effectiveness in diesel engine as an alternate and sustainable substitute to fossil fuel sources.

Kinematic viscosity (kg/m^3 at 40 ℃) is another important fuel property of biodiesel and plays a vital role in the fuel combustion process. The high value of kinematic viscosity significantly affects atomization of fuel, spray penetration and fluidity, especially in cold weather with low temperature. It tells about the stickiness of biodiesel. In the present study, the kinematic viscosity of ZASOB was found to be 4.34 mm^2/s, which is equivalent to the international standards. Kinematic viscosity of the ZASOB was found to be less than biodiesel of *Saussurea heteromalla, Cocos nucifera* and *Taraxacum officinale* (Rozina et al., 2017, Ayetor et al., 2015; Rozina et al., 2019).

Flashpoint is regarded as the temperature at which biofuel flashes upon ignition or the degree of the affinity of a chemical substance to make a flammable mixture in the existence of

oxygen gas. It aids to determine the storage temperature and transportation requirement of the fuel. Biofuels with a high value of the flashpoint (>66 ℃) are considered hazardous free and safe to store, which is acting as a vital safety asset for transport [36]. The flashpoint of the ZASOB in the current study was found to be 70 ℃, which is less likely to ignite accidentally and comparable to international standards.

Cold properties of synthesized biodiesel are significant parameters investigated as they critically affect fuel quality at low temperature. The pour point value of ZASOB was observed to be -6 ℃, and the cloud point in the current study was -11 ℃, which lies within the range of ASTM standards. Comparatively, the lower sulphur content in the ZASOB was (0.0003 wt. %) observed and indicated it as a clean and eco-friendly.

Table 3.2.4 - Comparison of Fuel properties of ZASO biodiesel with international standards

Property	*Zanthoxylum armatum*	ASTM D-6751			EN-14214		China GB/T 20828-2007	
	Mean	Mean	St.Dev	Mean	Mean	St.Dev	Mean	St.Dev
Flash Point (°C)	70	2.0	-	-	2.0	-	-	2.52
Pour Point (°C)	-6	≤0.5	≤0.8	≤0.5	≤0.5	≤0.8	≤0.5	1.0
Viscosity (mm²/s at 40 °C.)	4.34	≥93	≥130	≥120	≥93	≥130	≥120	0.2
Density (kg/m³ at 40 °C)	0.910	-15-16	_	_	-15-16	_	_	0.036
Cetan Number	-	1.9-6.0	_	3.4-5.0	1.9-6.0	_	3.4-5.0	2.52
Iodine Value (g I2/100 g)	-	≤120	_	≤120	≤120	_	≤120	2.1
Sulpher content	0.0003	≤0.05	≤0.05	≤0.20	≤0.05	≤0.05	≤0.20	0
Cloud point	-11	-3.0-12	_	_	-3.0-12	_	_	1
References		ASTM D-6751		EN-14214			China GB/T 20828-2007	

3.2.6 Reusability of catalyst and role of the plant extract in the catalyst preparation

Catalyst reusability is one of the significant parameters to stretch advantages at an industrial scale and conserves time spent re-synthesizing. The catalyst stability and economic viability for industrial-scale biodiesel production highly depend on its efficiency to reuse in a reaction process. The reusability of a heterogeneous catalyst depends on the type and nature of the catalyst and relies on the purification, separation, and transesterification process. In the current study, the reusability of synthesized silver oxide green nanoparticles was checked at optimum reaction conditions, *i.e.* catalyst loading (0.5 wt. %), time (2 h), temperature (90 ℃), and the molar ratio of 1:7. After completing the first cycle, the spent Nano catalyst was recovered from transesterification products by centrifugation, then washed with methanol to remove impurities and dried in an oven at 60 ℃ for 24 h. The oven-dried catalyst was calcined for 3 h at 500 ℃ to reuse for the following cycles. The results showed the catalytic activity was higher for the first three runs, and the obtained yield of biodiesel was found between 95 to 75%. Biodiesel yields were reduced after the third run up to 60 % due to leaching and poisoning of catalyst active sites by organic species like glycerides and glycerol, shrinking surface area, basicity and pore volume of catalyst (Figure 3.3.11). It was assumed that the reduction in the availability of active catalytic sites declined the methyl esters yield.
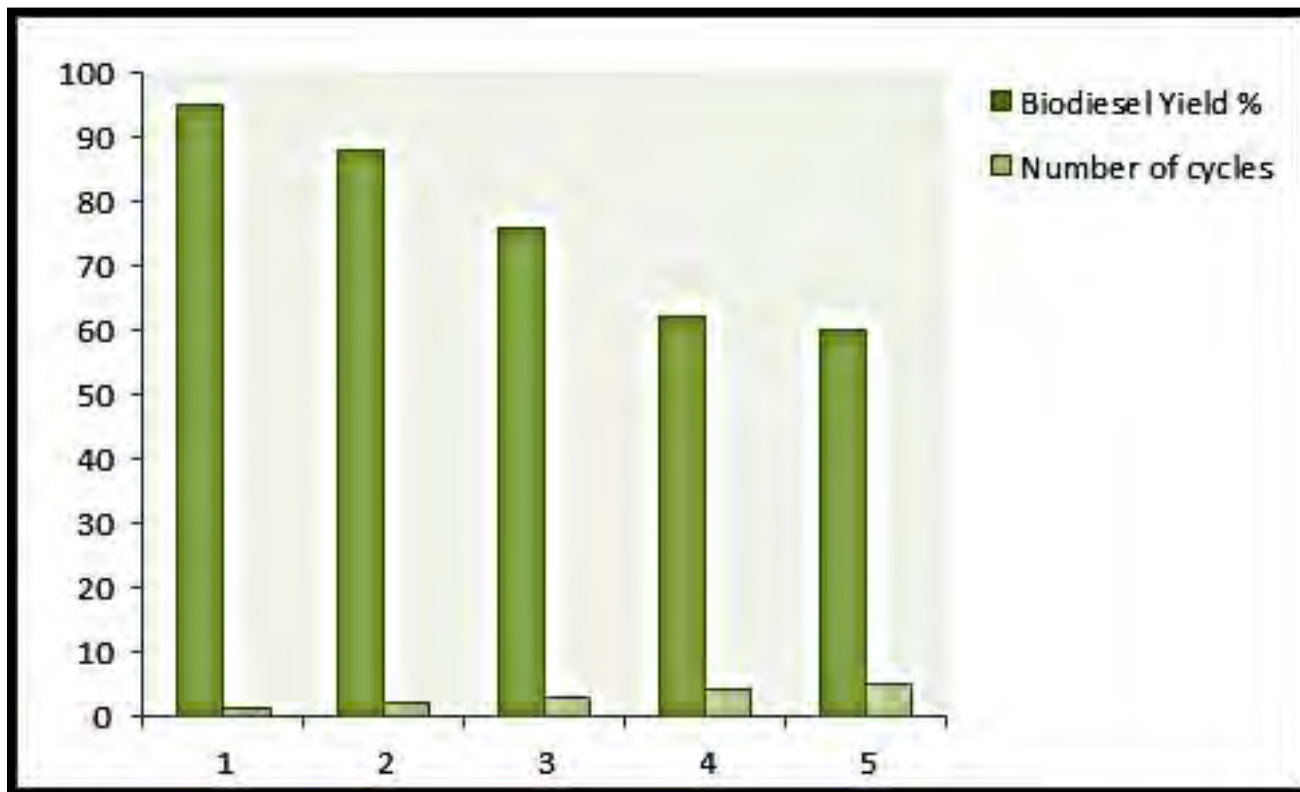
Figure 3.2.11. Reusability of Silver oxide NPs in a transesterification reaction

SECTION III

- Biodiesel Production from *Citrus medica* L seed oil using Green nano Catalyst of Copper oxide

Transitional metal oxides, like CuO, have demonstrated successful uses as cutting-edge nanomaterials in the realms of energy, biomedicine, and the environment. This excellent adsorption capacity of CuO NP greatly improves both their performance and applications. Hence, in this study we made an attempt to determine its efficacy in the process of transesterification.

3.3.1 Catalyst characterization

3.3.1.1 X-Ray Diffraction (XRD) of CuO

X-Ray Diffraction (XRD) is used to investigate crystal structure and phase purity of nano-particles. The pattern of X-Ray Diffraction of CuO revealed that all diffraction peaks are related to CuO nano-particles and there is no second phases like Cu_2O or $Cu(OH)_2$. The 2θ peaks identified in XRD pattern included 32.56^o, 34.95^o, 38.65^o, 42.7^o, 53.5^o, and 58.2^o which corresponded to crystal plane indices of (110), (002), (111), (202), (020) and (202) of CuO monoclinic phase (Figure 3.3.1). The crystalline size of NPs was found to be 50 nm.

3.3.1.2 Scanning Electron Microscopy (SEM) of CuO

Surface morphology of green nano-particles of CuO was studied by scanning electron microscopy (SEM). SEM micrographs of CuO powder can be seen in Figure 3.3.2 which revealed aggregated spherical morphology. The resultant spherical morphology could be because of the method of their green synthesis including reduction and combustion. Functional molecules in green extract assists in controlling shape of nano-particles by acting as shape directing or capping agent (Kannimuthu et al., 2021). Nevertheless, these capping molecules are destroyed during combustion step and lead to formation of spherical aggregates of CuO (Li et al., 2020).

3.2.1.3 Energy Diffraction X-ray (EDX) of CuO

Energy diffraction (EDX) is a technique used to find out chemical composition of synthesized powder and to check it for impurities. The EDX spectrum of CuO nano-particles disclosed that it contains only Cu and O elements illustrated in Figure 3.3.3. Moreover, based on the element analysis of the sample percentage of Cu and O was found to be 77.98% and 22.20%

respectively. It was demonstrated from EDX result that synthesized nano-particles are that of CuO. Results of EDX were in agreement with XRD pattern.

3.3.1.4 Thermogravimetric analysis (TGA) of CuO

Thermal analysis of CuO nano-particles was carried out with thermo gravitational analysis (TGA). Thermogram of CuO nanoparticles has been illustrated in Figure 3.3.4a along with corresponding derivative curve (Figure 3.3.4b). The TG curve expressed major weight loss in three broad steps. The first loss of 0.529% was observed in temperature range of 300 ºC-500 ºC associated to dehydration process from OH groups. The second sharp loss of 3.634% in weight was noted at relatively higher temperature in between 550 ºC -620 ºC. These broad endothermic transitions are attributed to desulfurization process. The third major loss of 1.489% was observed in temperature range of 640 ºC -850 ºC which is attributed to decomposition and transformation of molecules of CuO nano-particles. Derivative curve clarified these endothermic peaks (Figure 3.3.4b).

3.3.1.5 Fourier Transform Infrared Spectroscopy (FTIR)

Fourier-transform infrared spectroscopy (FTIR) in the wave length range of 515-4000 cm^{-1} was used to examine nature of synthesized green nano-particles of CuO. FTIR spectrum of CuO has been depicted in Figure 3.3.5. Absorption band at 608.78 cm^{-1} and 1063.97 cm^{-1} were attributed to SO$_4$ bending and stretching vibration respectively in the IR spectrum. Absorption band at 3117.72 cm^{-1} is attributed to O-H stretching vibration due to presence of physisorbed water molecules whereas, intense absorption peak at 1063.97 cm^{-1} is endorsed to CuO. Deep peak at 961.9 cm^{-1} indicated metal oxygen (Cu-O) bond hence, confirming formation of CuO nano-particles.
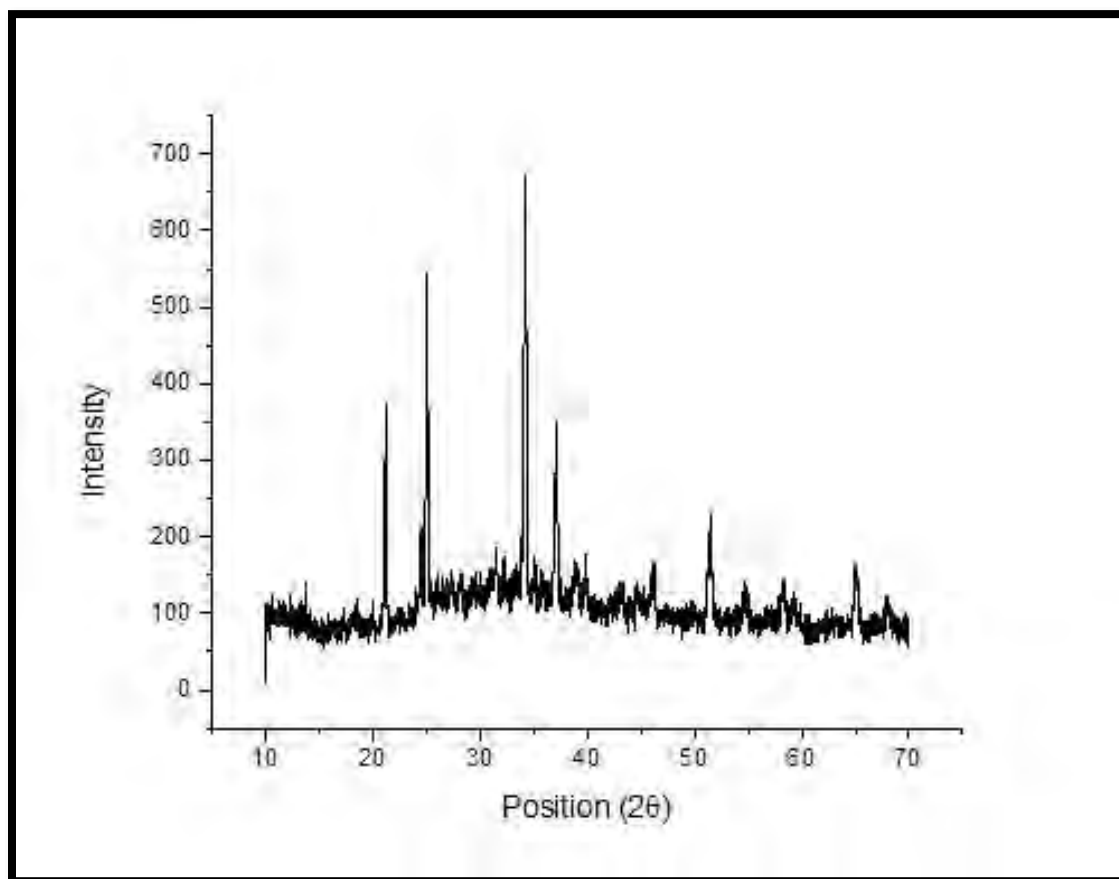
Figure 3.3.1. XRD pattern of calcined copper oxide green nano particles
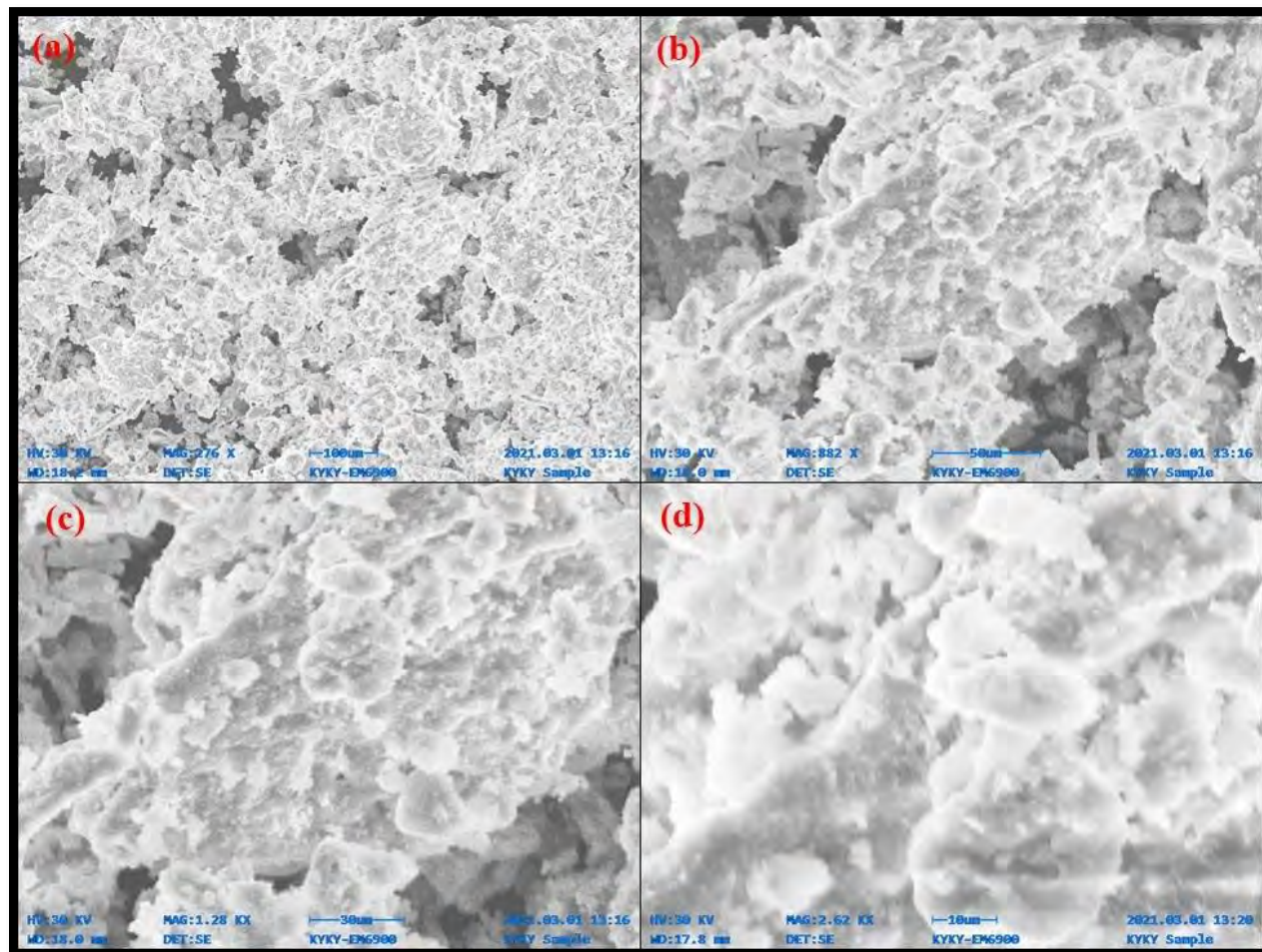
Figure 3.3.2. Scanning electron microscopy (SEM) of calcined copper oxide green nano particles
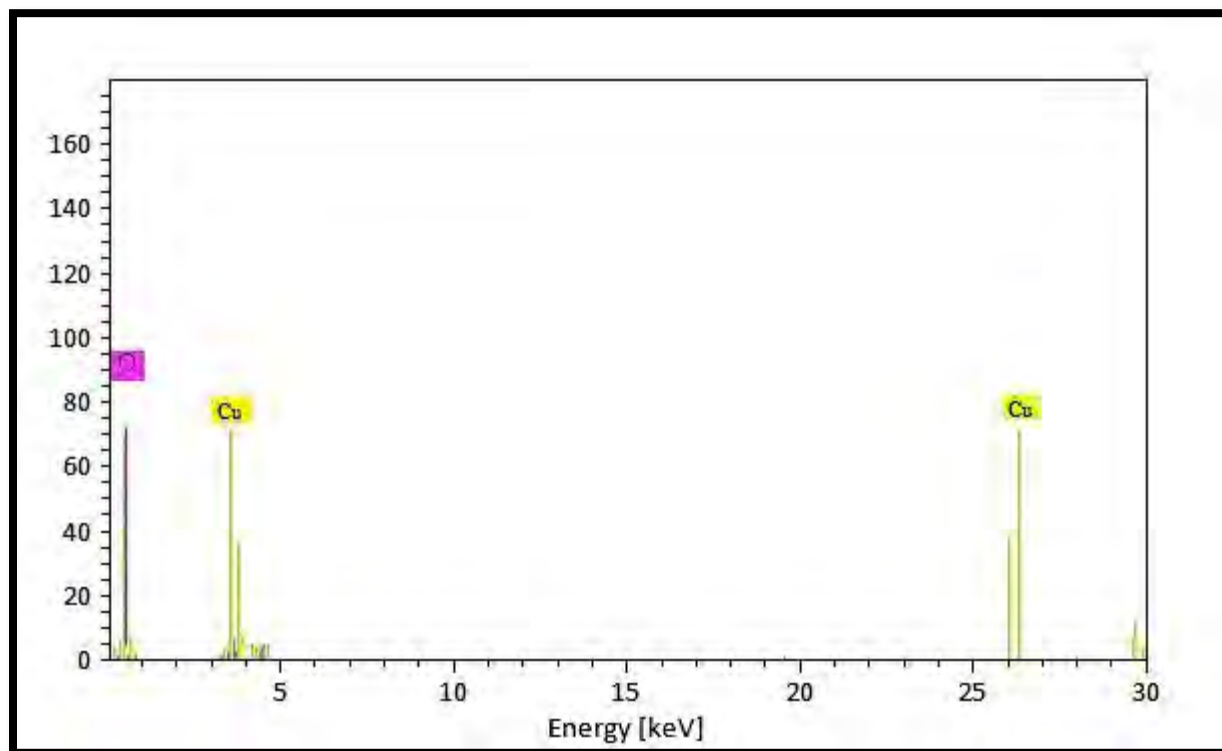
Figure 3.3.3. Energy diffraction X-Ray (EDX) of calcined copper oxide green nano particles
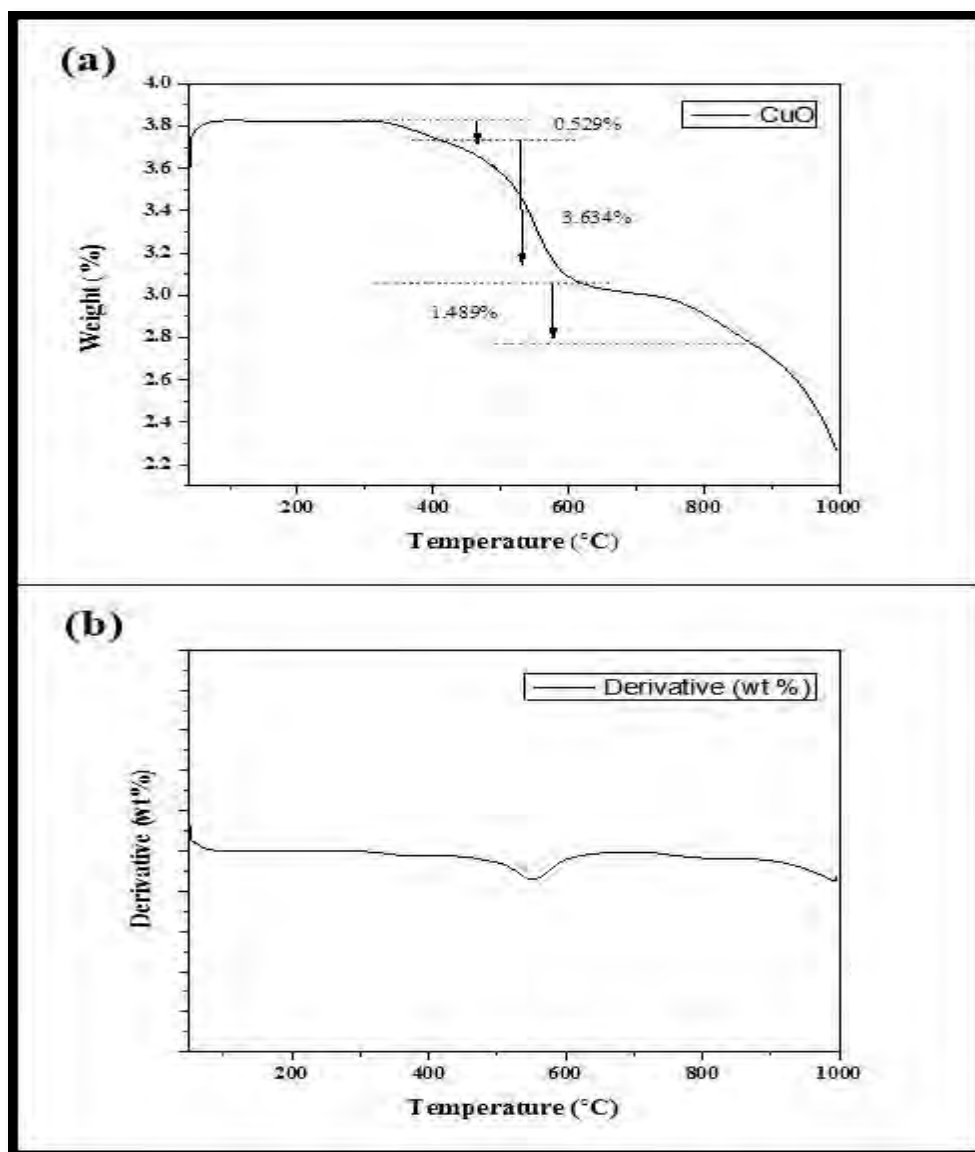
Figure 3.3.4. (a) TGA of copper oxide green nano particles (b) derivative Thermogram of copper oxide nano particles
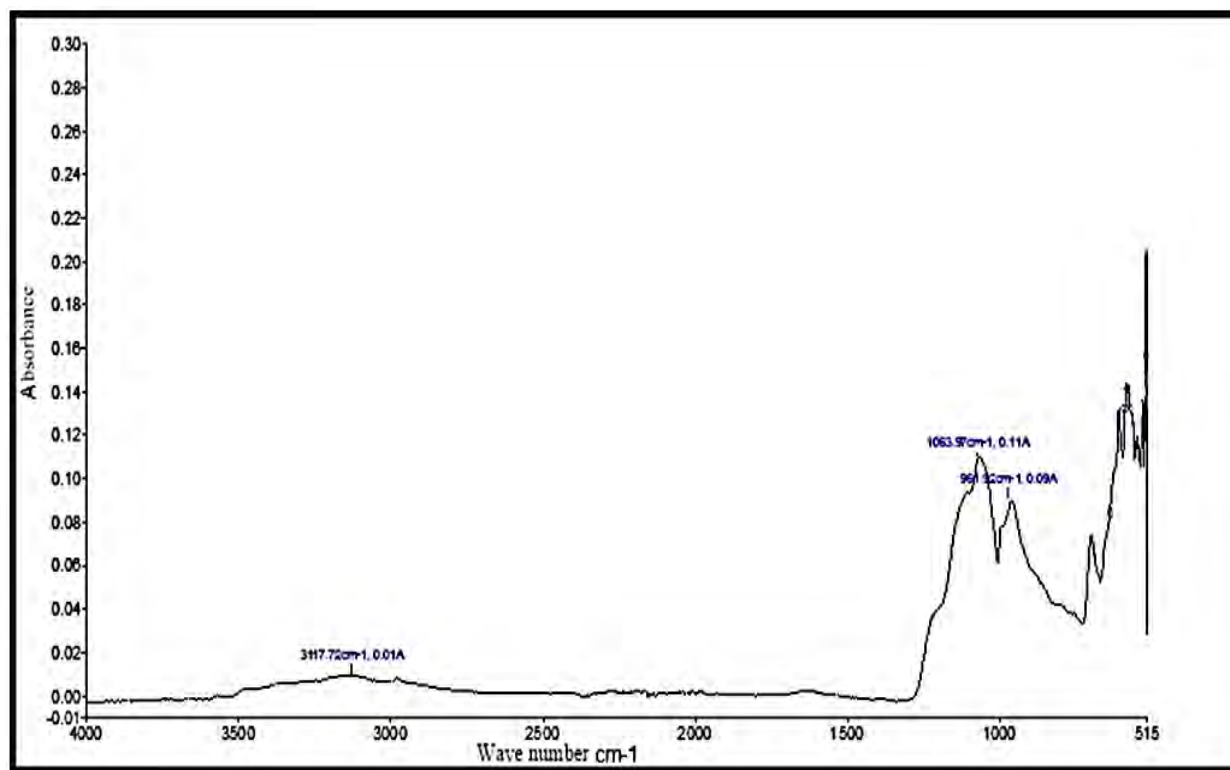
Figure 3.3.5. FTIR spectrum of copper oxide green nano particles

3.3.2. Biodiesel synthesis *via* transesterification

Crude seed oil of *Citrus medica* was evaluated for green synthesis of biodiesel via CuO nano-particles synthesized with *Portulaca oleracea* without any refining process due to its compatibility and high potential. It seemed yellow in color at room temperature. Non-edible seeds of *Citrus medica* have a high oil content of 33% (w/w) with a promising potential for biodiesel production. Physiochemical properties of CMBD have been illustrated in Table 3.3.1. The free fatty acid content of seed oil was found to be 2.1 (wt. %) lesser than restricted limit (3%) directing single step transesterification reaction with no additional esterification step. The percentage yield of biodiesel obtained through numerous experiments of transesterification results has been displayed in Table 3.3.2. Quadratic polynomial equation (9) in terms of coded factor was used to predict percent yield of methyl ester.

Biodiesel Yield = +78.57+0.9444 *A-0.7222* B-0.8889 *C-1.91* D-0.3750 *AB+1.75 *AC+0.1250 *AD+0.5000* BC-1.12* BD+0.7500 *CD-10.55* A²+9.45* B²+1.95 *C²-15.86 *D²
$$\hspace{10cm} (9)$$

Biodiesel yield is significantly affected by reaction parameters like catalyst concentration, reaction time, temperature and oil to methanol ratio. Hence, a series of experiments was performed to investigate optimal reaction conditions. For this purpose an experimental design of Central Composite Design was made using Response Surface Methodology (RSM) with the help trial version-13 of Design of Experiment (DOE). Quadratic model with four independent variables i.e. (A) oil to methanol ratio 3:1-14:1 (B) catalyst concentration of 0.18-1.48 wt. %, (C) reaction time 60-180 mins, and (D) temperature 50-120 ºC. Results of statistical analysis of variance (ANOVA) for the quadratic model have been described in Table 3.3.4.

Predicted versus actual yield of biodiesel are being compared in Figure 3.3.6 in which both data are disseminated near the straight line indicating satisfactory correlation between actual and predicted yield of methyl ester. Statistical analysis of variance (ANOVA) of Response Surface quadric model was carried out and obtained results have been displayed in Table 3.3.3. Results of ANOVA declared the Quadratic model as significant with p-value 0.0122 (<0.05).

Moreover, the lack of fit F-value in the present model was found not significant with F-value of 0.77. Overall, four independent variables of transesterification such as oil to methanol ratio, catalyst concentration, reaction time and reaction temperature were found to had a substantial influence on biodiesel production. Accuracy prediction of response values of the Quadratic model was calculated using Coefficient of determination (R^2) value. The value of predicted R^2 was 0.7391 and found close to the Adjusted R^2 of 0.8030 with variance lesser than 0.2. Adequate Precision of an experimental model measures the ratio of signal to noise. A ratio larger than 4 is required for the significant model. In the current Quadratic model ratio of 6.7755 specifies an adequate signal. Coefficient of variance (CV) reveals the capability of the experimental model and has to be <10%. The value of CV was found 9.03% (<10%) in the current model. It was concluded from all these values that the Quadratic model is significant.
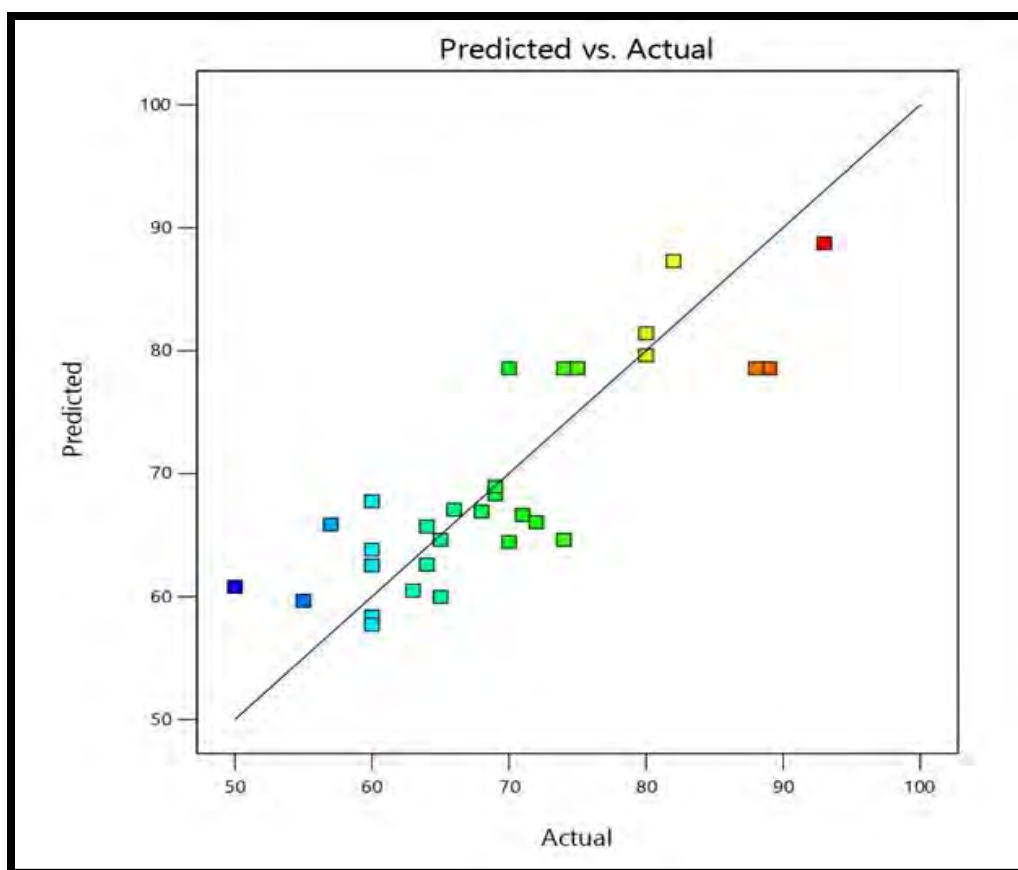
Figure 3.3.6. Comparison between the experimental biodiesel yield and the predicted yield of the model

Table 3.3.1- Experimental design by central composite design for transesterification reaction of *Citrus medica* seed oil

Process parameters	−1	+1
Alcohol to oil ratio	3:1	14:1
Catalyst loading	0.18	1.48
Reaction time	60	180
Temperature	50	120

Table 3.3.2 Detailed experimental result for transesterification reaction of *Citrus medica* seed oil

	Factor 1	Factor 2	Factor 3	Factor 4	Response 1
Run	A:Alcohol to oil molar ratio	B:Catalyst loading	C:Reaction time	D:Temperature	Yield
		wt.%	Min	°C	%
1	3:1	0.48	180	50	60
2	8:1	0.33	180	85	70
3	3:1	0.18	180	50	65
4	13:1	0.18	120	50	71
5	8:1	0.18	180	120	55
6	13:1	0.18	120	85	72
7	8:1	0.33	120	85	88
8	3:1	0.48	60	50	69
9	3:1	0.18	120	50	60
10	8:1	0.48	120	85	82

11	3:1	0.48	60	120	63
12	8:1	0.48	60	85	75
13	3:1	0.48	180	120	60
14	8:1	0.33	120	50	74
15	8:1	0.33	120	50	80
16	13:1	0.48	180	120	64
17	13:1	0.18	60	120	60
18	13.1	0.18	180	50	57
19	8:1	0.18	120	85	93
20	8:1	0.33	120	85	89
21	8:1	0.33	120	120	50
22	8:1	0.18	120	50	65
23	8:1	0.18	60	120	60
24	13:1	0.48	180	50	68
25	8:1	0.33	120	85	74
26	3:1	0.33	120	85	66
27	3:1	0.18	120	85	70
28	13:1	0.33	120	85	69
29	13:1	0.48	60	50	64
30	8:1	0.18	60	85	80

Table 3.3.3- ANOVA for Response Surface Quadratic model

Source	Sum of Squares	df	Mean Square	F-value	p-value	
Model	2210.95	14	157.93	1.72	0.0122	significant
A-Alcohol to oil molar ratio	16.06	1	16.06	0.2763	0.0268	
B-Catalyst loading	9.39	1	9.39	0.1616	0.0934	
C-Reaction time	14.22	1	14.22	0.2447	0.0480	
D-Temperature	68.20	1	68.20	1.17	0.1958	
AB	2.25	1	2.25	0.0387	0.8467	
AC	49.00	1	49.00	0.8431	0.3730	
AD	0.2500	1	0.2500	0.0043	0.0486	
BC	4.00	1	4.00	0.0688	0.7966	
BD	20.25	1	20.25	0.3484	0.0238	
CD	9.00	1	9.00	0.1549	0.6995	
A²	298.33	1	298.33	5.13	0.0387	
B²	239.30	1	239.30	4.12	0.0606	
C²	10.18	1	10.18	0.1752	0.6814	
D²	835.96	1	835.96	14.38	0.0018	
Residual	871.75	15	58.12			
Lack of Fit	528.45	10	52.84	0.7697	0.6621	not significant
Pure Error	343.30	5	68.66			
Cor Total	3082.70	29				

R² = 0.8030, Std. Dev = 0.2501, C.V. % = 9.03, Adeq Precision = 6.7755

Biodiesel Synthesis, Optimization and Characterization from Novel Non-edible oil Seeds via High Performance Phyto-nano catalysts

118

3.3.3 Influence of reaction parameters on transesterification reaction

3.3.3.1 Combined influence of methanol to oil ratio and catalyst loading

The combined effect of methanol to oil molar ratio and catalyst loading was investigated while fixing other reaction parameters at optimum conditions. Mutual interaction of methanol to oil molar ratio and catalyst loading has been displayed in the form of three-dimensional plot shown in Figure 3.3.7a. It was observed that maximum yield of 93% was obtained at run 19 with reaction conditions of methanol to oil ratio 8:1, catalyst loading 0.18 (wt.%), reaction time 120 min and temperature 85 °C. Enhancing the catalyst loading up to 0.33 wt. % slightly decreased percent yield to 88% with same methanol to oil ratio 8:1 (Run 7) (Aryasomayajula et al., 2020). A further decrease up to 82% was noticed with catalyst loading of 0.48 (wt. %) (Run 10). It was evident from 3-D plot that greater methanol to oil ratio of 13:1, with same amount of catalyst loading (0.18 wt. %) gave low yield of 72 % (Run 6) due to increase in glycerol solubility which leads to phase separation issues too (Ansori and Mahfud 2021). Both lower methanol to oil ratio and higher catalyst loading failed to carry on transesterification long way and lowest yield of 66% of FAMEs with methanol to oil ratio of 3:1 and catalyst loading of 0.33 (wt. %) (Run 26). Results of ANOVA declared that effect of methanol to oil molar ratio and catalyst loading is not significant with *p*-value 0.3730 (>0.05).

3.3.3.2 Combined influence of methanol to oil ratio and reaction time

3-D plot of combined influence of methanol to oil ratio and reaction time has been illustrated in Figure 3.3.7b. Increase in reaction time gradually enhanced reaction rate and high biodiesel yield of 93% was obtained at run 19 with reaction conditions of methanol to oil ratio 8:1, catalyst loading 0.18 (wt.%), reaction time 120 min and temperature 85 °C. It can be seen that higher methanol to oil ratio at run 6 with reaction time 120 min resulted in low yield of 72% while keeping other two reaction parameters constant. Methanol to oil ratio of 8:1 with reaction time 60 min resulted in decreased efficiency of biodiesel production and compact yield up to 80% (Run 30). It was observed that lower methanol to oil ratio 3:1, at greater reaction time of 120 min caused low yield of 70% (Run 27) due to insufficient amount of methoxide solution to get mixed with oil (Abdullah et al., 2019). Collective interaction of oil to methanol ratio and reaction time was found insignificant in the ANOVA result of the experimental model with p-

value 0.3730 (>0.05). Nevertheless, individually reaction time was found significant with *p*-value 0.0480 and methanol to oil molar ratio with p-value 0.0268 (<0.05).

3.3.3.3 Combined influence of methanol to oil ratio and temperature

The combined influence of methanol to oil ratio and temperature is one of the most substantial interactive parameters prompting transesterification. The collective effect of methanol to oil molar ratio and reaction temperature on transesterification reaction of *Citrus medica* seed oil has been demonstrated in 3-dimensional plot grounded on central composite design in Figure 3.3.7c. The highest yield of 93% of FAMEs was achieved with reaction conditions of methanol to oil ratio 8:1, catalyst loading 0.18 (wt.%), reaction time 120 min and temperature 85 °C (Run 19). Lower methanol to oil ratio 3:1 with same reaction temperature (85 °C) resulted in low yield 70% (Run 27). Higher methanol to oil ratio 13:1 at reaction temperature 50 °C resulted in low yield of 71% (Run 4). It can be viewed that low yield of 60% was achieved at methanol to oil ratio 3:1 and low reaction temperature 50 °C due to low mass transfer between different phases reacting mixture (Run 9) (Ayoola et al., 2020). Similarly, higher reaction temperature of 120 °C with methanol to oil ratio of 8:1, decreased reaction of transesterification and lowest yield of 55% was obtained (Run 5). It is attributed to the fact that rate of evaporation of methanol in the reacting mixture enhances beyond temperatures of 70 °C (Kumar et al., 2021). It was concluded from ANOVA results that combine influence of methanol to oil ratio and temperature is significant with *p*-value 0.0486 (<0.05).

3.3.3.4 Combined influence of reaction time and catalyst loading

The collective effect of catalyst loading (B) and reaction time (c) on transesterification has been depicted in the form of 3D plot in Figure 3.3.7d while keeping other two reaction parameters (reaction temperature and oil to methanol molar ratio) constant. Both variables showed analogous effect on biodiesel yield. Percent yield of biodiesel amplified with growing catalyst loading and reaction temperature until optimal values were achieved (Takase et al., 2018). Experimental results declared highest yield of 93% of FAMEs was achieved with reaction conditions of methanol to oil ratio 8:1, catalyst loading 0.18 (wt.%), reaction time 120 min and temperature 85 °C (Run 19). High catalyst loading (0.33 wt. %) and reaction time of 120 min caused low yield of 88% at run 7. Further increase in catalyst loading up to 0.48 wt. % and low reaction time 60 min gave low methyl ester yield of 75% (Run 12). Both high catalyst loading

(0.33 wt. %) and reaction time of 180 min mutually affected reaction rate and resulted in lowest yield of 70% at run 2. Combined influence of reaction time and catalyst loading was found insignificant in current model with p-value 0.7966 (>0.05). However, individually these both parameters i.e. reaction time and catalyst loading were found significant with p-value of 0.0480 and 0.0934 respectively.

3.3.3.5 Combined influence of catalyst loading and temperature

Catalyst loading and reaction temperature are the most influential reaction parameters of transesterification. Both have a significant role in controlling rate of transesterification reaction. The combined influence of catalyst loading and reaction temperature on percent yield of methyl esters has been presented in Figure 3.3.7e. Maximum yield of 93% of biodiesel was observed at run 19 with reaction conditions of methanol to oil molar ratio 8:1, catalyst loading 0.18 (wt.%), reaction time 120 min and temperature 85 °C. It was exposed from experimental results that high catalyst loading of 0.33 wt. % with same reaction temperature (85 °C) reduced yield up to 89% at run 20. Low yield of 80% was achieved at low reaction temperature of 50 °C and catalyst loading of 0.33 wt. % (Run 15). Furthermore, a high reaction temperature of 120 °C with catalyst loading of 0.33 (wt. %) resulted in lowest yield of 50% at run number 21. Results of ANOVA declared that collective interaction of catalyst loading and temperature significant with p-value 0.0238 (<0.05).

3.3.3.6 Combined influence of reaction time and temperature

Reaction time and temperature has considerable impact on biodiesel yield. The combined influence of reaction time and temperature on transesterification has been illustrated in Figure 3.3.7f. in the form of 3-D plot. FAMEs yield increased correspondingly with increase in reaction time and temperature up to a certain limit due upsurge in mass interaction (Thangarasu et al., 2020). Maximum methyl ester yield of 93% was achieved with reaction conditions of methanol to oil ratio 8:1, catalyst loading 0.18 (wt.%), reaction time 120 min and temperature 85 °C at run 19. Reaction temperature of 85 °C with lesser time of 60 min resulted in compact yield of 80% at run 30. High reaction temperature of 120 °C and low time of 60 min ensued lesser yield of 60% at run 23. FAMEs yield was further dropped to 65% at low reaction temperature of 50 °C and reaction time of 120 min (Run 22). The lowest yield of 55% was achieved at high reaction temperature (120) °C and reaction time of 120 min (Run 5). Results of ANOVA disclosed that

Combined influence of reaction time and temperature is not significant with p-value 0.6995 (>0.05). However, independently reaction time was found significant with p-value less than 0.05 and temperature as insignificant with p-value 0.1958.
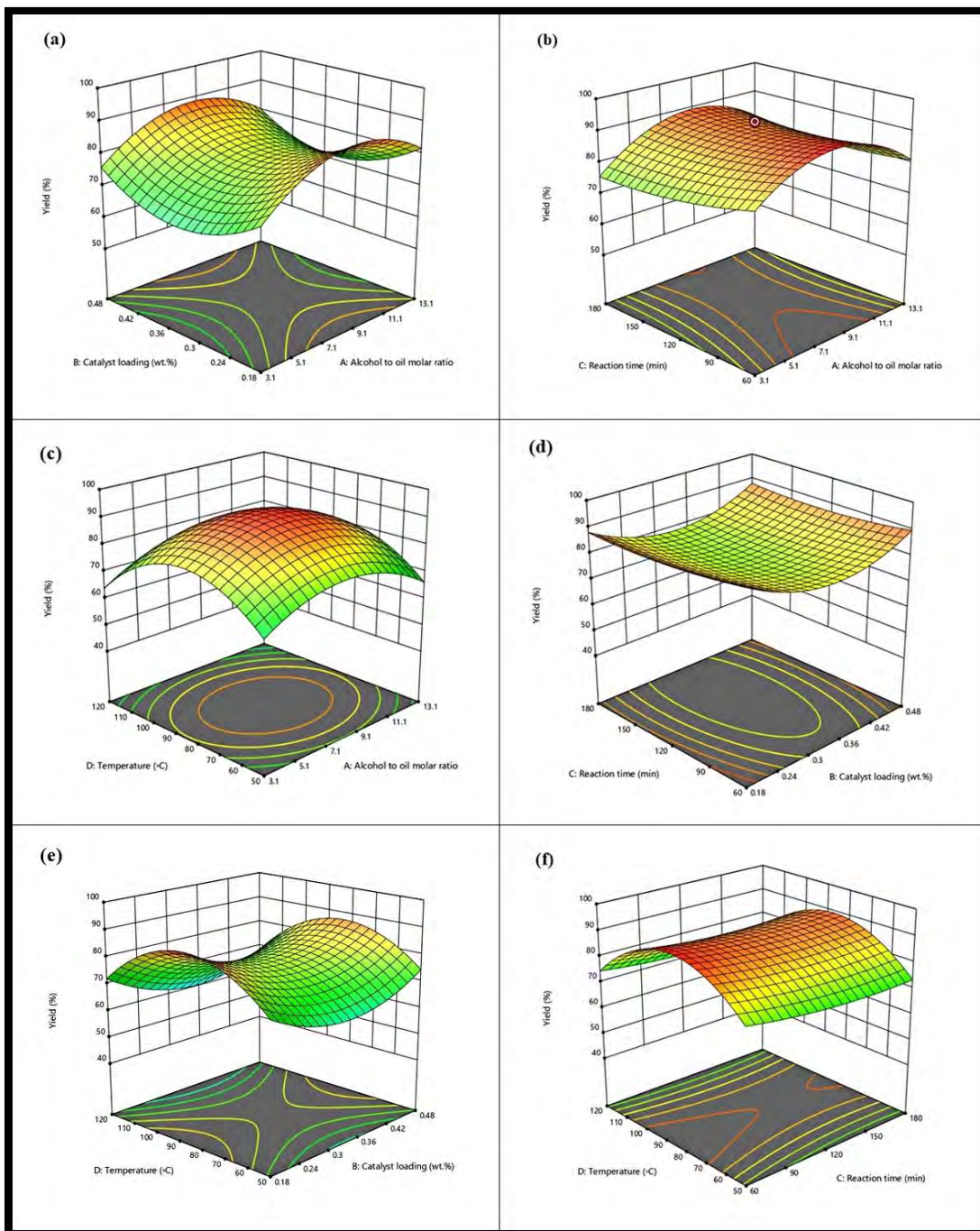
Figure 3.3.7. Influence of the reaction parameters of *Citrus medica* biodiesel.

3.3.4 Characterization of Biodiesel

3.3.4.1. FTIR Study

FTIR is one of the most significant techniques which are utilized for confirmation of methyl ester in the sample after conduction of transesterification reaction. Fourier-transform infrared spectroscopy (FTIR) is a technique which is used to study various bands corresponding to stretching and binding vibrations and different functional groups in synthesized sample of biodiesel. FTIR spectrum of seed oil of *Citrus medica* and biodiesel has been presented in Figure 3.3.8a and 3.3.8b respectively. Various stretches and bands were detected in FTIR spectrum of *Citrus medica* seed oil and biodiesel. A strong ester stretch representing carbonyl group (C=O) was detected in the FTIR region of 1728.67 cm^{-1} of CMBD. It was further inveterate by NMR results of methyl esters. Other stretches observed in synthesized biodiesel include sp^2 C-H stretching at 2923.46 cm-^{1}, sp^3 C-H at 2853.96 cm-^{1} and C-H bending (rocking) appeared at 1463.56 cm-^{1}. Whereas FTIR spectrum of seed oil of *Citrus medica* showed sp ≡C-H (alkynes) stretching at 3315.06 cm^{-1}, stretch of C-H (sp^2) appeared at 2831.60 cm^{-1} and C-H (sp^3) at 2939.48 cm^{-1}. Major difference in the Infra-Red region of 1750-1705 cm^{-1} and 1625-1430 cm^{-1} in FTIR spectrum of *Citrus medica* seed oil and synthesized biodiesel demonstrated considerable conversion during transesterification reaction.

Besides, another prominent Infra-Red region of the spectrum of seed oil and biodiesel which lies within ester peak area appeared around 1400-1000 cm^{-1}. Similarly, C-H$_2$ wagging frequency stretch which appeared at 1023.10 cm^{-1} in IR spectrum of seed oil vanished in the IR spectrum of CMBD. Another deep peak observed at 1292.76 cm^{-1} in IR spectrum of CMBD disappeared in the spectrum of seed oil. Broad peak at 1731.98 cm^{-1} in the spectrum of *Citrus medica* seed oil was split into 1728.67cm^{-1}, 1601.29 cm^{-1} and 1580.31 cm^{-1} in CMBD. Hence, all these variations in the IR spectrum of *Citrus medica* seed oil and biodiesel confirmed conversion of triglycerides into fatty acid methyl esters during transesterification.

3.3.4.2. ^{1}HNMR Spectroscopic Analysis

Spectroscopy technique of ^{1}HNMR and ^{13}CNMR is used for characterization and confirmation of synthesized biodiesel. ^{1}HNMR and ^{13}CNMR spectrum of CMSOD has been illustrated in Figure 3.3.9a and 3.3.9b. Peak of methoxy proton appeared at 3.677 ppm as a singlet in the spectrum of ^{1}HNMR. Characteristic peak of α-CH_2 protons was observed at 2.315 ppm. These both idiosyncratic peaks in the spectrum confirmed the presence of methyl esters in synthesized sample of biodiesel. The peak of free methanol which generally appears at 3.45 ppm was not detected in the ^{1}HNMR spectrum of CMSOD. Signal for conjugated double bonds and two outer hydrogen (-CH=CH-CH=CH-) was seemed at 5.355 ppm whereas, signal for inner two hydrogen of conjugated double bonds was observed at 7.281 ppm. Signal for methylene –CH_2– setting between non-conjugated double bonds appeared at 2.767 ppm, signal for –CH_2– next to carbonyl group appeared at 2.291 ppm. Signal for aliphatic –CH_2– stretch out at 1.628 and 1.26 ppm while end of aliphatic chain –CH_3 was observed at 0.893 ppm.

^{13}CNMR spectrum of *Citrus medica* biodiesel has been depicted in Figure 3.3.9b which illustrated structural characteristics methyl ester. Signal for ester carbonyl (─COO─) group appeared at 174.35 ppm whereas, characteristic methoxy carbon signal (O─CH_3) was observed at 51.47 ppm. Signal at 129.74 to 130.20 ppm were for unsaturated and outer nun-conjugated (-CH=CH-CH_2-CH=CH-) carbons. Inner carbons of nun-conjugated (-CH=CH-CH_2-CH=CH-) appeared at 127.89 ppm. Signals for aliphatic methylene carbons (-CH_2-s) of long carbon chain appeared at 27.21 to 31.93 ppm. Signal at for (-C-O) carbon group appeared at 76.64 to 77.48 ppm. Total conversion of *Citrus medica* seed oil into methyl ester was calculated and found 92 % which is near to obtained experimental yield (93%).

3.3.4.3. GC-MS

Chromatography and mass spectrometry (GC-MS) is a technique used to investigate the percent composition of fatty acid methyl ester (FAMEs) of synthesized biodiesel. It is one of the most important qualitative parameters of biodiesel. FAME's profile of synthesized biodiesel revealed that seed oil of *Citrus medica* is favorable for single step transesterification reaction. The chemical composition of biodiesel significantly affects its physiochemical properties like cetane number and viscosity. High degree of unsaturation in biodiesel is considered unwanted as

it affects engine efficiency (Mofijur et al., 2021). Five different peaks of fatty acid methyl esters were identified in GC-MS spectrum *Citrus medica* seed oil seed oil biodiesel. All these peaks were further acknowledged by library match software NO. NIST02. GC-MS spectrum of CMSOB has been presented in Figure 3.3.10 GC-MS analysis of *Citrus medica* seed oil biodiesel showed presence of saturated fatty acids like Tetradecanoic acid (14:1), Hexadecanoic acid methyl ester (16:0), Heptadecanoic acid, 14-methyl-, methyl ester (17:0) and unsaturated fatty acids like 7, 10- Octadecanoic acid methyl ester (18:0) and Hexadecenoic acid (16:1). 7, 10- Octadecanoic acid methyl ester was found as the major fatty acid methyl ester in the spectrum. In the current study, results GC/MS analysis disclosed that non-edible seed oil of *Citrus medica* is appropriate for the cleaner production of biodiesel.
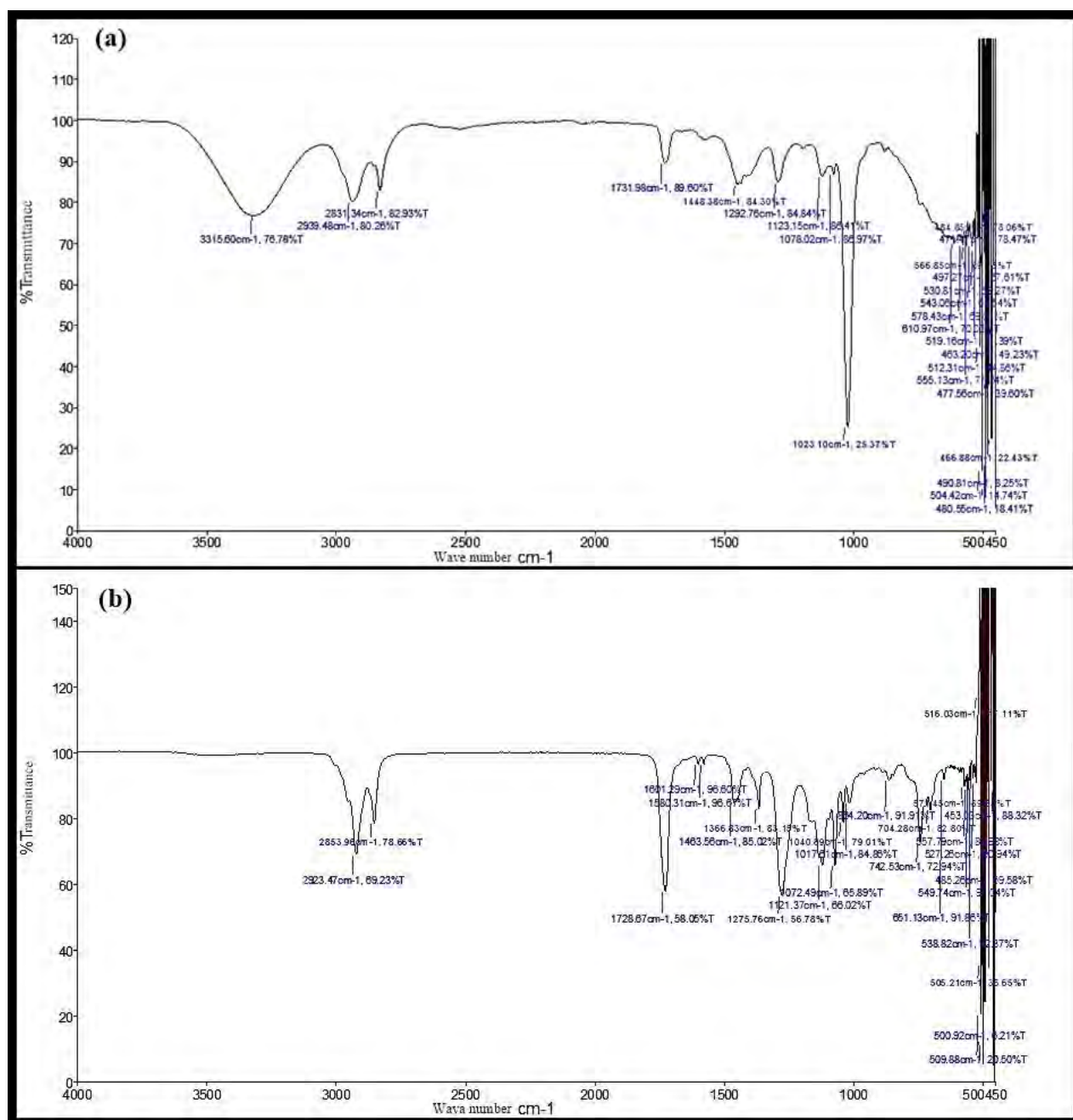
Figure 3.3.8. FTIR spectrum of **(a)** seed oil of *Citrus medica* **(b)** *Citrus medica* biodiesel
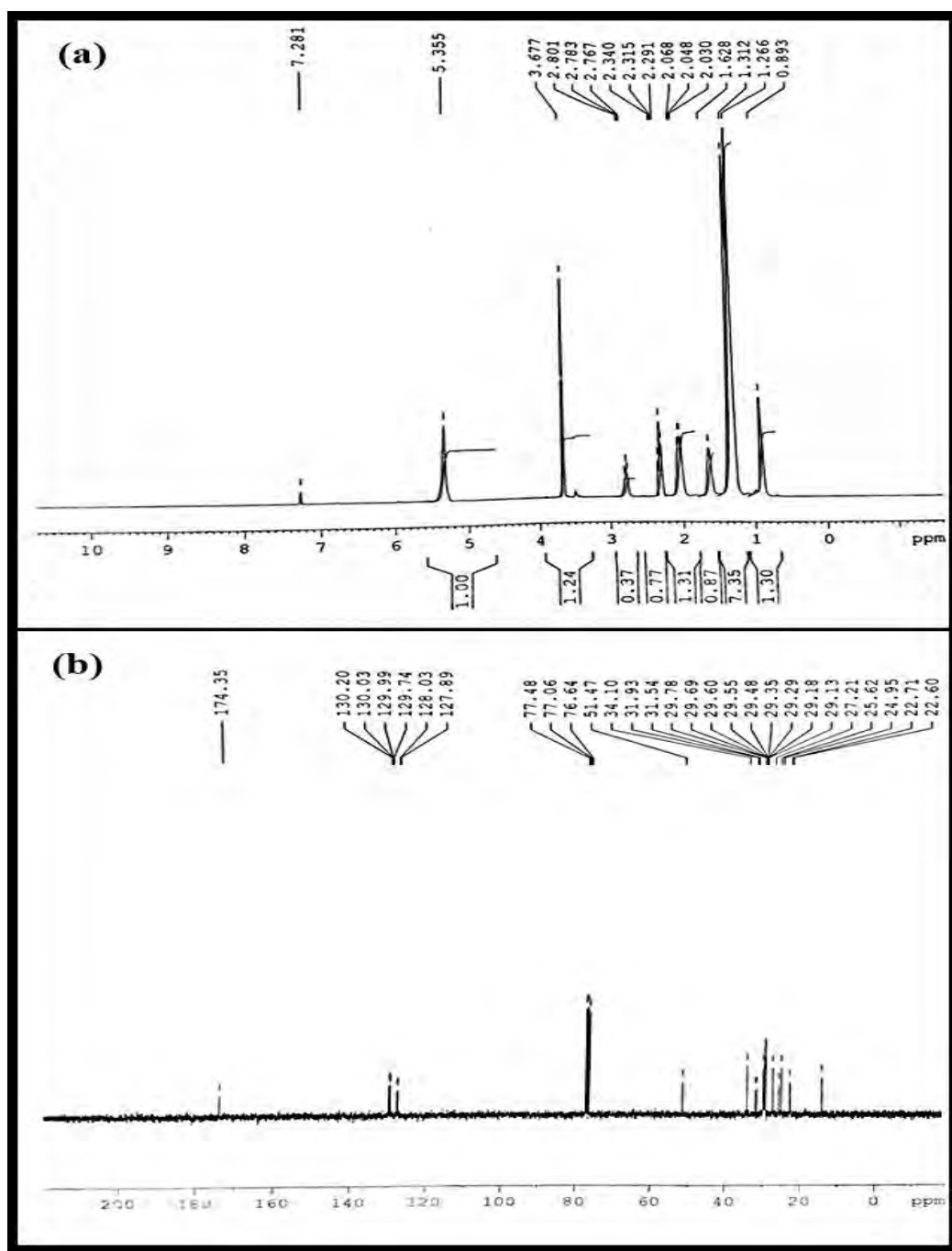
Figure 3.3.9. NMR spectrum of **(a)** ^{1}HNMR and **(b)** ^{13}CNMR of *Citrus medica*
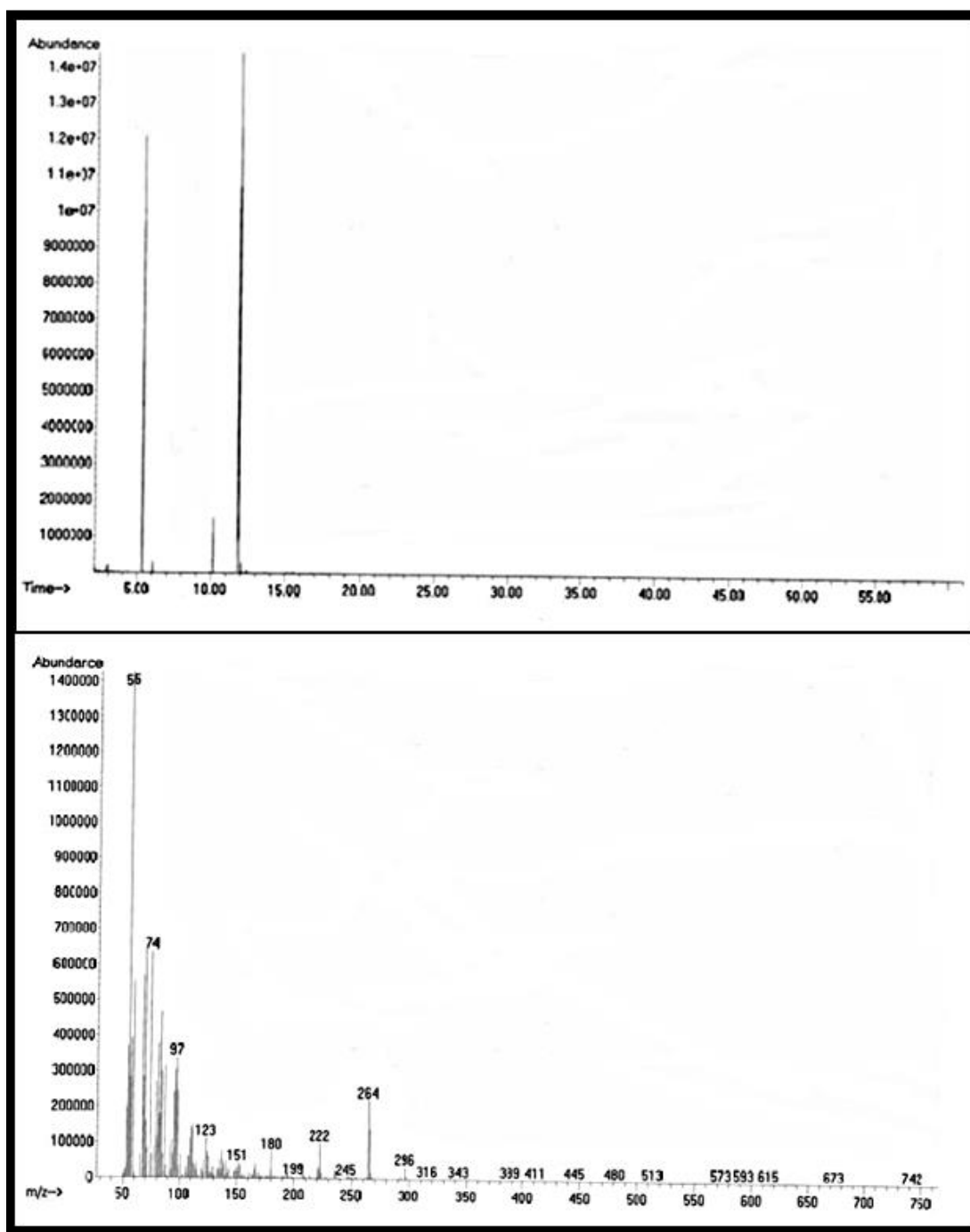
Figure 3.3.10. GC-MS spectrum of *Citrus medica* biodiesel

3.3.5 Fuel properties

Fuel properties of biodiesel produced from *Citrus medica* seed oil were investigated for assessment of fuel quality. Biofuels with higher density and viscosity result in poor fuel atomization and negatively affect engine efficiency. Fuel properties of biodiesel including density, viscosity, flash point, cetane number, pour point and cloud point depends upon the quality of vegetable oil used in transesterification and purification steps of biodiesel at the end of reaction. Density and viscosity of seed oil reduces after transesterification reaction. Fuel properties of *Citrus medica* biodiesel were evaluated and compared with ASTM D-675, European Union 14214 and China GB/T 20828-2007 standards. All these properties were found well matched with international standards. Fuel properties of *Citrus medica* biodiesel (B-100) and their comparison with international standards have been illustrated in Table 3.3.4.

The acid value of biodiesel is one of the significant parameters that needs to be considered in biodiesel production as it profoundly affects biodiesel quality and stability (Avhad and Marchetti 2015). According to ASTM D-675 and European Union 14214 acid value of biodiesel should be lesser than 0.5 (mg KOH/g). High acid value leads to saponification in transesterification and affects biodiesel aging (Behera et al., 2020). In the current study acid value of *Citrus medica* biodiesel was 0.1 (mg KOH/g) which lies under ASTM standard.

Density is one of the most important fuel properties of biodiesel affecting its application on diesel engines. It has a direct effect on fluid movement inside pipelines (Singh et al., 2021). High density of fuels causes disruption in engine operation and results in high exhaust gas emission with larger fuel consumption. Largely, biofuels have higher density as compared to petro-diesel (Guldhe et al., 2015). Mean density of *Citrus medica* biodiesel was found to be 0.81(mm^2/s) which lies within acceptable range of ASTM standard. *Citrus medica* biodiesel can be therefore easily injected into the cylinders and positively swaying fuel combustion in diesel engine.

Kinematic viscosity is another important fuel property influencing fuel combustion in diesel engines. It depends on feedstock used for biodiesel synthesis and varies accordingly. Biofuels with high viscosities result in incomplete combustion and causes pump resistance. Lower viscosity results in better fuel spraying and easy engine atomization. Biofuel with high

concentration of saturated fatty acids have inappropriate viscosity. It has been observed that viscosity of biodiesel enhances with increase in density. Kinematic viscosity of *Citrus medica* biodiesel was found to be 4.77 (mm^2/s) and is consistent with ASTM standard requirement.

A sample of diesel is considered useful and appropriate if the flash point value is greater than 38 ^{o}C (Davis et al., 2018). Higher flash point values of biodiesel made them safer and prevented unexpected and accidental ignition. Such fuels can be stored and manipulated safely. Flash point of *Citrus medica* biodiesel in present study was found 70 ^{o}C which is less likely to ignite accidentally and comparable to the limits of international standards.

The pour and cloud point of biodiesel is significantly affected by properties of the feedstock used for biodiesel production. Previous literature revealed that pour and cloud point of biodiesel is poor than that of petro-diesel (Borges et al., 2012). Cold flow properties of unsaturated and branched-chain fatty acids are considered better than long chain saturated methyl esters. Saturated components of biofuel crystalize at low temperature causing precipitation problems like clogged fuel lines. Pour point value of *Citrus medica* biodiesel was detected to be - 5 ^{o}C while cloud point in the present study was -9 ^{o}C which is consistent to the requirements of ASTM standards.

Sulphur content of *Citrus medica* biodiesel was 0.0001 wt. % demonstrating that produced biodiesel is non-toxic, clean and eco-friendly and is recommended for efficient use in fuel engines at broad scale level.

Table 3.3.4 - Comparison of fuel properties of CMBD with international standards ASTM D-6571, EN 14214 and China GB/T 20828-2007.

Property	Methods	*Citrus medica*		HSD ASTM D-951	ASTM D-6751	EN-14214	China GB/T 20828-2007
		Mean	St.Dev.				
Color	Visual	2.5	-	2.0	2.0		
Acid number (mg KOH/g)	ASTM-D974	0.100	0.1	0.8343	≤0.5	≤0.8	≤0.5
Flash Point (°C)	ASTM-D93	70	14	60-80	≥93	≥130	≥120
Pour Point (°C)	ASTM-D97	-5	5	_	-15-16	_	_
Viscosity (mm²/s at 40 °C.)	ASTM-D445	4.77	0.5	4.223	1.9-6.0	_	3.4-5.0
Density (kg/m³ at 40 °C)	ASTM-D1298	0.81	1.06	0.8343	≤120	_	≤120
Sulphur content (wt.%)	ASTM-D4294	0.0001	1	0.05	≤0.05	≤0.05	≤0.20
Cloud point (°C)	ASTM-D2500	-9	1	_	-3.0-12	_	_

3.3.6 Catalyst Reusability and recycling

Investigation of reusability of a nano-catalyst is one of the most significant characteristics of heterogeneous catalyst as they are recyclable and stable. Moreover, economical production of biodiesel demands recyclability capacity of the catalyst (Avhad et al., 2015). Reusability of CuO nano-particles was studied at optimum reaction conditions (catalyst concentration 0.18 (wt. %), oil to methanol ratio 1:8, time 120 min and temperature 85 ℃). No substantial change in percent yield of biodiesel was observed in initial few cycles and catalytic activity of nano-particles in transesterification was efficiently maintained. Biodiesel yield started to gradual decrease from 78% in fifth cycle to 70% in sixth cycle. It might have contributed to reduction in active sites of green nano-catalyst due to deposition of organic materials on its surface (Figure 3.3.11). The lowest yield of 66% of biodiesel was obtained in 7th cycle. The potential of reusability of CuO nano-particles in biodiesel production is useful in reducing raw cost for total production at large scale area.
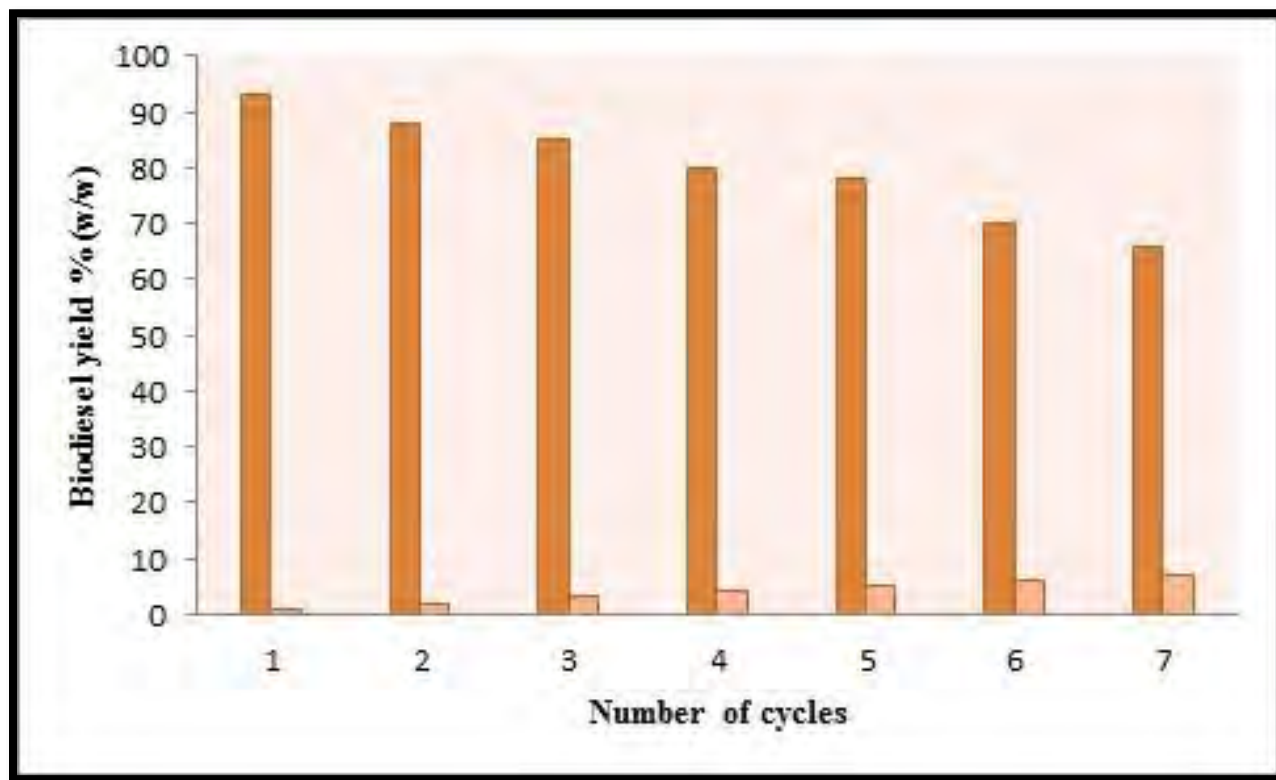
Figure 3.3.11. Reusibility of copper oxide NPs in transesterification reaction

SECTION IV

- Biodiesel Production from *Cichorium intybus* L seed oil using Green nano Catalyst of Magnesium oxideCopper oxide
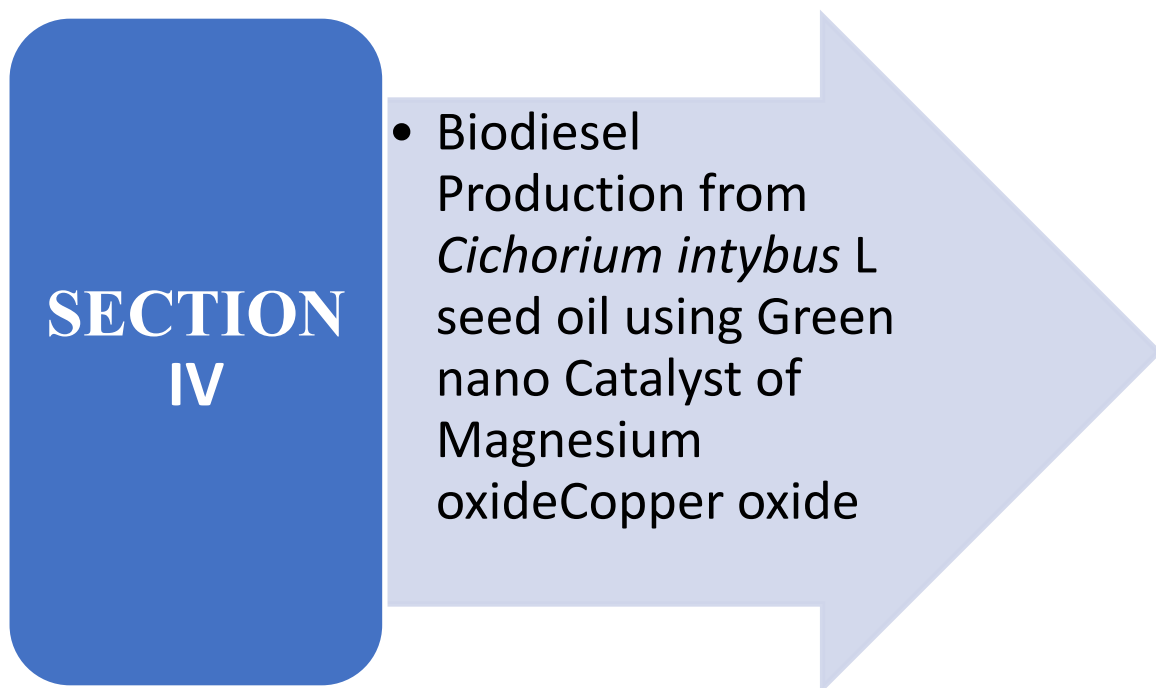
MgO has been successfully used to catalyze transesterification. By increasing the concentration of basic sites on the surface, catalytic activity of MgO can be increased. The increased activity is attributed to the reduced surface basicity. Since the large concentration of edge/corner sites and structural defects on their surface, it has been shown that the form and size of nanocrystalline magnesium oxide particles give them a high specific surface and reactivity. In this study leaves of *Parthenium hysterophorus* successfully reduced Mg $(NO_3)_2$ into MgO.

3.4.1. Catalyst Characterization

3.4.1.1 X-Ray Diffraction (XRD) of MgO

X-Rays diffraction technique is used to investigate crystallographic structure of prepared nano catalyst using powder diffractometer with Cu-Kα with radiation wavelength (λ) = 1.544ºA with scanning rate of 2º in 2θ min-1 in the scale range 2θ= 5-70º. X-Rays diffraction of MgO nano particles demonstrated solid crystal phase which was proved by the indexing of diffraction peaks in the data. Various diffraction peaks were developed at 2θ values of 36.5°, 42.2°, 62.2°, 75.8° and 78.5º (Figure 3.4.1). These reflection peaks corresponded to 111, 200,220, 311 and 222 *hkl* values which indicated the cubic structure of MgO nano particles (NPs). No additional peak or shifting has been observed in data which implies that there was no unreacted reactants or impurities incorporated to crystal structure in the prepared sample. Debye–Scherrer formula (6) at full width half maximum (FWHM) was used to calculate crystalline size of MgO NPs by using XRD pattern of most deep peaks at 2θ value of 42.2º (highest peak 200) and was found to be 36 nm in size.

3.4.1.2 Scanning Electron Microscopy (SEM) of MgO

Scanning electron microscopy (SEM) was used to investigate morphological characteristics of the surface of catalyst. SEM image of MgO NPs has been shown in Figure 3.4.2. The topical view of the nanostructures viewed spherical morphology with mean size below 50nm. This observation is further confirmed by the size measured by XRD pattern analysis. The bottom of the SEM micrograph showed masses with a few large clusters at some places at the

bottom. These clusters of masses were considered due to biological incapacitation capabilities of some phytochemicals present in the extract of plant species (Sharma et al., 2017).

3.4.1.3 Energy Diffraction X-ray (EDX) of MgO

EDX analysis was used to identify the chemical composition of MgO NPs and has been presented in Figure 3.4.3. EDX analysis confirmed the formation of the MgO Nano particles by showing representative peaks magnesium and oxygen in the spectrum. The weight percent of magnesium and oxygen was found 36.5% and 63.45% respectively in MgO nano particles. No other extra peak was observed in the EDX spectrum of MgO NPs which indicated that there is no impurity in the nanostructures.

The FTIR spectra of absorbance-mode zinc oxide nanoparticles are displayed in Figure 3.4.4. Two distinct IR peaks at 3200 cm^{-1} and 3325 cm^{-1}, which were attributed to Mg-O stretching, were visible in the MgO spectra. Adsorbed water molecules exhibit a peak in the O-H group at 1648 cm^{-1} and 2275 cm^{-1}. Metal oxides' FTIR spectra often show absorption peaks in the 1000–4000 cm^{-1} IR region. The production of the green magnesium oxide nano-catalyst was pure, as evidenced by the lack of any further superfluous peaks.

In order to investigate the mass breakdown properties of magnesium oxide, thermogravimetric analysis was used. A thermogram of MgO nanoparticles and a corresponding derivative thermogram are displayed in Figure 3.4.5 a and b. There were three main stages of breakdown for MgO. The initial loss of 0.87% of the initial weight occurred quickly during decomposition at temperatures between 160 °C and 400 °C. A weight loss of roughly 0.87% was observed in the bulk mass as a result of drying at the molecular surface.

The second phase of thermal deterioration (0.036%) was discovered at the temperature range of 401 °C to 520 °C, indicating noticeably greater thermal durability of MgO with effective catalytic activity. While the third step of heat degradation occurred between 521 °C and 700 °C, where more green nanoparticle conversion (0.027%) occurred, hastening the switch to thermal constancy. The weight percentage derivative curve in Fig. The endothermal peaks of MgO are shown in Figure 3.4.5a.
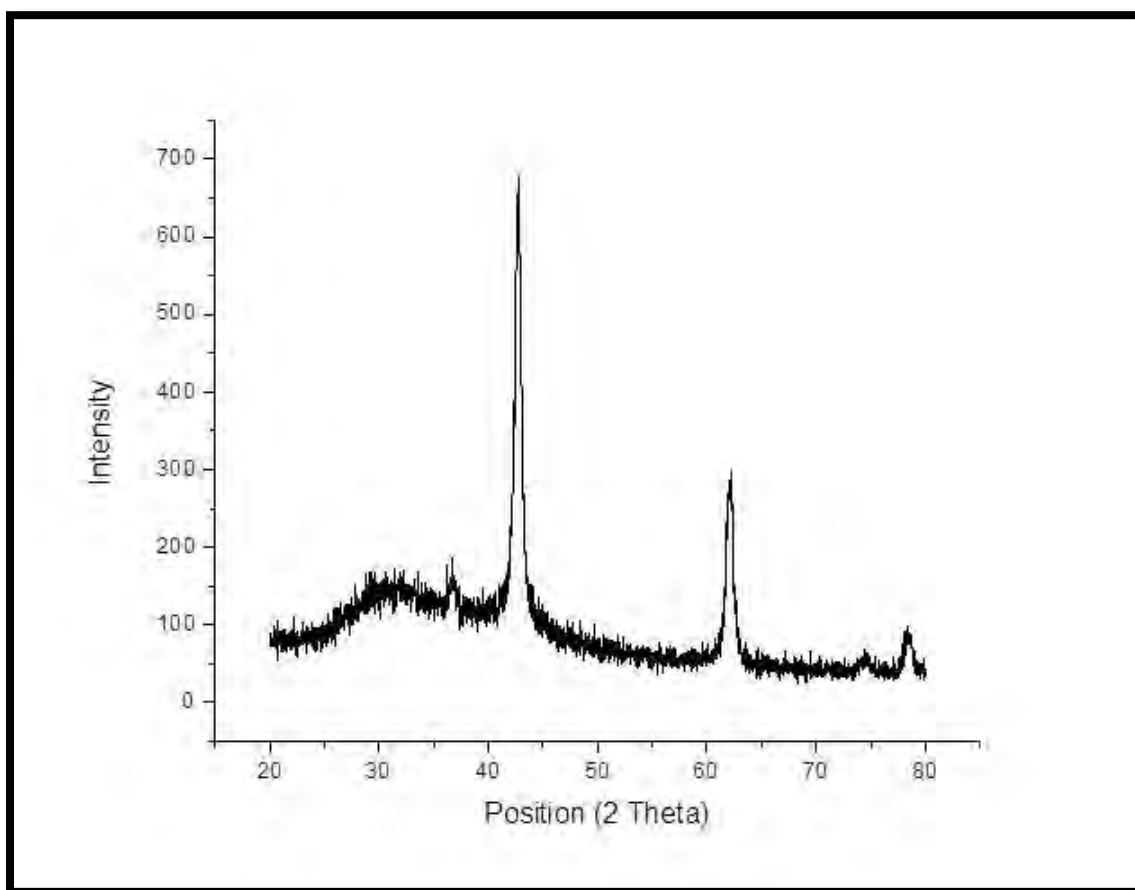
Figure 3.4.1. XRD pattern of calcined MgO green nano particles
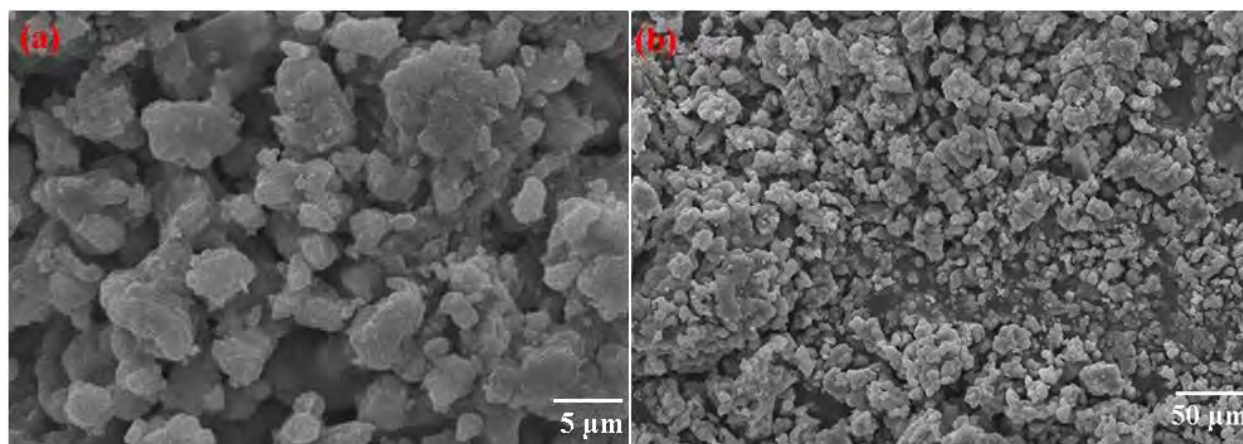
Figure 3.4.2. Scanning electron microscopy (SEM) of calcined MgO green nano particles
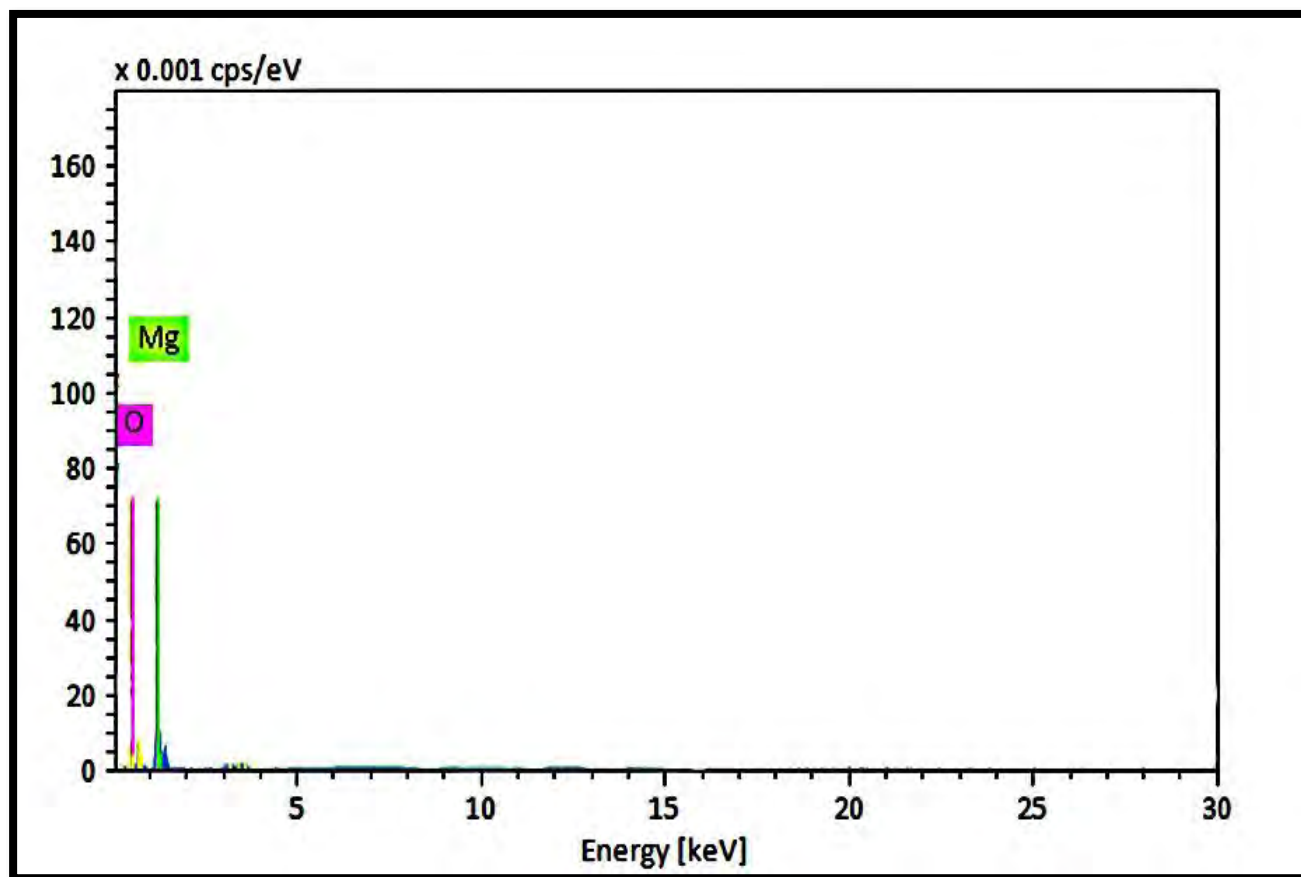
Figure 3.4.3. Energy diffraction X-Ray (EDX) of calcined MgO green nano particles
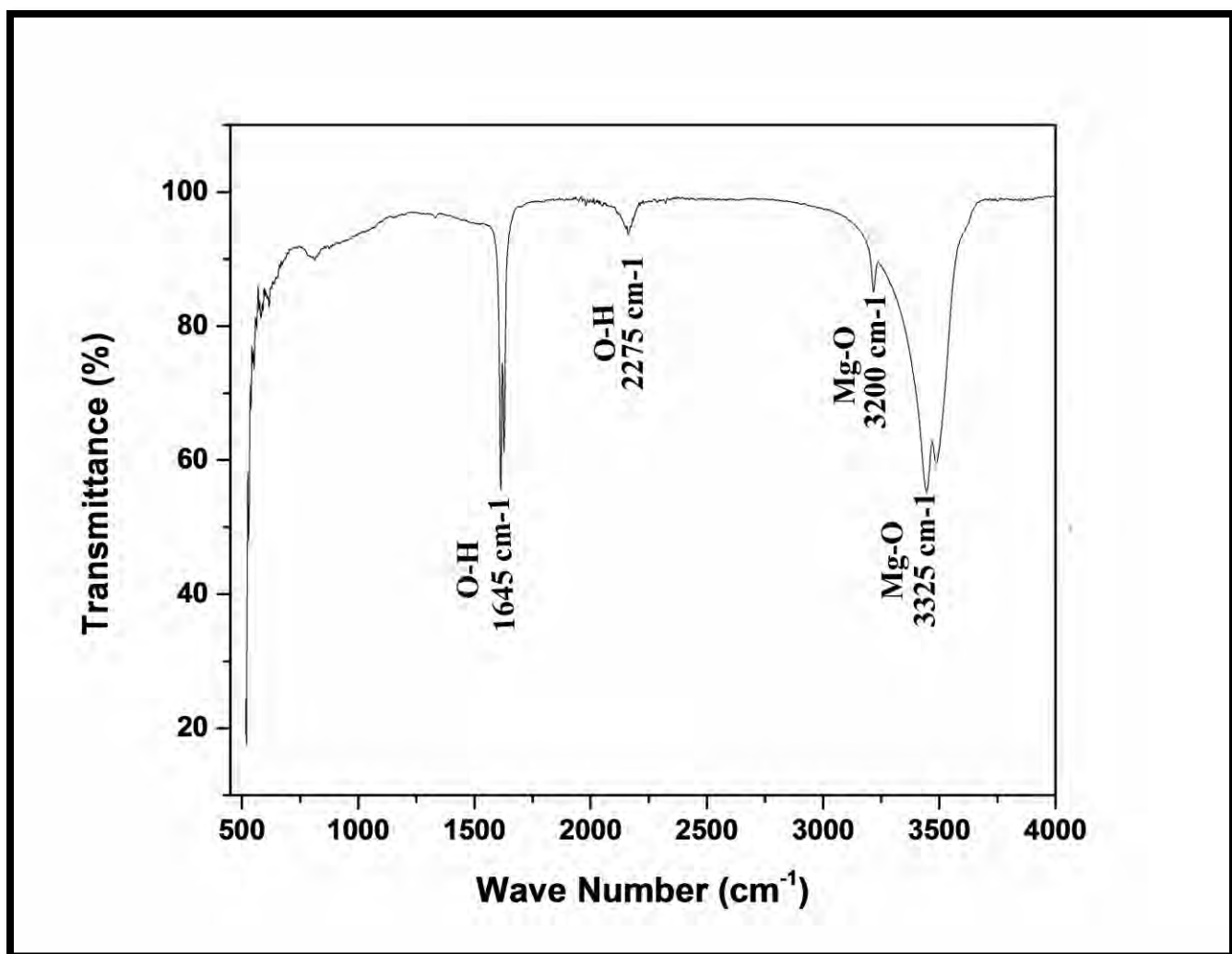
Figure 3.4.4. FT-IR spectrum of magnesium oxide nanocatalyst
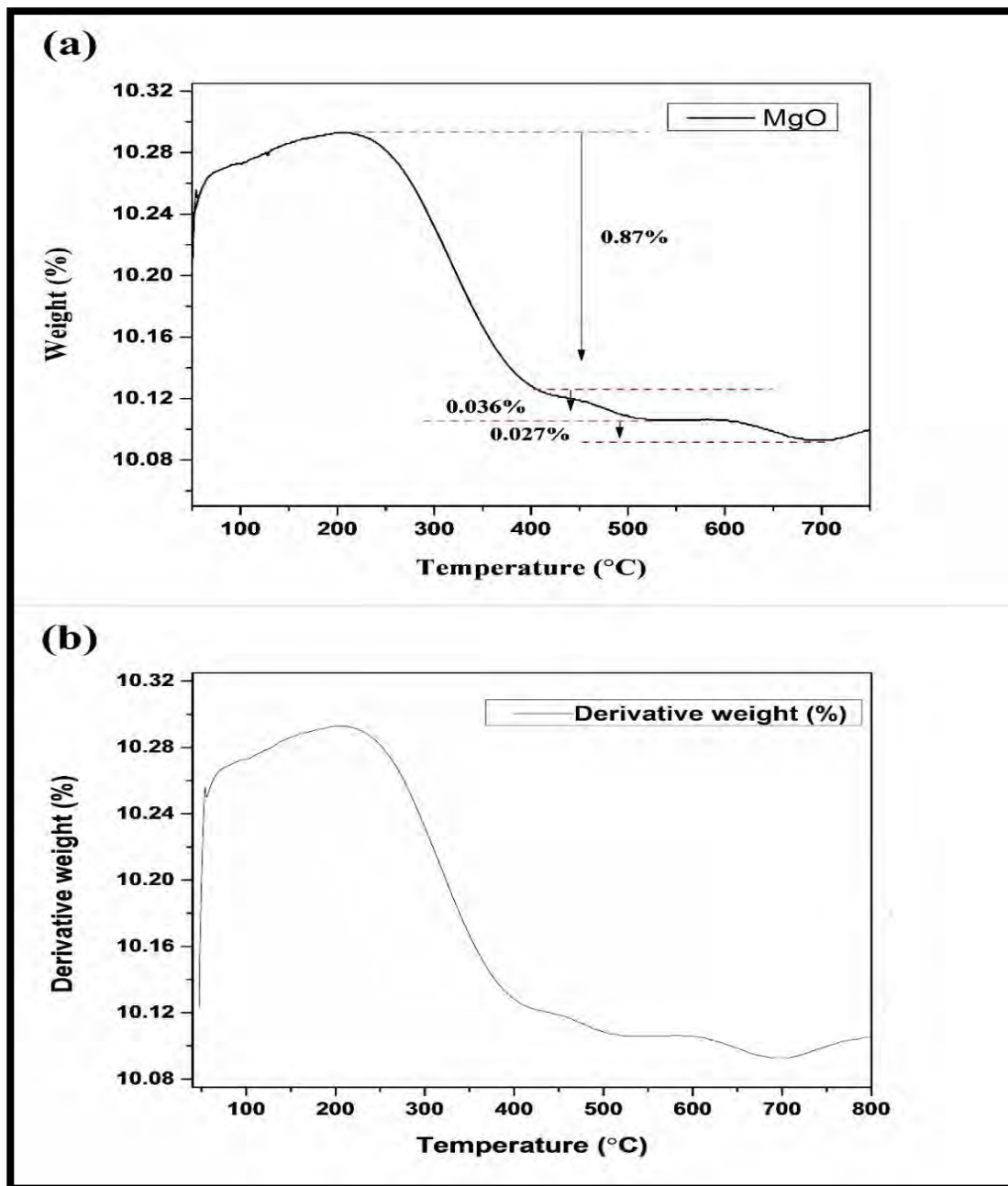
Figure 3.4. 5. (a) TGA of indium oxide nanocatalyst (b) derivative thermogram of indium oxide nanocatalyst

3.4.2. Biodiesel synthesis

Biodiesel synthesis of *Cichorium intybus* seed oil was carried out with MgO NPs. Before proceeding for transesterification reaction, oil was purified by filtration and moisture content was removed with preheating at 60 °C for about an hour. Experimental design of central composite design in terms of coded values for transesterification reaction has been presented in Table 3.4.1 and experimental results are displayed in Table 3.4.2 whereas, Table 3.4.3 depicts statistical analysis of variance (ANOVA) for response surface quadric model of methyl ester formation from *Cichorium intybus* seed oil. Moreover, significance, precision and fitness of the model for transesterification reaction was investigated by execution of data of four reaction parameters and was found significant with *p*-value lesser than 0.05. Insignificant terms of the quadric regression model were kept under consideration. Quadratic terms such as catalyst loading (B^2) and reaction time (C^2) exhibited the insignificant *p*-value greater than 0.05 whereas, quadric factors i.e. reaction temperature (D^2) and methanol to oil ratio (A^2) represented the most significant p-value (<0.05). However, they cannot be illuminated from the model as they are linked with hierarchy of model (Kawashima et al., 2009).

Model was found significant with p-value of 0.0002 (<0.05). The F-value of the model was 7.71which implies that the model is significant with a chance of 0.02% that an F-value greater than that could occur due to noise. Precision of model was found to be 95%. Moreover, the adjusted value of R² (0.9580) and predicted value (0.965) has a difference <0.2 which denoted a good correlation with regression polynomial of the model. Adequate precision represents the measure of signal to noise ratio and was found 11.078 in present model which is >4 and ensures the adequateness of the model to predict biodiesel yield. The Lack of Fit F-value of 2.11 implies the Lack of Fit is not significant relative to the pure error. There is a 21.25% chance that a Lack of Fit F-value this large could occur due to noise. Non-significant lack of fit was good as it indicated best fitness of the model to experimental data. Furthermore, a straight line was noticed in predicted and actual yield of biodiesel.
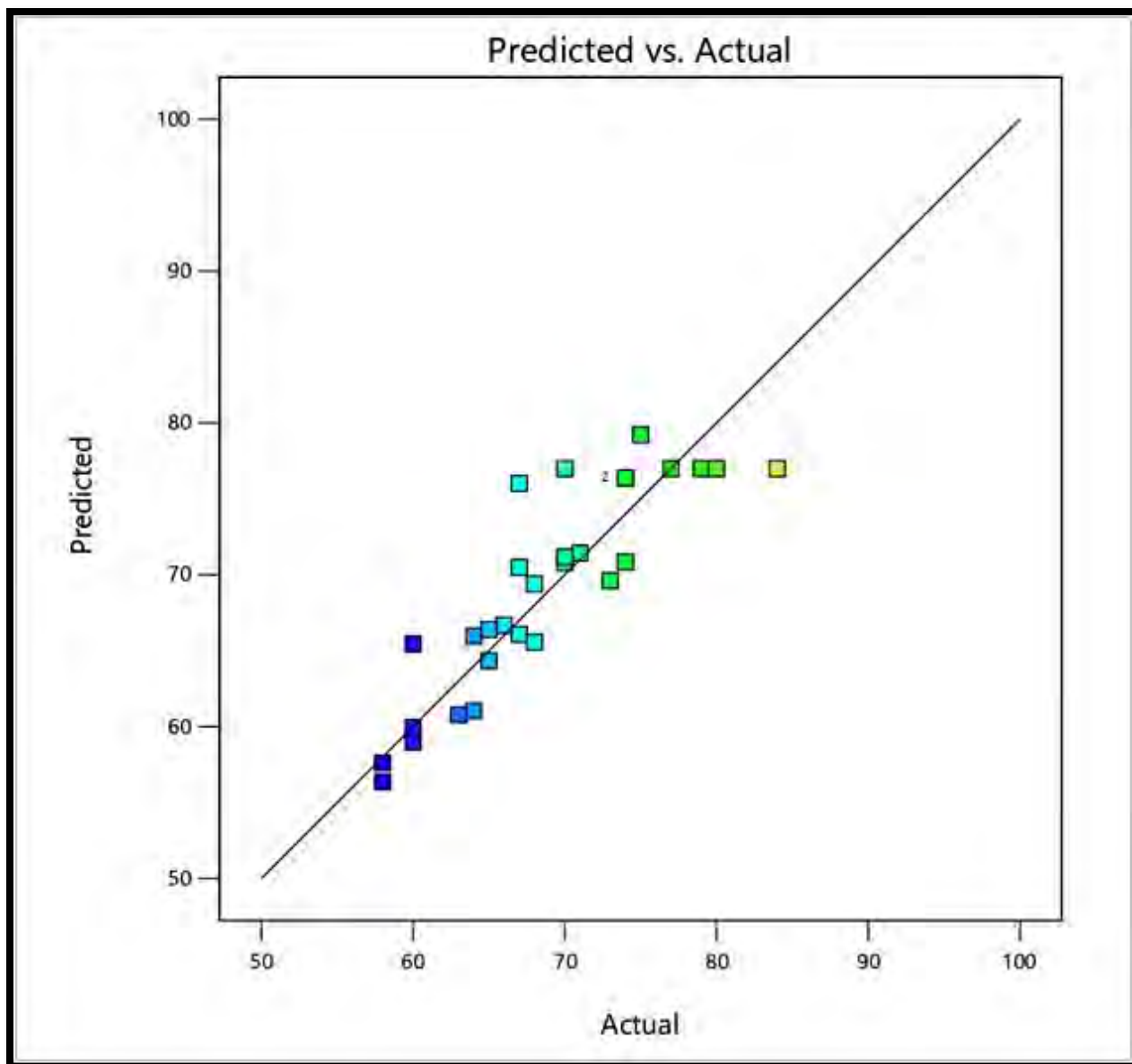
Figure 3.4.6. Comparison between the experimental and predicted yield of biodiesel in the model

Table 3.4.1- Experimental design by central composite design for transesterification reaction

Process parameters	−1	+1
Alcohol to oil ratio	3:1	15:1
Catalyst loading	0.22	1. 44
Reaction time	55	180
Temperature	50	120

Table 3.4.2- Detailed experimental result for transesterification reaction

Run	A:Alcohol to oil molar ratio	B:Catalyst loading	C:Reaction time	D:Temperature	Yield
		wt.%	min	°C	%
1	3:1	1.44	180	50	72
2	3:1	0.83	120	85	80
3	9:1	1.44	120	85	75
4	9:1	0.83	180	85	95
5	3:1	0.22	180	120	71
6	9:1	0.83	120	120	88
7	3:1	0.22	60	120	65
8	3:1	0.22	180	50	60
9	9:1	1.44	180	120	55
10	9:1	0.22	120	85	84
11	9:1	0.83	120	85	90
12	15:1	1.44	60	120	69
13	9:1	0.83	120	85	88
14	9:1	0.83	120	50	80
15	3:1	1.44	60	50	60
16	9:1	0.83	120	50	80
17	15:1	0.83	180	50	55
18	9:1	0.22	120	85	85
19	15:1	0.22	180	50	58
20	9:1	0.83	60	85	75
21	15:1	0.83	120	85	66
22	9:1	0.83	60	120	76
23	3:1	0.83	180	85	65
24	15:1	0.83	180	120	70
25	15:1	0.22	60	50	65
26	3:1	1.44	60	120	55
27	15:1	1.44	60	50	53

28	15:1	1.44	180	120	50
29	15:1	0.22	60	120	59
30	3:1	0.83	60	50	50

Table 3.4.3- ANOVA for Response Surface Quadratic model

Source	Sum of Squares	Df	Mean Square	F-value	p-value	
Model	2.43	14	0.1734	7.71	0.0002	significant
A- Methanol to oil Ratio	1.07	1	1.07	47.42	<0.0001	
B- Catalyst Loading	0.0409	1	0.0409	1.82	0.0275	
C- Time	0.0011	1	0.0011	0.0467	0.0318	
D Temperature	0.3612	1	0.3612	16.06	0.0011	
AB	0.0300	1	0.0300	1.33	0.0262	
AC	0.0004	1	0.0004	0.0184	0.0138	
AD	0.2184	1	0.2184	9.71	0.0071	
BC	0.0413	1	0.0413	1.84	0.0355	
BD	0.0335	1	0.0335	1.49	0.0411	
CD	0.0954	1	0.0954	4.24	0.0573	
A²	0.0002	1	0.0002	0.0070	0.0344	
B²	0.0063	1	0.0063	0.2787	0.0052	
C²	0.0818	1	0.0818	3.64	0.0459	
D²	0.0581	1	0.0581	2.59	0.0287	
Residual	0.3373	15	0.0225			
Lack of Fit	0.2726	10	0.0273	2.11	0.2125	not significant
Pure Error	0.0647	5	0.0129			
Cor Total	2.76	29				

R² = 0.9580, Std. Dev=0.1500, C.V. % = 1.68, Adeq Precision = 11.0708

3.4.3. Parametric interactions of Transesterification reaction

3.4.3. 1. Mutual Influence of methanol to oil ratio and Catalyst loading

The combined influence of methanol to oil molar ratio and catalyst loading on biodiesel synthesis from *Cichorium intybus* seed oil (CISO) has been presented in the form of 3D plots in Figure 3.4.7a. In the present study a range of 3:1 to 15:1 of methanol to oil molar ratio and catalyst loading of 0.22-1.4 wt. % was taken under consideration. Experimental data revealed a high yield of 95% at methanol to oil ratio of 9:1 and catalyst concentration of 0.83 (wt. %) under controlled reaction conditions i.e. reaction time 180 (min), and temperature 85 °C at constant stirring (Run 4). It is evident from current investigation that there is a close relation between these reaction parameters and methyl ester formation. 3 mol of biodiesel and 1 mol of glycerol are synthesized from 3 mol of alcohol and 1 mol of oil during transesterification reaction as per previous studies (Dossin et al., 2006). Rate of methanolysis can be enhanced with greater amount of methanol in order to promote methoxy species formation on the surface of green nano catalyst (MgO NPs). FAMEs yield increased from 65% to 85 % with increase in methanol to oil molar ratio and catalyst loading (Run 23 and 13). However, further increase in methanol content beyond optimum limit increases solubility of glycerol and creates separation problem (Run 28). Low yield of 66% was obtained at methanol to oil molar ratio of 15:1 with same amount of catalyst. It was attributed to the excess amount of methanol which shifted reaction equilibrium towards product side (Run 21) (Singh et al., 2021). The *p*-value of combine effect of methanol to oil molar ratio and catalyst loading was found lesser than 0.05 (0.0262) and proved to be one of the significant factors of the model.

3.4.3. 2. Mutual influence of methanol to oil ratio and reaction time

Methanol to oil molar ratio and reaction time is one of the significant parametric interactions of transesterification reaction. Mutual influence of methanol to oil molar ratio and reaction time on transesterification has been illustrated in 3D plot shown in Figure 3.4.7b. Parametric interaction of methanol to oil molar ratio and reaction time on biodiesel synthesis was investigated using experimental data while keeping other parametric conditions like temperature (85 °C) and catalyst loading (0.83 wt.%) constant. Maximum yield of 95% was obtained with methanol to oil molar ratio 9:1 at reaction time duration of 180 min at run number 4. An

optimum amount of alcohol is required to transform triglycerides to mono glycerides in transesterification. However, excess of methanol significantly reduced the yield of methyl ester. It was further dropped to 66% at methanol to oil ration 15:1 and reaction time 120 min at run number 21. It is attributed to glycerol solubility in the reacting mixture with high concentration of methanol (Ghadge and Raheman 2006).

Shrinkage in the reaction time up to 60 minutes with optimal methanol to oil molar ratio of 9:1 resulted in low yield of 75% at run number 21 due to insufficient reaction duration. Mutual influence of methanol to oil molar ratio and reaction time was found insignificant in the experimental model with p-value 0.8938 (>0.05).

3.4.3. 3. Mutual influence of methanol to oil molar ratio and temperature

Mutual influence of methanol to oil molar ratio and reaction temperature has been illustrated in Figure 3.4.7c. Percent yield of methyl ester raised up to 95% at methanol to oil molar ratio of 9:1 and reaction temperature 85 ^{o}C at constant reaction time (180 min) and catalyst concentration (0.83 wt.%). High reaction temperature (120 ^{o}C) and methanol to oil ratio of 15:1 resulted in low yield of 70% at run number 24. Increase in methanol to oil molar ratio up to 15:1 at reaction temperature 85 ^{o}C resulted in lowest yield of 66% (Run 21). Similarly, lesser methanol to oil molar ratio of 3:1 and temperature 85 ^{o}C reduced yield 65% (Run 23). Low reaction temperature of 50 ^{o}C and high methanol to oil molar ratio (15:1) gave low yield of 55% at run number 17. It was credited to the compact mass transfer rate of the reactants as they all are immiscible at lower temperature. Mutual influence of methanol to oil molar ratio and reaction temperature was found significant with *p*-value 0.0071 (<0.05).

3.4.3. 4. Mutual influence of catalyst loading and reaction time

Catalyst concentration and reaction time is one of the most influential parameters of transesterification reaction, momentously affecting yield of methyl ester and plays a vital role in optimization process. In our current investigation the mutual effect of MgO NPs and reaction time on methyl ester formation from *Cichorium intybus* seed oil was studied at constant methanol to oil molar ratio (9:1) and temperature of 85 ^{o}C. Results of ANOVA revealed a *p*-value of 0.1955 for parametric interaction of catalyst loading and reaction time. Three-dimensional (3D) plot of influence of catalyst loading and reaction time on biodiesel yield has been depicted in Figure 3.4.7d. A high yield of 95% has been observed with catalyst loading of

0.83 (wt. %) and reaction time 180 min at run number 4. Catalyst amounts lower than 0.83 (wt. %) at reaction time of 180 min was found insufficient to carry out transesterification reaction efficiently, giving the lowest yield of 50% due to unfinished transformation of triglycerides into methyl ester and resultant increase in viscosity of reacting mixture which renders the interaction between catalyst and the reacting mixture (Run 30). Increase in the percent yield of biodiesel was observed with increase in catalyst amount which could possibly because of availability of more reactive sites on catalysts surface during transesterification reaction but it was up to certain limit (Run 6) (Maneerung et al., 2015; Abdullah et al., 2019). Therefore, in the present study optimum catalyst loading was taken as 0.83 (wt. %) with reaction time 180 min in order to get maximum yield of methyl ester. Our current results are in line with previous findings where excess amount of catalyst results in reversible reaction (Dai et al., 2014).

3.4.3.5. Mutual influence of catalyst loading and reaction temperature

Catalyst loading and reaction temperature is another important parametric interaction of transesterification reaction. 3D plot of influence of reaction temperature and catalyst loading on biodiesel yield has been depicted in Figure 3.4.7e. A maximum of 95% was observed at reaction temperature 85 °C at constant reaction time 180 (min), oil to methanol ratio molar 1:9 and stirring intensity of 600 rpm (Run 4). Similar positive effects of reaction temperature on methyl ester formation from *Saussurea heteromalla* seed oil was observed at temperature of 55, 65 and 75 °C (Rozina et al., 2017). The yield of methyl ester was reduced up to 88% with raise in temperature and catalyst concentration (Run 6). Moreover, further increase in reaction temperature and catalyst concentration didn't support biodiesel yield and resulted in low productivity of 55 % (Run 9). Likewise, the process of transesterification reaction usually ceased at temperature lower than 50 °C. Results of ANOVA exposed that collective influence of these parameters is not significant with *p*-value (0.2411) greater than 0.05.

3.4.3.6. Mutual influence of reaction time and temperature

Generally, transesterification reaction needs appropriate time and temperature for proper mixing of reactants (methanol and oil) at constant rate. Mutual influence of reaction time and temperature on methyl ester formation has been illustrated in Figure 3.4.7f. It was observed that the percentage yield of biodiesel enhances with increase in reaction time as the reacting mixture gets sufficient time for the conversion of reactants into products. At run number 4, maximum

yield of 95% was obtained at reaction time of 180 (min) and temperature 85 $^{\circ}$C in controlled conditions of methanol to oil ratio of 6:1, catalyst amount (0.83 wt. %) and stirring intensity of 600 rpm. Maximum conversion of soya bean oil into methyl ester with K_2CO_3/MgO at reaction time of 2 h has been previously reported and matched well with our current finding (Onoji et al., 2017). Together higher reaction time (120 min) and temperature (120 $^{\circ}$C) were found to be accelerating the chemical process of hydrolysis of methyl esters into acids and consequent polar methanol in the reacting mixture therefore, declining percent yield of biodiesel (Run 6). Decrease in reaction time at run number 20 at same reaction temperature resulted in reduced percent yield up to 75%. Results of ANOVA demonstrated insignificant correlation between temperature and reaction time with p-value greater than 0.05 (0.0573).
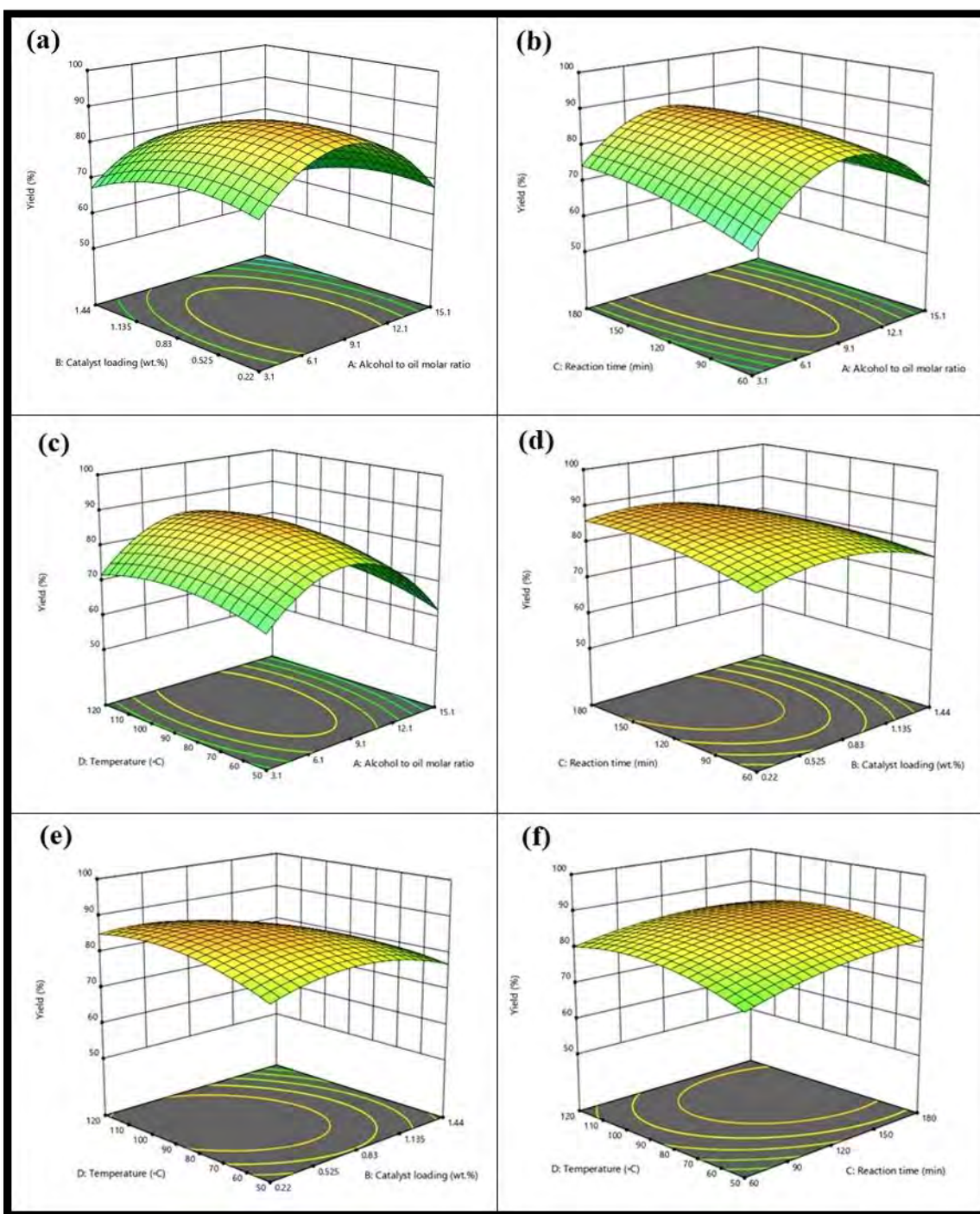
Figure 3.4.7. Influence of the reaction parameters of *Cichorium intybus* biodiesel.

3.4.4. Characterization of Biodiesel

3.4.4.1 FTIR Study

FTIR spectroscopy is one of the defined laboratory techniques used to confirm biodiesel production next to transesterification reaction. Presence of carbonyl and methyl group bands in the IR spectrum of biodiesel proves methyl ester production during transesterification. The Fourier-transform infrared spectroscopy (FTIR) of *Cichorium intybus* seed oil and biodiesel at the mid IR range of 500-4000 cm^{-1} has been used to identify various functional groups, bands and stretching presented in Figure 3.4.8. FTIR spectrum of CISO and CIBD showed variation in terms of absorbent frequency and band intensity because of minor difference between oil and diesel while, most part of spectrum was similar between both (Betiku et al., 2016). A normally deep and strong ester (C=O) stretching was observed at 1743.4 cm^{-1}. C-O axial stretching was noticed at 1377.5 cm^{-1} to 1000 cm^{-1}. Stretching of sp^2 C-H, sp^3 C-H, and C-H bending (rocking) appeared at 2922.78 cm^{-1}, 2853.3 cm^{-1} and 1464.47 cm^{-1} *Cichorium intybus* biodiesel respectively. Whereas, seed oil spectrum had sp C-H stretch appeared at 3329.7 cm^{-1}, C-H (sp^2) stretching was observed at 2831.91 cm^{-1} and 2854.6 cm^{-1}, C-H (sp^3) at 2925.5 cm^{-1}.

A great change was observed in the IR region 1700-500 cm^{-1} from ester to methyl ester showing impact of transesterification on oil. Chemically it can be depicted as change from R1-C (OR) =O for the ester group of CISO and while R1-C (OCH$_3$) =O for methyl ester group of *Cichorium intybus* biodiesel. IR region of 1743.4 cm^{-1} and 1377.5 cm^{-1} is a significant signal indicating substantial difference between *Cichorium intybus* seed oil and biodiesel. A typically detected changeable IR region during transesterification reaction lies within ester control peak area of the spectrum at around 1100-1000 cm^{-1}. Broad peak of 1425 cm^{-1} in *Cichorium intybus* seed oil was split into 1377.5 cm^{-1} and 1237.7 cm^{-1} in CISOD. Similarly, prominent peak at 1025.01 cm^{-1}, which indicates C-H$_2$ wagging frequency in oil was not observed in CIBD. Another intense peak which was observed in the IR region of biodiesel at 1160.15 cm^{-1} (C-O) was absent in *Cichorium intybus* seed oil IR spectrum. The occurrence of FAMEs (biodiesel) has been therefore, confirmed from all these peaks.

3.4.4.2. NMR Spectroscopic Analysis

In order to properly monitor transesterification reaction, the technique of NMR is employed which contributes characteristic signals of reaction in ^{1}HNMR and ^{13}CNMR spectrum. ^{1}HNMR spectrum of *Cichorium intybus* seed oil biodiesel has been presented in Figure 3.4.9a. Spectrum has chemical shifts at δ (ppm): 0.893 (CH$_3$ triplet), 1.266 (CH$_3$ multiplet), 1.628 (-CH2-C-OO multiplet), 5.355 (-CH=CH-) and 7.281 ppm. Signal at 1.628 and 1.27 ppm is for aliphatic group and its chemical shift is not affected by ester group or double bond molecules. Signals for two outer hydrogen atoms of the conjugated double bonds were detected at 5.355 ppm. Peak of Free methanol which is typically detected at 3.45 ppm was not observed in ^{1}HNMR spectrum.

One of the major significant peaks at 3.677 ppm indicated characteristic methoxy group (– OCH$_3$) and confirmed methyl ester formation which was absent in the spectrum of *Cichorium intybus* seed oil. Results obtained are in line with findings of previous literature (Joshi et al., 2011). Structural characteristics of synthesized biodiesel were studied with ^{13}CNMR spectrum. ^{13}CNMR spectrum of CIBD shown in in Figure 3.4.9b has chemical shifts at δ (ppm):173.18 for carbonyl carbon (-COO-), 129.95 for unsaturated and nun-conjugated carbons (-CH=CH-), 77.53 (-C-O) and 29.31 (-CH$_2$-)n ppm for aliphatic methylene group. All these peaks in NMR spectrum revealed the presence of methyl ester in *Cichorium intybus* seed oil biodiesel. Percent conversion rate of *Cichorium intybus* seed oil into biodiesel was calculated and was found 88.5%.
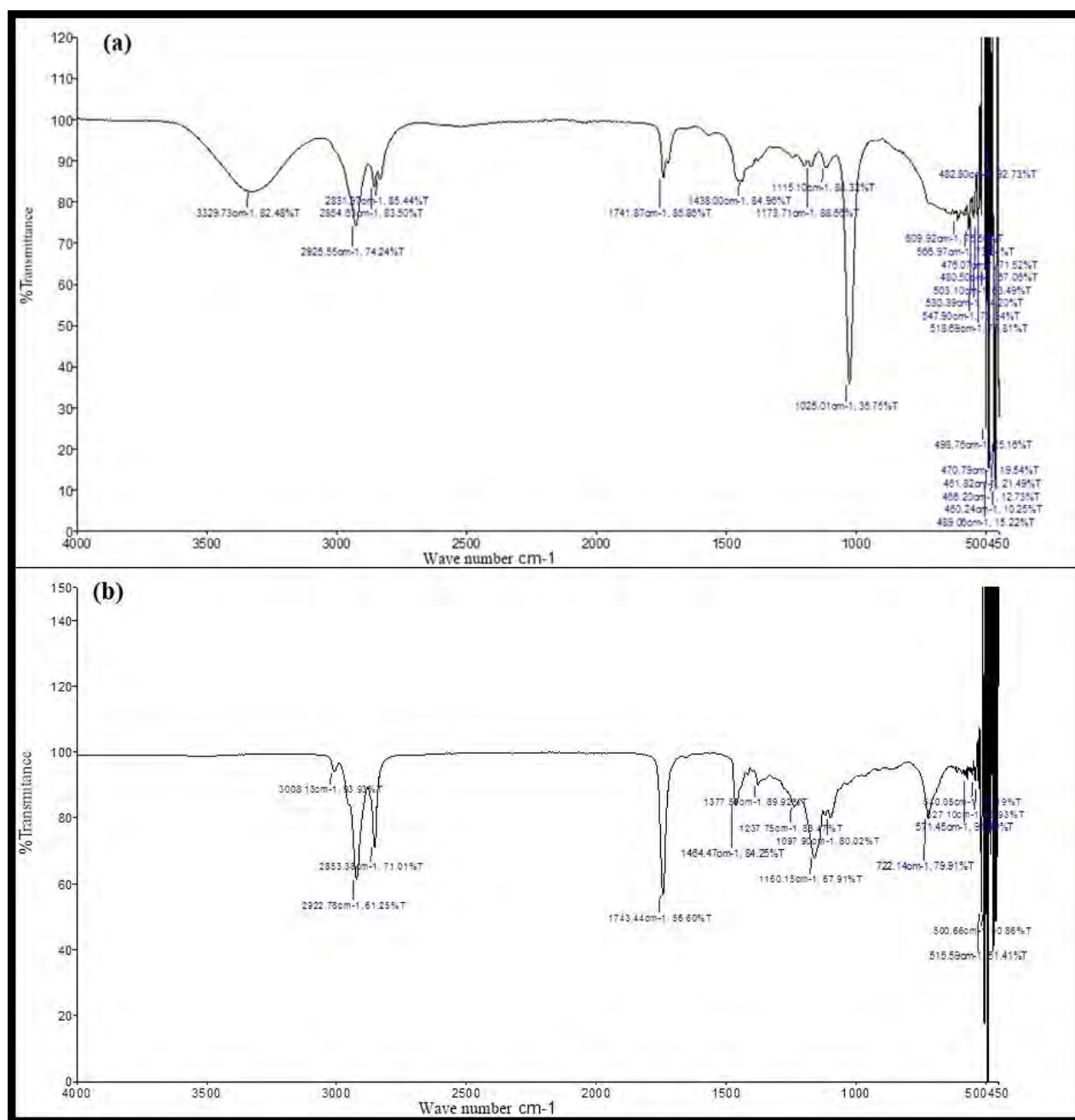
Figure 3.4.8. FTIR spectra of **(a)** seed oil of *Cichorium intybus* and **(b)** *Cichorium intybus* biodiesel
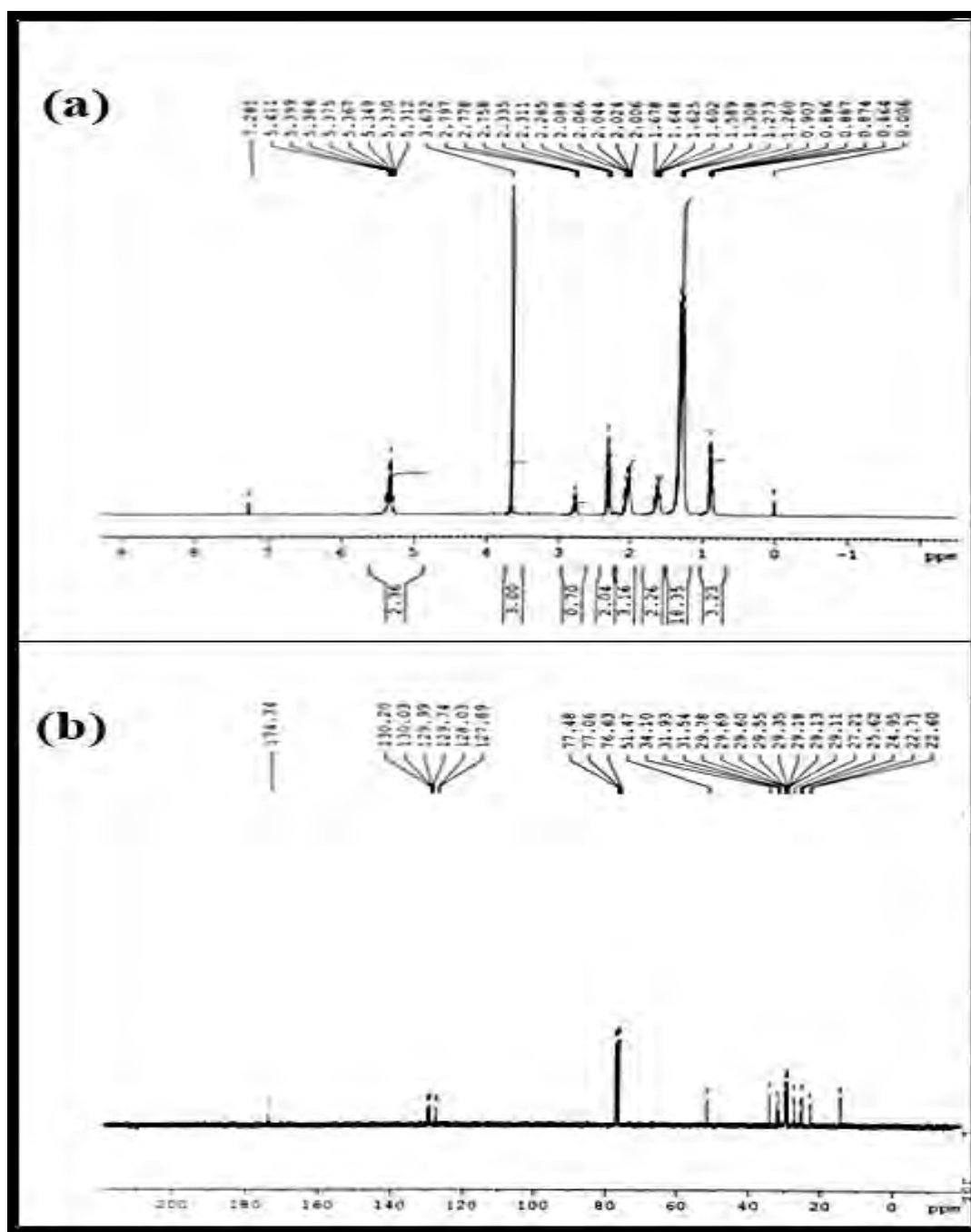
Figure 3.4.9. NMR spectrum of **(a)** ^{1}HNMR and **(b)** ^{13}CNMR of *Cichorium intybus* biodiesel
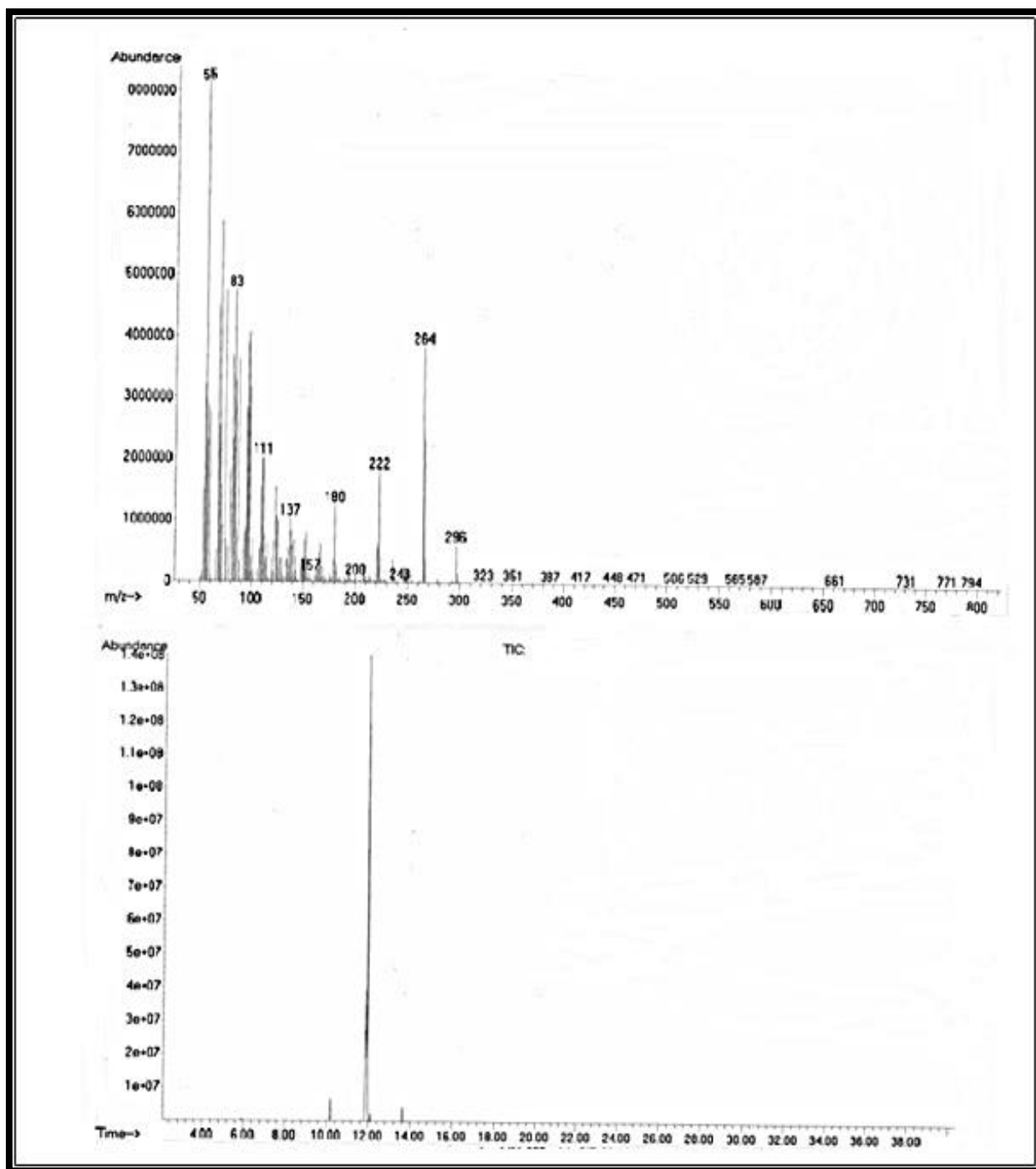
Figure 3.4.10. GC-MS spectrum of *Cichorium intybus* biodiesel

3.4.4.3. GC/MS

GC/MS analysis is used for chemical characterization of biodiesel to find out composition and percentage of various constituents of FAMEs in it. GC/MS spectrum gives us deep insight into purity and quality of biodiesel. It is one of the crucial factors which reflects suitability of a biomass source for biodiesel production. Biodiesel with large amount of saturated fatty acids is considered objectionable as it affects engine efficiency. GC/MS spectrum of *Cichorium intybus* biodiesel exposed six major peaks which correspond to different fatty acid methyl esters and presented in in Figure 3.4.10. These peaks were further compared with library reference data utilizing software (NO. NIST02). Retention time of fatty acid methyl esters was utilized to recognize them. Further confirmation was done through MS analysis. Peaks of unsaturated and saturated fatty acids which were identified include methyl Hexadecanoate (C16:0), methyl-11-ecosanoate (C20:0) one di-unsaturated; methyl 2-octenoate (C9:2) and two mono-unsaturated methyl Hexadec7-enoate (C16:1, m/z 264) and methyl Octadec-8-enoate (m/z296); were also observed. Methyl Hexadecanoate and methyl Hexadec7-enoate were found to be major fatty acid methyl esters with higher concentration. The percentage and composition methyl esters are greatly affected by saponification reaction during transesterification which reduces conversion efficiency of triglycerides into methyl esters. Outcomes of GC/MS analysis disclosed that seed oil of *Cichorium intybus* is suitable for production of methyl ester at broad scale level.

3.4.5. Fuel properties of *Cichorium intybus* Biodiesel

Fuel properties of biodiesel like kinematic viscosity, density, flash point, pour point, iodine value and sulfur content were used to measure its quality and effectiveness in diesel engines for future implications (Table 3.4.4). Fuel properties of synthesized biodiesel of *Cichorium intybus* seed oil were compared with international fuel standards *i.e.* ASTM D-6751 and European Union 14214 as shown in Table 3.4.4. One of the most important properties of biofuel is acid value. The acid value of biodiesel is under great influence of free fatty acids content of the fuel. Higher values of acid number negatively affect engine performance by causing corrosion in engine parts. However, acid value of CIBD was found 0.121 (mg KOH/gm) and well matched with international standards indicating its viability for efficient use in fuel

engines. Biodiesel density says about its quality, purity and fatty acid outline. It plays a vital role in determining diesel quality. The presence of unsaturated fatty acids highly influences biodiesel density. Biofuels with higher density disturbs fuel engine and are not recommended for practical use. Biodiesel density in our current study was found 0.811 (g/cm^3) which lies under range of international standards. It indicated that synthesized biodiesel can be used in diesel engine as an alternate and environment friendly substitute of petro diesel with no negative effect.

Kinematic viscosity (Kg/m^3 at 40 °C) of biodiesel plays a significant part in the process of combustion, blending fuels and spray fuels. It is also known as stickiness index of biofuels. Biofuels with high viscosity results in operability issues in ignition due to incomplete combustion and emission of particulate matter. In our current study, kinematic viscosity of *Cichorium intybus* biodiesel was found to be 4.44 (mm^2/s) which is equivalent to international standards. Flash point of biodiesel refers to temperature at which biofuel flash upon on ignition. It is considered as an important tool for safety measures and other aspects linked with engine performance like legal safety insurance and transportation for fire guidelines. It is exceedingly affected by the content of methanol in produced biodiesel. The higher the content of methanol smaller will be the flash point. Flash point of CIBD was 72.5 °C and found well matched with ASTM D-6751and European Union 14214 standards. However, biodiesel with higher flash points (>66 °C) are considered safer with lesser volatile nature as compared to petro diesel. Cold flow properties of biodiesel (pour point and cloud point) are also critical parameters which are kept under consideration especially in colder regions of the world. These properties depend upon type and quantity of impurities present in biodiesel. At lower temperature biodiesel turns milky due to emergence of crystal nuclei and affects flowing characteristics of biodiesel. It can be improved by adding commercially available additives and antioxidant. Pour point of methyl ester is directly related to viscosity of crude oil used for biodiesel synthesis. Pour and cloud point of *Cichorium intybus* biodiesel were found to be -8 °C and -12 °C respectively. Sulfur content of *Cichorium intybus* biodiesel was 0.0001 (wt. %) indicating that synthesized biodiesel is eco-friendly and harmless.

Table 3.4.4 - Comparison of Fuel properties of fuel properties of *Cichorium intybus* biodiesel with international standards**.**

Property	*Cichorium inthybus*		ASTM D-6751		EN-14214		China GB/T 20828-2007	
	Mean	**St.Dev**	**Mean**	**St.Dev**	**Mean**	**St.Dev**	**Mean**	**St.Dev**
Flash Point (°C)	72	2.0	-	-	2.0	-	-	2.52
Pour Point (°C)	-8	≤0.5	≤0.8	≤0.5	≤0.5	≤0.8	≤0.5	1.0
Viscosity (mm²/s at 40 °C.)	4.44	≥93	≥130	≥120	≥93	≥130	≥120	0.2
Density (kg/m³ at 40 °C)	0.74	-15-16	_	_	-15-16	_	_	0.036
Cetane Number	-	1.9-6.0	_	3.4-5.0	1.9-6.0	_	3.4-5.0	2.52
Iodine Value (g I2/100 g)	73.5	≤120	_	≤120	≤120	_	≤120	2.1
Sulphur content (wt.%)	0.0001	≤0.05	≤0.05	≤0.20	≤0.05	≤0.05	≤0.20	0
Cloud point (°C)	-12	-3.0-12	_	_	-3.0-12	_	_	1
References			ASTM D-6751		EN-14214		China GB/T 20828-2007	

3.4.6. Reusability of catalyst

The reusability of MgO nano particles was investigated to find out its economic viability, strength for methyl ester formation and application at industrial level. Transesterification reaction of *Cichorium intybus* seed oil was carried out at optimum reaction conditions (catalyst loading 0.83 wt. %, reaction time 180 min, temperature 85 ^{o}C and methanol to oil ratio 9:1) (Figure 3.4.11). It was evident from a number of experiments that efficiency of the catalyst decreases with increase in successive runs. A yield of 80% was observed at 5th cycle which further dropped to 60% in 6th cycle possibly because of deactivation of catalyst active site. A major decrease in catalytic activity was observed after 6th cycle. However, the catalytic activity of the catalyst was regained after another round of calcination.
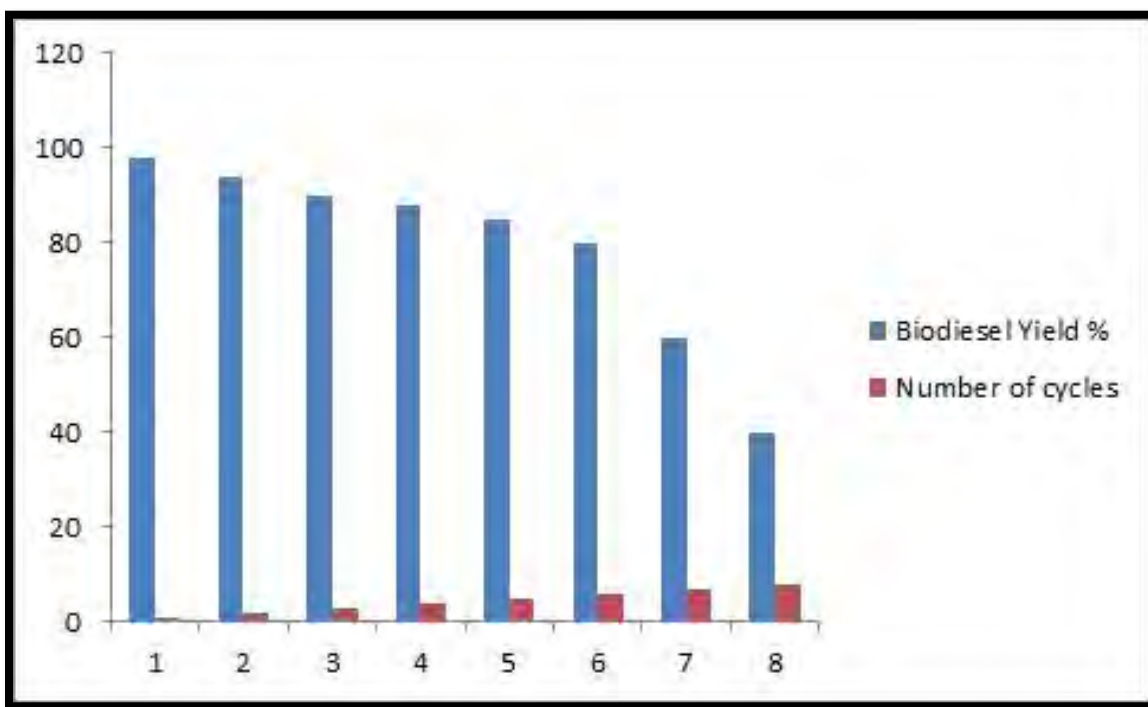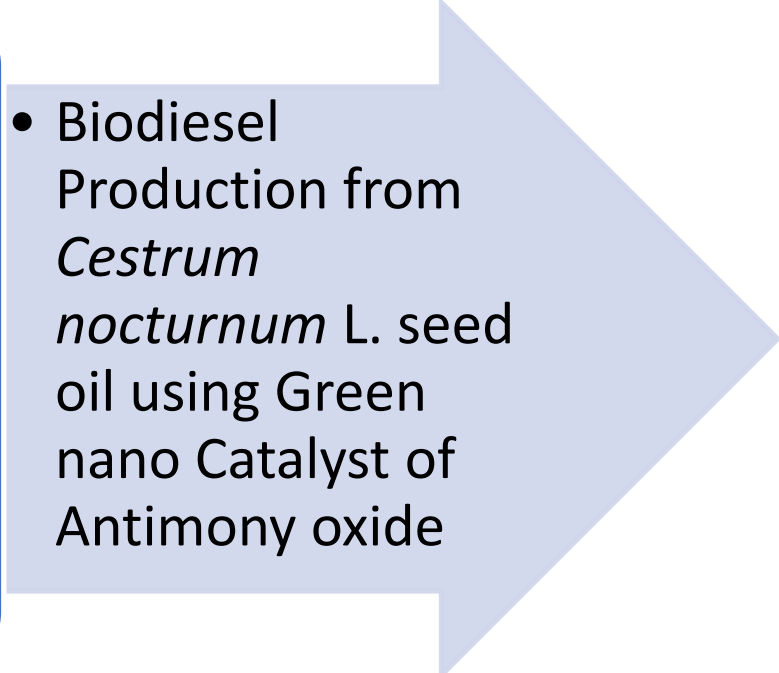
Figure 3.4.11. Reusibility of magnesium oxide nanocatalyst in transesterification

SECTION V

- Biodiesel Production from *Cestrum nocturnum* L. seed oil using Green nano Catalyst of Antimony oxide

To the best of our knowledge, there has been little research on the synthesis and properties of Sb₂O₃ nanoparticles. It is the first study conducted on Sb₂O₃ nanoparticles used in transesterification reaction.

3.5.1   Characterization of Sb₂O₃ Nano-catalyst

3.5.1.1 X-Ray Diffraction (XRD) of Sb₂O₃

Powder X-ray diffraction was used to analyze the crystalline structure of calcined antimony trioxides, (Sb₂O₃). XRD was used to determine the phase compositions of the samples as they were obtained Figure 3.5.1 depicts the Sb₂O₃ NPs' XRD pattern. All the diffraction peaks in the XRD patterns of Sb₂O₃ composites can be accurately indexed in accordance with the standard peaks of (Sb₂O₃). As shown by the spectrum, antimony trioxides exhibit six discernible peaks at 2 θ= 15.03°, 29.24°, 31.15°, 35.76°, 39.64°, 45.87°, 52.16°, 55.24°, and 64.25°, which correspond to (111), (222), (400), (331), (440), and (622) hkl, respectively (JCPDS: 06-0416). The Debye-Scherer formula (Eq. 1) was used to estimate the size of the relevant crystal from the deepest peak at 2θ value of 35.76° (222 hkl). Particle size was found to be 40 nm.

3.5.1.2 Scanning Electron Microscopy (SEM) of Sb₂O₃

The SEM method was used to investigate the surface morphology of Sb₂O₃ at different magnifications. Figure 3.5.2 shows SEM images of Sb₂O₃ nanoparticles, which reveal a uniform, cubic shape. O, and Sb elements are evenly distributed throughout the designated area in SEM micrographs.

3.5.1.3 Energy Diffraction X-ray (EDX) of Sb₂O₃

Chemical components of Sb₂O₃ NPs were investigated using EDX spectroscopic method. Figure 3.5.3 represents the EDX spectrum of antimony and oxygen in nanoparticles, showing the peak of these elements in pure form. Peaks at 0.5 KeV in the EDX spectrum are related to the binding energy of oxygen and peaks at 0.5, 3.5 and 25.6 KeV depicted binding energy of antimony respectively. Both antimony and oxygen have percentage values of 74.30% and 25.70% respectively.

3.5.1.4 Fourier Transform Infrared Spectroscopy (FTIR)

FT-IR spectroscopy studies have revealed details on the various functional groups found in Sb_2O_3 NPs. The FT-IR spectra of the Sb_2O_3 NPs show the transmittance % of various absorption peaks in Figure 4. Information regarding the numerous functional groups discovered in Sb_2O_3 NPs was provided by FT-IR spectroscopic research. Figure 3.5.4 displays the transmittance percentage of distinct absorption peaks in the FT-IR spectrum of Sb_2O_3 NPs. Water absorbed on the surface of the tested particles was suggested by a wide peak that occurred at 982.4 cm^{-1}. Broad band at The Sb-O bond was responsible for the deepest peak, which was measured at 1266 cm^{-1} and 2365.62 cm^{-1}. These peaks confirm the presence of phases of Sb_2O_3.

3.5.1.5 Thermogravimetric analysis (TGA) of Sb_2O_3

The thermal degradation of Sb_2O_3 precursor was investigated using a thermogravimetric analysis from room temperature to 1000 ∘C. Figure 3.5.5 a and b show the Sb_2O_3 thermogram and its ensuing derivative curve (wt.%), respectively. First significant weight loss of 4.32% was seen between 50 ∘C to 120 ∘C, which is related to desiccation and the removal of water from nanoparticle surfaces. At the temperature range between 150 ∘C to 420 °C, the second peak of weight loss showed a loss of 3.65%, which is due to the decomposition of the precursor to Sb_2O_3. With a weight loss of 4.37%, the third phase of Sb_2O_3 breakdown occurred at temperatures between 450 ∘C to 710 ∘C.
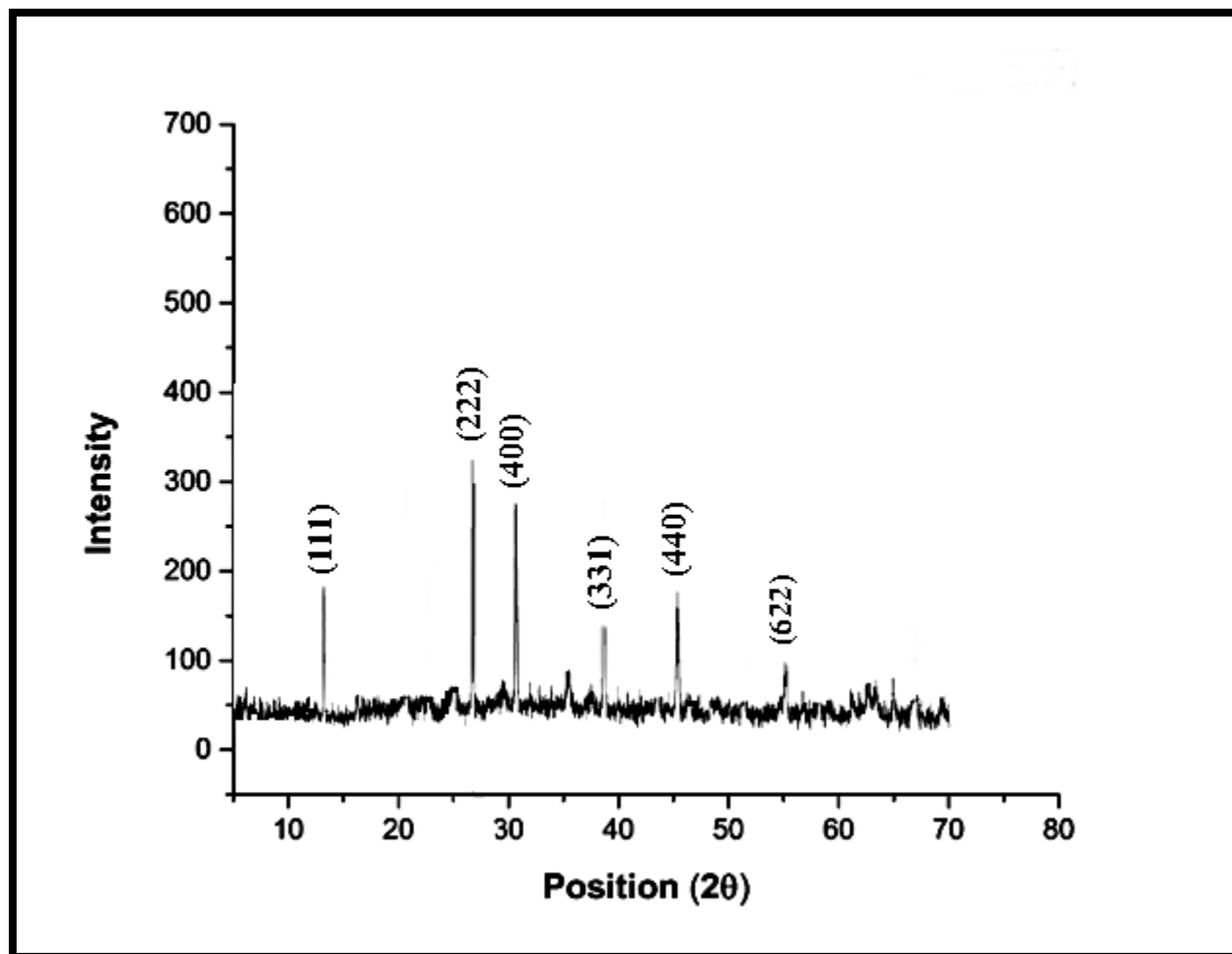
Fig. 3.5.1. XRD pattern of calcined antimony oxide nanocatalyst
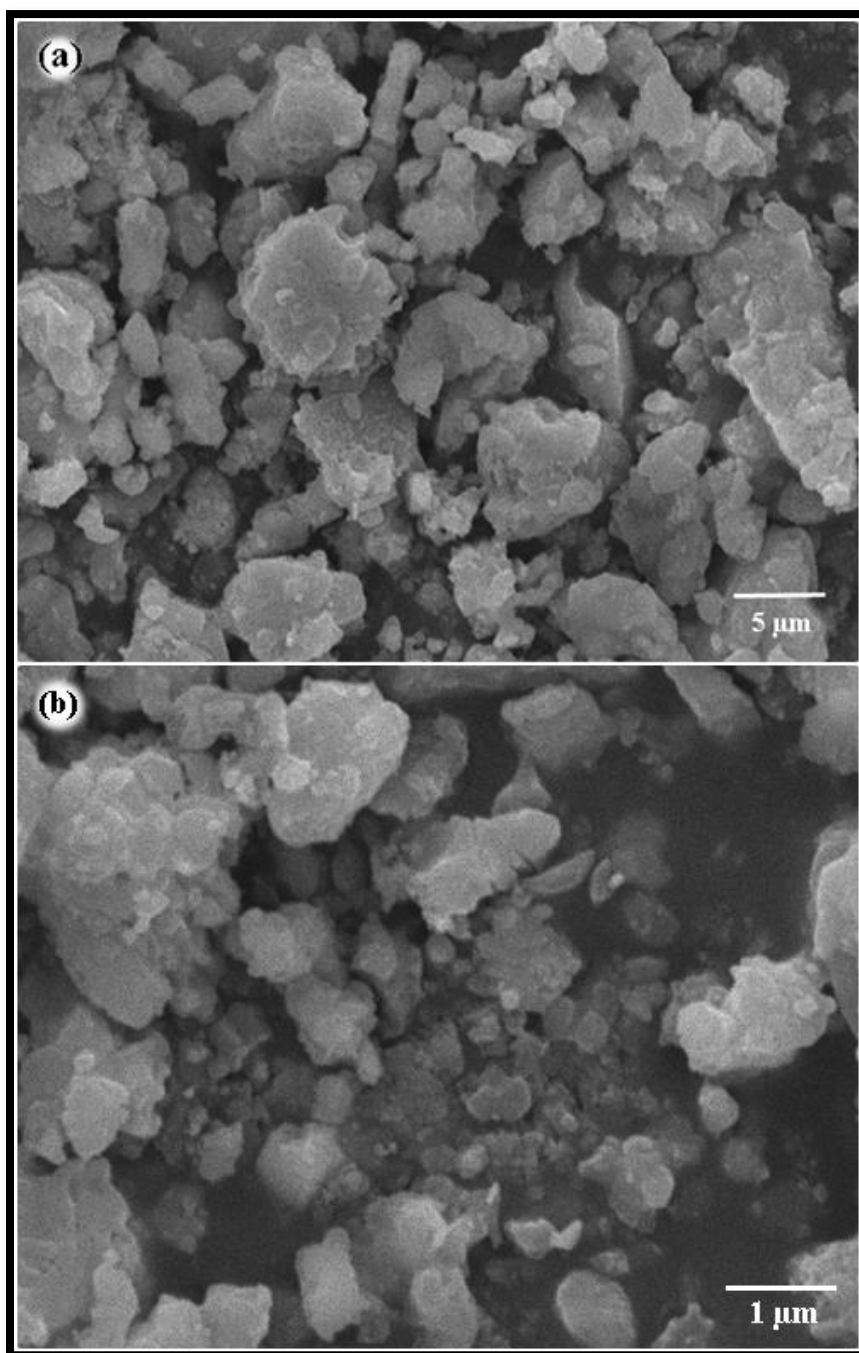
Fig. 3.5.2. Scanning electron micrographs of antimony oxide nanocatalyst
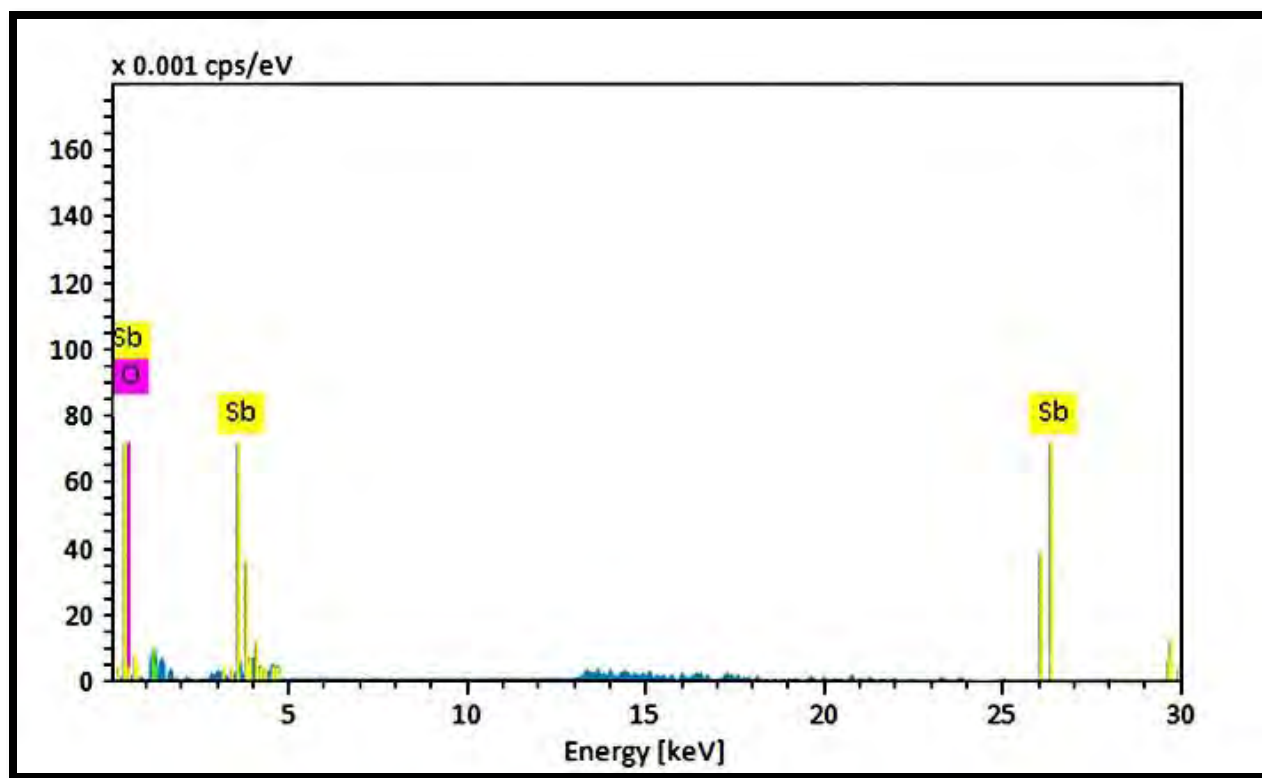
Figure 3.5.3. Energy diffraction X-Ray (EDX) of antimony oxide nanocatalyst
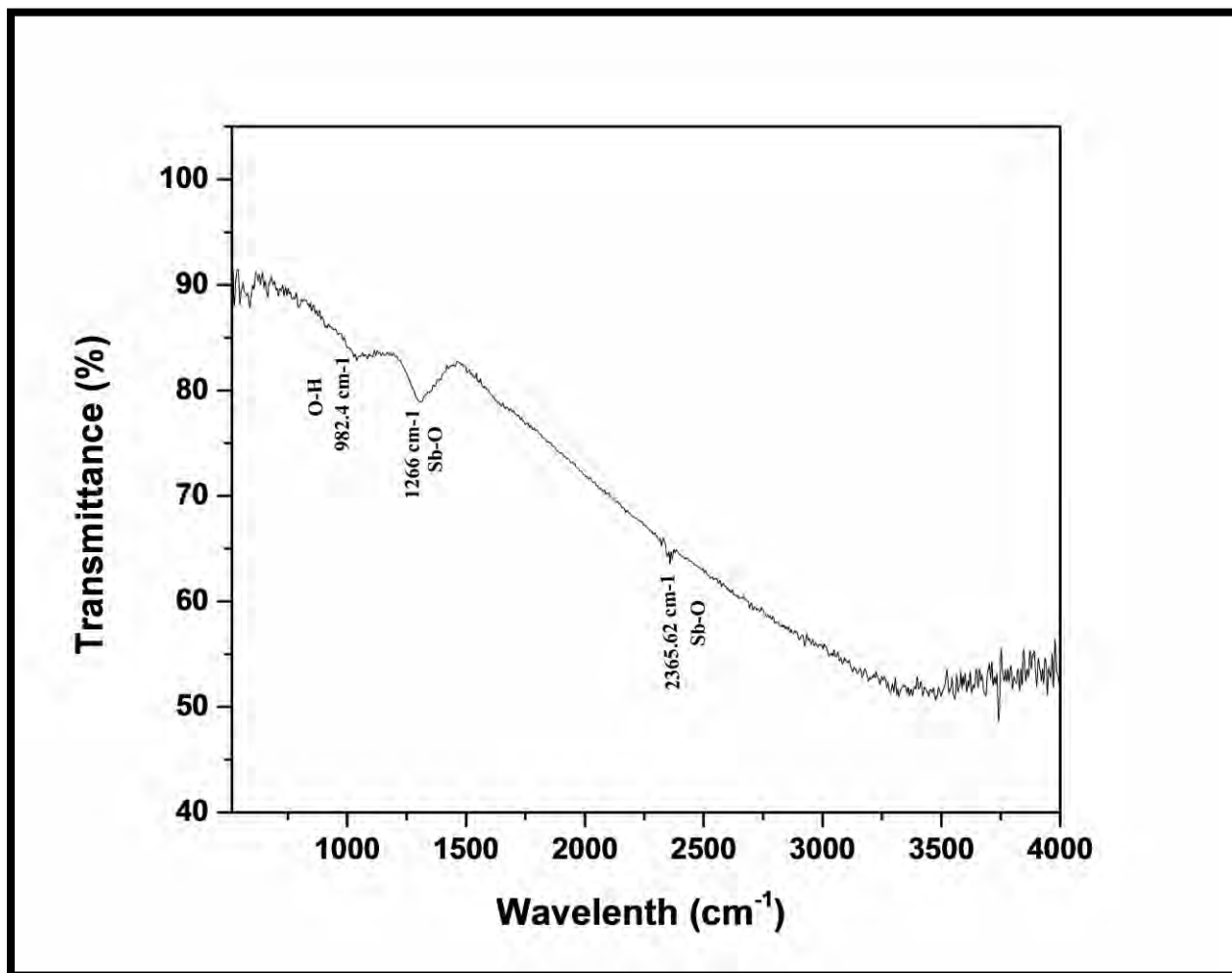
Figure 3.5.4. FT-IR spectrum of antimony oxide nanocatalyst
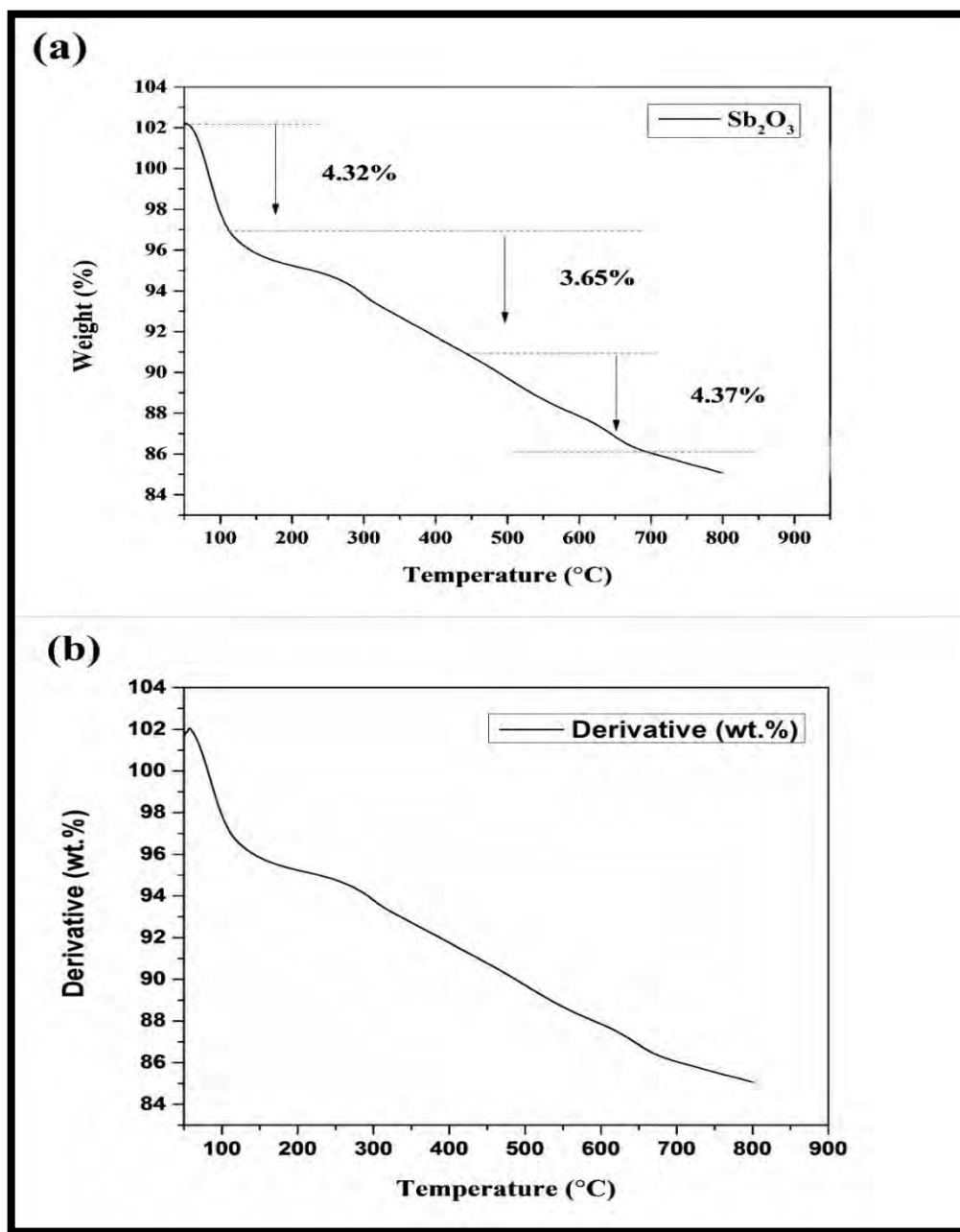
Figure 3.5.5. (a) TGA of antimony oxide nanocatalyst (b) derivative thermogram of antimony oxide nanocatalyst

3.5.2 Biodiesel synthesis using transesterification

In the current work, innovative and potential *Cestrum nocturnum* L. seed oil was used to create sustainable and environmentally friendly biodiesel. Before beginning the biodiesel synthesis process, it is crucial to determine the FFA level of the oil of a chosen feedstock. When compared to other reported non-edible seed sources, such as *Azadirachta indica* (Betiku et al., 2017), the oil content was discovered to be 28%, a significant increase.

At 25 ∘C, *Cestrum nocturnum* seed oil was discovered to be chocolate brown in hue. Since the FFA content of CNSO was found to be 1.5 (wt.%) in the current investigation, which is much lower, it is evident that CNSO is ideal for the operation of a single step base-catalyzed transesterification reaction. Oil with a high FFA level (more than 3%) is regarded as unfavorable since it necessitates an extra step of acid esterification, produces less biodiesel, and produces soap, which complicates the separation of reaction products and necessitates further purification processes.

As a result, *Cestrum nocturnum* seed oil can be used effectively to synthesize methyl esters without the need for an additional step of acid esterification. Using a green nano Sb_2O_3 catalyst made from the aqueous leaf extract of *Chenopodium album* L, *Cestrum nocturnum* seed oil was transesterified.

The yield of biodiesel is significantly impacted by the transesterification reaction's reaction conditions. In order to acquire the highest yield of methyl ester, studies were conducted to determine the ideal transesterification reaction conditions. The DOE (Design of Experiment) method was used to create the Central Composite Design (CCD), which had four autonomous variables with minimum and maximum ranges of values: (A) methanol to oil molar ratio of 2:1-15:1. (B) catalyst concentration of 0.16-0.96 wt.%, (C) temperature of 70-120 ºC, and (D) reaction time of 60-180 mins, (Table 3.5.1). In Figure 3.5.6, a comparison of the expected and actual yield is displayed. The distribution of the anticipated and actual values (obtained through experiments) are both close to the straight line, indicating a strong correlation between them. Table 3.5.3 displays the findings of a statistical examination of the response surface quadric model's variance. ANOVA findings showed that the experimental model had a significant *p*-value of 0.0003 (<0.05). The current model's lack of fit F-value, however, had an F-value of

2.14, which is deemed good for desirable model fit and was not significant in comparison to pure error. The most significant *p*-value for the transesterification process was less than 0.05 for the quadratic terms of catalyst loading (C^2) and methanol to oil ratio (A^2). The Adjusted R^2 of 0.869 is determined to be relatively near to the Predicted R^2 of 0.725, and the variance is less than 0.2. The signal-to-noise ratio is measured by enough precision. A ratio of at least 4 is preferred. The ratio of 9.509 in the current investigation denotes a sufficient signal. As a result, the experimental model is effective in forecasting methyl ester yield. The model's applied polynomial equation (6) is provided below.

Biodiesel Yield (wt. %) = +82.65+5.72 *A-5.20 *B+5.42 *C-0.2223 *D-2.85 *AB+0.6056 *AC+1.23 *AD-0.5178* BC-0.7521 *BD-2.20 *CD-15.54 *A²-1.64 *B²-3.98 *C²+2.92 *D²
(11)
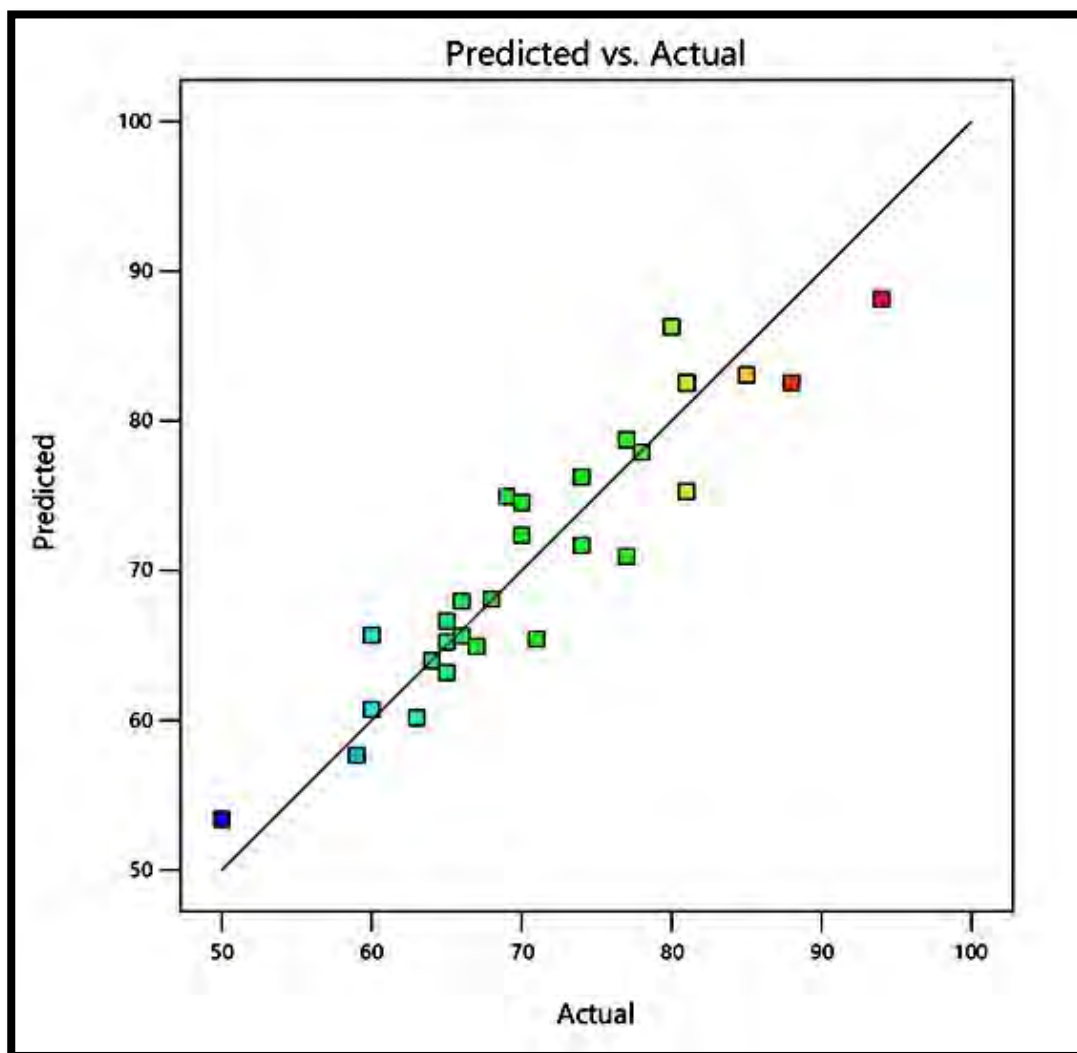
Fig. 3.5.6. Comparison between the experimental and predicted yield of biodiesel in the model

Table 3.5.1- Experimental design by central composite design for transesterification reaction

Process parameters	−1	+1
Methanol to oil ratio	2:1	15:1
Catalyst loading (wt. %)	0.16	0. 96
Reaction time (min)	60	180
Temperature (∘C)	70	120

Table 3.5.2- Detailed experimental result for transesterification reaction of *Cestrum nocturnum* Biodiesel

Run	Factor 1 A: Alcohol to oil molar ratio	Factor 2 B: Catalyst loading wt.%	Factor 3 C: Temperature °C	Factor 4 D: Reaction time (min)	Response Yield wt.%
1	2.1	0.96	70	180	65
2	8.1	0.56	95	180	94
3	8.1	0.56	70	120	70
4	2.1	0.96	120	180	66
5	15.1	0.56	95	180	88
6	2.1	0.16	70	60	60
7	8.1	0.56	120	120	77
8	15.1	0.96	120	180	59
9	8.1	0.56	95	120	74
10	2.1	0.96	70	60	71
11	8.1	0.56	70	60	66
12	2.1	0.16	120	60	64
13	15.1	0.56	95	60	50
14	2.1	0.56	95	180	69
15	2.1	0.16	70	180	63
16	15.1	0.96	70	180	68
17	15.1	0.56	70	180	70
18	8.1	0.56	95	60	80
19	2.1	0.96	95	180	65
20	8.1	0.16	95	120	64
21	2.1	0.96	120	60	67
22	8.1	0.16	95	60	56
23	15.1	0.16	95	180	74
24	8.1	0.56	95	120	81
25	8.1	0.16	95	120	78

26	1=8.1	0.56	120	60	65
27	15.1	0.16	120	180	60
28	15.1	0.56	95	120	81
29	8.1	0.56	70	60	77
30	8.1	0.16	95	180	85

Table 3.5.3- ANOVA for Response Surface Quadratic model

Source	Sum of Squares	df	Mean Square	F Value	p-value	
Model	2392.57	14	170.90	7.15	0.0003	significant
A-Methanol to oil Ratio	0.5000	1	0.5000	0.0209	0.0069	
B-Catalyst Concentration	12.80	1	12.80	0.5357	0.0455	
C-Temperature	59.75	1	59.75	2.50	0.0346	
D-Time	16.50	1	16.50	0.6906	0.0190	
AB	115.56	1	115.56	4.84	0.0440	
AC	138.06	1	138.06	5.78	0.0296	
AD	1.56	1	1.56	0.0654	0.0016	
BC	14.06	1	14.06	0.5886	0.0149	
BD	3.24	1	3.24	0.1357	0.0178	
CD	3.42	1	3.42	0.1431	0.0105	
A²	177.69	1	177.69	7.44	0.0156	
B²	94.31	1	94.31	3.95	0.0655	
C²	303.86	1	303.86	12.72	0.0028	
D²	68.72	1	68.72	2.88	0.1105	
Residual	358.39	15	23.89			
Lack of Fit	321.64	12	26.80	2.19	0.8827	not significant
Pure Error	36.75	3	12.25			
Cor Total	2750.97	29				

$R^2 = 0.869$, Std. Dev. = 3.89,   C.V. % = 6.82, Adeq Precision = 10.05

3.5.3 Influence of reaction parameters on transesterification reaction

3.5.3.1 Combined influence of methanol to oil molar ratio and catalyst loading

One important reaction parameter affecting biodiesel yield during transesterification is the methanol to oil molar ratio and catalyst loading. To transform oil into methyl ester and advance the reaction, enough methanol is needed. A stoichiometric calculation revealed that when three moles of alcohol are combined with one mole of oil, biodiesel (3 moles) and glycerol are produced (1 mol). In three-dimensional plots built on a central composite experimental design, the combined effects of the oil to methanol molar ratio and the catalyst loading on the transesterification reaction of *Cestrum nocturnum* seed oil have been shown in Figure 3.5.7a. At 0.56 wt.% of the catalyst and molar ratio of 8:1 the highest yield (94%) of methyl ester was produced (Run 2). About 70% of triglycerides are converted to methyl esters when the molar ratio of oil to methanol is decreased from 2:1 while the amount of catalyst remains same (Run 14). By decreasing the catalyst amount up to 0.16 weight percent, at a molar ratio of 15:1, the yield was reduced to 74% (Run 23). The development of undesirable reaction products was shown to be the reason why the percentage yield of biodiesel declined as catalyst amounts increased. At 15:1, an excessive amount of methanol reduced the biodiesel output by up to 88% (Run 5). By combining and solubilizing glycerol in FAMEs and encouraging its recombination with FAMEs, which results in the reformation of monoglycerides in the reacting mixture, this loss in yield is attributable to the reversible reaction of glycerolysis (Bateni et al., 2014). The extra methanol in the reacting mixture causes the concentration of the catalyst to dilate. Additionally, it decreases the output of biodiesel and hinders the separation of glycerol from FAMEs. The new study's findings are consistent with earlier research showing that too much methanol causes a reversible glycerolysis reaction. According to a recent publication, a rise in the molar ratio from 15:1 to 20:1 at 80 oC and 1% catalyst concentration led to a drop in biodiesel output (Salehian et al., 20013). With a *p*-value of 0.0440 (<0.05), the combined effect of the molar ratio and catalyst loading was found to be significant.

3.5.3.2 Combined influence of oil to methanol molar ratio and reaction temperature

Figure 3.5.7b shows the combined impact of the reaction temperature and oil to methanol molar ratio. As the reaction temperature for transesterification was increased to 95 ∘C at a catalyst concentration of 0.56 wt. % and oil to methanol ratio of 8:1, the percent yield of methyl ester improved up to 94% (Run 2). The boiling point of methanol, which is 65 ∘C, and saponification of glycerol, respectively, limit the biodiesel yield at run number 3 (84%) to additional temperature increases over the edge level (>90 ∘C). Additionally, a lower reaction temperature of 70 ∘C resulted in a 70% decrease in biodiesel output (Run 17). As oil, methanol, and catalyst all become immiscible at lower temperatures and require enough kinetic energy to react correctly and boost productivity in less time, the mass transfer rate of these substances is reduced (Berman et al., 2011). As a result, it can be inferred from the current study that the combined influence of the volumetric ratio of oil to methanol and the reaction temperature is worthwhile to take into account during the transesterification reaction. Results of the ANOVA indicated that this combined association had a *p*-value lesser than 0.05. (0.0296).

3.5.3.3 Combined influence of oil to methanol ratio and reaction time

Another crucial reaction parameter that has a significant impact on biodiesel yield is the volumetric ratio of oil to methanol. While other reaction parameters including temperature (95 ∘C) and catalyst loading (0.56 wt.%) were held constant, Figure 3.5.7c shows the combined effects of the oil to methanol ratio (A) and reaction time (D). Maximum yield of 94% was seen at molar ratio of 8:1 and a react time of 180 min at run number 2, which was attributed to an increase in the interaction of triglycerides with excess alcohol during transesterification. On the other hand, a shorter reaction time of 120 min of transesterification at run number 9 with a lower volumetric ratio of oil to methanol resulted in a relatively low yield of methyl ester (74%). It is most likely because the reactants did not have enough time to achieve an equilibrium state, which led to an incomplete conversion of the reactants into products. Due to an excess of methanol, which moved the reaction towards an undesirable reaction condition and facilitated reverse reaction, a reduction in biodiesel production (50%) was found at a higher oil to methanol ratio of 15:1 with reaction time of 1 h at run number 13. Previous research that used an iron doped zinc oxide catalyst to facilitate the chemical reaction of transesterification and reported a

91% yield of biodiesel at a high reaction time of 50 min attested to similar results. According to a study, a high catalyst loading results in a higher conversion of triglycerides into methyl ester in a shorter amount of time (Salaheldeen et al., 2015). The results of the ANOVA showed a substantial and robust association between the molar ratio and the reaction time, with a *p*-value of less than 0.05 (0.0016).

3.5.3.4 Combined influence of catalyst loading and reaction temperature

Figure 3.5.7d shows the combined impact of temperature and catalyst loading on biodiesel yield percentage. At reaction temperature of 95 ∘C, oil to methanol ratio of 8:1, and reaction time of 1 h, run number 2 produced the highest yield of 95%, which is attributable to the greatest contact of oil with methanol during transesterification (Degfie et al., 2019). This is consistent with the Arrhenius equation, which states that as reaction temperature rises, chemical reaction speed and methyl ester production increase continuously [48]. In contrast, run number 2 had a low biodiesel yield of 70% despite a shorter reaction time (120 min) and temperature of 70 ∘C. This low yield was most likely caused by incomplete conversion at a short reaction time because the reactants failed to achieve equilibrium state. Biodiesel yield decreased (77%) in run number 7 due to a high temperature of 120 ∘C, reaction time of 120 min. It is because a large amount of methanol causes the reaction to shift toward unfavorable conditions, which leads to a low biodiesel yield. In earlier literature (Sun et al., 2015), similar findings were reported. The combined effect of these parameters is significant, according to the ANOVA results, with a *p*-value of 0.0149 less than 0.05.

3.5.3.5 Combined influence of reaction time and catalyst loading

The combined effect of reaction time (D) and catalyst loading (B) during transesterification is shown in Figure 3.5.7e as a 3D plot while reaction temperature and the volumetric ratio of oil to methanol are kept constant. Due to equilibrium in the transesterification reaction, a maximum yield of 94% was attained at run number 2 at optimal reaction duration (3 h) and catalyst loading 0.56 wt.%. With other reaction parameters like reaction temperature and the volumetric ratio of oil to methanol held constant. Due to equilibrium in the transesterification reaction, the highest yield of 94% was reached at the optimum reaction duration (3 h) and catalyst loading of 0.56 wt.% at run number 2. Same catalyst load with time of 60 min resulted in of yield of 80% at Run 18. Catalyst loading of 0.16 wt.% and time 120 min rendered yield to

64% (Run 20). Both low catalyst load (0.16 wt. %) and time of 60 min decreased yield up to 56% (Run 22). According to the ANOVA results, the combined effect of these parameters is significant with a *p*-value of 0.0178less than 0.05.

3.5.3.6 Combined influence of reaction time and temperature

Figure 3.5.7f shows the combined effect of transesterification reaction duration and temperature at constant oil to methanol volumetric ratio 8:1 and catalyst loading 0.56 wt.% on biodiesel yield. Run 2 clearly shows that a 95% biodiesel yield was attained at a reaction temperature of 95 ∘C and a reaction period of 3 h. Any additional increase in reaction temperature and decrease in duration causes a 56% reduction in methyl ester production (Run 26). Increased reaction time and temperature are thought to hasten the process of alkyl esters hydrolyzing into acids and subsequent polar methanol in the reacting mixture, resulting in a decrease in biodiesel production (Liang et al., 2019). Both low temperature of 70 ∘C and time 60 min rendered yield to 66% at Run 11. According to the results of our recent analysis, the endothermic nature of the transesterification reaction causes a considerable percent yield decline when the biodiesel yield increases by a certain amount within an increase in reaction temperature and duration. The combined effect of reaction time and temperature on biodiesel yield was determined to be significant with a *p*-value (0.0105) less than 0.05, according to the results of an ANOVA.
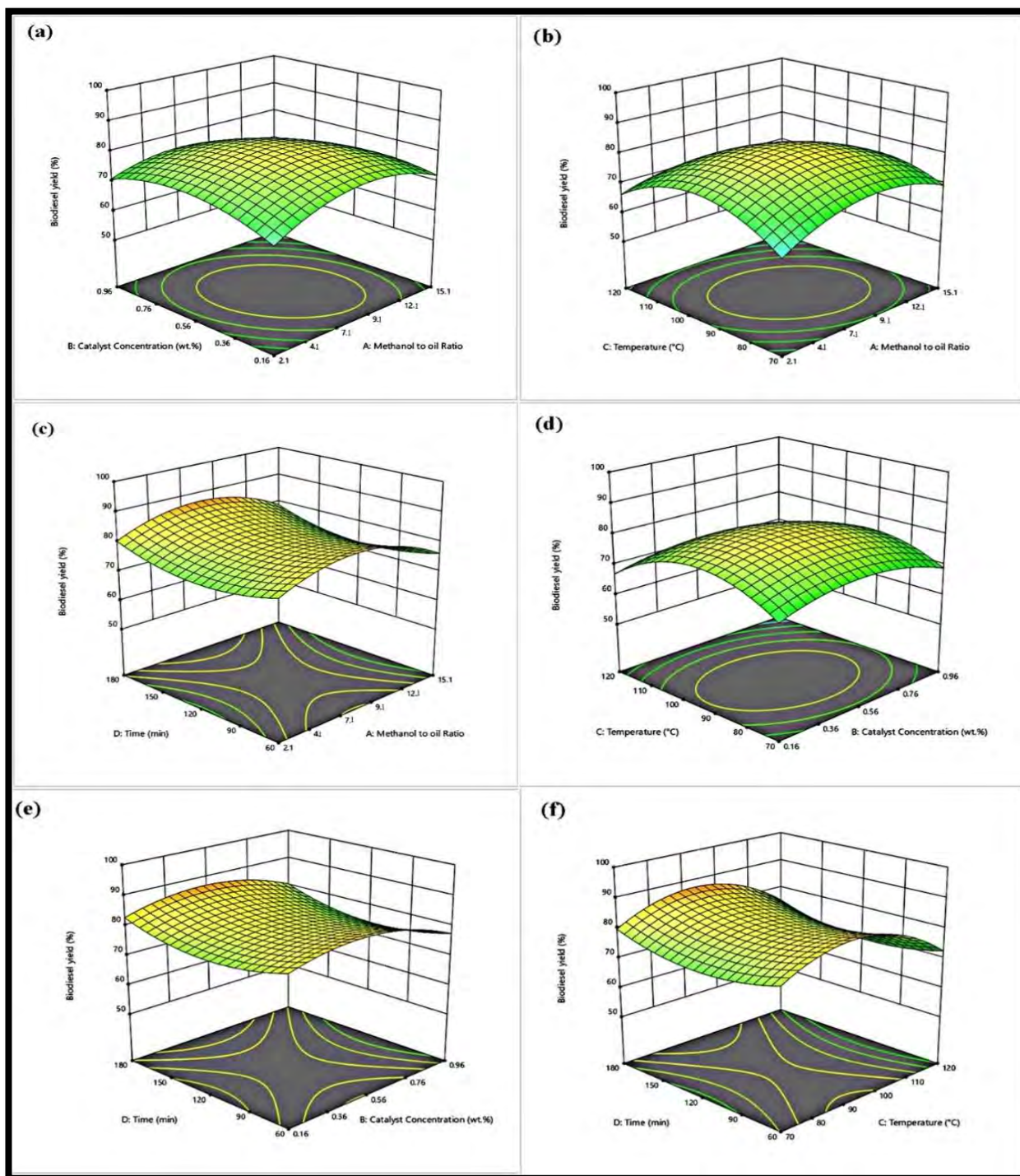
Figure 3.5.7. Impact of the reaction conditions of *Cestrum nocturnum* biodiesel

3.5.4. Characterization of Biodiesel

3.5.4.1. FTIR Study

FTIR spectroscopy is one of the defined laboratory techniques used to confirm biodiesel production next to transesterification reaction Presence of carbonyl and methyl group bands in the IR spectrum of biodiesel proves methyl ester production during transesterification. Various functional groups, bands, and stretching were identified using Fourier-transform infrared spectroscopy (FTIR) of *Cestrum nocturnum* L. seed oil and biodiesel at the mid IR range of 500-4000 cm^{-1} in Figure 3.5.8a. Because there are only slight differences between oil and diesel, the FTIR spectra of CNSO and CNBD revealed variation in terms of absorbent frequency and band intensity (Gardy et al., 2018). At 1743.55 cm^{-1}, a typically deep and powerful ester (C=O) stretching was seen. There was C-O axial stretching between 1377.63 cm^{-1} and 1098.19 cm^{-1}. *Cestrum nocturnum* biodiesel showed stretching of sp^2 C-H, sp^3 C-H, and C-H bending (rocking) at 2922.41 cm^{-1}, 2853.26 cm^{-1}, and 1464.86 cm^{-1}, respectively.

The impact of transesterification on oil was demonstrated by a significant shift from ester to methyl ester in the IR region between 1000 cm^{-1} -2000 cm^{-1} and 3100 cm^{-1}-3300 cm^{-1}. The change in R1-C (OR) = O for the ester group of CNSO and R1-C (OCH$_3$) = O for the methyl ester group of *Cestrum nocturnum* biodiesel can be represented chemically. An important signal suggesting a considerable difference between *Cestrum nocturnum* seed oil and biodiesel may be seen in the IR region between 1743.4 cm-1 and 1377.5 cm^{-1}. During transesterification reactions, the ester control peak area of the spectrum, which is located at about 1100-1000 cm^{-1}, is where changing IR regions are frequently identified. *Cestrum nocturnum* seed oil has a broad peak of 1425 cm-1 that was divided into two smaller peaks of 1377.5 cm-1 and 1237.7 cm-1. Like this, CNBD did not show a noticeable peak at 1246.92 cm-1, which implies C-H wag (-CH$_2$X) frequency in oil (Figure 3.5.8b). The *Cestrum nocturnum* seed oil IR spectra did not exhibit the 1159.80 cm^{-1} (C-O) strong peak that was seen in the IR region of biodiesel. Therefore, the presence of FAMEs (biodiesel) has been established from all of these peaks.

3.5.4.2. NMR Spectroscopic Analysis

NMR technology is used to effectively monitor transesterification reactions because it produces characteristic reaction signals in the ^{1}HNMR and ^{13}CNMR spectra. Figure 3.5.9a shows the ^{1}HNMR spectrum of the biodiesel made from *Cestrum nocturnum* seed oil. Chemical shifts in the spectrum occur at ppm values of 0.899 (CH_3 triplet), 1.263 (CH_3 multiplet), 1.628 (-CH_2-C-OO multiplet), 5.296-5.426 ppm (-CH=CH-), and 7.281 (-CH=CH-). The aliphatic group signal lies at 1.584 ppm to and 1.652 ppm, and neither ester groups nor molecules with double bonds change this signal's chemical shift. At 5.352 ppm, signals for the conjugated double bonds two exterior hydrogen atoms were found. The ^{1}HNMR spectrum did not contain the peak of free methanol, which is generally identified at 3.45 ppm.

One of the primary significant peaks, which was absent from the spectrum of *Cestrum nocturnum* seed oil, appeared at 3.675 ppm and revealed the distinctive methoxy group (- OCH_3) and validated methyl ester production. The outcomes are consistent with those reported in earlier studies (Knothe, 2001). Using the ^{13}CNMR spectrum, the structural properties of synthetic biodiesel were investigated. Chemical shifts for the CNBD ^{13}CNMR spectra are given in Figure 3.5.8b and are as follows (in ppm): 174.36 for carbonyl carbon (-COO-), 129.75-130.21 ppm for unsaturated and nun-conjugated carbons (-CH=CH-), 76.63-77.48 ppm for carbon atoms (-C-O), and 29.37 ppm for aliphatic methylene group. These peaks in the NMR spectrum demonstrated the existence of methyl ester in the biodiesel made from *Cestrum nocturnum* seed oil. The formula below was used to compute the conversion rate of *Cestrum nocturnum* seed oil into biodiesel, and the result was 90.5%.

3.5.4.3. GC/MS

Chemical characterization of biodiesel uses GC/MS analysis to determine the composition and percentage of different FAMEs in it. We gain extensive insight into the quality and purity of biodiesel from the GC/MS spectrum. It is an important indicator of whether a biomass source is suitable for the manufacture of biodiesel. Large amounts of saturated fatty acids in biodiesel are seen negatively since they reduce engine efficiency. Six significant peaks in the GC/MS spectrum of the biodiesel from *Cestrum nocturnum*, which are related to various fatty acid methyl esters and shown in Figure 3.5.10. These peaks were additionally compared

using software to library reference data (NO. NIST02). Fatty acid methyl esters were identified using their retention time. MS analysis was used to provide additional confirmation. Peaks of saturated and unsaturated fatty acids, including Hexadecanoic acid methyl ester (C16:0), 9, 12-Octadecadienoic acid methyl ester (C18:2), 9-Octadecenoic acid, (2)-methyl-, methyl ester (C18:1) and Octadecanoic acid, methyl ester (C18:0). Major fatty acid methyl esters with greater concentrations were identified to be 9, 12-Octadecadienoic acid methyl ester. The percentage and composition methyl esters are greatly affected by saponification reaction during transesterification which reduces conversion efficiency of triglycerides into methyl esters. Outcomes of GC/MS analysis disclosed that seed oil of *Cestrum nocturnum* is suitable for production of methyl ester at broad scale level.
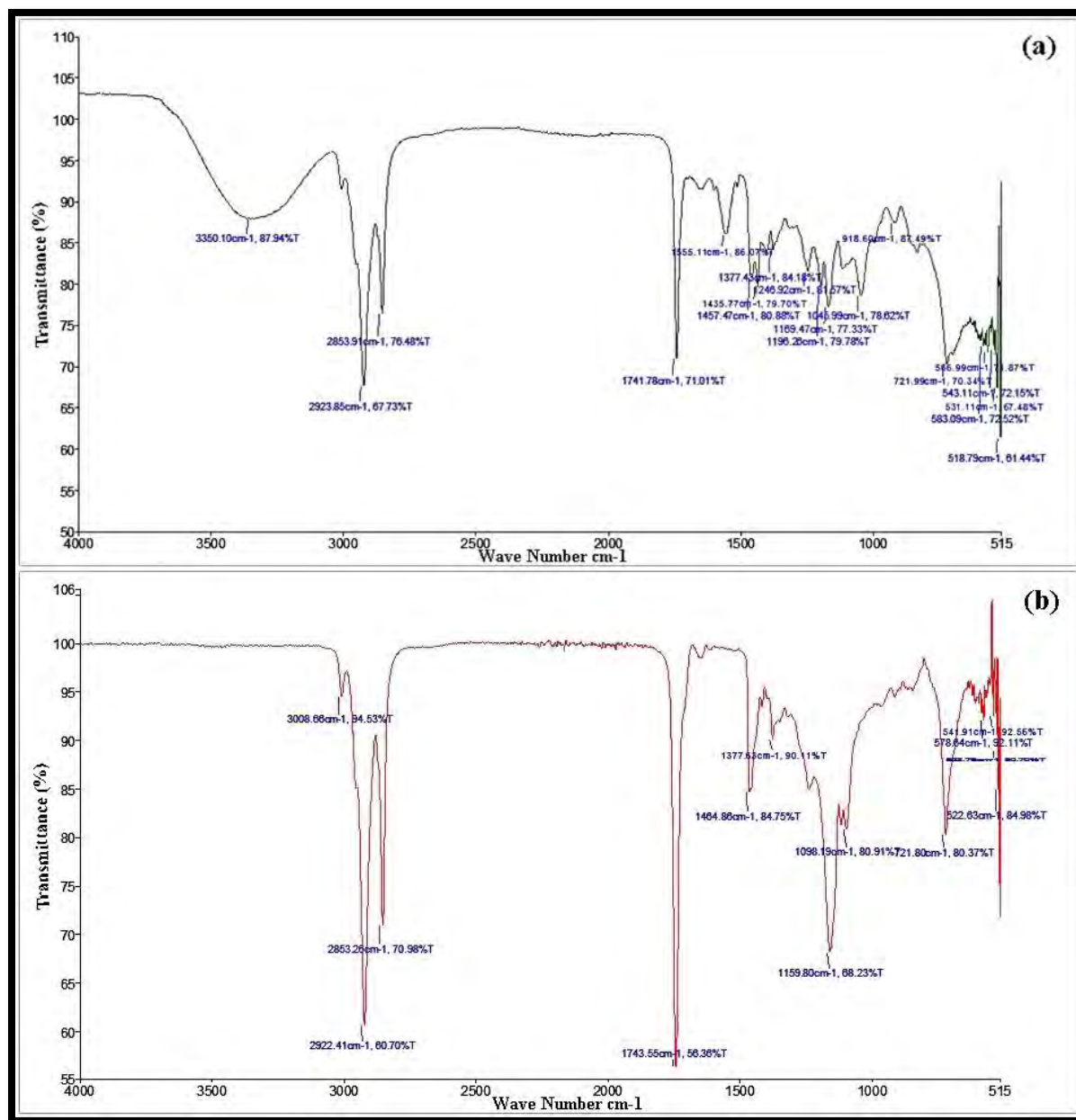
Figure 3.5. 8. FT-IR spectrum of **(a)** *Cestrum nocturnum* seed oil **(b)** *Cestrum nocturnum* biodiesel
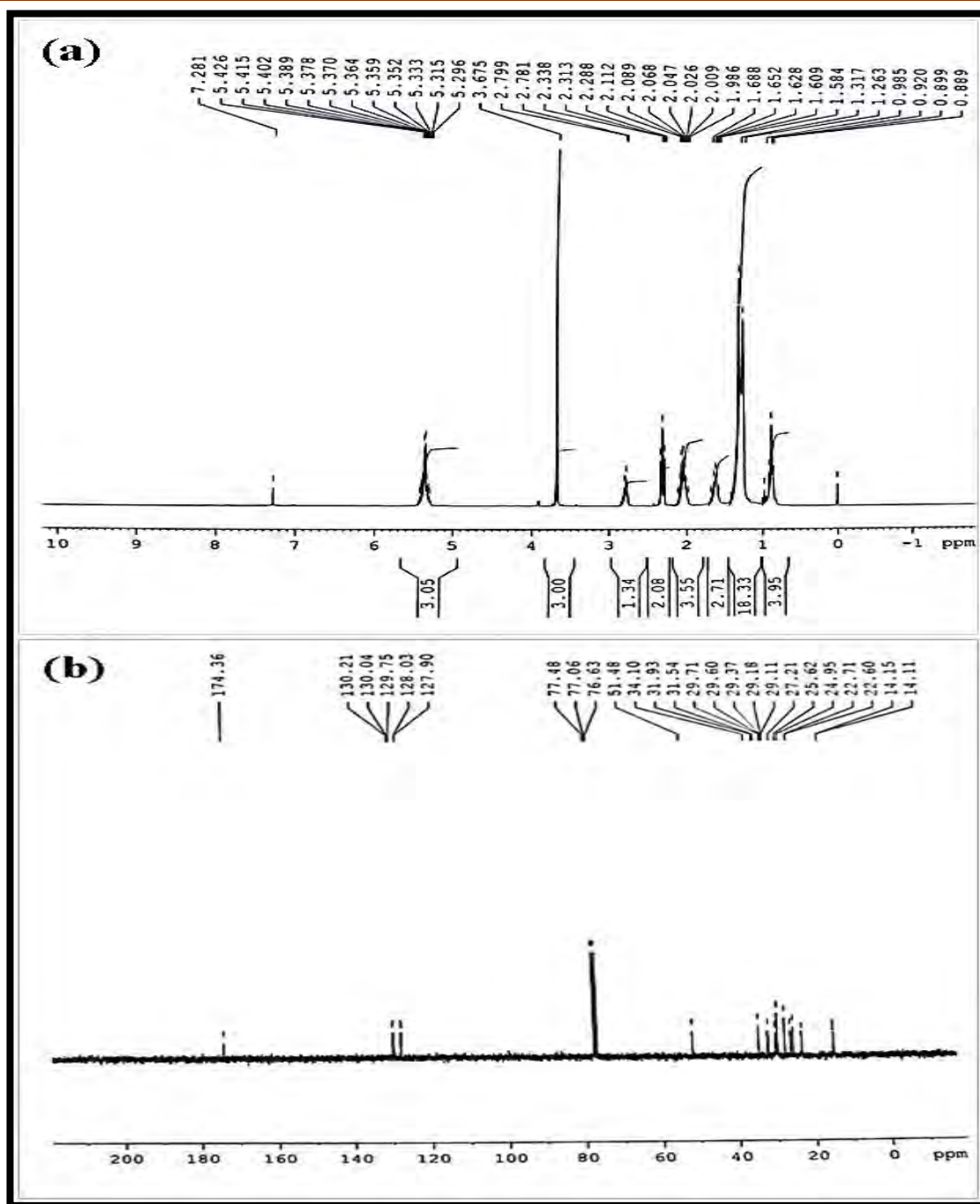
Figure 3.5.9. NMR spectrum of **(a)** ^{1}HNMR and **(b)** ^{13}CNMR of *Cestrum nocturnum* biodiesel
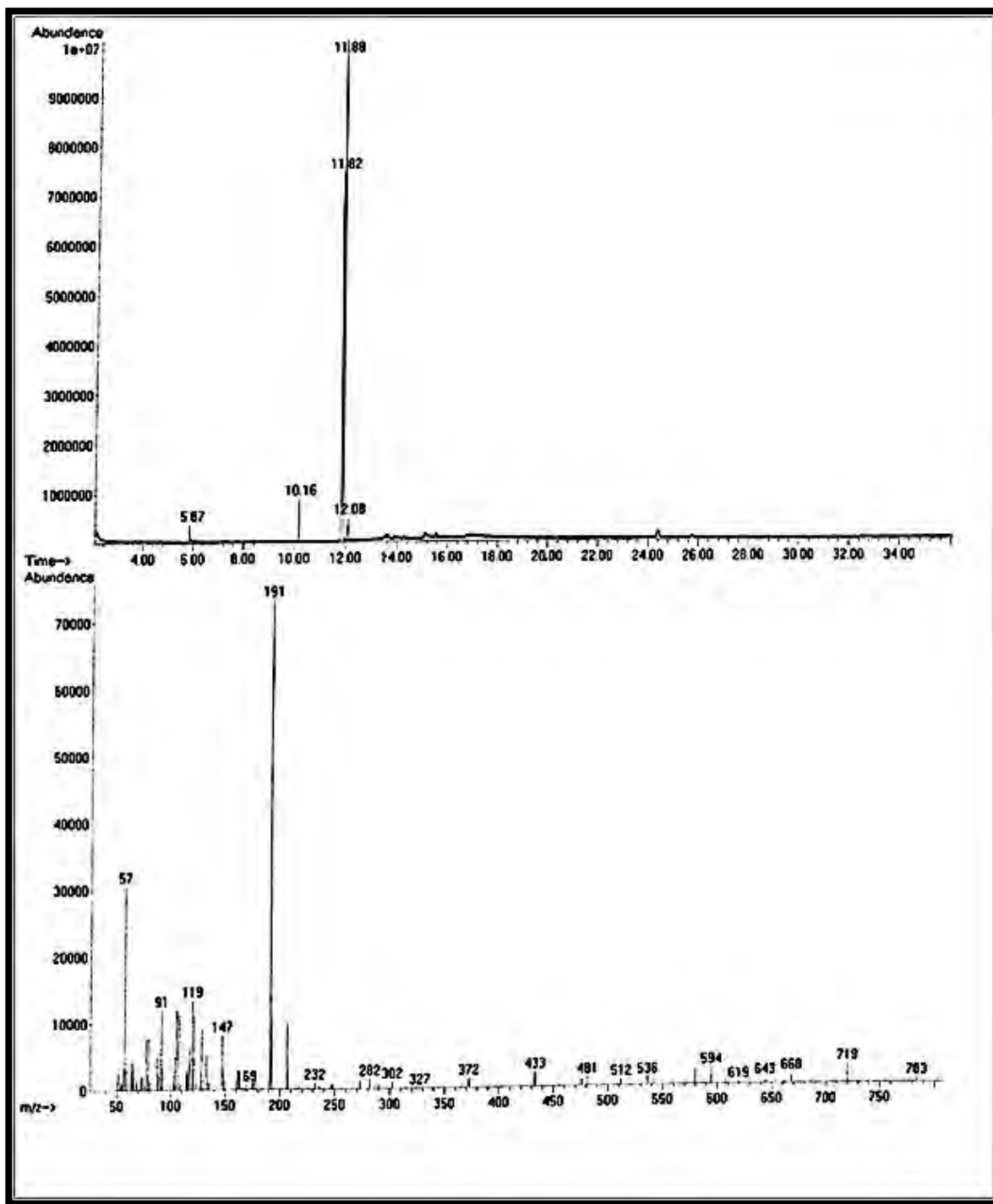
Figure 3.5.10 GC-MS spectrum of *Cestrum nocturnum* biodiesel

3.5.5. Fuel properties of *Cestrum nocturnum* Biodiesel

In order to evaluate the quality and efficiency of biodiesel in diesel engines for potential future applications, fuel parameters such as kinematic viscosity, density, flash point, pour point, iodine value, and sulfur concentration were used. As indicated in Table 3.5.4, the fuel characteristics of synthetic biodiesel made from *Cestrum nocturnum* seed oil were compared to those of international fuel standards such ASTM D-6751 and European Union 14214. Acid value is among the most crucial characteristics of biofuel. The amount of free fatty acids in the fuel has a significant impact on the acidity of biodiesel. Higher acid number levels cause corrosion in engine components, which has a detrimental impact on engine performance. However, it was discovered that CNBD's acid value was 0.342 (mg KOH/gm) and that it was well matched with international standards, indicating that it was viable for use in fuel engines (Table 3.5.4). The density of biodiesel gives information regarding its quality, purity, and fatty acid composition. It is crucial in determining the quality of fuel. The presence of unsaturated fatty acids substantially effects biodiesel density. Higher density biofuels disturb fuel engines and are not advised for practical use. In the current investigation, biodiesel density was found to be 0.815 (g/cm^3), which is below the range of international norms (Table 3.5.3). It said that synthetic biodiesel can be utilized as an environmentally benign alternative to petroleum diesel in diesel engines without having any detrimental effects.

The combustion, fuel blending, and spray fuel processes all heavily rely on biodiesel's kinematic viscosity (Kg/m^3 at 40 ∘C). The stickiness index of biofuels is another name for it. High viscosity biofuels cause problems with ignition because of partial combustion and particulate matter emission. The kinematic viscosity of *Cestrum nocturnum* biodiesel was determined in the current study to be 5.45 (mm^2/s), which is equivalent to international standards. The term "flash point" for biodiesel refers to the temperature at which the fuel ignites and flashes. It is regarded as a crucial instrument for safety precautions and other engine performance-related issues, such as legal safety insurance and transportation regulations for fire. It is greatly impacted by the methanol level of the biodiesel that is produced. The flash point will be smaller the higher the methanol content. The CNBD's flash point was 99 ∘C, which was found to be well matched to the European Union 14214 and ASTM D-6751 requirements. Though less volatile than petro diesel, biodiesel with greater flash values (>66 ∘C) is thought to be safer. Pour

point and cloud point are two important biodiesel cold flow qualities that must be taken into mind, especially in colder parts of the world. These characteristics rely on the kind and number of contaminants in biodiesel. Due to the formation of crystal nuclei at lower temperatures, biodiesel becomes milky and changes how it flows. Commercially available chemicals and antioxidants can be used to improve it. The viscosity of the crude oil used to make biodiesel is directly correlated with the pour point of the methyl ester. *Cestrum nocturnum* biodiesel pour and cloud points were discovered to be -11 °C and -8 °C, respectively. *Cestrum nocturnum* biodiesel has a sulfur level of 0.0001 (wt.%), showing that synthetic biodiesel is safe and favorable to the environment.

Table 3.5.4 - Comparison of Fuel properties of previously reported biodiesel sources with that of *Cestrum nocturnum* biodiesel fuel properties**.**

Property	Methods	*Cestrum nocturnum*		ASTM D-6751	EN-14214	China GB/T 20828-2007
		Mean	**St.Dev.**			
Color	Visual	1.5	-	2.0		
Acid number (mg KOH/g)	ASTM-D974	0.342	0.1	≤0.5	≤0.8	≤0.5
Flash Point (°C)	ASTM-D93	99	1.4	≥93	≥130	≥120
Pour Point (°C)	ASTM-D97	-11	0.2	-15-16	_	_
Viscosity (mm²/s at 40 °C.)	ASTM-D445	5.45	0.5	1.9-6.0	_	3.4-5.0
Density (kg/m³ at 40 °C)	ASTM-D1298	0.815	0.06	≤120	_	≤120

| Sulphur content (wt.%) | ASTM-D4294 | 0.0001 | 1 | ≤0.05 | ≤0.05 | ≤0.20 |
| Cloud point (°C) | ASTM-D2500 | -8 | 1 | -3.0-12 | _ | _ |

3.5.6. Catalyst Reusability

Sb_2O_3 nanoparticles' ability to be recycled was investigated in order to assess its stability and economic sustainability in subsequent cycles. The methods used to clean and separate the catalyst from the reaction mixture have a significant impact on the catalyst's ability to be reused (Suresh et al., 2018). Reusability of the generated Sb_2O_3 nanoparticles was carried out under ideal transesterification reaction conditions, including Met:Oil ratio of 8:1, catalyst loading of 0.56 (wt.%), reaction time of 180 min, and temperature of 95 ∘C.

After the first cycle of transesterification, green nanoparticles of Sb_2O_3 were recovered from the reaction mixture using the centrifugation process. The recovered particles were then cleaned with alcohol to remove impurities, dried in the oven, and then calcined for 180 min at 500 °C in the muffle furnace in preparation for reuse in the following transesterification cycles. Up to cycle seven, catalytic activity was investigated. Up to five consecutive cycles of experimental trials showed the maximum catalytic performance, producing high FAME yields of 93 to 77%. Sixth cycle was marked by a decline in methyl ester production of up to 70%. Yield fell even more, reaching 65% in the seventh cycle (Figure 3.5.11).

Chemical analysis attributes this drop in catalytic activity to the poisoning of dynamic Sb_2O_3 NP sites by organic components present in the mixture of transesterification reactants, which resulted in a decreased methyl esters production. Nevertheless, after washing and calcination in a muffle furnace, the nanoparticles' catalytic activity can be recovered.
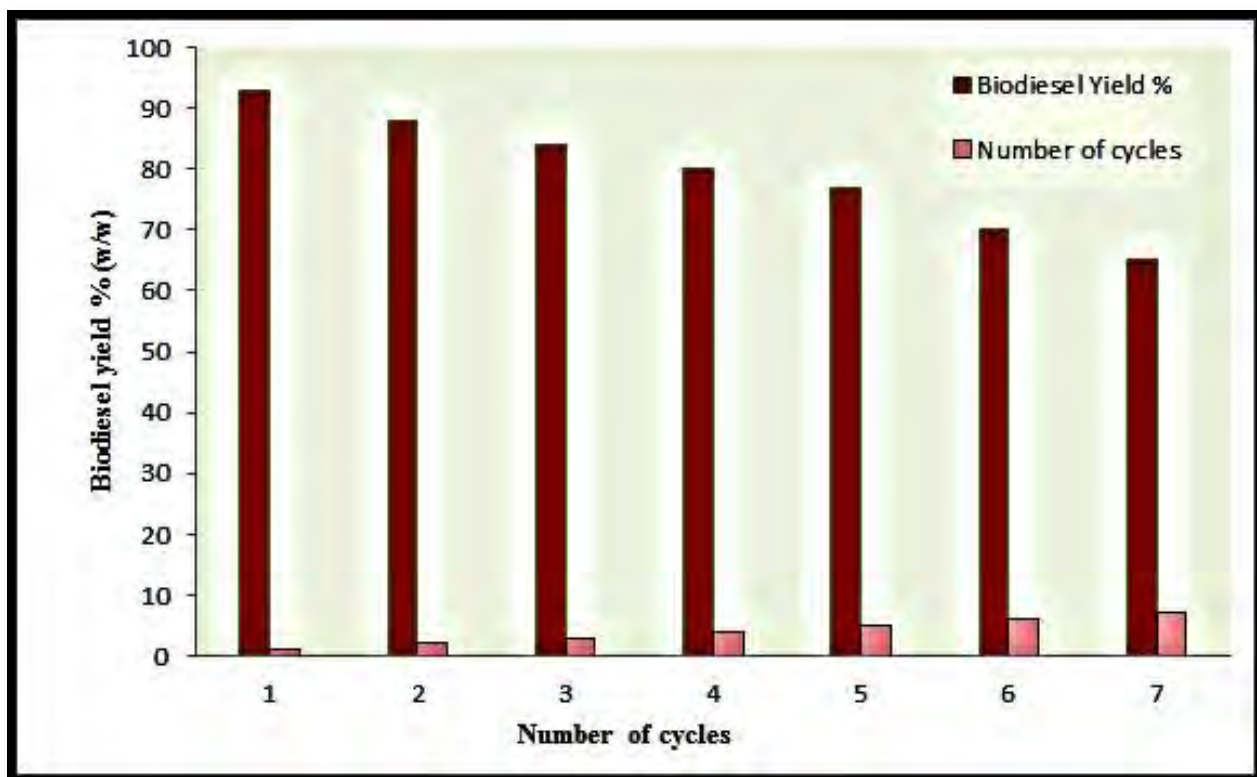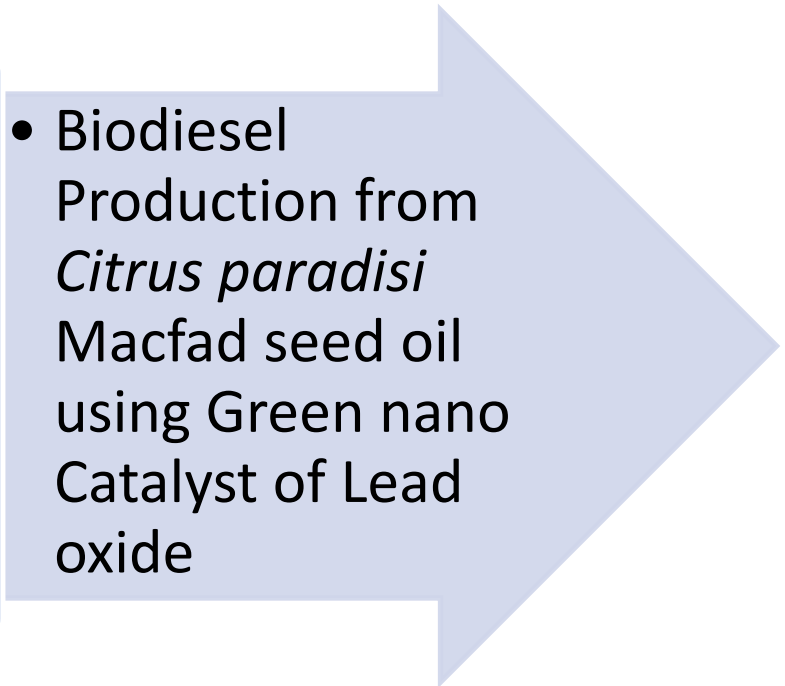
Figure 3.5.11. Reusibility of antimony oxide nanocatalyst in transesterification

SECTION VI

- Biodiesel Production from *Citrus paradisi* Macfad seed oil using Green nano Catalyst of Lead oxide

PbO nanoparticles have been investigated as a very effective, straightforward, affordable, and recyclable catalyst for the quick synthesis of biodiesel. Leaf extract of *Nasturtium officinale* efficiently reduced $PbSO_4$ into PbO in the current investigation.

3.6.1 Characterization of PbO Nano-catalyst

3.6.1.1 X-Ray Diffraction (XRD) of PbO

One of the crucial methods for identifying the fundamental makeup, dimensions, and crystalline structure of produced phyto-nanoparticles is X-ray diffraction. Figure 3.6.1 shows the XRD diffractogram of a nano zinc oxide catalyst. Peaks in Diffracted Energy spectrum were observed at 2θ values of 25.26, 29.36, 32.06, 45.58, 52.45, 55.03, and 64.43, which were associated with the lattice planes 010, 111, 002, 011, 020, 121, 220, and 311 hkl, respectively. The crystalline size of lead oxide nanoparticles using the XRD pattern of the deepest peak at 2θ value of 32.06 (highest peak 002).

The average size of lead oxide nanoparticles was 42 nm, suggesting that lead oxide is a naturally occurring phyto-catalyst. Results for PbO from SEM and X-Ray Diffraction are congruent with one another.

3.6.1.2 Scanning Electron Microscopy (SEM) of PbO

The surface morphology (shape, structure, and size) of nanoparticles was investigated using SEM. A SEM image of lead oxide nanoparticles is shown in Figure 3.6.2. Due to the polarity and electrostatic attraction of the nano-particles, the topical view of the nano catalyst revealed orthorhombic and uniform granular morphology with negligible agglomeration. Due to the agglomeration of smaller nanoparticles, larger nanoparticles were seen in the SEM image. Our findings are consistent with earlier observations that have been recorded (Arulmozhi and Mythili 2013).

3.6.1.3 Energy Diffraction X-ray (EDX) of PbO

Energy diffraction was used to examine the elemental structure of lead oxide nanoparticles (EDX). Figure 3.6.3 displays the EDX spectrum of PbO. The spectrum's great purity revealed the key phase of Pb and O. There were 56.14% and 43.86% mass percent of Pb and O, respectively. Additionally, the EDX spectrum showed no other pointless peak, proving that green nanoparticles are devoid of contaminants and additional elements.

3.6.1.4 Fourier Transform Infrared Spectroscopy (FTIR)

Figure 3.6.4 shows the FTIR spectra of absorbance-mode zinc oxide nanoparticles. The PbO spectra showed two unique IR peaks, namely those at 1023 cm^{-1} and 2381 cm^{-1}, which were attributed to Pb-O stretching. The O-H group of adsorbed water molecules has a peak at 787 cm^{-1}. The absorbance peaks in the FTIR spectra of metal oxides are typically in the 400–600 cm^{-1} IR range. The absence of any further unnecessary peaks demonstrated the purity of the produced green lead oxide nano-catalyst.

3.6.1.5 Thermogravimetric analysis (TGA) of PbO

Thermogravimetric analysis was used to examine the bulk breakdown characteristics of lead oxide. In Figure 3.6.5a and b, a thermogram of PbO nanoparticles and a matching derivative thermogram are shown. PbO underwent three primary phases of decomposition. At first, 1.7% of the original weight was rapidly lost during decomposition at temperatures between 100 ◦C and 200 ◦C. Due to dehydration at the molecular surface, weight loss of about 1.7% was seen in the bulk mass.

Indicating significantly higher thermal durability of PbO with effective catalytic activity, the second phase of thermal deterioration (0.16%) was found at the temperature range of 210 °C to 400 °C. While the third stage of thermal degradation was observed at the temperature range of 500 °C to 700 °C, further conversion (0.14%) of green nanoparticles took place and which further sped up the transition to thermal constancy. The derivative curve (wt.%) shown in Figure 3.6.5b represents the endothermal peaks of PbO.
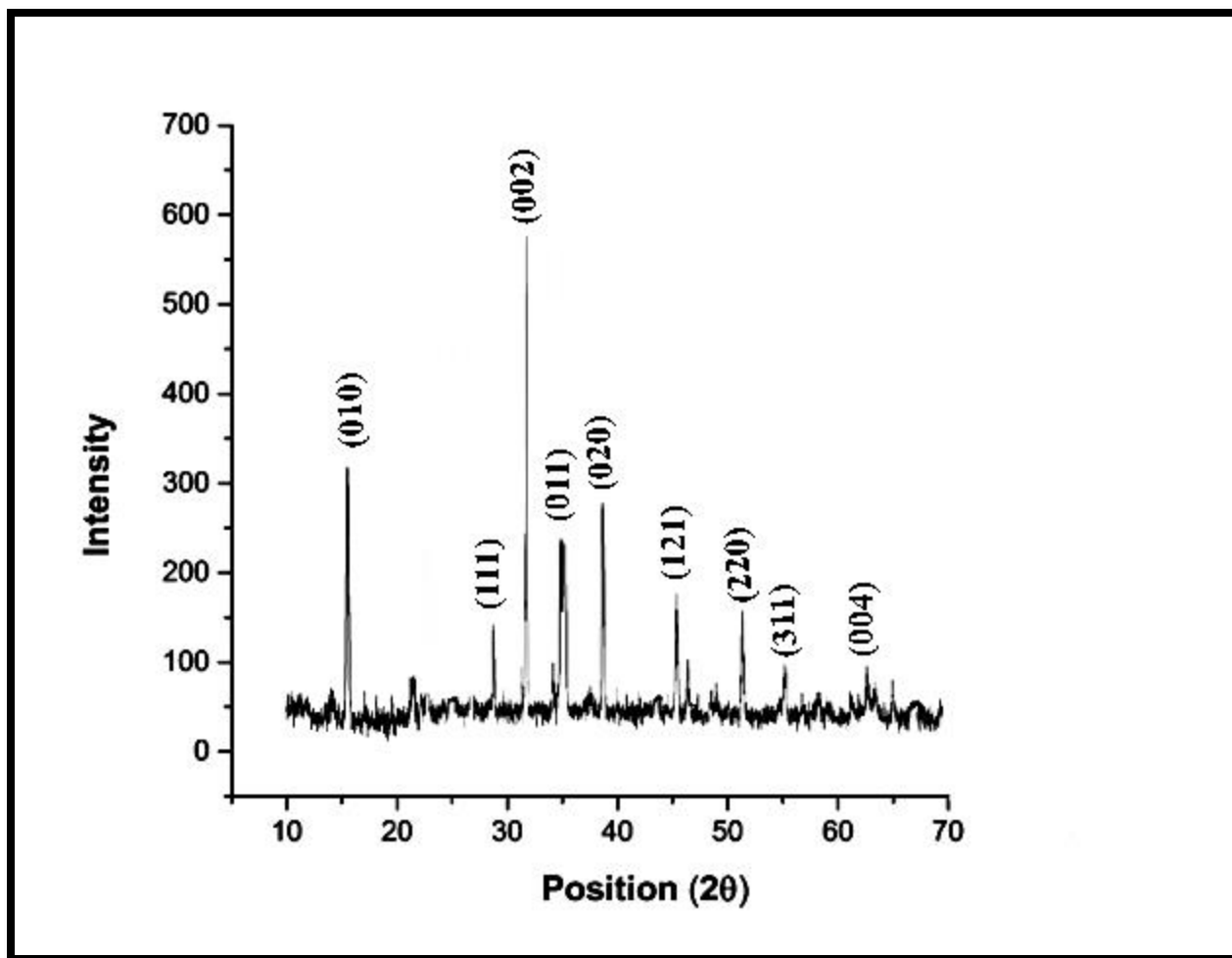
Figure 3.6.1. XRD pattern of calcined lead oxide nanocatalyst
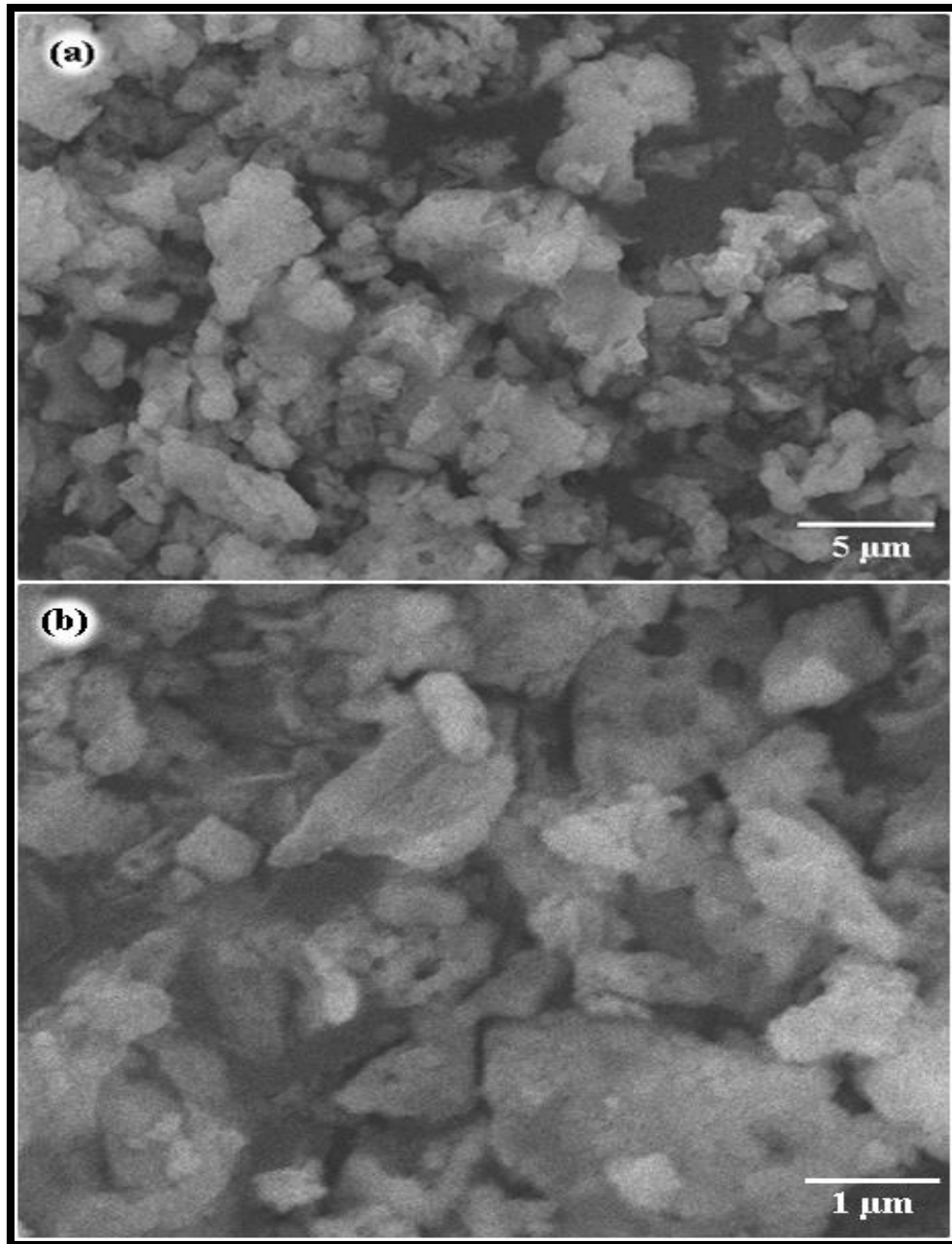
Figure 3.6.2. Scanning electron micrographs of lead oxide nanocatalyst
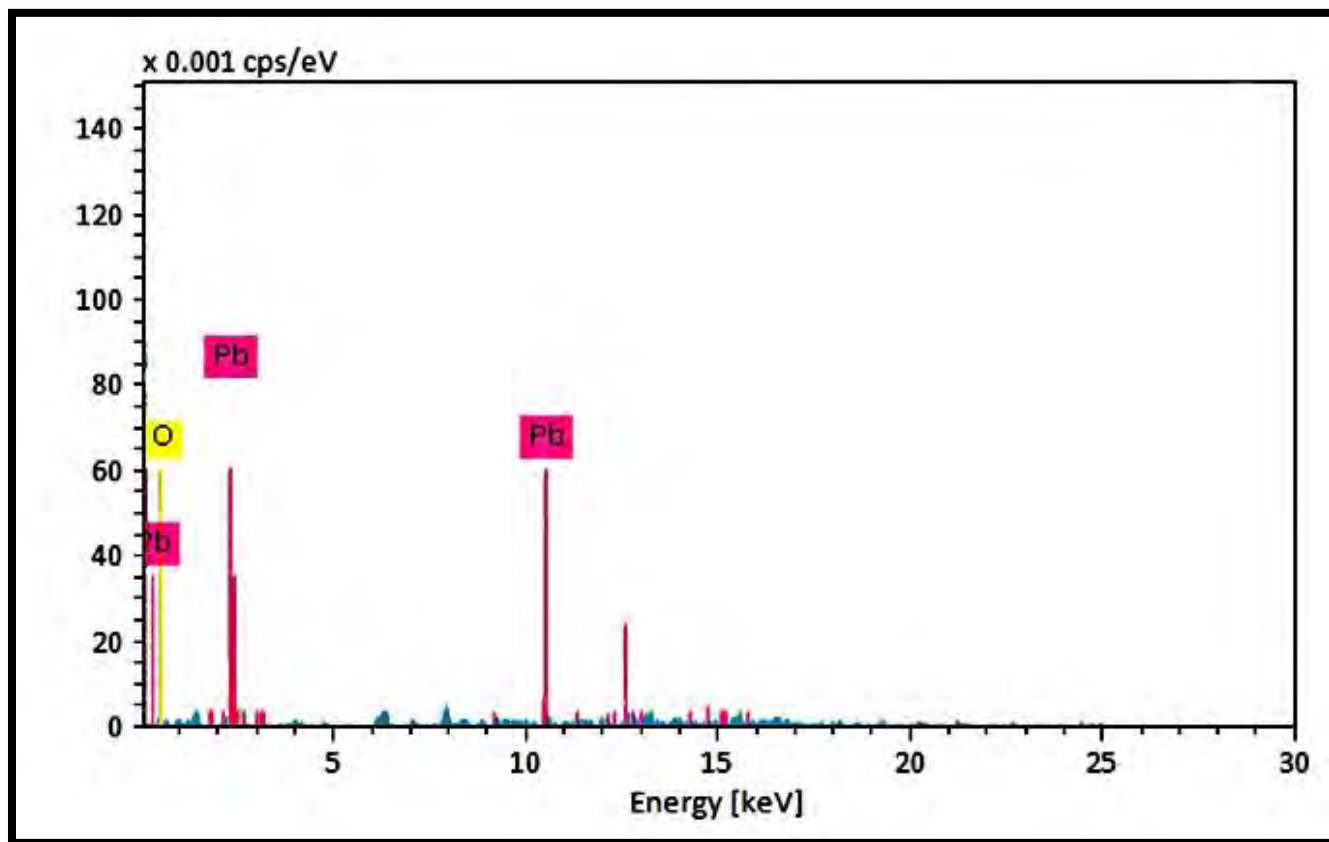
Figure 3.6.3. Energy diffraction X-Ray (EDX) of lead oxide nanocatalyst
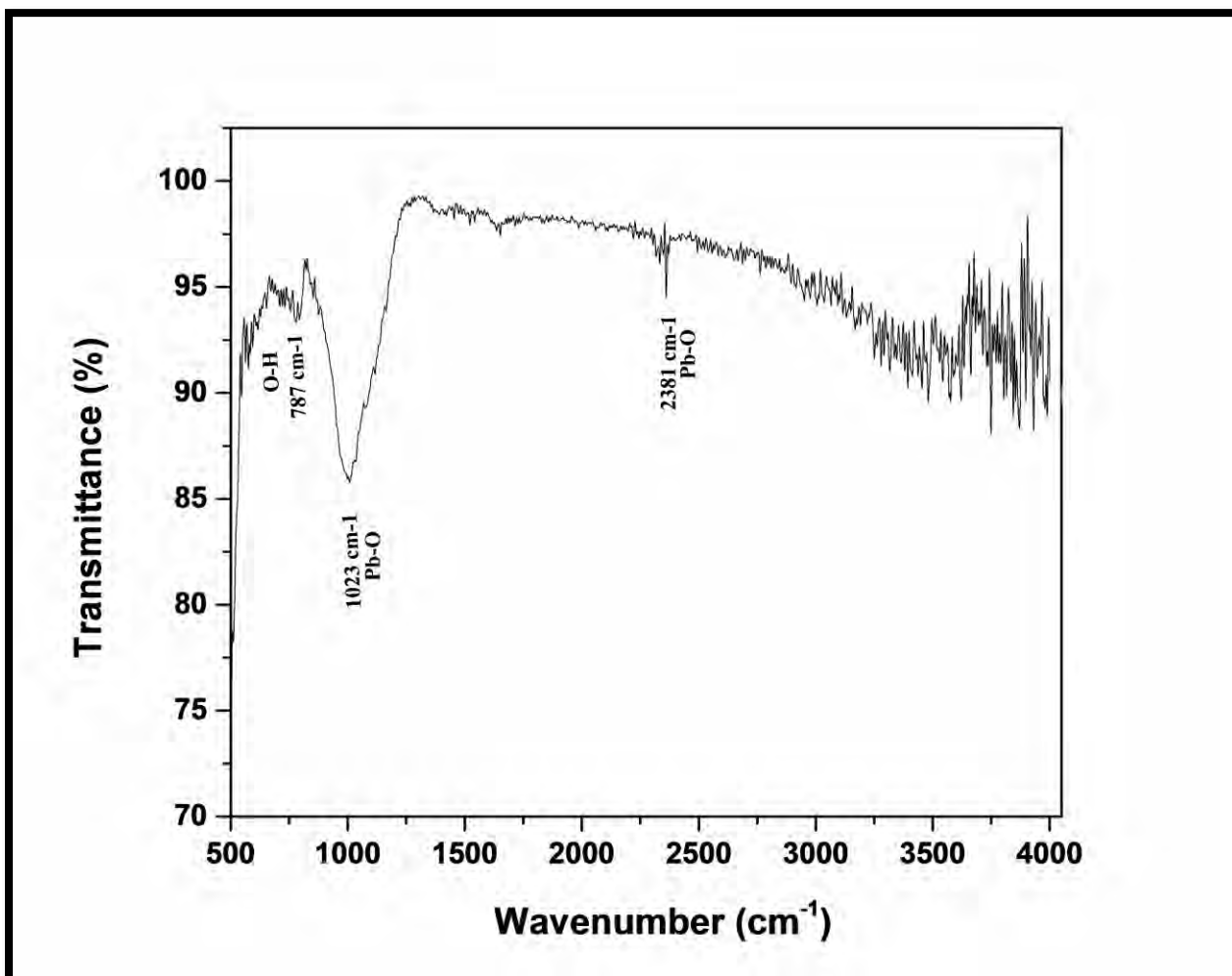
Fig. 4. FT-IR spectrum of indium oxide nanocatalyst
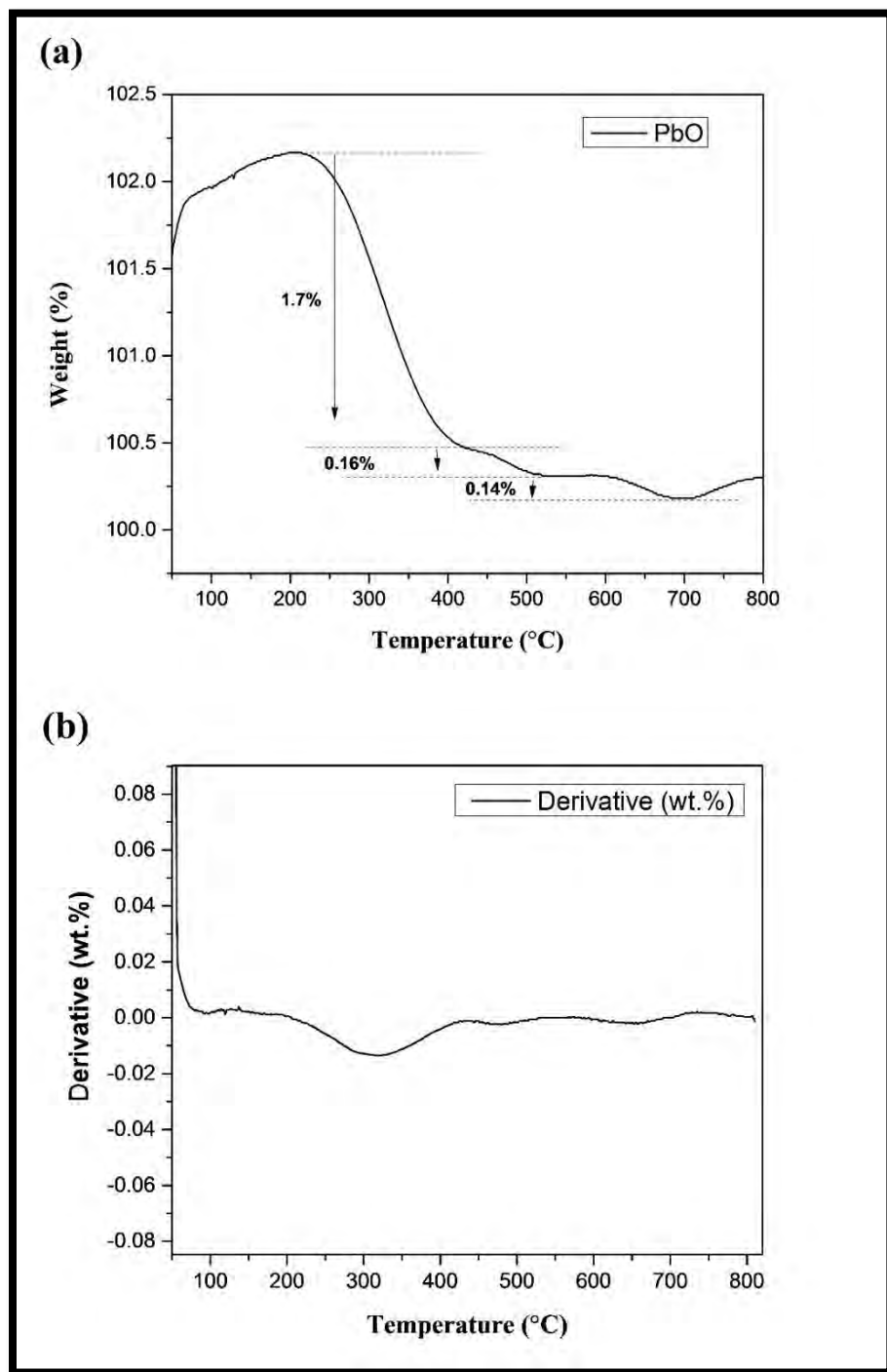
Figure 3.6.5. (a) TGA of lead oxide nanocatalyst (b) derivative thermogram of indium oxide nanocatalyst

3.6.2 Biodiesel synthesis via transesterification

Due to its compatibility and high potential, *Citrus paradisi* Macfad crude seed oil was tested for the green synthesis of biodiesel using PbO nanoparticles made from Portulaca oleracea. At room temperature, it looked yellow. *Citrus paradisi* Macfad non-edible seeds have a high oil content of 30% (w/w) and have a promising future in the production of biodiesel. It was discovered that the free fatty acid content of seed oil was 2.06 (wt. %) less than the restricted limit of 3 percent, leading to a single-step transesterification process without a subsequent esterification step.

Reaction variables including catalyst concentration, reaction duration, temperature, and oil to methanol ratio have a substantial impact on biodiesel yield. So, a number of tests were run to determine the ideal circumstances for reactions. With the aid of trial version 13 of Design of Experiment, a Central Composite Design experimental design was created for this purpose utilizing Response Surface Methodology (RSM) (DOE). Model is quadratic and has four independent variables: (A) oil to methanol ratio of 3:1–12:1, (B) catalyst concentration of 0.17–0.47 wt%, (C) temperature of 50–110 ∘C. and (D) reaction duration of 60–150 mins, (Table 3.6.1). Table 3.6.2 shows the percentage production of biodiesel that was attained through various transesterification trials. Table 3.6.3 summarizes the findings of a statistical analysis of variance (ANOVA) for the quadratic model. The percent production of methyl ester was predicted using the quadratic polynomial equation (6) in terms of coded factor.

Biodiesel Yield% $=+85.64+1.56*A-1.78*B-0.5629*C+2.76*D-2.00*AB-1.25*AC+1.50*AD+0.4534*BC+1.38*BD-1.60*CD-12.05*A^2-5.26*B^2-6.45*C^2+0.6770*D^2$

(12)

In Figure 3.6.6, the projected and actual yields of biodiesel are compared. Both sets of data are distributed close to a straight line, demonstrating a good connection between the two yields of methyl ester. The Response Surface quadric model underwent statistical analysis of variance (ANOVA), and the outcomes are shown in Table 3.6.3. The quadratic model was deemed significant by the ANOVA results with a *p*-value of < 0.0001. Additionally, the present model's lack of fit F-value, which was 0.736, was deemed to be non-significant. Overall, it was

discovered that the generation of biodiesel was significantly influenced by four distinct transesterification factors, including the oil to methanol ratio, catalyst concentration, reaction time, and reaction temperature. The Coefficient of determination (R^2) value was used to determine how accurately the response values of the quadratic model were predicted. The adjusted R^2 was 0.871, while the expected R^2 was 0.779, with a variance of less than 0.2. The ratio of signal to noise is a measure of an experimental model's precision. The significant model requires a ratio greater than 4. The experimental model's competence is revealed by the coefficient of variance (CV), which must be less than 10%. In the current model, the value of CV was found to be 6.95 percent (10%). All of these numbers led to the conclusion that the quadratic model is important.

Table 3.6.1- Experimental design by central composite design for transesterification reaction

Process parameters	−1	+1
Methanol to oil ratio	3:1	12:1
Catalyst loading (wt. %)	0.17	0. 47
Reaction time (min)	60	150
Temperature (◦C)	50	110

\

Table 3.6.2- Detailed experimental result for transesterification reaction of *Citrus paradisi* Biodiesel

	Factor 1	Factor 2	Factor 3	Factor 4	Response
Run	A: Alcohol to oil molar ratio	B: Catalyst loading wt.%	C: Temperature °C	D: Reaction time (min)	Yield wt.%
1	7.1	0.32	80	105	93
2	7.1	0.32	50	105	77
3	3.1	0.17	110	60	65
4	3.1	0.47	80	105	60
5	3.1	0.17	110	150	58
6	7.1	0.32	50	60	69
7	12.1	0.32	80	105	72
8	7.1	0.47	80	105	85
9	3.1	0.32	50	105	54
10	3.1	0.32	50	105	63
11	7.1	0.17	80	105	80
12	7.1	0.47	80	105	75
13	12.1	0.32	80	150	74
14	7.1	0.32	50	150	66
15	7.1	0.47	80	150	90
16	7.1	0.32	50	60	70
17	12.1	0.17	80	105	68
18	3.1	0.17	50	60	60
19	7.1	0.32	80	60	71
20	3.1	0.47	50	150	67
21	12.1	0.32	110	105	60
22	3.1	0.47	50	60	57
23	7.1	0.32	110	60	63
24	7.1	0.17	80	60	57

25	7.1	0.47	50	105	55
26	7.1	0.17	110	105	80
27	3.1	0.32	80	150	64
28	3.1	0.17	80	105	54
29	7.1	0.45	80	105	75
30	12.1	0.17	110	150	70

Table 3.6.3- ANOVA for Response Surface Quadratic model

Source	Sum of Squares	df	Mean Square	F Value	p-value	
Model	3045.00	14	217.50	8.99	< 0.0001	significant
A-Methanol to oil Ratio	43.56	1	43.56	1.80	0.0396	
B-Catalyst Concentration	62.44	1	62.44	2.58	0.0290	
C-Temperature	6.47	1	6.47	0.2674	0.0126	
D-Time	150.47	1	150.47	6.22	0.0248	
AB	64.00	1	64.00	2.65	0.0247	
AC	25.00	1	25.00	1.03	0.0255	
AD	36.00	1	36.00	1.49	0.0413	
BC	3.42	1	3.42	0.1413	0.0123	
BD	30.25	1	30.25	1.25	0.0411	
CD	43.26	1	43.26	1.79	0.0010	
A²	529.19	1	529.19	21.88	0.0003	
B²	113.45	1	113.45	4.69	0.0469	
C²	141.38	1	141.38	5.84	0.0288	
D²	1.57	1	1.57	0.0647	0.8027	
Residual	362.86	15	24.19			
Lack of Fit	362.86	13	27.91	3.368	0.736	not significant
Pure Error	0.0000	2	0.0000			
Cor Total	2750.97	29				

$R^2 = 0.871$, Std. Dev. = 3.89,   C.V. % = 6.95, Adeq Precision = 9.9533
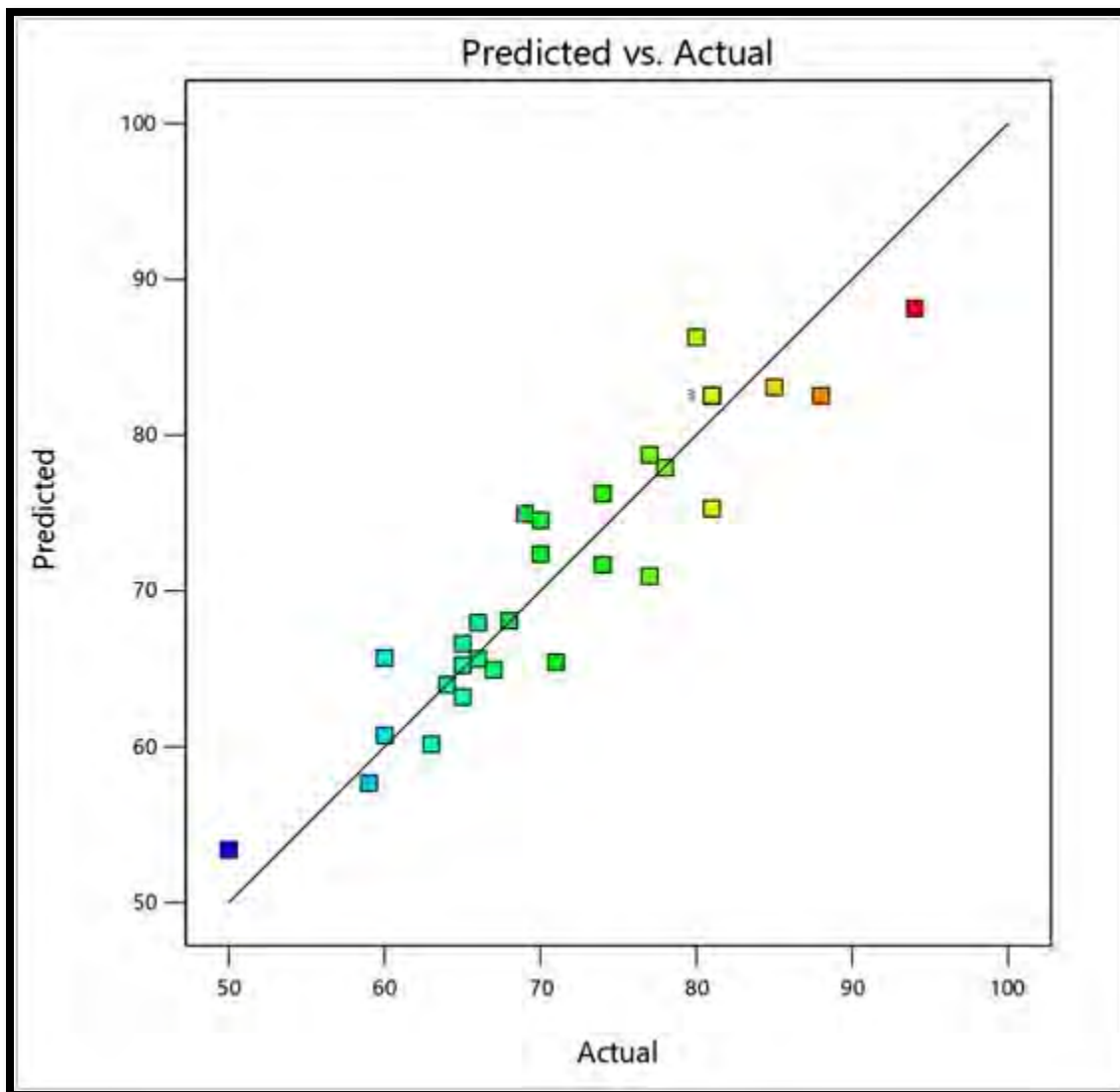
Figure 3.6. 6. Comparison between the experimental and predicted yield of biodiesel in the model

3.6.3 Influence of reaction parameters on transesterification reaction

3.6.3.1 Combined influence of methanol to oil ratio and catalyst loading

While keeping the other reaction parameters at their ideal values, the combined effect of the methanol to oil molar ratio and the catalyst loading was studied. The three-dimensional plot in Figure 3.6.7a illustrates the relationship between the catalyst loading and the methanol to oil molar ratio. The highest yield of 93% was noted to be attained at run 1 with the following reaction parameters: methanol to oil ratio of 7:1, catalyst loading of 0.32 (wt.%), reaction time of 105 min., and temperature of 80 ◦C. With the same methanol to oil ratio (Run 8) of 7:1, increasing the catalyst loading up to 0.47 wt.% significantly reduced percent yield to 85%. A catalyst loading of 0.47 (wt.%), a further drop of up to 60% was observed with low molar ratio of 3:1 (Run 4). The 3-D figure clearly showed that a higher methanol to oil ratio of 12:1 with the catalyst loading of 0.17 wt.% resulted in a poor yield of 68% (Run 17) due to an increase in glycerol solubility, which also causes problems with phase separation (Baskar et al., 2017). The lowest yield of 54% of FAMEs was achieved with a methanol to oil ratio of 3:1 and catalyst loading of 0.17 (wt.%), since larger catalyst loading as well as lower methanol to oil ratios both failed to conduct transesterification out to completion (Run 28). According to the ANOVA results, the influence of the catalyst loading and methanol to oil molar ratio is not significant with a *p*-value of 0.0247 (>0.05).

3.6.3.2 Combined influence of methanol to oil ratio and temperature

One of the most important interacting parameters driving transesterification is the interaction between the influence of temperature and the methanol to oil ratio. In a three-dimensional plot based on a central composite design in Figure 3.6.7b, the combined effects of the methanol to oil molar ratio and reaction temperature on the transesterification reaction of *Citrus paradisi* seed oil have been shown. The reaction conditions of methanol to oil ratio 7:1, catalyst loading 0.32 (wt.%), reaction duration 105 min., and temperature 80 ◦C resulted in the highest yield of 93% of FAMEs (Run 1). Low yield of 70% was achieved with a lower methanol to oil ratio of 3:1 at the same reaction temperature (85 ◦C) (Run 27). Low yield of 63 % was achieved with a higher methanol to oil ratio of 13:1 at reaction temperature of 50 ◦C. (Run 10). Due to the limited mass transfer between the various phases of the reacting mixture, a low yield

of 54% was obtained at a methanol to oil ratio of 3:1 and a low reaction temperature of 50 ◦C (Run 9) (Aransiolaet al., 2013). Like this, low yield of 60% was obtained at a higher reaction temperature of 110 ◦C and a methanol to oil ratio of 12:1 (Run 21). It is believed to be caused by the fact that the rate of methanol evaporation in the reacting mixture increases beyond temperatures of 70 ◦C (Meng et al., 2009). Based on the findings of the ANOVA, it was determined that the combined effect of temperature and the methanol to oil ratio is significant with a *p*-value of 0.0255 (<0.05).

3.6.3.3 Combined influence of methanol to oil ratio and reaction time

Figure 3.6.7c shows a 3-D depiction of the combined effects of the methanol to oil ratio and reaction time. At run 1, with reaction parameters of methanol to oil ratio of 7:1, catalyst loading of 0.32 (wt.%), reaction time of 105 min, and temperature of 80 ◦C, a high biodiesel yield of 93% was attained. As can be observed, despite keeping the other two reaction parameters constant, a greater methanol to oil ratio of 12:1 at run 13 with a reaction time of 150 min led to a low yield of 74%. A reduction in the production efficiency of biodiesel and a compact yield of up to 80% were observed with a methanol to oil ratio of 7:1 and a reaction period of 60 min (Run 19). According to research, a lower methanol to oil ratio of 3:1 and a longer reaction time of 150 min resulted in a poor yield of 64% (Run 27) because not enough methoxide solution combined with the oil (Maina et al., 2017). The experimental model's ANOVA results showed that the combined interaction between oil to methanol ratio and reaction duration was statistically significant (*p*-value 0.0413).

3.6.3.4 Combined influence of catalyst loading and temperature

The most important transesterification reaction parameters are catalyst loading and reaction temperature. Both play a big part in regulating the transesterification reaction's pace. Figure 3.6.7d shows the combined effect of catalyst loading and reaction temperature on the % yield of methyl esters. At run 1 with reaction conditions of methanol to oil molar ratio 7:1, catalyst loading 0.32 (wt.%), reaction period 105 min., and temperature 80 ◦C, maximum yield of 93% of biodiesel was observed. According to experimental findings, yield was lowered by up to 89% due to a high catalyst loading of 0.45 weight percent at the same reaction temperature (80 ◦C) (Run 29). Low reaction temperature of 50 ◦C and catalyst loading of 0.47 wt% resulted in a lowest yield of 50%. (Run 25). Furthermore, run number 26 had the low yield of 80% due to a

high reaction temperature of 110 ◦C and a catalyst loading of 0.17 (wt.%). With a *p*-value of 0.0123 (<0.05), the ANOVA results showed that the combined interaction of catalyst loading and temperature was significant.

3.6.3.5 Combined influence of reaction time and catalyst loading

While maintaining the other two reaction parameters (reaction temperature and oil to methanol molar ratio) constant, the combined effect of catalyst loading (B) and reaction duration (D) on transesterification has been shown in the form of a 3D figure in Figure 3.6.7e. Both factors had a similar impact on biodiesel production. As catalyst loading and reaction temperature increased, the percentage of biodiesel produced increased (Alaswad, et al., 2015). According to experimental results, a reaction with a methanol to oil ratio of 7:1, a catalyst loading of 0.32 (wt.%), a reaction period of 105 min, and a temperature of 80 ◦C produced the greatest yield of 93% of FAMEs (Run 1). Low yield of 88% at run 15 was caused by high catalyst loading (0.45 wt.%) and a reaction duration of 150 min. Methyl ester yield of 57% was achieved with a further decrease in catalyst loading up to 0.17 wt.% and a brief reaction period of 60 min (Run 24). With a *p*-value of 0.0411 (<0.05), the combined influence of catalyst loading, and reaction time was found to be significant in the current model.

3.6.3.6 Combined influence of reaction time and temperature

Temperature and reaction time both have a significant impact on biodiesel yield. In Figure 3.6.7f, a 3-D figure illustrating the combined effect of reaction time and temperature on transesterification is shown. Up to a certain point due to an increase in mass interaction, FAMEs yield rose accordingly with an increase in reaction time and temperature (Gupta et al., 2018). At run 1, the highest methyl ester yield of 93% was attained using the following reaction parameters: methanol to oil ratio of 7:1, catalyst loading of 0.32 (wt.%), reaction time of 105 min., and temperature of 80 ◦C. At run 6, a reaction temperature of 50 ◦C and a shorter reaction period of 60 min produced a compact yield of 69%. A lower yield of 63% resulted from a high reaction temperature of 110 ◦C and a brief reaction period of 60 min at run 23. At a low reaction temperature of 50 ◦C and a reaction period of 150 min, the FAMEs yield was further reduced to 66%. (Run 14). The combined influence of reaction time and temperature is significant, according to the ANOVA results, with a *p*-value of 0.0010 (<0.05).
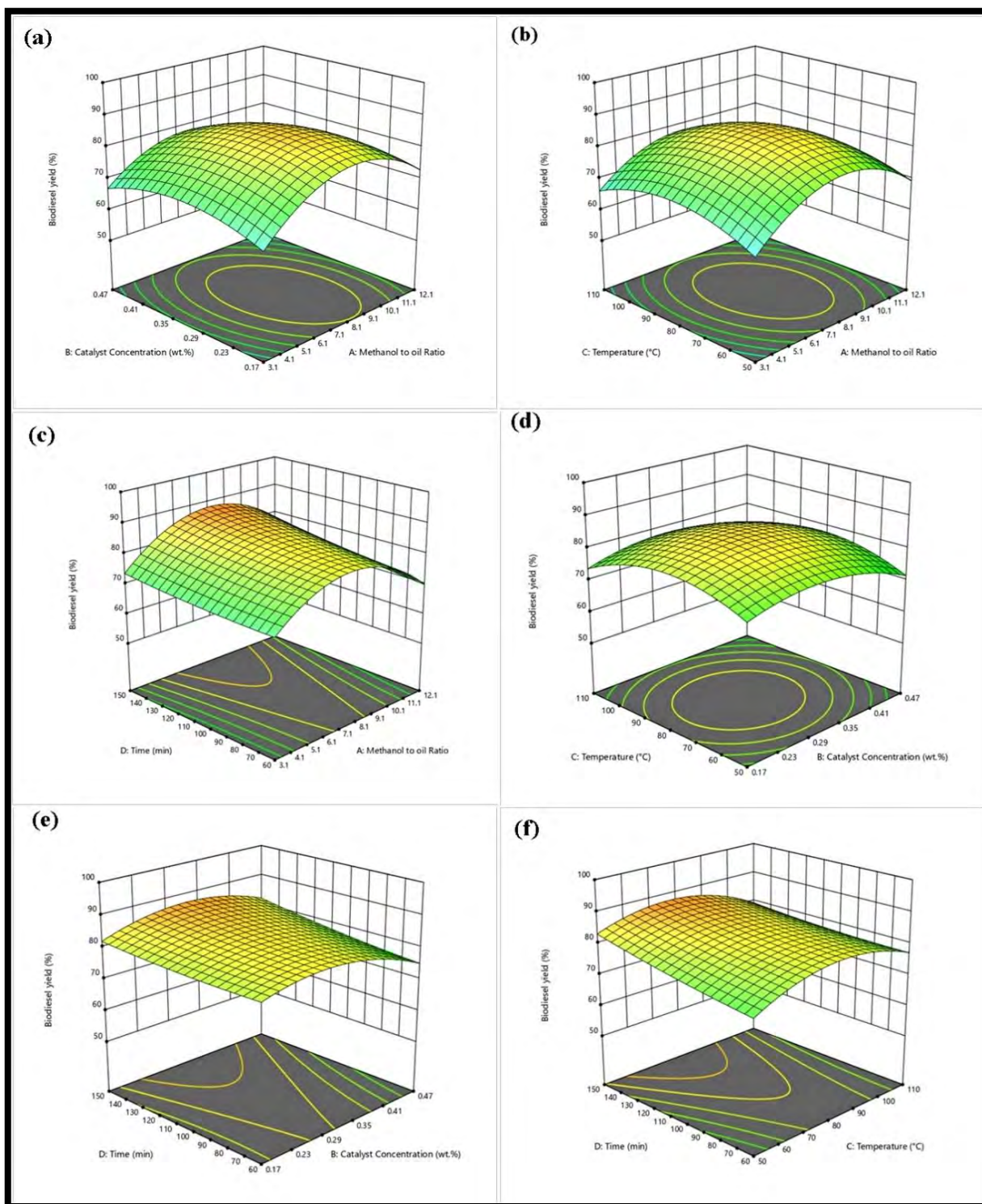
Figure 3.6.7. Impact of the reaction conditions of *Citrus paradisi* biodiesel.

3.6.4 Characterization of Biodiesel

3.6.4.1. FTIR Study

One of the established laboratory methods used to confirm biodiesel generation after the transesterification reaction is FTIR spectroscopy. The IR spectrum of biodiesel shows carbonyl and methyl group bands, which is evidence that methyl ester is produced during transesterification. The area of the biodiesel spectrum thought to be most susceptible to chemical and molecular modification is the IR region associated with the carbonyl group. Fourier-transform infrared spectroscopy (FTIR) of *Citrus paradisi* seed oil and biodiesel at the mid IR range of 500-4000 cm^{-1} was utilized. Because there are only slight differences between oil and diesel, the FTIR spectra of CISO and CIBD revealed variation in terms of absorbent frequency and band intensity (Albuquerque et al., 2009). At 1741.58 cm^{-1}, a typically deep and powerful ester (C=O) stretching was seen. There was C-O axial stretching between 1361.20 cm^{-1} and 1015 cm^{-1}. *Citrus paradisi* biodiesel showed stretching of sp^2 C-H, sp^3 C-H, and C-H bending (rocking) at 2923.35 cm^{-1}, 2843.81 cm^{-1}, and 1463.72 cm^{-1}, respectively. While the sp C-H stretch in the seed oil spectrum was seen at 3387.9 cm^{-1}, and the sp C-H (sp^2) stretching was seen at 2923.75 cm^{-1} respectively.

The impact of transesterification on oil was demonstrated by a significant shift from ester to methyl ester in the IR region between 1000-2000 and 2200-3300 cm^{-1}. The change in R1-C (OR) = O for the ester group of CISO and R1-C (OCH$_3$) = O for the methyl ester group of *Citrus paradisi* biodiesel can be represented chemically. An important signal suggesting a considerable difference between *Citrus paradisi* seed oil and biodiesel may be seen in the IR region between 1741.58 cm^{-1} and 1377.5 cm^{-1}. During transesterification reactions, the ester control peak area of the spectrum, which is located at about 1100-1000 cm^{-1}, is where changing IR regions are frequently identified. *Citrus paradisi* seed oil has a broad peak of 3287.94 cm^{-1} that was divided into two smaller peaks of 2923.35 cm^{-1} and 2843.81 cm^{-1}. Similar to this, CIBD did not show a noticeable peak at 1013.33 cm^{-1}, which implies C-H^2 wagging frequency in oil. The *Citrus paradisi* seed oil IR spectra did not exhibit the 1415.99 cm^{-1} (C=C) strong peak that was seen in the IR region of biodiesel. Therefore, the presence of FAMEs (biodiesel) has been established from all of these peaks.

3.6.4.2. NMR Spectroscopic Analysis

NMR technology is used to effectively monitor transesterification reactions because it produces characteristic reaction signals in the ^{1}HNMR and 13CNMR spectra. Figure 3.6.9a shows the 1HNMR spectrum of the biodiesel made from *Citrus paradisi* seed oil. Chemical shifts in the spectrum occur at ppm values of 0.898 (CH3 triplet), 1.265 (CH$_3$ multiplet), 1.640 (-CH2-C-OO multiplet), 5.281-5.422 ppm (-CH=CH-), and 7.280 (-CH=CH-). The aliphatic group's signal lies at 1.617-1.640 ppm and 1.253 ppm, and neither ester groups nor molecules with double bonds change this signal's chemical shift. At 5.281-5.422 ppm, signals for the conjugated double bonds' two exterior hydrogen atoms were found. The ^{1}HNMR spectrum did not contain the peak of free methanol, which is generally identified at 3.45 ppm.

One of the primary significant peaks, which was absent from the spectrum of *Citrus paradisi* seed oil, appeared at 3.659 ppm and revealed the distinctive methoxy group (- OCH3) and validated methyl ester production. The outcomes are consistent with those reported in earlier studies (Pinzi et al., 2014). Using the ^{13}CNMR spectrum, the structural properties of synthetic biodiesel were investigated. Chemical shifts for the ^{13}CNMR spectra of *Citrus paradisi* biodiesel is given in Figure 3.6.7b and are as follows (in ppm): 174.26 for carbonyl carbon (-COO-), 129.71-130.15 ppm for unsaturated and nun-conjugated carbons (-CH=CH-), 76.63-77.48 ppm for carbon atoms (-C-O), and 29.09-29.76 ppm for aliphatic methylene group. These peaks in the NMR spectrum demonstrated the existence of methyl ester in the biodiesel made from *Citrus paradisi* seed oil. The conversion rate of *Citrus paradisi* seed oil into biodiesel was calculated and the result was 92%.

3.6.4.3. GC/MS

Chemical characterization of biodiesel uses GC/MS analysis to determine the composition and percentage of different FAMEs in it. We gain extensive insight into the quality and purity of biodiesel from the GC/MS spectrum. It is an important indicator of whether a biomass source is suitable for the manufacture of biodiesel. Large amounts of saturated fatty acids in biodiesel are seen negatively since they reduce engine efficiency. Five primary peaks in the *Citrus paradisi* biodiesel's GC/MS spectrum, which are represented in Figure 3.6.10, correspond to various fatty acid methyl esters. These peaks were additionally compared using software to library reference data (NO. NIST02). Fatty acid methyl esters were identified using

their retention time. MS analysis was used to provide additional confirmation. Peaks of saturated and unsaturated fatty acids, including Decanoic acid, methyl ester (C10:0), dodecanoic acid methyl ester (C12:0), 5, 8-Octadecadienoic acid methyl ester (C18:2), 9-Octadecenoic acid, (2)-methyl-, methyl ester (C18:1) and Octadecanoic acid, methyl ester (C18:0). Major fatty acid methyl esters with greater concentrations were identified to be 5, 8-Octadecadienoic acid methyl ester. During transesterification, the saponification reaction has a significant impact on the percentage and composition of methyl esters, which lowers the efficiency at which triglycerides are converted into methyl esters. Results of GC/MS analysis showed that *Citrus paradise* seed oil is suitable for manufacturing methyl ester on a large scale.
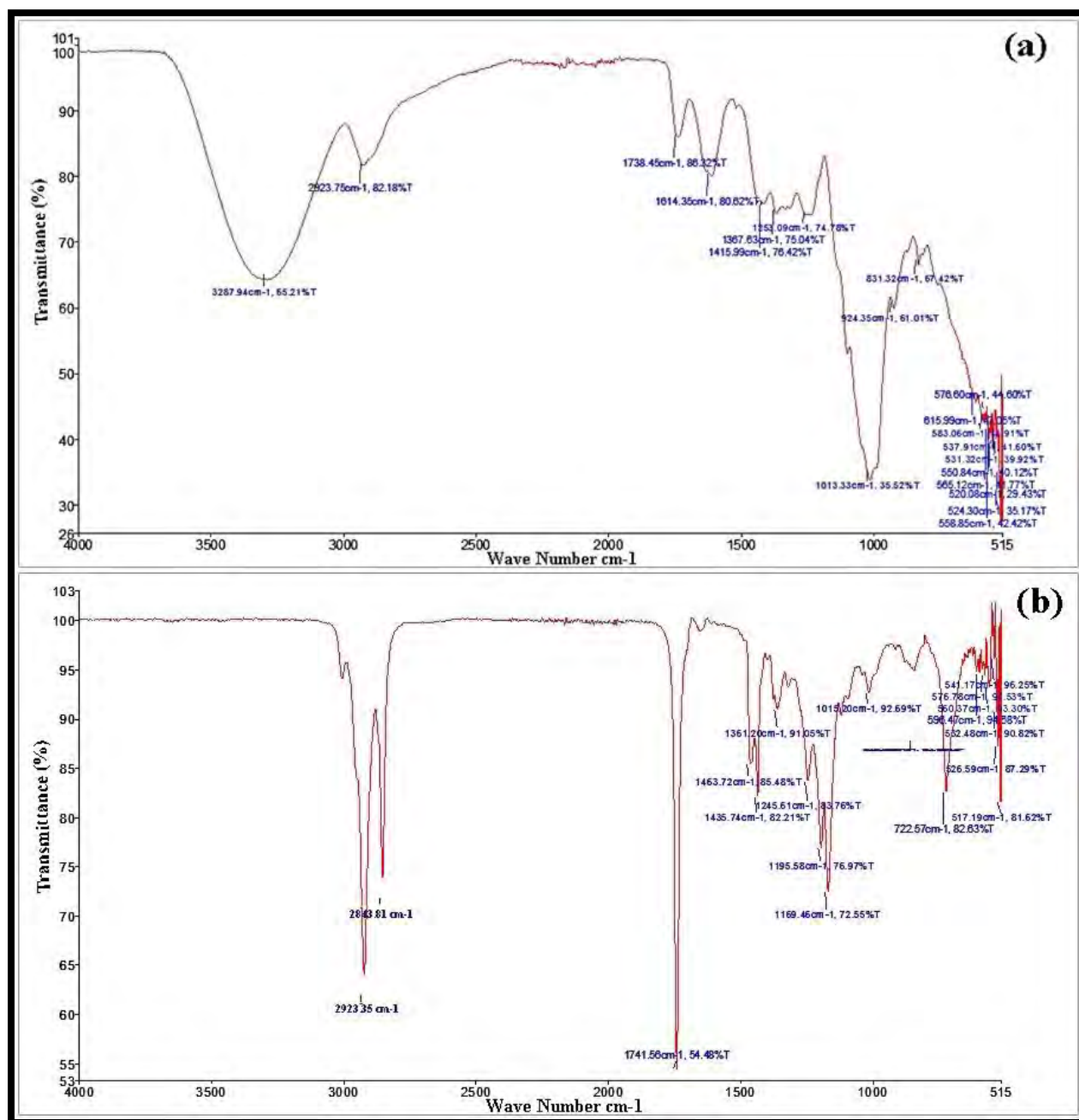
Figure 3.6.8. FT-IR spectrum of **(a)** *Citrus paradisi* seed oil and **(b)** biodiesel
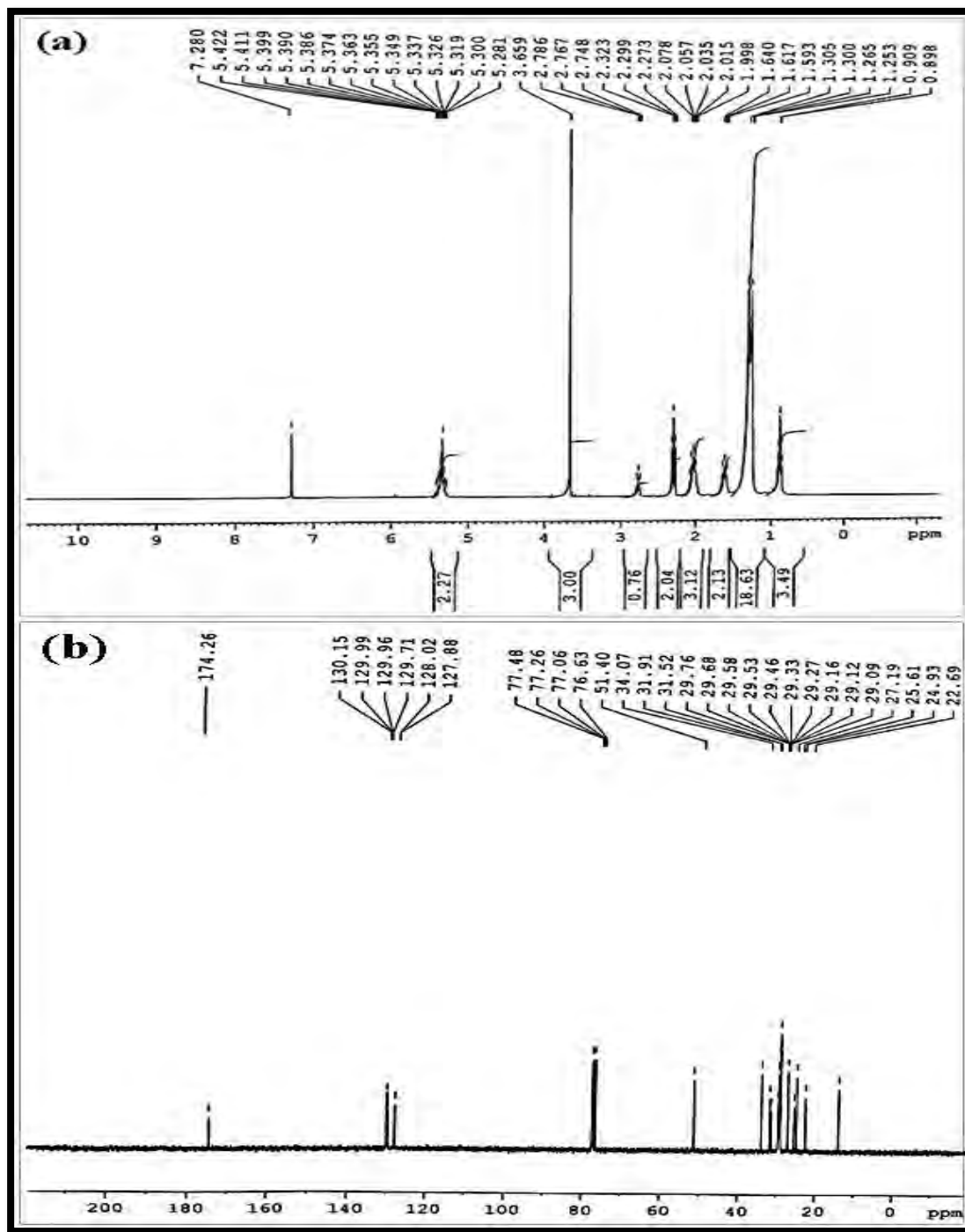
Figure 3.6.9. NMR spectrum of **(a)** ^{1}HNMR and **(b)** ^{13}CNMR of *Citrus paradisi* biodiesel
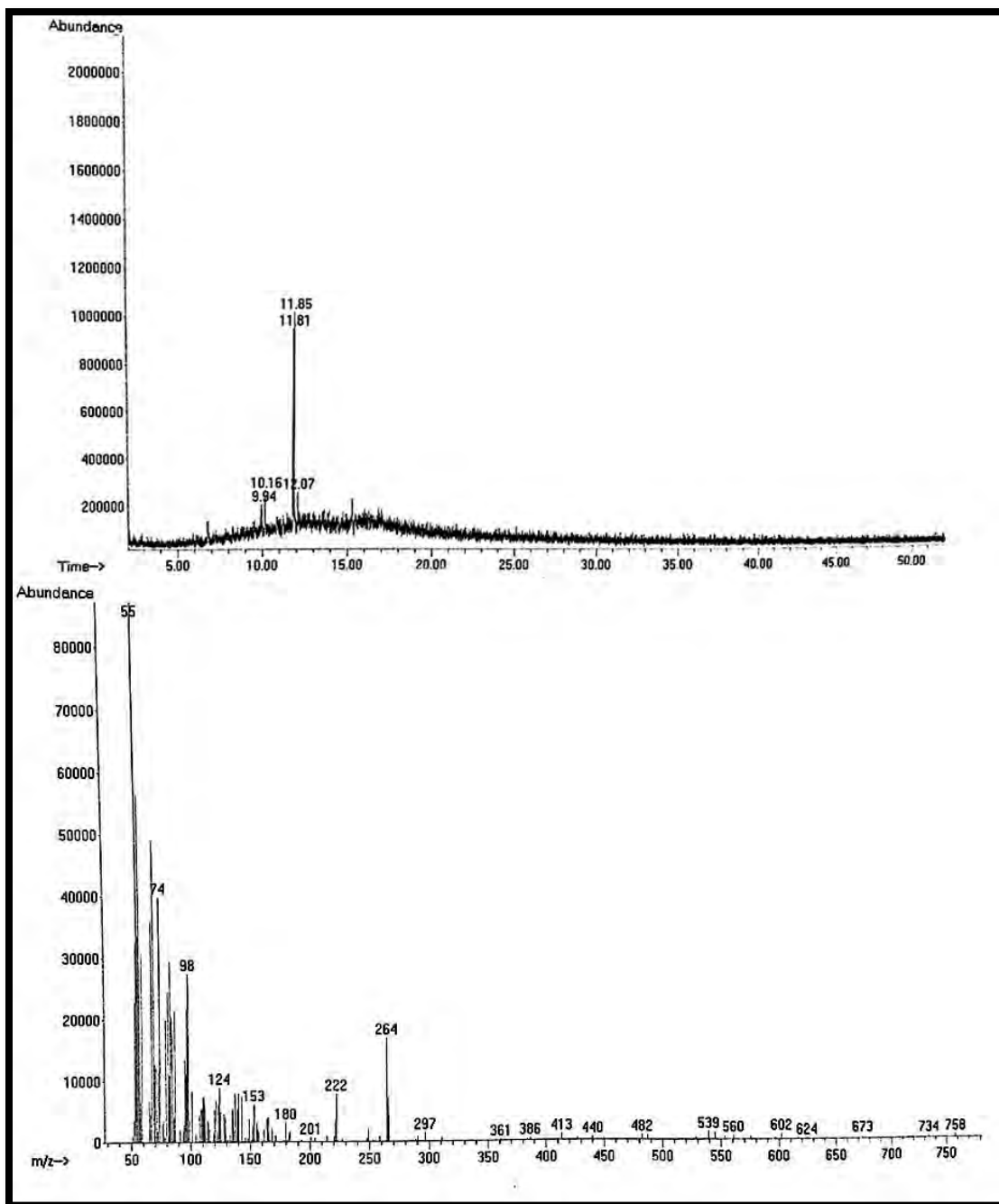
Figure 3.6.10 GC-MS spectrum of *Citrus paradisi* biodiesel

3.6.5. Fuel properties of *Citrus paradisi* Biodiesel

In order to evaluate the quality and efficiency of biodiesel in diesel engines for potential future applications, fuel parameters such as kinematic viscosity, density, flash point, pour point, iodine value, and sulfur concentration were used (Table 3.6.4). The fuel characteristics of synthetic biodiesel made from *Citrus paradisi* seed oil were compared to those of international fuel standards such ASTM D-6751 and European Union 14214. Acid value is among the most crucial characteristics of biofuel. The amount of free fatty acids in the fuel has a significant impact on the acidity of biodiesel. Higher acid number levels cause corrosion in engine components, which has a detrimental impact on engine performance. However, it was discovered that CIBD's acid value was 0.145 (mg KOH/gm) and that it was well matched with international standards, indicating that it was viable for use in fuel engines (Table 3.6.4). The density of biodiesel gives information regarding its quality, purity, and fatty acid composition. It is crucial in determining the quality of fuel. Unsaturated fatty acid content has a significant impact on biodiesel density. Higher density biofuels disrupt fuel engines and are not advised for practical use. In the current investigation, biodiesel density was found to be 0.512 (g/cm^3), which is below the range of international norms (Table 5). It said that synthetic biodiesel can be used as an environmentally friendly alternative to petroleum diesel in diesel engines without having any negative effects.

Biodiesel's kinematic viscosity (Kg/m^3 at 40 ◦C) is an important factor in the combustion, fuel blending, and spray fuel processes. It is sometimes referred to as the biofuel's stickiness index. Because of partial combustion and particulate matter emission, high viscosity biofuels are difficult to ignite. In the present investigation, *Citrus paradisi* biodiesel was discovered to have kinematic viscosity of 4.25 (mm^2/s), which is equivalent to international norms. The term "flash point" for biodiesel refers to the temperature at which the fuel ignites and flashes. It is regarded as a crucial instrument for safety precautions and other engine performance-related issues, such as legal safety insurance and transportation regulations for fires. It is greatly impacted by the methanol level of the biodiesel that is produced. The flash point will be smaller the higher the methanol content. The *Citrus paradisi* biodiesel flash point was 95 ◦C, which was well matched to ASTM D-6751 and European Union 14214 specifications. However, biodiesel with higher flash points (>66 ºC) is thought to be safer and less volatile than petro diesel. Cold flow

characteristics of biodiesel (pour point and cloud point) are important factors to keep in mind, particularly in colder parts of the world. These characteristics rely on the kind and number of contaminants in biodiesel. Due to the formation of crystal nuclei at lower temperatures, biodiesel becomes milky and changes how it flows. Commercially available chemicals and antioxidants can be used to improve it. The viscosity of the crude oil used to make biodiesel is directly correlated with the pour point of the methyl ester. *Citrus paradisi* biodiesel's pour and cloud points were discovered to be -12 °C and -9 °C, respectively. *Citrus paradisi* biodiesel has a sulfur level of 0.0002 (wt.%), showing that synthetic biodiesel is safe and favorable to the environment.

Table 3.6.5 - Comparison of Fuel properties of previously reported biodiesel sources with that of *Citrus paradisi* biodiesel fuel properties**.**

Property	Methods	*Citrus paradisi*		ASTM D-6751	EN-14214	China GB/T 20828-2007
		Mean	**St.Dev.**			
Color	Visual	1.5	-	2.0		
Acid number (mg KOH/g)	ASTM-D974	0.145	0.1	≤0.5	≤0.8	≤0.5
Flash Point (°C)	ASTM-D93	95	1.2	≥93	≥130	≥120
Pour Point (°C)	ASTM-D97	-12	0.4	-15-16	_	_
Viscosity (mm²/s at 40 °C.)	ASTM-D445	4.25	0.3	1.9-6.0	_	3.4-5.0
Density (kg/m³ at 40 °C)	ASTM-D1298	0.512	1.12	≤120	_	≤120
Sulphur content (wt.%)	ASTM-D4294	0.0002	1	≤0.05	≤0.05	≤0.20
Cloud point (°C)	ASTM-D2500	-9	1	-3.0-12	_	_

3.5.6 Reusability of catalyst

One of the key factors that extends benefits at an industrial scale and reduces time spent on resynthesis is catalyst reusability. The catalyst's capacity to be reused in a reaction process has a significant impact on both its stability and economic viability for biodiesel synthesis on an industrial scale. The kind and nature of the catalyst, as well as the purification, separation, and transesterification processes, all affect a heterogeneous catalyst's ability to be reused. In the current study, the reusability of produced green lead oxide nanoparticles was evaluated under ideal reaction circumstances, including catalyst loading of 0.32 weight percent, reaction time of 105 min, reaction temperature of 80 ∘C, and volumetric molar ratio of 7:1 for oil to methanol. After the first cycle was finished, the spent nano catalyst was separated from the transesterification products using centrifugation. It was then cleaned with methanol to get rid of any impurities before being dried in a 60 ∘C oven for 24 hours. The oven-dried catalyst was previously calcined for three hours at 500 ∘C to reuse it for subsequent cycles. The results demonstrated that the catalytic activity was strong for the first three runs and the generated biodiesel yield ranged from 93 to 85%. However, the biodiesel yields were decreased after the third cycle by up to 60% as a result of the catalyst's surface area, basicity, and pore volume decreasing, as well as organic species including glycerides and glycerol leaking into and poisoning the catalyst's active sites (Figure 3.6.11). It was therefore assumed that the decline in the yield of methyl esters was caused by the reduction in the availability of catalytic active sites.
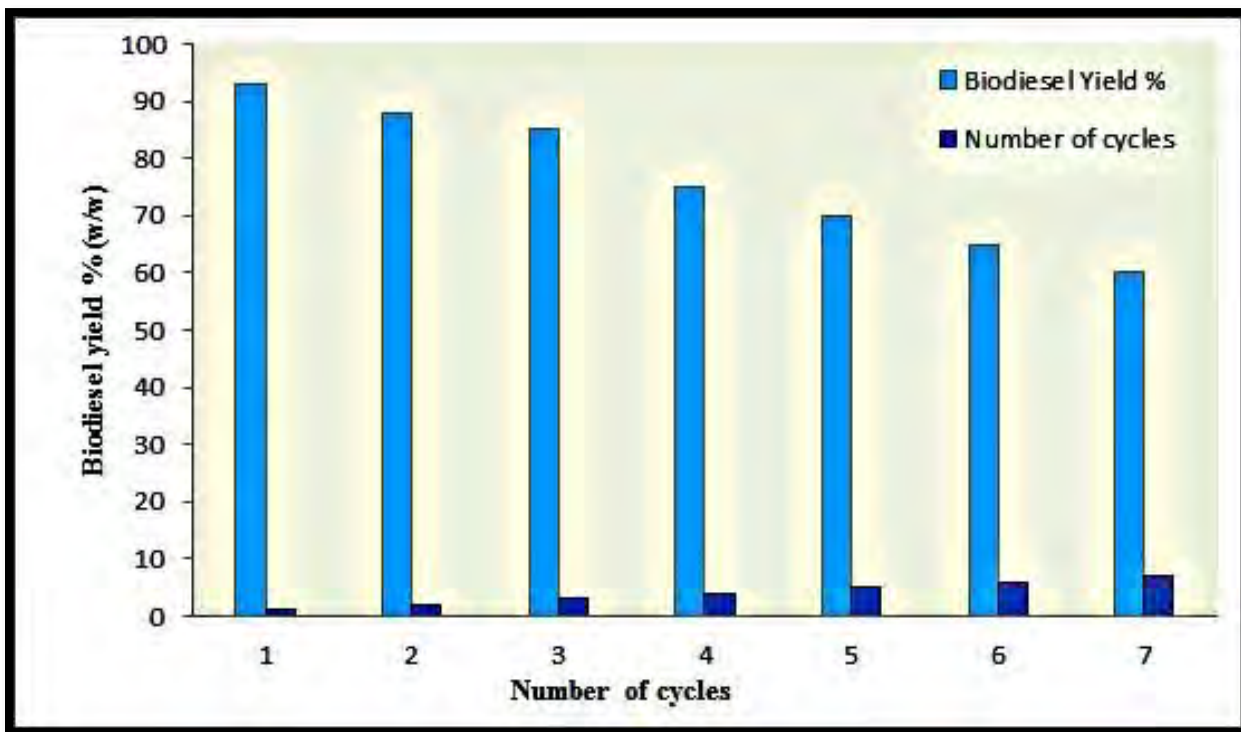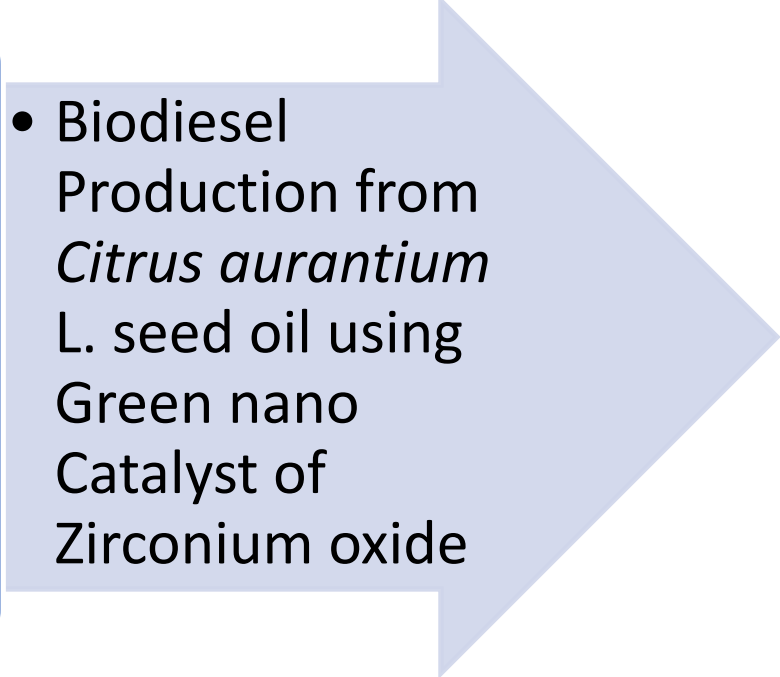
Figure 3.6.11. Reusibility of lead oxide nanocatalyst in transesterification

SECTION VII

- Biodiesel Production from *Citrus aurantium* L. seed oil using Green nano Catalyst of Zirconium oxide

Zirconium is the most evident transition metal with acidic-basic and redox property that gives it farfetched potential for activation and stabilization of catalyst while their utility as a dopant or support. Hence, zirconium and its modified forms have been systematically used in several industrial applications such as alkylation, esterification, transesterification, isomerization, condensation. Aqueous leaves extract of *Alternanthera pungens* successfully reduced Zirconium nitrate to ZrO_2.

3.7.1 Catalyst characterization

3.7.1.1 X-Ray Diffraction (XRD) of ZrO_2

X-Ray Diffraction (XRD) of ZrO_2 NPs was carried out to determine particle size and crystal structure. Diffraction peaks appeared in the pattern showed good crystalline nature of particles and confirmed high purity production of zirconia nano-particles via green technology. X-Ray Diffraction pattern of green NPs of ZrO_2 is given in Figure 3.7.1. The average size of ZrO_2 nano particles was calculated using XRD pattern of most deep peaks at 2θ value of 30.27^o (highest peak 101). Average Size of ZrO_2 was found 42 nm.

3.7.1.2 Scanning Electron Microscopy (SEM) of ZrO_2

SEM analysis of ZrO_2 NPs was used to examine topography of and fractured cross-section. SEM micrograph ZrO_2 NPs presented good surface characteristics (Figure 3.7.2). Larger particles were observed due to agglomeration or overlapping of small particles of ZrO_2 NPs. Morphology of ZrO_2 mostly appeared spherical. SEM Micrograph of ZrO_2 NPs has been depicted in Figure 3.7.2 showing spherical morphology with uniform particle structure.

3.7.1.3 Energy Diffraction X-ray (EDX) of ZrO_2

Energy diffraction (EDX) was used to identify the chemical composition of synthesized nano-particles of ZrO_2. Two characteristic peaks of Zr and O were observed in the spectrum shown in Figure 3.7.3. The percentage amount of Zirconium was 42.56% and oxygen was found 57.36%. Results of EDX spectrum clearly justified the purity of nano-particles and recommended it for methyl ester formation.

3.7.1.4 Fourier Transform Infrared Spectroscopy (FTIR)

FT-IR absorption spectrum was used to identify ZrO_2 nano-particles in the absorbance mode. A wave length range of 515-4000 cm^{-1} was used to determine absorbance of ZrO_2 nano-particles. FT-IR Spectrum of ZrO_2 nano-particles has been displayed in Figure 3.7.4. Distinctive characteristic absorption bands of ZrO_2 NPs were obtained at 526.46 cm^{-1} and 550.20 cm^{-1} related to representative c- ZrO_2 phase.

3.7.1.5 Thermogravimetric analysis (TGA) of ZrO_2

TGA thermogram of ZrO_2 nano-particles has been depicted in Figure 3.7.5. It represents thermal curve between changes in mass of sample versus temperature. TGA is used to find out thermal and oxidative stability, its lifetime, moisture and volatile content of the sample material. Loss in mass took place in three bases phases. No obvious change was observed till temperature of 400 °C. In the first step of decomposition, 0.029% loss in mass was detected at temperature range of 400-600 °C which revealed high thermal stability of ZrO_2 nano-particles. Another noticeable change (0.032%) in sample mass took place at temperature range of 600-800 °C. In third step 0.032% of mass loss was detected at temperature 800-1000 °C and afterward, particles gradually moved towards stability.

.,
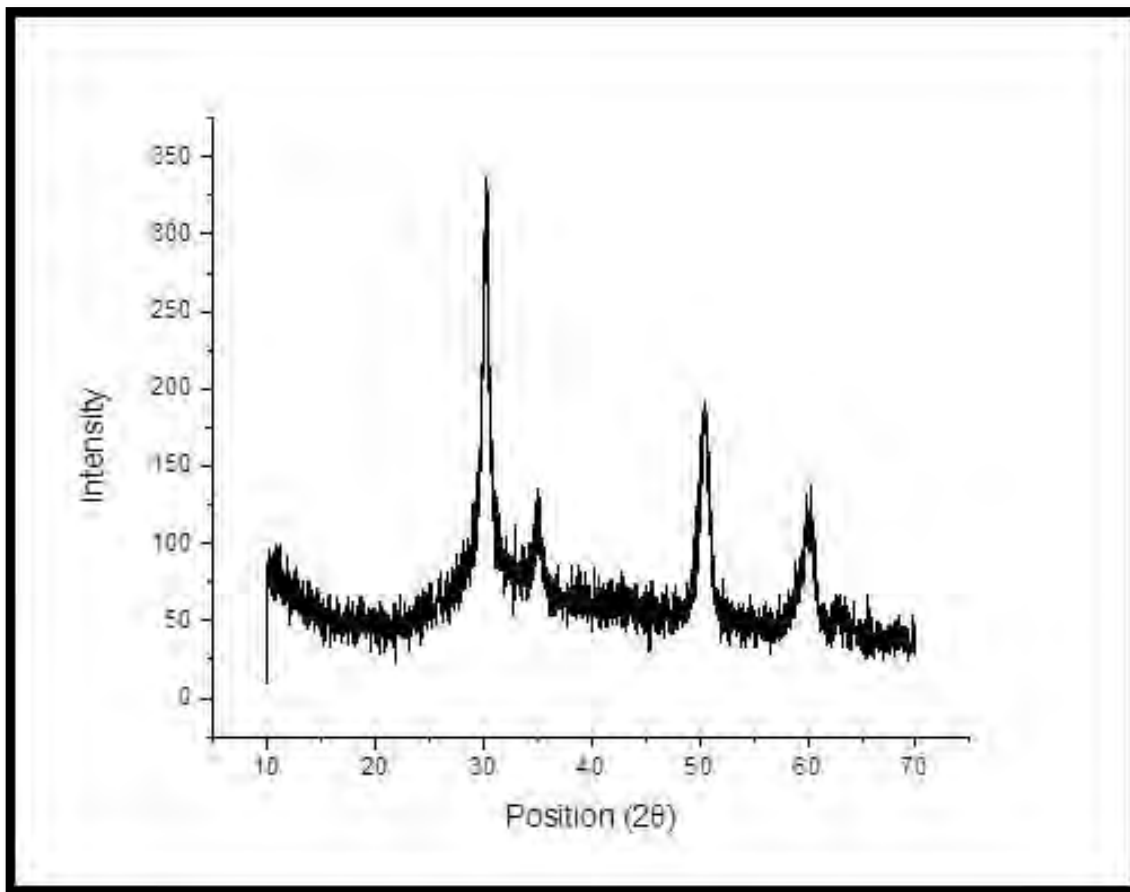
Figure 3.7.1. XRD pattern of calcined ZrO$_2$ green nano particles
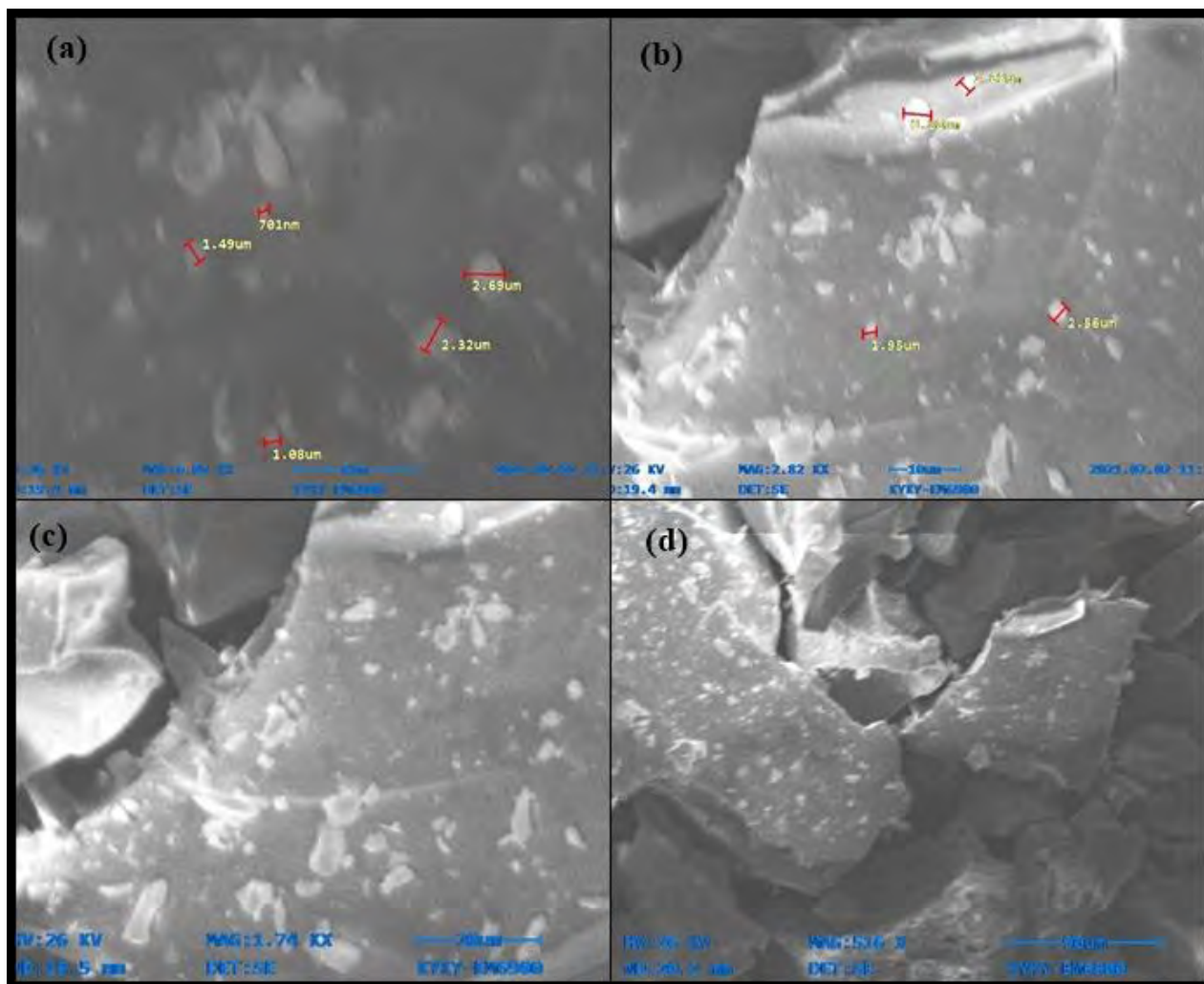
Figure 3.7. 2. Scanning electron microscopy (SEM) of calcined ZrO_2 NPs.
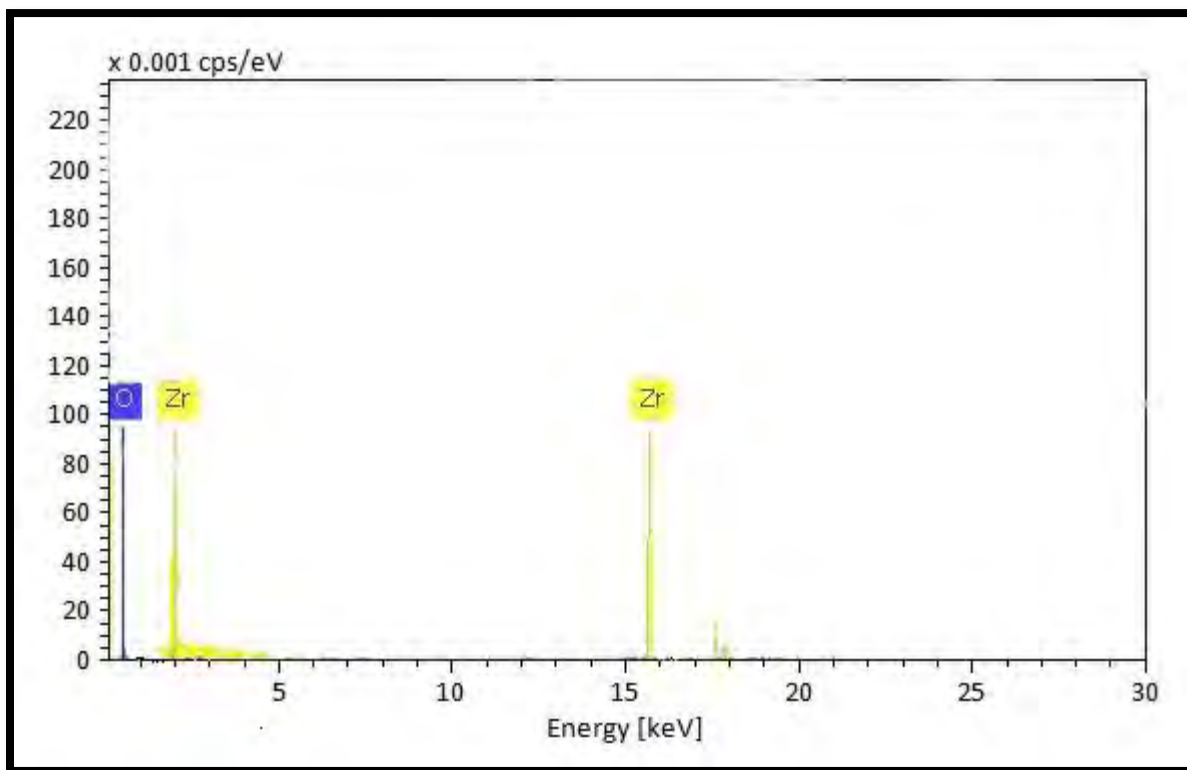
Figure 3.7.3. Energy diffraction X-Ray (EDX) of calcined ZrO_2 green nano particles
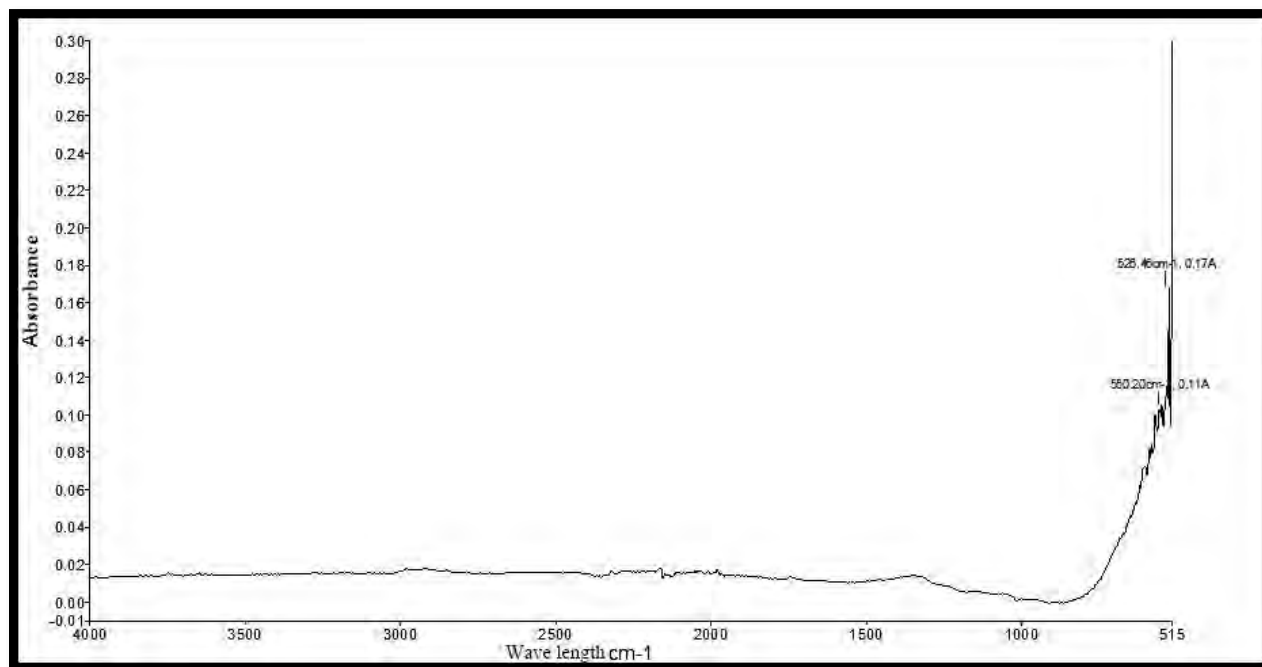
Figure 3.7.4 FTIR spectrum of calcined ZrO$_2$ green nano particles
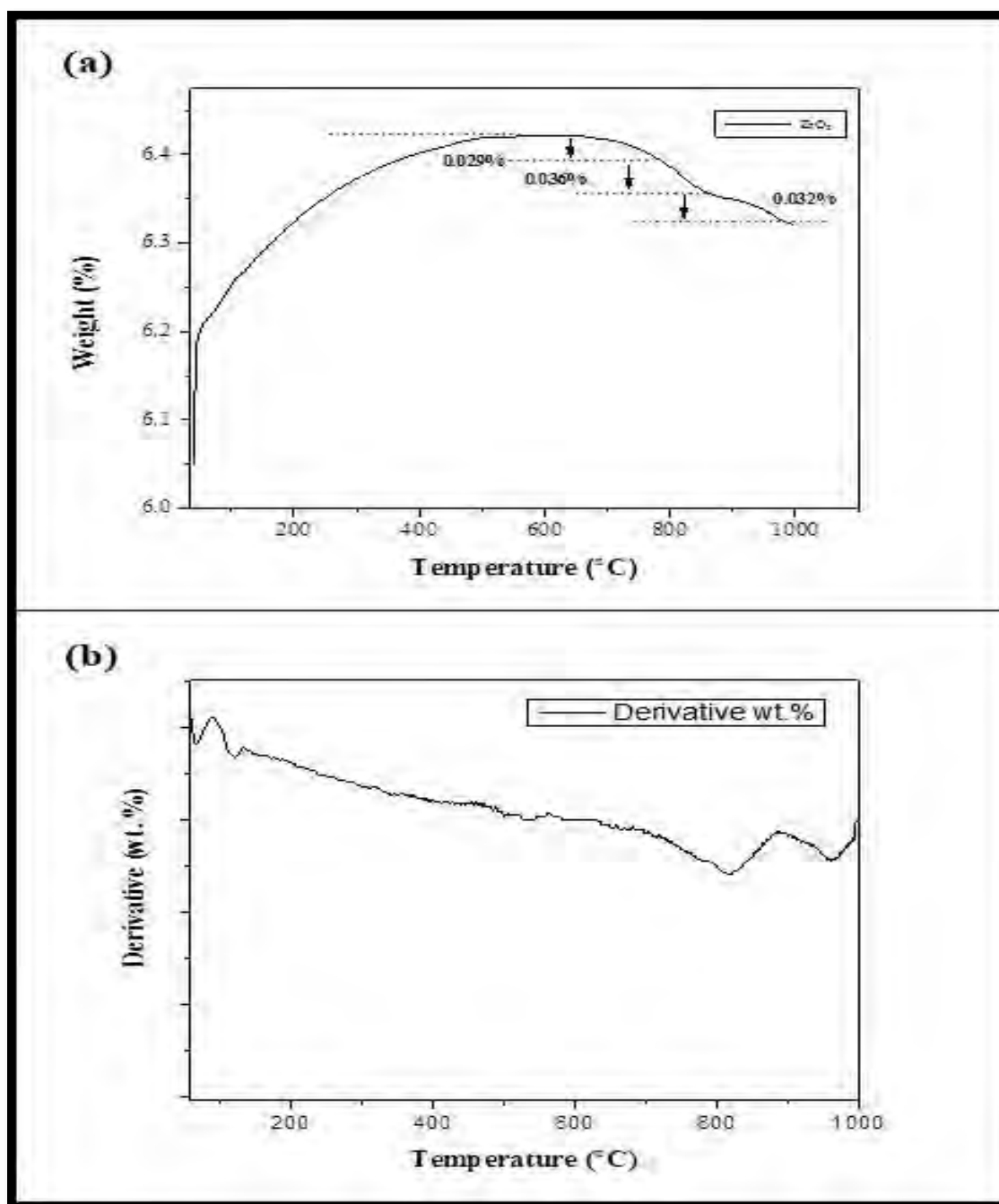
Figure 3.7.5. (a) TGA of ZrO$_2$ green nano particles **(b)** derivative thermogram of silver oxide nano particles

3.7.2 Biodiesel synthesis

Seeds of *Citrus aurantium* contain high content of oil (38% of total dry weight) which is substantially greater than other reported non-edible seed oil producing plants (Vidhu et al., 2014). Seed oil color was observed yellow at room temperature. The free fatty acid content of the oil was investigated prior to transesterification reaction and was found to be 0.14%, reflecting single step transesterification reaction. Transesterification reaction of *Citrus aurantium* seed oil was carried with zirconium oxide nano catalyst. The experimental design in terms of coded values by central composite design (CCD) has been given in Table 3.7.1 Experimental results of transesterification reactions are mentioned in Table 3.7.2 whereas; the outcomes of statistical analysis of variance (ANOVA) for Response Surface Quadratic model have been described in Table 3.7.3. Percent yield of methyl ester was predicted by quadratic polynomial equation (6) in terms of coded factor of biodiesel.

Biodiesel (yield %) = +81.35*A+1.258*B-2.97*C+6.11*D+0.7255*AB+0.5000*AC+8.25*AD-0.8371*BC-4.29*BD+2.00*CD-5.46* A²-17.31* B²-1.72* C²-8.69 *D²   (13)

The model was further validated by using four sets of data shown in figure 4. This revealed that the predicted results match well with experimental results. The application of data is intended to discover the significance, fitness and accuracy of the model for methyl ester production. Coded values gotten from estimation of data were used to make quadratic regression model and some insignificant terms of the model were kept in consideration. It was revealed from the results of ANOVA that yield of biodiesel and four influencing variables have substantial correlation with a confidence level of 97%. F-test and p-value was utilized to measure the significance of the resultant model, smaller the value of *p* (<0.05) greater is the significance of the model. Altogether, all variables of transesterification reaction i.e. reaction time, catalyst loading, alcohol to oil ratio and temperature had a significant effect on transesterification reaction and resultant biodiesel yield. Model was declared as significant by results obtained from ANOVA with a *p*-value lesser than <0.0001 for effective calculation of biodiesel yield. Figure 3.7.6 shows comparison between predicted values versus actual values was found comparable to each other as they are spread near to the straight line of the plot.

Coefficient of determination (R^2) was used as a precursor to measure accuracy prediction of response values of the experimental model. It was found to be equal to the value of 0.89, which is regarded as an acceptable range in the model and quadratic terms like alcohol to oil ratio (A^2), time of reaction (B^2), catalyst concentration (C^2) and temperature of reaction (D^2) were also found significant because their p-value was lesser than <0.05. The ratio of signal to noise was measured by precision value of the model and it should be >4. A high precision value of 9.15 of the models was observed which met with the required value. The lake of fit value of the model was 4.2, small enough to compare with pure error and negligible. All these conclude that the model is significant.

Table 3.7.1- Experimental design by central composite design for transesterification reaction

Process parameters	−1	+1
Reaction time	20	90
Alcohol to oil ratio	2:1	11:1
Catalyst loading	0.16	0.58
Temperature	35	90

Table 3.7.2 - Detailed experimental result for transesterification reaction

Run	A:Alcohol to oil ratio	B:Reaction time (min)	C: Catalyst loading(g)	D: Temperature (ºC)	Yield (wt%)
1	9.1	30	0.35	55	45
2	10.1	30	0.16	35	35
3	6.1	45	0.25	65	60
4	7.1	55	0.58	55	30
5	11.1	85	0.26	35	90
6	5.1	20	0.19	45	92
7	3.1	75	0.58	30	75
8	6.1	65	0.35	65	96
9	5.1	45	0.25	65	40
10	8.1	20	0.20	85	35
11	10.1	45	0.26	65	55
12	8.1	75	0.48	75	50
13	8.1	65	0.16	70	94
14	5.1	45	0.26	65	90
15	9.1	35	0.20	75	93
16	6.1	45	0.20	55	92
17	7.1	65	0.58	90	45
18	8.1	25	0.16	45	22
19	3.1	65	0.16	55	34
20	8.1	55	0.26	45	50
21	6.1	55	0.16	65	90
22	5.1	60	0.20	45	89
23	9.1	70	0.35	35	66
24	10.1	65	0.45	75	85

25	5.1	50	0.26	45	35
26	8.1	65	0.20	65	89
27	3.1	40	0.35	75	89
28	9.1	45	0.25	45	64
29	5.1	45	0.40	55	60
30	5.1	35	0.35	90	45

Table 3.7.3- ANOVA for Response Surface Quadratic model

Source	Sum of Squares	df	Mean Square	F Value	p-value
Model	5616.17	18	356.3045	9.3679	<0.0001
A-Alcohol to oil ratio	101.26	1	101.26	4.7829	0.008
B-Reaction time	12.569	1	12.569	2.157534	0.004
C- Catalyst loading	1234.236	1	1234.236	18.141	0.0009
D- Temperature	3.465	1	3.465	9.1974	<0.0001
AB	3.10	1	3.10	0.05428	0.4810
AC	130	1	130	1.67389	0.1293
AD	0.32	1	0.32	0.00559	0.4784
BC	316.40	1	316.40	6.46937	0.0128
BD	255	1	255	4.47036	0.0543
CD	2,007	1	2,007	15.2071	0.0014
A²	1,432.60	1	1,432.60	30.71540	<0.0001
B²	35.3469	1	35.3469	0.63852	0.0003
C²	1278.218	1	1278.218	17.4562	0.0036
D²	650.3729	1	650.3729	8.2905	0.0074
Residual	65.18396	9	65.18396		
Lack of Fit	904	10	90.4	4.21452	0.0534
Pure Error	126.4162	6	22.3044		
Cor Total	1,2875.35	25			

R^2 = 0.89 , Std. Dev. = 10.40,   **C.V. % = 15.69, Adeq Precision = 9.15**
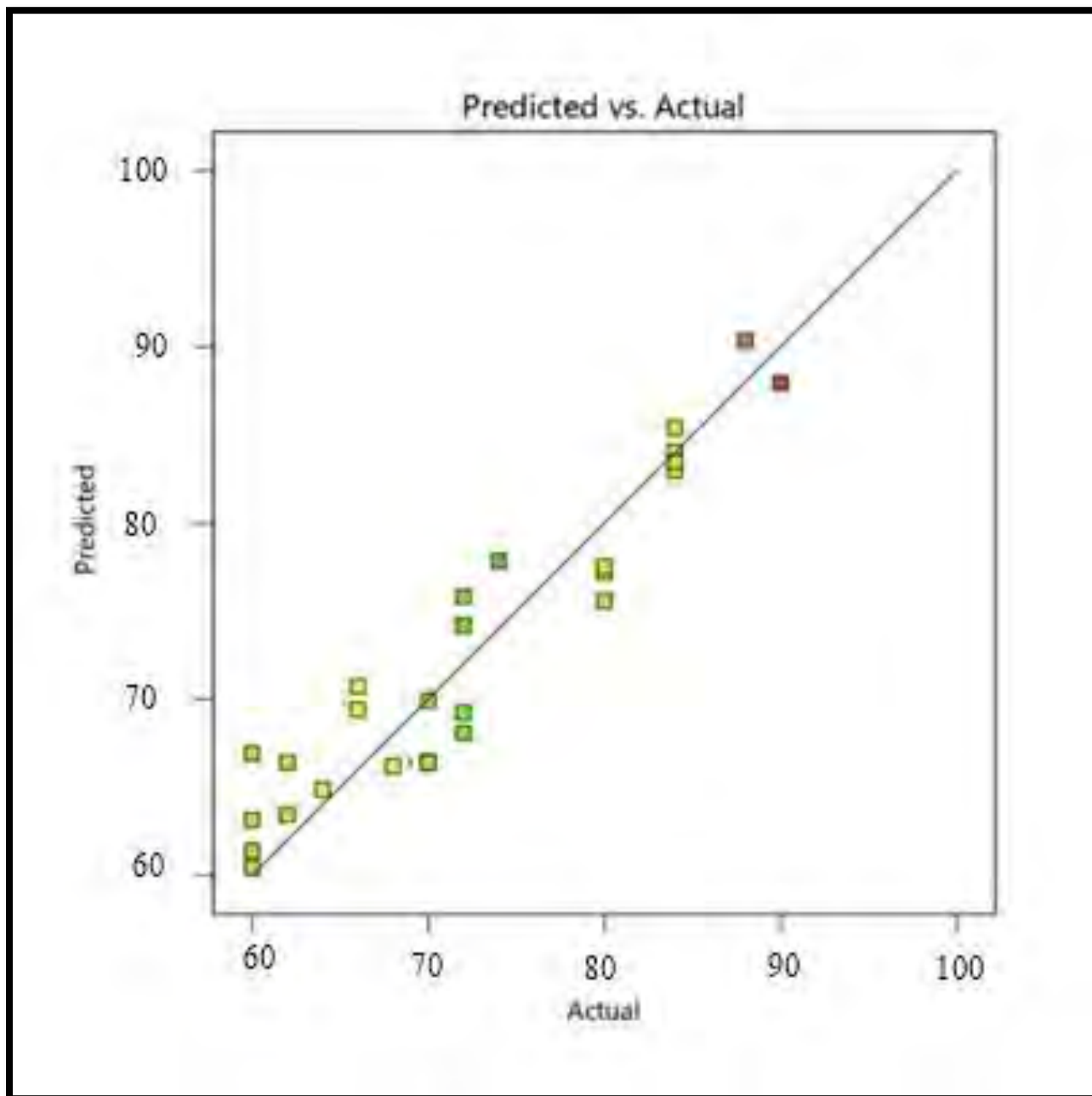
Figure 3.7.6. Comparison between the experimental biodiesel yield and the predicted yield of the model

3.7.3 Influence of reaction parameters on transesterification reaction

3.7.3.1 Combined influence of methanol to oil ratio and reaction time

The combined effect of methanol to oil ratio and reaction time has been depicted in 3D plots shown in Figure 3.7.7a. It is one of the significant parameters of transesterification reaction. Parametric interactions of methanol to oil molar ratio and reaction time on biodiesel synthesis was studied during transesterification reaction using experimental data while keeping other parametric conditions like temperature (87.5 $^\circ$C) and catalyst loading (0.5 wt.%) constant. A high yield of 94% was observed with methanol to oil molar ratio 6:1 at reaction time duration of 120 min at run number 6. A high percent yield of biodiesel was observed with high content of alcohol, which converts more triglycerides to mono glycerides; however, same result was observed in the current study that further addition in alcohol content substantially decreased the yield of biodiesel. Stoichiometric measurement of transesterification reaction revealed that a reaction between 3 mol of alcohol and 1mol of oil results in formation of 3 mol of methyl ester and one mol of glycerol (Tan et al., 2017). Biodiesel yield dropped to 60% at methanol to oil ration 10:1 and reaction time 85 mins as increasing alcohol amount beyond its limit enhances glycerol solubility and makes it challengeable to separate it from biodiesel (Quintero et al., 2003). It rose up to 65% with methanol to oil molar ratio of 3:1 and to 89% in run number 20 at methanol to oil molar ratio of 6:1 and time 85 minutes. Decrease in the reaction time from 85 to 55 minutes at run number 21 with same methanol to oil molar ratio (6:1) resulted in lower yield of 85%. Combine effect of methanol to oil ratio and reaction time was found insignificant in the results of ANOVA with p-value 0.4810 (>0.05). Results of our investigation are in harmony with previous findings (Rehan et al., 2018).

3.7.3.2 Combined influence of reaction temperature and catalyst loading

Reaction temperature and catalyst loading is another important parameter that may intensely influence biodiesel yield during transesterification reaction. Figure 3.7.7b depicts 3D plots of combined influence of reaction temperature and catalyst loading on biodiesel yield. Uniform lines of 3D plot represented good mutual correlation between reaction temperature and catalyst loading on yield of methyl ester. Highest yield of 94% was obtained run number 6 with catalyst loading of 0.5 wt.% and reaction temperature 87.5 $^\circ$C at constant reaction time (120 min)

and alcohol to oil ratio (6:1). Decrease in reaction temperature with same amount of catalyst concentration (0.5 wt.%) resulted in rapid fall in methyl ester formation. Lowest yield of 65% was obtained with catalyst loading 0.5 wt.% and reaction temperature 55 °C (Run 14). Increase in both reaction temperature and catalyst loading (120 °C and 0.62 wt.% respectively) beyond a certain limit resulted in decrease in biodiesel yield up to 88% (Run 15). Decline in yield of methyl ester was observed at high catalyst loading of 0.75 wt.% at optimum temperature of 87.5 °C which is attributed to saponification reaction with increase in catalyst concentration (Run 16). Same results are observed with feedstock of *Astrocaryum aculeatum* (Mendonça et al., 2019). Low reaction temperature (55 °C) and high catalyst loading (0.75 wt.%) favored reversible reaction and reduced biodiesel yield up to 85% (Run 27). The lowest reaction temperature was found to be insufficient to precede methyl ester formation efficiently. Results of ANOVA signposted that combined influence of reaction temperature and catalyst loading on biodiesel yield was significant with p-value 0.0014 (<0.05) and showed good mutual correlation.

3.7.3.3 Combined influence of reaction time and catalyst loading

An adequate reaction time and appropriate amount catalyst is required in the course of transesterification reaction. Combined influence of reaction time and catalyst loading on biodiesel yield has been presented in Figure 3.7.7c reaction time of 120 min and temperature of 87.5 °C resulted in highest yield (94%) at constant methanol to oil ratio (6:1) and temperature (87.5 °C) at run number 6. Low reaction time was found insufficient to accomplish transesterification reaction even with high amount of catalyst loading and resulted in lower yield of biodiesel (Run 5 and 13). A further decline in yield (65%) with low reaction time (50 min) was predicted at Run 4. It is because an appropriate reaction time is required to ensure efficient mixing with proper stirring at constant rate for suitable chemical interaction of oil and alcohol during transesterification reaction (Sandhya et al., 2020). However, overpassing a certain limit even high reaction time (120 min) with high catalyst loading favored reversible reaction and a yield of 78% and 88% of biodiesel was obtained at Run number 16 and 26 respectively. It is attributed to a saponification reaction and ultimate rapid decline in productivity. The combined influence of reaction time and catalyst loading on biodiesel yield was found significant in ANOVA outcomes with p-value 0.0128 which is lesser than 0.05.

3.7.3.4 Combined influence of reaction time and temperature

Mutual effect of reaction time and temperature at constant oil to methanol molar ratio 1:6 and catalyst loading 0.5 wt.% on biodiesel yield has been demonstrated in 3D plot in Figure 3.7.7d. Both reaction time and temperature have significant effects on biodiesel synthesis. It is revealed from Run 6 that 94% yield of biodiesel was achieved at reaction temperature 87.5 °C and reaction time 2 h. Decrease in methyl ester yield up to 80% was predicted at high reaction temperature of 120 °C and reaction time 85 min (Run 24). Higher reaction time and temperature are reflected to accelerate the chemical process of hydrolysis of methyl esters into acids and consequent polar methanol in the reacting mixture therefore, declining percent yield of biodiesel (Anwar et al., 2010). The lowest yield of biodiesel (50%) was obtained at lowest temperature of 55 °C and reaction time 85 min (Run 11). 89% yield of biodiesel was obtained at reaction temperature 87.5 °C and reaction time 85 min. Lowest yield was observed at run 24 with reaction temperature 120 °C and time 85 min. Results of ANOVA illustrated insignificant correlation between temperature and reaction time with p-value greater than 0.05 (0.0543) and were found significant.

3.7.3.5 Combined influence of methanol to oil molar ratio and temperature

The combined effect of methanol to oil molar ratio and reaction temperature has been illustrated in Figure 3.7.7e. Yield percent of biodiesel raised up to 94% at methanol to oil molar ratio of 6:1, reaction temperature 87.5 °C at constant reaction time (120 min) and catalyst concentration (0.5 wt.%). Decrease in reaction temperature (55 °C) with same methanol to oil molar ratio of 6:1 resulted in lower yield of 65% (Run 14). It is attributed to compact mass transfer rate of oil, methanol and catalyst as they all are immiscible at lower temperature and need proper kinetic energy to react appropriately and enhance productivity in shorter time period (Vidhu and Philip 2014). 55 % yield of methyl ester was obtained at run 23 with methanol to oil molar ratio of 3:1 and temperature 87.5 °C. Further increase in methanol to oil molar ratio up to 10:1 at reaction temperature 87.5 °C resulted in lowest yield of 50% (Run 30). Combined effect of methanol to oil molar ratio and reaction temperature was found insignificant with p-value 0.47 (>0.05).

3.7.3.6 Combined influence of methanol to oil ratio and catalyst loading

The combined effect of methanol to oil molar ratio and catalyst loading has been illustrated in Figure 3.7.7f. In order to carry on the transesterification reaction sufficient amount of methanol is needed to convert oil into methyl ester and push the reaction onward. Maximum yield of methyl ester (93%) was obtained at methanol to oil molar ratio of 6:1 and catalyst loading of 0.5 wt.% (Run 6). Greater catalyst loading (0.62 wt.% and 0.75 wt.%) resulted in low yield of biodiesel (88% and 78% respectively) at same methanol to oil molar ratio of 6:1(Run 26 and 16). High methanol to oil molar ratio of 10:1 and catalyst loading of 0.62 wt.% resulted in low yield of 60% (Run 12). Excess methanol is responsible for shifting reaction towards undesirable condition of transesterification, expediting reverse reaction and subsequent low yield of methyl ester. Methanol to oil molar ratio of 3:1 and catalyst loading of 0.62 wt. % was found deficient to accomplish biodiesel synthesis and decline in percent yield of biodiesel up to 56% was observed (Run 19). In current study collective influence of methanol to oil molar ratio and concentration of catalyst was found not significant with p-value (0.1293) > 0.05 for methyl ester formation.
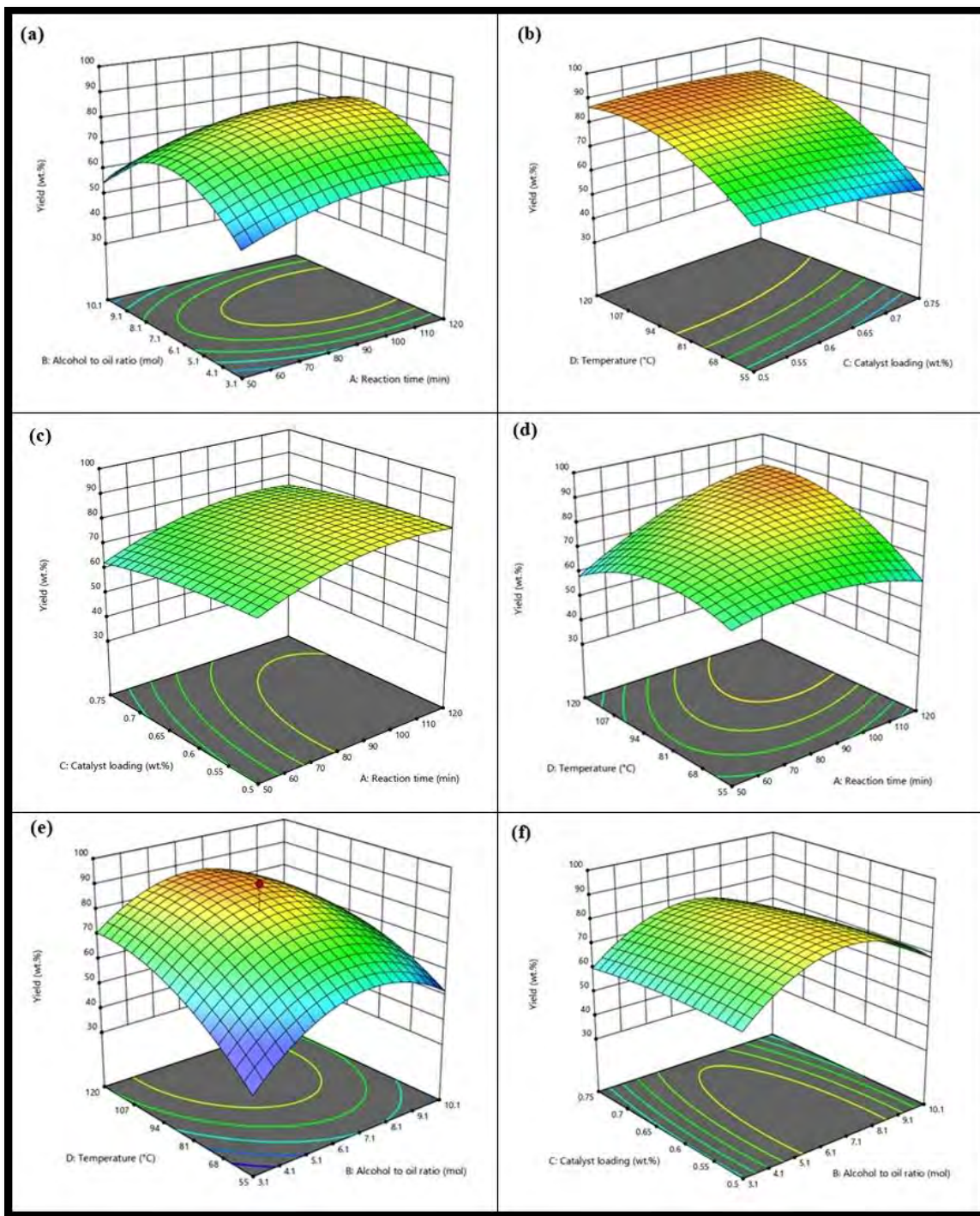
Figure 3.7.7. Influence of the reaction parameters of *Citrus aurantium* biodiesel.

3.7.4 Physiochemical Characterization of biodiesel

3.7.4.1 FTIR

Position of carbonyl stretch in FT-IR spectrum is considered significant to displacement effect and structural modification of the sample molecules (Tabatabaei et al., 2015). Spectrum of FT-IR in the mid infra-red region was utilized for recognition of functional groups and bands conforming to different stretches and vibrations in CASO and biodiesel. FT-IR spectrum of CASO and synthesized biodiesel has been shown in Figure 3.7.8. A characteristic peak for carbonyl group appeared at 1743.52 cm^{-1} which was further confirmed by NMR spectrum of biodiesel. Stretching vibrations CH_3, CH_2, and CH were observed at 2922.62 cm^{-1}, 2853.31 cm^{-1} and 3008.20 cm^{-1} respectively in the FT-IR spectrum of biodiesel. Whereas, bending vibration of these groups were observed at 1464.47 cm^{-1}, 1160.26 cm^{-1} and 721.92 cm^{-1} respectively. FT-IR spectrum of CASO and biodiesel were found to be nearly same with some variations and shifting which can be considered for identification purpose. Shifting in the transmission peaks were observed in the region of 3330.83 cm^{-1}, 1741.80 cm^{-1} and 1437.10 cm^{-1} to 3008.20 cm^{-1}, 1743.52 cm^{-1} and 1464.47 cm^{-1} in methyl ester respectively. Conversion of triglycerides into fatty acid methyl esters was further confirmed from disappearance of peaks of oil spectrum at 1025.19 cm^{-1}, 1172.61 cm^{-1} and 532.20 cm^{-1} wave length in the spectrum of CASO biodiesel.

3.7.4.2 NMR

CASO biodiesel was further characterized by ^{1}HNMR and ^{13}CNMR spectroscopy which has been depicted in Figure 3.7.9a. The distinguishing peak of methoxy protons was detected at 3.675 ppm as a singlet whereas, triplet of α-CH_2 protons was observed at 2.313 ppm. These two peaks are considered as distinctive for the endorsement of existence of methyl esters in sample biodiesel. A peak of free methanol which is commonly observed at 3.45 ppm was found absent in ^{1}HNMR spectrum of CASO biodiesel. Protons of β-CH2 (β-methylene) were observed at 1.262-1.648 ppm which represents atoms of hydrogen attached to carbon number 3 in aliphatic fatty chain. Peaks at 0.008 ppm and 0.868 ppm of spectrum represented terminal methyl protons while olefinic hydrogen (-CH=CH-) was perceived at 5.294-5.370 ppm indicating double bonds integrated for two hydrogen atoms.

^{13}CNMR spectrum was used to study structural characteristics of biodiesel synthesized from CASO (Figure 3.7.9b). Characteristic peak of ester carbonyl (─COO─) and C─O was observed at 174.73 ppm and 51.47 ppm respectively. Peaks existed around 127.89-130.20 ppm indicated the presence of unsaturation in biodiesel sample. Signals at 22.60-31.93 ppm presented aliphatic methylene carbons of long carbon chains present in fatty acid methyl esters of CASO.

3.7.4.3 GC-MS

Chemical composition of synthesized biodiesel was studied with Gas chromatography and Mass spectrometry (GC/MS). GC/MS is an analytical technique used to analyze fragmentations of fatty acid methyl esters. GC/MS chromatogram of CASO biodiesel with representative mass spectrum of 5, 8-Octadecanoic acid methyl ester has been given in Figure 3.7.10. Six major peaks were observed in chromatogram. All these peaks correspond to different fatty acid methyl esters found in biodiesel sample and were further identified from library match software named NO. NIST02 for confirmation. Retention time of various fatty acid methyl esters was kept in consideration for their identification which was further confirmed by MS analysis (Taravus et al., 2009). Saturated methyl ester fragmentations were found are Heptadecanoic acid, 14-methyl-, methyl ester (17:1), 16-Octadecanoic acid (18:1), methyl ester, Eicosanoic acid, methyl ester (20:4), Unsaturated fatty acid methyl esters are Hexadecanoic acid methyl ester (16:0), 5, 8-Octadecanoic acid methyl ester (18:2) and 13-Docosenoic acid, methyl ester (22:1). 5, 8-Octadecanoic acid methyl ester (C18:2) was the major fatty acid methyl ester. Base peak of major fatty acid methyl esters was observed at m/z 74, 55 and 143 corresponding to 5, 8-Octadecanoic acid methyl ester, Hexadecanoic acid methyl ester and Heptadecanoic acid, 14-methyl-, methyl ester respectively. GC/MS analysis of CASO biodiesel reflected that seed oil of *Citrus aurantium* is suitable for biodiesel production at industrial level and can lead to transition towards circular economy.

Figure 3.7.8. FTIR spectra of **(a)** seed oil of *Citrus aurantium* **(b)** *Citrus aurantium* biodiesel
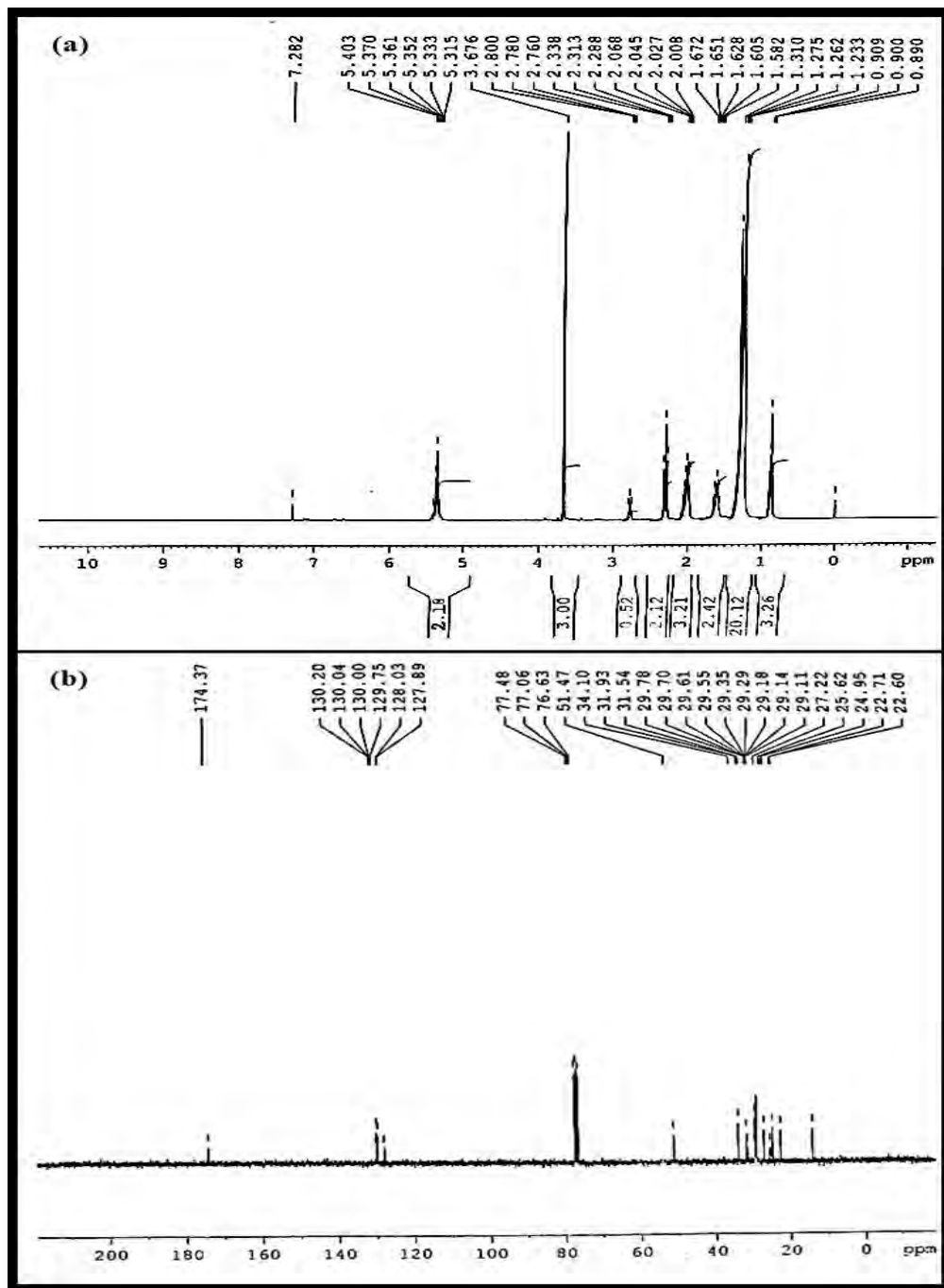
Figure 3.7.9. NMR spectrum of **(a)** ^{1}HNMR and **(b)** ^{13}CNMR of CASOD
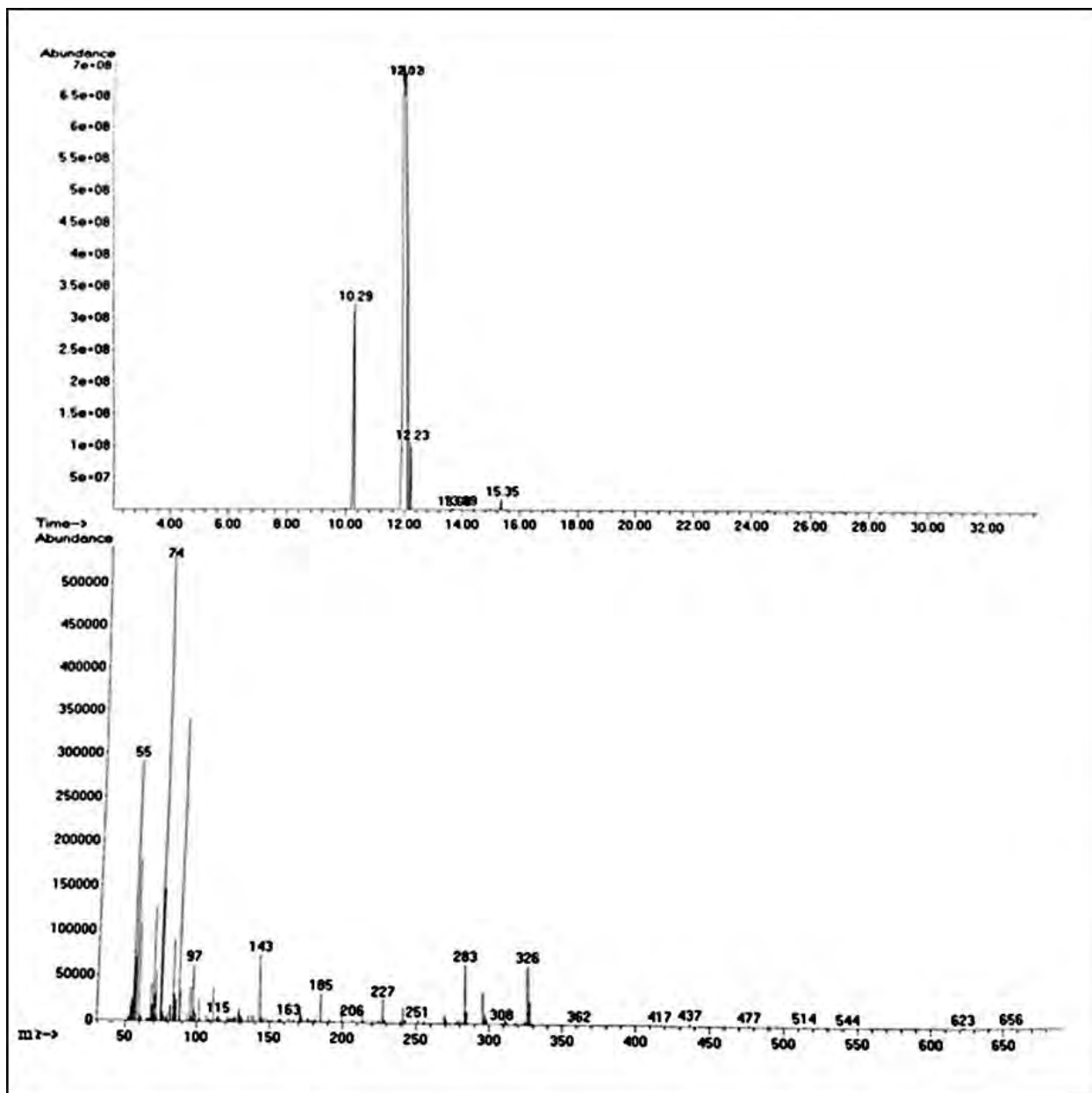
Figure 3.7.10. GC-MS spectrum of *Citrus aurantium* biodiesel

3.7.5 Fuel properties of biodiesel

Fuel properties or quality of biodiesel should be comparable to petro-diesel as they affect engine efficiency. Fuel properties of *Citrus aurantium* seed oil methyl ester were examined and found well matched with international standards of ASTM D-6571, EN 14214 and China GB/T 20828-2007. Investigated fuel properties of biodiesel comprised; flash point, density (Kg/m^3 at 40 °C), viscosity (mm^2/s at 40 °C), pour point, cloud point, acid value and sulphur content. Comparison of fuel properties of *Citrus aurantium* biodiesel with international standards has been given in Table 3.7.4.

One of the most significant properties of biodiesel that negatively affects engine quality is acid number. Acid number is in direct relation with free fatty acid content of sample diesel, higher the amount of free fatty acids greater will be acid value. The acid value of *Citrus aurantium* biodiesel in our current study was found to be 0.177 (mg KOH/g). Another important fuel property is kinematic viscosity. It harshly affects various aspects of diesel fuel *i.e.* atomization of fuel in combustion chamber, soot and deposit formation in vehicle engine (Mofijur et al., 2020). According to ASTM D-445 the acceptable range of viscosity for biodiesel is from 1.9 to 6.0 *mm^2/s.* The kinematic viscosity of *Citrus aurantium* biodiesel was found to be 3.91 (mm²/s at 40 °C) which is in line with international standard.

The efficiency of fuel atomization was found under influence of density of biodiesel. The presence of unsaturated fatty acids which have more than two double bonds in biodiesel moderately increases its density. Mean density of CABD was recorded to be 0.74 (kg/m³ at 40 °C) at 15 °C which meet well with international standard. Pour and cloud point, both fundamentally regulate operation of diesel engine in cold weather at low temperature. Pour point can be defined as the temperature at which wax content is out of solution enabling the fuel to flow (Ong et al., 2020). Increase in amount of saturated fatty acids results in increase in pour point. The pour point of clean diesel ranges from 15 °C to 40 °C. It is greater than the pour point of conventional fossil fuel diesel and diesel synthesized from waste vegetable oils. In current investigation, the pour point and cloud point of *Citrus aurantium* biodiesel was recorded as -7 °C and -12 °C respectively. Both pour point and cloud point meet ASTM standards. Flash point represents the least temperature of the fuel at which it flash upon when ignited with an ignition

source. It has been noticed that methyl ester produced from biomass exhibits higher flash point as compare to petro diesel giving it advantage in saponification. Average flash point of *Citrus aurantium* biodiesel in the current study was 71 °C which is comparable to ASTM D-657, EN 14214 and China GB/T 20828-2007 standard.

Table 3.7.5 - Comparison of fuel properties of *Citrus aurantium* biodiesel with international standards ASTM D-6571, EN 14214 and China GB/T 20828-2007.

Property	Methods	*Citrus aurantium*		ASTM D-6751	EN-14214	China GB/T 20828-2007
		Mean	St.Dev.			
Color	Visual	2	-	2.0		
Acid number (mg KOH/g)	ASTM-D974	0.177	0.1	≤0.5	≤0.8	≤0.5
Flash Point (°C)	ASTM-D93	71	14	≥93	≥130	≥120
Pour Point (°C)	ASTM-D97	-7	5	-15-16	_	_
Viscosity (mm²/s at 40 °C.)	ASTM-D445	3.91	0.5	1.9-6.0	_	3.4-5.0
Density (kg/m³ at 40 °C)	ASTM-D1298	0.74	1.06	≤120	_	≤120
Sulphur content (wt.%)	ASTM-D4294	0.0002	1	≤0.05	≤0.05	≤0.20
Cloud point (°C)	ASTM-D2500	-12	1	-3.0-12	_	_

3.7.6 Catalyst reusability

Reusability of the catalyst separated from the reaction mixture was studied at optimum reaction conditions of oil to methanol molar ratio (6:1), catalyst concentration (0.5 wt.%) and reaction time (120 min). Reusability action of the catalyst was assessed with consecutive transesterification reactions with recycled catalyst. The performance of the catalytic activity after each transesterification reaction has been illustrated in Figure 3.7.11. Experimental results indicated that efficiency of the catalyst decreased with increases in the number of cycles. A high yield of 94% was obtained in the first run with catalyst loading 0.5 wt.% which decreased up to 89% and ultimately 72% in 5th run and 66% in 7th run respectively. A major decrease in the activity of the catalyst was noticed in the 5th cycle. This decrease in % yield with increase in number of cycles of the catalyst was assumed due to poisoning of active sites of the catalyst and its leaching due to organic species (glycerides and glycerol) present in the reacting mixture. Recyclability of the catalyst up to 7th run indicated relatively better performance of zirconium oxide. Zirconium oxide nano-particles are to be enhancing their environmental sustainability from circular economy perspective.
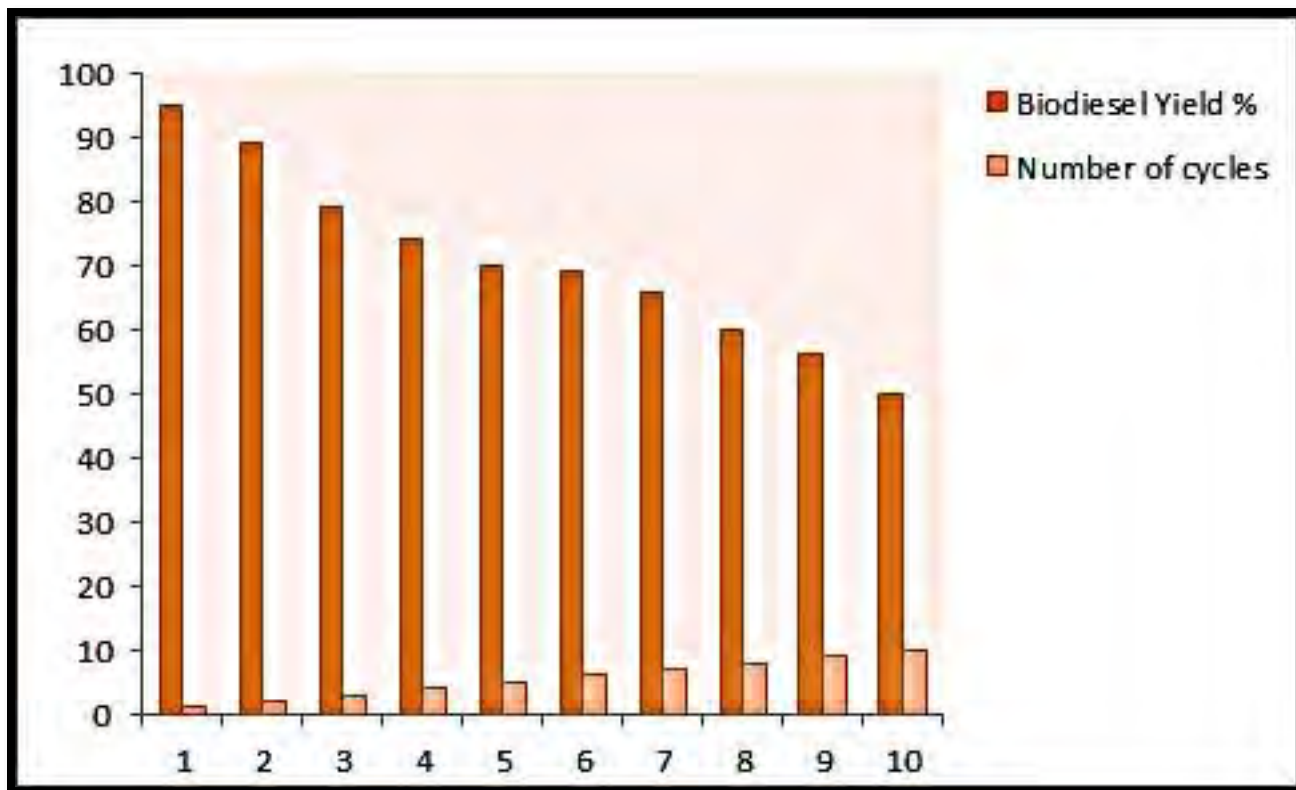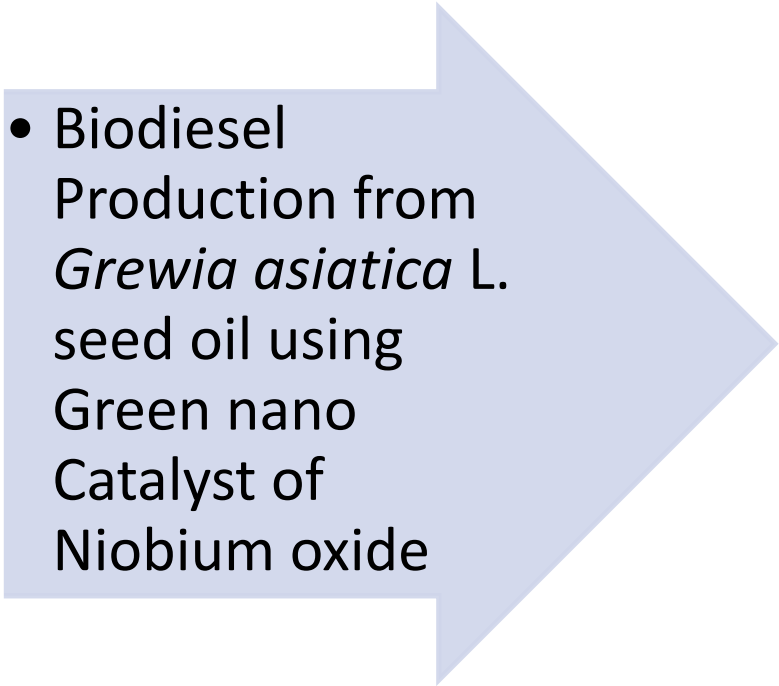
Figure 3.7.11 Reusibility of ZrO$_2$ NPs in transesterification reaction.

SECTION VIII

- Biodiesel Production from *Grewia asiatica* L. seed oil using Green nano Catalyst of Niobium oxide

Nb_2O_5 has not been used previously in synthesis of biodiesel. Green nanoparticles of Nb_2O_5 are also synthesized for the first time using aqueous leaf extract of *Fumaria indica*.

3.8.1 Catalyst characterization

3.8.1.1 X-Ray Diffraction (XRD) of Nb_2O_5

X-Ray Diffraction is a regularly employed method for investigating basic composition, size and crystal structure of nanocatalyst calcined at various temperature and time. Figure 3.8.1 shows the XRD pattern of green Nb_2O_5 NPs. Energy diffraction peaks at 2θ values of 9.1º, 7.34º, 25.60 º, 26.03º, 27.21 º, 29.05 º, 36.36 º, 37.31º, 44.01º, 47.62º, 48.93 º, 51.36º, 45.21º, 46.02 º, 49.15º, 51.14º, 55.07 º, 58.52º, and 59.46 º corresponded to 301, 304, 110, 405, 402, 313, 803, 007, 703, 709, 704, 708, 813, and 626 *hkl* respectively. Crystalline size of Nb_2O_5 NPs was determined with XRD pattern of most deep peak appeared at 2θ value of 25.60 º (highest peak 110).

The reflection peaks have revealed the monoclinic phase lettuce structure. The average size of nanoparticles in the current study was around 31 nm, which clearly demonstrated that Nb_2O_5 particles manufactured using a green method are nanoparticles in nature. Green NPs of Nb_2O_5 were formed, as shown by comparison of the XRD pattern with the standard. Results of Nb_2O_5 X-Ray Diffraction were discovered in agreement with SEM.

3.8.1.2 Scanning Electron Microscopy (SEM) of Nb_2O_5

SEM was used to examine the surface morphology of green nanoparticles of Nb_2O_5. The nano catalyst's topology was seen to have a uniform cubical shape. Figure 3.8.2 shows a micrograph of a SEM that demonstrates a rectangular and largely homogeneous particle structure. Due to the agglomeration of smaller nanoparticles in the SEM examination, larger nanoparticles are also seen.

3.8.1.3 Energy Diffraction X-ray (EDX) of Nb_2O_5

The chemical makeup of synthesized nanoparticles was identified using energy diffraction (EDX). Peaks of Nb and O seen in the spectrum provided evidence that Nb_2O_5

nanoparticles had formed (Figure 3.8.3). Nb and O made up, respectively, 25.22% and 74.88% of the total. The lack of additional unnecessary peaks in the EDX spectrum demonstrated the purity and lack of other elements in green nanoparticles.

3.8.1.4 Fourier Transform Infrared Spectroscopy (FTIR)

The spectrum of Nb_2O_5 nanoparticles was discovered using Fourier-transform infrared spectroscopy in the absorbance mode. The absorbance of Nb_2O_5 nanoparticles was measured over the wavelength range of 515 cm^{-1} to 4000 cm^{-1}. Figure 3.8.4 shows the FT-IR spectrum of Nb_2O_5 nanoparticles. Physiosorbed water molecules (OH stretch) are responsible for the distinctive characteristic absorption at 935 cm^{-1}, and the strong bands at 1478 cm^{-1} and 2465 cm^{-1} are ascribed to Nb-O stretching. These groups collectively mediate the reduction of Nb_2O_5 nanoparticles.

3.8.1.5 Thermogravimetric analysis (TGA) of Nb_2O_5

The thermal stability of Nb_2O_5 nanoparticles is examined by thermo gravitational analysis (TGA). Figure 3.8.5a shows the thermogram of synthesized nanoparticles and the related derivative thermogram (Figure 3.8.5b). Three stages of heat deterioration were visible in both thermograms. At temperatures between 50 °C and 100 °C, 0.86% of the mass of Nb_2O_5 nanoparticles was lost during the early stage. This loss is related to water being removed from molecular surfaces and evaporation.

Thermal degradation (0.98%) was observed in the second step at temperatures between 110 ◦C and 200 ◦C, revealing considerably increased thermal stability of Nb_2O_5 nanoparticles and enhanced catalytic activity. Particles underwent additional change (1.36%) in the third stage, which happened at temperatures between 201 °C and 950 °C. In Figure 3.8.5b endothermic peaks of derivative curve (wt.%), are clearly visible.
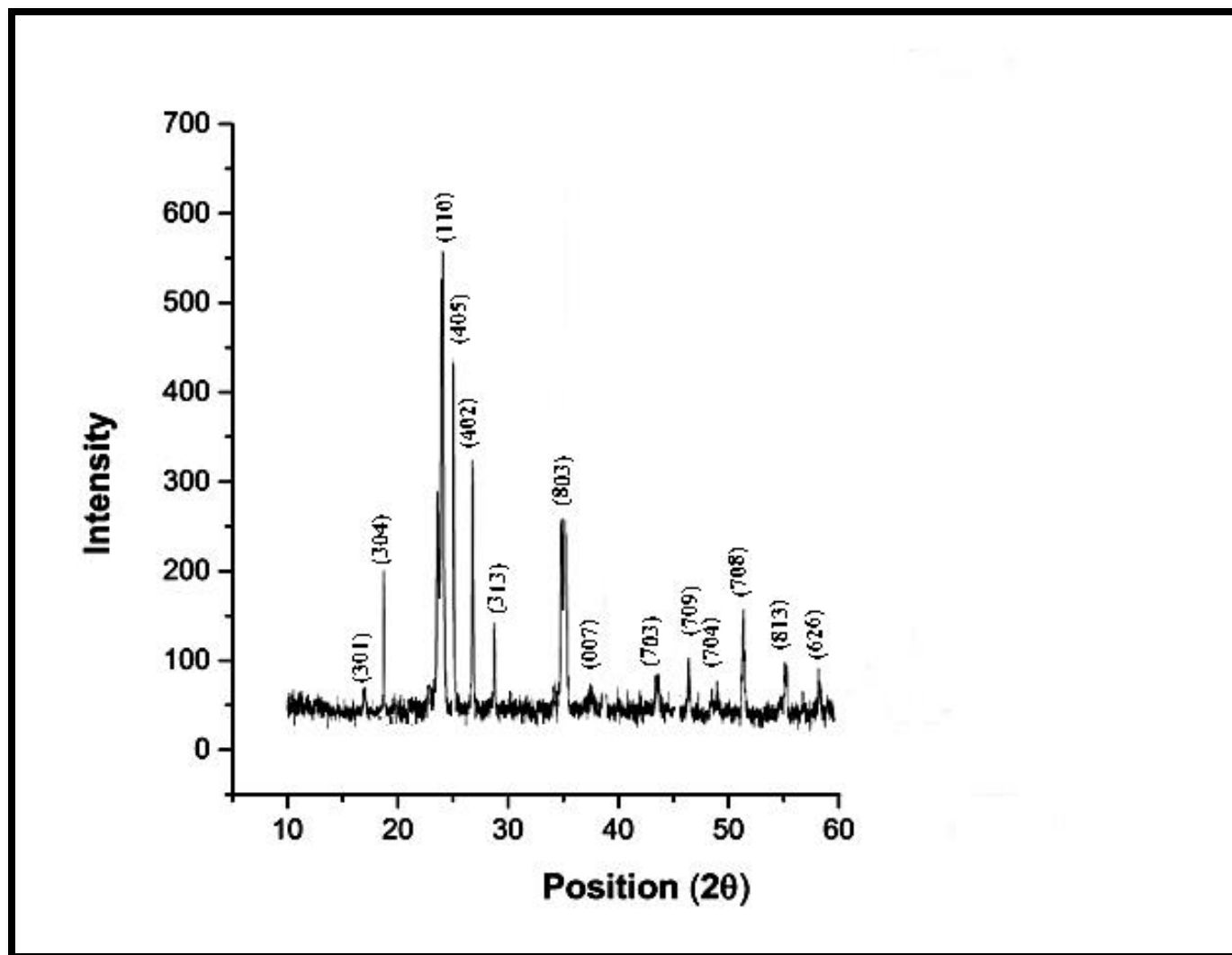
Figure 3.8.1. XRD pattern of calcined niobium oxide nanoparticles
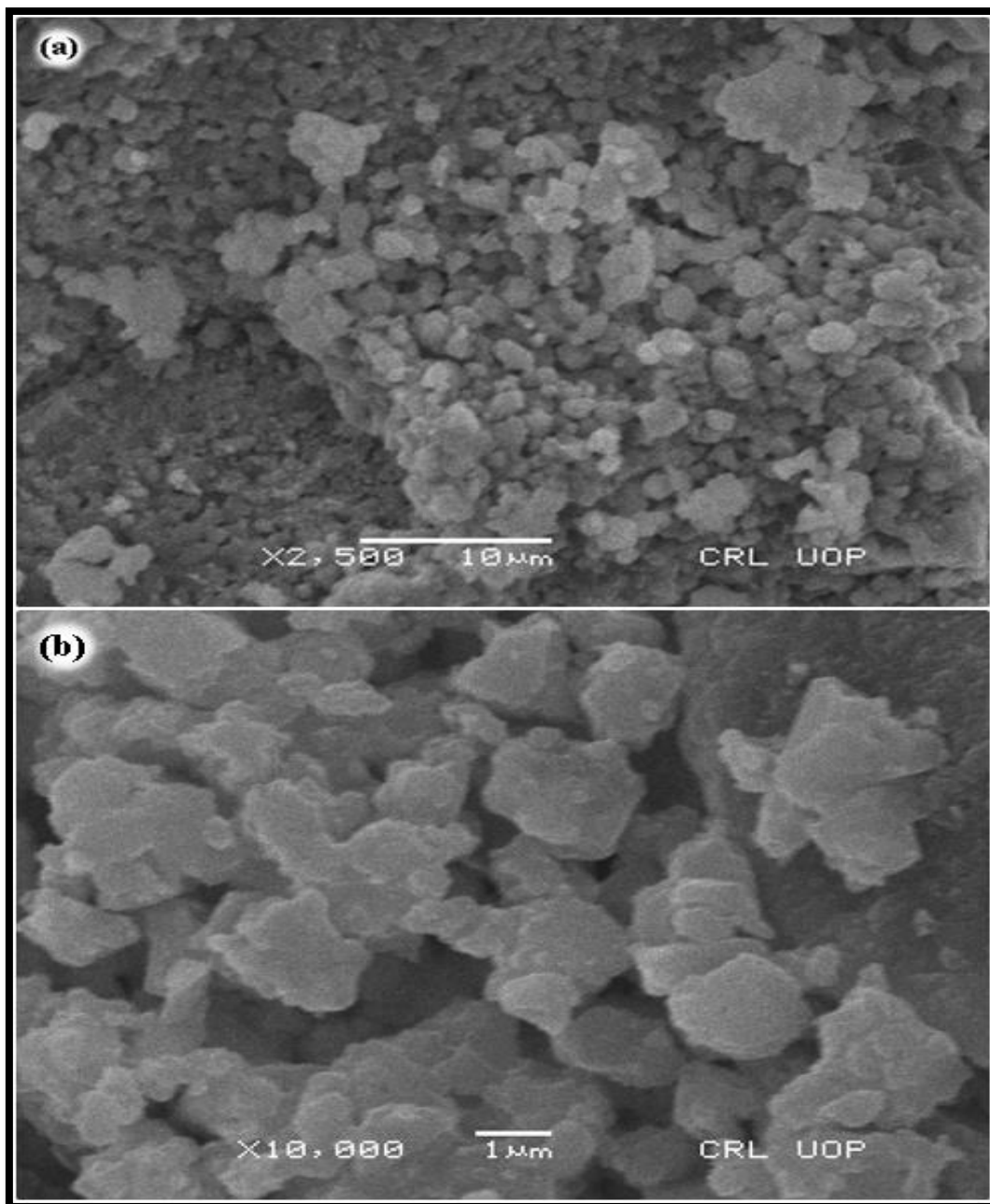
Figure 3.8.2. Scanning electron microscopy (SEM) of niobium oxide nanoparticles
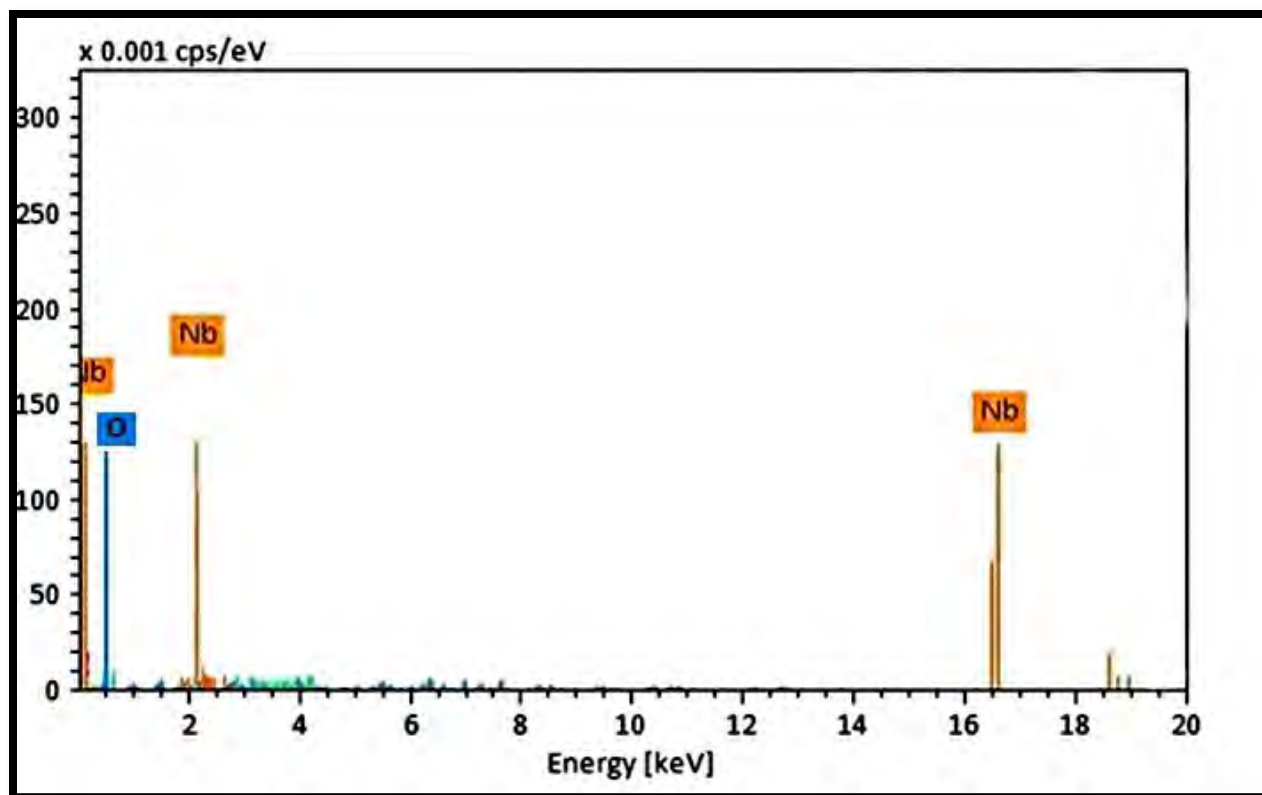
Figure 3.8.3. Energy diffraction X-Ray (EDX) of niobium oxide nanoparticles
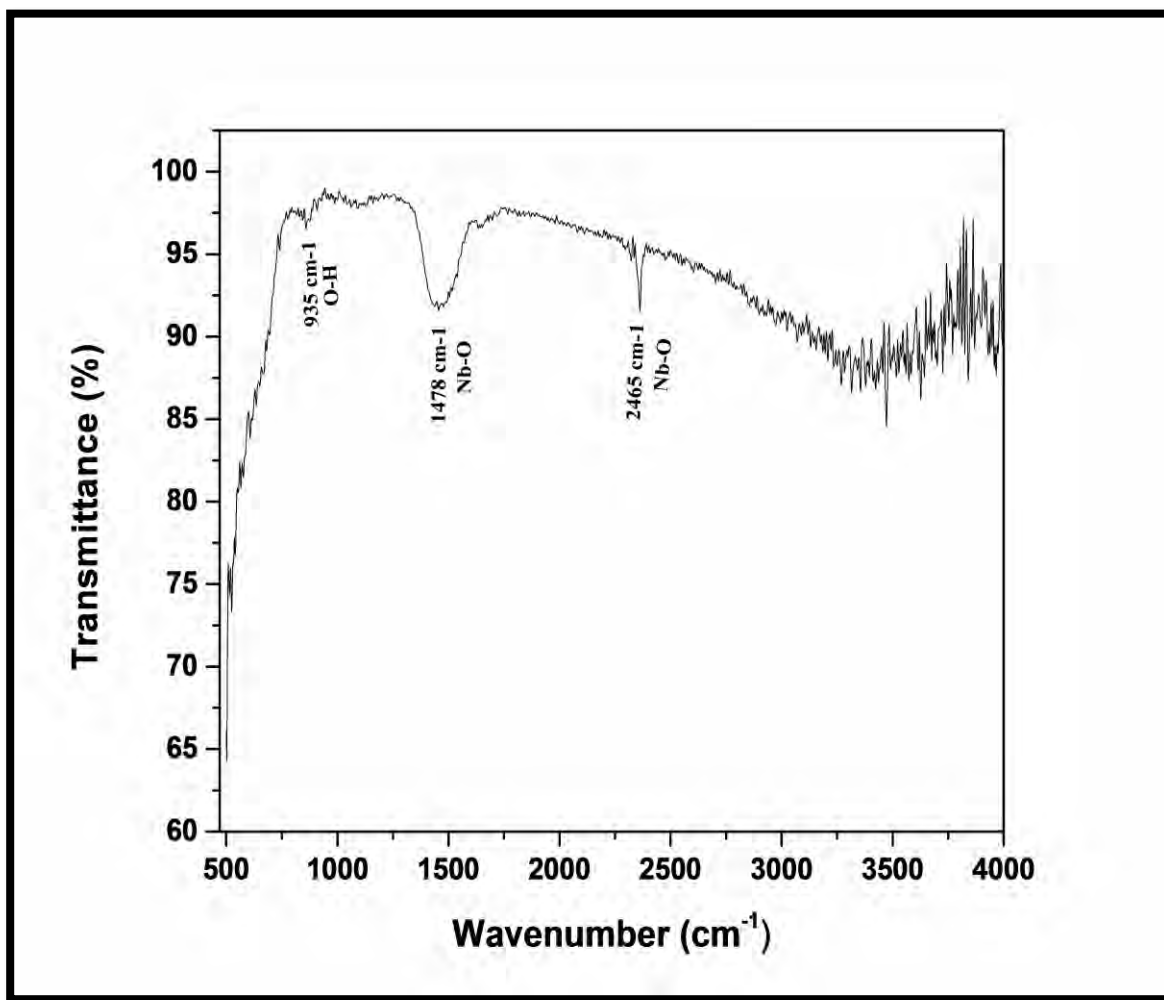
Figure 3.8.4. FTIR spectrum of niobium oxide nanoparticles
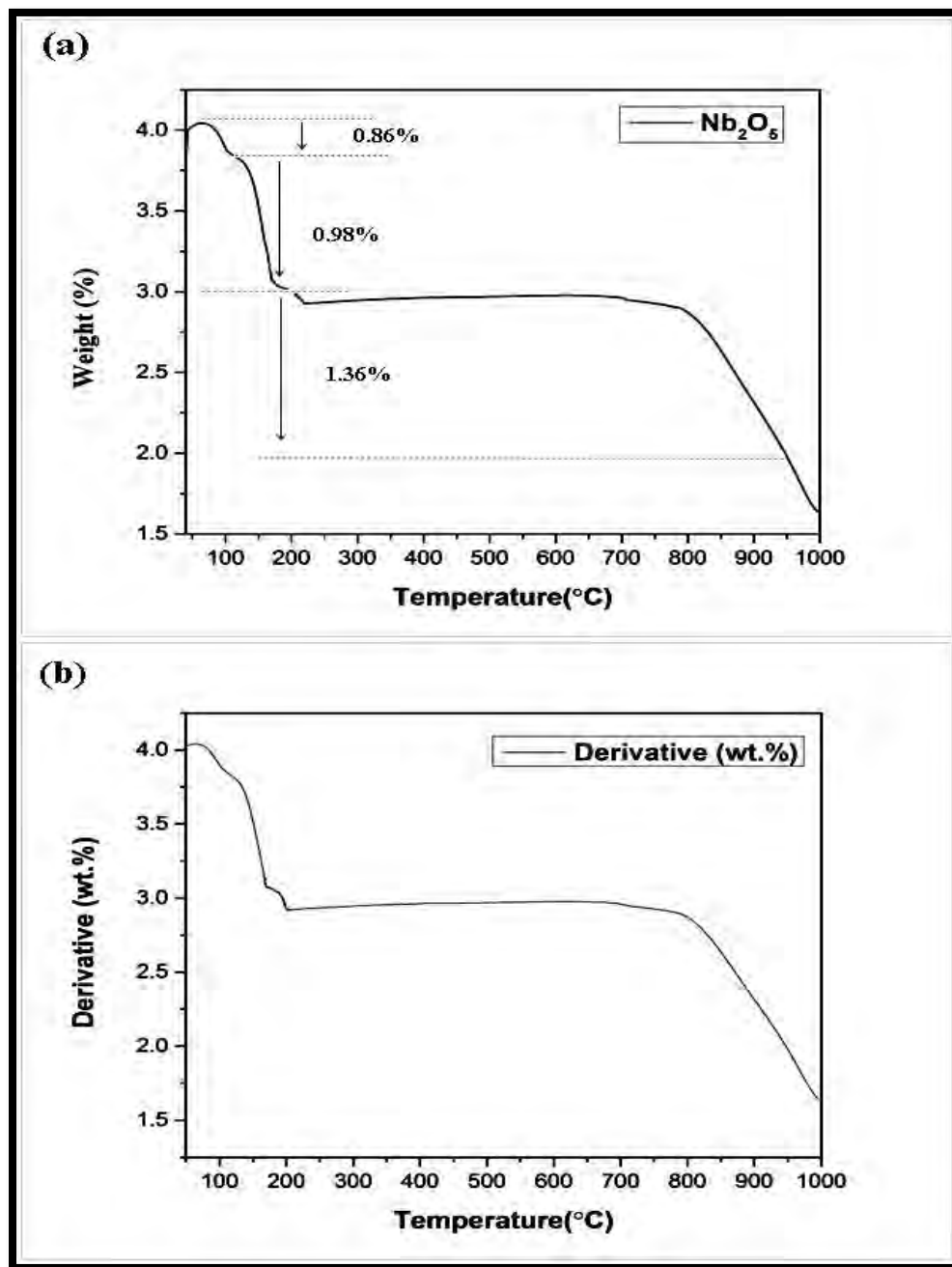
Figure 3.8.5. (a) TGA of niobium oxide nanocatalyst (b) derivative thermogram of niobium oxide nanocatalyst

3.8.2 Biodiesel synthesis via transesterification

In this study, green nano-particles of iron oxide were used to create methyl ester from unique, inedible *Grewia asiatica* seed oil. Compared to other reported species, the seed oil content of was 25% of the total dry weight (Ong et al., 2020). A single step transesterification reaction was produced by seed oil, which had a significantly reduced free fatty acid content of 0.72 (wt.%). A higher than 3% FFA content in seed oil is considered undesirable and requires an additional step of acid esterification, which limits the amount of triglycerides that may be converted to methyl esters during the transesterification reaction (Falowo et al., 2020). As a result, *Grewia asiatica* L. seed oil can be effectively used for the production of methyl ester in a single step. Aqueous *Fumaria indica* (Hausskn.) Pugsley leaf extract was used to create phyto-nano iron oxide particles, which were then used to transesterify the extracted seed oil.

Response Surface Methodology was extensively used to determine the ideal transesterification reaction conditions in order to obtain the highest methyl ester yield possible. As shown in Tables 3.8.1 and 3.8.2, the central composite design (CCD) was created using four independent transesterification variables with lower and higher values, including catalyst concentration of 0.32-0.88 weight percent (A), temperature of 60–120 ∘C (B), and the methanol to oil molar ratio of 3:1–15:1. Figure 3.8.6 shows the contrast between the predicted and actual yield of methyl ester. 8 showed that both of these values are distributed quite close to the straight line, indicating a strong link between them. In Table 3.8.3, comprehensive findings from the Response Surface Quadric model's statistical analysis of variance are shown. The significance of the quadric model was determined with a low p-value of 0.0001 (0.05). Additionally, the quadric model's lack of fit F-value, which had a value of 8.41, was judged to be insignificant in comparison to the pure error. In addition, the most significant term among the quadratic terms of the transesterification catalyst loading (A^2) had a *p*-value of 0.0001 and was followed by catalyst load (B^2), The adjusted R^2 value of 0.8870 was sufficiently near to the predicted value of 0.7811, and there was a variance of 0.2 between the two. We were able to measure the model's signal to noise ratio thanks to enough precision. It was discovered in the present model to be 10.299, proving that the experimental model can accurately forecast methyl ester yield. A favourable

ratio is one that is greater than 4 (Muanruksa and Kaewkannetra 2020). Below is the polynomial equation (8) used in the experimental model.

Biodiesel Yield (wt. %) = +81.22-1.33*A-1.61*B+0.5251*C+2.98*D+0.4375*AB-1.56 *AC+0.4375 *AD-0.5625 *BC-0.2846 *BD-0.0625 *CD-14.92 *A²+2.54 *B²-5.19 *C²+1.82 *D² (14)

Table 3.8.1- Experimental design by central composite design for transesterification reaction

Process parameters	−1	+1
Methanol to oil ratio	3:1	15:1
Catalyst loading (wt. %)	0.32	0. 88
Reaction time (min)	60	180
Temperature (∘C)	60	120

Table 3.8.2- Detailed experimental result for transesterification reaction of *Grewia asiatica* Biodiesel

	Factor 1	Factor 2	Factor 3	Factor 4	Response
Run	A: Alcohol to oil molar ratio	B: Catalyst loading wt.%	C: Temperature °C	D: Reaction time (min)	Yield wt.%
1	3.1	0.32	60	60	68
2	3.1	0.32	120	60	65
3	9.1	0.32	120	180	69
4	9.1	0.32	60	120	87
5	15.1	0.32	120	60	64
6	3.1	0.32	60	180	67
7	9.1	0.585	120	120	83
8	15.1	0.32	120	180	64
9	9.1	0.32	120	180	67
10	15.1	0.585	60	120	68
11	9.1	0.32	60	60	60
12	9.1	0.32	60	180	90
13	9.1	0.32	120	180	58
14	9.1	0.585	90	180	77
15	15.1	0.32	90	180	70
16	9.1	0.85	90	120	79
17	15.1	0.32	90	60	65
18	9.1	0.32	90	120	65
19	15.1	0.85	60	180	62
20	9.1	0.88	120	180	56
21	9.1	0.585	60	120	76
22	3.1	0.32	60	120	70
23	9.1	0.32	60	60	60
24	3.1	0.85	60	180	65

25	3.1	0.85	60	60	60
26	15.1	0.85	120	60	58
27	9.1	0.88	60	120	58
28	9.1	0.85	60	60	68
29	15.1	0.85	120	180	62
30	15.1	0.85	60	180	70

Table 3.8.3- ANOVA for Response Surface Quadratic model

Source	Sum of Squares	df	Mean Square	F Value	p-value	
Model	2294.34	14	163.88	8.41	< 0.0001	significant
A-Methanol to oil Ratio	32.00	1	32.00	1.64	0.0195	
B-Catalyst Concentration	45.48	1	45.48	2.33	0.0474	
C-Temperature	5.16	1	5.16	0.2645	0.0145	
D-Time	182.22	1	182.22	9.35	0.0080	
AB	3.06	1	3.06	0.1571	0.0074	
AC	39.06	1	39.06	2.00	0.0173	
AD	3.06	1	3.06	0.1571	0.0274	
BC	5.06	1	5.06	0.2597	0.0177	
BD	1.34	1	1.34	0.0688	0.0166	
CD	0.0625	1	0.0625	0.0032	0.0456	
A²	662.21	1	662.21	33.98	< 0.0001	
B²	14.80	1	14.80	0.7595	0.0372	
C²	93.83	1	93.83	4.81	0.0444	
D²	11.67	1	11.67	0.5989	0.0410	
Residual	292.36	15	19.49			
Lack of Fit	145.36	10	14.54	0.4944	0.8394	not significant
Pure Error	147.00	5	29.40			
Cor Total	2586.70	29				

$R^2 = 0.8870$, Std. Dev. = 4.41,   C.V. % = 8.09, Adeq Precision = 10.299
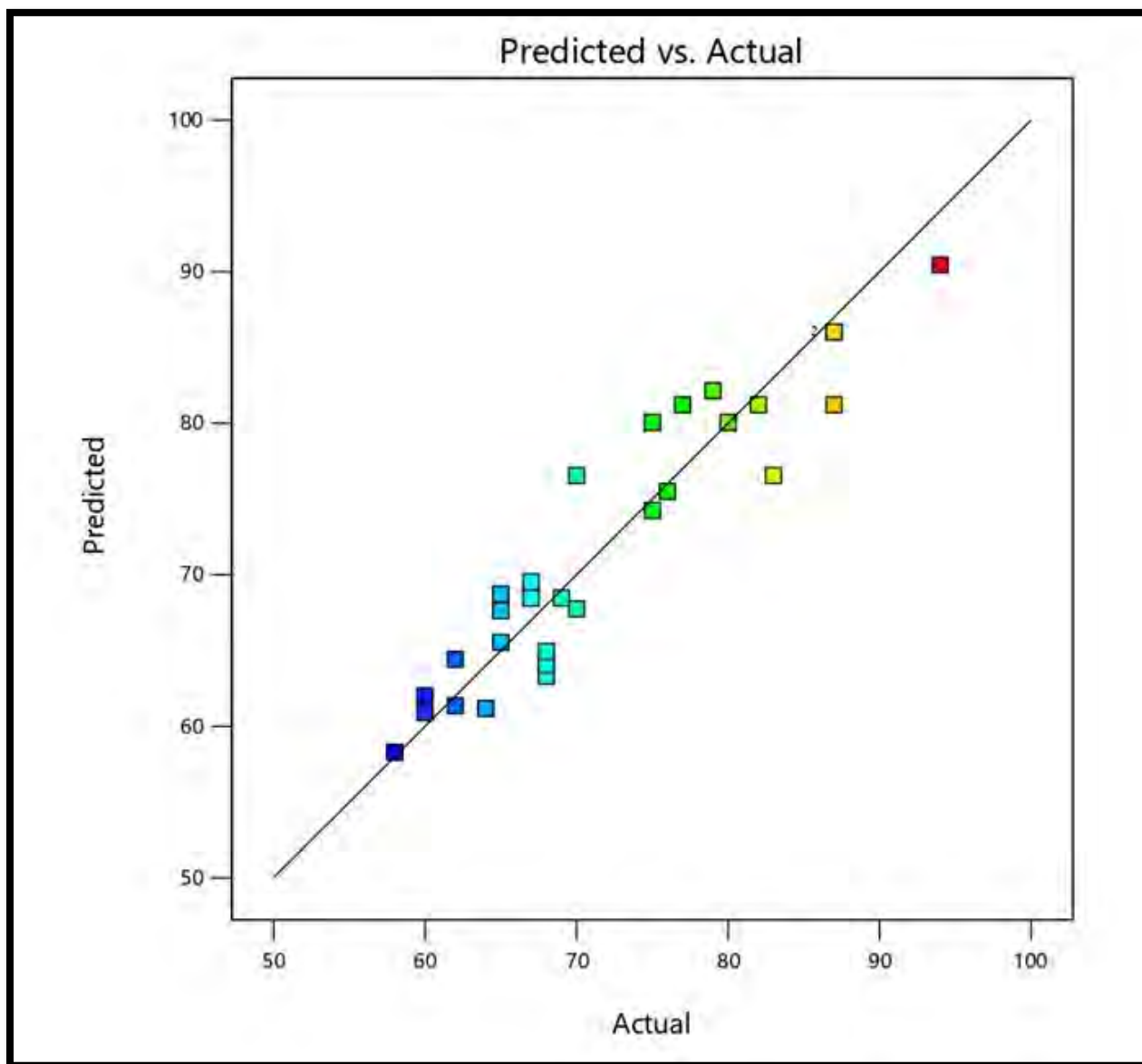
Figure 3.8.6. Comparison between the experimental and predicted yield of biodiesel in the model

3.8.3 Impact of reaction Parameters on Transesterification

3.8.3.1 Combined influence of oil to methanol molar ratio and catalyst loading

Transesterification is significantly influenced by the relationship between catalyst amount and Met:Oil ratio. Plots in three dimensions are shown in Figure 3.8.7a as an example of this mutual interaction. The highest production of 90% biodiesel was seen at a catalyst loading of 0.32 (wt. %), a Met:Oil ratio of 9:1, 180 min, and a temperature of 60 ∘C. (Run 12). At Run 19, the synthesis of methyl ester decreased by 62% as a result of higher catalyst concentration of 0.85 (wt. %) and higher Met:Oil ratio of 15:1. At Run 10, a catalyst loading of 0.58 (wt. %) with a Met:Oil ratio of 15:1 resulted in a low yield of 68%. When the amount of methanol in the reactant mixture exceeds the optimal level, it thins the concentration of the catalyst, favoring reversible reactions. As a result, glycerolysis occurs in the reacting mixture, facilitating the recombination of glycerol with FAMEs and the reformation of monoglycerides (Naveenkumar and Baskar 2020). Low yield of 67% was added by a lower Met:Oil ratio of 3:1 and a catalyst concentration of 0.32 (wt.%) (Run 6). The findings of the ANOVA verified the significant relationship between Met:Oil and catalyst loading with a p-value of 0.0074 (<0.05).

3.8.3.2 Combined influence of oil to methanol ratio and reaction temperature

Figure 3.8.7b shows the impact of the ratio of Met:Oil and reaction temperature on the methyl ester yield that results. A higher yield of 90% was obtained at optimum temperature of 60 ∘C, the ratio of Met:Oil was 9:1. (Run 12). At Run 3, the same Met:Oil (6:1) and 120 oC conditions produced an 69% yield. A maximum output of 70% was attained at 90 ∘C with a Met:Oil ratio of 15:1 at Run 15. The excess of methanol is blamed for the rise in methyl ester yield because it stimulates the catalyst to produce methoxy species, which drive the reaction forward (Bohlouli and Mahdavian 2019). Results of the experimental investigation showed that a constant rise in temperature has a significant impact on reaction rate. The study found that 60 °C was the ideal temperature for transesterification because it lowers activation energy and improves contact between the catalyst and the reactants, resulting in the greatest conversion of reactants into products. The methyl ester yield drops to 64% at Run 8 due to higher molar ratios of 15:1 and 120 ∘C. This correlation was substantial according to the ANOVA results (*p*-value 0.0173).

3.8.3.3 Combined influence of oil to methanol molar ratio and reaction time

The Met:Oil ratio and reaction time have a substantial interaction effect on the generation of biodiesel. The combined effect of Met:Oil, duration at constant temperature (60 °C), and catalyst loading (0.32 wt.%) was explained in Figure 3.8.7c. The catalyst loading of 0.32 (wt.%) with a met:oil ratio of 9:1 produced the highest output of biodiesel, 90% (Run 12). At reaction time 120 (min), yield was slightly reduced to 87% with the same Met:Oil (Run 4). Yield decreased even further, to 65%, at Met:Oil 15:1 and 60 (min) (Run 17).A surplus of alcohol increases the solubility of glycerol, making biodiesel purification challenging (Mokbli et al., 2018). There are specific oil to methanol molar ratios to yield methanolysis, as shown in numerous research (Yazdani et al., 2019). At Met:Oil 6:1 and time 55 (min), around 64% yield was attained (Run 19). It unquestionably led to incomplete conversion and a low yield of methyl ester because there was not time to adequately combine the reactants and reach equilibrium going forward (Feyzi and Shahbazi 2019). With the lowest Met:Oil ratio of 3:1 and time 120 (min), the minimum yield of 70% was attained (Run 18). Results from the ANOVA showed a significant association between molar ratio and reaction time, with a *p*-value of 0.0274 less than 0.05.

3.8.3.4 Combined influence of catalyst loading and reaction temperature

Figure 3.8.7d illustrates the impact of mutual interaction between catalyst loading, temperature, at constant Met:Oil ratio 9:1 oil and the and time (180 min) on transesterification. It is attributed to complete contact of seed oil with methanol during transesterification at these reaction conditions (Roy et al., 2019). At Met:Oil, of 9:1, with a catalyst concentration of 0.32 (wt.%), time 180 min., and a temperature of 60 oC, the highest output of 90% biodiesel was obtained (Run 12). With a temperature of 120 ∘C and a reduced catalyst loading of 0.32 wt.%, about 67% yield was produced (Run 9). It is believed that the minimum boiling point of alcohol is to blame for the transesterification's forward reaction being slowed down. At Run 14, a reaction temperature of 90 ∘C and a Nb_2O_5 loading of 0.58 wt.% resulted in about 77% yield (Run 14). When MgO concentration was increased from 0.5 to 2%, it was shown to improve the yield of FAME in soybean oil. However, as concentration increased further, the yield of

biodiesel declined. Thus, their findings are in complete agreement with the findings of our current investigation (Elkelawy et al., 2019). At the highest Nb_2O_5 loading of 0.88 wt.% and temperature of 120 ◦C, a minimum yield of 56% was obtained (Run 20). However, the extra catalyst concentration over this threshold reduced the FAME yield due to an increase in reaction mixture viscosity and a decrease in catalytic activity, which reduced interaction between the catalyst and reactants and caused a low product concentration (Ambat et al., 2020). Combination impact was deemed significant by having a *p*-value of 0.0177.

3.8.3.5 Combined influence of catalyst loading and reaction temperature

The combined impact of time and catalyst concentration on FAME synthesis is depicted in a 3D figure in Figure 3.8.7e. The maximum biodiesel production of 90% was attained after 180 min at a constant Met:Oil of 9:1 at a temperature of 60 ◦C. (Run 12). A yield of nearly 76% was attained with a nano catalyst concentration of 0.58 (wt.%)) and a run time of 120 min (Run 21). Cut yield to 68% with a catalyst concentration of 0.88 (wt.%) over 60 min (Run 28). A 60 min of reaction time and a catalyst concentration of 0.32 (wt.%) led to a minimum yield of 60%. (Run 23). The yield was further decreased to 58% after 180 min of reaction time and at a catalyst concentration of 0.88 (wt.%) as triglycerides partially converted to biodiesel (Run 27). Therefore, it was inferred from this investigation that joint effect of Met:Oil and reaction temperature is worthy to be keep under consideration in transesterification reaction. Significant relationship between Met:Oil and reaction time was declared by ANOVA results with *p*-value of 0.0166 lesser than 0.05.

3.8.3.6 Combined influence of reaction time and temperature

The productivity of biodiesel with constant catalyst loading (0.32 wt.%) and Met:Oil 9:1 has been shown to be affected jointly by time and temperature in Figure 3.8.7f. It can be proven that the reaction time was too short to achieve chemical equilibrium and that the catalyst needed time to interact, resulting in a lower-quality product. After 2 hours, the forward reaction was in full swing, equilibrium had been reached, and a maximum conversion yield of 90% had been noted at run 12. With a longer reaction period, a steady elevation in FAME yield was observed.

At a fix Met:Oil (9:1) and catalyst loading (0.32 wt.%), the highest productivity of 90% biodiesel was attained in 180 minutes at 60 ∘C (Run 12). From Run 18 with time 120 min and temperature 90 oC, about 65% of the yield was revealed. Time of 180 min at a high temperature of 120 ∘C resulted in a further 58% reduction in methyl ester synthesis (Run 13). This investigation revealed that reaction productivity increased with rising temperature and reaction duration up to a certain point, beyond which a significant decline in percent yield was seen, which is due to the endothermic nature of transesterification. Minimum productivity was 60% was achieved at reaction time 60 min and temperature of 60 ∘C at Run 11. ANOVA results with a *p*-value of 0.0456 (<0.05) showed a significant association between time and temperature on transesterification.
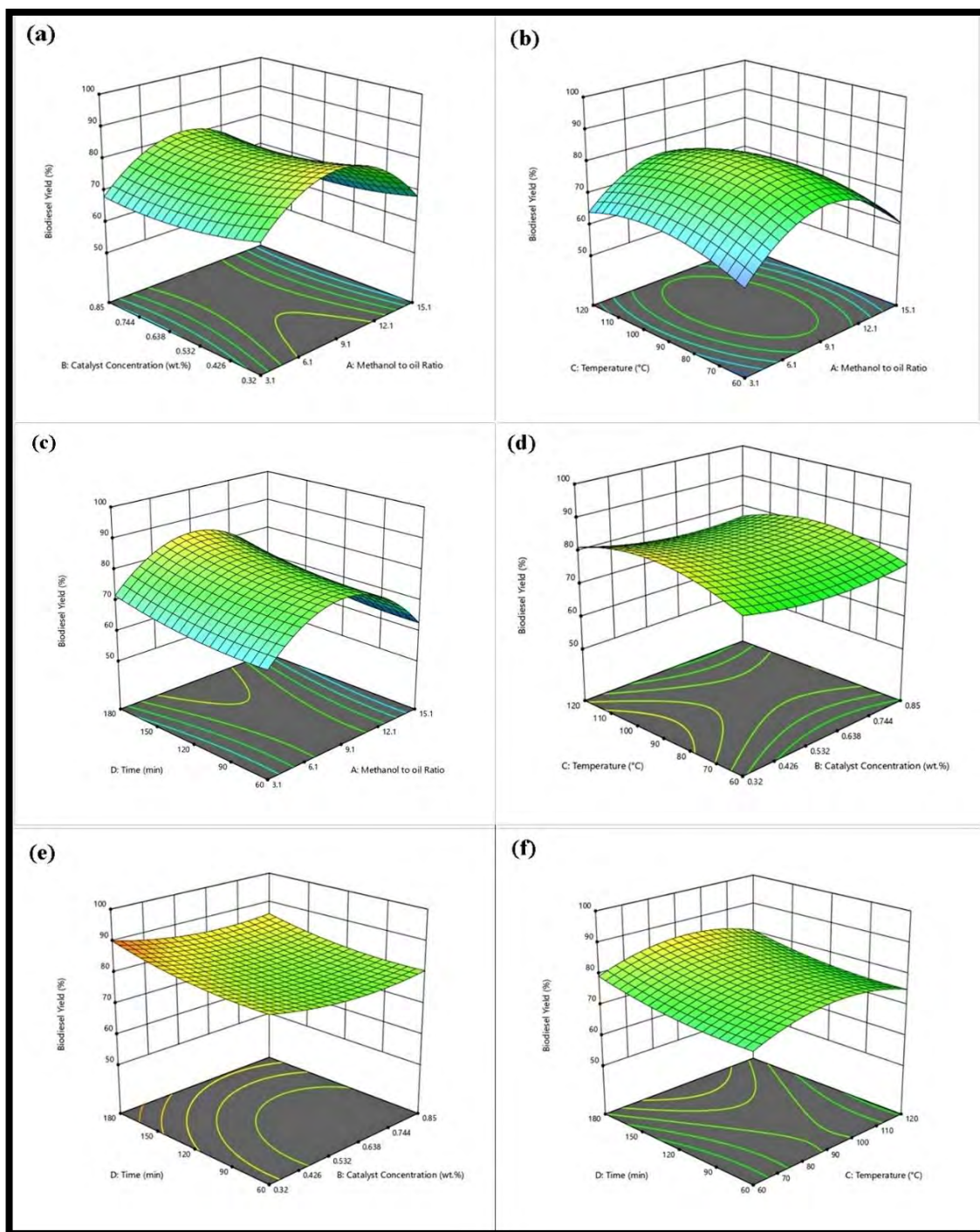
Figure 3.8. 7. Impact of the reaction conditions of *Grewia asiatica* biodiesel.

3.8.4. Biodiesel characterization

3.8.4.1 FTIR spectroscopic Study

One of the widely utilized methods for examining the structural composition of biodiesel is FTIR spectroscopic analysis. Once transesterification is complete, it aids in the confirmation of methyl ester production. Figure 3.8.8 a and b, which show the FTIR spectra of synthetic methyl ester and oil from *Grewia asiatica*, respectively, show the numerous bands and stretches of functional groups that may be found in triglycerides and methyl ester. In the biodiesel spectrum, a key band for the carbonyl group (C=O) could be seen at 1743.52 cm^{-1} in the infrared, while a band for the methyl group (CH_3) could be seen at 1464.47 cm^{-1}. These two bands' presence is proof that methyl ester formed at the conclusion of transesterification. Stretch for CH (sp^2) was observed at 2853.31 cm^{-1}, while the characteristic peak of C-H (sp^3) occurred in the IR region at 2922.62 cm^{-1}. The carbonyl group's IR region is thought to be the most susceptible to chemical and molecular changes in the biodiesel spectrum of all the other peaks (Rozina et al., 2021). Stretch (O=C-O-C) for aliphatic esters detected at 1160.26 cm^{-1}.

A very variable portion of the oil and biodiesel spectra was found between 1000 and 2000 cm^{-1} and 3300 and 2800 cm^{-1}. The resulting stretch peak in the spectra at 1098.06 cm^{-1} was the wagging frequency for $C-H_2$. When compared to the spectrum of methyl ester, intense peaks at 3321.97 cm^{-1} that occurred in the spectrum of *Grewia asiatica* seed oil vanished in the spectrum of methyl ester. In the spectra of methyl ester, the deep stretch for (O-H) at 1023.10 cm^{-1} was gone. These analyzed peaks on the spectrum of methyl ester and seed oil from *Grewia asiatica* have confirmed that transesterification converts oil triglycerides into methyl esters.

3.8.4.2 NMR Spectroscopic Analysis

The ^{1}HNMR spectroscopic approach was used to confirm and measure *Grewia asiatica* biodiesel (GABD). In biodiesel samples at various life cycle stages, such as after transesterification, purification, heat treatment, and storage, NMR spectroscopy is frequently used to investigate transesterification reaction and quantify the amount of saturated and unsaturated fatty acid methyl esters (Maneerung et al., 2016). Figure 3.8.9a depicts the corresponding absorbance peak of the *Grewia asiatica* biodiesel ^{1}HNMR spectrum. The ^{1}HNMR

spectrum of biodiesel revealed a distinctive peak for the methoxy group (- OCH_3) at 3.670 ppm, indicating effective transesterification and subsequent methyl ester synthesis. In the 1HNMR spectra of GABD, no unwanted methanol signal was found. Typically, it is detected around 3.45 ppm.

The proton peak for the triplet methylene (-CH_2) in the ^{1}HNMR spectra of CHBD was discovered at 2.283-2.333 ppm. At 1.261–1.309 ppm, a singlet-like peak for -CH_2 (-methylene) protons was seen in the spectra. The hydrogen element on the C-3 of the aliphatic straight fatty chain of a hydrocarbon corresponds to these protons of -methylene. peak of incorporated terminal methyl protons at 0.864–0.918 ppm. The signal observed at 5.311-5.401 ppm was considered to be olefinic hydrogen, which has two carbon atoms linked by a double bond (-CH=CH-). Allylic hydrogen was responsible for the peak that was seen at 2.757-2.777 ppm (-CH_2). These ^{1}HNMR peaks have demonstrated the existence of methyl esters in the biodiesel sample. The entire conversion of triglycerides into FAME was calculated and it was found to be 93%.

The position of the esters carbonyl (-COO-) and C-O group, as well as other structural details, were explored using the biodiesel from *Grewia asiatica* ^{13}CNMR spectrum. Figure 3.8.9b shows the ^{13}CNMR spectrum of *Grewia asiatica* biodiesel that has been manufactured. Methoxy carbon was defined in the ^{13}CNMR spectra by a peak at 51.40 ppm. At 174.26 ppm, a signal for the carbonylic group (-COOH) was detected. The peak at 127.88-128.02 ppm, which represented the internal non-conjugated carbon atoms, allowed for the detection of the degree of unsaturation, which is represented by the double bond between carbon atoms (-CH=CH-), in the biodiesel sample. Additionally, chemical shifts seen between ppm values 129.71 to 130.15 ppm showed that the ^{13}CNMR spectra contained exterior carbons of non-conjugated carbons (-CH=CH-). C-O group signal was detected between 76.63 to 77.48 ppm. The peak at 29.09–29.76 ppm was caused by a long sequence of ethane carbon (–CH_2)n. Finally, the peak for the carbon atom in aliphatic methylene (-CH2-s) was found to be between 31.52 to 34.07 ppm.

3.8.4.3. GC/MS Analysis

The fatty acid profile has a significant impact on biodiesel quality. The ester components of the biodiesel sample were identified for this purpose using GC/MS analysis. Figure 3.8.10 shows the gas chromatogram of *Chamaerops humilis* biodiesel, which exhibits eight distinct peaks of saturated and unsaturated methyl esters. These peaks were further confirmed by MS analysis using the library match program NO. NIST02. Hexadecanoic acid methyl ester (C16:0), tridecanoic acid methyl ester (C14:0) and Octadecanoic acid, methyl ester (C18:0) were both found in saturated methyl esters. Unsaturated methyl ester composed of 5, 8-Octadecadienoic acid methyl ester (C18:2), and 9-Octadecenoic acid, (2)-methyl-, methyl ester (C18:1). The chromatogram with the highest abundance of 5, 8-Octadecadienoic acid methyl ester at retention time 11.85 min was found to be a significant fatty acid methyl ester. Typically, a biodiesel sample with a high content of saturated and monounsaturated fatty acid methyl esters is thought to be advantageous for obtaining the highest energy yield and oxidative stability. However, biodiesel high in polyunsaturated methyl esters has less oxidative stability but more attractive cold flow characteristics (Atabani et al., 2013). The methyl ester of *Grewia asiatica* has been shown by GC/MS analysis to be a very capable source of biofuel that can be generated on an industrial scale.
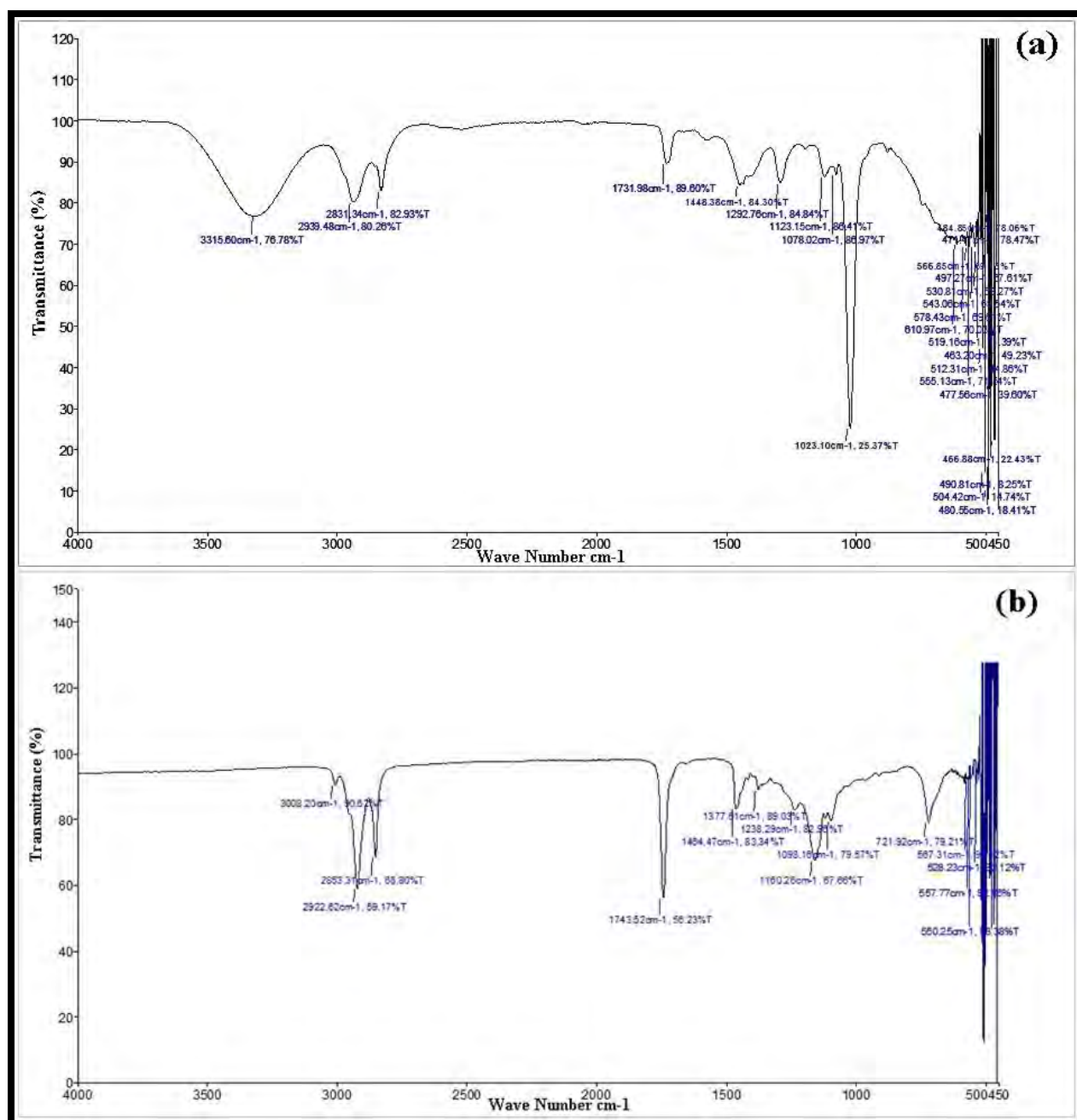
Figure 3.8.8. FT-IR spectrum of **(a)** *Grewia asiatica* seed oil and **(b)** biodiesel
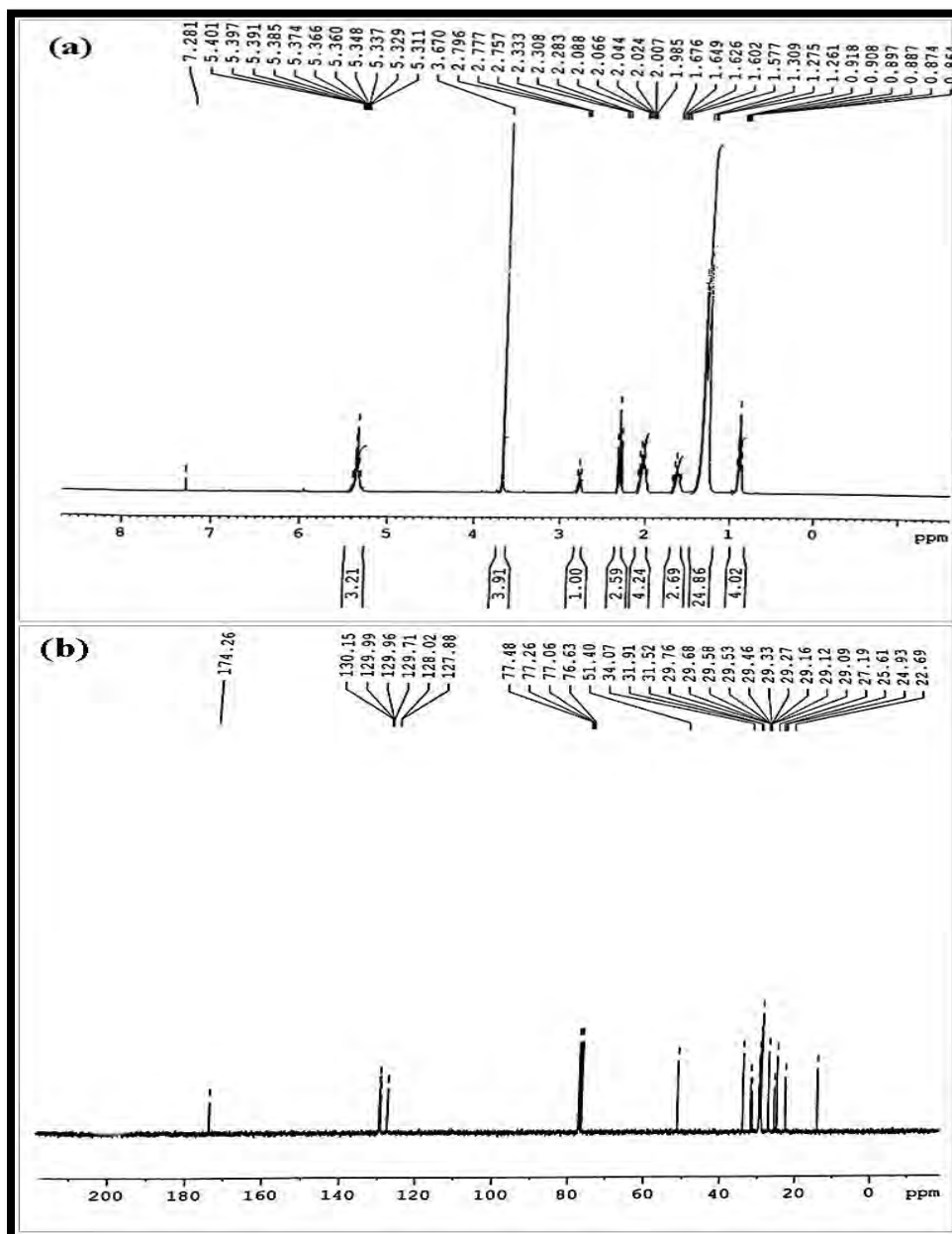
Figure 3.8.9. NMR spectrum of **(a)** ^{1}HNMR and **(b)** ^{13}CNMR of *Grewia asiatica* biodiesel
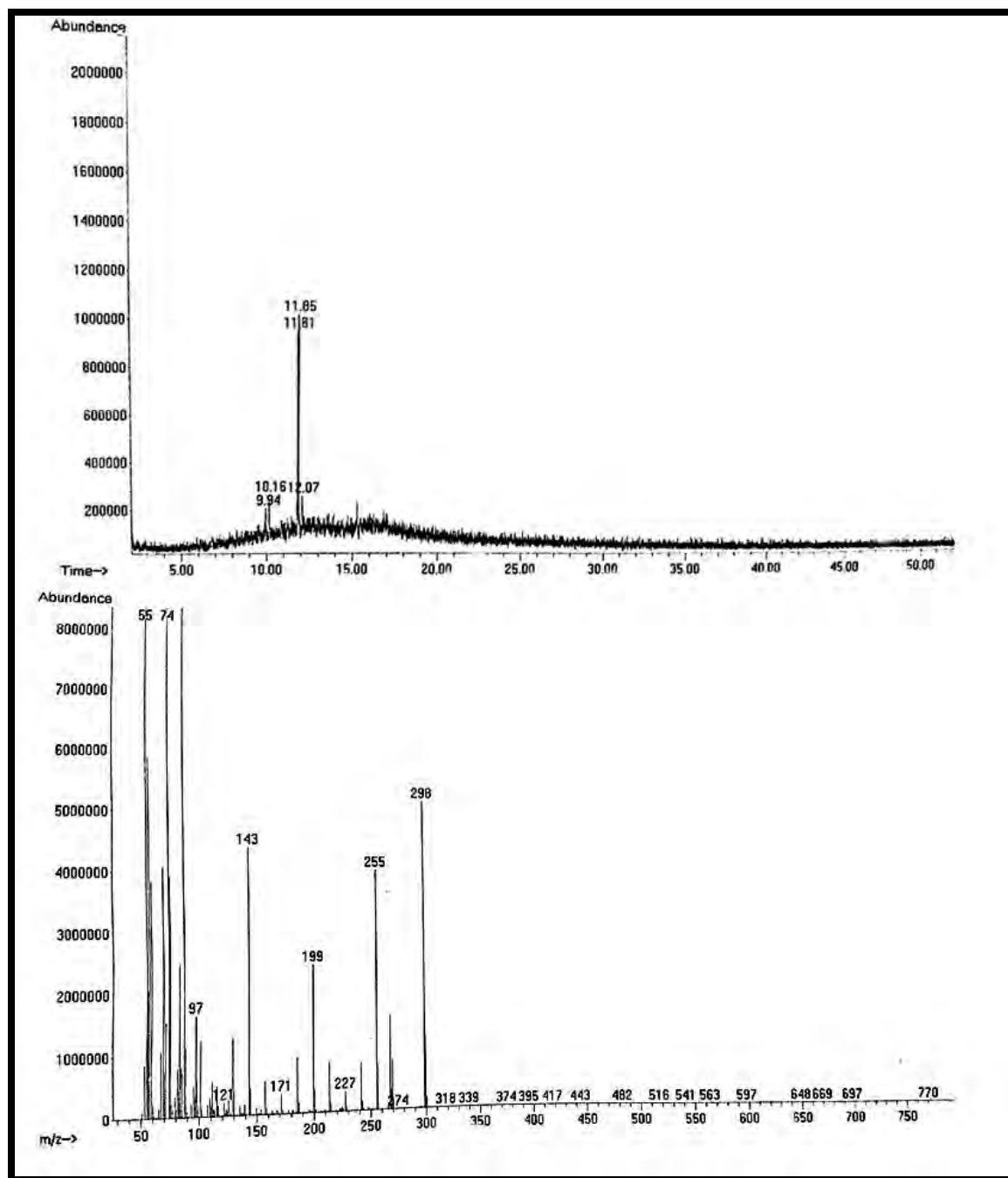
Figure 3.8.10 GC-MS spectrum of *Grewia asiatica* biodiesel

3.8.5. Analysis of Fuel Properties of biodiesel

Prior to practical application, it is necessary to do an analysis of the fuel qualities of a sample of synthetic methyl ester that must be comparable to international standards like ASTM D-6571, EN 14214, and China GB/T 20828-2007. The structure of the fatty acid profile in the seed oil used for transesterification has a significant impact on the physiochemical properties of biodiesel. Table 4 lists the biodiesel fuel qualities of *Grewia asiatica* that were investigated.

Acid value has a significant impact on the fuel's quality. The acid value of biodiesel therefore has a significant impact on engine performance. In order to neutralize the free fatty acids present in liquid fuel, a certain amount of potassium hydroxide is needed, and this is what it denotes. Old diesel engines' rubber components experience problems and corrode when biodiesel's acid value exceeds the permitted level. The methyl ester of *Grewia asiatica* had an acid value of 0.200 (mg KOH/gm), which was well within the range of fuel that is generally acceptable on a global scale.

Kinematic density significantly affects the fuel property of biodiesel, which directly regulates engine performance, fuel flow through pipeline systems, and injector nozzles. The viscosity of biodiesel is increased by fuels with higher density, which causes incomplete combustion and increased particulate matter generation (Ali et al., 2020). Kinematic density CHBD, which was determined to be 4.81 (mm2/s), fitted international fuel criteria very well.

Fuel atomization and fuel injector lubrication are significantly influenced by the kinematic viscosity of the fuel. Lower viscosity fuel results in leakage issues and provides less lubrication for injection pumps, which leads to increased power loss in the fuel engine. Similar to how increased viscosity ensures adequate fuel supply for the injection pump and subsequent engine efficiency (Saman et al., 2020). Kinematic viscosity of *Grewia asiatica* in the current experiment was 3.76 (mm^2/s), which is below the range of the international fuel standard.

The term "flash point" refers to the temperature at which fuel begins to burn when an ignition source is present. Fuel having a greater flash point has a lower danger of catching fire accidentally during storage and transportation (Borah et al., 2019). In comparison to traditional

fossil fuels, biodiesels have greater flash points, making them safer to handle. According to Table 3.8.4, the biodiesel made from *Grewia asiatica* had a flash point of 97 °C.

The pour and cloud points of the gasoline affect how well diesel engines work in colder parts of the world where the temperature drops into the negatives. The fatty acid makeup of the seed oil used in transesterification directly influences the pour point of the biodiesel that is produced. The biodiesel made from *Grewia asiatica* had a pour point of -6 °C, which complied with international fuel regulations. The biodiesel temperature at which fuel crystallization begins is referred to as the cloud point. In the course of our examination, we determined that the cloud point was -9 ∘C, which is below the fuel restriction stipulated by international standards. In comparison to petro diesel, which has a sulphur concentration of 50 ppm, GABD sulphur content was determined to be 0.0001% less than that figure. This tiny amount of sulphur improves the quality of the biodiesel, making it pollution-free and environmentally friendly (Shaah et al., 2021).

Table 3.8.4 - Comparison of Fuel properties of previously reported biodiesel sources with that of *Grewia asiatica* biodiesel fuel properties.

Property	Methods	*Grewia asiatica*		ASTM D-6751	EN-14214	China GB/T 20828-2007
		Mean	**St.Dev.**			
Color	Visual	2.0	-	2.0		
Acid number (mg KOH/g)	ASTM-D974	0.200	0.1	≤0.5	≤0.8	≤0.5
Flash Point (°C)	ASTM-D93	97	14	≥93	≥130	≥120
Pour Point (°C)	ASTM-D97	-6	5	-15-16	_	_
Viscosity (mm²/s at 40 °C.)	ASTM-D445	3.76	0.5	1.9-6.0	_	3.4-5.0
Density (kg/m³ at 40 °C)	ASTM-D1298	4.81	1.06	≤120	_	≤120
Sulphur content (wt.%)	ASTM-D4294	0.0001	1	≤0.05	≤0.05	≤0.20
Cloud point (°C)	ASTM-D2500	-9	1	-3.0-12	_	_

3.8.7. Catalyst Reusability

Nb_2O_5 nanoparticles' ability to be recycled was investigated in order to assess its stability and economic sustainability in subsequent cycles. The methods used to clean and separate the catalyst from the reaction mixture have a significant impact on the catalyst's ability to be reused (Bokhari et al., 2015). Reusability of the generated Nb_2O_5 nanoparticles was carried out under ideal transesterification reaction conditions, including Met:Oil ratio of 9:1, catalyst loading of 0.32 (wt.%), reaction time of 180 min, and temperature of 60 °C.

After the first cycle of transesterification, green nanoparticles of Nb_2O_5 were recovered from the reaction mixture using the centrifugation process. The recovered particles were then cleaned with alcohol to remove impurities, dried in the oven, and then calcined for 180 min at 500 °C in the muffle furnace in preparation for reuse in the following transesterification cycles. Up to cycle seven, catalytic activity was investigated. Up to five consecutive cycles of experimental trials showed the maximum catalytic performance, producing high FAME yields of 90 to 70%. Fifth was marked by a decline in methyl ester production of up to 70%. Yield fell even more, reaching 60% in the sixth cycle and 55% in the seventh (Figure 3.8.11).

Chemical analysis attributes this drop-in catalytic activity to the poisoning of dynamic Nb_2O_5 NP sites by organic components present in the mixture of transesterification reactants, which resulted in a decreased methyl esters production. Nevertheless, after washing and calcination in a muffle furnace, the nanoparticles' catalytic activity can be recovered.
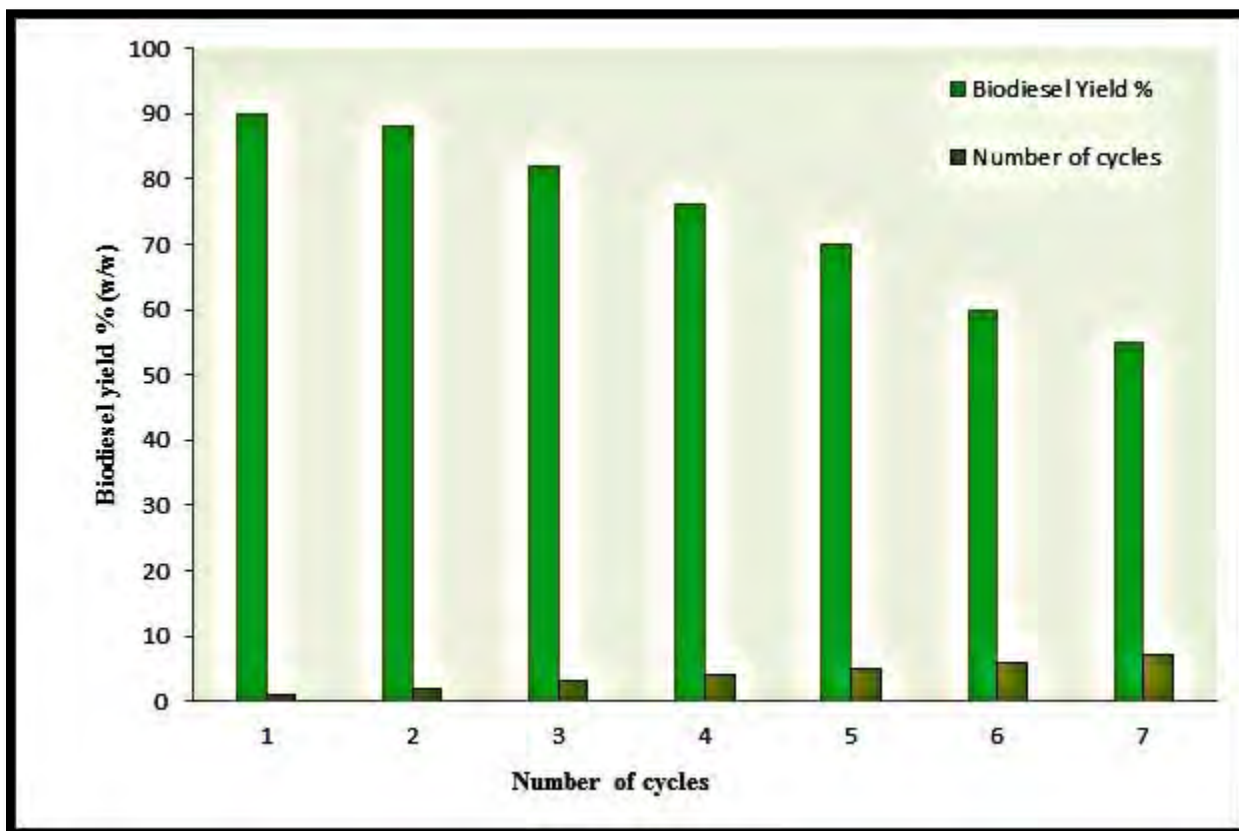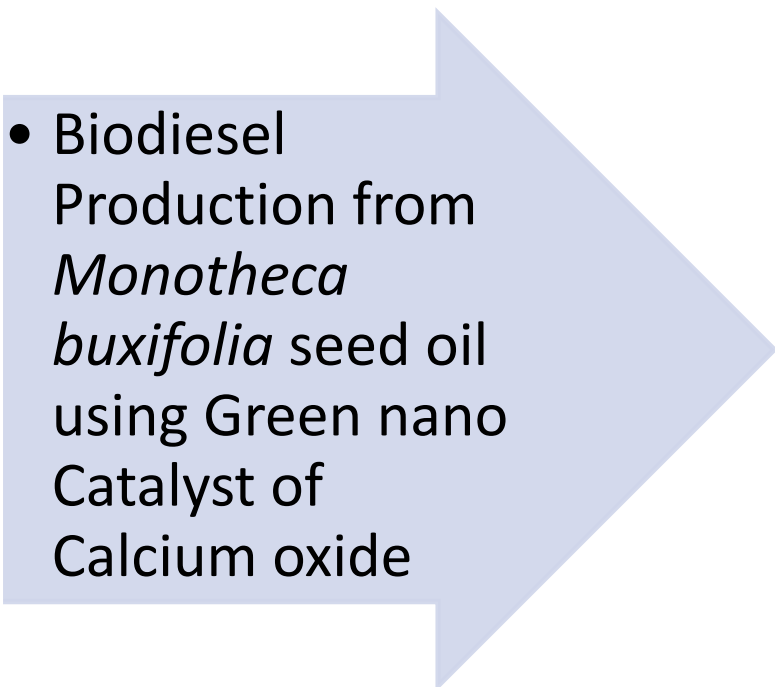
Figure 3.8.11. Reusibility of niobium oxide nanocatalyst in transesterification

SECTION IX

- Biodiesel Production from *Monotheca buxifolia* seed oil using Green nano Catalyst of Calcium oxide

In our present research work green CaO NPs are synthesized for the first time using aqueous leaf extract of *Boerhavia procumbens*. *Boerhavia procumbens* contain a variety of biological chemical compounds such as flavonoids, alkaloids, vitamins, phenols and terpenoids. *Boerhavia procumbens* was selected due to its functional properties like antioxidant, anti-inflammatory, antispasmodic, diuretic, laxative, stomachic, expectorant, purgative and rejuvenates. Besides, the significance of using natural based and cheaper biomass material such as *Boerhavia procumbens* could synthesize metal oxide with aqueous medium hence, circumventing the presence of toxic chemical solvents.

3.9.1 Catalyst Characterization

Techniques like XRD, SEM, EDX and TGA were used to characterize green nano catalyst of CaO.

3.9.1.1 X-Ray Diffraction (XRD) of CaO

Structural and crystalline phase of calcium oxide (CaO) was investigated by powder X-Ray Diffraction technique. High crystalline structure of the powder has been revealed in XRD pattern shown in Figure 3.9.1. Sharp peaks were observed at 2θ values of 32.34°, 37.37°, 54.23° and 63.47° corresponding to the lattice plane (111), (200), (202) and (311) *hkl* respectively (JCPD 77-9574). The crystalline size of calcium oxide nanoparticles in nanometer was calculated with XRD pattern of most deep peak at 2θ value of 37.37° (highest peak 200). Particle size of the synthesized CaO nano-catalyst was found 32 nm indicating the nano nature of green particles with larger surface area.

3.9.1.2 Scanning Electron Microscopy (SEM) of CaO

Surface morphology of CaO was investigated by Scanning Electron Microscopy (SEM) analysis was performed at 10 μm and 5 μm magnifications. SEM micrograph of CaO nano-catalyst has been shown in Figure 3.9.2 (a-c). Conferring to the SEM micrographs synthesized nano particles encompass homogenous, regular and square shape particles. Slight agglomeration of particles can be observed in micrographs attributed to electrostatic attraction and polarity of

nano-particles. Moreover, various sizes of particles indicated that the nano catalyst has bigger surface area with more active sites to carry out transesterification reaction (Karthika et al., 2021).

3.9.1.3 Energy Diffraction X-ray (EDX) of CaO

Elemental composition of calcium oxide nano-catalyst was studied with Energy diffraction X-Ray (EDX). EDX spectrum of CaO NPs has been presented in Figure 3.9.3. Peak at 3.7 keV spotted in the EDX spectrum is related to the binding energy of calcium whereas, peak at 0.4 keV is associated to the binding energy of oxygen.

Results of EDX revealed that there is no other additional element in the spectrum representing the purity of synthesized nano-particles of CaO. The atomic percentage of oxygen was 40.49 (w/w %) whereas; calcium had a percentage of 59.51 (w/w %).

3.9.1.4 Fourier Transform Infrared Spectroscopy (FTIR)

FTIR spectroscopic analysis was used to find out various functional groups in CaO nano-particles. FTIR spectrum of calcium oxide NPs was investigated in the mid infra-red region of 500-4000 cm^{-1} and has been presented in Figure 3.9.4. Five major peaks were observed in the spectrum. Transmittance spectrum peaks observed at 1339.16 cm^{-1}, 878.75 cm^{-1} and 834.02 cm^{-1} is attributed to Ca-O. Stretch observed at 2428.71 cm^{-1} indicates the presence of hydroxyl groups (O-H). C=C stretch was observed at wave number of 1789.09 cm^{-1}.

3.9.1.5 Thermogravimetric analysis (TGA) of CaO

Thermal stability and decomposition property of calcium oxide NPs was explored with Thermogravimetric analysis (TGA). Thermogram of CaO nano-particles along with corresponding derivative curve (wt. %) including their Endothermic peaks has been presented in Figure 3.9.5 a and b. In our current investigation, thermal decomposition of calcium oxide NPs happened in consecutive three major stages. In first stage of decomposition 0.24% loss in total mass occurred at temperature range of 55-150°C which was attributed to the process of dehydration and evaporation of adsorbed and surface water from synthesized nano-particles. Similarly, dehydration process further continued and about 0.68% loss in mass of CaO was observed in the second phase of decomposition at temperature range of 150-200 °C. A straight

line can be observed beyond 200∘C with no conspicuous change which continued up to 750 ∘C. It has revealed high thermal stability of CaO in the process of decomposition. Third stage of decomposition happened at temperature range of 750-850∘C and resulted in a loss of 0.95% in mass of CaO.
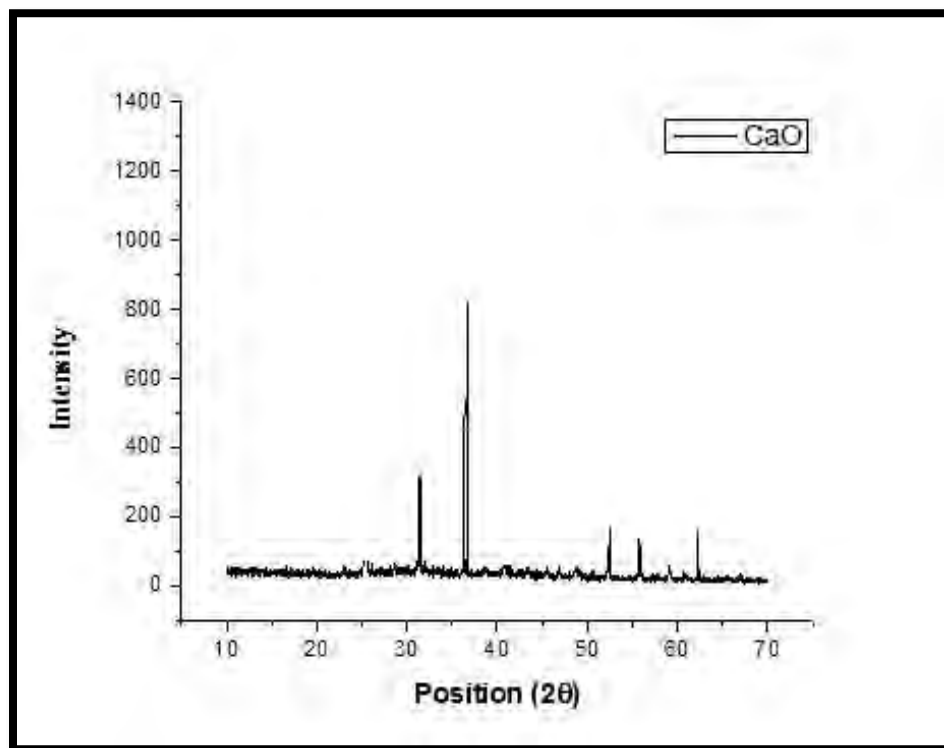
Figure 3.9.1. XRD pattern of calcined Calcium oxide green nano particles
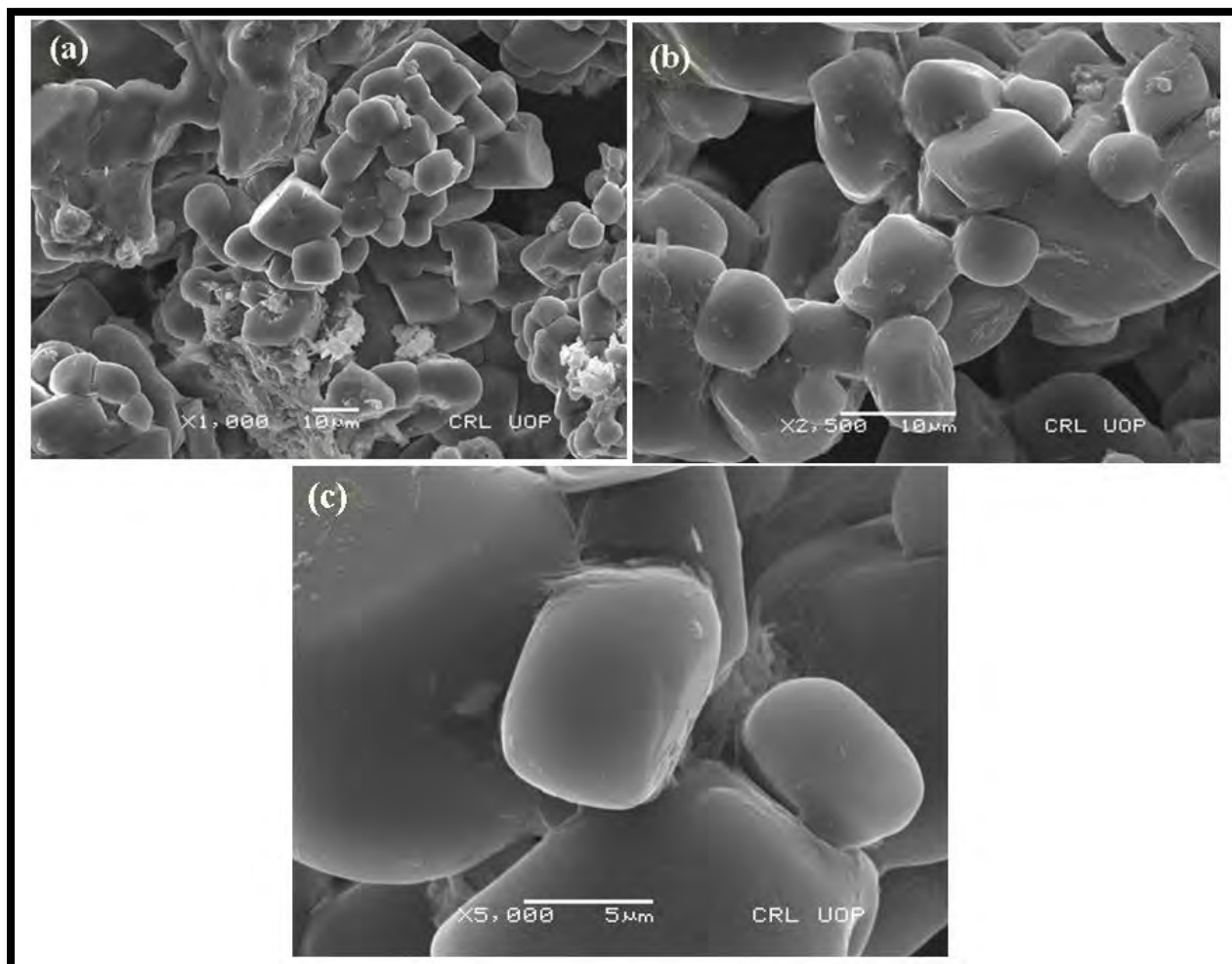
Figure 3.9.2. Scanning electron microscopy (SEM) of calcined Calcium oxide green nano particles
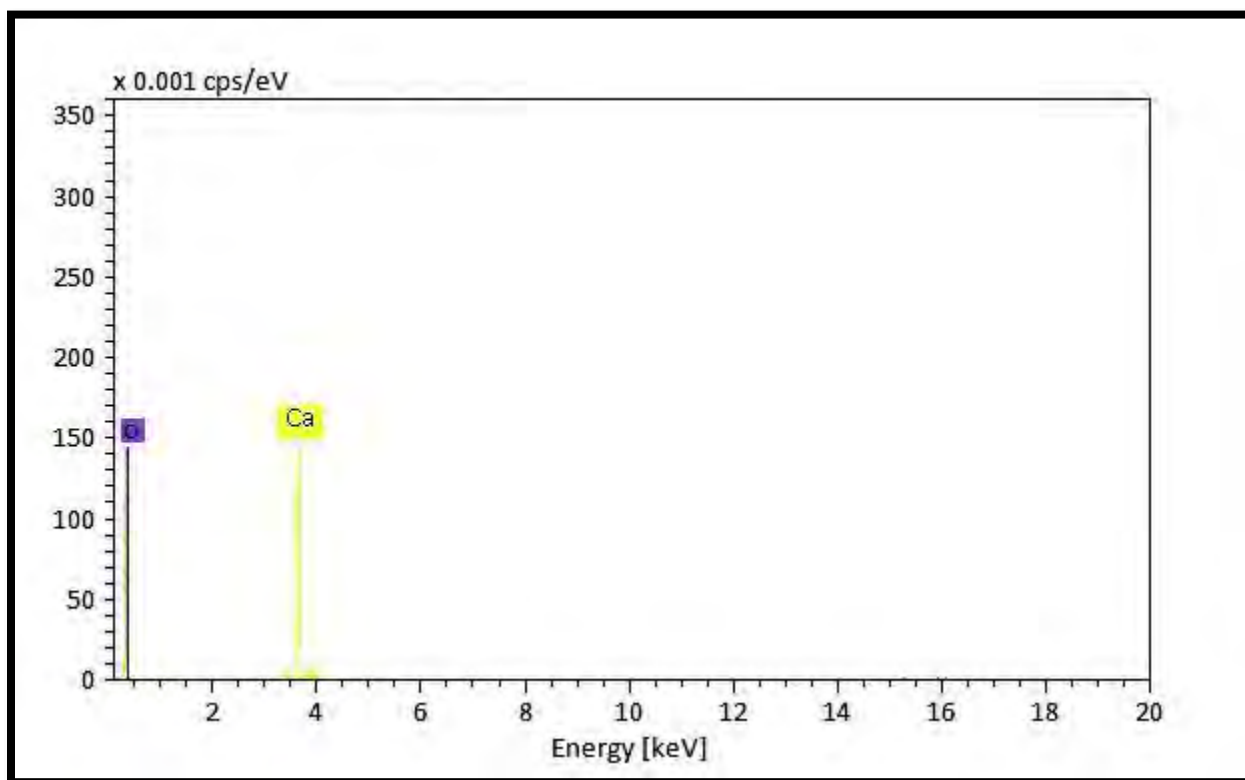
Figure 3.9. 3. Energy diffraction X-Ray (EDX) of calcined Calcium oxide green nano particles
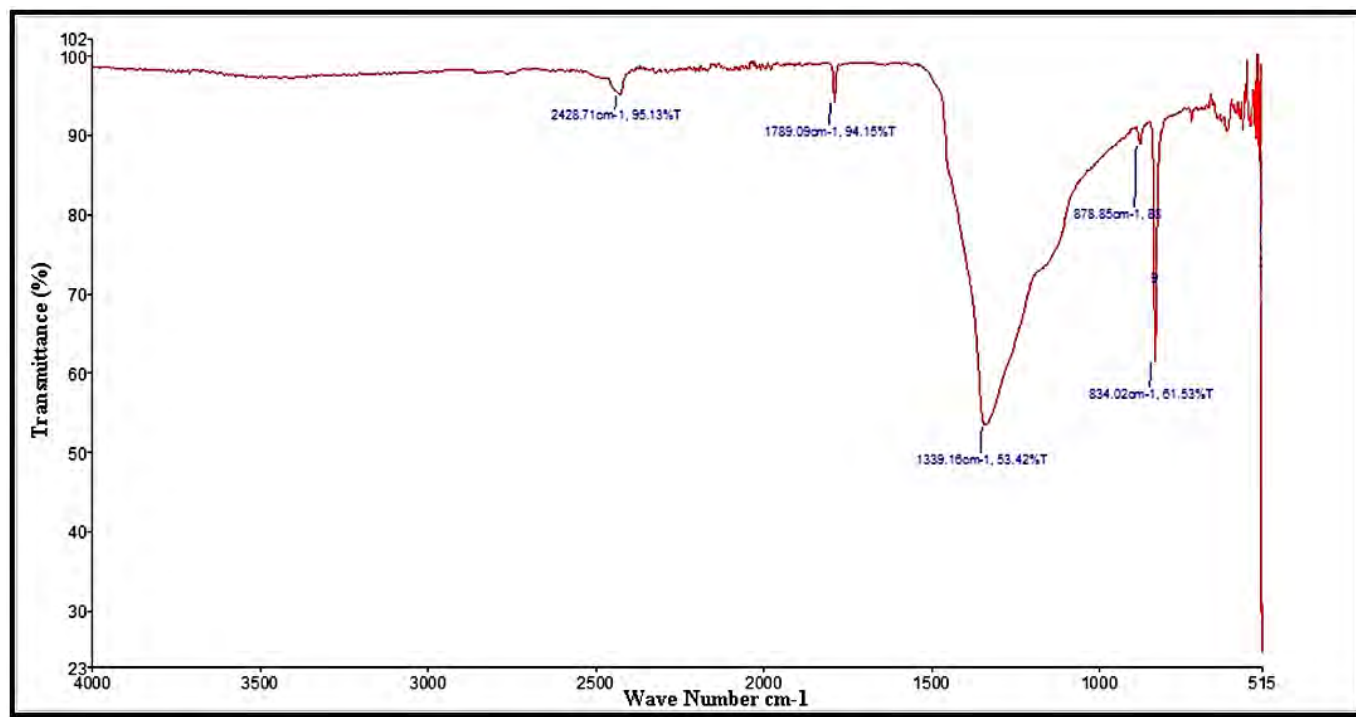
Figure 3.9. 4. FTIR spectrum of calcium oxide green nano particles
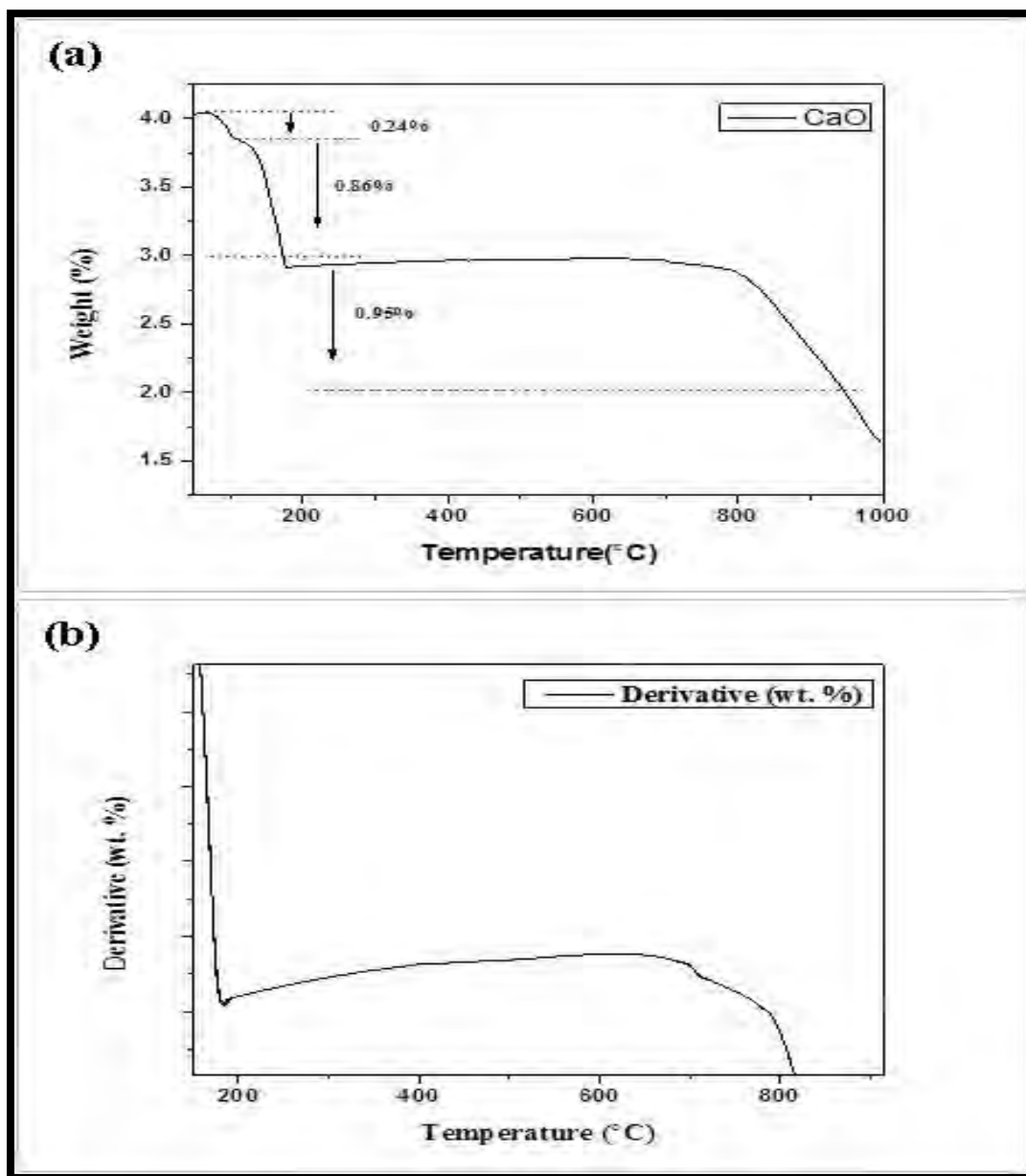
Figure 3.9.6. (a) TGA of Calcium oxide green nano particles (b) derivative thermogram of Calcium oxide nano particles

3.9.2 Biodiesel synthesis via transesterification

Sustainable biodiesel was synthesized from novel and non-edible seed oil of *Monotheca buxifolia*. It has been previously reported that those feedstocks which have oil content higher than 20% would only be considered for biodiesel production (Adepoju et al., 2020). *Monotheca buxifolia* has seed oil content of 45% (w/w) which is significantly high amount hence, recommendable for broad scale synthesis of biodiesel. Moreover, wild and easy availability of *Monotheca buxifolia* made it a highly potential source for renewable biodiesel production. The free fatty acid content of seed oil was determined prior to transesterification and was measured to be 0.45 (wt. %). Considerably lower FFA content specified single step transesterification. Oil source with FFA content higher than 3% needs an additional step of acid esterification and results in incomplete conversion of triglycerides in to fatty acid methyl esters during transesterification (Adewuyi, 2020). Green nano-particles of CaO synthesized with *Boerhavia procumbens* aqueous leaf extract were used to catalyze transesterification of extracted seed oil.

Transesterification reaction is under influence of reaction parameters. Therefore, analysis of optimal reaction conditions of transesterification has to be carried out at which maximum yield of biodiesel is obtained. In our current investigation, Central composite design (CCD) was prepared by DOE (Design of experiment) using four independent variables of transesterification with lower and higher values i.e. methanol to oil molar ratio 3:1-15: 1 (A), catalyst concentration of 0.22-1.44 wt.% (B), reaction time 55-180 min (C) and temperature 50-120 ºC (D) (Table 3.9.1). Figure 3.9.6 describes the comparison between predicted versus actual yield of transesterification. Both predicted and actual values are found to be distributed near the straight line demonstrating a good correlation among them. Results of Statistical analyses of variance (ANOVA) of response surface quadric model have been demonstrated in Table 3.9.3. Quadric model was found significant with a low p-value of 0.0001 (<0.05). The lack of fit F-value of experimental model relative to the pure error was not significant and has a value of 0.2554. Not significant lack of fit value is considered good for the quadric model with a chance of 25.54% that could be caused by noise. Among quadratic terms of transesterification methanol to oil ratio (A^2) was found most significant with p-value of 0.0007 (<0.05) followed by catalyst loading (B^2) with p-value 0.0298 and reaction time (C^2) with *p*-value 0.0476. On the basis of results shown in

Table 4 the predicted R² value was 0.8531 which is closer to the adjusted R² value of 0.8613 with variance lesser than 0.2. Adequate Precision of the model and was found greater than 4 (6.9493). In the current experimental model greater value of Adequate Precision demonstrated that experimental model can be efficiently utilized in predicting biodiesel yield. Polynomial equation (8) applied in the Quadric model is given below.

Biodiesel Yield (wt. %) = +86.50-0.8894 *A-2.18*B+2.20*C+1.43*D-1.31*AB-2.56 *AC+0.8125*AD-1.56 *BC-2.69 *BD-0.9002 *CD-15.40*A²-4.83*B²-2.20*C²-3.83*D²   (15)
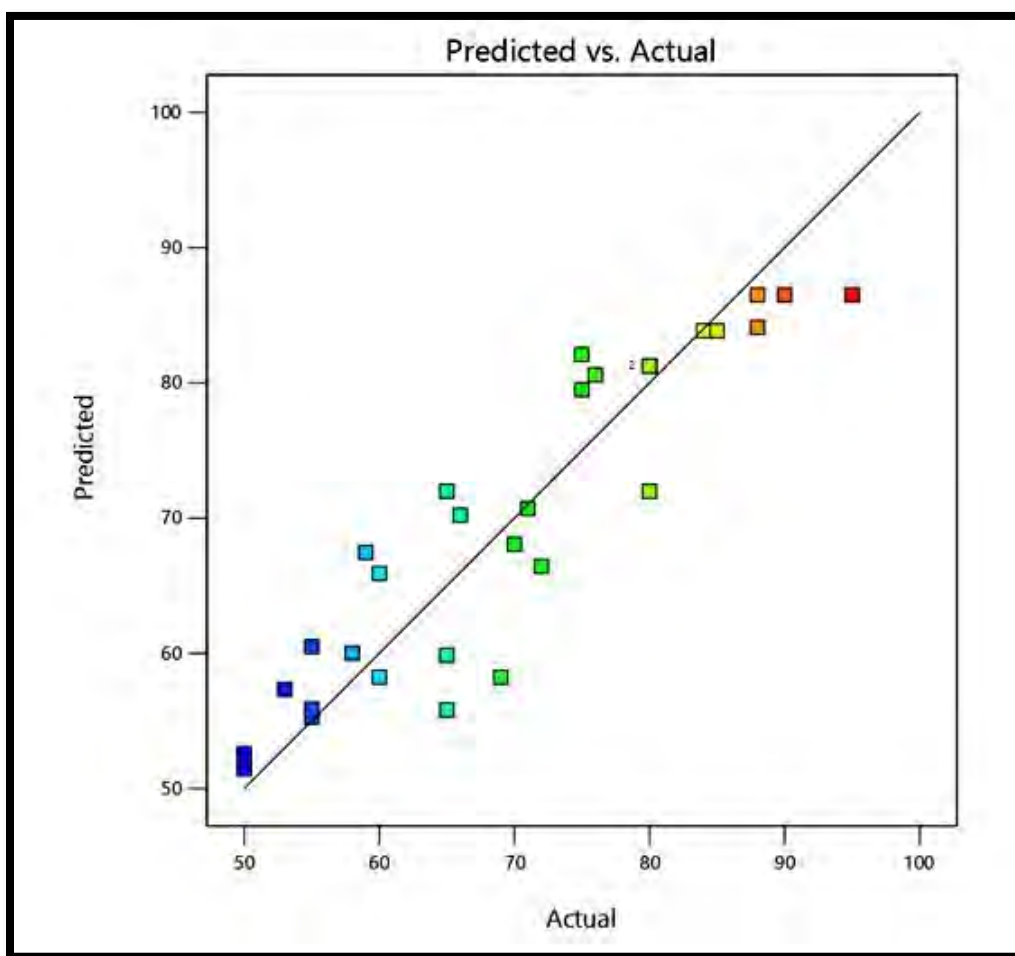
Figure 3.9.6. **Comparison between the experimental and predicted yield of biodiesel in the model**

Table 3.9.1- Experimental design by central composite design for transesterification reaction

Process parameters	−1	+1
Alcohol to oil ratio	3:1	15:1
Catalyst loading	0.22	1. 44
Reaction time	55	180
Temperature	50	120

Table 3.9.2- Detailed experimental result for transesterification reaction of *Monotheca buxifolia* biodiesel

Run	A: Methanol to Oil molar Ratio	B: Catalyst loading (wt. %)	C: Reaction Time (min)	D: Temperature (◦C)	Yield (wt. %)
1	9:1	1.44	180	50	72
2	3:1	0.83	120	85	80
3	9:1	1.44	120	85	75
4	9:1	0.83	180	85	95
5	3:1	0.22	180	85	71
6	9:1	0.83	180	120	88
7	9:1	0.22	60	85	65
8	3:1	0.22	180	50	60
9	3:1	1.44	180	120	55
10	9:1	0.22	180	85	84
11	9:1	0.83	120	85	90

12	15:1	1.44	60	120	69
13	9:1	0.83	120	85	88
14	9:1	0.83	120	50	80
15	9:1	0.83	60	50	60
16	9:1	0.83	180	50	80
17	15:1	1.44	180	85	55
18	9:1	0.83	120	85	85
19	15:1	0.83	180	50	58
20	9:1	0.83	60	85	75
21	15:1	0.83	60	85	66
22	9:1	0.83	60	120	76
23	3:1	0.83	180	85	65
24	15:1	0.83	180	120	70
25	9:1	0.22	180	50	65
26	3:1	1.44	60	120	55
27	15:1	1.44	60	50	53
28	15:1	1.44	180	120	50
29	9:1	0.22	60	120	59
30	3:1	0.38	180	50	50

Table 3.9.3- ANOVA for Response Surface Quadratic model

Source	Sum of Squares	Df	Mean Square	F-value	p-value	
Model	4042.09	14	288.72	5.68	0.0001	significant
A-Alcohol to oil molar ratio	14.79	1	14.79	0.2908	0.0476	
B-Catalyst loading	88.45	1	88.45	1.74	0.0170	
C-Reaction time	90.17	1	90.17	1.77	0.0228	
D-Temperature	39.85	1	39.85	0.7837	0.0900	
AB	27.56	1	27.56	0.5421	0.0329	
AC	105.06	1	105.06	2.07	0.0711	
AD	10.56	1	10.56	0.2077	0.0451	
BC	39.06	1	39.06	0.7682	0.0946	
BD	115.56	1	115.56	2.27	0.0224	
CD	13.48	1	13.48	0.2652	0.0141	
A²	929.87	1	929.87	18.29	0.0007	
B²	91.47	1	91.47	1.80	0.0298	
C²	15.61	1	15.61	0.3071	0.0476	
D²	54.27	1	54.27	1.07	0.1179	
Residual	762.71	15	50.85			
Lack of Fit	647.71	11	58.88	2.05	0.2554	not significant
Pure Error	115.00	4	28.75			
Cor Total	4804.80	29				

R^2 = 0.8613, Std. Dev = 6.13, C.V. % = 9.22, Adeq Precision = 6.9493

3.9.3. Influence of reaction parameters on transesterification reaction

Three dimensional response surface plots of reaction parameters have been presented in Figure 3.9.7 a, b, c, d, e and f. These plots were found useful in understanding different interactive effects of four variables and thereby contributing to the recognition of extreme response levels. Usually, yield of methyl ester is expected to increase under optimal reaction conditions. A sudden drop in biodiesel yield beyond optimal levels was observed. Successive sub-sections could deeply elucidate the interactive effects of the transesterification reaction.

3.9.3.1 Combined influence of methanol to oil molar ratio and catalyst loading

Combined interaction between methanol to oil molar ratio and catalyst loading has great impact on biodiesel yield. Mutual effect of these reaction parameters on transesterification of *Monotheca buxifolia* seed oil has been illustrated in three dimensional plots presented in Figure 3.9.7a. Maximum yield of 95% was obtained at molar ratio of 9:1 and catalyst loading 0.83 (wt. %) at constant reaction time (180 min) and temperature (85 $^{\circ}$C) (Run 4). About 84% yield of methyl ester was achieved at Run 10 with molar ratio of 9:1 and catalyst amount of 0.22 (wt. %). It was further reduced to 71% with lower molar ratio of 3:1 and catalyst loading of 0.22 (wt. %) at Run 5. It was noticed that lower molar ratio of 3:1 with same amount of catalyst (0.83 wt. %) resulted in 65% yield at Run 23. Both High molar ratio of 15:1 and catalyst amount of 1.44 (wt. %) resulted lowest yield of 55% (Run 17). Excess amount of methanol in reacting mixture results in dilution of catalyst concentration and favors glycerolysis (a reversible reaction). Consequently, recombination of glycerol with FAMEs results in reformation of monoglycerides (Singh et al., 2019). Results of ANOVA declared the mutual interaction of molar ratio and catalyst loading as significant with p-value 0.0329 (<0.05). Moreover, individually both catalyst loading and molar ratio were found significant with p-value 0.0170 and 0.0476 respectively.

3.9.3.2 Combined influence of methanol to oil ratio and reaction time

Parametric interaction of Methanol to oil ratio and time was profoundly investigated while keeping catalyst loading (0.83 wt. %) and reaction temperature (85 $^{\circ}$C) constant. Interaction between these reaction parameters has a noticeable effect on biodiesel yield. Figure 3.9.7b describes mutual effect of molar ratio and reaction time. High yield of 95% was obtained at molar ratio of 9:1 and time of 180 (min) (Run 4). The molar ratio of 9:1 and time of 120 reduced yield up to 90% at Run 11. Further reduction in molar ratio of 1:3 and time of 120 min resulted in lower yield of 80% at Run 2. Parametric interaction at lesser time of 60 min and high molar ratio of 15:1 was found inappropriate and a low yield of 66% was obtained (Run 21). It is due to insufficient reaction time for the reactants to mix properly and reach equilibrium state hence, results in unsatisfactory conversion of reactants into products (Pandit et al., 2017). The molar ratio of 3:1 and maximum reaction time of 180 min further reduced yield up to 65% at Run 23. A correlation between molar ratio and time was found non-significant observed in results of ANOVA with p-value greater than 0.05 (0.0711).

3.9.3.3 Combined influence of methanol to oil molar ratio and temperature

Parametric interaction of molar ratio and temperature was studied at constant catalyst loading of 0.83 (wt. %) and reaction time of 180 (min). The combined effect of molar ratio and temperature of transesterification has been demonstrated in Figure 3.9.7c. Maximum yield of 95% was obtained at molar ratio of 9:1 and temperature of 85 $^{\circ}$C (Run 4). Higher temperature of 120 $^{\circ}$C and molar ratio of 9:1 resulted in 88% yield at Run 6. At this stage, yield of methyl ester was significantly limited by boiling point of methanol (65 $^{\circ}$C) and saponification reaction (Kouzu and Hidaka 2012). 58% yield was obtained with lowest temperature of 50 $^{\circ}$C and molar ratio of 15:1 at Run 19. A lower molar ratio of 3:1 and temperature of 50 $^{\circ}$C resulted in lowest yield of 50% at Run 30. Therefore, it was concluded from the current investigations that the combined effect of molar ratio and temperature is commendable and has to be considered during transesterification. In current investigation, results of ANOVA revealed this combined correlation as significant by having a p-value < 0.05 (0.0451).

3.9.3.4 Combined influence of time and catalyst loading

Parametric relation of reaction time and catalyst concentration was investigated at constant molar ratio of 9:1and temperature of 85 °C. Mutual influence of time and catalyst loading on transesterification has been exhibited in the form of 3D plot in Figure 3.9.7d. Maximum yield of 95% was obtained at catalyst loading 0.83 (wt. %) and time of 180 (min) (Run 4). Higher catalyst loading of 1.44 wt. % and reaction time of 120 min resulted in 75% yield at Run 3. Decrease in FAME conversion at this stage is attributed to surplus quantity of catalyst in the reacting mixture which increased viscosity of the fluid encouraging a poor mass transfer between the three phases in transesterification (Ajith et al., 2020). Low catalyst loading of 0.22 wt. % and maximum time of 180 min resulted in yield of 84% at Run 10. Catalyst loading of 0.83 wt. % and time of 120 min resulted in yield of 88% at Run 13. Shorter time of 60 min and catalyst loading of 0.83 wt. % rendered yield up to 75% (Run 20). Percent yield was further reduced to 65% with catalyst amount of 0.22 wt. % and time of 60 min at Run 7. Mutual effect of time and catalyst loading was found not significant with p-value (0.0946) > 0.05 for methyl ester formation. However, individually both catalyst loading and reaction time was significant with p-value less than 0.05.

3.9.3.5 Combined influence of catalyst loading and reaction temperature

The combined influence of catalyst loading and reaction temperature was studied at constant molar ratio of 9:1and reaction time 180 (min). Mutual interaction of catalyst loading and temperature during transesterification has been presented in Figure 3.9.7e. Maximum yield of 95% was obtained at catalyst loading 0.83 (wt. %) and reaction temperature of 85 °C (Run 4). 80% yield was obtained with same amount of catalyst loading (0.83 wt. %) and lowest reaction temperature of 50 °C which indicated that low reaction temperature failed to convert triglycerides into methyl esters (Run 16). Catalyst loading of 0.22 wt. % with high reaction temperature of 120 °C was found insufficient to complete the reaction of transesterification and resulted in a reduced yield of 59% at Run 29. Moreover, high reaction temperature slows down forward reaction due to low boiling point of methanol (65 °C). Similarly, both the lowest temperature of 50 °C and catalyst loading of 0.22 wt. % resulted in low yield of 65% (Run 25). Catalyst concentration of 1.44 wt. % and temperature of 50 °C resulted in 72% at Run 1. Results of

ANOVA exposed that mutual interaction of these parameters is significant with p-value (0.0224) lesser than 0.05. However, individual catalyst loading was found significant with p-value of 0.0228 and temperature was not significant with a *p*-value of 0.0900.

3.9.3.6 Combined influence of time and temperature

The combined influence of time and temperature was examined at constant molar ratio of 9:1 and catalyst loading 0.83 (wt. %). The combined influence of time and temperature on methyl ester formation has been demonstrated in Figure 3.9.7f. It was manifested from Run 4 that maximum yield of 95% was obtained at reaction time 180 (min) and temperature of 85 $^\circ$C. About 85% yield was obtained at time 120 min and temperature of 85 $^\circ$C (Run 18). Methyl ester yield was reduced to 80% yield at Run 14 with lowest temperature of 50 $^\circ$C and time of 120 min which was most probably due to endothermic nature of transesterification reaction. Further decrease in time duration up to 60 min with high reaction temperature of 120 $^\circ$C has compact yield to 76% (Run 22). A substantial decline in percent yield happened up to 60% with both low reaction temperature of 50 $^\circ$C and time of 60 min at Run 15. The collective effect of reaction time and temperature on biodiesel synthesis was found significant in results of ANOVA with p-value (0.0141) lesser than 0.05.
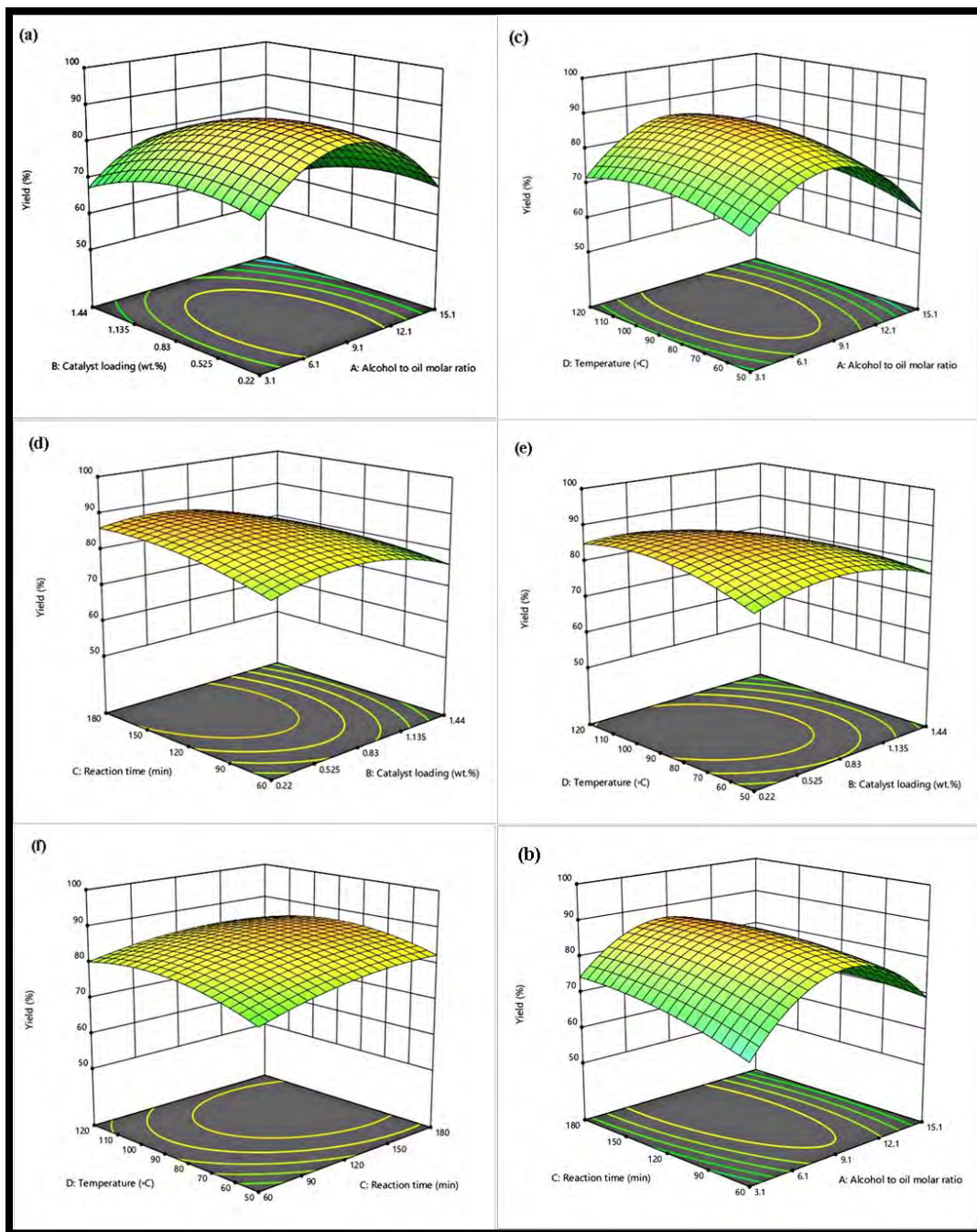
Figure 3.9.7. Influence of the reaction parameters of MBBD biodiesel.

3.9.4 Characterization of Biodiesel

3.9.4.1 FTIR Analysis

FT-IR analysis along with NMR is the most commonly implemented method used to confirm presence of methyl esters in biodiesel sample after transesterification. Fourier-transform infrared spectroscopic analysis of *Monotheca buxifolia* seed oil and biodiesel was carried out in the mid infra-red region of 500-4000 cm^{-1} for determination of various functional groups existing in it. FTIR spectrum of *Monotheca buxifolia* seed oil and resultant biodiesel has been presented in Figure 3.9.8 a and b respectively. A number of stretches and bands were detected in FTIR spectrum of triglycerides and methyl ester representing different functional groups. Two key bands in IR the region of 1743.57 cm^{-1} for carbonyl group (C=O) and 1435.44 cm^{-1} for methyl group (CH$_3$) were observed in the spectrum of methyl ester which have confirmed the conversion of triglycerides into methyl esters. Other important characteristic peaks of biodiesel were spotted in IR region of C-H (sp^3) at 2922.85 cm^{-1} and 2853.28 cm^{-1} for C-H (sp^2) stretching. Previous literature has regarded the region of the carbonyl group as the most sensitive peak to change in chemical and molecular structure among all other peaks (Mares et al., 2021). Existence of aliphatic esters (O=C-O-C) in the synthesized biodiesel was specified by the stretch appeared at wavenumber 1159.41 cm^{-1}.

Moreover, the most prominently variable IR region in the spectrum of seed oil and methyl ester appeared around 1300-1800 cm^{-1} and 3300-280 cm^{-1}. Stretch peak for C-H$_2$ wagging frequency located at 1098.60 cm^{-1} in the IR spectrum of biodiesel. A deep peak detected at 3330.87 cm^{-1} for (O-H) stretch in IR spectrum of seed oil was found absent in the spectrum of biodiesel. Another deep peak in the IR spectrum of *Monotheca buxifolia* seed oil at 1025.19 cm^{-1} also vanished in the spectrum of methyl ester. Consequently, the conversion of *Monotheca buxifolia* seed oil into methyl ester during transesterification has been clearly indicated by all these discussed peaks of the IR spectrum.

3.9.4.2 NMR Spectroscopic Analysis

Quantitative information about chemical substances existing in synthesized biodiesel sample was obtained *via* ^{1}HNMR a spectroscopic analysis. ^{1}HNMR spectroscopic analysis is a frequently used analytical technique for getting confirmation about conversion of biomass into fatty acid methyl esters after transesterification. Protons of methylene group adherent to ester moiety in synthesized methyl ester were considered to confirm reaction product. ^{1}HNMR spectrum of *Monotheca buxifolia* biodiesel has been illustrated in Figure 3.9.9a. Representative peak of methoxy group (– OCH_3) appeared at 3.654 ppm in the ^{1}HNMR spectrum which confirmed the existence of methyl esters in biodiesel sample. ^{1}HNMR spectrum of *Monotheca buxifolia* biodiesel (MBBD) lacked undesirable methanol peak at 3.45 ppm. A triplet peak for α methylene proton (α-CH_2) was patterned at 2.318 ppm whereas, peak of β- methylene (β-CH_2) protons indicating atoms of hydrogen positioned on carbon number 3 of aliphatic fatty chain appeared as singlet at 1.251-1.98 ppm. Besides, respective peaks of terminal methyl protons were spotted at 0.851 and 0.994 ppm in the spectrum. Signal peak of olefinic hydrogen (-CH=CH-) positioned at 5.277-5.394 ppm whereas, peak of allylic hydrogen (-CH_2-) appeared at 2.799 ppm in the spectrum. These two peaks consisted of two hydrogen atoms per each non conjugated double bond. Occurrence of all these peaks in ^{1}HNMR spectrum of biodiesel has inveterate the formation of methyl esters from triglycerides of *Monotheca buxifolia* seed oil. Moreover, total percent conversion of triglycerides into methyl esters was also calculated and was found to be 94 % which is near to the optimum yield of biodiesel obtained in our current study.

Structural characteristics of biodiesel such as position of esters carbonyl (-COO-) and C-O group in methyl ester of MBBD were investigated with ^{13}CNMR spectrum and have been presented in Figure 3.9.9b. Characteristic signal peak of methoxy carbon appeared at 51.36 ppm in the spectrum. Carbonyl (C-O) group in methyl ester was detected at 77.48 ppm whereas, signal for long chain of ethylene carbon (-CH_2-)$_n$ appeared at 29.08-29.75 ppm. Signal for carbonyl group (-COOH) was spotted at 174.21 ppm. Signals for unsaturation (-CH=CH-) in biodiesel spectrum was positioned at 127.70 ppm corresponding to inner nun-conjugated carbon. Chemical shifts at δ (ppm) 129.69-129.94 signified the outer carbon of nun-conjugated carbon (-

CH=CH-). Furthermore, signal for aliphatic methylene (-CH2-s) carbon was detected at the region of 34-27 ppm in the ^{13}CNMR spectrum.

3.9.4.3. GC/MS

GC/MS analysis of *Monotheca buxifolia* biodiesel sample was executed to find out the presence of different types of FAMEs and examine the purity of synthesized biodiesel. Every feedstock of biodiesel possesses its own fatty acid structure. Nearly most of the significant fuel properties of biodiesel intensely rely on the content of various fatty acids of the oil source from which it has been synthesized (Ma et al., 2021). It is therefore needed to investigate fatty acid compositions of biodiesel in detail. The quality and chemical composition (degree of saturation and unsaturation) of biodiesel deeply affect fuel properties of biodiesel such as viscosity and cetane number. Library match software NO. NIST02 was used to analyze individual peaks of fatty acid methyl esters using their retention time which were further validated by MS analysis. A chromatograph of *Monotheca buxifolia* biodiesel along with library match has been depicted in Figure 3.9.10. Four prominent peaks were distinguished in the chromatograph of MBBD including both saturated and unsaturated fatty acid methyl esters. Saturated fatty acids comprised of Hexadecanoic acid methyl ester (C16:0) and Octadecanoic acid, methyl ester (C18:0). Unsaturated fatty acids included 5, 8-Octadecadienoic acid methyl ester (C18:2) and 9-Octadecenoic acid methyl ester (C18: 1). The major fatty acid methyl ester with highest abundance was found to be 9-Octadecenoic acid methyl ester. Degree of unsaturation was found competitively lesser in methyl ester sample which is considered as suitable for smooth and steady fuel combustion in engines (Foroutan et al., 2021). GC/MS analysis of synthesized biodiesel has disclosed that seed oil of *Monotheca buxifolia* possesses efficient conversion ability into fatty acid methyl esters and can be utilized for wide scale synthesis of biodiesel.

Figure 3.9.8. FTIR spectrum of **(a)** seed oil of *Monotheca buxifolia* **(b)** *Monotheca buxifolia* biodiesel
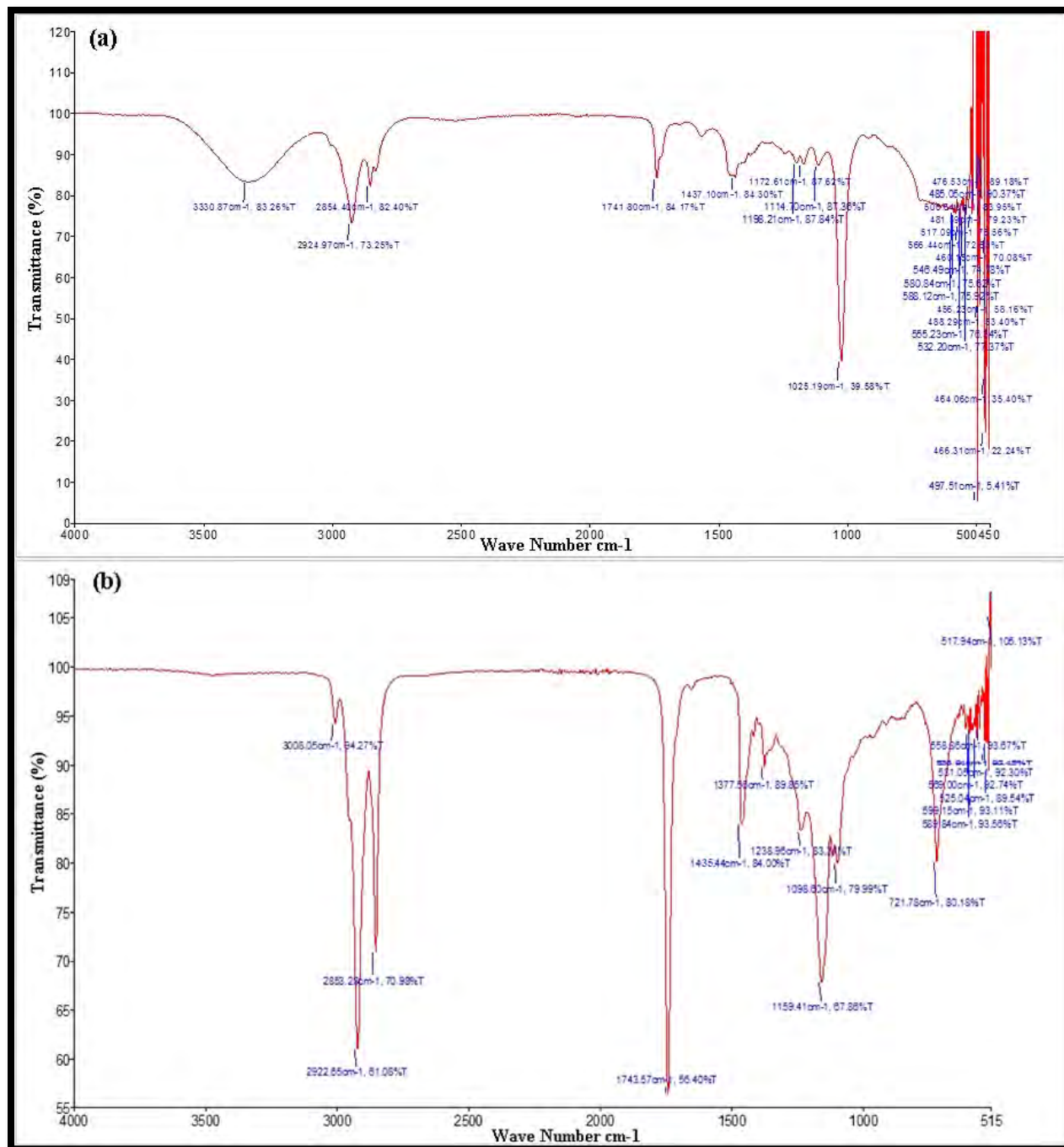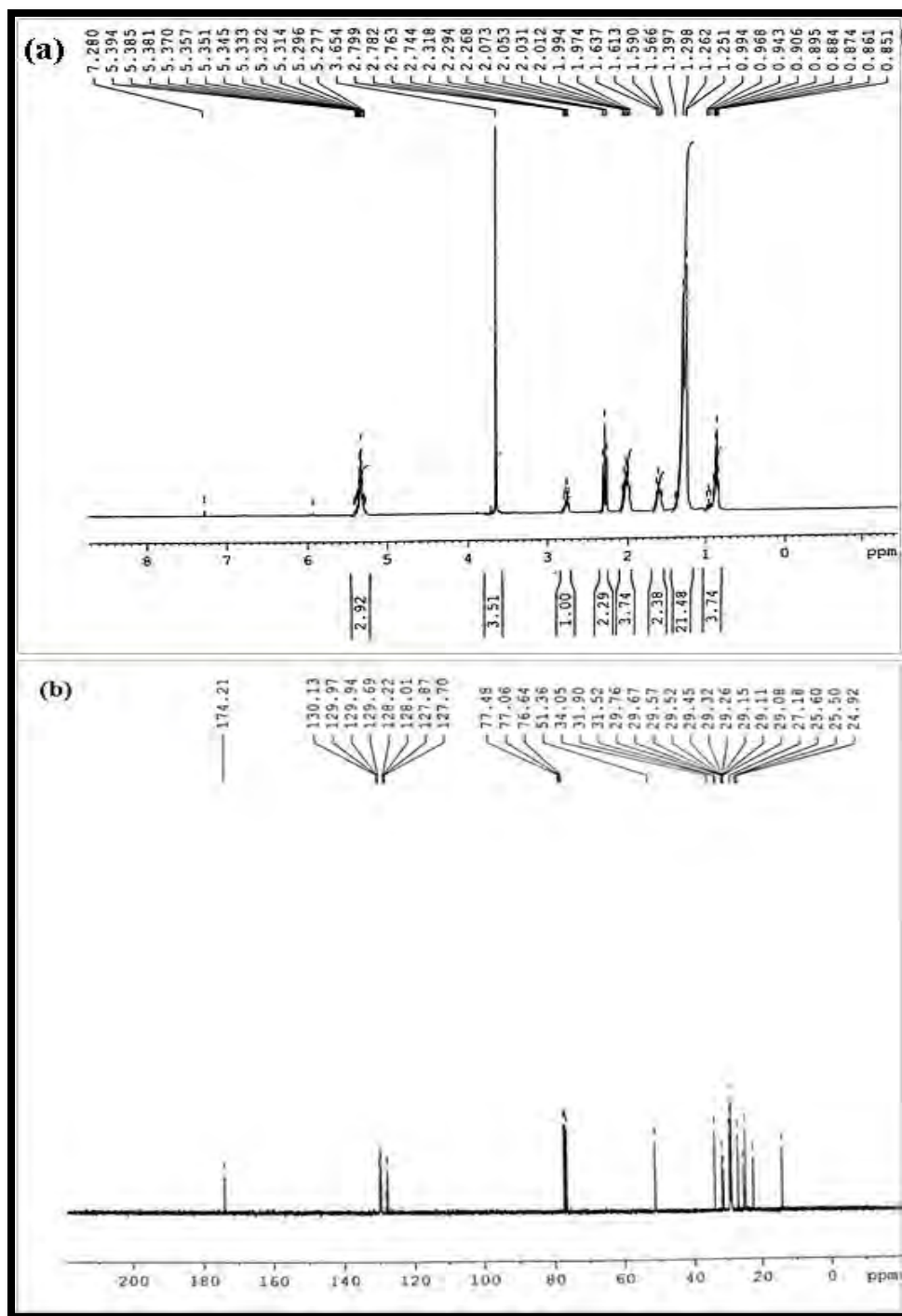
Figure 3.8.9. NMR spectrum **(a)** ^{1}HNMR and **(b)** ^{13}CNMR of MBBD
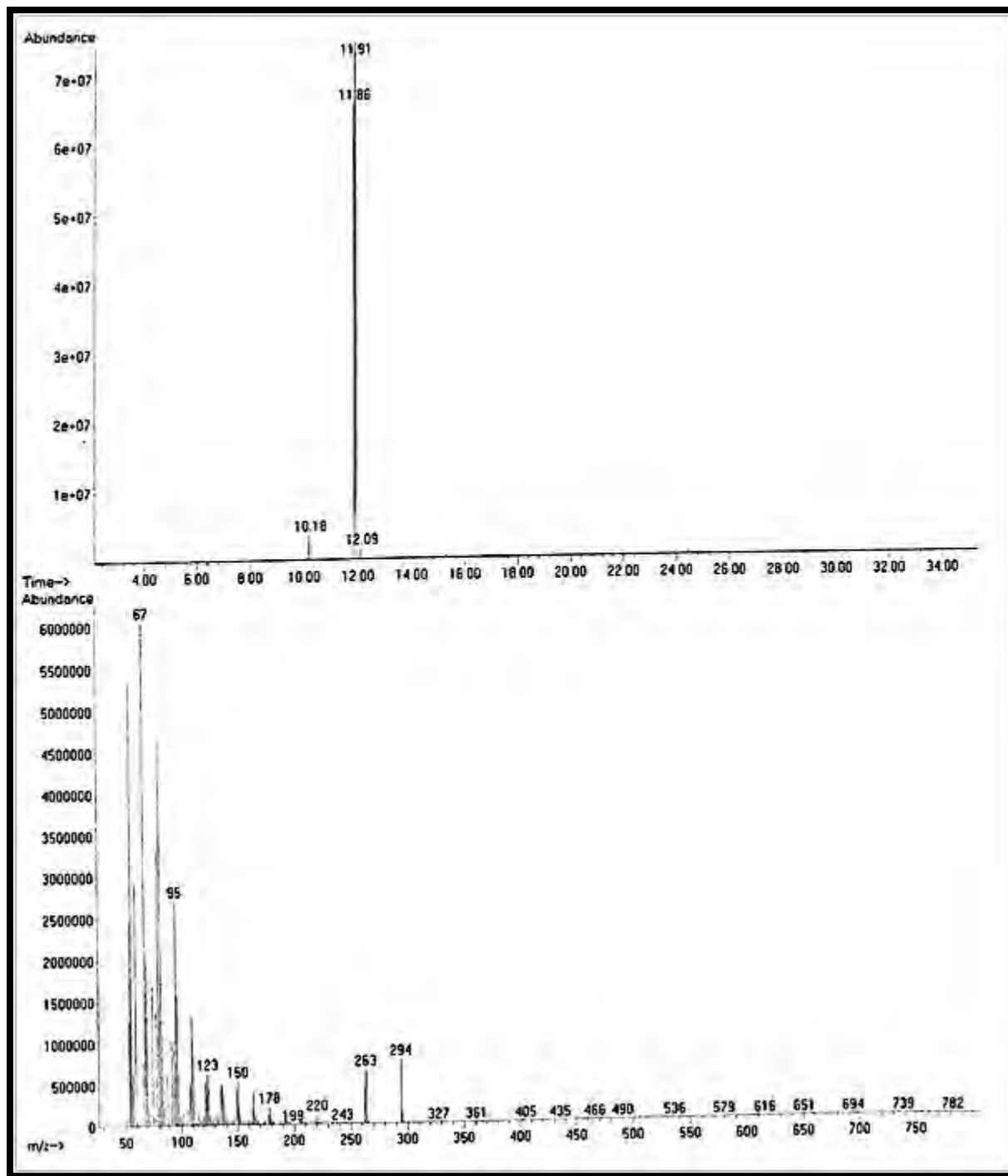
Figure 3.9.10. GC-MS spectrum of *Monotheca buxifolia* biodiesel

3.9.5. Fuel Properties of biodiesel

Determination of fuel properties of biodiesel is among the most significant criteria required to be taken under consideration before its practical implication. Fuel properties of biodiesel must fall under limits of existing international standards of fuel. Fuel properties of biodiesel vary from feedstock to feedstock and depend upon fatty acid composition of the source oil. Biodiesel fuels produced from oils with more mono-unsaturated fatty acid content have comparatively better fuel properties (Fatah et al., 2012). All these fuel properties of *Monotheca buxifolia* biodiesel were in good accordance with international standards of fuel and depicted in Table 3.9.4.

Acid value highly affects the degradation of biodiesel. Acid value has a substantial impact on the quality of fuel and engine efficiency. Biodiesel with higher acid value results in problems in rubber parts of the fuel system by causing corrosion particularly in old diesel engines. The acid value of synthesized *Monotheca buxifolia* methyl ester was calculated 0.325 mg KOH/gm which lies within given international limits of fuel.

Kinematic density of biodiesel plays a vital role during fuel injection in diesel engines, particularly at low temperature. It has an impact on energy content and air to fuel ratio in combustion chamber. Usually, biofuels have higher density as compared to petro-diesel. High degree of unsaturation leads to higher density of fatty acid methyl esters (Hammouda et al., 2017). Density of *Monotheca buxifolia* biodiesel was 0.821 (kg/m³) which is in line with required international fuel standards (Table 3.9.4).

Viscosity has a great impact on fuel atomization and engine deposit formation upon injection in combustion chamber. Fuels with higher viscosities tend to produce more engine deposits and emissions as a result of incomplete combustion. It increases with increase in chain length of fatty acids and degree of saturation. It is associated with alcohol moiety too such as the viscosity of ethyl ester is comparatively higher than that of methyl esters (Roy et al., 2019). Generally, it has been noticed that the value of biofuel viscosity increases with the time of storage which might be attributed to the oxidation process happening in it. Viscosity of synthesized *Monotheca buxifolia* biodiesel was found to be 5.35 mm²/s in our current investigation.

Flash point of the fuel is lowest ignition temperature of a fuel and inversely related to volatility of fuel. Flash point of fuels should be higher in order to ensure safe handling during transportation. Flash point of synthesized biodiesel agreed with prescribed international standards of biodiesel (Cruz et al., 2020). Flash point of biodiesel is higher as compared to petro-diesel hence, are lesser hazardous during transportation. The Flash point of *Monotheca buxifolia* biodiesel in our current study was measured 95 °C as depicted in Table 4 which is quite higher than conventional diesel (55 °C) (Li et al., 2019).

Cloud point and pour point are two of three main cold filter plugging points which characterize the cold flow properties of a fuel. Temperature at which first cloud layer appears in the fuel indicating the onset of crystallization during cold season is known as cloud point whereas, pour point can be expressed as the minimum temperature at which the fuel still upholds its ability to flow. Beyond this limit of temperature, fuel does not remain liquid anymore due extreme crystallization (de Jesus et al., 2020). It has been reported that cold flow properties of longer chain FAMEs are poor as compared to unsaturated and branched-chain FAMEs. Biofuels which are highly concentrated in saturated fatty acids have higher viscosities and ultimately worse cold-flow properties. In this study, cloud point of *Monotheca buxifolia* biodiesel was found -8 °C and pour point was -9 °C which are equivalent to the limits set by international standards.

Sulphur content of synthesized methyl ester was found 0.0002%, a quite negligible amount falling in the range of <1ppm as compared to conventional petro-diesel (50 ppm). Sulphur content of biodiesel lesser than 1 ppm has a great advantage over conventional fossil fuel which results in pollution free and environment friendly fuel combustion with low SO_X gas emission making it suitable for commercial use with no negative consequences (Istadi et al., 2020).

Table 3.9.4 - Comparison of fuel properties of *Monotheca buxifolia* biodiesel with international standards**.**

Property	Methods	*Monotheca buxifolia*		ASTM D-6751	EN-14214	China GB/T 20828-2007
		Mean	St.Dev.			
Color	Visual	1.5	-	2.0		
Acid number (mg KOH/g)	ASTM-D974	0.325	0.1	≤0.5	≤0.8	≤0.5
Flash Point (°C)	ASTM-D93	95	1.2	≥93	≥130	≥120
Pour Point (°C)	ASTM-D97	-9	0.4	-15-16	_	_
Viscosity (mm²/s at 40 °C.)	ASTM-D445	5.35	0.5	1.9-6.0	_	3.4-5.0
Density (kg/m³ at 40 °C)	ASTM-D1298	0.821	1.06	≤120	_	≤120
Sulphur content (wt. %)	ASTM-D4294	0.0002	1	≤0.05	≤0.05	≤0.20
Cloud point (°C)	ASTM-D2500	-8	1	-3.0-12	_	_

3.9.6. Reusability of the catalyst

Reusability signifies one of the most imperative benefits of heterogeneous nano-catalyst over conventional homogenous catalysts. In this study, reusability of the CaO NPs was investigated at optimal reaction conditions of transesterification predicted via Design of Expert 13 Software. The reusability of the catalyst was evaluated after each cycle of reaction. CaO NPs were separated from the reacting mixture and afterward washed with methanol and n-hexane in order to eliminate residual biodiesel or glycerol. Reusability of the CaO NPs was studied up to seven cycles as depicted in Figure 3.9.11. Experimental results revealed that green nano-particles of calcium oxide can be efficiently reused up to five successive cycles with little change in the percent yield of biodiesel. After fifth cycle of transesterification the yield of biodiesel dropped significantly resulting in low yield of 75% in the sixth cycle. Yield was further reduced to 65% in seventh cycle of reaction due to deposition of organic species present in the reacting mixture of transesterification. Poisoning of active sites of CaO nano-particles resulted in shrinkage of whole surface area of particles and pore volume hence, attenuating the catalyst activity (Hosseini et al., 2020). However, catalytic activity of nano-particles can be recovered after washing them and repeating calcination.
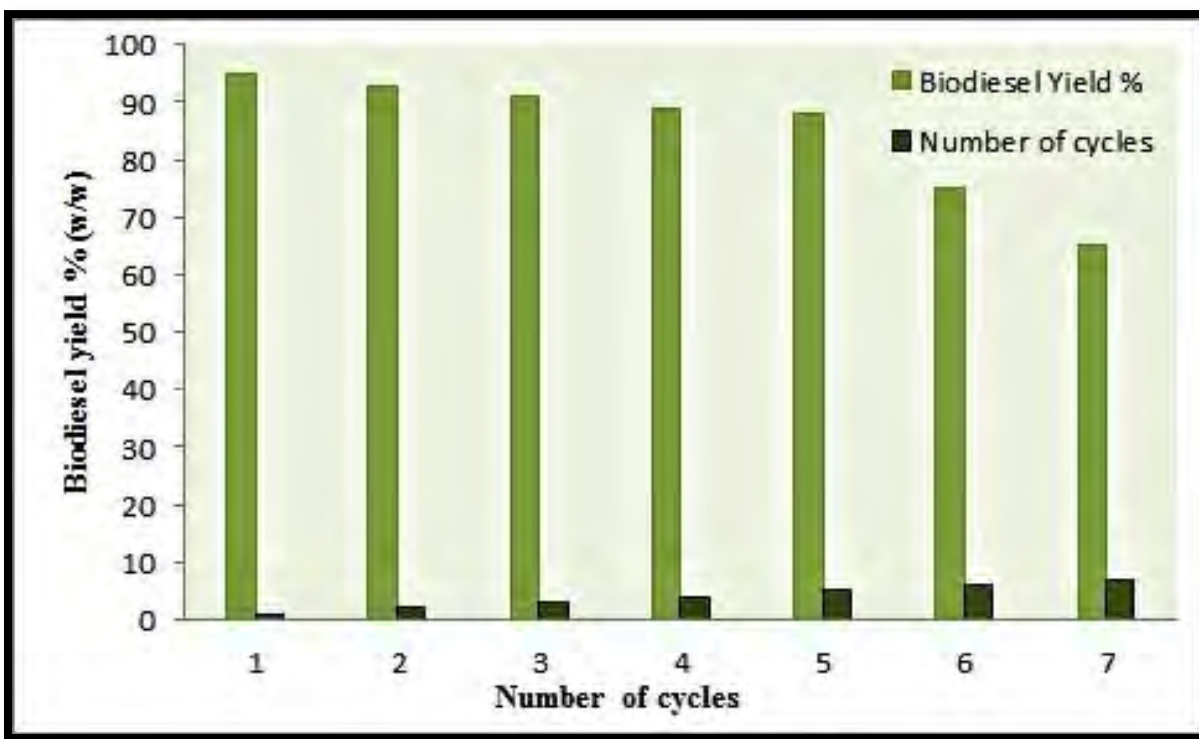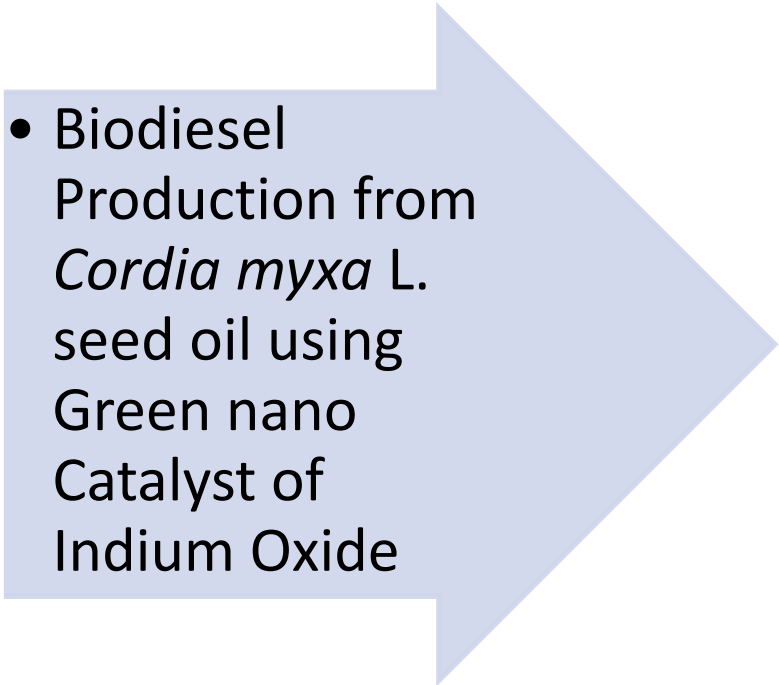
Figure 3.9.11. Reusibility of Calcium oxide NPs in transesterification reaction

SECTION X

- Biodiesel Production from *Cordia myxa* L. seed oil using Green nano Catalyst of Indium Oxide

Indium oxide nanoparticles are not previously used in production of biodiesel. Hence, it is first investigation carried out to explore the potential of indium oxide nanoparticles in transesterification. The green mediated synthesis of nanoparticles offers advantages over chemical synthesis. This environmentally friendly approach is therefore considered a pronounced alternative way to synthesize nanoparticles. In this study *Boerhavia diffusa* leaf extract was successfully used to synthesize indium oxide nanoparticles.

3.10.3. Characterization of In_2O_3 Nano-catalyst

3.10.1.1 X-Ray Diffraction (XRD) of In_2O_3

Powder X-Ray Diffraction was carried out to examine the crystalline structural of indium oxide (In_2O_3). The XRD pattern of In_2O_3 NPs has been shown in Figure 3.10.1. As confirmed by spectrum, indium oxide has six detectable peaks at 2θ = 22.07◦, 30.15◦, 35.4◦2, 45.53◦, 51.61◦, 61.35◦ corresponding to (211), (222), (400), (431), (440), (622) *hkl* respectively (JCPDS: 06-0416). The estimation of the respective crystal size was acquired from deepest peak at 2θ value is 30.15◦ (200 *hkl*).

The approximate crystalline size of In_2O_3 particles was determined to be 40.21 nm. All evident peaks of XRD spectrum of In_2O_3 confirmed cubic structure in the standard data (JCPDS 6-416).

3.10.1.2 Scanning Electron Microscopy (SEM) of In_2O_3

SEM technique was employed to explore the surface morphology of In_2O_3 at magnification of X2,500, X5,000 and X10, 000. SEM micrographs of In_2O_3 NPs are displayed in Figure 3.10.2 (a and b) which indicate a homogeneous, unvarying, and cubic morphology.

3.10.1.3 Energy Diffraction X-ray (EDX) of In_2O_3

EDX spectroscopic technique employed to explore chemical elements of In_2O_3 NPs. EDX spectrum of In_2O_3 nanoparticles has been shown in Figure 3.10.3 which illustrates peak of indium and oxygen without any impurity. In the spectrum EDX, peak at 0.5 KeV is allied with binding energy of oxygen while peak at 3.5 KeV and 24.2 KeV is linked with binding energy of indium. The percentage value of indium and oxygen was 74.30% respectively.

3.10.1.4 Fourier Transform Infrared Spectroscopy (FTIR)

FT-IR spectroscopic analysis gave details about various functional groups found in In_2O_3 NPs. The FT-IR spectrum of In_2O_3 NPs is displayed in Figure 3.10.4 showing transmittance percent of various absorption peaks. Wide peak appeared at 3218.31 cm^{-1} was suggested for adsorbed water on the surface of sampled particles. Broad band found at 1091.69 cm^{-1} reflected the stretching vibration of the In-O bond.

3.10.1.5 Thermogravimetric analysis (TGA) of In_2O_3

Thermogravimetric analysis of In_2O_3 precursor was carried out from ambient temperature to 1000 ◦C to examine its thermal decomposition. Thermogram of In_2O_3 and consequent derivative curve (wt. %) has been exhibited in Figure 3.10.5. First major weight loss of 0.264% was observed at 50-120 ◦C which is associated with desiccation and elimination of water from the surface of nanoparticles. Second peak of weight loss indicated loss of 0.085% which occurred at temperature range 150-220 ◦C which is attributed to decomposition of In_2O_3 precursor. Third phase of In_2O_3 decomposition happened at temperature range 250-550 ◦C accompanying weight loss of 0.265%.
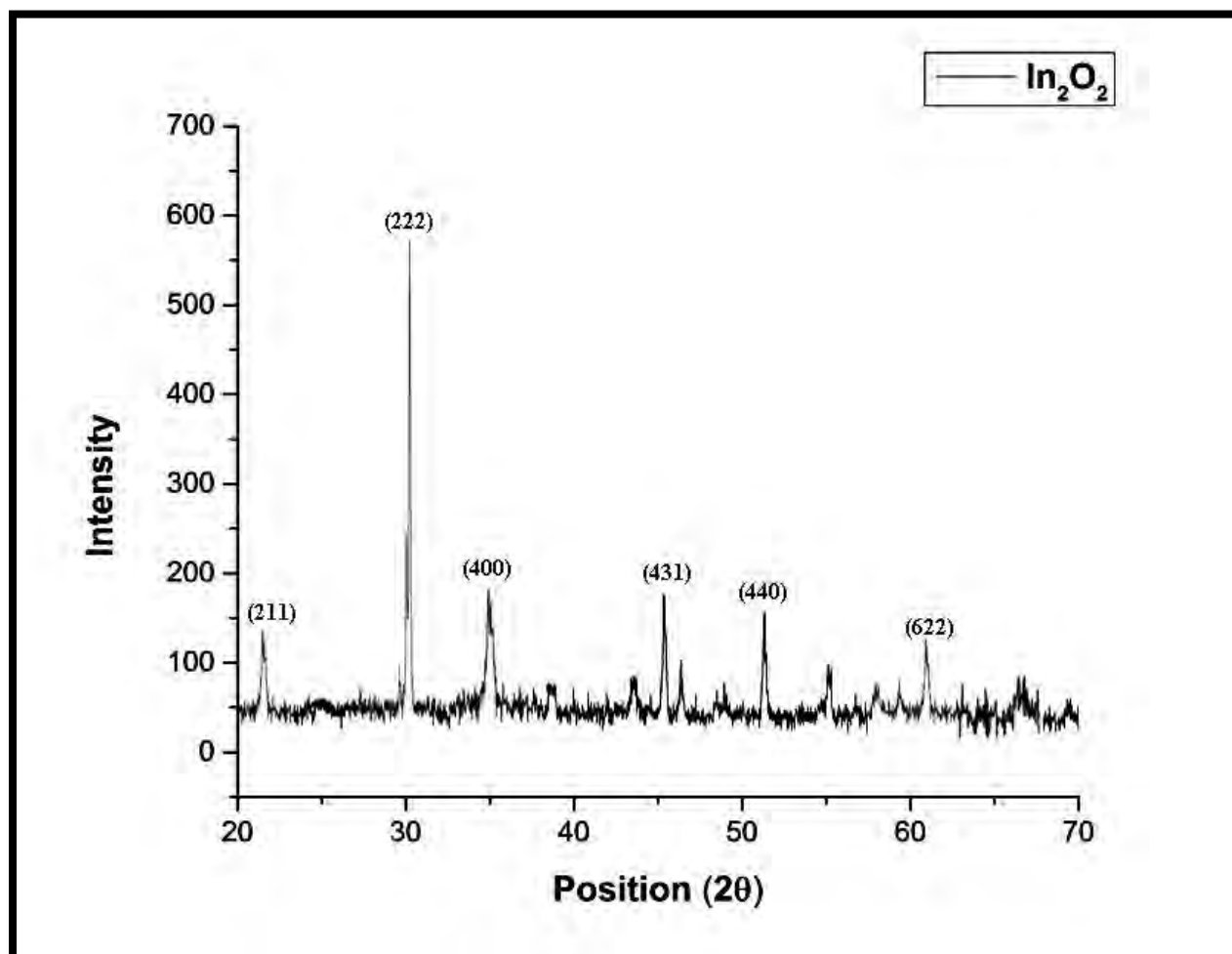
Figure 3.10. 1. XRD pattern of calcined indium oxide nanocatalyst
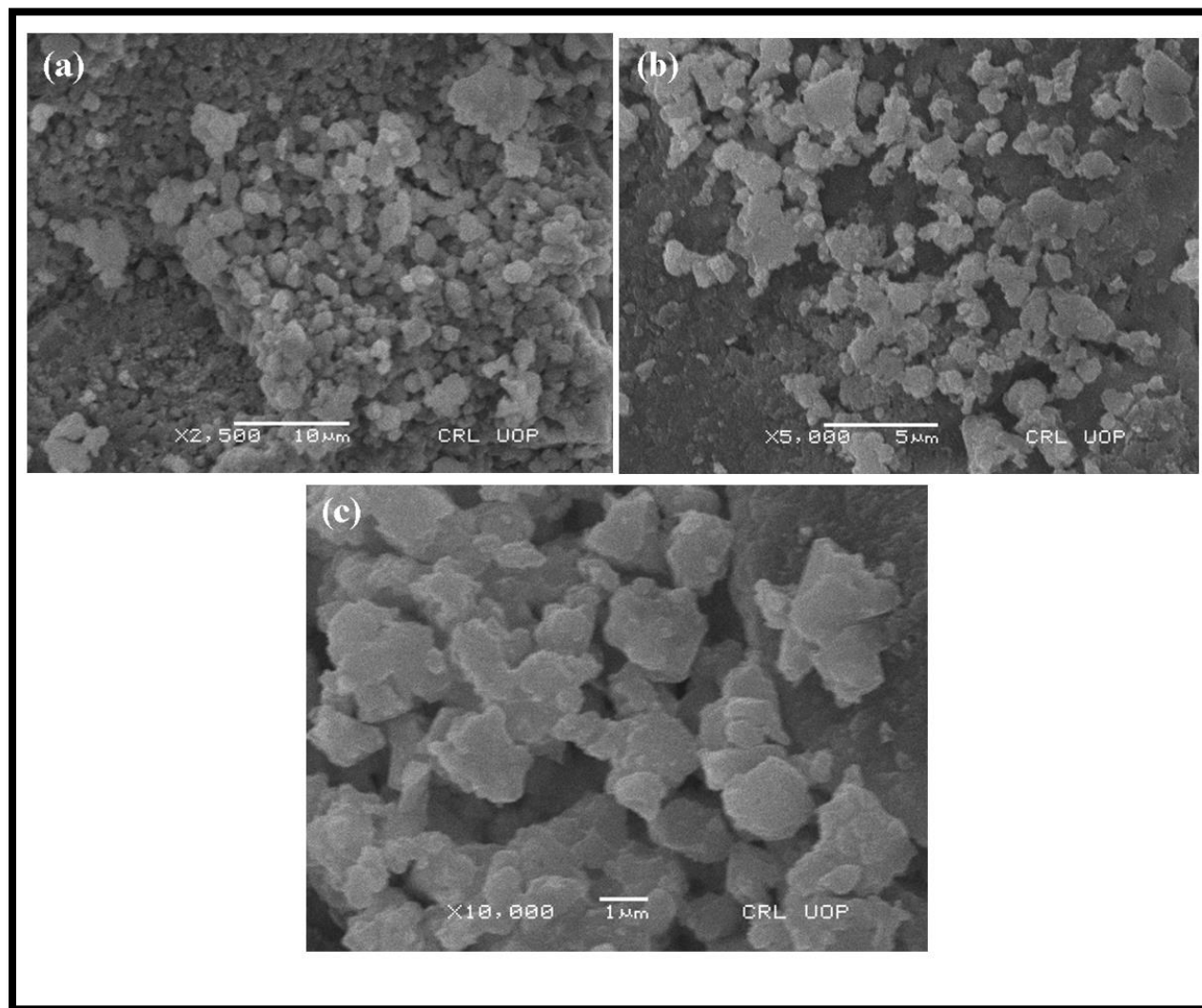
Figure 3.10. 2. (a-b) Scanning electron micrographs of indium oxide
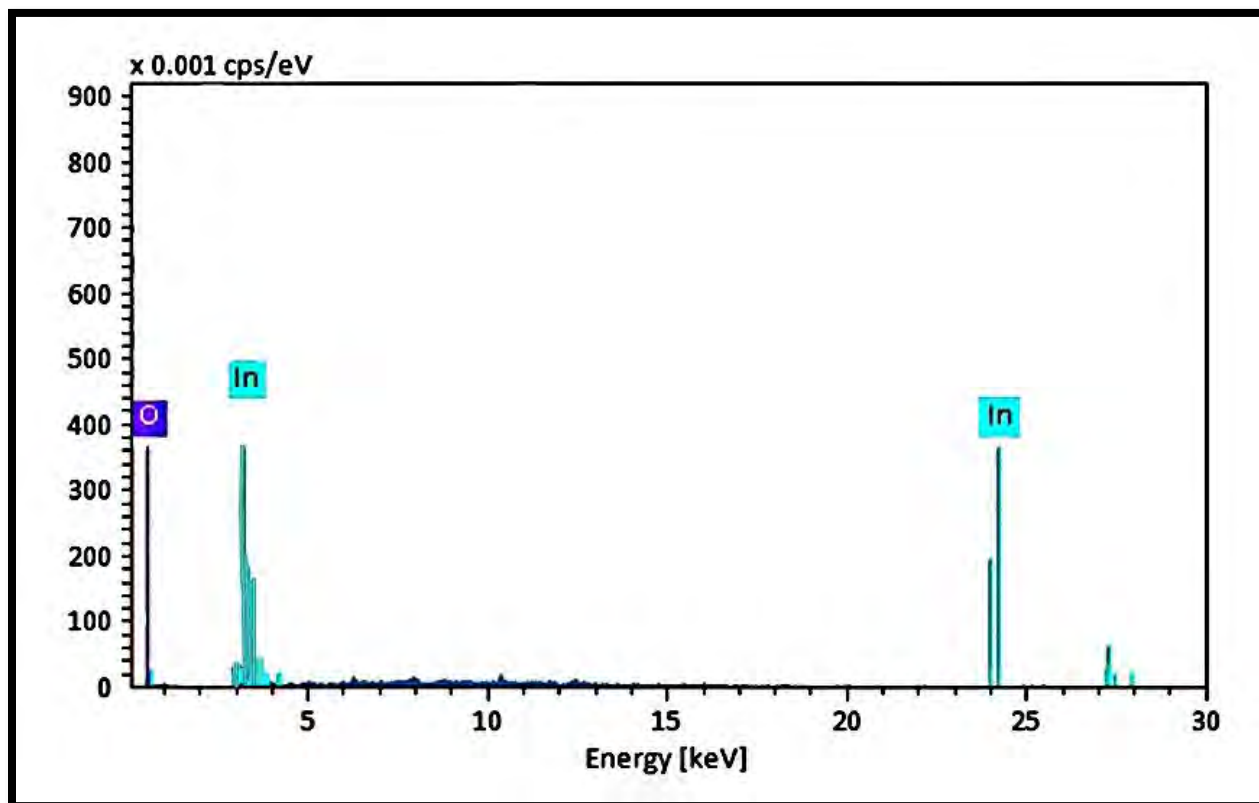
Figure 3.10. 3. Energy diffraction X-Ray (EDX) of indium oxide nanocatalyst
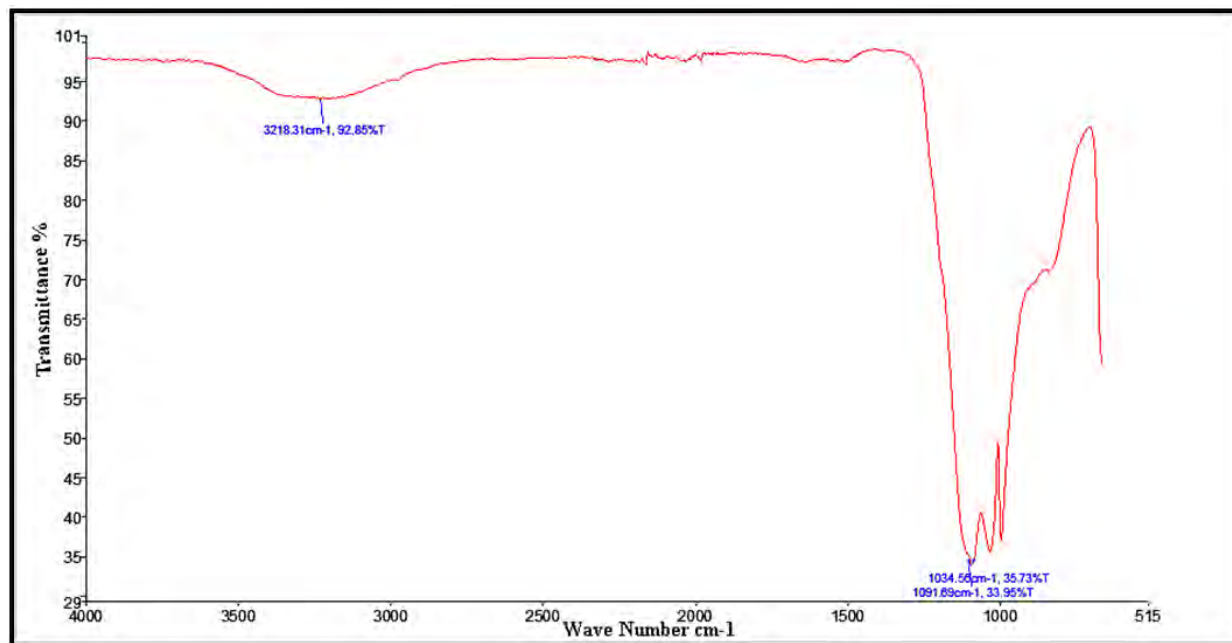
Figure 3.10. 4. FT-IR spectrum of indium oxide nanocatalyst
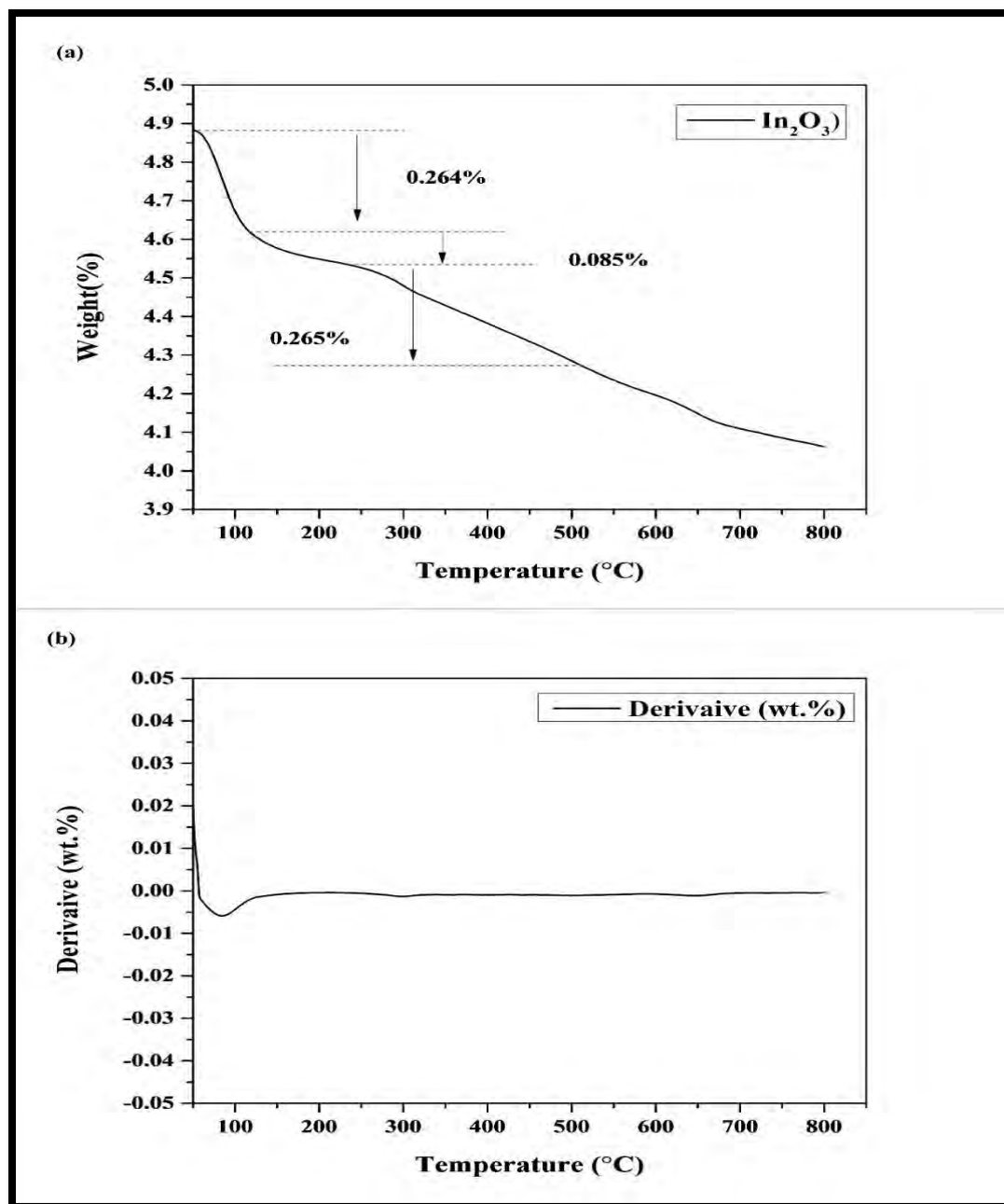
Figure 3.10. 5. (a) TGA of indium oxide nanocatalyst (b) derivative thermogram of indium oxide nanocatalyst

3.10.2 Biodiesel synthesis *via* Transesterification

In present investigation, novel, and potentially suitable seed oil of *Cordia myxa* was utilized to synthesize methyl ester. The FFA content of the oil must be determined prior to methyl ester formation. Table 3 presents the physical characteristics of *Cordia myxa* seed oil. According to prior reports, feedstocks with an oil content of more than 20% are regarded as suitable for synthesis of biodiesel (Tian et al., 2020). The oil content of *Cordia myxa* seeds was measured to be 37% (w/w), which is much greater than the advised percent value (Rahimi et al., 2021). The FFA concentration of *Cordia myxa* seed oil in this study was observed to be 0.62 mg KOH/g which is much lower and reflected the perfect functioning of a single-step transesterification. Non-edible *Cordia myxa* seed oil was used as renewable source to produce biodiesel with green nano catalyst of In_2O_3 produced with *Boerhavia diffusa* aqueous leaf extract.

CCD was designed using minimum and maximum values for four autonomous variables (Table 3.10.1). In order to achieve the highest yield of FAME and recognize optimal reaction conditions of transesterification, 30 separate experimental tests were carried out (Table 3.10.2). In Figure 3.10.6, the projected and actual yields of biodiesel are compared. Both sets of data are distributed close to a straight line, demonstrating a good connection between the two yields of methyl ester. They were found in proximity with one another, implying that they are aligned. Findings of ANOVA exhibited the experimental model as significant with a *p*-value of 0.0002 (<0.05) (Table 3.10.3). F-value of 7.39 in terms of the pure error and is refereed adequate for the model fit. The Predicted R^2 value of 0.724 was close to the adjusted R^2 of 0.873 with variance is <0.2. Precision of the model was determined to be adequate (8.99) in the current analysis. Applied polynomial Eq. (6) is given below.

Yield of Methyl ester (wt. %) = +85.00+0.0005 *A-0.3502 *B+1.82 *C+2.51 *D+0.6340 *AB-1.05 *AC+0.2354 *AD+0.3052 *BC-0.4425 *BD-4.31 *CD-10.91*A²-3.00 *B²+1.72* C²-11.32 D²

(17)

Biodiesel Synthesis, Optimization and Characterization from Novel Non-edible oil Seeds via High Performance Phyto-nano catalysts

308

Table 3.10.1- Experimental design by central composite design for transesterification reaction

Process parameters	−1	+1
Methanol to oil ratio	3:1	12:1
Catalyst loading (wt. %)	0.10	1. 5
Reaction time (min)	60	180
Temperature (∘C)	55	110

Table 3.10.2- Detailed experimental result for transesterification reaction of *Cordia myxa* Biodiesel

	Factor 1	Factor 2	Factor 3	Factor 4	Response
Run	A: Alcohol to oil molar ratio	B: Catalyst loading wt.%	C: Reaction time min	D: Temperature °C	Yield wt.%
1	7:1	1.5	120	82.5	80
2	3:1	0.11	60	110	70
3	7:1	0.8	180	110	92
4	7:1	0.8	180	82.5	95
5	12:1	1.5	180	55	65
6	3:1	1.5	180	110	60
7	7:1	0.11	120	82.5	85
8	7:1	0.11	180	82.5	77
9	3:1	0.11	60	55	57
10	3:1	0.8	180	110	64
11	7:1	0.8	60	110	70
12	3:1	1.5	60	55	50
13	3:1	0.8	180	55	65

14	7:1	0.8	120	82.5	90
15	3:1	0.8	60	82.5	65
16	3:1	0.11	180	55	67
17	7:1	0.11	180	110	74
18	12:1	0.8	180	82.5	75
19	12:1	0.11	180	55	60
20	7:1	0.8	120	110	65
21	12:1	1.5	180	82.5	55
22	12:1	0.8	120	82.5	88
23	7:1	0.8	180	55	68
24	3:1	1.5	180	55	60
25	12:1	0.8	180	110	55
26	7:1	0.8	180	110	60
27	3:1	0.8	120	82.5	70
28	7:1	0.8	60	55	57
29	7:1	0.8	180	110	79
30	7:1	0.11	60	82.5	64

Table 3.10.3- ANOVA for Response Surface Quadratic model

Source	Sum of Squares	df	Mean Square	F Value	p-value	
Model	3566.62	14	254.76	7.39	0.0002	**Significant**
A-Alcohol to oil molar ratio	4.624	1	4.624	1.341	0.0497	
B-Catalyst loading	2.29	1	2.29	0.0665	0.0300	
C-Reaction time	59.65	1	59.65	1.73	0.0082	
D-Temperature	117.41	1	117.41	3.40	0.0148	
AB	6.44	1	6.44	0.1869	0.0417	
AC	17.65	1	17.65	0.5118	0.0324	
AD	0.8882	1	0.8882	0.0258	0.0446	
BC	1.49	1	1.49	0.0432	0.0381	
BD	3.13	1	3.13	0.0909	0.0672	
CD	297.56	1	297.56	8.63	0.0102	
A²	323.54	1	323.54	9.38	0.0079	
B²	30.80	1	30.80	0.8932	0.0596	
C²	8.25	1	8.25	0.2391	0.0319	
D²	438.45	1	438.45	12.71	0.0028	
Residual	517.25	15	34.48			
Lack of Fit	393.50	10	39.35	1.59	0.3176	**not significant**
Pure Error	123.75	5	24.75			
Cor Total	4083.87	29				

$R^2 = 0.873$, Std. Dev. = 5.87,   C.V. % = 8.36, Adeq Precision = 8.99
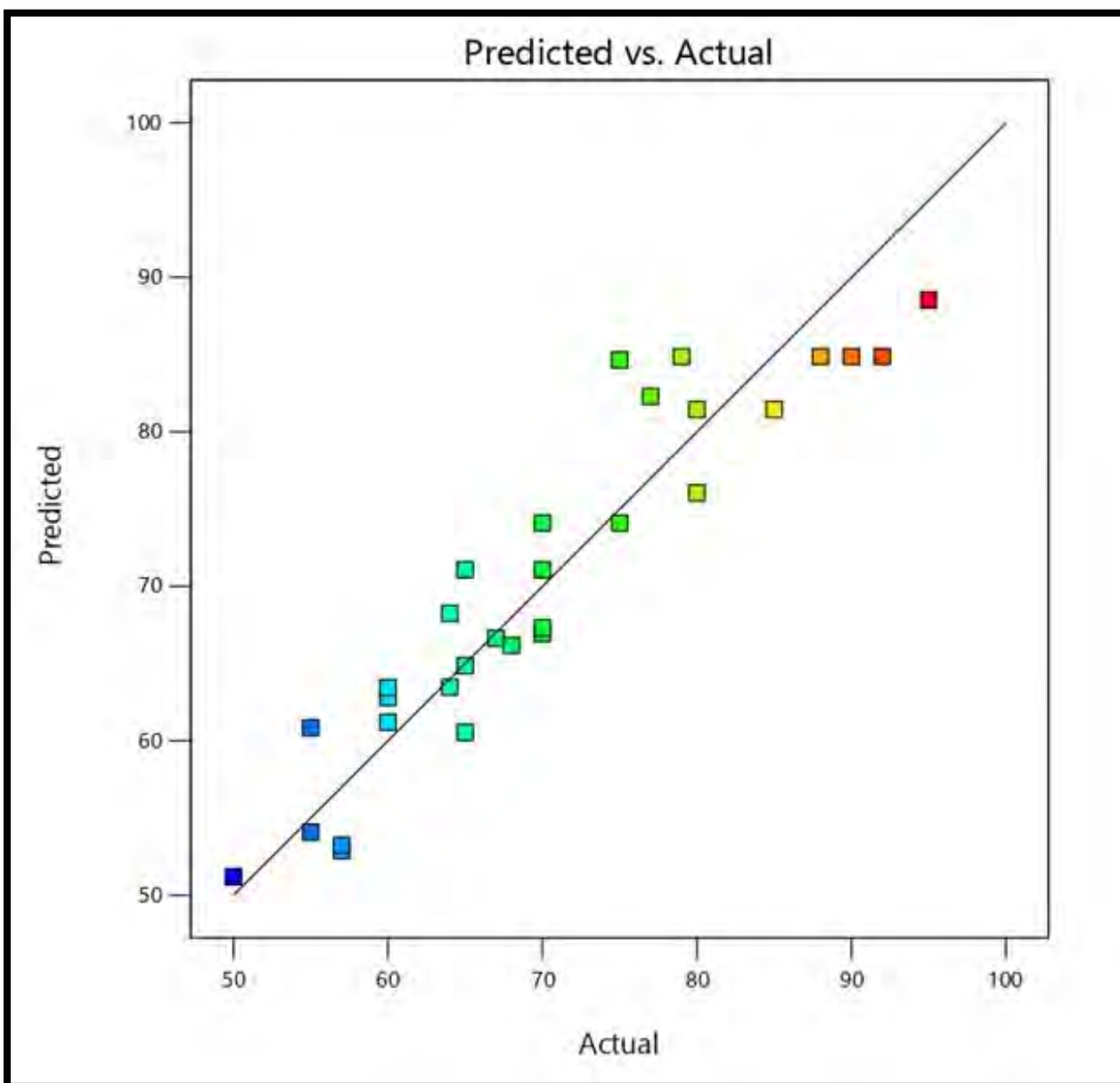
Figure 3.10.6 Comparison between the experimental biodiesel yield and the predicted yield of the model

3.10.3. Effect of Reaction variables on Transesterification

3.10.3.1 Combined influence of methanol to oil molar ratio and catalyst loading

Mutual correlation of Met:Oil and catalyst load was studied at constant temperature (82.5 ∘C) and time (180 min). These are one of the important reaction interactions which substantially influences biodiesel yield throughout the process of transesterification. The parametric interaction of Met:Oil and catalyst load is displayed in Figure 3.10.7a in the frame of 3D plot. Sufficient amount of methanol is required for conversion of *Cordia myxa* seed oil into biodiesel. Highest FAMEs yield was achieved at Met:Oil 7:1 and catalyst load of 0.8 (wt.%) (Run 4). FAME yield was rendered to 77% with minimum catalyst load of 0.11 (wt.%) at Run 8. High Met:Oil of 12:1 and , catalyst load 0.8 (wt.%), gave a yield of 75% at Run 18. Both higher Met:Oil and catalyst load 1.5 (wt.%) gave lowermost yield of 55% at Run 21. It was observed that increasing the catalyst beyond 0.8 (wt.%) reduced biodiesel yield. Similarly, excess of methanol drops the output of transesterification by causing glycerolysis and encouraging reversible reaction (Rezania et al., 2019). A significant correlation was observed between Met:Oil and catalyst load in results of ANOVA by having *p*-value of 0.0417.

3.10.3.2 Combined influence of methanol to oil ratio and reaction time

The interaction between Met:Oil and time has significant influence on transesterification which is exhibited in the frame of 3-D plot presented in Figure 3.10.7b. Highest FAME yield of 95% was achieved at Met:Oil 7:1, and time 180 (min) at constant catalyst load (0.8 wt.%) and temperature (82.5 ∘C) (Run 4). Decrease in time of chemical reaction up to 120 min cut out yield from 95% to 90% at Run 14 with same Met:Oil (7:1). It's most likely because the reactants didn't have enough time to react effectively, following in partial conversion of reacting compounds into products. Higher Met:Oil 12:1 at Run 22 resulted in FAMEs yield of 88%. Excess methanol in the reactant mixture causes thinning of the catalyst concentration. It obstructs the parting of glycerol from FAMEs, resulting in a low biodiesel output. The latest findings are consistent with prior findings, which show that a surplus of methanol causes a retrograde glycerolysis process (Ayoub et al., 2021). Lowest Met:Oil 3:1 and time of 120 min triggered FAME yield of 70% at Run 27. A minimum yield of 65% was achieved at Run 16 with Met:Oil 3:1 and time duration of 60 min. It is attributed to deficient time resulting in the least interaction of reactants. ANOVA

results has declared the relationship between Met:Oil and time as significant with *p*-value 0.0324.

3.10.3.3 Combined influence of methanol to oil molar ratio and temperature

The interaction of Met:Oil and temperature has great impact on FAME yield during transesterification. It is demonstrated in the frame of 3-D plot shown in Figure 3.10.7c. Greatest yield of 95% was observed at Met:Oil 7:1, and temperature 82.5 ∘C at constant catalyst load (0.8 wt.%), and time (180 min) at Run 4. High temperature of 110 ∘C and Met:Oil 7:1 dropped yield to 79% at Run 29. Met:Oil 3:1 and temperature 55 ∘C produced FAME yield of 65% at Run 13. About 64% yield was detected at Run 10 with highest temperature of 110 ∘C and low Met:Oil 3:1. The high concentration of methanol encouraged unfavorable conditions, resulting in a low biodiesel production (Li et al., 2020). Yield was further reduced to 55% 110 ∘C and highest Met:Oil 12:1 at Run 25. It was previously reported that increasing the Met:Oil above 15:1 at 80°C and a catalyst load of 1% resulted in a drop in biodiesel production (Silitonga et al., 2020). ANOVA outcome has declared the relation between Met:Oil and temperature as significant with *p*-value 0.0446 (<0.05).

3.10.3.4 Combined influence of time and catalyst loading

A strong interaction between catalyst load and time is evident from Figure 3.10.7d. Highest yield of 95% was achieved at Met:Oil 7:1 and temperature 82.5 ∘C (Run 4). Maximum catalyst load of 1.5 (wt.%) and time 120 min reduced FAMEs yield to 80% (Run 1). At this stage decline in FAME yield is ascribed to excessive catalyst amount in the mixture of reactant which enhanced fluid viscosity hence, pushing a reduced mass transfer in transesterification. The lowest catalyst load of 0.11 (wt.%) and time 120 min produced FAMEs yield of 85% (Run 7) which implies that even long reaction time with insufficient amount of catalyst is not able to proceed reaction in forward direction (Adepoju et al., 2020). Minimum FAMEs yield of 64% was achieved with time 60 min and catalyst loading 0.11 (wt.%) at Run 30. This is most likely owing to partial conversion at a short period in which reactants failed to reach equilibrium. The correlation between catalyst loading and time was shown significant in ANOVA table exhibiting *p*-value lesser than 0.05 (0.0381).

3.10.3.5 Combined influence of catalyst loading and reaction temperature

A positive interaction between catalyst load and temperature was discovered in our current investigation which has been exhibited in Figure 3.10.7e. Highest FAME yield of 95% was achieved at catalyst load 0.8 (wt.%), temperature 82.5 ∘C at constant Met:Oil 7:1, and time 180 min (Run 4). Yield was lowered to 92% with catalyst load of 0.8 (wt.%), and temperature 110 ∘C at Run 3. However, an additional rise in temperature above 90 ∘C (edge level) has drastically lessened biodiesel yield. Minimum catalyst load 0.11 (wt.%), and high temperature of 110 ∘C reduced yield to 74% (Run 17). About 68% FAMEs yield was observed at Run 23 with lowermost temperature of 55 ∘C and catalyst loading 0.8 (wt.%). Maximum catalyst loading 1.5 (wt.%), and low temperature of 55 ∘C reduced yield to 60% at Run 24 which signified that temperature lesser than optimum level failed to give sufficient kinetic energy for proper mixing of reactants (Demirbas et al., 2016). Significant correlation was observed between catalyst loading and temperature in ANOVA table having *p*-value of 0.0672.

3.10.3.6 Combined influence of time and temperature

Mutual interaction with time and temperature and their influence on FAMEs yield has been shown in Figure 3.10.7f. Highest FAME yield of 95% was calculated at time 180 min and temperature 82.5 ∘C at constant Met:Oil (7:1) and catalyst load of (0.8 wt.%) (Run 4). About 70% yield was calculated with time 60 min and temperature 110 ∘C (Run 11). The recent study found that increasing temperature and duration rises biodiesel yield up to a certain point (Ajith et al., 2020). Following that, due to the endothermic nature of the transesterification, there is a considerable fall in percent yield. Maximum temperature 110 ∘C for maximum time 180 min gave lowest yield of 60% at Run 26. Low time of 60 min and temperature 110 ∘C compact FAMEs yield to 57% at Run 27. It is due to insufficient kinetic energy in a short time. About 65% FAMEs yield was observed with time 120 min and temperature 110 ∘C at Run 20. The chemical reaction of hydrolysis of alkyl esters into acids is thought to be accelerated by increasing the reaction duration and temperature. Biodiesel production is being reduced by the consequent polar CH_3OH in the reaction mixture (Meghwal et al., 2022). The relation between time and temperature was declared as significant in the results of ANOVA having *p*-value of 0.0102 which is less than 0.05.
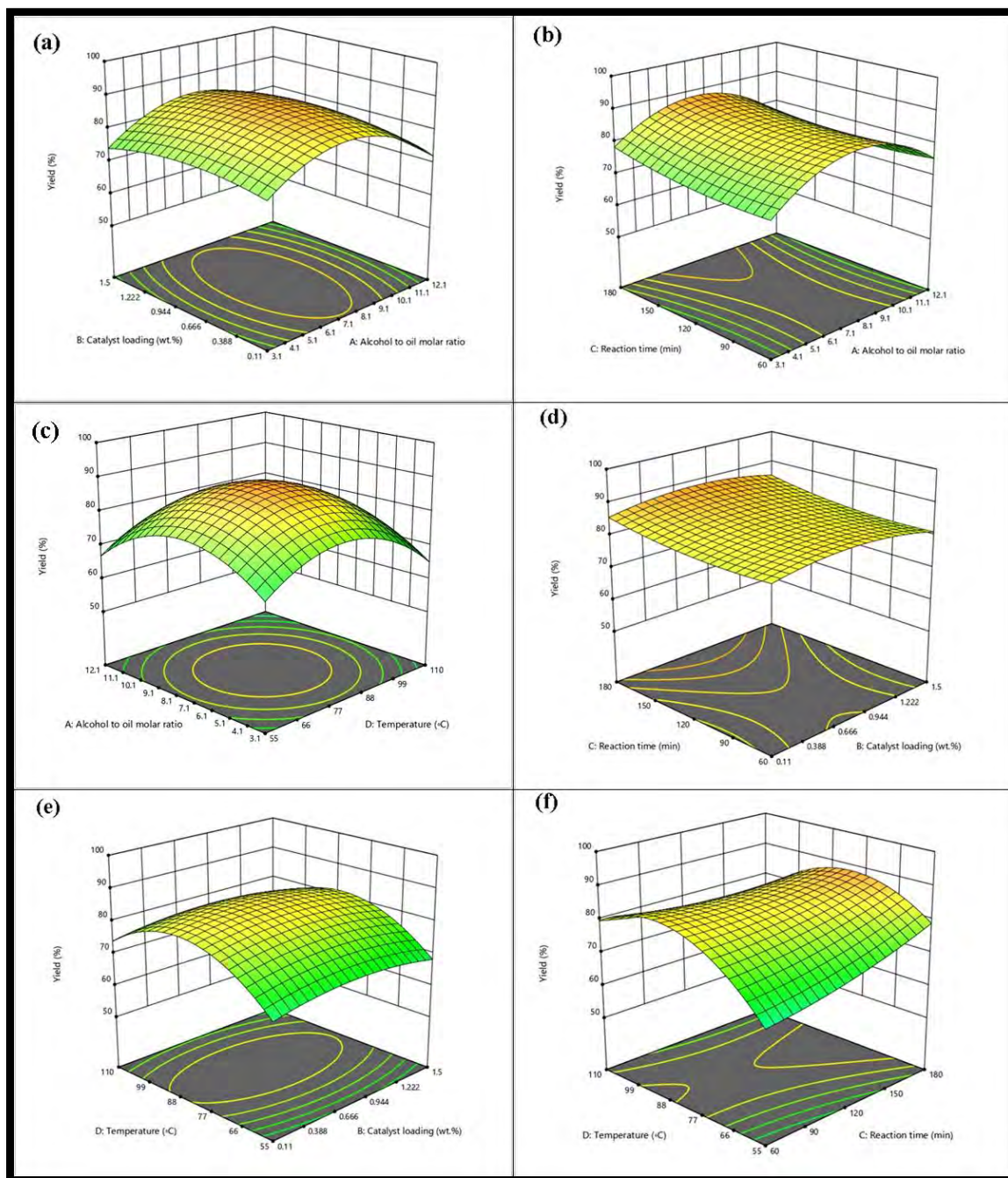
Fig. 4. Impact of the reaction conditions of *Cordia myxa* biodiesel.

3.10.4. Characterization of Biodiesel

3.10.4.1 FTIR spectroscopic Study

FT-IR spectroscopic analysis is also used as an effective tool for validation of methyl ester formation after transesterification (Ansori and Mahfud 2021). FT-IR spectroscopic analysis un mid infra-red region has been employed to identify structural composition of *Cordia myxa* seed oil *and* biodiesel. Figure 3.10.8 (a and b) illustrated IR spectrum of *Cordia myxa* seed oil and biodiesel respectively, describing bands and stretches of various functional groups. The major representative band of carbonyl group (C=O) appeared at 1743.63 cm^{-1} in the spectrum of biodiesel while, vibration band for group of methyl (CH$_3$) was noticed at 1464.47 cm^{-1}. The presence of carbonyl and methyl group in the spectrum of biodiesel has confirmed production of methyl ester during transesterification. The IR area depicting carbonyl group is the most vulnerable to chemical and molecular change among all other peak areas in the spectrum of biodiesel (Moreira et al., 2020). The distinguishing peak of C-H (sp^3) occurred in the IR area of 2922.65 cm^{-1} while, CH (sp^2) stretch appeared at 2853.28 cm^{-1}. Stretching vibration for aliphatic esters (O=C-O-C) was detected at 1161.28 cm^{-1}.

The IR region in spectrum of oil and biodiesel with maximum variability was detected around 1200-1800 cm^{-1} and 3300-2800 cm^{-1}. Stretch observed at 1097.28 cm^{-1} was allotted to the wagging frequency of C-H$_2$. Peak appeared at 1741.53cm^{-1} in the spectrum of *Cordia myxa* seed oil was gone in the spectrum of biodiesel. Similarly, intense peak of (C=C) situated at 1460.32 cm^{-1} also gone in the IR spectrum of methyl ester. Exploration of mentioned stretches and band of the IR spectrum of *Cordia myxa* oil and methyl ester have proven the transformation of triglycerides into FAME in the process of transesterification.

3.10.4.2 NMR Spectroscopic Analysis

^{1}HNMR is a spectroscopic technique applied for confirmation and quantification of synthesized biodiesel of *Cordia myxa* It is broadly used to estimate the concentration of saturated and unsaturated FAME in sample of biodiesel at various steps like post transesterification, purification, heat treatment, and after storing (Ingle et al., 2021). ^{1}HNMR spectrum of *Cordia myxa* biodiesel has been displayed in Figure 3.10.8a. Occurrence of FAME in biodiesel was

confirmed by distinctive peak for methoxy group (– OCH$_3$) spotted at 3.672 ppm in the ^{1}HNMR spectrum. Peak of methanol which normally appeared at 3.45 ppm was not found in spectrum of CMBD.

^{1}HNMR spectrum of CMBD presents triplet peak for proton of α-methylene (α-CH$_2$) at 2.088-2.335 ppm. Signal for β-CH$_2$ (β-methylene) protons was noted as a singlet at 1.260-1.308 ppm in the spectrum corresponding to hydrogen atom positioned on carbon-3 of aliphatic chain of hydrocarbon. Peak observed at 0.864-0.907 ppm is attributed to terminal protons methyl group. peak spotted at 5.312-5.411 ppm was signified for olefinic hydrogen with a pair of carbon atom connected with a double bond (-CH=CH-). The peak reflected at 2.758-2.797 ppm is linked to allylic hydrogen (-CH$_2$). All discussed peaks of ^{1}HNMR spectrum have confirmed methyl esters formation in biodiesel sample. Determining of the total conversion of triglycerides into FAME was carried out and calculated value was 93 %.

^{13}CNMR spectrum of biodiesel synthesized from *Cadia myxa* seed oil have been exhibited in Figure 3.10.8b. ^{13}CNMR spectroscopy was used to examine structural characteristics of CMBD methyl ester. Methoxy carbon showed appearance in the form of distinctive peak observed at 51.47 ppm. Signal at 174.35 ppm is attributed to carbonylic group (-COOH). Peak positioned at 127.89-128.03 ppm is assigned to double bond between internal non-conjugated carbon atoms (-CH=CH-) indicating level of unsaturation in biodiesel. The chemical shifts for outer carbon of non-conjugated carbons (-CH=CH-) was detected at 129.74-120.18 ppm in the spectrum of ^{13}CNMR. Signal at 76.64-77.48 ppm was assumed for C-O group of methyl ester. Peak found at 29.13-29.78 ppm implied long series of ethene carbon (-CH$_2$-)$_n$ chain. Peak found at 31.53-34.10 ppm described aliphatic-methylene (-CH$_2$-s) carbon in biodiesel sample.

3.10.4.3. GC/MS Analysis

The fatty acid profile composition of *Cordia myxa* biodiesel was examined by GC/MS analysis. It is the most used technique for quantification of biodiesel due to its high accuracy (Fatah et al., 2012). Figure 3.10.10 exhibits gas chromatogram of CMBD. Recognized methyl esters were further verified by MS analysis employing library match software NO. NIST02. GC/MS spectrum exhibited four distinct methyl ester peaks of were observed in chromatogram. Hexadecanoic acid methyl ester (16:0) and Octadecanoic acid, methyl ester (18:0) are saturated

methyl esters obtained at retention time 10.24 min and 12.17 min respectively. The presence of saturated fatty acid methyl-esters is considered as beneficial for biodiesel quality (Campli et al., 2021). However, due to its high melting points it can cause gelling of fuel at low temperatures. Unsaturated methyl ester included 9, 12-Octadecadienoic acid methyl-ester (18:2) and 9-Octadecenoic acid, (2)-methyl, methyl ester (18:1). Unsaturated fatty acid methyl esters have low melting points which help to endure low temperatures but are more predisposed to oxidation. 9, 12-Octadecadienoic acid methyl ester is major FAME with greater concentration obtained at retention time 11.89 min. FAME profiling of *Cordia myxa* biodiesel indicated it an efficient feedstock for biofuel production at commercial scale.
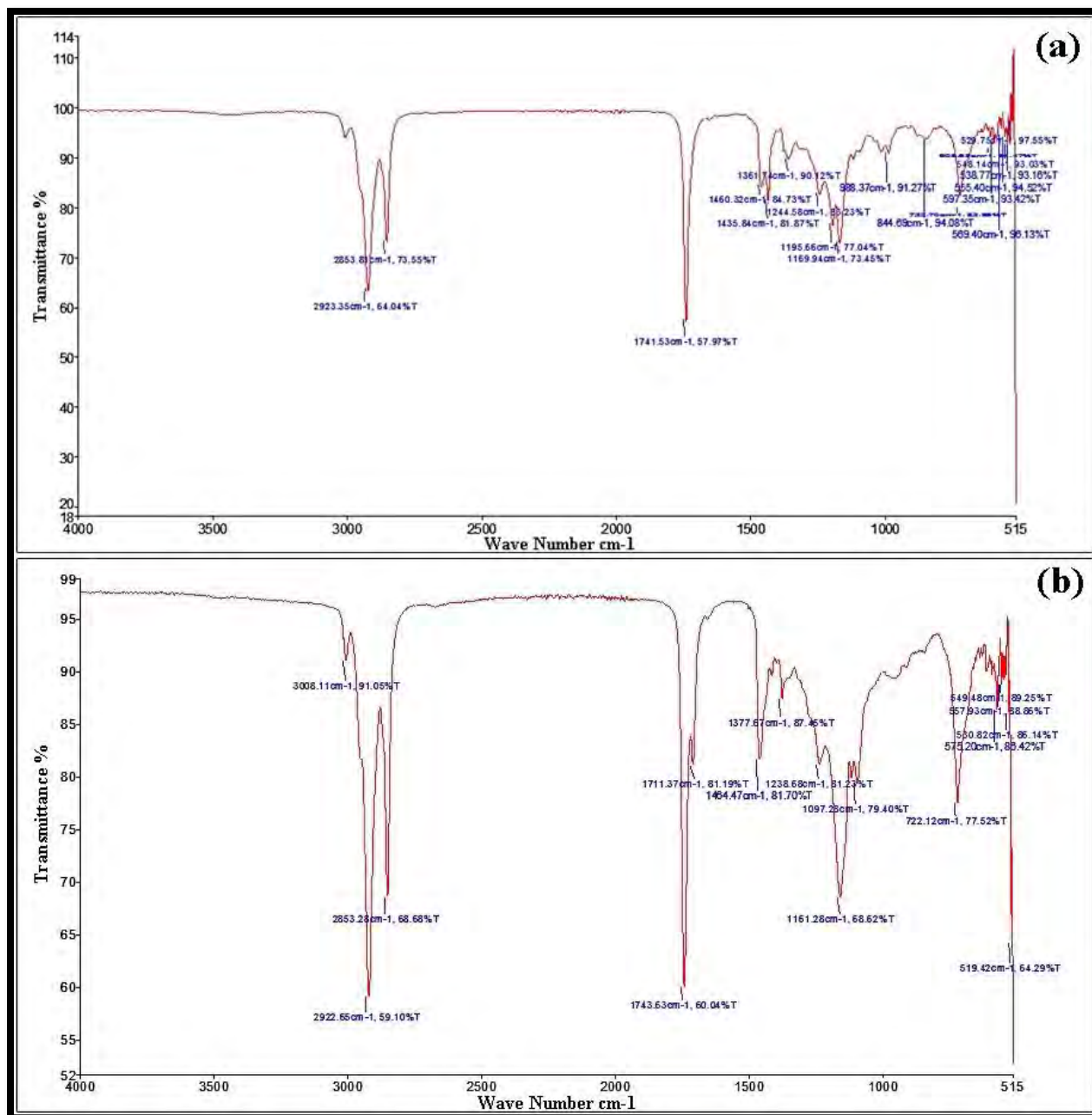
Figure 3.10.8 FT-IR spectrum of **(a)** *Cordia myxa* seed oil **(b)** *Cordia myxa* biodiesel
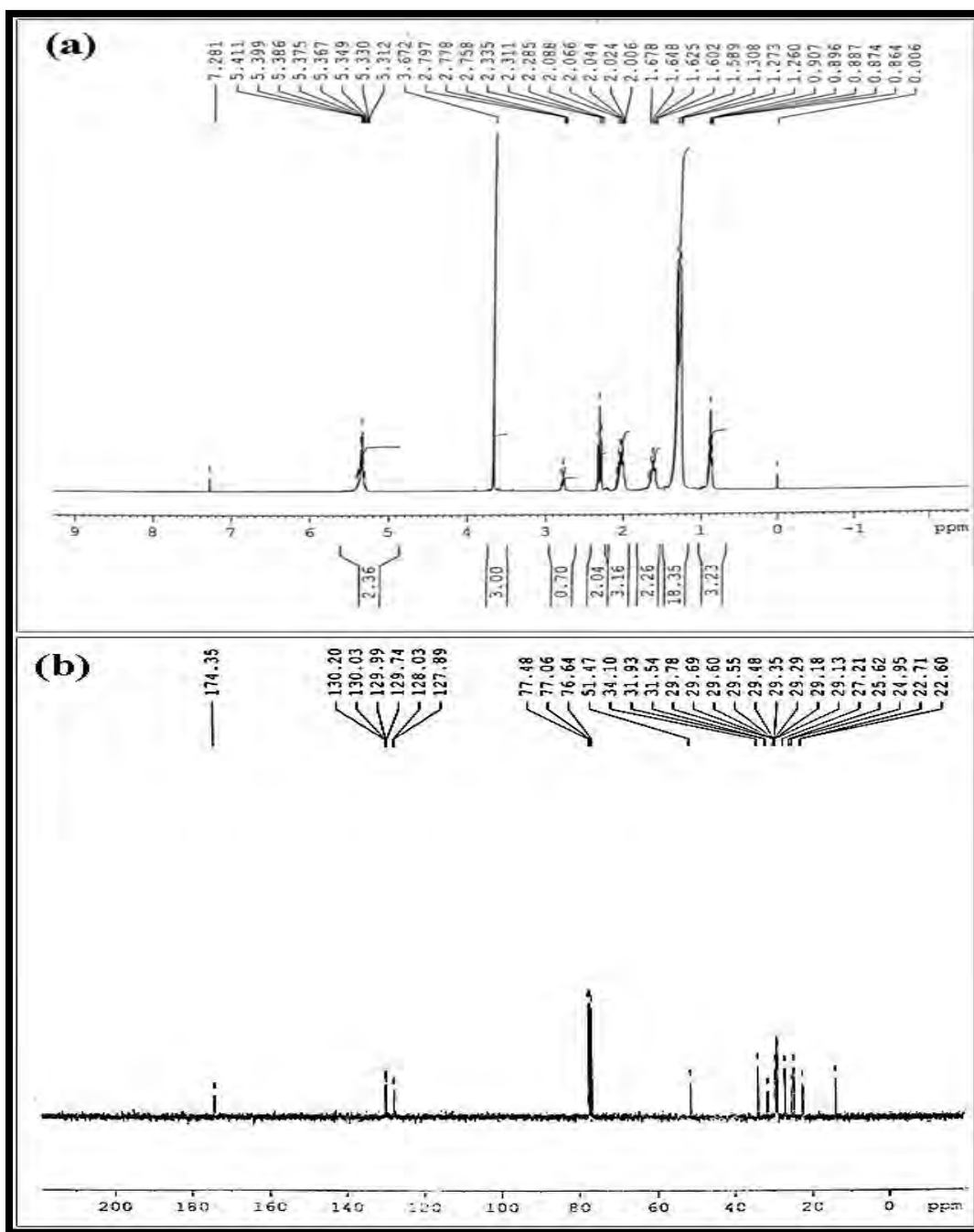
Figure 3.10.9 NMR spectrum of **(a)** ^{1}HNMR and **(b)** ^{13}CNMR of *Cordia myxa* biodiesel
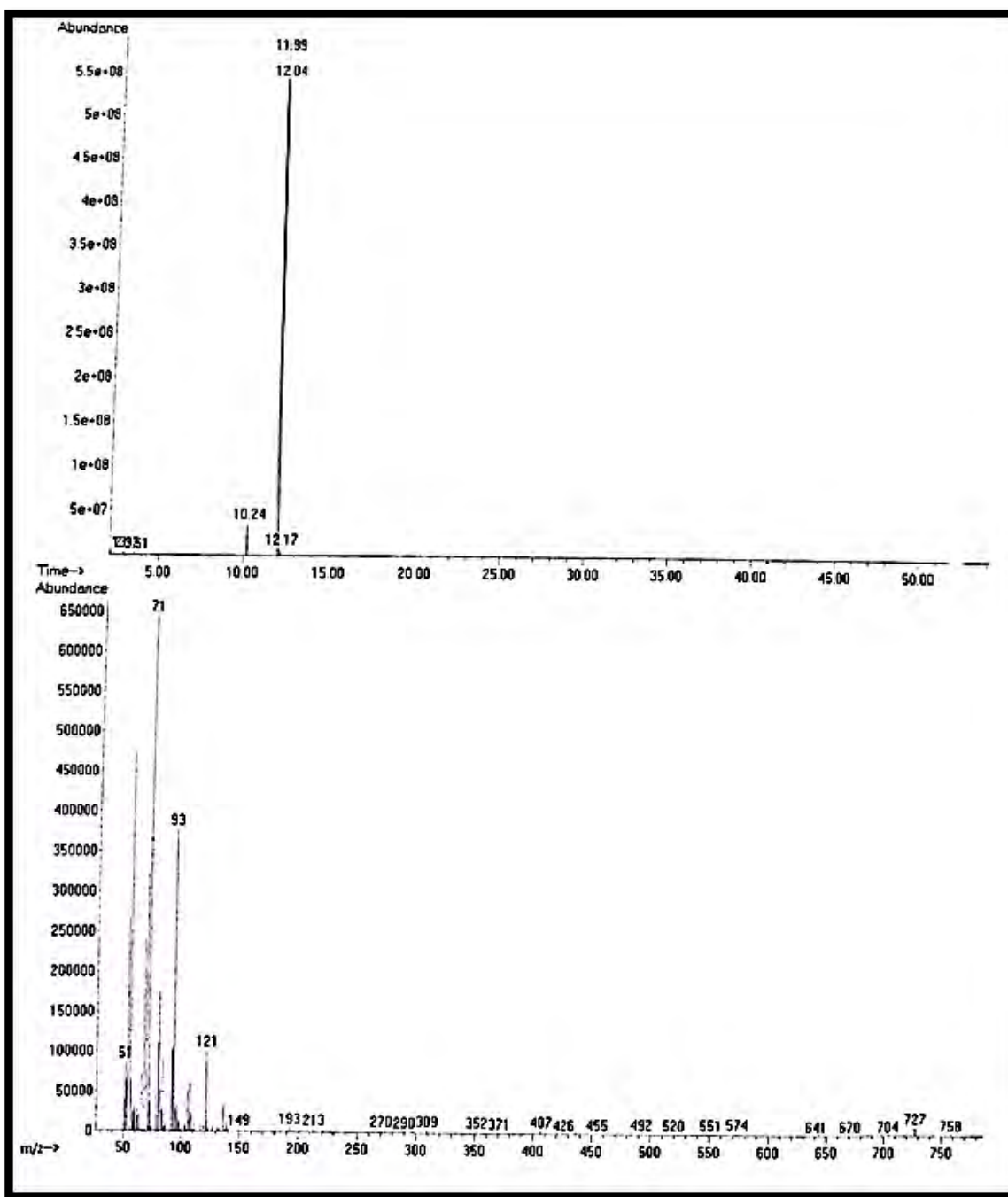
Figure 3.10.10 GC-MS spectrum of *Cordia myxa* biodiesel

3.10.5. Determination of Fuel properties of biodiesel

Fatty ester profile composition of biodiesel varies from feedstock to feedstock which subsequently influences its fuel properties (Mofijur et al., 2021). All fuel properties of *Cordia myxa* biodiesel fall under international standards of ASTM D-6571, EN 14214 and China GB/T 20828-2007.

The flammability hazard of a fuel is assessed by measuring the flash point. It characterizes the slightest temperature at which a fuel ignites upon exposure to a flame or spark (Behera et al., 2020). Flash point has an inverse relation with volatility; higher the flash point lower will be the volatility. Biofuels are safe to handle, transport and store. The flash point of *Cordia myxa* biodiesel which is 95 ◦C falls under ASTM standard (Table 3.10.4).

Kinematic viscosity is one the key characteristics of biodiesel which highly influences the pattern of fuel spray. High viscosity results in large size fuel droplets which leads to inappropriate mixing of air and fuel causing poor combustion and high particulate matter emission. Likewise, viscosity lower than the standard declines peak heat release rate leading to reduced rate of air fuel mixing (Rozina et al., 2019). The mean value of kinematic viscosity of *Cordia myxa* biodiesel was 6.24 (mm^2/s) which lies with in boundaries of international fuel standards.

Density has great impact on fuel injection hence, energy content in combustion chamber and performance of engine are highly influenced by density of the fuel (Torabi et al., 2020). High content of unsaturated fatty acids results in high density of biodiesel. Composition of methyl esters and their purity have high impact on density of biodiesel. Kinematic density CMBD found to be 0.877 (kg/m³) found equivalent to international fuel standards.

Pour point is the significant cold flow property of the fuel. It is relatively higher than conventional Petro diesel. It is greatly affected by the amount of saturated fatty acids (Takaseet al., 2018). Pour point was calculated to be -12 ◦C which fit well within accepted international limits of fuel. Cloud point is the minimum temperature at which small knobs of crystals appear in fuel sample. At temperatures lower than the cloud point these crystals fused to form clusters and prevents pouring of the fuel. These crystals might block filters or drop down to the storage

tank. Mean value of the cloud point of *Cordia myxa* methyl ester was analyzed to be -10 ∘C which match well with ASTM standard.

       The measurement of concentration of free fatty acid is known as acid value (Vidhu and Philip 2014). It depends upon the type of raw feedstock. The acid value of *Cordia myxa* biodiesel was found to be 0.245 (mg KOH/gm) which lies under international fuel standards. Sulphur is an objectionable element present in fuel which results in soot formation during combustion. Sulphur emission in form of oxides causes environmental pollution and acid rain. Minimum sulphur content of 0.0002% (less than 1 ppm) was observed in CMBD.

Table 3.10.4 Comparison of fuel properties of *Cordia myxa* L biodiesel with international standards**.**

Property	Methods	*Cordia myxa*		ASTM D-6751	EN-14214	China GB/T 20828-2007
		Mean	**St.Dev.**			
Color	Visual	2	-	2.0	-	-
Acid number (mg KOH/g)	ASTM-D974	0.245	0.1	≤0.5	≤0.8	≤0.5
Flash Point (°C)	ASTM-D93	95	1.2	≥93	≥130	≥120
Pour Point (°C)	ASTM-D97	-12	0.3	-15-16	_	_
Viscosity (mm²/s at 40 °C.)	ASTM-D445	6.24	0.1	1.9-6.0	_	3.4-5.0
Density (kg/m³ at 40 °C)	ASTM-D1298	0.877	1.1	≤120	_	≤120
Sulphur content (wt.%)	ASTM-D4294	0.0002	-	≤0.05	≤0.05	≤0.20
Cloud point (°C)	ASTM-D2500	-10	-1	-3.0-12	_	_

3.10.6. Catalyst Reusability

Reusability of In_2O_3 NPs was analyzed at optimum reaction settings of transesterification such as Met:Oil of 7:1, catalyst loading of 0.8 (wt. %), time 180 min and temperature of 82.5 °C. It included a series of chemical reactions of transesterification carried out to verify its stability and viability (Roy et al., 2019). In_2O_3 NPs were first separated by centrifugation from reaction mixture and purified by washing with alcohol. Recovered In_2O_3 NPs nanoparticles were dried and calcined at 500 ∘C for 3 hours.

In_2O_3 NPs catalytic action was examined up to 7th consecutive cycles of transesterification. Catalytic performance was found to be excellent till six consecutive rounds gave high FAME yield. About 95% yield was observed in first, which was reduced to 90% in 3rd and up to 80% in 5th cycle. A sudden drop in FAME yield up to 61% was distinguished in 7th. cycle (Figure 3.10.11). Decline in catalytic activity of In_2O_3 NPs is attributed to inactivation of vibrant sites of In_2O_3 NPs by organic components formed during transesterification. Yet, catalytic activity can be resumed after washing and calcination as mentioned earlier.
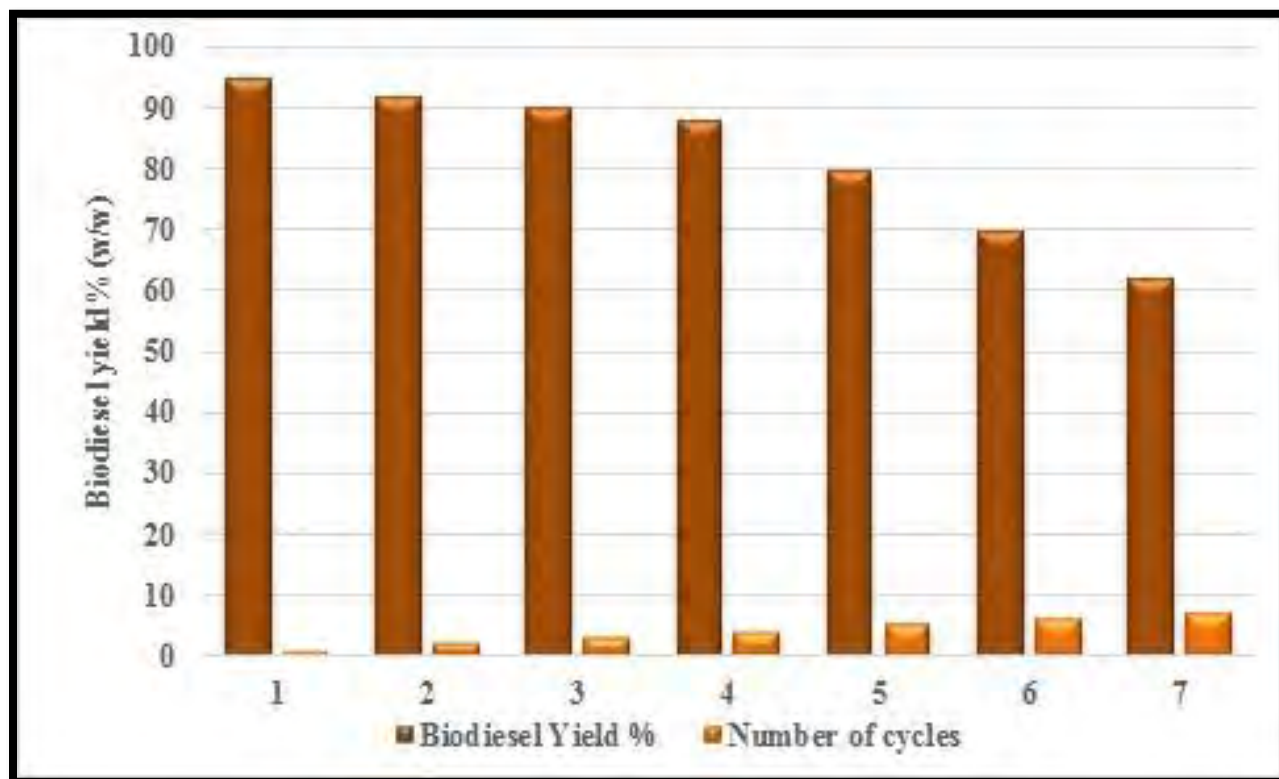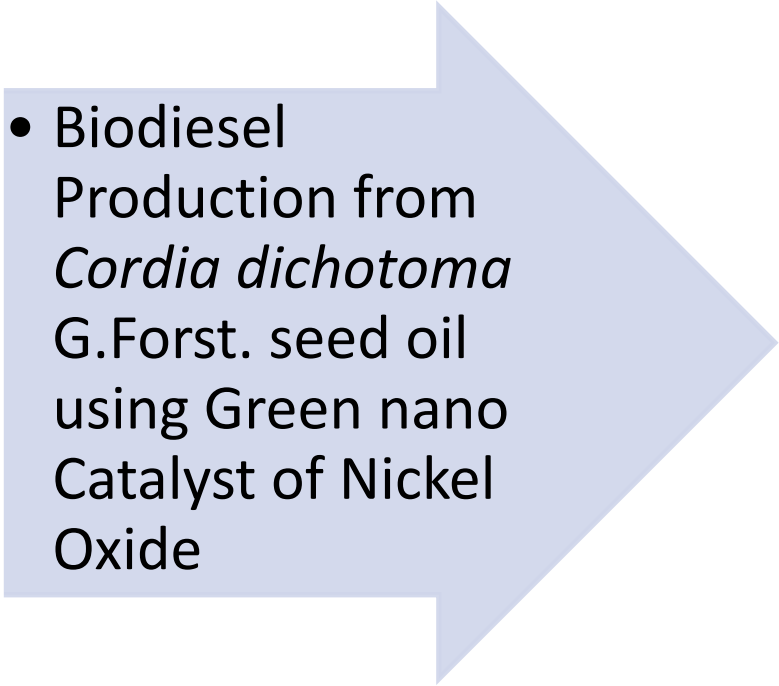
Figure 3.10.11. Reusibility of indium oxide NPs in transesterification reaction

SECTION XI

- Biodiesel Production from *Cordia dichotoma* G.Forst. seed oil using Green nano Catalyst of Nickel Oxide

Nanoparticles of nickel oxide (NiO) have intense significance due to their unique electronic, magnetic and catalytic properties used in the energy, biomedicine, magnetism, and electronics. Nickel oxide NPs have greater chemical stability, and electron transfer capacity being applied in activities such as anti-inflammatory, photocatalytic, and antibacterial. In this study, Nickel oxide NPs were prepared with leaf extract of *Anagallis arvensis* L., which is an eco-friendly and non-hazardous method of preparation.

3.11.1. Characterization of NiO nanoparticles

3.11.1.1 X-Ray Diffraction (XRD) of NiO

Techniques like EDX, XRD and SEM were employed to analyze synthesized nanoparticles of NiO to investigate its crystallographic phase, surface topography, thermal stability, and elemental composition. The Powder X-Ray Diffraction technique was utilized to examine structural and crystalline phase of nickel oxide. XRD pattern of NiO nanoparticles has been depicted in Figure 3.11.1.

XRD pattern of nickel oxide exhibited five distinctive peaks at $2\theta = 37.172\circ$, $43.47\circ$, $63.70\circ$, $74.93\circ$, and $79.87\circ$ corresponding to intensity of (111), (200), (220), (311), (222) *hkl* respectively. The deepest peak was located at 2θ value is $43.47\circ$ (highest peak 200 *hkl*).

The mentioned crystal planes revealed the pure formation of cubic NiO. The average calculated particle size of NiO NPs was about 38.5 nm. The nature and position of diffraction peaks was compared by the JCPDS database (00-001-1239).

3.11.1.2 Scanning Electron Microscopy (SEM) of NiO

Technique of SEM was utilized to explore the surface morphology and topography of NiO nano-catalyst at three different magnifications i.e. X500, X5,000 and X10, 000. SEM images of NiO nano-catalyst are exhibited in Figure 3.11.2. SEM micrographs of NiO NPs explicated spherical morphology. Aggregation of particles can be observed due to their electrostatic attraction towards each other and high surface energy.

3.11.1.3 Energy Diffraction X-ray (EDX) of NiO

The composition of nickel oxide nanoparticles was explored by EDX technique, and the resultant spectrum has been demonstrated in Figure 3.11.3. Absence of additional element EDX spectrum of NiO NPs revealed the purity of synthesized nanoparticles. In EDX spectrum, peak at 0.5 KeV is connected to oxygen binding energy whereas peak at 1.02 KeV and 8.6 KeV is linked with binding energy of nickel. The percentage (%) value of Ni and oxygen was 73.26% and 26.84% respectively.

3.11.1.4 Fourier Transform Infrared Spectroscopy (FTIR)

FTIR spectroscopy was performed to understand function groups pertaining to the synthesized nanoparticles. FTIR spectrum of nickel oxide NPs has been displayed in Figure 3.11.4. Broad peak at 3219.53 cm^{-1} was attributed to absorbed water on the surface of NiO nanoparticles. Bending vibration of H-OH was spotted on 1646.02 cm^{-1}. Oxides of metals generally give transition band below 1000 cm^{-1} which arise from interatomic vibrations. A deep peak appeared at 981.99 cm^{-1} in IR-spectrum showing Ni-O bonds which provided strong evidence of the existence of NiO.

3.11.1.5 Thermogravimetric analysis (TGA) of NiO

Thermogravimetric analysis of NiO nanoparticles was performed to find out thermal stability and decomposition process from ambient temperature to 1000 ◦C. Thermogram of NiO and its subsequent derivative curve (wt. %) has been presented in Figure 3.11.5 a and b respectively. At initial step, the precursor weight loss of 1.58% was observed from 200 to 300 ◦C which is related to dehydration of NiO NPs and removal of physically adsorbed water. A loss of 4.13% has occurred in next phase of decomposition which is contributed to thermal decomposition of NiO precursor at temperature range 300-360 ◦C. Third peak of weight loss was located between 380-660 ◦C associated with weight loss of 1.41%. Above mentioned TGA results have revealed High thermal stability of NiO nanoparticles.
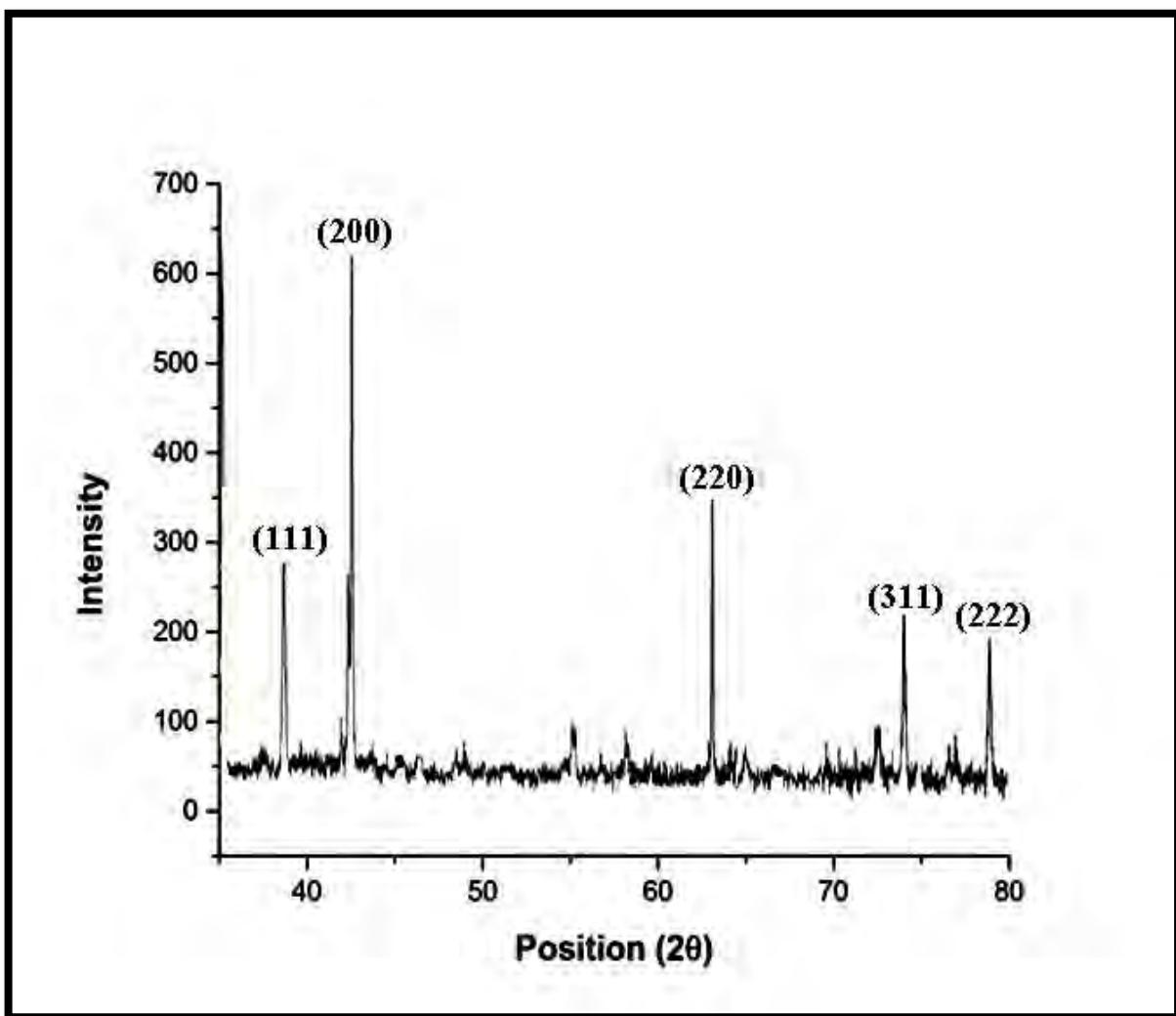
Figure 3.11.1 XRD pattern of calcined nickel oxide green nano particles
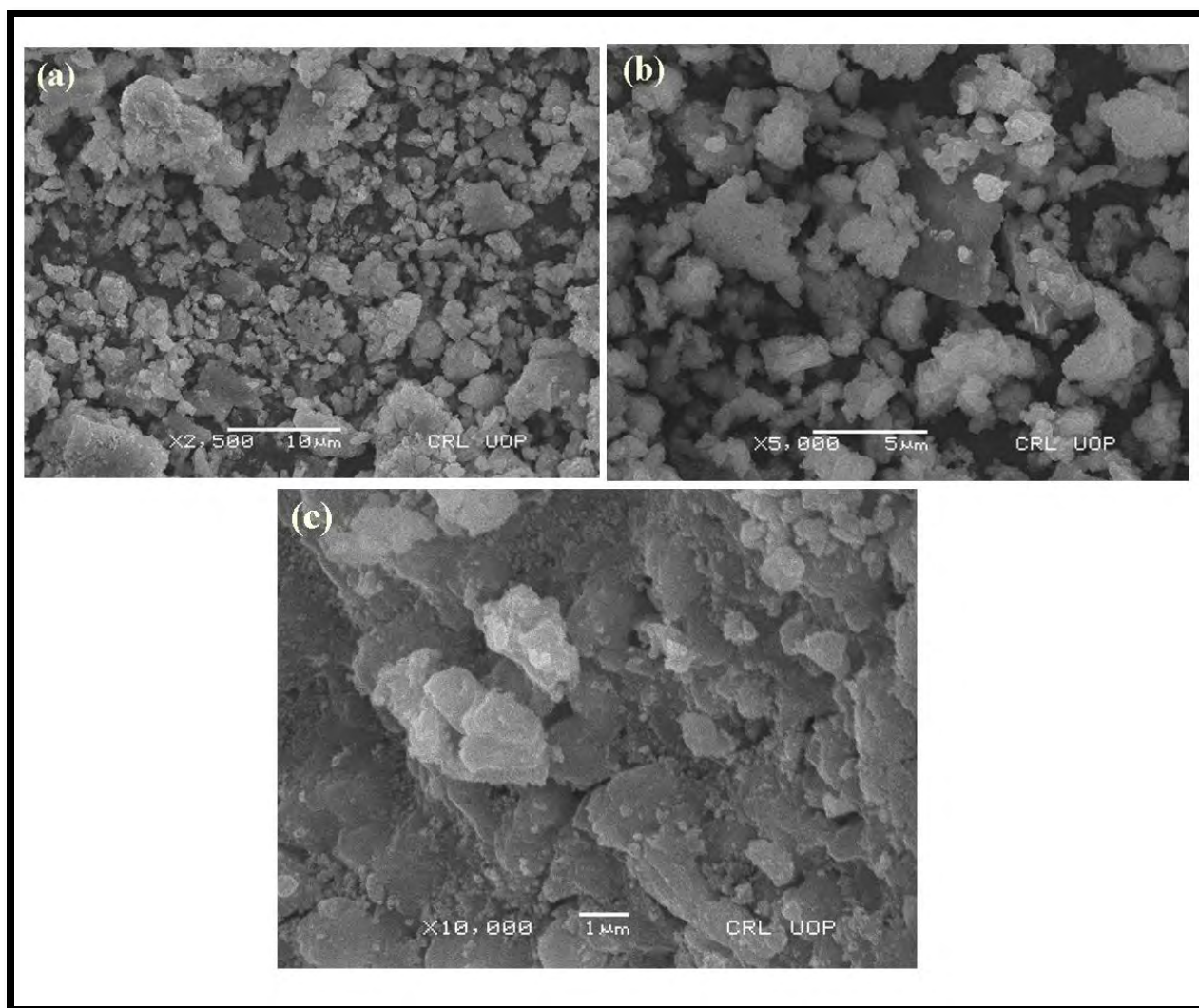
Figure 3.11.2 Scanning electron microscopy (SEM) of calcined nickel oxide green nano particles
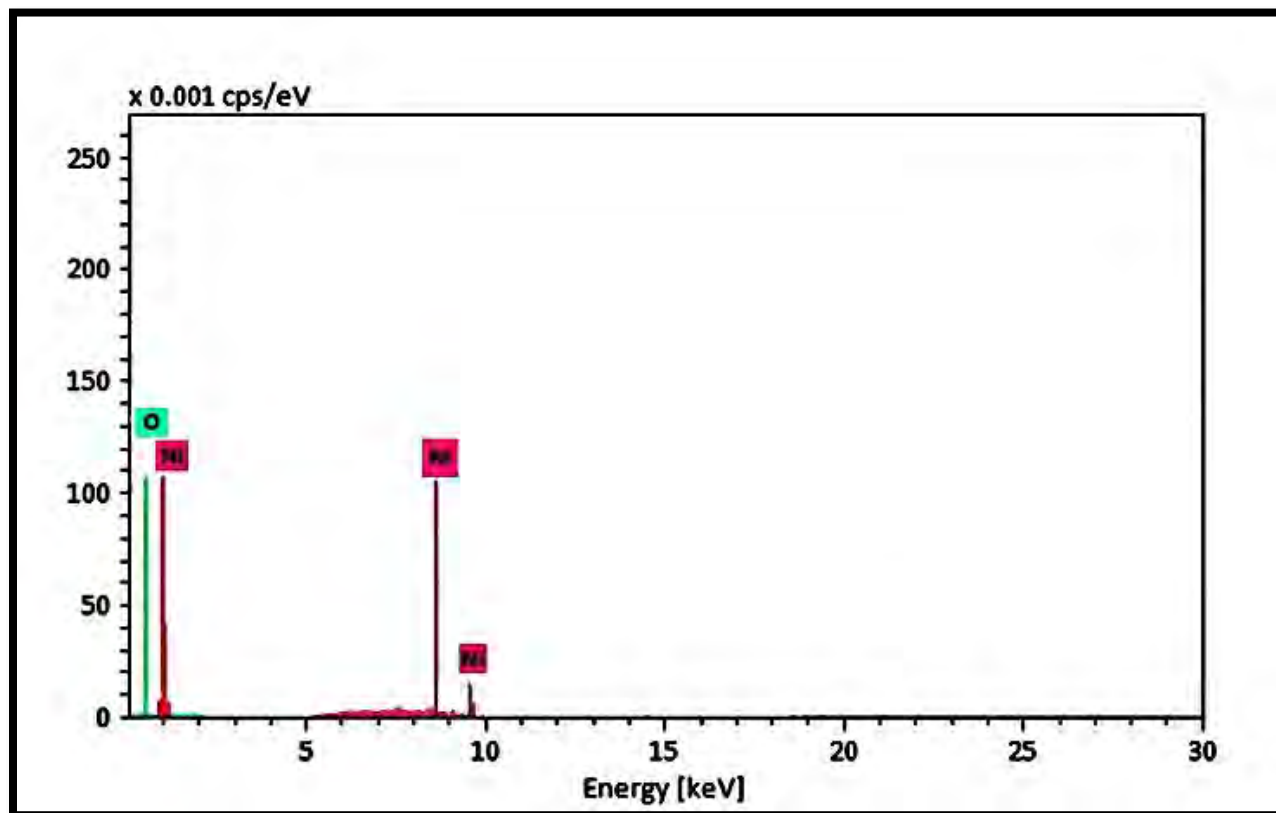
Figure 3.11.3 Energy diffraction X-Ray (EDX) of calcined nickel oxide green nano particles
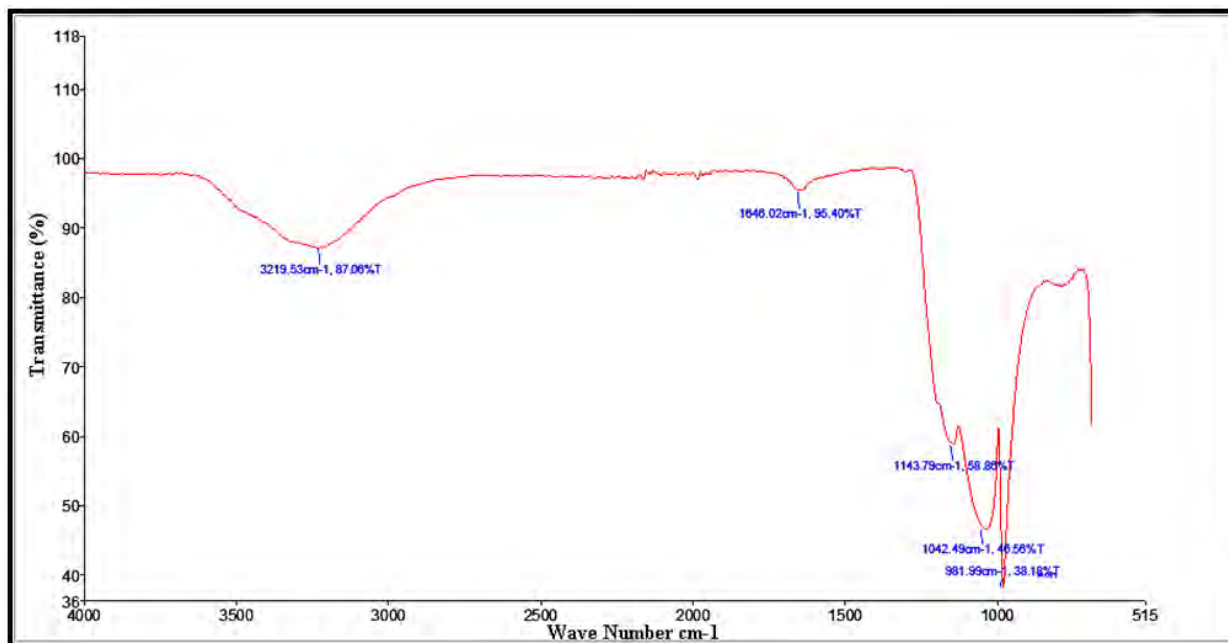
Figure 3.11.4 FTIR spectrum of nickel oxide green nano particles
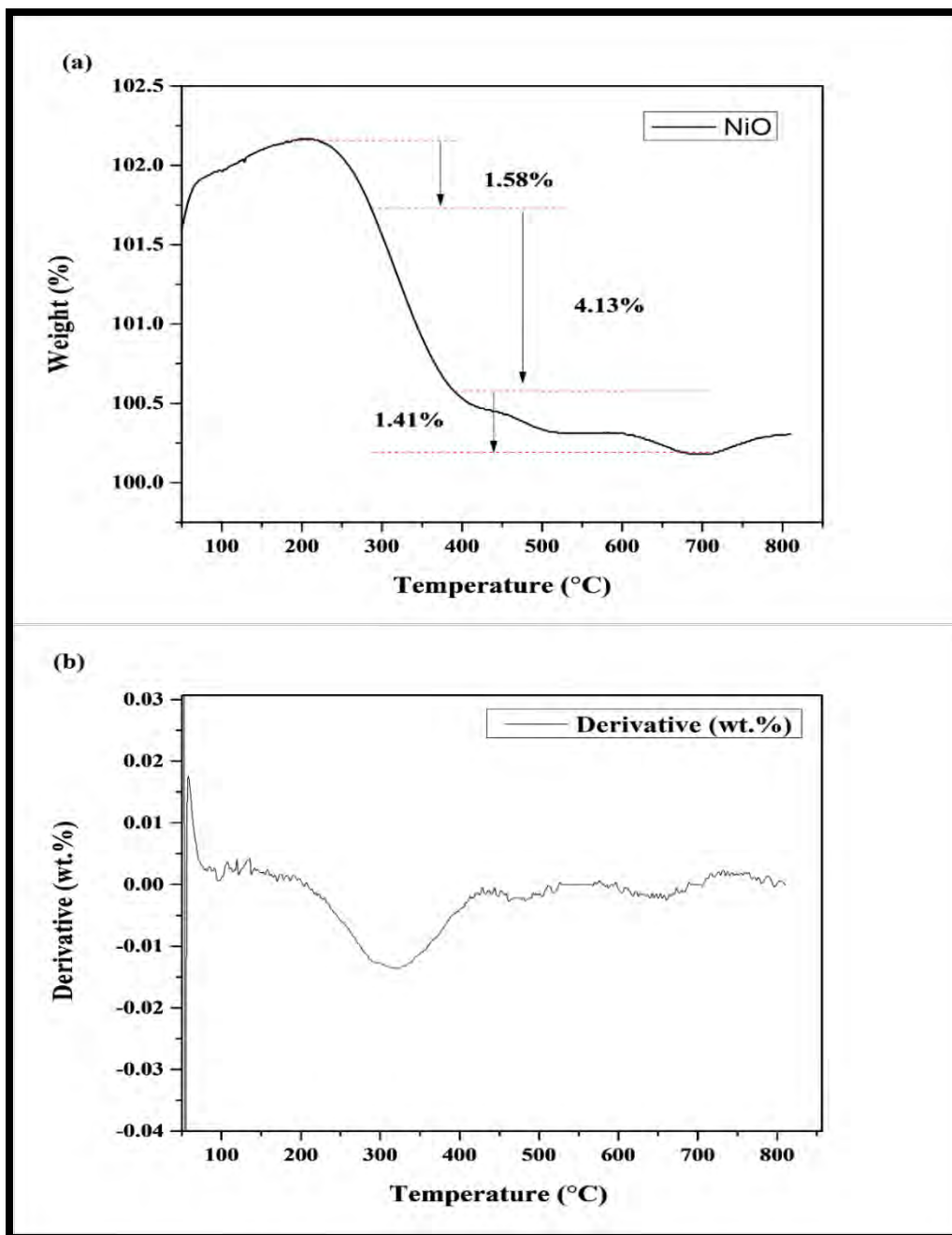
Figure 3.11.5 (a) TGA of nickel oxide green nano particles (b) derivative thermogram of nickel oxide nano particles

3.11.2 Biodiesel synthesis *via* transesterification

Cordia dichotoma belongs to family Boraginaceae. It is a novel and nonedible seed oil feedstock, efficiently used in transesterification. Maximum seed oil content of 35%. (w/w) was determined with FFA concentration of 0.41 mg KOH/g recommending one step reaction of transesterification. The highest FAME yield of 94% was achieved during transesterification using seed oil of *Cordia dichotoma* and of NiO NPs as catalyst.

Impact of reaction conditions on transesterification have been studied to explore optimum values which give maximum yield of biodiesel. For this purpose, thirty experimental trials were performed using Central Composite Design (CCD). These variables of transesterification had the lowest and highest value including Met:Oil 2:1-10:1 (A), catalyst load of 0.16-0.98 wt.% (B) reaction time 50-180 min (C) and temperature 55-100 ºC (D) as shown in Table 3.11.1. Experimental results of thirty different trials have been shown in Table 3.11.2. Figure 3.11.6 displayed a good correlation among predicted *vs.* actual yield of biodiesel having values distributed nearby the straight line. ANOVA of experimental model has been carried out and obtained results are displayed in Table 3.11.3. The significance of experimental model and independent variables was assessed by F and *p*-value. A minimum *p*-value of 0.0003 (<0.05). has confirmed the Quadric experimental model as significant with Lack of fit F-value of 1.19. Quadratic terms with most significant values were Temperature (*p*-value 0.0119) followed by Met:Oil (A^2) with *p*-value of 0.0171 (<0.05). Model reliability and accuracy of was evaluated by predicted R² value which was 0.735 which was quite closer to adjusted R² value of 0.879 with a variance <0.2. Experimental model had Adequate precision is 7.25. Value greater than 4 is recommended prompting efficient predicted yield of biodiesel. The following polynomial Eq. 6 was used in the model.

Yield of Methyl ester (wt. %) = +78.45+5.50 *A-4.44 *B+2.33 *C+1.72 *D-1.62 *AB+1.50 *AC+2.38 *AD+1.00 *BC+1.63 *BD-0.2500 *CD-6.56 *A²+4.94 *B²+0.9386 *C²-14.56 *D² (18)
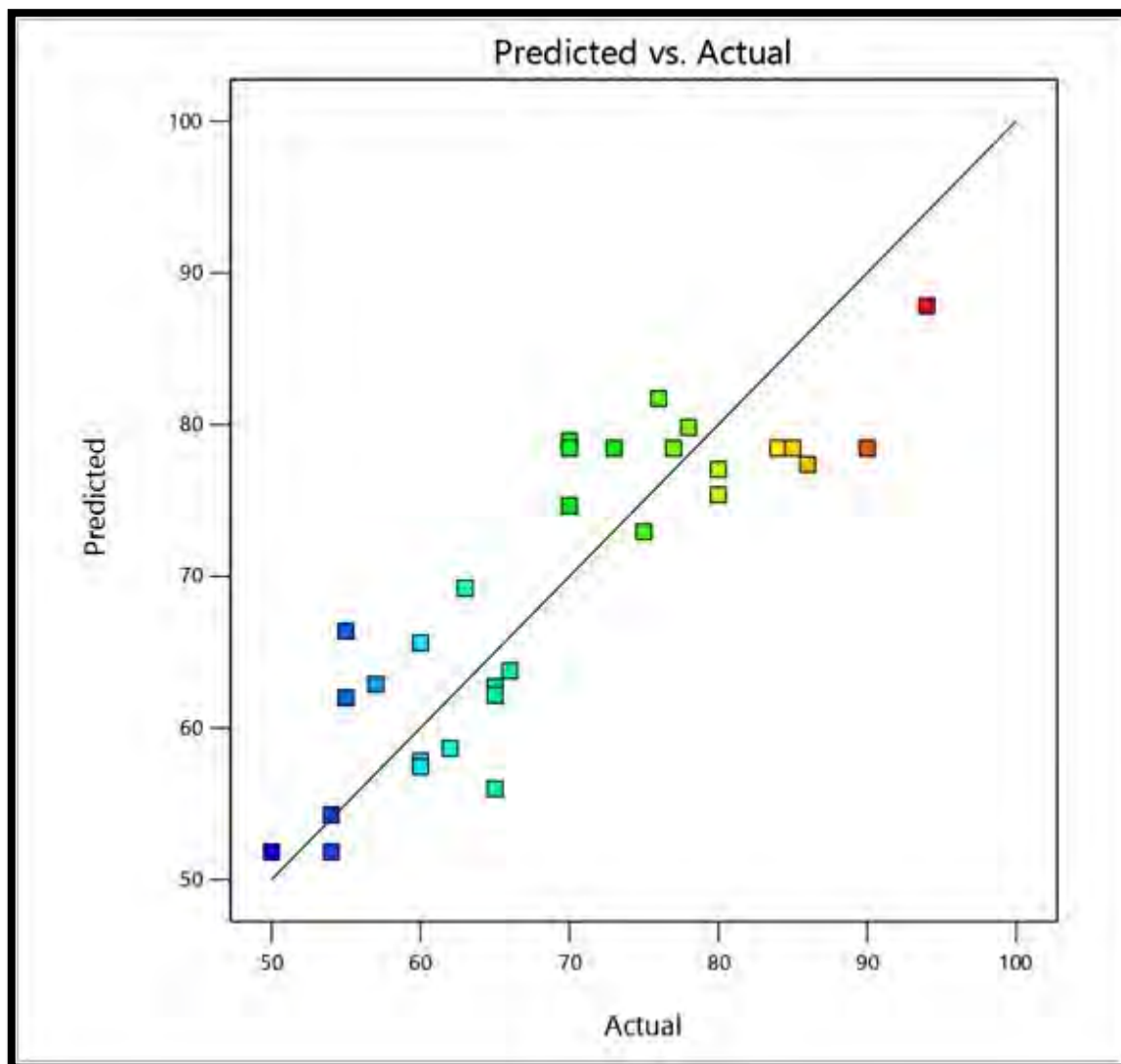
Figure 3.11.6 Comparison between the experimental biodiesel yield and the predicted yield of the model

Table 3.11.1- Experimental design by central composite design for transesterification reaction

Process parameters	−1	+1
Methanol to oil ratio	2:1	10:1
Catalyst loading (wt. %)	0.16	0. 98
Reaction time (min)	50	180
Temperature (∘C)	55	100

Table 3.11.2- Detailed experimental result for transesterification reaction of *Cordia dichotoma* G.Forst. biodiesel

	Factor 1	Factor 2	Factor 3	Factor 4	Response
Run	A: Alcohol to oil molar ratio	B: Catalyst loading wt.%	C: Reaction time Min	D: Temperature ∘C	Yield wt.%
1	7:1	0.16	50	55	63
2	7:1	0.16	50	80	65
3	12:1	0.98	115	80	55
4	7:1	0.98	115	55	65
5	7:1	0.16	115	100	65
6	7:1	0.16	115	100	57
7	12:1	0.16	115	80	80
8	2:1	0.98	50	55	50
9	12:1	0.98	50	55	54
10	7:1	0.16	50	80	80
11	2:1	0.57	115	80	65
12	12:1	0.16	115	100	70
13	7:1	0.57	180	80	76
14	7:1	0.57	115	80	84

15	7.1	0.57	115	80	73
16	7:1	0.98	115	80	70
17	7:1	0.16	115	100	77
18	7:1	0.16	115	80	94
19	7.1	0.57	115	80	90
20	12:1	0.16	180	80	85
21	12.1	0.57	115	80	86
22	7:1	0.57	115	100	60
23	12.1	0.16	180	100	78
24	2:1	0.16	50	80	54
25	12.1	0.16	50	100	70
26	2:1	0.16	180	80	60
27	12.1	0.98	50	100	66
28	7:1	0.16	50	55	62
29	7:1	0.98	180	80	60
30	12.1	0.98	180	100	75

Table 3.11.3- ANOVA for Response Surface Quadratic model

Source	Sum of Squares	df	Mean Square	F Value	p-value	
Model	3048.54	14	217.75	3.24	0.0003	**Significant**
A-Alcohol to oil ratio	544.50	1	544.50	8.10	0.0122	
B-Catalyst loading	355.56	1	355.56	5.29	0.0362	
C-Reaction time	98.00	1	98.00	1.46	0.0458	
D-Temperature	53.39	1	53.39	0.7947	0.0568	
AB	42.25	1	42.25	0.6289	0.0401	
AC	36.00	1	36.00	0.5358	0.0354	
AD	90.25	1	90.25	1.34	0.0246	
BC	16.00	1	16.00	0.2382	0.0325	
BD	42.25	1	42.25	0.6289	0.0401	
CD	1.0000	1	1.0000	0.0149	0.0305	
A²	111.54	1	111.54	1.66	0.0171	
B²	63.19	1	63.19	0.9406	0.0475	
C²	2.28	1	2.28	0.0340	0.0562	
D²	549.36	1	549.36	8.18	0.0119	
Residual	1007.76	15	67.18			
Lack of Fit	708.93	10	70.89	1.19	0.4510	**not significant**
Pure Error	298.83	5	59.77			
Cor Total	4056.30	29				

$R^2 = 0.879$, Std. Dev. = 6.20,   C.V. % = 11.94, Adeq Precision = 7.25

3.11.3 Influence of Reaction variables on Transesterification

3.11.3.1 Combined influence of methanol to oil molar ratio and catalyst loading

The interaction of Met:Oil and catalyst concentration have grave impact on transesterification reaction which has been presented in Figure 3.11.7a in the form of 3-D plot. Met:Oil of 7:1 and catalyst loading of 0.16 (wt. %) ensued in highest yield of 94% of biodiesel at reaction time 115 min and temperature of 80 °C (Run 18 Table 2). Higher Met:Oil of 12:1 and catalyst concentration of 0.16 (wt. %) rendered yield to 80% (Run 7). Decrease in Met:Oil up to 2:1 and increase in catalyst concentration up to 0.57 (wt. %) at Run 11 has dramatically rendered biodiesel yield to 65%. Further increase in catalyst loading to 0.98 (wt. %) with highest Met:Oil of 12:1 resulted in lowest yield of 55% at Run 3. It is envisioned that excess amount of methanol beyond the optimum value causes lowering of catalyst concentration therefore, encouraging glycerolysis in the reaction mixture. Glycerolysis allows the recombination of FAMEs and glycerol producing monoglycerides (Ayoub et al., 2021). Higher catalyst amount of 0.98 (wt. %) with Met:Oil of 12:1 gave minimum yield of 70% at Run 16. Significant interaction of Met:Oil and catalyst concentration with *p*-value of 0.0401 (<0.05) was obtained in ANOVA.

3.11.3.2 Combined influence of methanol to oil ratio and reaction time

Mutual interaction of Met:Oil and reaction time plays a key role in determining biodiesel yield as elucidated in Figure 3.11.7b. Effect of Met:Oil and time was studied at constant temperature (80 °C) and catalyst loading (0.16 wt. %). Maximum yield (94%) of methyl ester was achieved at Met:Oil of 7:1 and time of 115 min. FAME yield was marginally lowered to 85% at reaction time 180 (min) with Met:Oil 12:1 (Run 20). Alcohol used in excess amount creates problems like difficulty in biodiesel purification due to greater solubility of glycerol (Thangarasu et al., 2020). A further drop in yield up to 54% was observed at Met:Oil 2:1 and time 50 (min) (Run 24). It is attributed to insufficient time and amount of methanol required for proper mixing of reactants, hence, resulted in partial conversion and minimum yield of methyl ester (Hammouda et al., 2017). Reduced yield of 60% was acquired with lowest Met:Oil of 2:1 and maximum reaction time 180 (min) (Run 26). This relationship in our current investigation has significant value in ANOVA results with *p*-value of 0.0354 lesser than 0.05.

3.11.3.2 Combined influence of methanol to oil ratio and reaction time

Interaction of Met:Oil and reaction temperature on FAME yield has been displayed in Figure 3.11.7c. Extreme yield of 94% was attained at Met:Oil of 7:1 and temperature of 80 °C (Run 18). This intensification in methyl ester yield may be attributed to the sufficient amount of methanol which recharged catalytic activity forming methoxy species to shift transesterification reaction in the forward direction (Ayetor et al., 2015). High reaction temperature of 100 °C with same optimum Met:Oil (7:1) reduced yield up to 77% at Run 17 (Table 2). Experimental work revealed that the rate of reaction is under great influence of temperature fluctuation. In this study, optimum temperature of transesterification was found to be 80 ℃. It refers to a temperature at which activation energy is lowered and the interaction between catalyst and reactants is enhanced leading to maximum conversion of reacting compounds into useful products. Both higher molar ratio of 12:1 and temperature 100 °C further reduced methyl ester yield to 70% in Run 12. ANOVA results have confirmed this correlation as significant with *p*-value 0.0246.

3.11.3.4 Combined influence of time and catalyst loading

The impact of time and catalyst concentration on synthesis of methyl ester in frame of 3D-plot has been demonstrated in Figure 3.11.7d. The highest productivity of transesterification was found to be 94% achieved at time 115 min and catalyst amount of 0.16 (wt. %) at constant oil Met:Oil (7:1) and temperature (80 °C) (Run 18). Approximately 84% yield of biodiesel was calculated at nano catalyst concentration of 0.57 (wt. %) with same time (115 min) at Run 14. Further increase in catalyst concentration up to 0.98 (wt. %) and time 180 min lowered yield to 60% (Run 29). A yield of 65% was obtained with lowest reaction time of 50 min and catalyst concentration of 0.16 (wt. %) due to partial conversion of triglycerides into biodiesel (Run 2). It was concluded from this investigation that collective effect of catalyst concentration and time has considerable influence on transesterification reaction. A significant relationship between catalyst concentration and time was observed in ANOVA results with *p*-value of 0.0325.

3.11.3.5 Combined influence of catalyst loading and reaction temperature

The effect of the cumulative relationship of catalyst concentration and temperature at constant time (115 min) and oil Met:Oil, ratio of 7:1 during transesterification have been

illustrated in Figure 3.11.7e. Maximum yield of 94% was calculated with catalyst amount of 0.16 (wt. %) and temperature (80 °C) at Run 18. It is ascribed to maximum interface of triglycerides with methanol at these reaction parameters (Bai et al., 2021). About 62% FAME yield was calculated for Run 26 with catalyst loading of 0.16 (wt. %) and temperature of 55 °C. Both high temperature of 100 °C and catalyst loading of 0.57 (wt. %) resulted in reduced yield of 60% for Run 22. Approximately, 57% FAME yield was calculated with temperature 100 °C and optimum value (0.18 wt. %) of catalyst loading (Run 6). It is due to the low boiling point of methanol which has slow the rate of the forward reaction of transesterification. However, further addition in catalyst concentration beyond optimum value lessened biodiesel yield. It is because of surge in viscosity of reactants and low catalytic activity due to depressed interaction between catalyst and reaction medium (Foroutan et al., 2022). The lowest yield of 65% was obtained at maximum NiO loading of 0.98 wt. % and temperature of 55 °C (Run 4). Results of ANOVA have revealed the combined influence as significant with *p*-value 0.0401.

3.11.3.6 Combined influence of time and temperature

The combined impact of time and temperature on biodiesel production was studied at constant catalyst loading (0.16 wt. %) and Met:Oil 7:1 which has been displayed in Figure 3.11.7f. The chemical equilibrium of transesterification needed sufficient time for proper interaction with catalyst. After 115 min, reaction in the forward direction was proceeded and equilibrium was achieved, resulting in maximum yield of 94 % at Run 18 with time 115 min and temperature of 80 °C at fix Met:Oil (7:1) and catalyst loading (0.16 wt. %). About 80% yield of biodiesel was obtained with a minimum time of 50 min and temperature of 80 °C at Run 10. Methyl ester production was further decreased to 65% with time 115 min and high temperature of 100 °C (Run 5). Minimum productivity of 63% was calculated at time 50 min and temperature of 55 °C at Run 1. It has been noticed that increase in methyl ester yield occur with increase in reaction temperature only up to certain limit beyond which a significant drop results. It is ascribed to the endothermic nature of transesterification reaction (Doudin et al., 2021). A significant correlation between time and temperature on chemical reaction of transesterification with p-value 0.0305 (<0.05) was concluded from the outcomes of ANOVA.
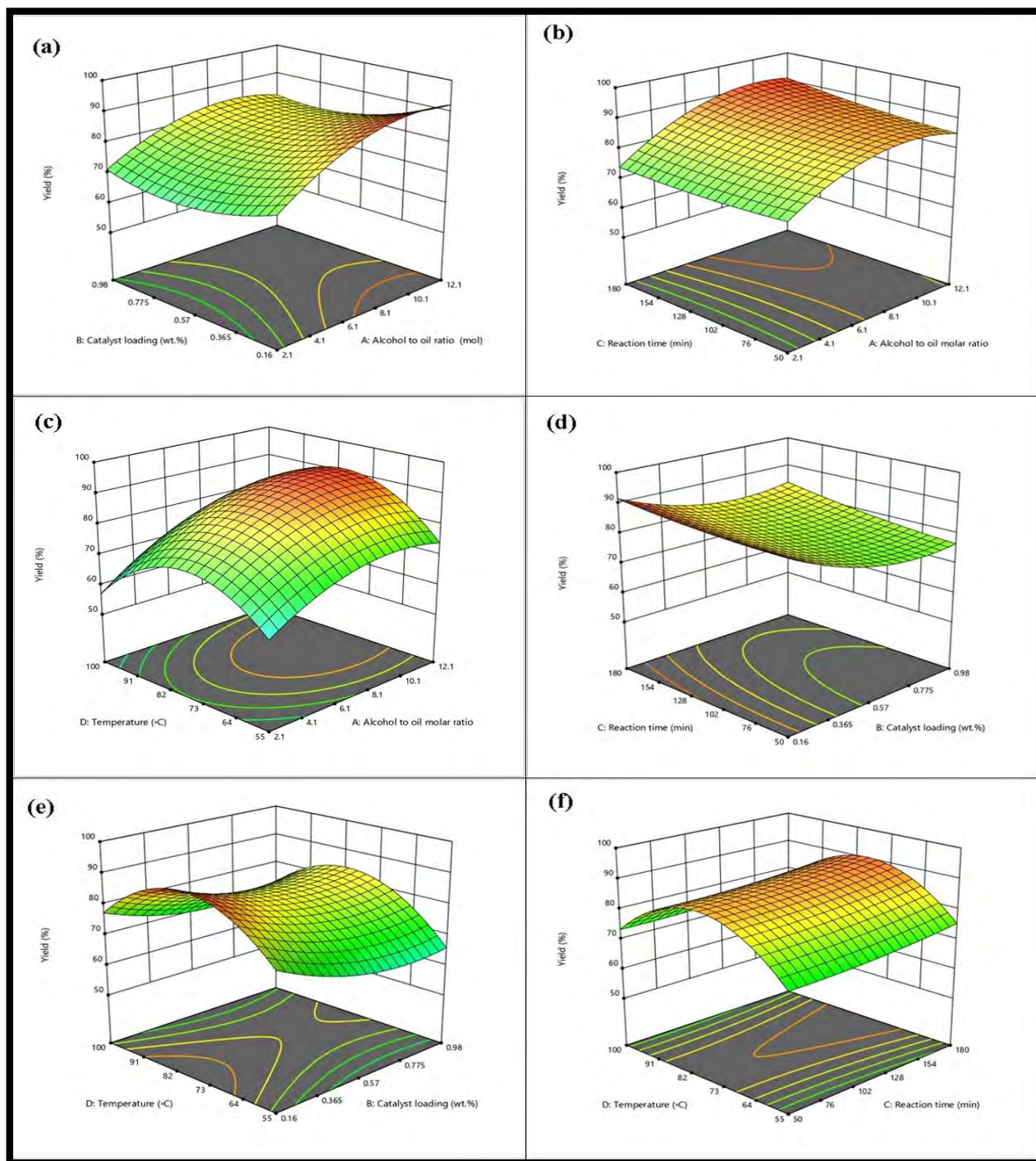
Figure 3.11.7 Influence of the reaction parameters of *Cordia dichotoma* biodiesel.

3.11.4. Characterization of *Cordia dichotoma* Biodiesel

3.11.4.1 FTIR spectroscopic Analysis

Both NMR and FT-IR are widely used in endorsement of FAME formation following to completion of transesterification. FTIR spectroscopic analysis was used to explore structural composition of both *Cordia dichotoma* seed oil and biodiesel. FT-IR spectrum of *Cordia dichotoma* oil and biodiesel have been demonstrated in Figure 3.11.8 a and b respectively. IR spectra described different bands and stretches of functional groups existing in triglycerides and methyl ester. Intense band in the IR the area of 1743.60 cm^{-1} represented carbonyl group (C=O) and stretching band for methyl group (CH$_3$) was detected at 1464.44 cm^{-1} in the spectrum of biodiesel. The presence of carbonyl and methyl group bands in the IR spectrum of CDBD has proved methyl ester production during transesterification. IR region associated with carbonyl group is considered as the most chemically and molecularly changeable part in the biodiesel spectrum (Arumugam and Ponnusami 2019). Characteristic vibration band for CH (sp^2) was located at 2853.25 cm^{-1} stretching band at 1161.32 cm^{-1} was assigned to aliphatic esters (O=C-O-C).

Comparison of the IR spectrum of oil and biodiesel revealed the intensely varying part located 3000-3500 cm^{-1} and 1000-2000 cm^{-1}. Stretch peak at 1097.46 cm^{-1} in the spectrum represented the wagging frequency for C-H$_2$. Intense peak observed at 2925.84 cm^{-1} in spectrum of *Cordia dichotoma* seed oil totally disappeared in the spectrum of biodiesel. Stretching vibration for (O-H) appeared at 1023.03 cm^{-1} in oil spectrum was gone in spectrum of methyl ester. All these analyzed peaks of the spectrum of *Cordia dichotoma* seed oil and biodiesel have substantiated impact on methyl esters formation.

3.11.4.2 NMR Spectroscopic Analysis

NMR spectroscopy is an outstanding technique used in biofuel analysis. It is used to identify and quantify various constituents of synthesized biodiesel after transesterification (alcoholysis). ^{1}HNMR spectrum of *Cordia dichotoma* biodiesel used in this work is presented in Figure 3.11.9a. A characteristic strong ester signal (– OCH$_3$) was spotted at 3.671 ppm which confirmed methyl ester formation in biodiesel sample. Spectrum was found free of undesirable

methanol peak which is commonly spotted at 3.45 ppm indicating purity of synthesized biodiesel. Signal positioned at 0.863-0.907 ppm signified terminal methyl protons whereas, singlet peak for β-methylene (β-CH₂) protons was detected at 1.260-1.309 ppm in the ^{1}HNMR spectrum. The mentioned β-methylene protons corresponded to hydrogen atom situated on carbon-3 of aliphatic chain of hydrocarbon. The triplet peak for α-CH₂ appeared at 2.285-2.335 ppm. The peak detected at 2.758-2.796 ppm signified allylic hydrogen (-CH₂). Single for hydrogen of unsaturated moieties (-CH=CH-) was observed at 5.311-5.410 ppm in the spectrum. The percent amount of FAME in sampled biodiesel was measured to be 92 % in total.

^{13}CNMR spectrum of *Cordia dichotoma* methyl ester has been given in Figure 3.11.9b. ^{13}CNMR spectroscopic analysis is used to examine structural attributes of methyl ester such as the position of C-O and esters carbonyl (-COO-) group. Signal appeared at 51.47 ppm in the ^{13}CNMR spectrum was attributed to methoxy carbon. Characteristic peak for carbonylic carbon (-COOH) was detected at 174.34 ppm. Signal for core non-conjugated carbon atoms appeared at 127.89-128.03 ppm representing degree of unsaturation in the form of double bond between carbon atoms (-CH=CH-) in sample of biodiesel. Moreover, outward carbon of non-conjugated carbons (-CH=CH-) were observed at δ ppm value 129.74-130.03. Characteristic peak for C-O group of methyl ester was spotted at 76.63-77.48 ppm in the spectrum. Peak detected at 29.11-29.78 ppm is ascribed to ethene carbon (-CH₂-)$_n$ with lengthy sequence. At last, peak situated at 31.54-34.10 ppm was considered for carbon of aliphatic-methylene (-CH₂-s). All stated peaks of ^{1}HNMR spectrum of *Cordia dichotoma* biodiesel have ascertained the synthesis of methyl esters.

3.11.4.3. GC/MS Analysis

GC/MS analysis was executed to quantify ester derivatives present in *Cordia dichotoma* biodiesel. Gas chromatogram of CDBD has been displayed in Figure 3.11.10. Identified methyl esters were verified by MS analysis using library match software NO. NIST02. Fatty acid methyl ester composition has substantial impact on fuel related characteristics of biodiesel such as viscosity and cetane number. Four different FAME peaks were observed in gas chromatogram of *Cordia dichotoma* biodiesel.   9-Octadecenoic acid, (2)-methyl-, methyl ester (18:1) was identified as main FAME with maximum concentration detected at retention time of 11.91 min. Dodecanoic acid methyl ester (12:0), and Octadecanoic acid (18:0), methyl ester was found to be

saturated methyl esters. The presence of saturated FAME in synthesized biodiesel sample results in better stability of biodiesel and greater cetane number. Methyl ester with unsaturated nature included 5, 8-Octadecadienoic acid methyl ester (18:2), and 9-Octadecenoic acid, (2)-methyl-, methyl ester (18:1). Saturated fatty acids are believed to be stable than unsaturated one. High concentration of unsaturated fatty acid methyl esters negatively influences biodiesel quality due to their easy oxidation. GC/MS analysis of methyl ester revealed that the oil from *Cordia dichotoma* is a highly fitting feedstock for conversion to biofuel.
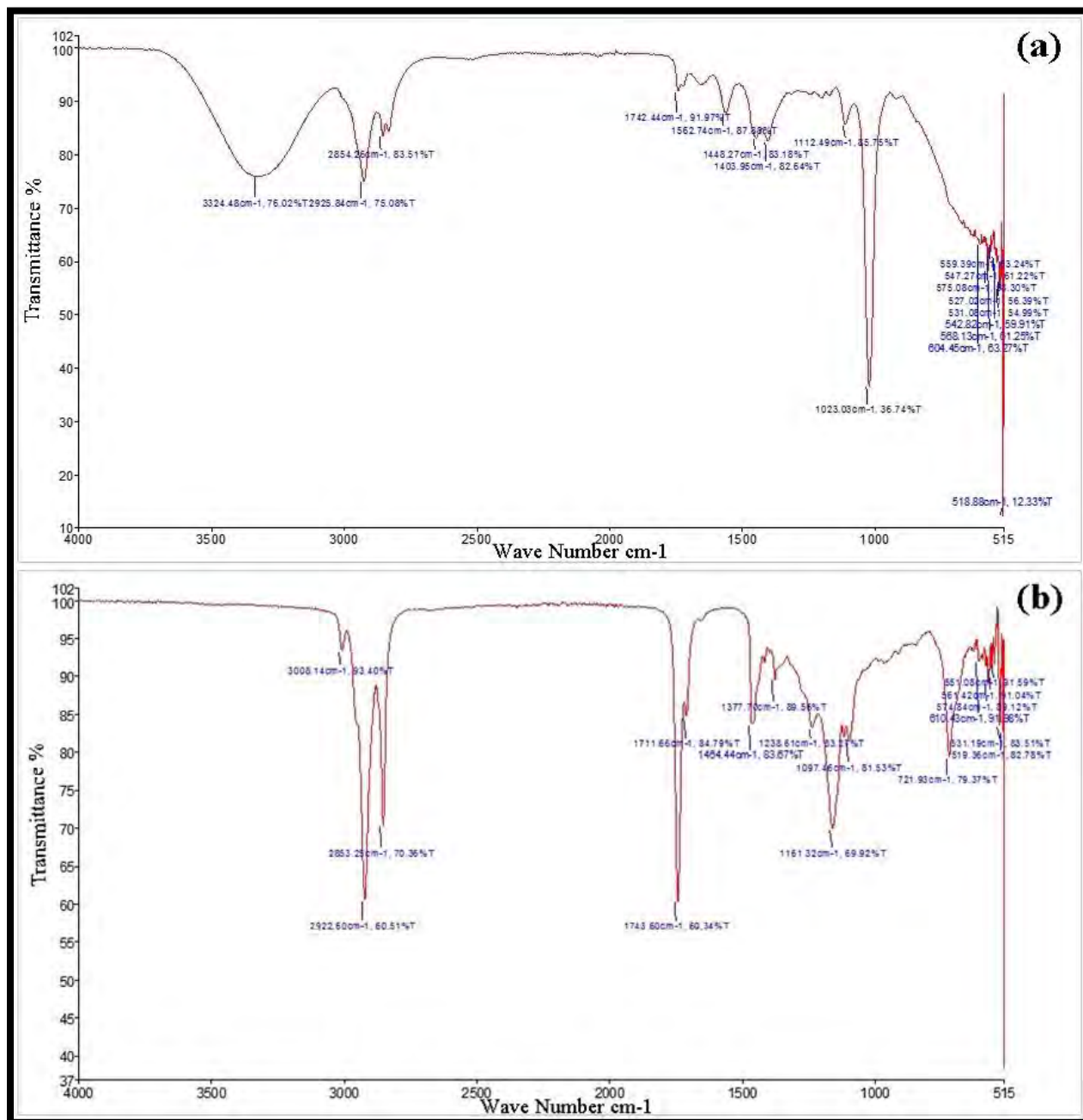
Figure 3.11.8 FTIR spectrum of **(a)** seed oil of *Cordia dichotoma* **(b)** biodiesel
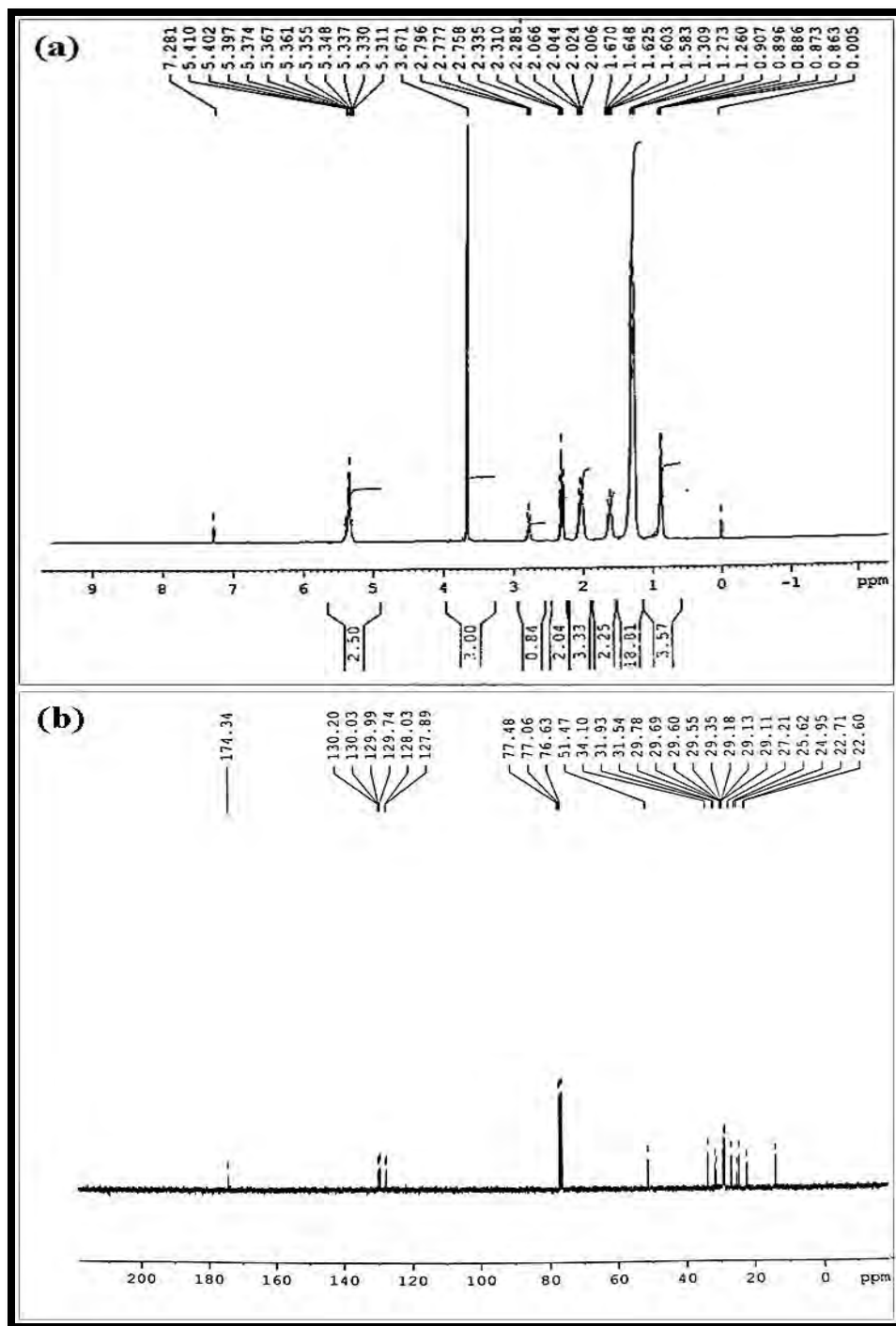
Figure 3.11.9 NMR spectrum **(a)** ^{1}HNMR and **(b)** ^{13}CNMR of *Cordia dichotoma*
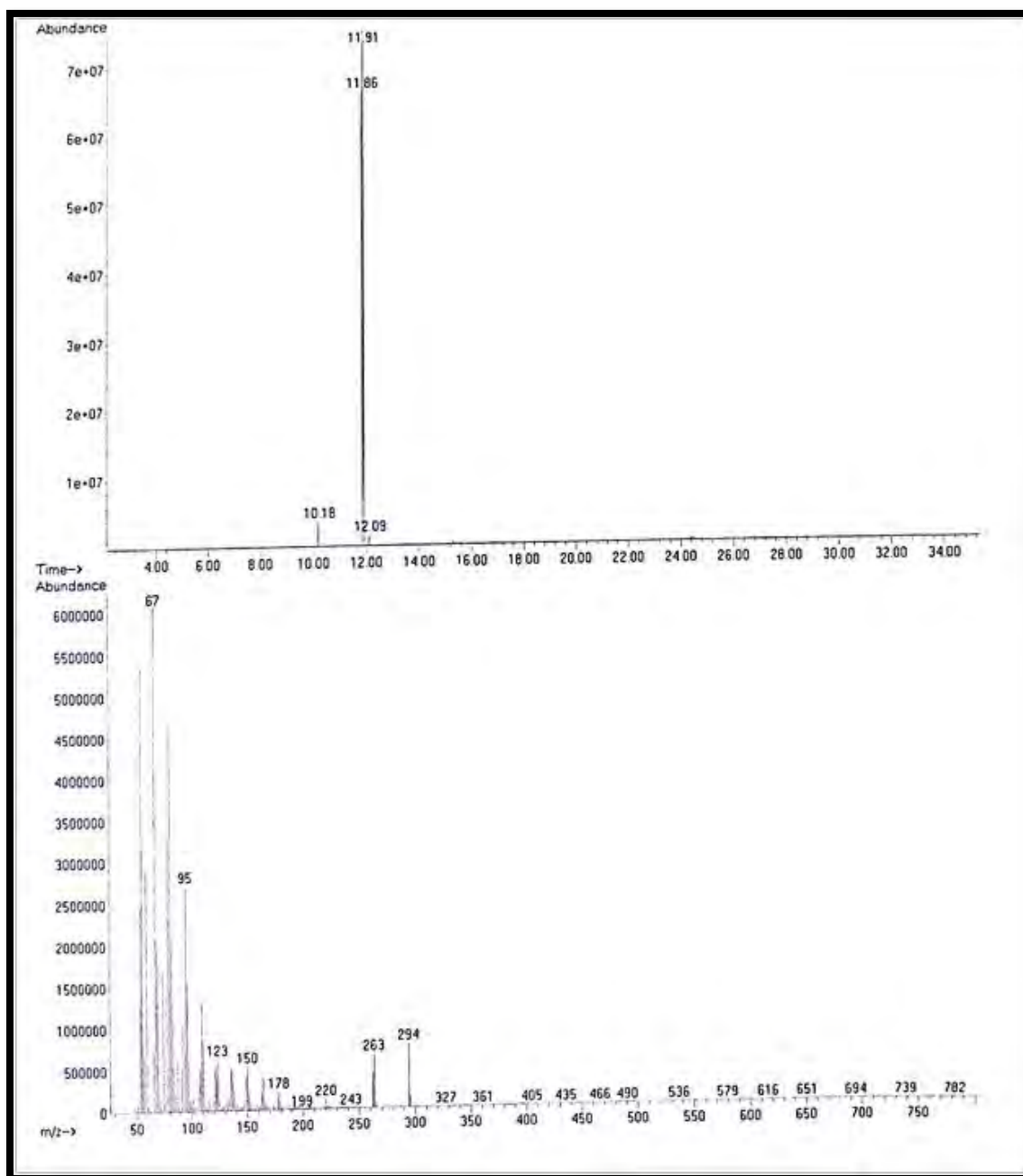
Figure 3.11.10 GC-MS spectrum of *Cordia dichotoma* biodiesel

3.11.5. Determination of Fuel properties of biodiesel

Quality standards of biodiesels are essential for their industrial application as they may affect engine performance and durability (Ameen et al., 2022). Generally, lower, and upper limits are set in all biodiesel standards. Fuel properties of *Cordia dichotoma* methyl ester were found similar to international standards and have been presented in Table 4. Biodiesel has a biodegradable and non-toxic nature. Flash point is the measure of propensity of a sample fuel to form inflammable mixture with oxygen present in air. Flash point of biodiesel is higher than conventional petro-diesel hence, making it easy to manage, store and transport (Alsaiari et al., 2022). Higher flash point of fuel diminishes accidental fire risks and ensures safe storage. Flash point of *Cordia dichotoma* biodiesel was 99 ◦C as appeared in Table 3.11.4.

Kinematic viscosity is one of the basic characteristics of biodiesel playing a dominant role in fuel combustion, emission of exhaust gases like carbon monoxide (Panahi et al., 2019). Fuel with high viscosity creates problems in cold weather as viscosity rises with decreasing atmospheric temperature. It also increases with increase in length of carbon chain in fatty acid methyl ester due to rise in random molecular interaction. Kinematic viscosity of CDBD was 8.24 (mm^2/s) which equivalent to international fuel standard.

Kinematic density has great influence on air to fuel ratio in the engine ignition chamber (El-Kemary et al., 2013). High degree of unsaturation increases density of the fuel. In contrast, higher carbon chain length leads to lower fuel density. Other key fuel properties like cetane number and heating value rely on density. Density depends upon composition of FAMEs and their purity. Kinematic density of CDBD was found to be 0.962 (kg/m³) which is analogous to international fuel standards.

Cold flow attributes of biodiesel (pour point and cloud point) are largely dependent upon type of oil used in transesterification and degree of saturated fatty acid (Zik et al., 2020). High amount of saturated fatty acids renders biodiesel performance at low temperature in cold weathers due to their high melting point resulting in solid crystals formation which in turn restricts flow and causes fuel starvation in diesel engines. The pour point is known as the lowermost temperature at which the movement of the fuel can be detected whereas, cloud point represents the temperature at which cloudiness (floating crystals) is observed in the fuel sample.

Pour point of *Cordia dichotoma* biodiesel was -10 ∘C as shown in Table 3.11.4. Cloud point was measured to be -8 ∘C and compares well with accepted international requirements of fuel.

Acid number signifies the amount of free fatty acids in fuel sample. It is influenced by factors like the type of feedstock used in biodiesel synthesis, production process and level of refinement. Acid number can be increased amid storage as hydrolytic cleavage of methyl ester bonds happens (Dharmaraj et al., 2006). The acid value of *Cordia dichotoma* methyl ester was found to be 0.157 (mg KOH/gm) and lies under set limit of international fuel standards.

Sulphur content of CDBD was 0.0001% (less than 1 ppm) as appeared in Table 3.11.4. Lesser concentration of sulphur diesel fuel enhances engine life and minimizes environmental pollution due to low emission of SO_2. It has been revealed from the discussed results that *Cordia dichotoma* is an adequate feedstock to produce biodiesel which meets the requirements of fuel characteristics.

Table 3.11.4. Comparison of fuel properties of *Cordia dichotoma* biodiesel with international standards**.**

Property	Methods	*Cordia dichotoma*		ASTM D-6751	EN-14214	China GB/T 20828-2007
		Mean	St.Dev.			
Color	Visual	2	-	2.0	-	-
Acid number (mg KOH/g)	ASTM -D974	0.157	0.2	≤0.5	≤0.8	≤0.5
Flash Point (°C)	ASTM -D93	99	1.6	≥93	≥130	≥120
Pour Point (°C)	ASTM -D97	-10	1.1	-15-16	_	_
Viscosity (mm²/s at 40 °C.)	ASTM -D445	5.24	0.2	1.9-6.0	_	3.4-5.0
Density (kg/m³ at 40 °C)	ASTM - D1298	0.962	1.2	≤120	_	≤120
Sulphur content (wt.%)	ASTM - D4294	0.0001	-	≤0.05	≤0.05	≤0.20
Cloud point (°C)	ASTM - D2500	-8	-1	-3.0-12	_	_

3.11.6. Reusability effect of nanoparticles

Reusability of NiO nanoparticles was explored in sequential steps to ascertain its stability and commercial feasibility. For this purpose, it was first separated from reaction mixture via centrifugation after completion of transesterification. Previous literature has revealed that purification and separation method of nanoparticles has significant impact on reusability (Khan et al., 2021). Reusability tests of NiO nanoparticles was performed at optimum reaction parameters of transesterification *i.e.* Met:Oil of 7:1, catalyst load of 0.16 (wt. %), time 115 min and temperature of 80 °C.

After recovery, NiO nanoparticles were rinsed with alcohol, desiccated in oven, and lastly calcined at 500 ◦C for 180 min. Reusability was tested up to 7th consecutive cycles. NiO nanoparticles remained stable until five successive cycles (high FAME yield of 94 to 70%). Methyl ester yield drop up to 67% for the 6th cycle. Further use to 7th cycle resulted in reduced yield to 60% which may be attributed might be attributed to deactivation of dynamic sites of NiO nanoparticles by organic elements present in reactants mixture of transesterification (Figure 3.11.11). However, reusability of NiO nanoparticles can possibly be revived after purification and calcination.
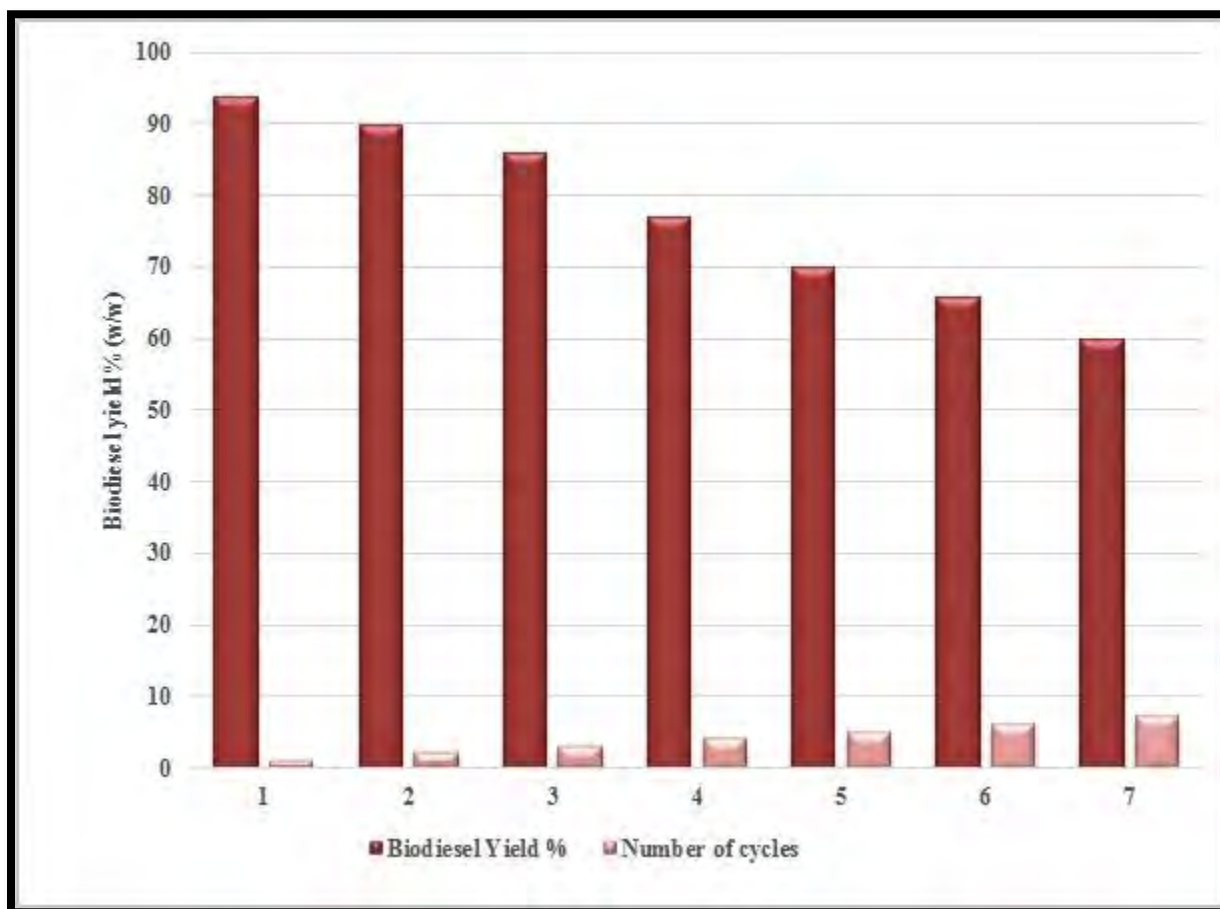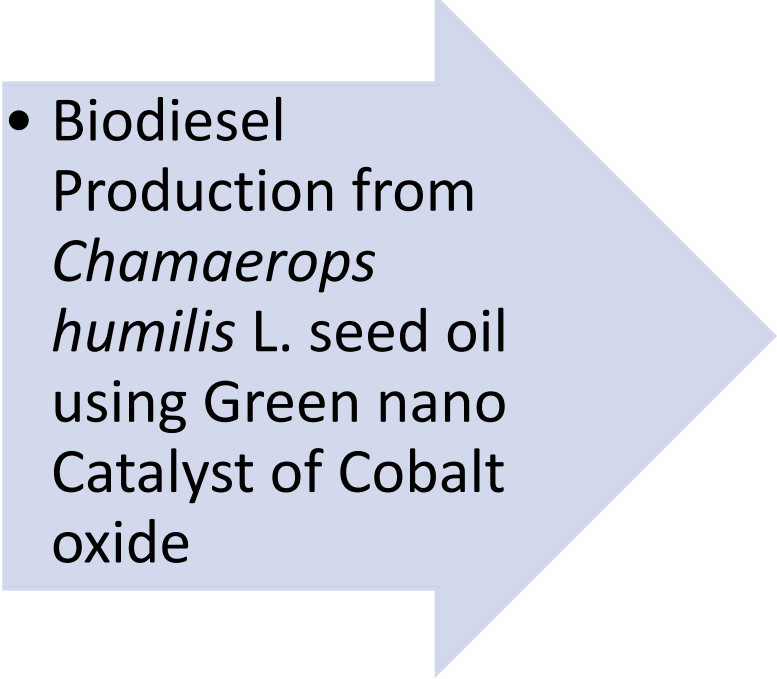
Figure 3.11.11 Reusibility of nickel oxide NPs in transesterification reaction

SECTION XII

- Biodiesel Production from *Chamaerops humilis* L. seed oil using Green nano Catalyst of Cobalt oxide

Cobalt oxide is a metal oxide with a wide range of applications due to its environment-friendly nature, corrosion and oxidation stability and low cost. Cobalt oxide nanoparticles (CoO NPs) are multifaceted with multiple uses in lithium-ion batteries, heterogeneous catalysis, supercapacitor, magnetic semiconductors, and gas-sensors (Chekin et al., 2016). Conventionally, CoO NPs were synthesized by various physical and chemical methods like ion implantation, sol–gel method, sputter deposition, melt-mingling, and laser vaporization having common disadvantage of producing toxic products incongruous for the environment (Jang et al., 2017). Co is a well-known ferromagnetic substance that is widely utilized in permanent magnets as an alloying element Orooji et al., 2022. Co nanoparticles have a variety of size-dependent structural, electrical, magnetic, and catalytic capabilities (Iravani and Varma, 2020). Abbasi et al. (2021) synthesized CoO NPs with *Rhamnus virgata* leaf extract and studied it for antibacterial activity, revealing promising biological potential. According to Bibi et al. (2017), *Punica granatum* could be used to synthesize cobalt-oxide NPs for photo-catalytic applications. However, in our current study, green mediated synthesis of CoO NPs was carried out with *Galium boreale* leaf extract which is eco-friendly and non-hazardous to the environment. CoO NPs are not previously investigated for transesterification of seed oils.

3.12.1 Catalyst characterization

3.12.1.1 X-Ray Diffraction (XRD) of CoO

X-Ray Diffraction technique was castoff to confirm purity and size of crystals of cobalt oxide. XRD diffractogram of cobalt oxide nanoparticles has been illustrated in Figure 3.12.1. Diffracted Energy peaks of XRD diffractogram exhibited pure crystalline nature of CoO nanoparticles with 2θ values at 32.5 º, 35.2 º, 37.05 º, 44.11 º, 60.80 º which corresponds to (220), (311), (400), (422) and (440) respectively. The XRD pattern of deepest peaks at 2θ value of 37.05º (highest peak 400) was used to find out crystalline size of cobalt oxide nanoparticles.

Crystalline size of cobalt oxide nanoparticles was 40 nm revealing the nano nature of synthesized green nanoparticles. XRD results of CoO are aligned with SEM.

3.12.1.2 Scanning Electron Microscopy (SEM) of CoO

SEM micrograph of cobalt oxide nanoparticles has been demonstrated in Figure 3.12.2. Cobalt oxide NPs appeared to cubic in shape with homogenous morphology. The cluster of particles detected in SEM micrograph is ascribed to polar and electro-static pull of nanoparticles towards each other. Our results are in accordance with previous studies (Abbasi et al. 2021).

3.12.1.3 Energy Diffraction X-ray (EDX) of CoO

Energy diffraction X-Ray analysis was used to investigate elemental composition of cobalt oxide nanoparticles. EDX spectrum of CoO has been exhibited in Figure 3.12.3. EDX analysis confirmed the existence of both cobalt at 0.13, 2.1, and 3.75 keV whereas, oxygen at 0.5 keV indicating high purity of synthesized particles. Mass percent of Co and O was 83.10% and 16.90% respectively. Lack of other extraneous peak the EDX spectrum revealed that nanoparticles have no impurities and additional elements.

3.12.1.4 Fourier Transform Infrared Spectroscopy (FTIR)

FTIR spectroscopic analysis of cobalt oxide nanoparticles demonstrated the presence of various functional groups. FTIR spectrum of cobalt oxide nanoparticles have been shown in Figure 3.12.4. FTIR spectrum of CoO nanoparticles represented four major absorption peaks. Besides, the absorption band observed at 551.08 cm^{-1} signifies Co–O stretching vibration mode while peak at 542.45 cm^{-1} was allotted to the relating vibration of O–Co–O bond (Nguyen et al. 2021). Sharp peak at 1377.91 cm^{-1} and 2164.69 cm^{-1} were assigned to O–H stretching of the moisture content.

3.12.1.5 Thermogravimetric analysis (TGA) of CoO

Thermogravimetric analysis (TGA) was used to examine thermal stability of cobalt oxide NPs along with the property of decomposition. Figure 3.12.5a depicts thermogram of CoO and Figure 3.12.5b presents the subsequent derivative curve (wt. %) with their endothermic peaks. Thermal decomposition of cobalt oxide nano catalyst occurred in three successive main phases. Initially, catalyst decay of 0.26% of the total mass happened in at temperature range of 50-170∘C due to desiccation and loss of water from the surface of nanoparticles. Correspondingly, this

process of desiccation continued in the next phase where 0.69% loss in total mass of CoO took place at temperature range of 175-200 ∘C. Away from 200 ∘C, a straight line was observed which persisted till 700 ∘C (Fig. 6). Third phase of disintegration was spotted at temperature range of 800-900 ∘C in which 0.98% loss took place in total mass of CoO. Results of TGA, in our current study has disclosed high thermal stability of CoO.
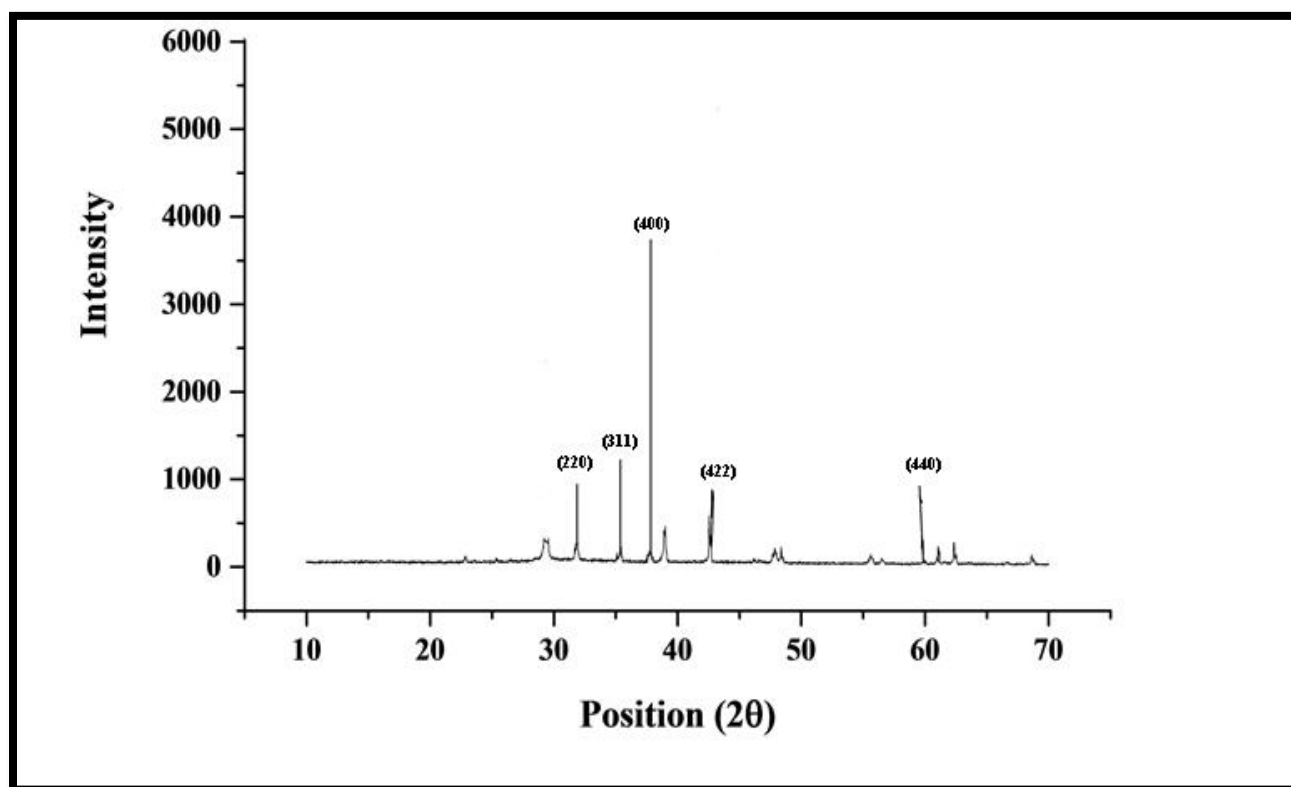
Figure 3.12.1 XRD pattern of calcined Cobalt oxide NPs
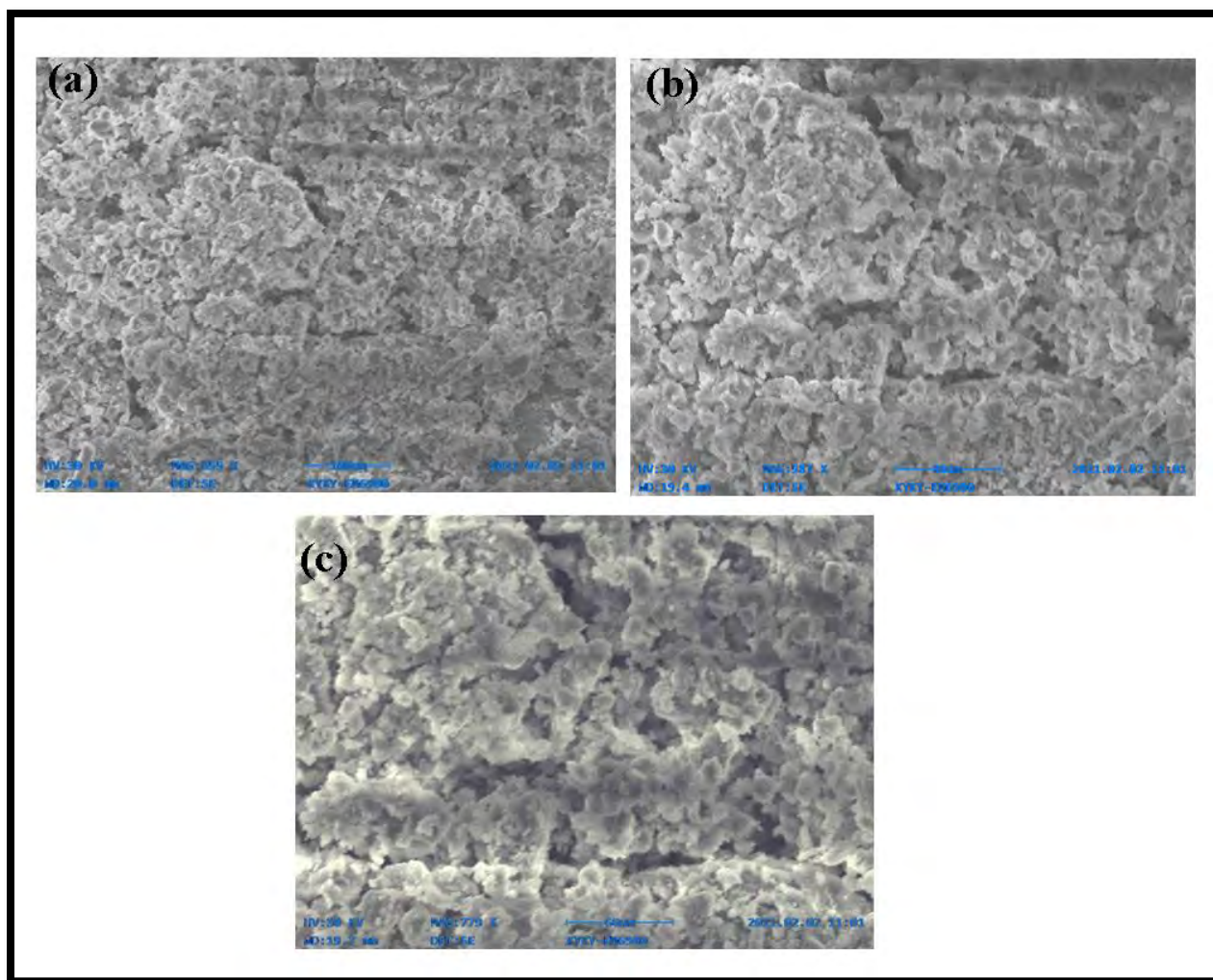
Figure 3.12.2 Scanning electron microscopy (SEM) of Cobalt oxide NPs
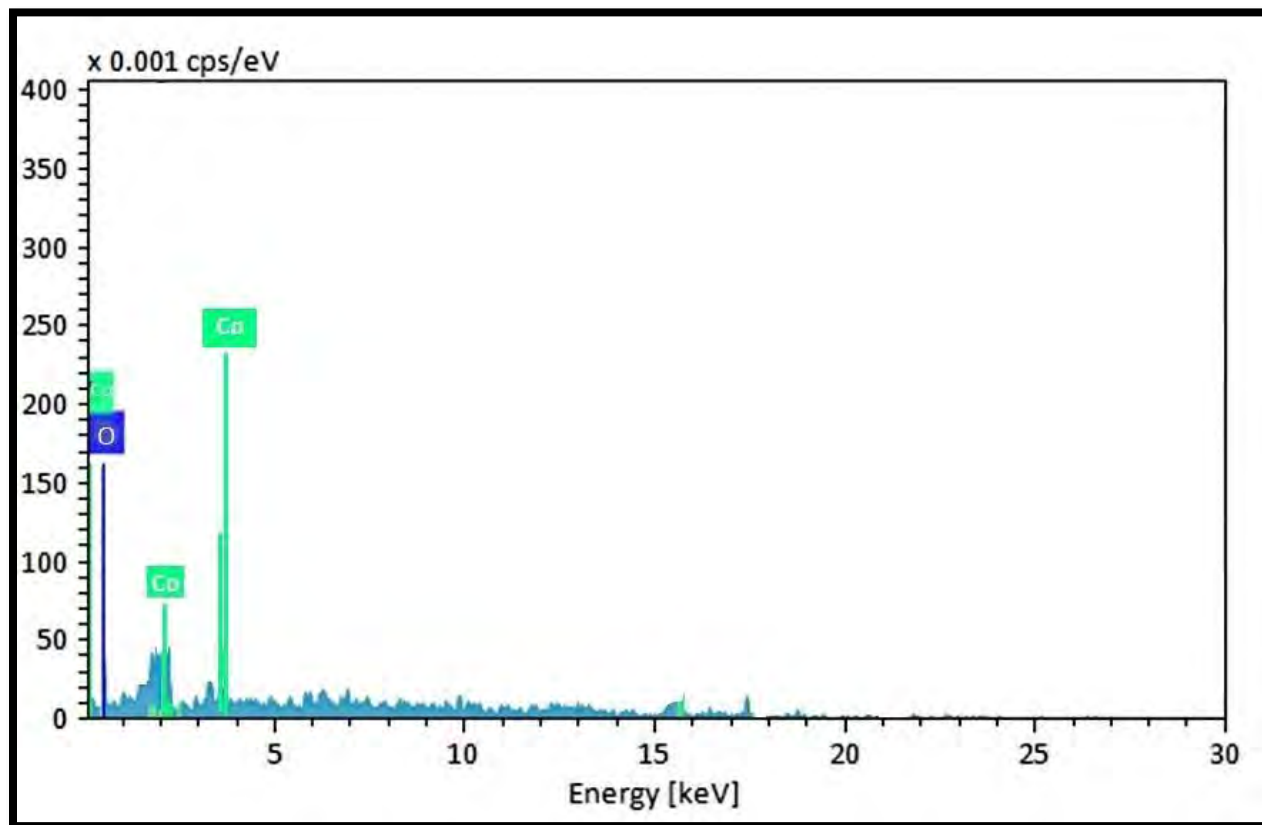
Figure 3.12.3 Energy diffraction X-Ray (EDX) of Cobalt oxide NPs
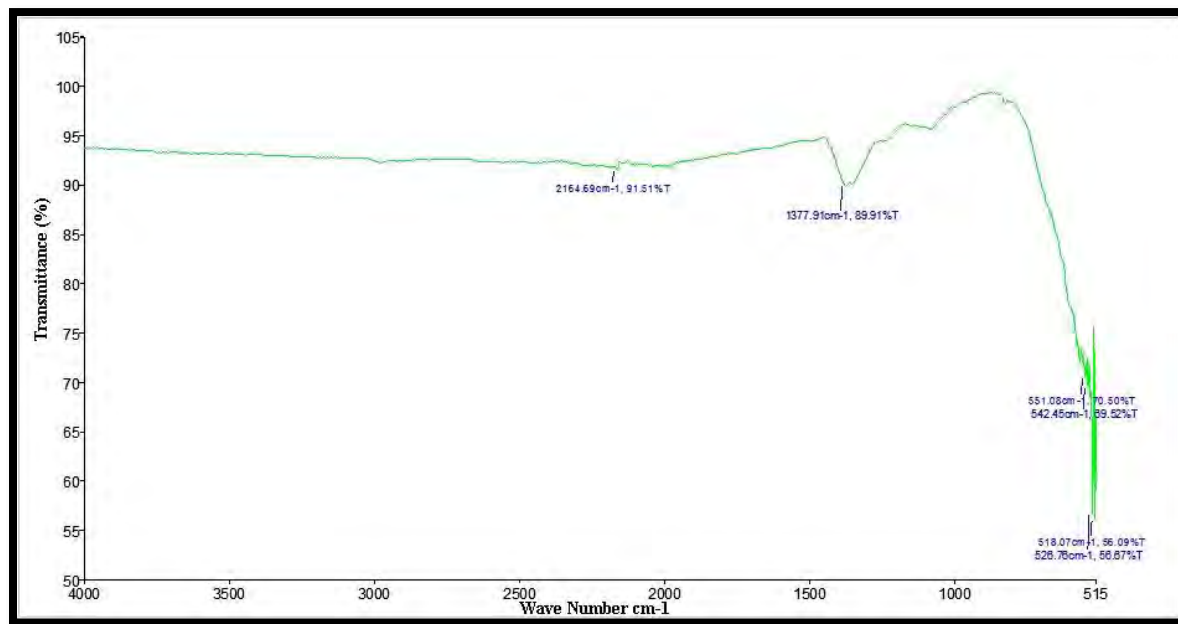
Figure 3.12.4 FTIR spectrum of Cobalt oxide NPs
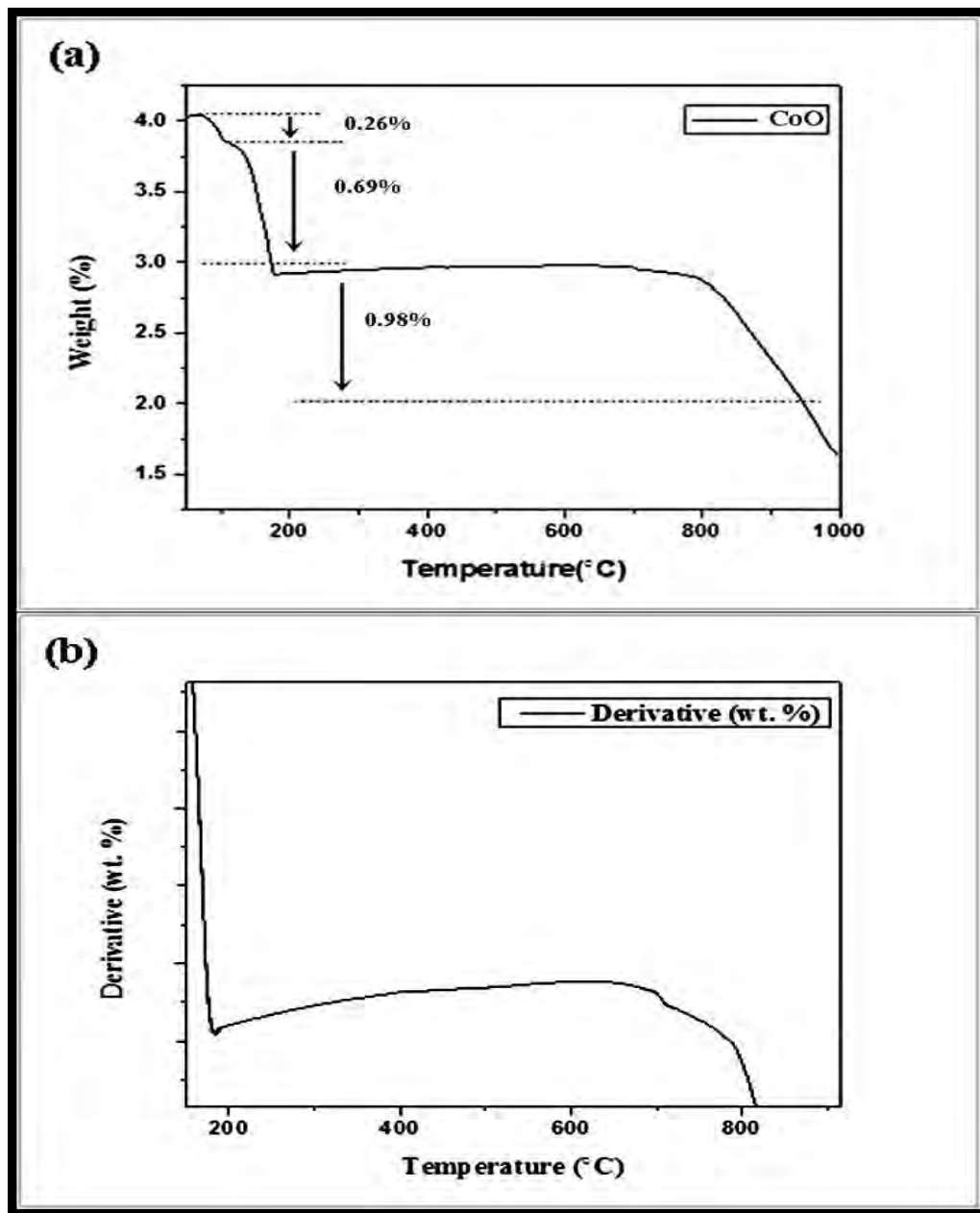
Figure 3.12.5 (a) TGA of Cobalt oxide nanoparticles with (b) derivative thermogram

3.12.2 Biodiesel synthesis via transesterification

Chamaerops humilis is a fetching palm belonging to the family Arecaceae. The novel, nonedible seed oil of *Chamaerops humilis* was used in transesterification for production of methyl ester. Seeds were found to have maximum oil content of 30%. (w/w) which is much more than the required amount (20%). FFA quantity of seed oil was 1.43 mg KOH/g which suggested one step transesterification. Maximum yield of 92% of biodiesel was obtained utilizing *Chamaerops humilis* seed oil and cobalt oxide nano particles during transesterification.

Reaction parameters have significant influence on f transesterification and are required to be explored for optimum values at which maximum yield of methyl ester is obtained. Four specific variables affecting transesterification were considered with minimum and maximum values such as reaction time 55-180 min (A), Met:Oil 2:1-11: 1 (B), catalyst amount of 0.18-0.91 wt.% (C) and temperature 60-120 ℃ (D) (Table 3.12.1). A series of 30 experiments were conducted using Box Behnken Design (BBD) (Table 3.12.2). The relationship among predicted versus actual yield has been demonstrated in Figure 3.12.6 which revealed a closed relation among them as their values are observed dispersed nearby the straight line.

Outcomes of ANOVA of experimental model can be seen in Table 3.12.3. F-value and p-value test used to assess the significance of independent variables. Quadric experimental model was confirmed significant with minimum *p*-value of 0.0008 (<0.05). Lack of fit F-value of the model was 0.2524. The most significant quadratic terms of transesterification were Met:Oil (A^2) with *p*-value of 0.0019 (<0.05). Reliability and accuracy of experimental model was measured by Predicted R² value which was 0.7906 quite close to the adjusted R² of 0.897 having a variance smaller than 0.2. Adeq precision of experimental model is 7.75 which is greater than 4 hence, eliciting efficient predicted yield of methyl ester in the experimental model. Following polynomial Eq. 5 was employed in the Quadric model.

Biodiesel Yield (wt. %) = +82.65+5.72 *A-5.20 *B+5.42* C-0.2223* D-2.85* AB+0.6056 *AC+1.23 *AD-0.5178* BC-0.7521* BD-2.20* CD-15.54* A²-1.64 *B²-3.98 *C²+2.92* D²　(5)
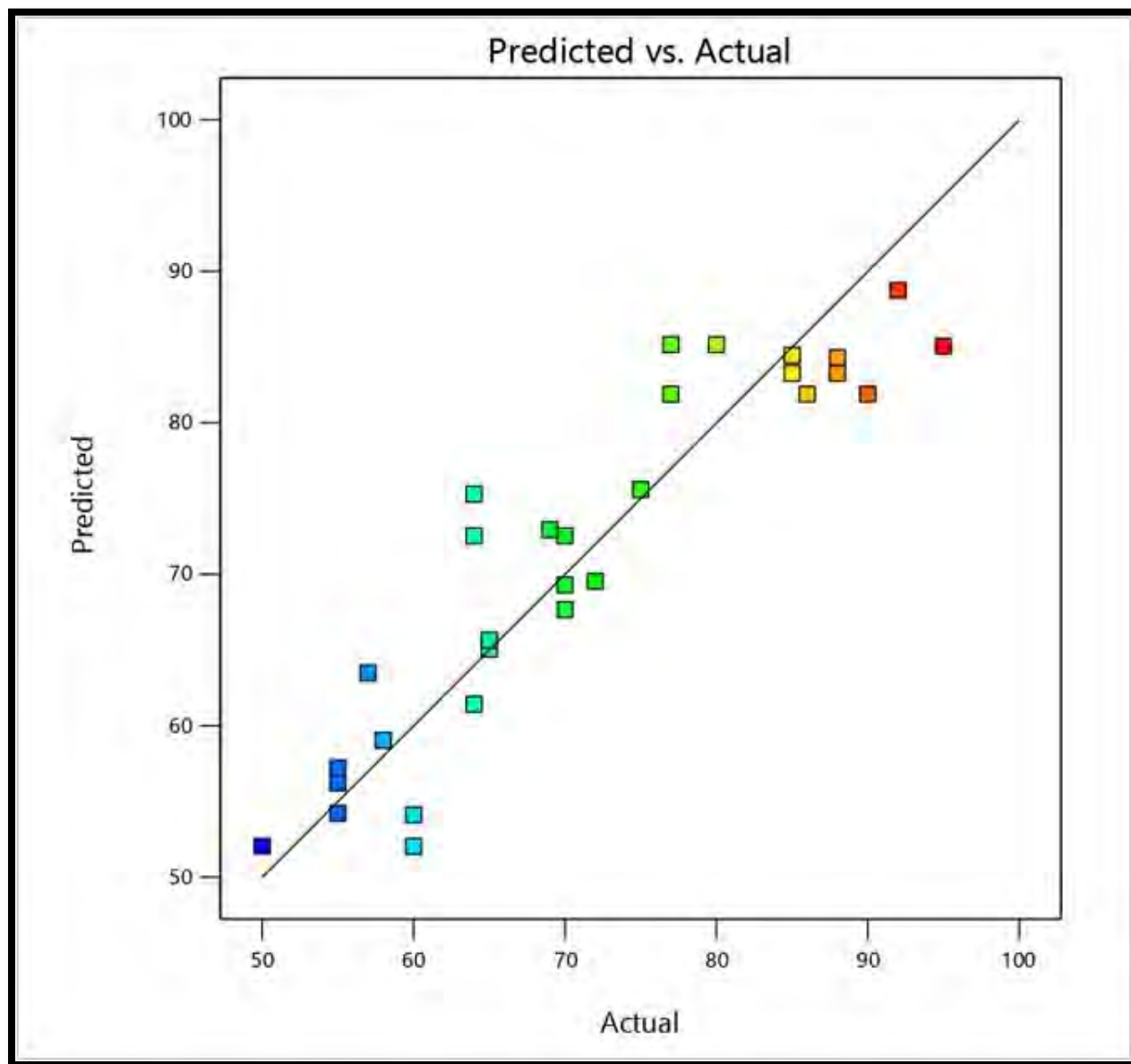
Figure 3.12.6 Comparison between the experimental and the predicted yield of biodiesel in model

Table 3.12.1- Experimental design by central composite design for transesterification reaction

Process parameters	−1	+1
Alcohol to oil ratio	2:1	11:1
Catalyst loading	0.18	0. 91
Reaction time	55	180
Temperature	60	120

Table 3.12.2- Detailed experimental result for transesterification reaction of *Chamaerops humilis* biodiesel

Run	Factor 1 A: Alcohol to oil molar ratio	Factor 2 B: Catalyst loading wt.%	Factor 3 C: Reaction time min	Factor 4 D:Temperature °C	Response Yield wt.%
1	2 : 1	0.91	55	120	60
2	6:1	0.18	180	120	88
3	2:1	0.91	180	120	55
4	6:1	0.18	117.5	90	85
5	6:1	0.91	55	60	60
6	2:1	0.91	55	60	50
7	6:1	0.54	117.5	90	90
8	6:1	0.91	117.5	60	80
9	11:1	0.91	180	60	72
10	11:1	0.18	55	120	75
11	6:1	0.54	117.5	120	85
12	2:1	0.54	55	60	55

13	6:1	0.91	117.5	90	64
14	6:1	0.54	180	90	85
15	6:1	0.54	117.5	90	86
16	6:1	0.54	180	90	88
17	11:1	0.18	180	60	77
18	6:1	0.18	180	60	57
19	6:1	0.54	55	60	64
20	6:1	0.18	55	60	58
21	6:1	0.54	180	120	70
22	6:1	0.54	180	120	65
23	2:1	0.18	180	60	70
24	2:1	0.54	117.5	90	64
25	11:1	0.54	180	90	69
26	6:1	0.54	180	60	92
27	11:1	0.54	55	60	70
28	2:1	0.91	180	60	65
29	6:1	0.18	117.5	60	77
30	6:1	0.54	55	120	55

Table 3.12.3- ANOVA for Response Surface Quadratic model

Source	Sum of Squares	df	Mean Square	F Value	p-value	
Model	4037.95	14	288.42	5.82	0.0008	Significant
A-Alcohol to oil molar ratio	588.50	1	588.50	11.88	0.0036	
B-Catalyst loading	486.98	1	486.98	9.83	0.0068	
C-Reaction time	606.87	1	606.87	12.25	0.0032	
D-Temperature	0.9211	1	0.9211	0.0186	0.0133	
AB	129.86	1	129.86	2.62	0.0263	
AC	5.88	1	5.88	0.1188	0.0351	
AD	24.37	1	24.37	0.4920	0.0238	
BC	4.29	1	4.29	0.0866	0.0426	
BD	9.05	1	9.05	0.1827	0.0051	
CD	80.81	1	80.81	1.63	0.0209	
A²	695.23	1	695.23	14.04	0.0019	
B²	7.93	1	7.93	0.1601	0.0347	
C²	63.81	1	63.81	1.29	0.0742	
D²	27.17	1	27.17	0.5485	0.0404	
Residual	743.02	15	49.53			
Lack of Fit	631.85	11	57.44	2.07	0.2524	not Significant
Pure Error	111.17	4	27.79			
Cor Total	4780.97	29				

$R^2 = 0.897$, Std. Dev. = 7.30,   C.V. % = 13.49, Adeq Precision = 7.75

3.12.3 Impact of reaction Parameters on Transesterification

3.12.3.1 Combined influence of methanol to oil molar ratio and catalyst loading

The relation between Met:Oil and catalyst amount has significant influence on transesterification. This mutual interaction has been demonstrated in the form of plots in three dimensions presented in Figure 3.12.7a. Highest yield of 92% of biodiesel was observed at Met:Oil of 6:1 and catalyst loading of 0.54 (wt. %), time 180 min and temperature of 60 $^\circ$C (Run 26). Both Higher Met:Oil of 11:1 and catalyst concentration of 0.91 (wt. %) led to decrease in methyl ester formation of 72% at Run 9. Catalyst loading of 0.18 (wt. %) with Met:Oil of 11:1 caused low yield of 77% at Run 17. When the amount of methanol exceeded beyond optimum level in the mixture of reactants it causes thinning of catalyst concentration hence, reversible reaction is favored and glycerolysis happens in the reacting mixture, easing the recombination of glycerol with FAMEs and reformation of monoglycerides takes place (Ma et al., 2021). Lower Met:Oil of 2:1 and catalyst concentration of 0.18 (wt. %) added low yield of 70% (Run 23). Higher catalyst amount of 0.19 (wt. %) ensued minimum yield of 65% (Run 26). The significant reaction with *p*-value of 0.0263 (<0.05) was validated between Met:Oil and catalyst loading in results of ANOVA.

3.12.3.2 Combined influence of methanol to oil ratio and reaction time

Mutual effect of Met:Oil ratio and reaction time on biodiesel production is also noticeable effect. Figure 3.12.7b elucidated collective effect of Met:Oil and time at constant temperature (80 $^\circ$C) and catalyst loading (0.18 wt. %). Highest yield of 92% of biodiesel was obtained at Met:Oil of 6:1 and catalyst loading of 0.54 (wt. %). The yield was marginally lowered to 90% at reaction time 117 (min) with same Met:Oil (Run 7). Yield was further drop to 70% at Met:Oil 11:1 and time 55 (min) (Run 27). Excess alcohol makes purification of biodiesel difficult by improving glycerol solubility (Mokbli et al. 2018). Numerous studies have depicted definite oil to methanol molar ratios to derive methanolysis (Alavijeh, et al. 2020). About 64% yield was obtained at Met:Oil 6:1 and time 55 (min) (Run 19). It certainly due to inadequate time for mixing reactants properly and attain equilibrium henceforth, resulted in incomplete

conversion and low yield of methyl ester (Ambat, et al., 2020). Minimum yield of 55% was obtained with lowest Met:Oil of 2:1 and time 55 (min) (Run 18). A significant relationship between molar ratio and reaction time was declared by ANOVA results with *p*-value of 0.0351 lesser than 0.05.

3.12.3.3 Combined influence of methanol to oil molar ratio and temperature

Effect of mutual interaction of Met:Oil and reaction temperature on resultant yield of methyl ester is depicted in Figure 3.12.7c. A larger yield of 92% was achieved with Met:Oil of 6:1 and optimum temperature of 60 °C (Run 26). Same Met:Oil (6:1) and temperature of 90 °C succeeded in a yield of 88% at Run 16. About 70% yield was obtained at higher 120 °C with optimum Met:Oil of 6:1 at Run 21. The source for increase in yield of methyl ester is credited to the surplus of methanol that stimulates catalyst forming methoxy species push the reaction in forward direction (Biggs et al., 2015). Results of experimental work disclosed that rate of reaction is under great influence of a steady rise in temperature. The optimum temperature for transesterification on this study was 60 ℃, owing to its property of lowering activation energy and enhancing interaction between catalyst and reactants, hence, leading to the maximum conversion of reactants into products. Higher molar 11:1 and temperature 90 °C render methyl ester yield to 69% at Run 25. ANOVA results showed this correlation as significant (*p*-value 0.0238).

3.12.3.4 Combined influence of time and catalyst loading

The joint impact of time and concentration of catalyst on FAME production in frame of 3D-plot has been illustrated in Figure 3.12.7d. Highest productivity of 92% of biodiesel was achieved at time 180 min and catalyst amount of 0.54 (wt. %) at constant oil Met:Oil (6:1) and temperature (60 °C) (Run 26). About 80% yield was gained at nano catalyst concentration of 0.91 (wt. %) and time 117.5 min at Run 8. Catalyst concentration of 0.91 (wt. %) time 117.5 min cut yield to 77% (Run 29). Minimum yield of 58% was achieved with reaction time 55 min and at catalyst concentration of 0.18 (wt. %) (Run 20). The yield was further reduced to 57% reaction time 180 min and at catalyst concentration of 0.18 (wt. %) as triglycerides converted into biodiesel partially (Run 20). Therefore, it was inferred from this investigation that joint effect of Met:Oil and reaction temperature is worthy to be keep under consideration in transesterification

reaction. A significant relationship between Met:Oil and reaction time was declared by ANOVA results with *p*-value of 0.0426 lesser than 0.05.

3.12.3.5 Combined influence of catalyst loading and reaction temperature

Influence of the mutual relationship of catalyst loading and temperature at fix time (180 min) and oil Met:Oil, ratio of 6:1 in transesterification has been presented in Figure 3.12.7e. It is credited to full interaction of seed oil with methanol at these reaction conditions in transesterification (Chang et al., 2021). The largest yield of 92% of biodiesel was attained at Met:Oil, of 6:1 and catalyst concentration of 0.54 (wt. %), time 180 min and temperature of 60 ^{o}C (Run 26). About 88% yield was obtained with temperature of 120 ^{o}C and lower catalyst loading of 0.18 wt. % (Run 2). It is attributed to the minimum boiling point of alcohol which slow down the forward reaction of transesterification. About 85% yield was obtained reaction temperature of 90 ^{o}C and CoO loading of 0.54 wt. % at Run 14. An increase in yield of FAME of soybean oil was observed with an increase in MgO amount from 0.5 to 2 %, but later, biodiesel yield was decreased with a further rise in concentration. Consequently, their results fully agree with our current research outcomes (Chekin, et al. 2016). Minimum yield of 60% was achieved at highest CoO loading of 0.91 wt. % and temperature of 60 ^{o}C (Run 6). Nevertheless, the additional catalyst concentration beyond this limit, narrowed FAME yield due to rise in viscosity of reaction concoction and drop-in activity of catalytic as a result depressing contact between catalyst and reactants resulting in low product concentration (Diehl et al. 2007). Results of ANOVA has declared combine effect significant with *p*-value 0.0051.

3.12.3.6 Combined influence of time and temperature

Joint effect of time and temperature on productivity of biodiesel at constant catalyst loading (0.54 wt. %) and Met:Oil 6:1 has been exhibited in Figure 3.12.7f. It can be vindicated that the chemical equilibrium was not attained within shorter reaction time and needed enough time for interaction with catalyst, hence, leading to lower product. After 2 h, forward reaction proceeded, equilibrium was achieved, and maximum conversion yield of 92 %, was detected. Constant elevation in FAME yield was noted with an increase in reaction time. The highest productivity with 92% productivity of biodiesel was achieved with time 180 min and

temperature of 60 $^{\circ}$C at fix Met:Oil (6:1) and catalyst loading (0.54 wt. %) (Run 26). About 85% yield was revealed from Run 11 with time 117.5 min and temperature of 120 $^{\circ}$C. Methyl ester production was further reduced to 65% with time 180 min and high temperature of 120 $^{\circ}$C (Run 22). This study unveiled that increase in reaction productivity with raise in reaction temperature and time till specific limit beyond which a substantial drop in the percent yield was observed which is attributed to endothermic nature of transesterification. Minimum productivity of 55% was notified reaction time 55 min and high temperature of 120 $^{\circ}$C at Run 30. Significant correlation between time and temperature on transesterification was reflected in outcomes of ANOVA with *p*-value 0.0209 (<0.05).
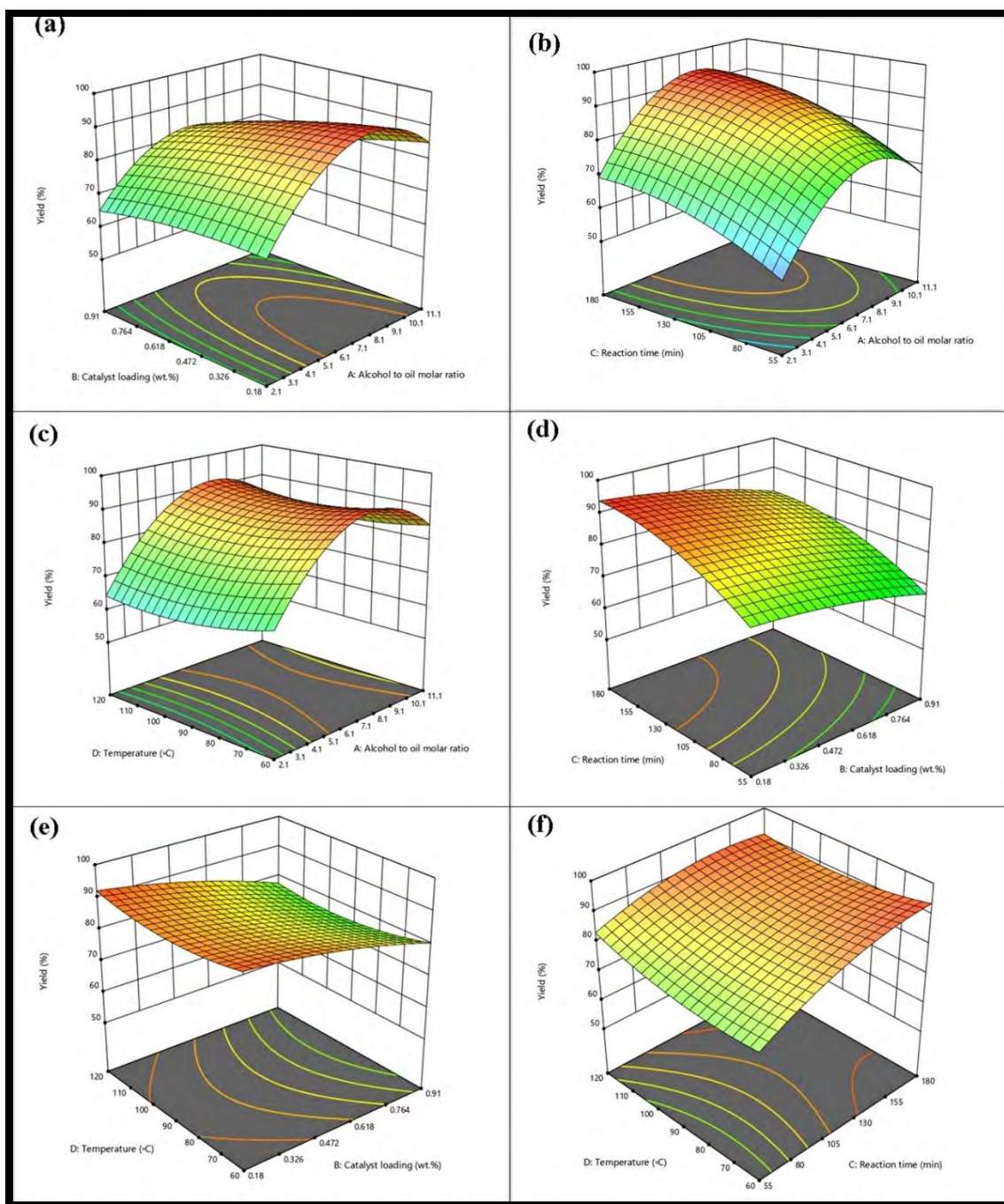
Figure 3.12.7 Influence of the reaction parameters of Transesterification on biodiesel yield

3.12.4. Biodiesel characterization

3.12.4.1 FT-IR spectroscopic Study

FT-IR spectroscopy helps in confirmation of methyl ester formation once transesterification is completed. FT-IR spectroscopic evaluation is one of the extensively used techniques for studying structural composition of biodiesel. FT-IR spectrum of *Chamaerops humilis* oil and synthesized methyl ester is illustrated in Figure 3.12.8 a and b respectively, displaying various bands and stretches of functional groups found in triglycerides and methyl ester. Representative key band of carbonyl group (C=O) was observed in the IR the area of 1743.48 cm^{-1} and band for methyl group (CH$_3$) was spotted at 1464.61 cm^{-1} in the spectrum of biodiesel. Silitonga, et al. (2020) observed carbonyl peak in biodiesel spectrum of *Ceiba pentandra* in the IR area of 1743.73 cm^{-1} which aligns with our current findings. The existence of these two bands has confirmed methyl ester formation at the end of transesterification. Characteristic peak of C-H (sp^3) appeared in the IR region of 2922.52 cm^{-1} whereas, stretch for CH (sp^2) was spotted at 2853.23 cm^{-1}. IR region of the carbonyl group among all other peaks is considered as vulnerable to transformation in both chemically and molecularly in the spectrum of biodiesel Stretch for aliphatic esters (O=C-O-C) spotted at 1160.07 cm^{-1}.

A greatly variable part in the spectrum of oil and biodiesel was observed about 1000-2000 cm^{-1} and 3100-2800 cm^{-1}. Similar result was observed by Rozina et al. 2021 in the IR spectrum of *Calophyllum inophyllum* biodiesel (Arumugam et al., 2019). The wagging frequency for C-H$_2$ ensued as stretch peak at 1098.06 cm^{-1} in the spectrum. Intense peaks at 3321.97 cm^{-1} seemed in the spectrum of *Chamaerops humilis* seed oil disappeared in the spectrum of methyl ester. Deep stretch for (O-H) found at 1022.46 cm^{-1} was gone in the spectrum of methyl ester. The peaks of the spectrum of *Chamaerops humilis* seed oil and methyl ester have validated the transformation of triglycerides of oil into methyl esters during transesterification.

3.12.4.2 NMR Spectroscopic Analysis

The spectroscopic technique of ^{1}HNMR was applied for confirmation and quantification of *Chamaerops humilis* biodiesel (CHBD). NMR spectroscopy is widely applied to examine transesterification reaction and to calculate amount of saturated and unsaturated fatty acid methyl

esters in biodiesel sample at different life cycle stages such as after transesterification, purification, thermal treatment, and storage (Singh et al. 2019). Corresponding absorbance peak of ^{1}HNMR spectrum of *Chamaerops humilis* biodiesel is shown in Figure 3.12.9a.   The distinguishing peak for methoxy group (–OCH$_3$) emerged at 3.670 ppm in the ^{1}HNMR spectrum of biodiesel which has approved successful transesterification and resultant methyl ester production. Unwanted peak of methanol was not detected in ^{1}HNMR spectrum of CHBD. It is generally noted at 3.45 ppm.

^{1}HNMR spectrum of CHBD has proton peak for triplet α methylene (α-CH$_2$) was found at 2.283-2.333 ppm. Peak for β-CH$_2$ (β-methylene) protons was observed at 1.261-1.309 ppm and appeared as a singlet in the spectrum. These protons of β-methylene correspond to hydrogen element located on C-3 of aliphatic straight fatty chain of hydrocarbon. Peak at 0.864-0.918 ppm embodied terminal methyl protons. Hydrogen named as olefinic with a pair of carbon atom associated with a double bond (-CH=CH-) was assumed from the peak spotted at 5.311-5.401 ppm. The peak observed at 2.757-2.777 ppm corresponded to allylic hydrogen (-CH$_2$). These mentioned peaks of ^{1}HNMR spectrum have proven the presence of methyl esters in sample of biodiesel. The total transformation of triglycerides into FAME which was measured to be 93 %.

^{13}CNMR spectrum of *Chamaerops humilis* biodiesel assisted in exploring its structural characteristics including the position of esters carbonyl (-COO-) and C-O group. ^{13}CNMR spectrum of synthesized biodiesel of *Chamaerops humilis* have been demonstrated in Figure 3.12.9b. Peak at 51.42 ppm characterized methoxy carbon in ^{13}CNMR spectrum. Signal for carbonylic group (-COOH) was observed at 174.29 ppm. Degree of unsaturation representing double bond between carbon atoms (-CH=CH-) in sample of biodiesel was detected from the peak located at 127.89-128.03 ppm which represented the internal non-conjugated carbon atoms. Besides, chemical shifts observed at δ ppm value 129.73-130.18 indicated the presence of outer carbon of non-conjugated carbons (-CH=CH-) in the spectrum of ^{13}CNMR. Signal for C-O group in biodiesel was observed at 76.62-77.47 ppm. The peak observed at 29.09-29.77 ppm signified lengthy sequence of ethene carbon (-CH$_2$-)$_n$. Lastly, peak for carbon atom present in aliphatic-methylene (-CH$_2$-s) was situated at 31.53-34.09 ppm.

3.12.4.3. GC/MS Analysis

The fatty acid profile intensely affects the quality of biodiesel. For this purpose, identification of ester constituents of biodiesel sample was carried out by GC/MS analysis. The gas chromatogram of *Chamaerops humilis* biodiesel is presented in Figure 3.12.10 reflecting eight separate peaks of saturated and unsaturated methyl esters which were additionally verified by MS analysis using library match software NO. NIST02. Saturated methyl esters contained tridecanoic acid methyl ester (C14:0) and Octadecanoic acid methyl ester (C18:0). Methyl ester with unsaturated comprised of 15-Octadecenoic acid methyl ester (C19:1) and 9-Octadecenoic acid, (2)-methyl-, methyl ester (C18:1), 13-Docosenoic acid, methyl ester (C23:1) and Docosenoic acid methyl ester (C23:0). 15-Octadecenoic acid methyl ester was discovered to be significant fatty acid methyl ester with highest abundance in chromatogram achieved at retention time of 11.847 min. Usually, high concentration of saturated and monounsaturated fatty acid methyl esters in biodiesel sample is considered as favorable for getting maximum energy yield and oxidative stability. However, biodiesel rich in polyunsaturated methyl esters have desirable cold flow properties but lesser oxidative stability (Tahir et al. 2019). GC/MS analysis of *Chamaerops humilis* methyl ester has represented it as a highly competent source of biofuel which can be produced at industrial scale.
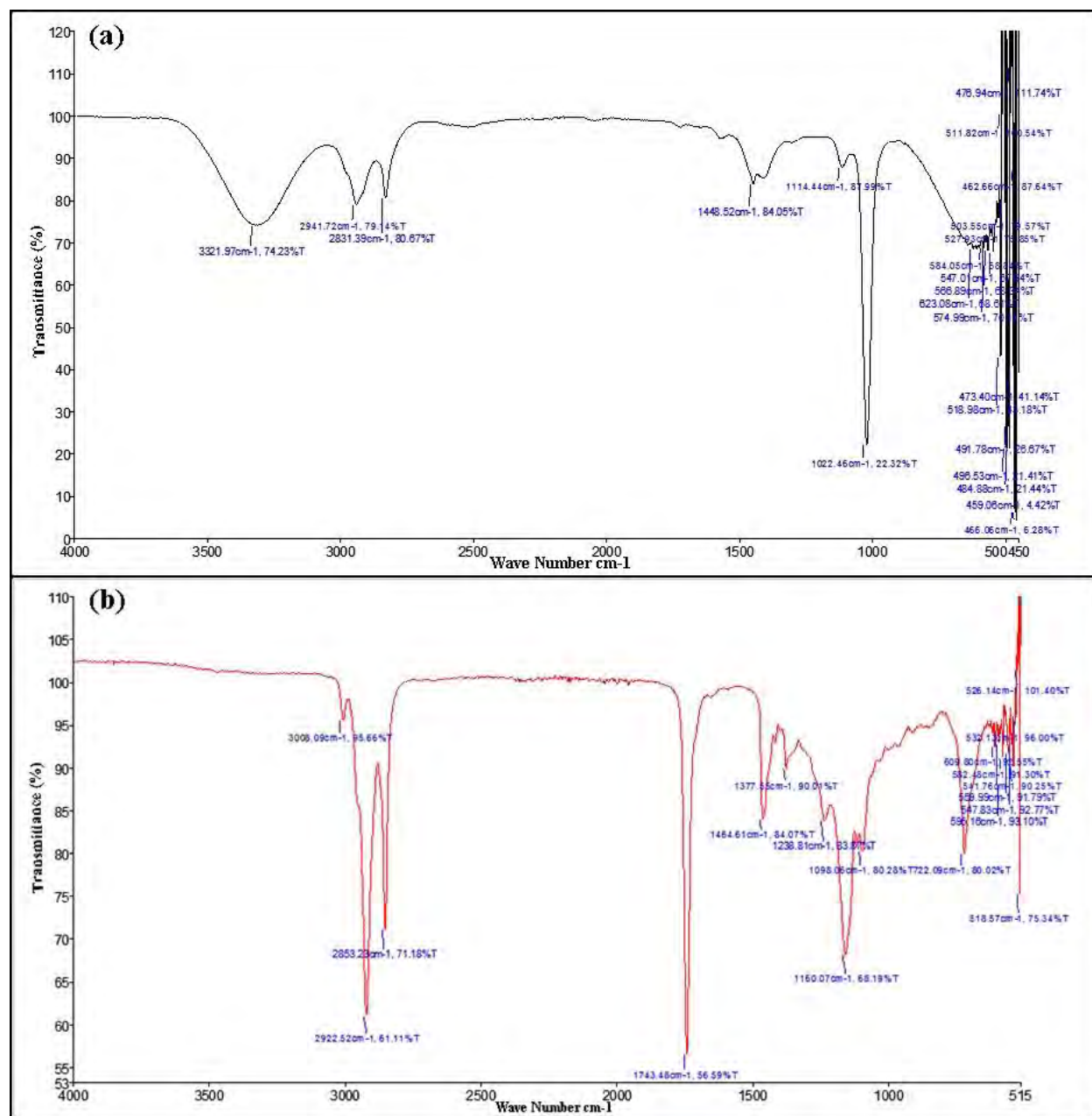
Figure 3.12.8 FTIR spectrum of *Chamaerops humilis* **(a)** seed oil and **(b)** biodiesel
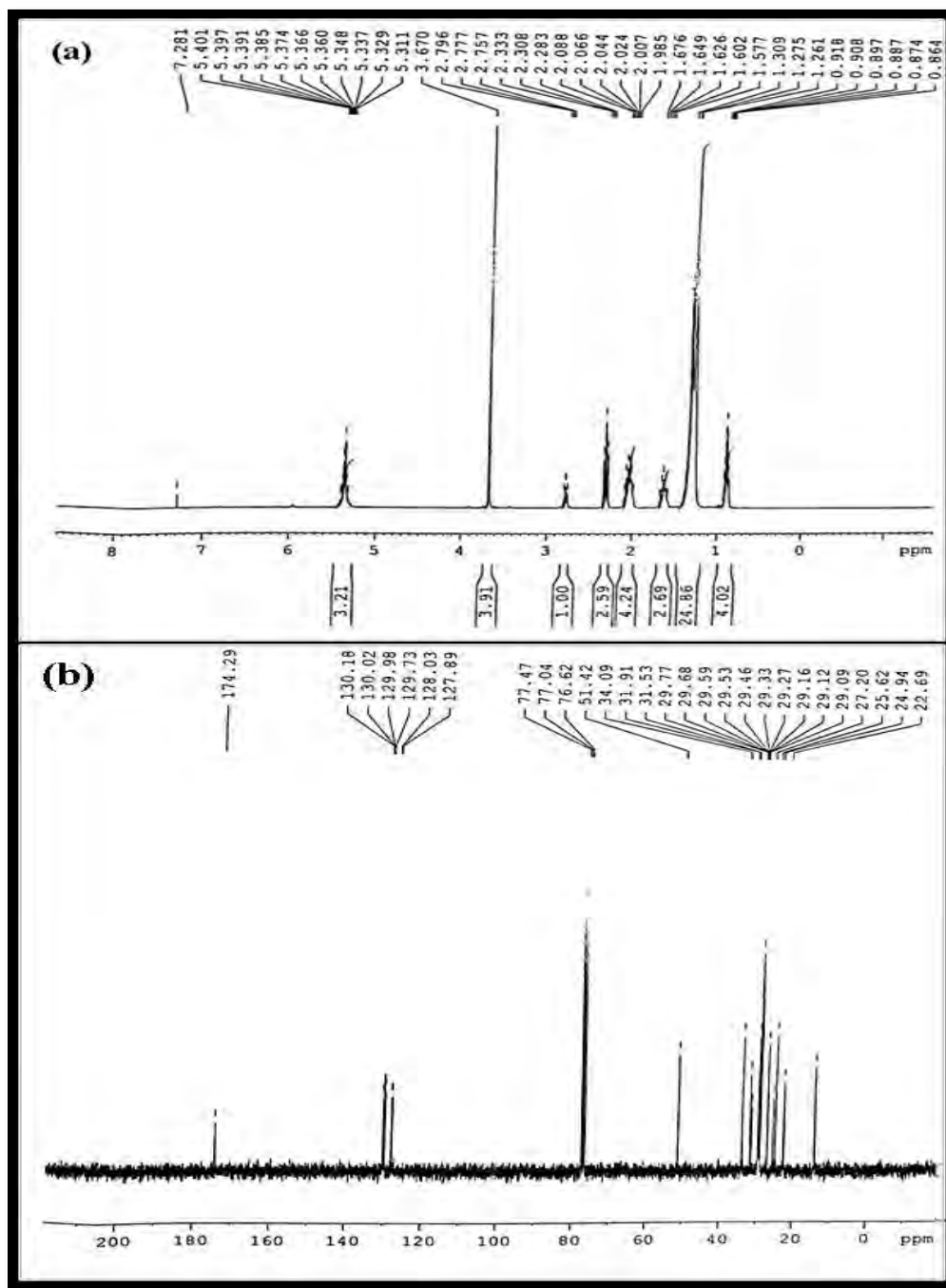
Figure 3.12.9 (a) ^{1}HNMR and **(b)** ^{13}CNMR of *Chamaerops humilis* biodiesel
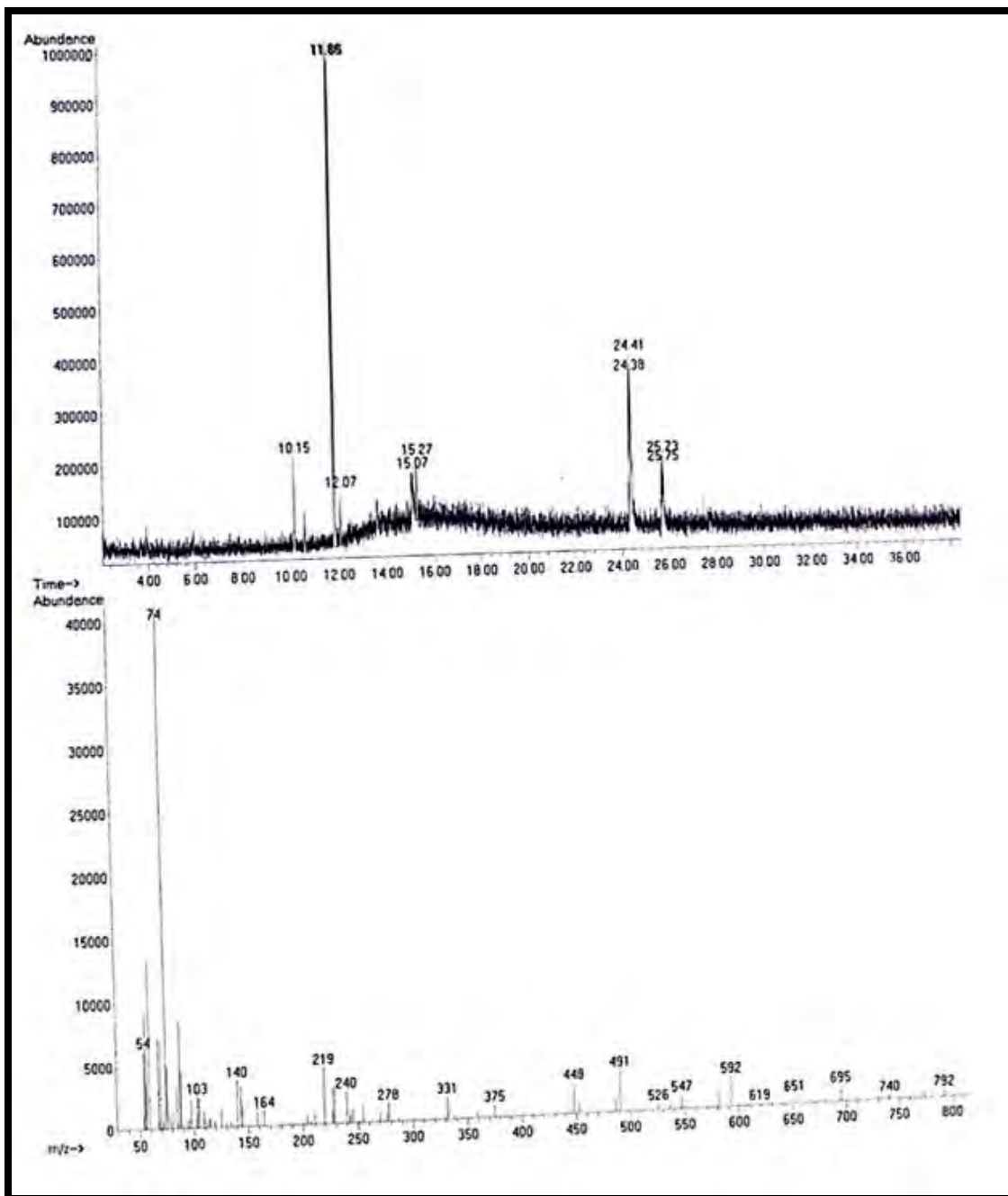
Figure 3.12.10 GC-MS spectrum of *Chamaerops humilis* biodiesel

3.12.5. Analysis of Fuel Properties of biodiesel

Analysis of fuel properties of synthesized methyl ester sample is required prior to its practical application and must be equivalent to compared with international standards of ASTM D-6571, EN 14214 and China GB/T 20828-2007. The fatty acid profile structure of the seed oil utilized in transesterification has great influence on physiochemical characteristics of biodiesel. Examined fuel properties of *Chamaerops humilis* biodiesel have been presented in Table 3.12.4.

The quality of the fuel is highly affected by acid value. Hence, the acid value of biodiesel has considerable impact on engine performance. It signifies the total amount of potassium hydroxide which is required in neutralizing free fatty acids found in liquid fuel. The acid value of biodiesel higher than required limit cause troubles in rubber parts of old diesel engines and results in corrosion. The acid value of *Chamaerops humilis* methyl ester was measured to be 0.179 (mg KOH/gm) and fit well within accepted international limits of fuel.

Kinematic density has a significant impact on the fuel property of biodiesel which directly controls engine efficiency, the passage of fuel within pipelines system and nozzles of injector. Fuels with higher density elevates the viscosity of biodiesel and results in incomplete combustion with more particulate matter formation (Yandri, et al. 2021). Kinematic density CHBD found to be 0.977 (mm^2/s) matched well with international fuel standards.

Kinematic viscosity of fuel has a great impact on fuel atomization and lubrication of fuel injector. Fuel with lower viscosity causes leakage problems and offers minimum lubrication in injection pumps as a result more power loss happens in fuel engine. Likewise, elevated viscosity renders sufficient fuel supply in injection pump and consequent engine efficiency (Hayyan et al. 2014). In our current investigation the kinematic viscosity of CHBD was 7.34 (mm^2/s) which lies under the given range of international fuel standard.

The temperature at which fuel starts burning on provision of ignition source is known as flash point. Fuel with higher flash point have minimum risk of accidental fire during transportation and storage (Govindan, and Hasanagi 2008). Biodiesels have the advantage of having higher flash points in contrast to conventional fossil fuels, hence, are safer to be handled. Flash point of *Chamaerops humilis* biodiesel was 97 ◦C as shown in Table 3.12.4.

The operability of diesel engines in colder regions of the world where the temperature reaches minus is stirred by pour and cloud point of the fuel. The fatty acid composition of seed oil utilized in transesterification directly affect the pour point of synthesized biodiesel. Pour point of *Chamaerops humilis* biodiesel was -11 ∘C which met international standards of fuel. Cloud point describes the temperature of biodiesel at which fuel crystallization starts. Cloud point in our present investigation was found to be -9 ∘C which lies under set limit of international standards of fuel. Sulphur content of CHBD was measured to be 0.0002% far more lesser than value 1 ppm in contrast to petro diesel which is 50 ppm. This negligible amount of sulphur has positive impact on biodiesel quality making it pollution free and environment friendly (Lee et al. 2019).

Table 3.12.4 Comparison of fuel properties of *Chamaerops humilis* biodiesel with international standards**.**

Property	Methods	*Chamaerops humilis*		ASTM D-6751	EN-14214	China GB/T 20828-2007
		Mean	St.Dev.			
Color	Visual	2	-	2.0	-	-
Acid number (mg KOH/g)	ASTM -D974	0.179	0.1	≤0.5	≤0.8	≤0.5
Flash Point (°C)	ASTM -D93	97	1.4	≥93	≥130	≥120
Pour Point (°C)	ASTM -D97	-11	0.1	-15-16	_	_
Viscosity (mm²/s at 40 °C.)	ASTM -D445	7.34	0.2	1.9-6.0	_	3.4-5.0
Density (kg/m³ at 40 °C)	ASTM -D1298	0.977	1.4	≤120	_	≤120
Sulphur content (wt.%)	ASTM -D4294	0.0002	-	≤0.05	≤0.05	≤0.20
Cloud point (°C)	ASTM -D2500	-9	-1	-3.0-12	_	_

3.12.6. Catalyst Reusability

Investigation of reusability of cobalt oxide nanoparticles was accomplished to determine its stability and economic viability to be reused in subsequent cycles. Method of purification and separation of catalyst from reaction mixture substantially affect reusability of a catalyst (Zhao et al. 2018). Reusability of the produced cobalt oxide nanoparticles was executed at optimum reaction terms of transesterification like Met:Oil of 6:1, catalyst loading of 0.54 (wt. %), time 180 min and temperature of 60 °C.

The centrifugation method was used to recover green nano particles of Co from reaction mixture after first cycle of transesterification. Recovered particles were then washed with alcohol to eliminate contaminations, dehydrated in the oven, and calcined in the muffle furnace for 180 min at 500 ∘C for reuse in the succeeding rounds of transesterification. Catalytic activity was tested up to 7th cycles. Maximum catalytic performance was observed up to five consecutive experimental trials which resulted in high FAME yield of 92 to 79%. Drop in the yields up to 79% of methyl ester was noted in fifth. Yield was further reduced to 70% in 6th and 66% in 7th cycle (Figure 3.12.11).

This decrease in catalytic activity is chemically ascribed to intoxication of dynamic sites of CoO NPs by organic constituents present in mixture of reactants of transesterification which declined yield of methyl esters. Nevertheless, catalytic action of the nanoparticles can be regained after washing and calcination in muffle furnace.
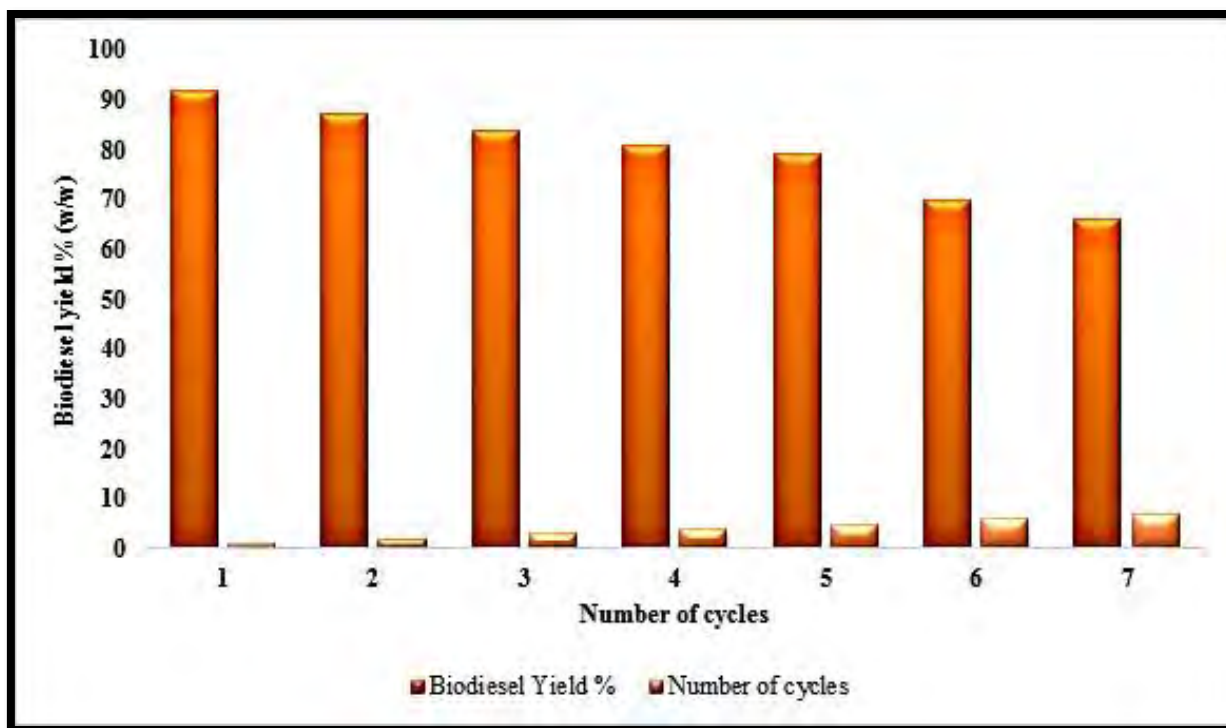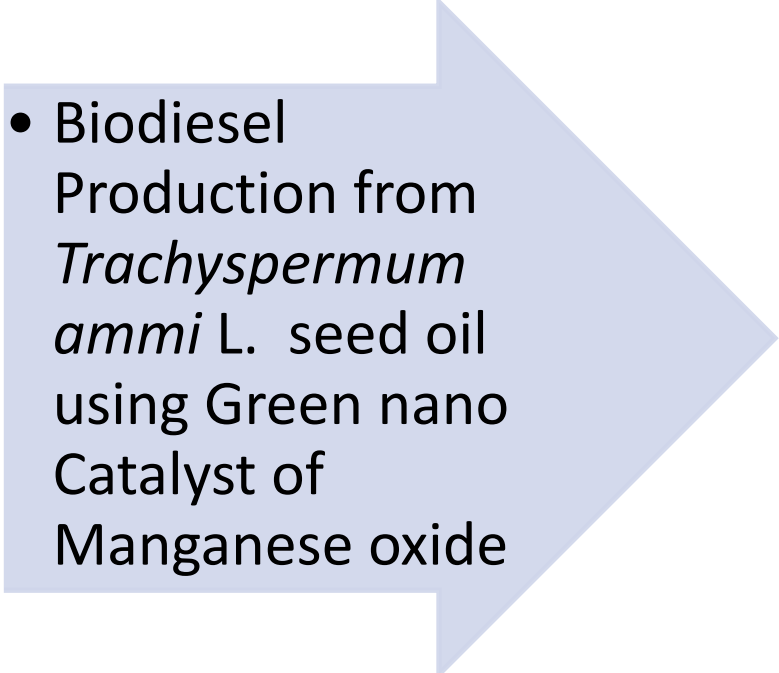
Figure 3.12.11 Reusibility of Cobalt oxide NPs in transesterification reaction

SECTION XIII

- Biodiesel Production from *Trachyspermum ammi* L. seed oil using Green nano Catalyst of Manganese oxide

Manganese oxide with various crystal morphologies has drawn interest of researchers due to its high fraction of surface atoms, non-toxicity, and wide range of applications, including catalytic activity. MnO2 nanoparticles are one of the most notable metal oxides due to their distinctive characterization. Their optical constant is large, and their band gap is small (Cai et al., 2019). MnOx has received extensive study in bulk, but the synthesis of MnOx materials at the nanoscale opens up new possibilities for nanotechnology. Due to its high surface area, manganese oxide at the nanoscale has more effective catalytic characteristics for electrochemical water oxidation (Koutani et al., 2022). Presently green nano catalyst of manganese oxide prepared with *Colchicum aitchisoni* leaf extract that can be immobilized in the system to speed up the entire reaction process.

3.13.1 Characterization of Manganese oxide Nanoparticles

3.13.1.1 X-Ray Diffraction (XRD) of MnO$_2$

The pattern of X-ray diffraction of MnO2 nanoparticles is shown in Figure 3.13.1. Five different peaks emerged in the XRD spectrum of MnO2 at 2 θ values = 21.91◦, 30.01◦, 29.42◦, 37.52◦, and 52.01◦, corresponding to (020), (200), (121), (211), and (122) *hkl*, respectively. There were no extra diffraction peaks linked to contaminations, indicating that the synthesized MnO2 was of good quality. The average size of MnO2 NPs was calculated using the XRD pattern of the intense peak at 2 θ value of 29.42◦ (121 *hkl*).

The tetragonal phase was assigned to MnO2 NPs and was confirmed in the standard data (JCPDS 6-416) by all identified peaks in the XRD spectrum. MnO2 NPs has a calculated mean particle size of 34 nm.

3.13.1.2 Scanning Electron Microscopy (SEM) of MnO$_2$

SEM analysis of MnO2 was performed to study the topography and cross-section of nanoparticles. Figure 3.13.2 shows a SEM micrograph of MnO2. The shape of MnO2 nanoparticles was spherical, and the particle arrangement was found uniform. Larger particles were present due to aggregation of smaller ones.

3.13.1.3 Energy Diffraction X-ray (EDX) of MnO$_2$

Energy diffraction was used to determine the chemical composition and purity of MnO$_2$ nanoparticles (EDX). The distinctive peaks of Mn were found at 0.5 and 6.1 keV, respectively, while the peak of O was found at 0.5 keV. Figure 3.13.3 shows the EDX spectrum MnO$_2$. Mn and O percent amounts were discovered to be 56.56 and 43.44%, respectively. The purity of produced nanoparticles has been demonstrated by the EDX spectrum.

3.13.1.4 Fourier Transform Infrared Spectroscopy (FTIR)

FT-IR analysis of the various functional groups on the MnO$_2$ nanoparticle surface is depicted in Figure 3.13.4. An FTIR study based on catalytic performance during transesterification provided additional information on the catalyst surface. The O-Mn-O stretching vibration mode of bridging oxygen atoms is responsible for the peak at 3218.31 cm^{-1} and 1091.69 cm^{-1}. A symmetric stretching vibration with intercalated water molecules may be the cause of the transmittance band in the 996.4 cm^{-1} region (O–H).

3.13.1.5 Thermogravimetric analysis (TGA) of MnO$_2$

MnO$_2$ nanoparticle thermal stability and the decomposition process from room temperature to 1000 ◦C were investigated using thermogravimetric analysis. The MnO$_2$ thermogram and its following derivative curve (in weight%) are shown in Figure 3.13.5 a and b, respectively. The dehydration of MnO$_2$ NPs and the removal of physically adsorbed water caused the precursor weight loss of 0.78% in the initial step between 150 ◦C to 400 ◦C. The subsequent phase of decomposition saw a loss of 0.021%, which was caused by the thermal decomposition of MnO$_2$ precursor at temperatures between 400 ◦C and 550 ◦C. The third peak of weight loss occurred between 551 ◦C and 730 ◦C and was accompanied by a 0.013% weight reduction. The aforementioned TGA measurements showed that MnO$_2$ nanoparticles have a high thermal stability.
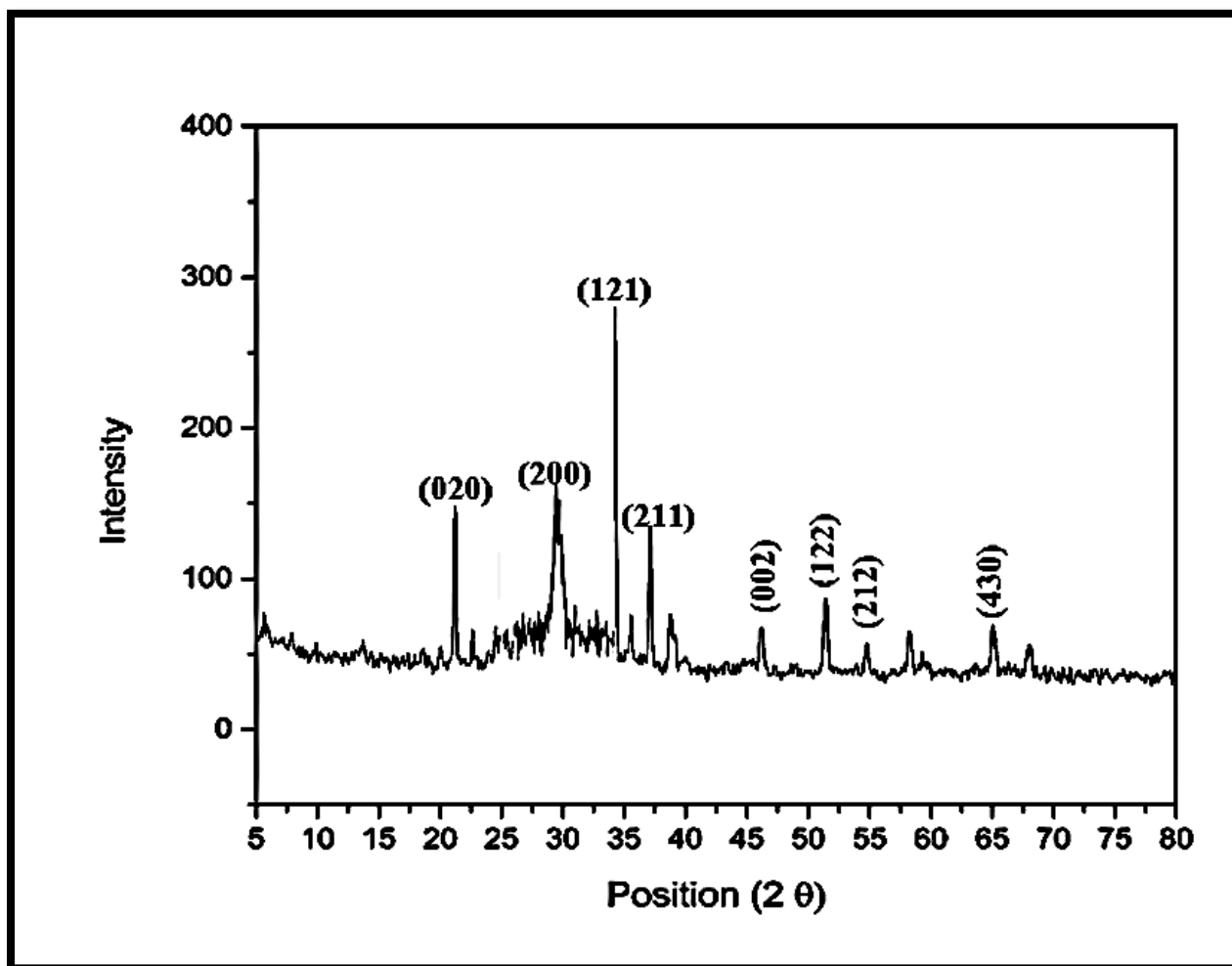
Figure 3.13.1 XRD pattern of calcined manganese oxide NPs
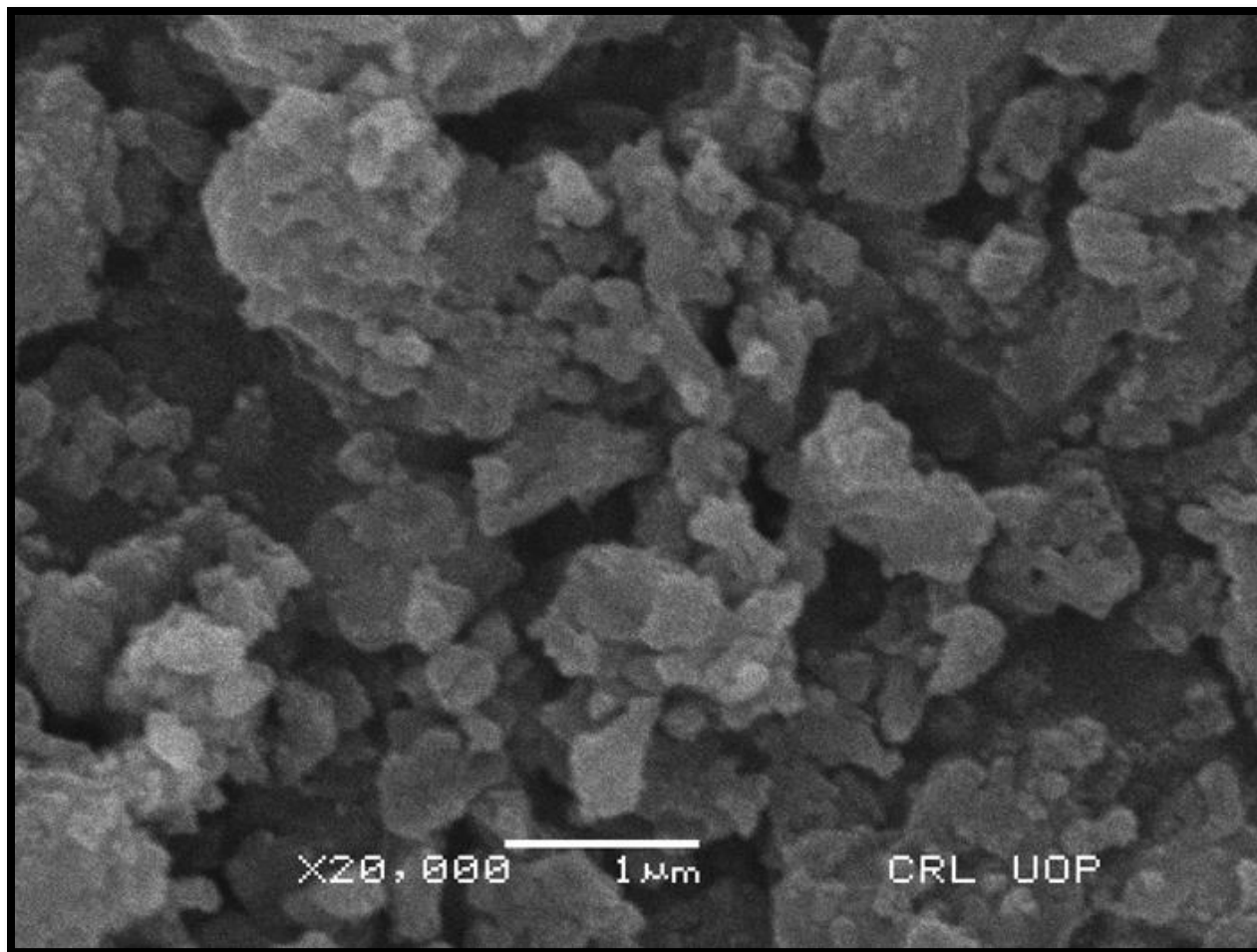
Figure 3.13.2 Scanning electron microscopy (SEM) of manganese oxide NPs
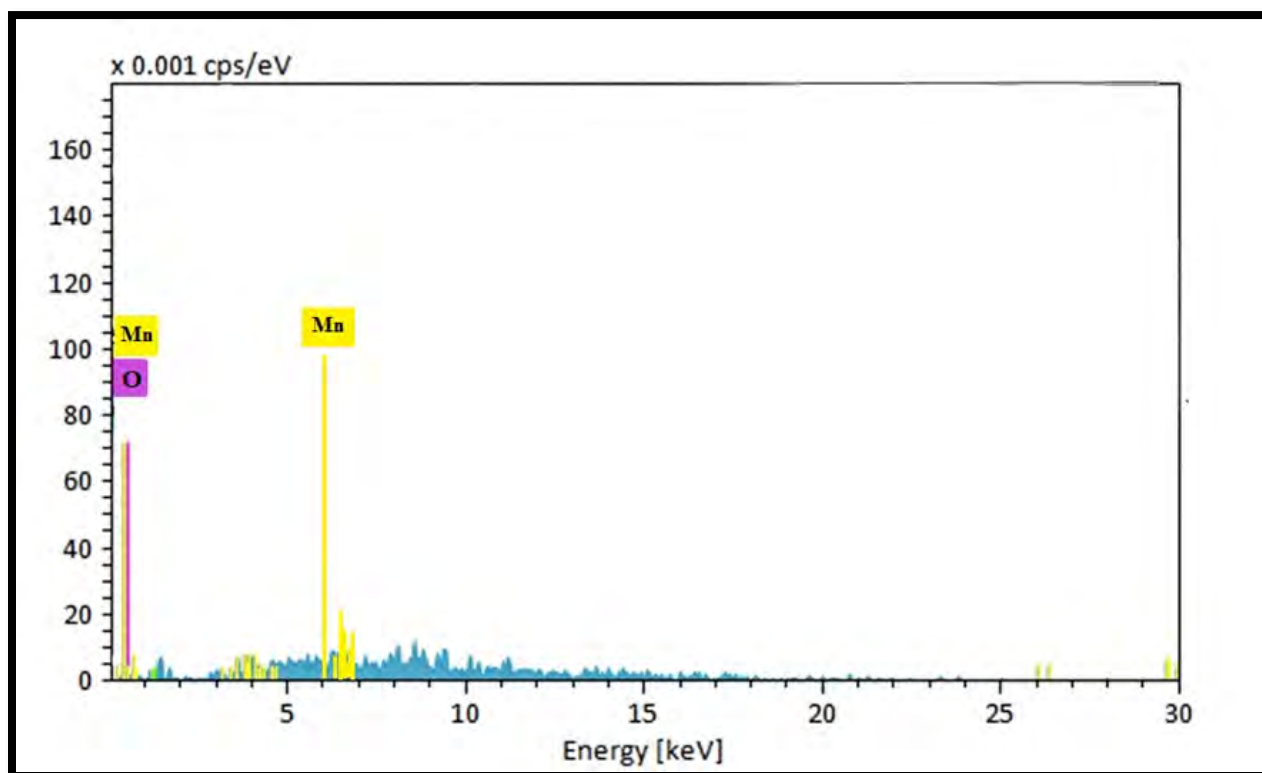
Figure 3.13.3 Energy diffraction X-Ray (EDX) of manganese oxide NPs
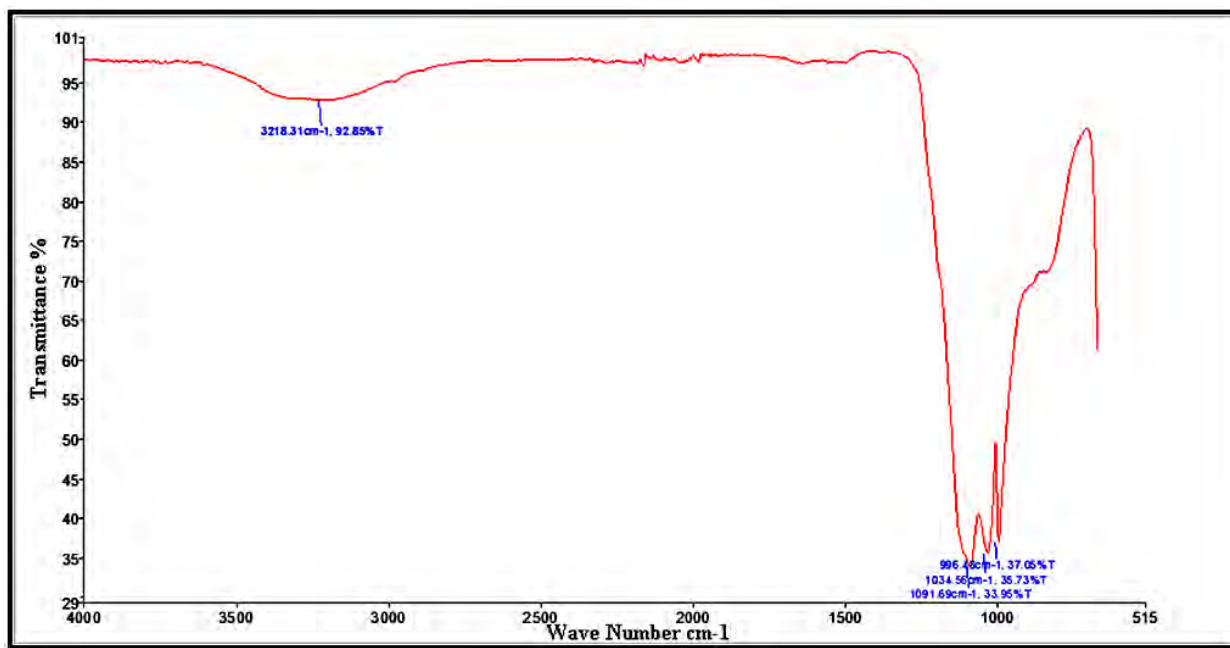
Figure 3.13.4 FTIR spectrum of manganese oxide NPs
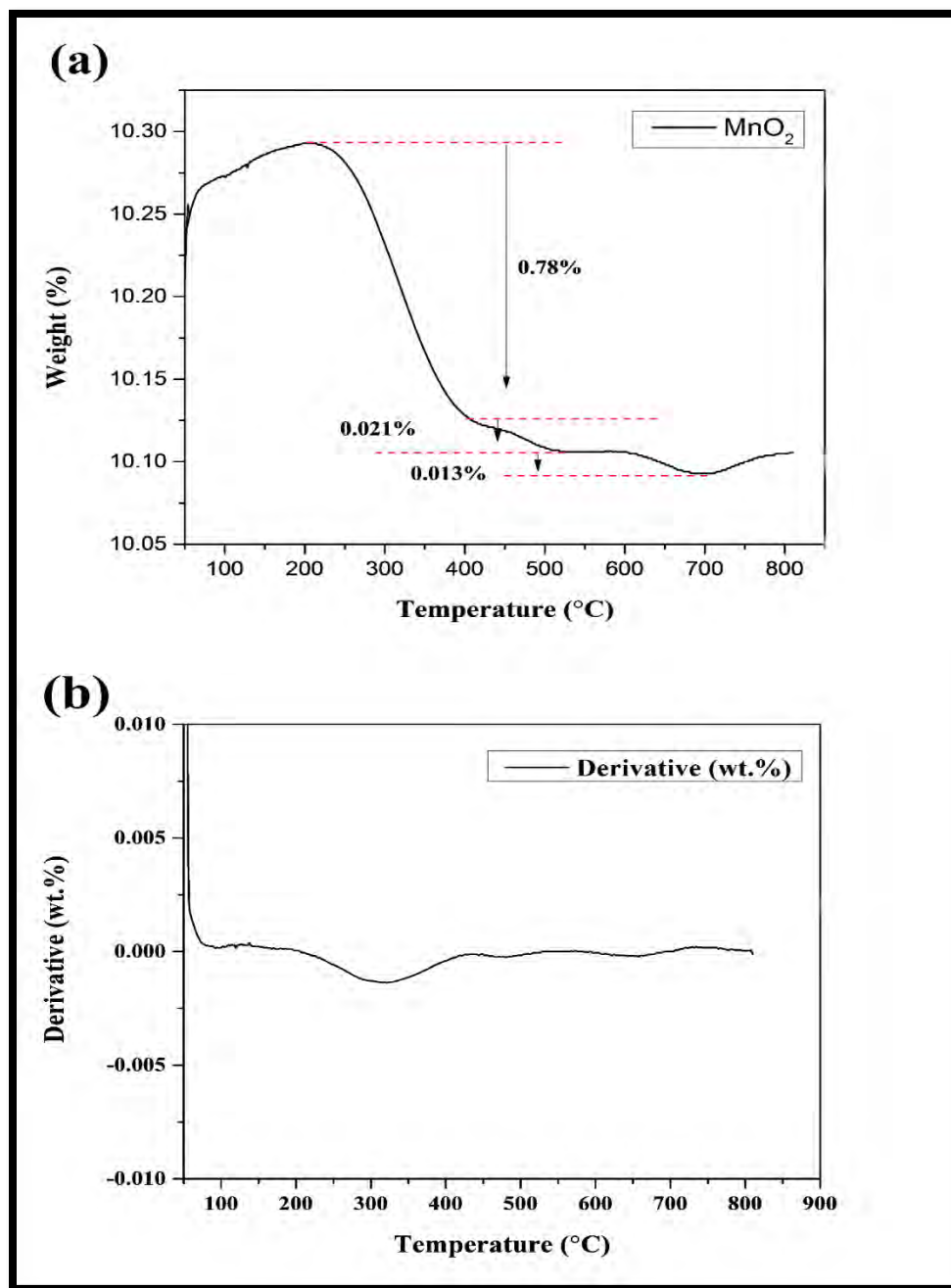
Figure 3.13.5 (a) TGA of manganese oxide nanoparticles with (b) derivative thermogram

3.13.2. Biodiesel synthesis

The current study used *Trachyspermum ammi* seed oil, which has potential for usage, to produce sustainable and green biodiesel. The FFA content of a selected feedstock's oil must be identified prior to biodiesel manufacturing. According to earlier reports, only feedstocks with an oil concentration of more than 20% will be taken into account for the production of biodiesel (Lawan et al., 2019). About 27% oil content was found to be present, which is far more than the permitted percentage limit (Yazdani, et al., 2021).

At 25°C, it was found that the *Trachyspermum ammi* (L.) Sprague seed oil had a distinct bright green tint. FFA concentration of TASO was found to be 2.5 (wt. percent) in the current experiment, which is substantially lower and indicates that it is ideal for transesterification reaction with single-step base-catalyzed. The seed oil that has a greater FFA content, or >3%, is considered undesirable since it needs an additional acid esterification step. Even without the addition of an acid esterification step, *Trachyspermum ammi* seed oil is used as a dependable source for the production of biodiesel. Even without an additional acid esterification step, *Trachyspermum ammi* seed oil is employed as a dependable source for the creation of methyl esters. Utilizing a *Colchicum aitchisoni* leaf extract-produced green nanocatalyst of MnO_2, the *Trachyspermum ammi* seed oil was transesterified.

The percent yield of methyl ester was calculated using a quadratic polynomial equation in terms of coded variables such (A) the methanol to oil ratio, (B) catalyst concentration, (C) reaction temperature, and (D) transesterification reaction time (Table 3.13.1). The yield of biodiesel obtained over a series of transesterifications is shown and exhibited in Table.3.13.2.

Biodiesel Yield % = +80.48-2.37*A+3.27*B-1.05*B+2.87*D-2.30*AB+2.98*AC-3.11*AD-0.7500*BC+2.62*BD-0.2500*CD-15.03*A^2-15.31 *B²+11.19 *C²+3.69 *D²
(19)

Table 3.13.3 lists the findings of the statistical analysis of variance (ANOVA) for the RSM together with the central composite design coded values for the four factorial experimental designs. Figure 3.13.6 compares the expected and actual yields (provided as supplementary material). The yields, both actual and expected, were found to be strongly correlated and

distributed along a straight line. Data analysis to determine a model's relevance, accuracy, and methyl ester synthesis fitness. Coded values obtained during data estimation were employed, together with a few minor model variables, to develop a quadratic regression model. F-test and p-value were used to calculate the significance of the resulting model; the less the value of p ($0 < .05$), the more significant the model. Transesterification processes and the yield of biodiesel that results are largely influenced by parameters related to transesterification. ANOVA results with a p-value of 0.0013 were utilized to determine the model's significance. The R^2 coefficient, which measures how well something is determined, was 0.83, which is acceptable. The signal-to-noise ratio, which was determined using the model's accuracy value, should be 4. The model's higher precision value, 9.47 (>4), was within the necessary range. The model's lack of fit value was 5.16, which was negligible and smaller than pure error. All of this points to the conclusion that the model is significant and reliable.
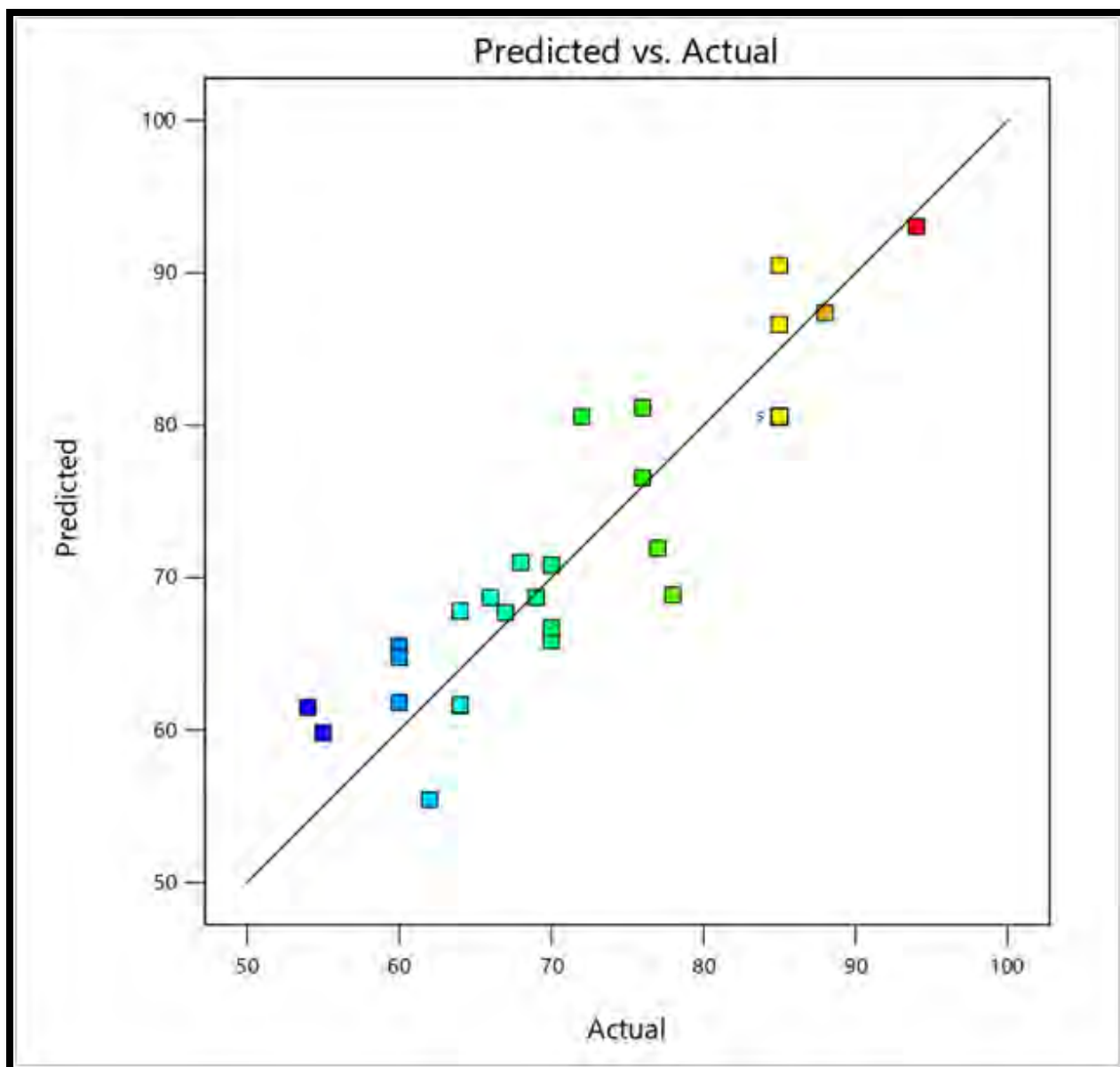
Figure 3.13.6 Comparison between the experimental and the predicted yield of biodiesel in model

Table 3.13.1- Experimental design by central composite design for transesterification reaction

Process parameters	−1	+1
Methanol to oil ratio	2:1	14:1
Catalyst loading (wt. %)	0.26	0.95
Reaction time (min)	60	180
Temperature (∘C)	60	120

Table 3.13.2- Detailed experimental result for transesterification reaction of *Trachyspermum ammi* Biodiesel

Run	Factor 1 a:Methanol to oil Ratio	Factor 2 C:Catalyst Concentration wt.%	Factor 3 B:Temperature °C	Factor 4 D:Time Min	Response Biodiesel Yield %
1	14:1	0.26	120	180	68
2	8:1	0.95	120	120	55
3	2:1	0.95	120	60	55
4	14:1	0.605	90	120	70
5	14:1	0.95	60	180	60
6	8:1	0.95	120	180	53
7	14:1	0.26	60	60	70
8	2:1	0.26	90	120	89
9	8:1	0.605	90	60	70
10	14:1	0.95	90	120	64
11	8:1	0.95	120	180	77
12	8:1	0.605	60	120	70

13	8:1	0.26	90	120	94
14	8:1	0.95	90	180	60
15	14:1	0.26	60	120	70
16	8. :1	0.605	90	120	85
17	8:1	0.605	90	120	85
18	2:1	0.26	90	120	58
19	8:1	0.605	90	180	88
20	8:1	0.26	90	60	76
21	8:1	0.605	90	120	85
22	14:1	0.26	120	120	64
23	8:1	0.605	60	120	60
24	2:1	0.95	120	180	76
25	15:1	0.26	90	60	80
26	2:1	0.26	120	60	78
27	14:1	0.95	60	60	70
28	2:1	0.26	90	60	58
29	8:1	0.26	60	60	62
30	14:1	0.26	60	180	60

Table 3.13.3- ANOVA for Response Surface Quadratic model

Source	Sum of Squares	Df	Mean Square	F Value	p-value	
Model	2847.37	14	203.38	5.16	0.0003	**significant**
A-Methanol to oil Ratio	72.37	1	72.37	1.83	0.0136	
B- Catalyst Concentration	190.67	1	190.67	4.83	0.0440	
C- Temperature	19.64	1	19.64	0.4980	0.0412	
D-Time	147.27	1	147.27	3.73	0.0024	
AB	72.25	1	72.25	1.83	0.0256	
AC	121.00	1	121.00	3.07	0.0303	
AD	132.25	1	132.25	3.35	0.0470	
BC	9.00	1	9.00	0.2282	0.0398	
BD	110.25	1	110.25	2.80	0.0153	
CD	1.0000	1	1.0000	0.0254	0.0256	
A²	424.96	1	424.96	10.77	0.0050	
B²	607.06	1	607.06	15.39	0.0014	
C²	324.60	1	324.60	8.23	0.0117	
D²	35.34	1	35.34	0.8959	0.3589	
Residual	591.60	15	39.44			
Lack of Fit	450.76	10	45.08	1.60	0.3149	**not significant**
Pure Error	140.83	5	28.17			
Cor Total	3438.97	29				

$R^2 = 0.876$, Std. Dev. = 6.28,   C.V. % = 8.65, Adeq Precision = 9.47

3.13.3. Interaction of variables on transesterification Reaction

3.13.3.1. Combined interaction of oil to methanol ratio and catalyst concentration

The combined interaction of methanol to oil ratio and catalyst concentration was studied while other reaction variables reaction time (2 h) and temperature (80 ° C) were held constant. The Met:Oil and catalyst concentration mutual influence is depicted as a 3D figure in Figure 3.13.7a. The greater yield of 94% was achieved at Run 13 with a 8:1 and catalyst loading 0.26 wt.%. Increasing the molar ratio to 14:1 and catalyst concentration of 0.60 wt.% lower resulted in a somewhat lower yield of 70% (Run 4). With a 0.95 wt.% increase in catalyst concentration, a further drop of up to 64% was seen (Run 10). When the amount of catalyst was increased to 0.95 wt.% at lower molar ratio constant of 2:1, the yield fell to 58%. (Run 18). Owing to the formation of undesirable reaction products, it was shown that increasing the catalyst amount decreased biodiesel yield. The reversible glycerolysis reactions, which include mixing and solubilizing glycerol in methyl ester and encouraging glycerol recombination with FAME, lead to the reformation of monoglycerides in the reaction, mixture, and solution (Hasan et al., 2019). With a p-value (<0.05) of 0.0256, the ANOVA findings show that the influence of the Met:Oil and catalyst load is not statistically significant.

3.13.3.2. Combined interaction of oil to methanol ratio and reaction temperature

The combined impact of the reaction temperature and the Met:Oil ratio is displayed in Figure 3.13.7b. When the transesterification temperature was raised to 90°C with a catalyst amount of 0.26 wt% and a 8:1 Met:Oil, the output of methyl ester was boosted by up to 94%. A lower yield of 89% was observed with a low Met:Oil of 2:1 at the same temperature (90 ∘C) (Run 8). Yield of 70% was obtained with a comparable reaction temperature (60 ∘C) and increased molar ratio (up to 14:1) (Run 15). However, at run number 22, maintaining the same Met:Oil of 14:1 while increasing the temperature to 120 °C significantly lowers the biodiesel production (64%). This is because evaporation of the amount of methanol exceeding the required operating temperature of 70 ° C. (Moreira et al., 2020). Based on the findings, it was found that the relationship between temperature and Met:Oil is significant, with a p-value of 0.0303 (<0.05).

3.13.3.3. Combined interaction of oil to methanol ratio and reaction time

A 3D depiction of the relationship between the Met:Oil and reaction time can be seen in Figure 3.13.7c. Controlling additional reaction variables including temperature and catalyst concentrations, the parametric relationship of the Met:Oil and time on the synthesis of biodiesel was studied. The greatest yield of 94% was observed at 120 min, a molar ratio of 8:1, a catalyst concentration of 0.26 wt.%, and a transesterification reaction temperature of 90 °C (Run 13). A higher Met:Oil of 14:1 with 60 min at Run 25 results in a reduced yield of 80% while keeping the other two reaction parameters constant. This is what causes the enhanced interaction of triglycerides with additional alcohol during transesterification. In contrast, run number 28 produces much less biodiesel (58%) due to a shorter reaction time of 60 min combined with a lower molar ratio of 2:1. Most likely, there wasn't enough time for the reactant to react properly, which resulted in insufficient product conversion. Yield was lowered to 60% at a 14:1 molar ratio and a 180 min reaction duration because elevating the amount of alcohol above its predetermined limit increased glycerol solubility and made it difficult to remove it from synthetic biodiesel due to insufficient methoxide solution to react with oil (Run 30) (Hammouda et al., 2017). The ANOVA results showed a strong relationship between the molar ratio and time, which was deemed significant with a *p*-value of 0.05 (0.0470).

3.13.3.4. Combined interaction of catalyst concentration and reaction temperature

Temperature and catalyst concentration are the two key reaction variables in transesterification. Both are crucial in controlling the transesterification reaction rate. The combined impact on the yield of FAMEs is seen in Figure 3.13.7d. A strong inverse link between catalyst concentration and reaction temperature on FAMEs yield was shown by the 3D plot's consistent lines. The catalyst concentration of 0.26 wt.%, the temperature of 90 ∘C, the duration of 120 min, and the molar ratio of 8:1 of resulted in the greatest yield of 94% (Run 13). It adheres to the Arrhenius equation, which stipulates that raising the reaction temperature gradually enhances the chemical reaction and raises the yield of methyl ester (Iravani and Varma 2020). Using a higher catalyst concentration (0.605 wt.%) and a temperature of 60 °C at Run 12 rendered yield up to 70%. A poor yield of 55% was achieved at 120 °C and 0.95 wt.% catalyst concentration (Run 2). Additionally, Run 6 lowest yield of 53% was attained at a higher

temperature of 120 °C and a catalyst concentration of 0.95 wt.%. According to the findings of the ANOVA, the combined influence of temperature and catalyst concentration on methyl ester yield was significant with a *p*-value of 0.0398 (<0.05) and showed a strong mutual connection.

3.13.3.5. Combined interaction of catalyst concentration and reaction time

The combined effect of catalyst concentration and reaction time on transesterification is depicted as a 3D plot in Figure 3.13.7e. Both factors have a similar impact on biodiesel yield. Up until optimal values were obtained, methyl ester yield increased as reaction temperature and catalyst concentration increased. With 0.2 wt.% catalyst concentration, 120 min a constant 8:1 molar ratio, and a temperature of 90°C, the highest yield of 94% FAME was obtained (Run 13). The yield of 70% was obtained at 60 min with catalyst concentration of 0.605 wt.% (Run 9). The transesterification reaction could not be completed in a fast reaction time even with a high catalyst loading (0.95 wt.%), which reduced the amount of biodiesel produced (Run 11). At Run 14, a yield loss of 60% and a 180 min reaction time were anticipated. With a *p*-value of 0.0153 (<0.05), the ANOVA findings showed that the combined influence of time and catalyst concentration on methyl ester yield was significant.

3.13.3.6. Combined interaction of reaction time and reaction temperature

In a 3-D plot in Figure 3.13.7f, the combined effects of reaction time and temperature on the transesterification reaction are shown. Due to an increase in mass interaction, FAMEs synthesis increased as time and reaction temperature were raised up to a specific point (Ewis et al., 2020). At Run 13, the greatest yield (94%) was obtained over a 120 min period at an ambient temperature of 90 °C using a constant molar ratio (8:1) and catalyst concentration (0.26 wt.%). A 76% drop in methyl ester synthesis was anticipated with a reaction duration of 60 min and a higher temperature of 90°C (Run 20). Lower biodiesel percent yield is the outcome of the chemical process of biodiesel hydrolysis being accelerated by higher temperature and reaction time into polar methanol and acids in the reacting mixture (Liu et al., 2008). The lowest yield of methyl ester (59%) was reported at a lower temperature of 60°C for a period of 60 min (Run 29). A 70% yield of biodiesel was obtained at the lowest reaction temperature of 50°C and the longest period of 180 min (Run 3). According to the findings of the ANOVA, the interaction between

time and temperature and biodiesel yield was found to be significant with a p-value (0.0089) 0.05.
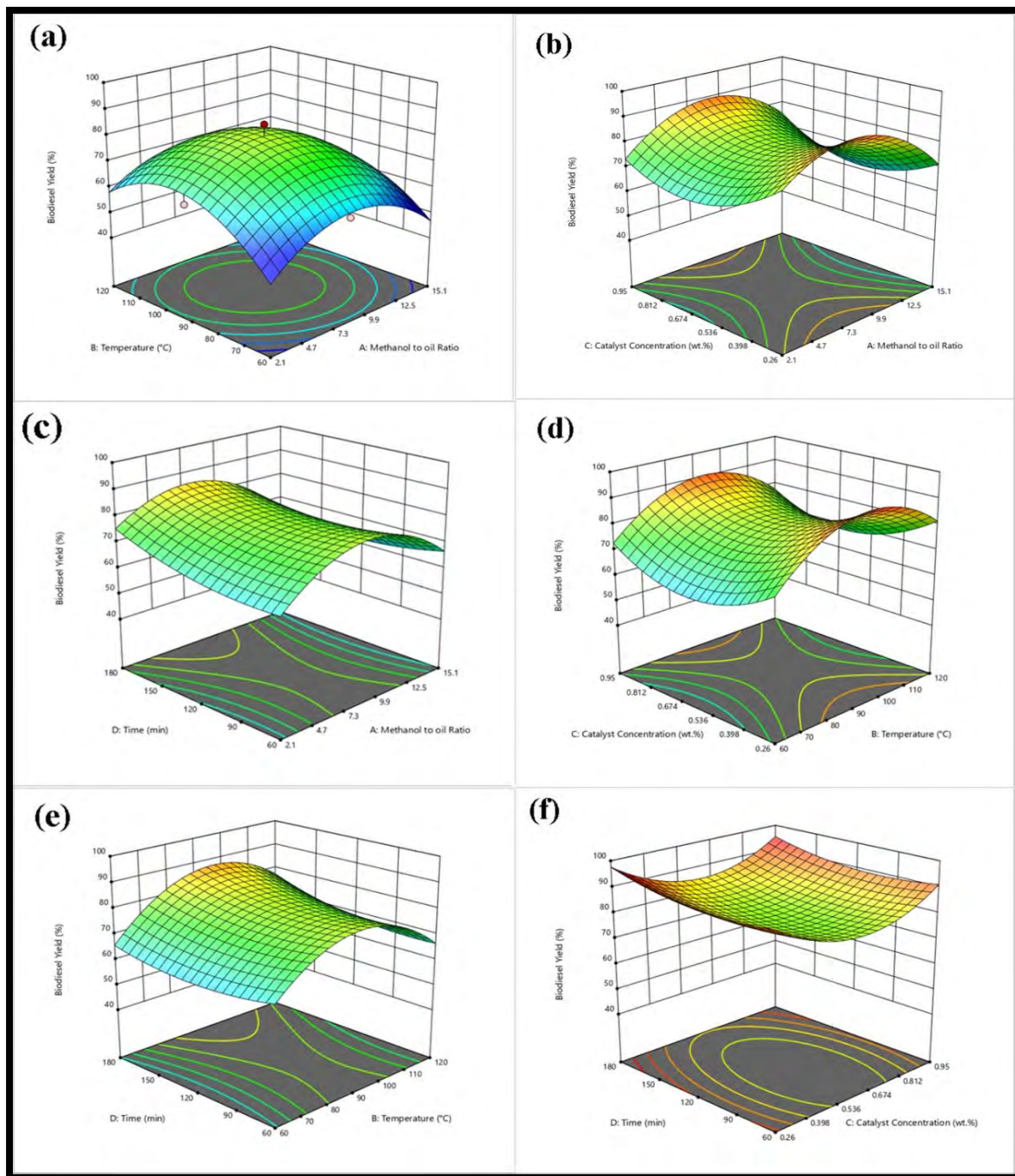
Figure 3.13.7 Influence of the reaction parameters of Transesterification on biodiesel yield

3.13.4. Methyl Ester Characterization

3.13.4.1. FT-IR analysis

FT-IR is the most significant analysis for determining whether methyl ester is still present in a substance after a transesterification procedure. The FT-IR technique is used to analyze various functional groups as well as the multiple bands that correspond to bending and stretching vibrations in a synthetic sample of methyl ester. The FTIR spectra of biodiesel and Cannabis sativa seed oil are shown in Figure 3.13.8 (a) and (b), respectively. The characteristic peak of the carbonyl group appeared at 1743.57 cm^{-1}, which was confirmed by the NMR spectra of the methyl ester. The carbonyl group was found at 1740 cm-1 in the spectra of *Trachyspermum ammi* methyl ester (Adewuyi, 2020). Stretching vibrations of CH_3 and CH_2 were found in the biodiesel's FT-IR spectra at 2853.81 cm^{-1} and 2923.35 cm^{-1}, respectively. The bending vibrations of these groups were determined to be 1435.82 cm^{-1}, 1244.58 cm^{-1}, and 844.69 cm^{-1}, respectively. The C-H stretching vibration was detected in the FTIR spectra of seed oil at 3331.06 cm^{-1}, 2853.75 cm^{-1}, and 2923.63 cm^{-1}. It was determined that the FTIR of TASO and FAMEs were nearly identical, with a few tiny variations and shifts that may be used to distinguish them. The conversion of triglycerides into fatty acid methyl esters was further confirmed by the elimination of oil spectrum peaks at 2854.24 cm-1, 1244.53 cm-1, and 519.87 cm^{-1} wavelengths in the spectra of *Trachyspermum ammi* methyl ester.

3.13.4.2. NMR Analysis

Figure 3.13.9 (a and b) displays the ^{1}HNMR and ^{13}CNMR of TABD. The prominent peak of the (- OCH_3) methoxy group, which appeared at 3.676 ppm in the ^{1}HNMR spectrum of the biodiesel, was used to confirm the synthesis of FAMEs in the sample. At 2.313–2.338 ppm, a triplet peak for the (-CH_2) methylene proton was visible. At 1.582-1.651 ppm, the singlet peak of aliphatic fatty chain protons called methylene (CH_2) developed. The spectra showed peaks of terminal methyl protons at 0.890. In the spectra of methyl ester, a signal peak of (-CH_2-) allylic hydrogen appeared at a value of 2.027 ppm, suggesting two hydrogen atoms per non-conjugated double bond. The synthesis of FAMEs from *Trachyspermum ammi* seed oil has been

demonstrated by precisely described peaks in the ^{1}HNMR spectrum. In a similar vein, 92% of triglycerides were converted into fatty acid methyl esters.

The ^{13}CNMR spectroscopy was used to analyze the structural characteristics of the methyl ester of *Trachyspermum ammi* seed oil, including the existence of carbonyl (-COO) and C-O, which are shown in Figure 3.13.9b. The methoxy group's carbon signal peak in the spectrum of biodiesel appears at 51.16 ppm. At 77.48-76.63 ppm, the carbonyl group (C-O) peak was found. At 29.11-29.29 ppm, a signal for a long $(-CH_2-)_n$ ethylene chain carbon was detected. At 174.37 ppm, the characteristic signal for the (-COOH) carbonyl group was detected. Signals connected to the inner nun-conjugated carbon atom at 127.01 ppm were found to have unsaturation (-CH=CH-) in spectra. Exterior nun-conjugated carbon (-CH=CH-) was suggested by the signal at (ppm) 129.55-129.78. In the ^{13}CNMR spectrum, a signal for $(-CH_2-s)$ aliphatic methylene carbon was discovered at 27.22 ppm.

3.13.4.3. GC-MS of Methyl ester

It is believed that biodiesel's quantity and chemical makeup significantly affect the fuel's physical and chemical characteristics. Because the carbon chain has been lengthened in biodiesel, it has a greater cetane number and viscosity (Akubude et al., 2019). Fatty acid methyl esters were quantified and the composition of TASO was determined using GC-MS to guarantee the quality of the biodiesel that was produced. GC-MS analysis is the most crucial factor in assessing if a biomass source is suitable for biodiesel synthesis. Larger quantities of unsaturated fatty acids are considered harmful since they stifle gasoline engines (Tan et al., 2017). Four distinct FAMEs were found in in the GC-MS spectra of the CSME, and they were confirmed using the library match program NO. NIST02, as shown in Figure 3.13.10. In the GCMS spectrum of the marijuana biodiesel, 7 main peaks were designated. The methyl ester of 5, 8-Octadecadienoic acid methyl ester (C18:2) was identified as the main fatty acid with the highest abundance. Dodecanoic acid methyl ester (C12:0) and Octadecanoic acid, methyl ester (C18:0), two saturated fatty acids, were detected in the spectrum. The primary unsaturated fatty acids found in TABD were 5, 8-Octadecadienoic acid methyl ester (C18:2)   and   9-Octadecenoic

acid, (2)-methyl-, methyl ester (C18:1). The results of the GC/MS spectrum showed that *Trachyspermum ammi* seed oil is suitable for the production of industrial biodiesel.
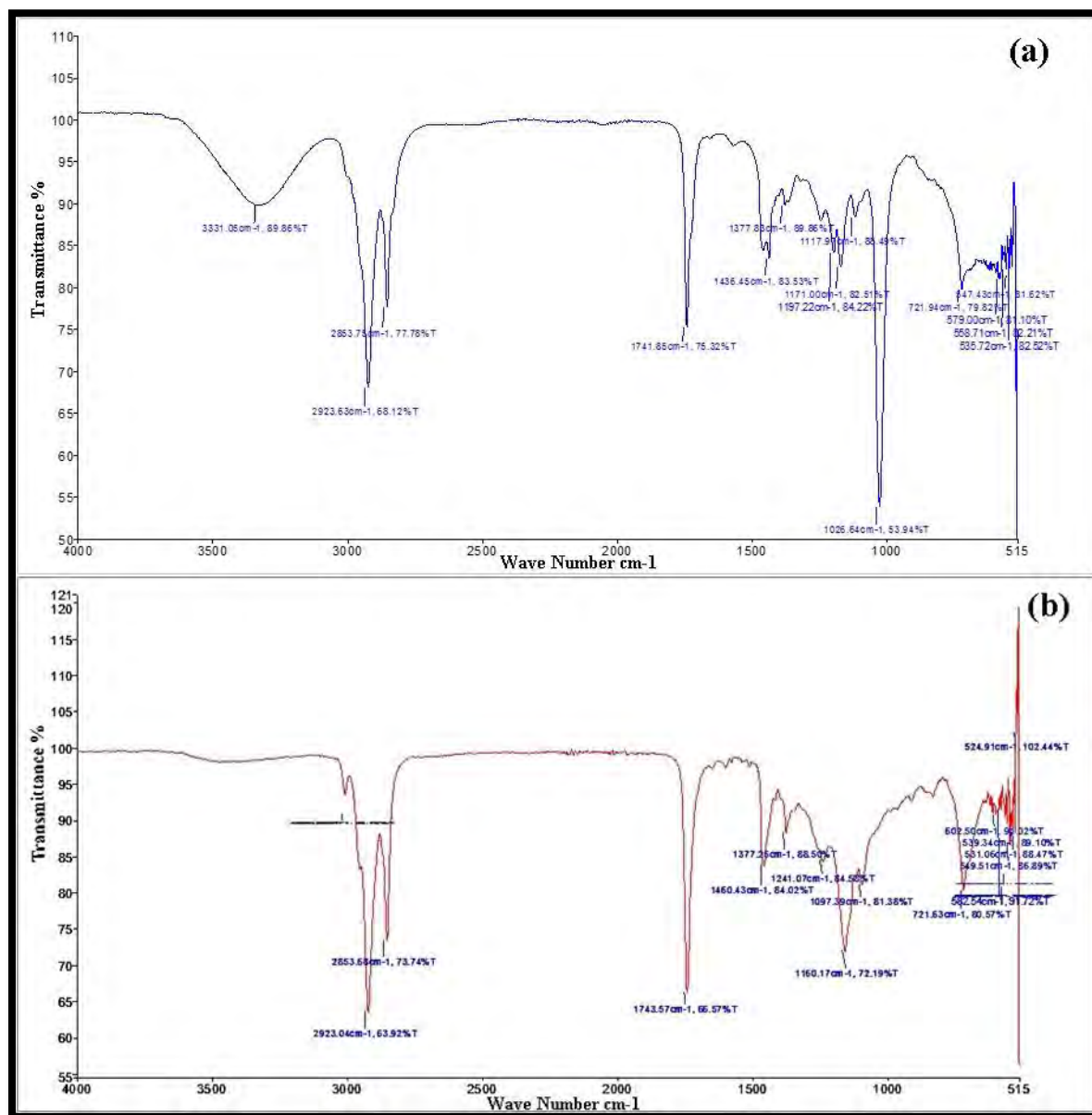
Figure 3.13.8 FTIR spectrum of *Trachyspermum ammi* **(a)** seed oil and **(b)** biodiesel
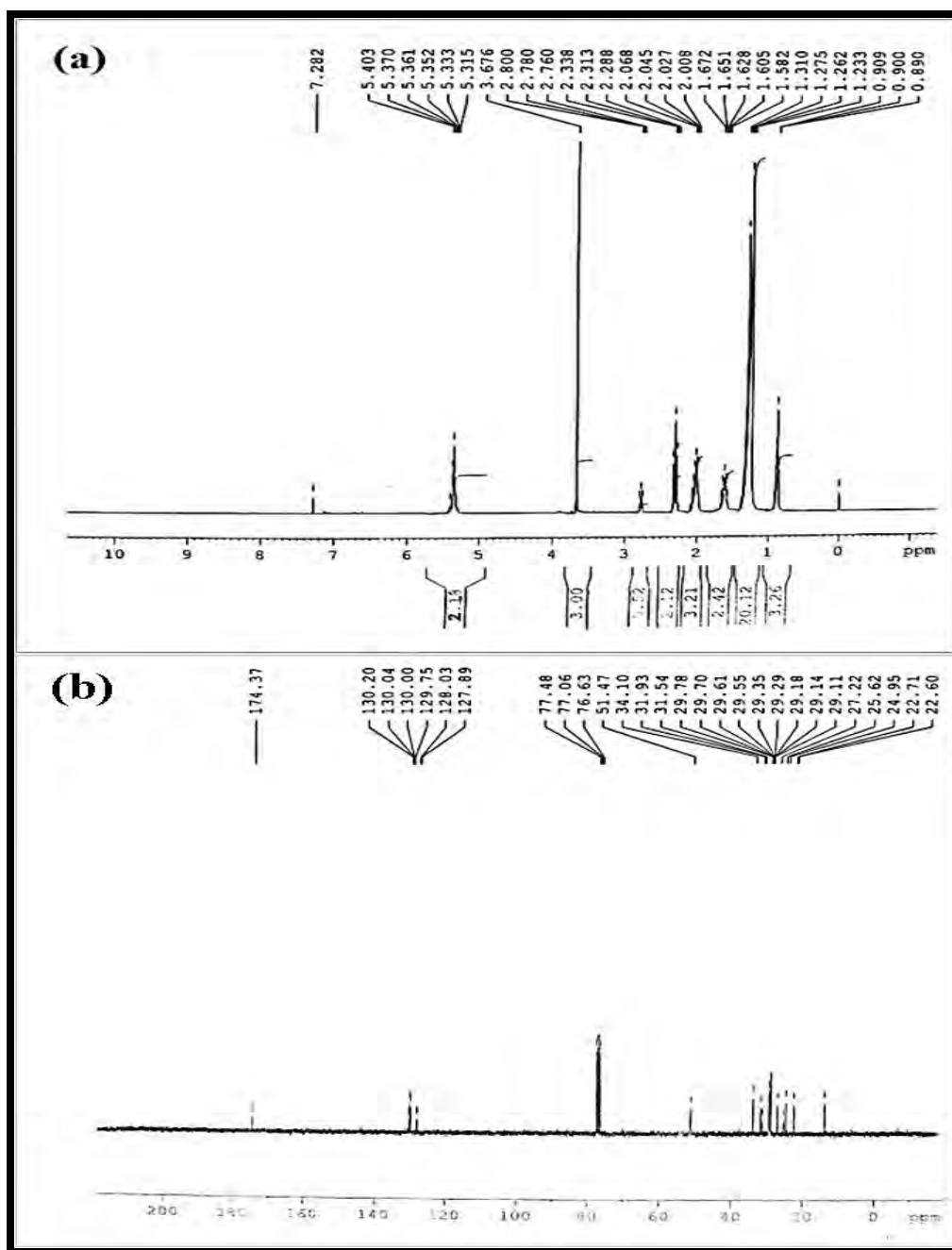
Figure 3.13.9 (a) ^{1}HNMR and **(b)** ^{13}CNMR of *Trachyspermum ammi* biodiesel
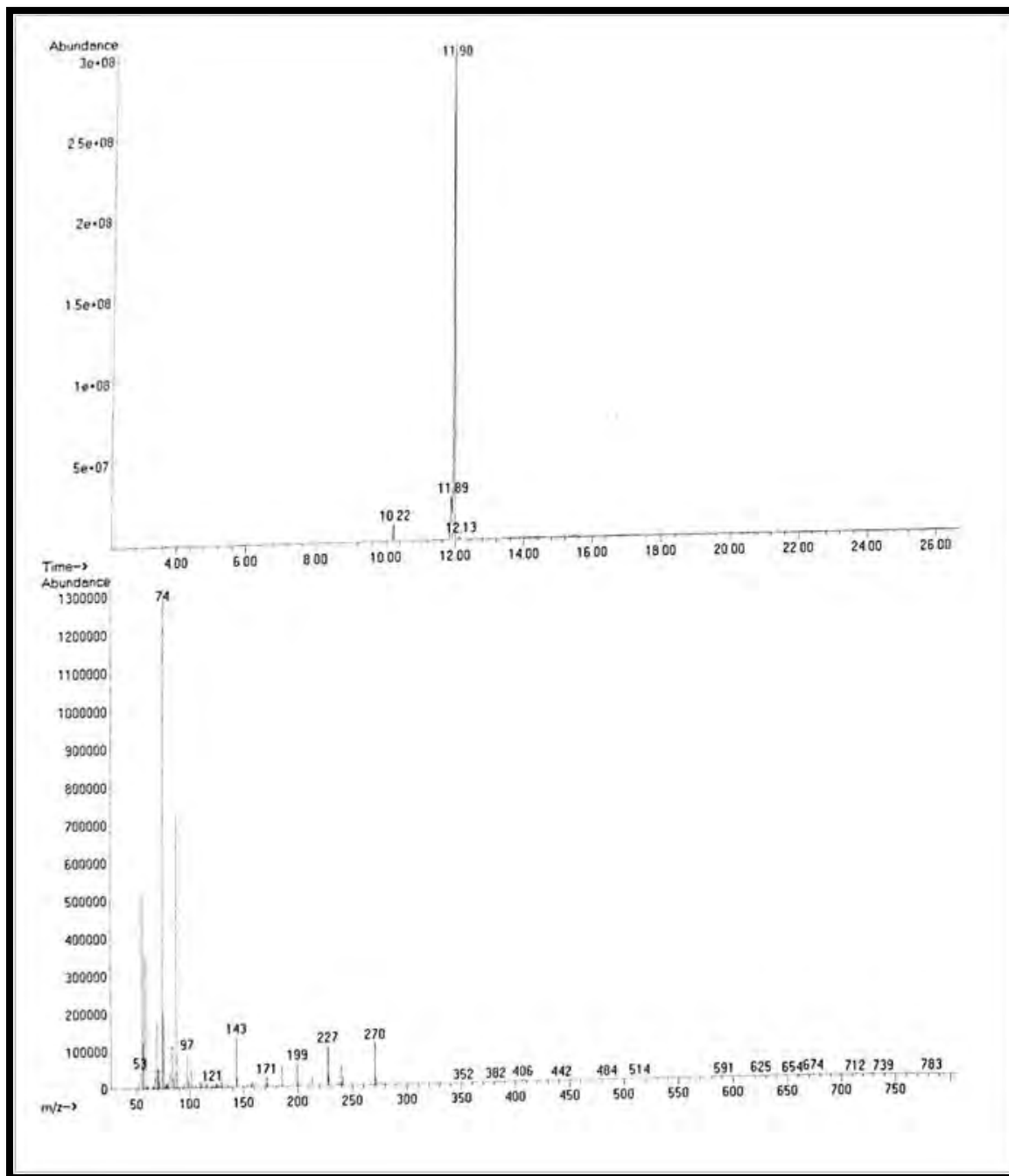
Figure 3.13.10 GC-MS spectrum of *Trachyspermum ammi* biodiesel

3.13.5. *Trachyspermum ammi* biodiesel fuel properties

Because of the efficiency of engines, biodiesel should have similar qualities and characteristics to petroleum diesel (Sedghamiz et al.,2019). When the fuel properties of *Trachyspermum ammi* seed oil were examined, it was found that they were a good match for international standards including EN 14214, ASTM D-6571, and China GB/T 20828-2007. The pour point, acid value, viscosity, flash point, density, cloud point, and sulfur content of biodiesel fuel were all examined. Table 3.13.4 compares the fuel properties of biodiesel made from *Trachyspermum ammi* to global standards.

One of the key characteristics of biodiesel that has a negative effect on engine performance is acid number. The amount of free fatty acids in diesel determines the acid number; the more free fatty acids, the higher the acid value. In our current study, the acid value of *Trachyspermum ammi* biodiesel was 0.124 (mg KOH/g), which was much lower than the acid value of jatropha biodiesel, which is 0.4 mg KOH/g (Gandhi and Gogate 2021). An additional important feature of gasoline is kinematic viscosity. It negatively affects the combustion chamber's ability to atomize diesel fuel as well as the engine's ability to produce soot and deposits (Kumar et al., 2020). According to ASTM D-445, the allowed range of viscosity for biodiesel is 1.9 to 6.0 mm^2/s. *Trachyspermum ammi* biodiesel meets international requirements with a kinematic viscosity of 5.45 (mm^2/s at 40°C). CSME is less viscous (4.24 mm^2/s) than coconut oil (Ong et al., 2019).

The presence of unsaturated fatty acids with more than two double bonds somewhat increases the density of biodiesel. The mean density of CSME at 15 °C was 0.814 (kg/m^3 at 40°C), which satisfies global requirements. Both the cloud and the pour point control how a diesel engine operates in the winter at lower temperatures. The pour is the temperature at which the interaction of the wax component with the fuel ceases, allowing fuel to flow (Ong et al., 2020). As the concentration of saturated fatty acids grows, the pour point also rises. Diesel has a pour point that ranges from 15 to 40 ◦C. In this investigation, the pour point and cloud points of *Trachyspermum ammi* were determined to be -8 and -10 ◦C, respectively. Biodiesel made from cannabis sativa has a lower pour point than biodiesel made from *Salvadora persica* and *Elaeagnus angustifolia* (Rozina et al., 2017). The pour and cloud points adhere to ASTM

standards. A fuel's flash point is the lower temperature at which it flashes when it is ignited with an ignition source. It has been discovered that biodiesel produced from biomass has a higher flash point than petroleum-based diesel, giving it an advantage during the saponification process. The average flash point of the cannabis sativa biodiesel used in the experiment was 99 °C, which is higher than the (55 °C) petroleum diesel.

     Trachyspermum ammi methyl ester's Sulphur concentration was found to be 0.0001% when compared to petroleum diesel, which is a very small amount and is within the range of 1 ppm (50 ppm). It was found that the amount was even smaller than previously known biodiesel feedstocks including cotton seeds, rape seeds, and safflower seeds (Galvan et al., 2020). When compared to petroleum fuels, biodiesel has a significant benefit in that it prevents pollution, burns cleanly, and is suitable for commercial production. Its sulphur level should be less than 1 ppm (Yunusa et al., 2021). It has been demonstrated that the biodiesel produced from *Trachyspermum ammi* has all the same fuel properties as EN 14,214, ASTM D-951, and China GB/T 20828-2007.

Table 3.13.4 Comparison of fuel properties of *Trachyspermum ammi* L biodiesel with international standards**.**

Property	Methods	*Trachyspermum ammi*		ASTM D-6751	EN-14214	China GB/T 20828-2007
		Mean	**St.Dev.**			
Color	Visual	1.5	-	2.0	-	-
Acid number (mg KOH/g)	ASTM-D974	0.124	0.2	≤0.5	≤0.8	≤0.5
Flash Point (°C)	ASTM-D93	99	1.5	≥93	≥130	≥120
Pour Point (°C)	ASTM-D97	-10	0.5	-15-16	_	_
Viscosity (mm²/s at 40 °C.)	ASTM-D445	4.24	0.1	1.9-6.0	_	3.4-5.0
Density (kg/m³ at 40 °C)	ASTM-D1298	0.814	0.3	≤120	_	≤120
Sulphur content (wt.%)	ASTM-D4294	0.0001	-	≤0.05	≤0.05	≤0.20
Cloud point (°C)	ASTM-D2500	-8	-1	-3.0-12	_	_

3.13.6. Catalyst Reusability

Catalyst reusability is one of the most important factors for extending benefit at industrial scale and reducing the number of hours required for resynthesizing. The stability and economic viability of the catalyst for industrial-scale biodiesel synthesis depend on its ability to be recycled in a reaction process. The kind and nature of the catalyst, as well as the techniques for separation, purification, and its transesterification, all affect how reusable a heterogeneous catalyst can be. This work examined the reusability of generated tungsten oxide nanoparticles under optimal reaction circumstances, including catalyst concentration (0.26 wt.%), Met:Oil of 8:1, temperature (90 °C), and reaction time 120 min. Recycled catalyst was used in a number of transesterification procedures to verify the catalyst's capacity for reuse. According to the results of the research, the catalyst efficiency decreased as the number of cycles increased. A maximum yield of 94% was achieved using a catalyst concentration of 0.26 wt. % in the first run, falling to 85% in the third run, 77% in the fourth run, and 70% in the fifth run. Leaching from glycerides and glycerol in the reacting mixture and poisoning of active sites were attributed for the decline in percent yield as the number of cycles of the nanocatalyst increased (Figure 3.13.11). Up to the seventh cycle, the catalyst's recyclability indicated that MnO_2 performed better. MnO_2 nanoparticles have been found to increase environmental sustainability from the standpoint of the circular economy.
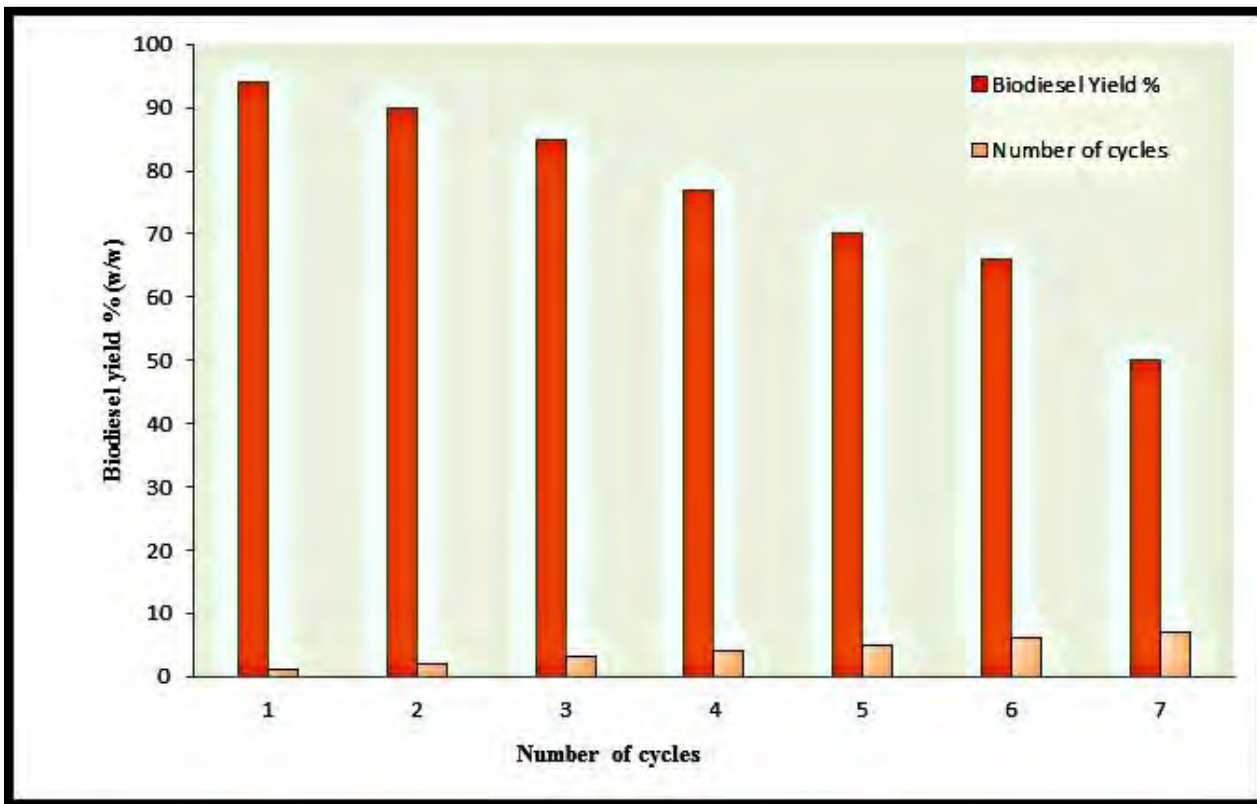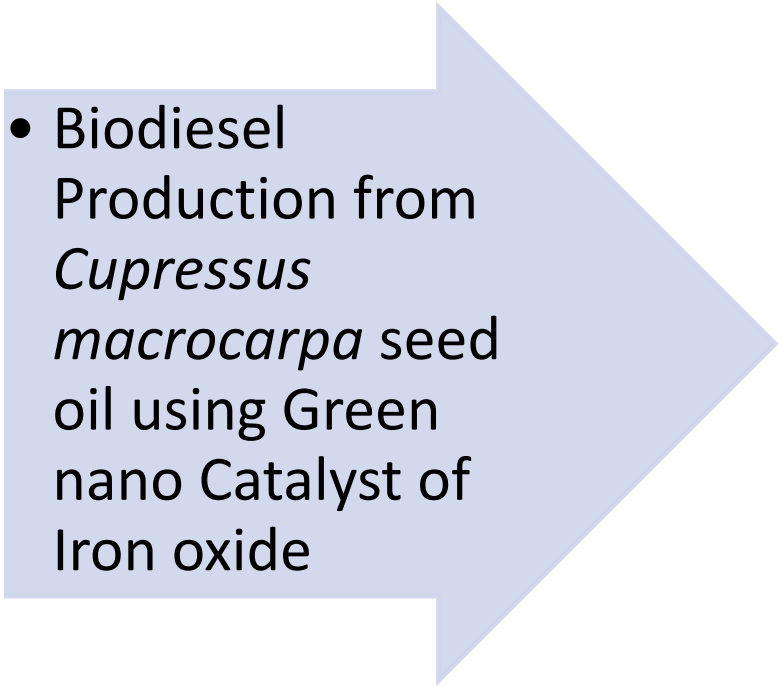
Figure 3.13.11 Reusibility of manganese oxide NPs in transesterification reaction

SECTION XIV

- Biodiesel Production from *Cupressus macrocarpa* seed oil using Green nano Catalyst of Iron oxide

Fe_2O_3 possess low toxicity, superparamagnetic characteristics, and ease of separation, magnetic properties which have drawn attention to their nanoscale particles for use in thermal therapy, drug delivery, and medical diagnostics such as magnetic resonance imaging (MRI). However, in current study Fe_2O_3 are used to catalyze transesterification reaction. Fe_2O_3 are efficiently synthesized with green mediated method using *Salvia moocroftiana* leaf extract.

3.14.1 Catalyst Characterization

Various techniques like XRD, SEM, TGA and EDX were used in our current study for characterization of green nano particles of Fe_2O_3.

3.14.1.1 X-Ray Diffraction (XRD) of Fe_2O_3

Powder X-Ray Diffraction technique was used to study crystalline structure of iron oxide nano-particles. XRD pattern of Fe_2O_3 has been shown in Figure 3.14.1. Green nanoparticles Fe_3O_4 were to have a face-centered cubic lattice crystalline structure. The diffracted Energy peaks of Fe_2O_3 nanoparticles recognized at 2θ values of 14.83◦, 20.35◦, 24.82◦, 29.87◦, 33.23◦ and 35.719◦ which corresponded to the lattice plane (004), (100), (012), (111), (114) and (110) *hkl* respectively.

Crystalline size of iron oxide nanoparticles by using at full width half maximum (FWHM) XRD pattern of most deep peaks at 2θ value of 24.82◦ (highest peak 012).

The average size of Fe_2O_3 nanoparticles was found 30 nm concluding that green particles Fe_2O_3 are Nano in nature. Results of X-Ray Diffraction and SEM of Fe_3O_4 nano-particles are aligned with one another.

3.14.1.2 Scanning Electron Microscopy (SEM) of Fe_2O_3

Surface electron microscopy technique was used to study surface morphology of Fe_2O_3 nanoparticles. SEM micrograph of Fe_2O_3 nano-particles at different magnification has been shown in Figure 3.14.2. It can be observed that nano-particles are uniformly distributed. Spherical and granular homogenous morphology was revealed from topical view of the nano-particles with slight agglomeration due to polarity and electrostatic attraction of particles. Presence of larger nano-particles in SEM micrograph indicated aggregation of small nano-

particles. SEM results of the current investigation are aligning with previously documented observations (Saqib et al., 2019).

3.14.1.3 Energy Diffraction X-ray (EDX) of Fe_2O_3

Elemental analysis of iron oxide nano-particles was carried out with Energy diffraction (EDX). EDX spectrum of iron oxide NPs has been shown in Figure 3.14.3. Peaks around 1 and 6.5 keV observed in the spectrum are associated to the binding energy of Fe whereas, peak at 0.5 keV is related to the binding energy of oxygen. Hence, presence of both iron and oxygen in the NPs was confirmed in the EDX spectrum. No other unrelated element was observed in the spectrum indicating the purity of nano-particles. Atomic percentage of oxygen and iron obtained from EDX quantification was found to be 49.28% and 51.72% respectively.

3.14.1.4 Fourier Transform Infrared Spectroscopy (FTIR)

FTIR spectroscopic analysis of iron oxide NPs was carried out to investigate various functional groups responsible for capping and stabilization of green nano-particles. FTIR spectrum of iron oxide NPs was studied in the mid infra-red region of 500-4000 cm^{-1}. FTIR spectrum of iron oxide NPs showed strong bands around 3445.4 cm^{-1}, 3217. 60 cm^{-1} and 2160.03 cm^{-1} which are attributed to H-O bending vibration while peak at 812.68 cm^{-1} and 1612.95 cm^{-1} are attributed to Fe-O stretch (Figure 3.14.4).

3.14.1.5 Thermogravimetric analysis (TGA) of Fe_2O_3

Thermo gravitational analysis (TGA) of iron oxide nano-particles was used to investigate its thermal stability and decomposition property. Thermogram of iron oxide NPs with corresponding derivative curve has been shown in Figure 3.14.5 a and b. Endothermic peaks of nano-particles are presented in derivative curve (wt. %) in Fig. 6b. Thermal decomposition was observed in three major stages. First stage of decomposition is attributed to dehydration and evaporation of adsorbed and surface water from nano-particles. About 0.223% loss in mass was detected in initial of decomposition at temperature range of 50-150 ∘C. Dehydration process was further continued to the second stage of decomposition up to 200 ∘C which further resulted in 0.92% loss in the mass of iron oxide. Beyond 200 ∘C straight line was observed till 750 ∘C indicating that no prominent change happened in the mass of nano-particles revealing high

thermal stability of the nanoparticles. However, a loss of 1.075% was detected in the third stage of decomposition at temperature range of 760-950 ◦C.
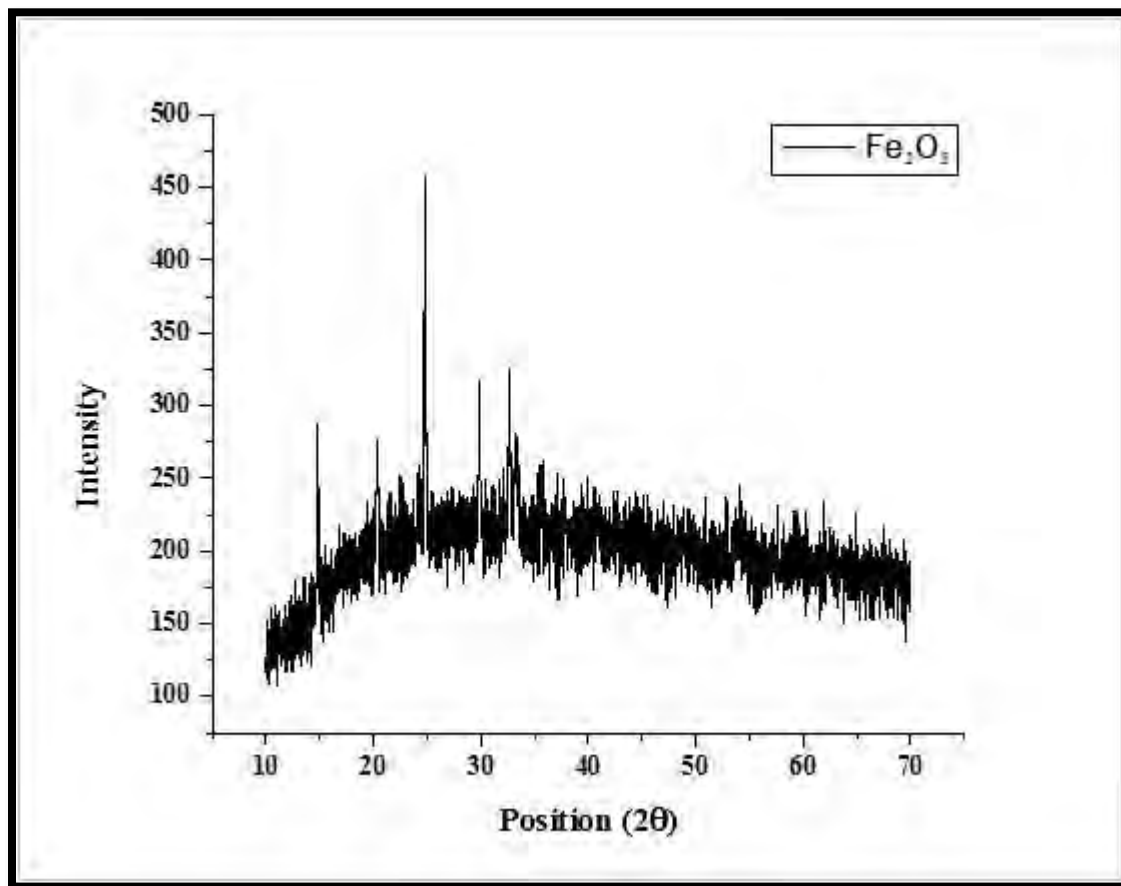
Figure 3.14.1 XRD pattern of calcined Iron oxide green nano particles
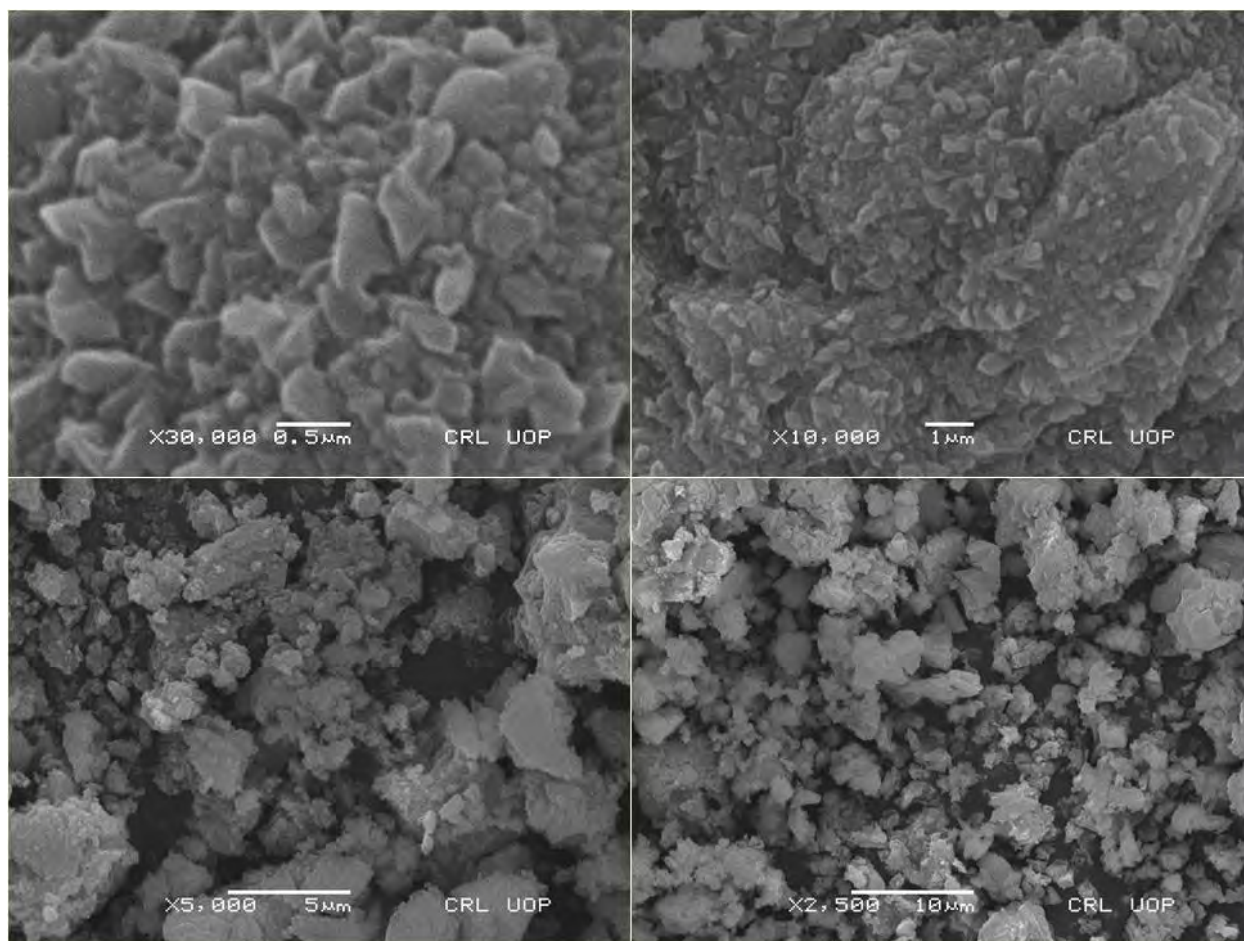
Figure 3.14.2 Scanning electron microscopy (SEM) of calcined Iron oxide green nano particles
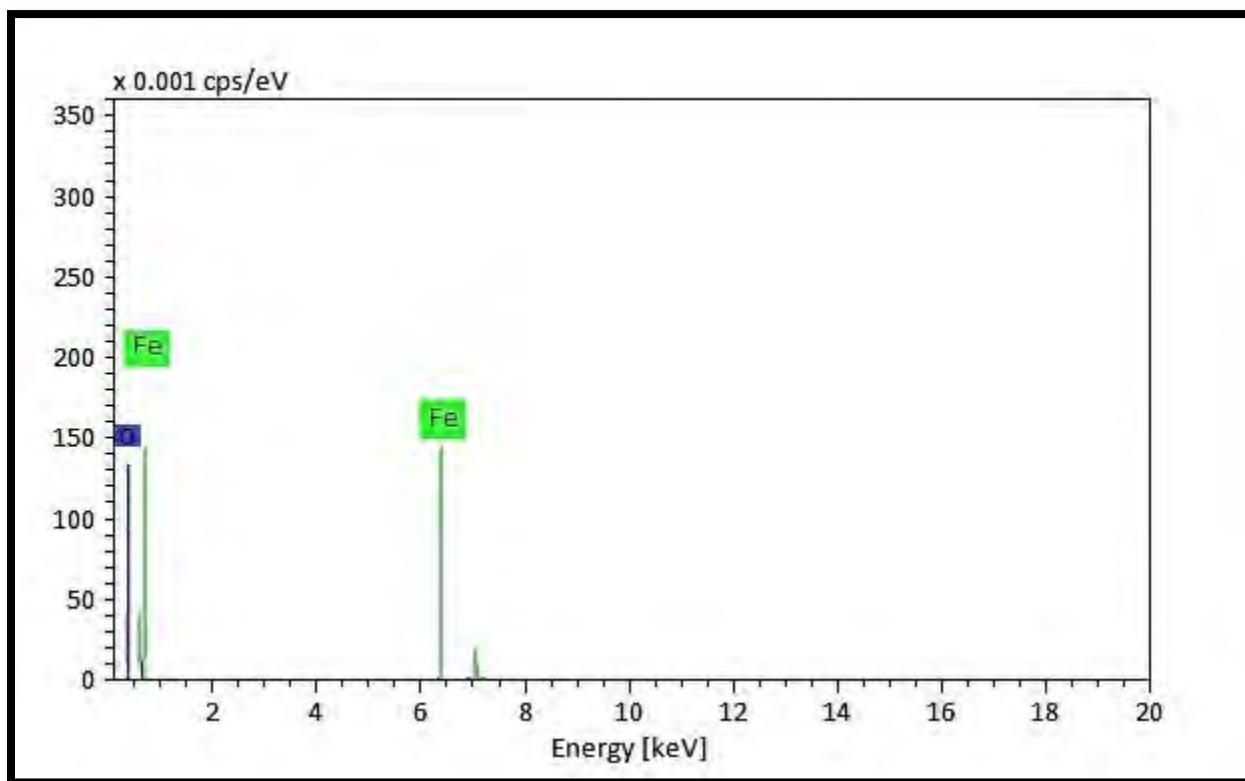
Figure 3.14.3 Energy diffraction X-Ray (EDX) of calcined Iron oxide green nano particles
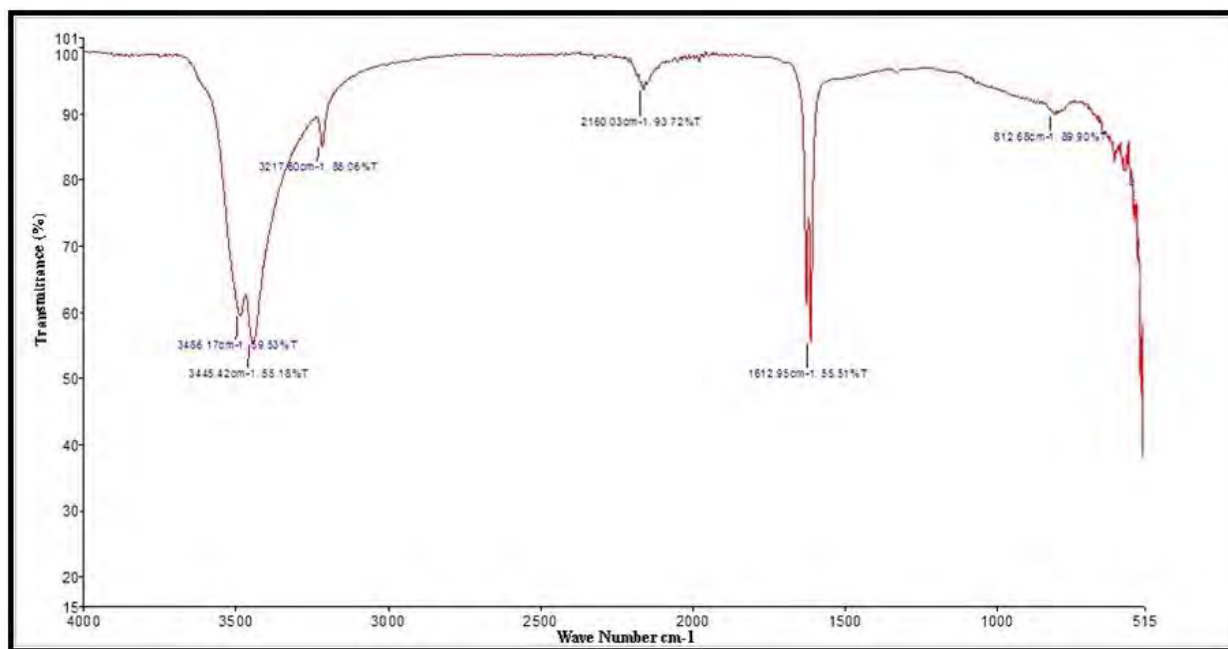
Figure 3.14.4 FTIR spectrum of Iron oxide green nano particles
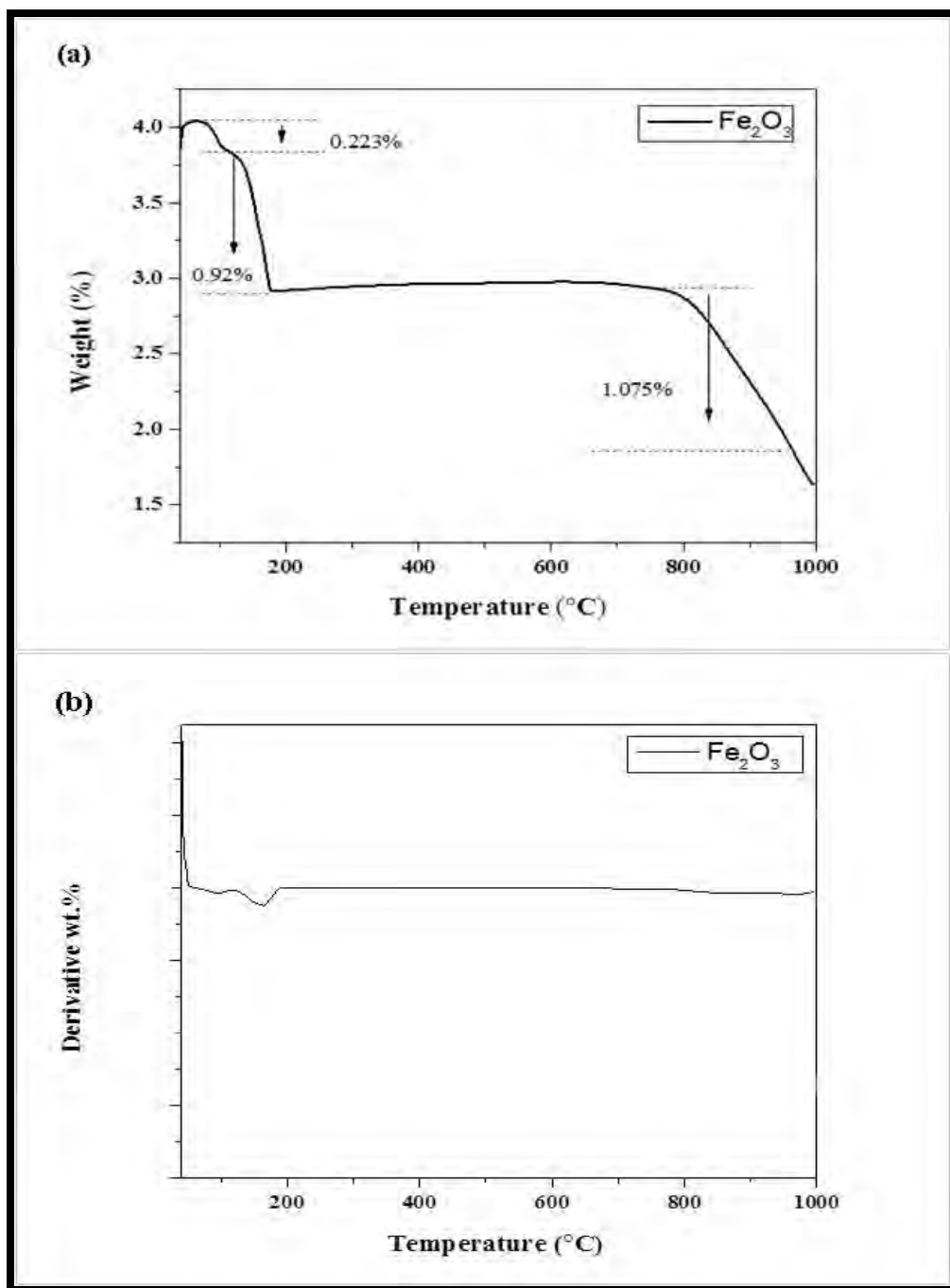
Figure 3.14.5 (a) TGA of Iron oxide green nano particles (b) derivative thermogram of Iron

oxide nano particles

3.14.2 Biodiesel synthesis *via* transesterification

In this study, methyl ester was synthesized from novel and non-edible seed oil of *Cupressus macrocarpa* using green nano-particles of iron oxide. Seed oil content of was 26% of total dry weight which is significantly higher than previously reported species (Yaşar et al., 2020). A considerably lower free fatty acid content of seed oil was 0.53 (wt. %) resulted in single step transesterification reaction. Previous literature has documented that FFA content of seed oil higher than 3% is undesirable and needs an additional step of acid esterification which results in limited conversion of triglycerides in to methyl esters during transesterification reaction (Zaharin et al., 2017). Consequently, *Cupressus macrocarpa* seed oil can be efficiently utilized for single step methyl ester formation. Transesterification of extracted seed oil was carried out with phyto-nano particles of iron oxide synthesized with aqueous leave extract of *Salvia moocroftiana*.

Optimal reaction conditions of transesterification were profoundly investigated using Response Surface Methodology in order to get maximum yield of methyl ester. Central composite design (CCD) was prepared using four independent variables of transesterification with lower and higher values such as catalyst concentration of 0.2-1.2 wt.% (A), temperature 60-150 ºC (B), methanol to oil molar ratio 3:1-16:1 (C), reaction time 60-180 min (D) as depicted in Table 3.14.1and Table 3.14.2. The comparison between predicted versus actual yield of methyl ester has been illustrated in Figure 3.14.6 which revealed that both of these values are distributed near the straight line demonstrating a good correlation among them. Detailed results of statistical analysis of variance of the Response Surface Quadric model have been presented in Table 3.14.3. Quadric model was declared significant with a small *p*-value of 0.0001 (<0.05). Moreover, lack of fit F-value of the quadric model was found not significant in relation to the pure error with a value of 1.06. Not significant lack of fit value is desirable for the quadric model with a chance of 52.29% that a Fit F-value this large could happen due to noise. Besides, among quadratic terms of the transesterification catalyst loading (A^2) was the most significant term with a p-value of 0.0004 (<0.05) followed by methanol to oil molar ratio (C^2) with p-value 0.0009. Predicted value of R² was 0.8311 close enough to the Adjusted R² of 0.9155 and the variance among them was found <0.2. Adequate Precision gave us the measure of signal to noise ratio of the model. It was found 10.3992 in the current model demonstrating that experimental model can

efficiently predict yield of methyl ester. A ratio greater than 4 is regarded as favorable. Polynomial equation (8) employed in the experimental model has been given below.

Biodiesel Yield (wt. %) = +83.88-3.21 *A-3.13 *B+0.1667 *C+1.80 *D+0.1250 *AB+1.58 *AC+0.6250 *AD-2.33* BC-1.87 *BD+2.62 *CD-14.13 *A²+1.87 *B²-12.71* C²+3.87* D² (20)

Table 3.14.1- Experimental design by central composite design for transesterification reaction

Process parameters	−1	+1
Catalyst loading (wt. %)	0.2	1.2
Temperature (ºC)	60	150
Methanol to oil molar ratio	3:1	16:1
Reaction time (min)	60	180

Table 3.14.2- Detailed experimental result for transesterification reaction of *Cupressus macrocarpa* biodiesel

Run	Factor 1 A: Catalyst amount (wt. %)	Factor 2 B:Temperature (ᵒC)	Factor 3 C:Methanol to oil molar ratio	Factor 4 D:Reaction Time (min)	Yield (wt. %)
1	0.7	105	9:1	120	80
2	0.2	150	16:1	180	60
3	0.7	60	3:1	60	67
4	1.2	150	3.1	180	55
5	0.2	105	9:1	120	70
6	1.2	60	9:1	180	69
7	1.2	150	16:1	60	57
8	0.2	60	3:1	180	65
9	0.7	60	9:1	180	58
10	0.2	60	9:1	120	68
11	0.7	150	9:1	120	90
12	0.7	150	9:1	120	77
13	0.2	60	3:1	120	66
14	0.2	60	9:1	180	89
15	0.2	60	16:1	120	55
16	0.7	105	3:1	120	69
17	1.2	60	9:1	180	62
18	0.7	105	16:1	120	64
19	0.2	150	3:1	60	75
20	0.7	105	16:1	120	72

21	0.7	60	9:1	60	57
22	0.2	60	16:1	180	80
23	1.2	105	9:1	120	68
24	0.7	60	16:1	60	65
25	1.2	150	3:1	60	55
26	0.7	105	9:1	120	80
27	1.2	150	16:1	180	60
28	0.7	60	9:1	60	85
29	0.7	60	9:1	120	93
30	0.7	60	16:1	120	67

Table 3.14.3- ANOVA for Response Surface Quadratic model

Source	Sum of Squares	Df	Mean Square	F-value	p-value	
Model	3602.97	14	257.35	10.84	< 0.0001	significant
A-Catalyst amount	185.31	1	185.31	7.81	0.0144	
B-Temperature	176.44	1	176.44	7.43	0.0164	
C-Methanol to oil molar ratio	0.5000	1	0.5000	0.0211	0.6867	
D-Reaction Time	58.33	1	58.33	2.46	0.1393	
AB	0.2500	1	0.2500	0.0105	0.0197	
AC	40.14	1	40.14	1.69	0.0245	
AD	6.25	1	6.25	0.2633	0.6159	
BC	86.66	1	86.66	3.65	0.0768	
BD	56.25	1	56.25	2.37	0.0460	
CD	110.00	1	110.00	4.63	0.0493	
A²	515.99	1	515.99	21.74	0.0004	
B²	9.08	1	9.08	0.3825	0.5462	
C²	412.71	1	412.71	17.39	0.0009	
D²	38.80	1	38.80	1.63	0.2219	
Residual	332.34	14	23.74			
Lack of Fit	241.14	10	24.11	1.06	0.5229	not significant
Pure Error	91.20	4	22.80			
Cor Total	3935.31	28				

$R^2 = 0.9155$, Std. Dev = 4.87, C.V. % = 6.89, Adeq Precision = 10.3992
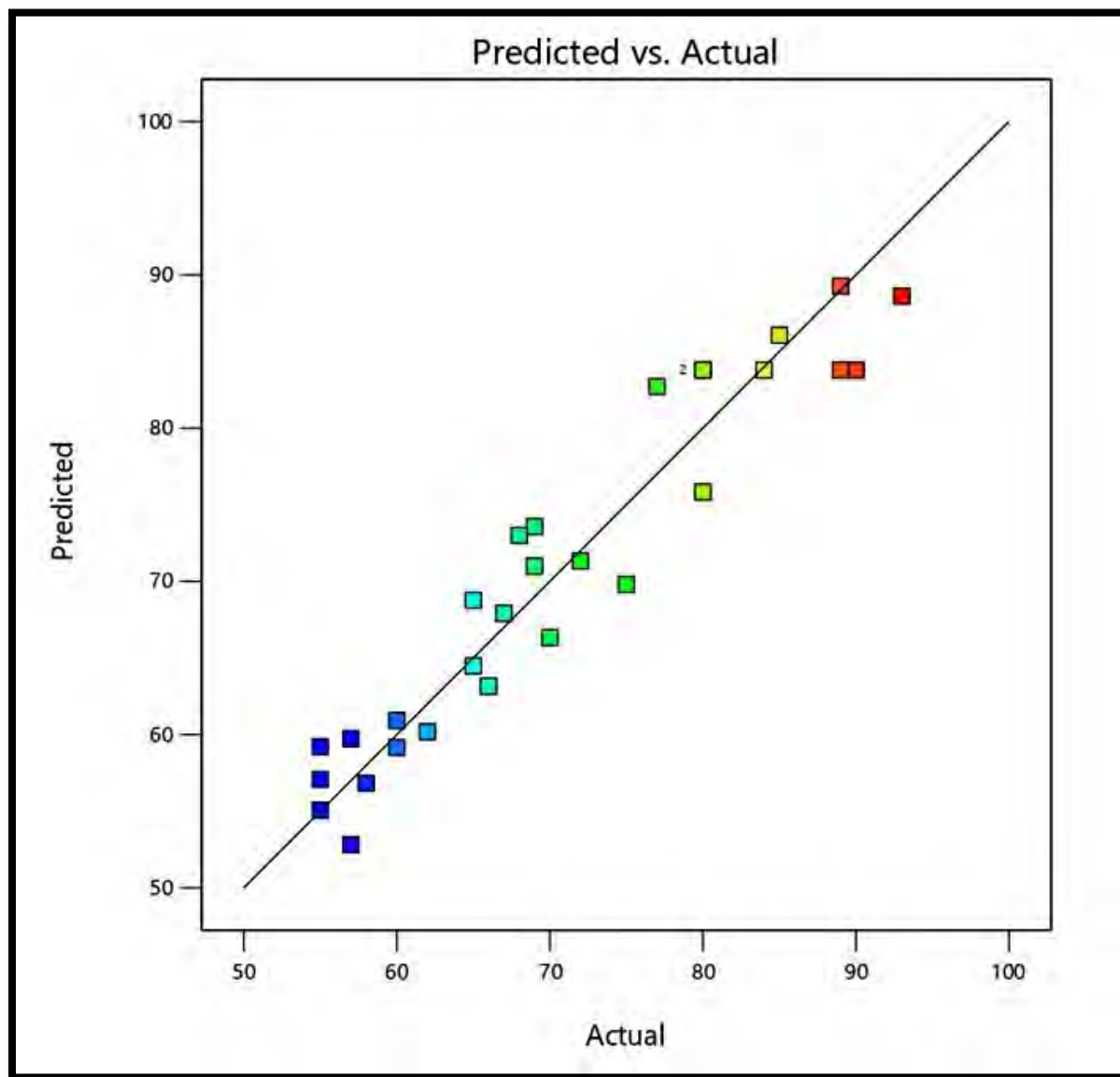
Figure 3.14.6 Comparison between the experimental biodiesel yield and the predicted yield of the model
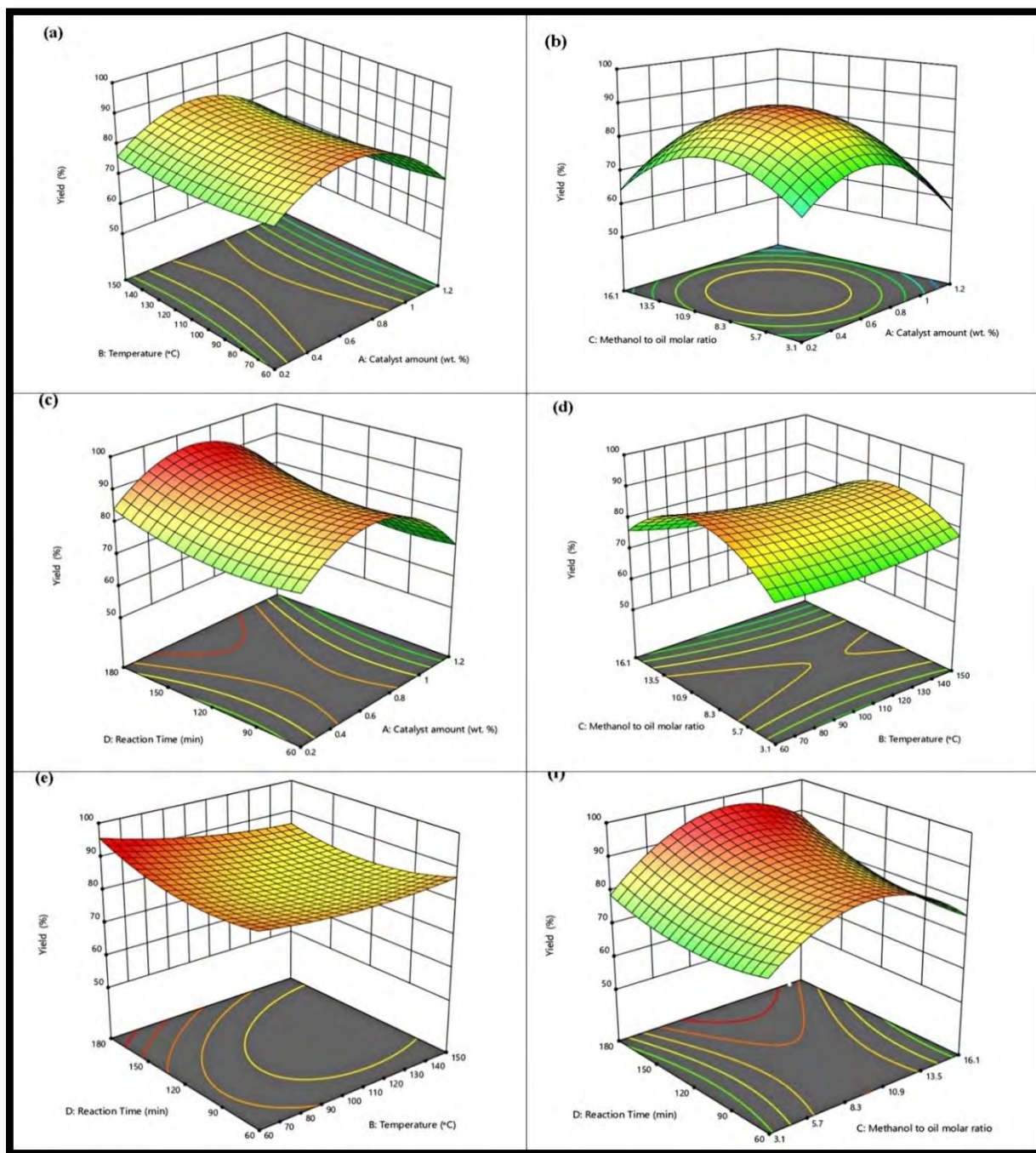
Figure 3.14.7 Influence of the reaction parameters of *Cupressus macrocarpa* biodiesel.

3.14.3. Influence of reaction parameters on transesterification reaction

3-Dimensional response surface plots for the product have been presented in Figure 3.14.7, a, b, c, d, e and f. These plots help to understand various interactive effects of variables, thereby contributing to the identification of maximum response levels. In general, biodiesel yield is expected to increase under optimal reaction conditions and sudden yield drop beyond optimal levels has been observed. Subsequent sub-sections could explain the interactive effects of the transesterification process.

3.14.3.1 Combined influence of catalyst loading and reaction temperature

The combined effect of catalyst loading and reaction temperature of CMBD has been presented in Figure 3.14.7a. Maximum yield of 93% was obtained at catalyst loading of 0.7 wt. % and temperature 60 (^{o}C) while keeping reaction time (120 min), methanol to oil ratio (9:1) constant (Run 29). 80% yield was achieved at catalyst loading of 0.7 wt. % and high temperature of 105 ^{o}C which implies that high temperature renders methyl ester formation due to low boiling point (65 ^{o}C) of methanol (Run 1). Yield was further reduced to 77% at maximum temperature of 150 ^{o}C and catalyst loading of 0.7 wt. % at Run 12. Lower catalyst loading of 0.2 wt. % and high temperature of 105 ^{o}C further reduced yield up to 70 % at Run 5. Reaction temperature of 60 ^{o}C with catalyst loading of 0.2 wt. % reduced yield to 68%. It was attributed to low catalyst loading which was found insufficient to complete transesterification reaction. High catalyst loading of 1.2 wt. % and temperature 105 ^{o}C resulted in lower yield of 68% at Run 23. This decrease in FAME content could be attributable to a decreased mass transfers and interaction of the reactants with the catalyst, which would cause emulsification leading to difficulties in separating end products and decreased FAME yield (Rahman et al., 2020). Mutual catalyst loading and reaction temperature was found significant in ANOVA results with p-value 0.0197 (<0.05). Similarly, independently catalyst loading was found significant with p-value 0.0144 and temperature with p-value 0.0164 (< 0.05).

3.14.3.2 Combined influence of methanol to oil molar ratio and catalyst loading

Combined interaction of molar ratio and catalyst loading during transesterification has been presented in the form of 3D plot shown in Figure 3.14.7b. Maximum yield of 93% was obtained at methanol to oil ratio 9:1 and catalyst loading of 0.7 wt. % at constant reaction time of 120 min and temperature 60 (^{o}C). Low yield of 68% was obtained at low catalyst loading of 0.2 wt. % and molar ratio of 9:1 at Run 10. It is because lesser amount of catalyst was found insufficient to continue transesterification till the end. Higher molar ratio of 16:1 and catalyst loading of 0.7 wt. % failed to complete transesterification and a yield 67% was obtained at Run 30. High concentration of methanol favors reversible reaction and consequently lowers methyl ester formation (Jahirul et al., 2021). It was further reduced to 55% with molar ratio of 16:1 and low catalyst loading of 0.2 wt. % at Run 15. Both low molar ratio of 3:1 and catalyst loading of 0.2 wt. % resulted in low yield of 66% at Run 13. Combine interaction of molar ratio and catalyst loading was found significant in ANOVA results with p-value 0.0245 (<0.05). However, independently catalyst loading was found significant with p-value 0.0144 and methanol to oil ratio was insignificant with p-value 0.6867 (>0.05).

3.14.3.3 Combined influence of reaction time and catalyst loading

Combined interaction between reaction time and catalyst loading has substantial effect on biodiesel yield during transesterification and are kept under consideration. In our current study various experimental trials were carried out to investigate this interaction. Mutual effect of reaction time and catalyst loading on transesterification reaction of *Cupressus macrocarpa* seed oil has been demonstrated in three-dimensional plot shown in Figure 3.14.7c. High yield of 93% was obtained at reaction time of 120 min and catalyst loading of 0.7 w. %t at constant temperature 60 ^{o}C and molar ratio 9:1. High reaction time 180 in and low catalyst loading (0.2 wt. %) resulted in yield of 89% at Run 14. Low reaction time of 60 min with catalyst loading of 0.7 wt. % further reduced yield up to 85% at Run 28. Catalyst loading of 1.2 wt. % and reaction time of 180 min rendered methyl ester yield to 62 % (Run 17). The percentage yield of methyl ester was further reduced to 77% at reaction time 120 min and low catalyst loading of 0.2 wt. % at Run 10 due to insufficient amount of catalyst to carry out transesterification. It is because the reaction of transesterification is tri-phasic (oil, methanol and catalyst) and sufficient amount of

thermal energy is required to facilitate the dispersion of particles in various stages and low catalyst loading failed to reduce activation energy to that level (Cruz et al., 2020).

The lowest

yield of 69% was achieved at maximum catalyst loading of 1.2 wt. % and reaction time of 180 min at Run 6. Higher catalyst loading for long period of time results in production of unwanted products during transesterification. In present investigation, combined effect of reaction time and catalyst loading was found not significant in the results of ANOVA with *p*-value (0.6159) > 0.05 for methyl ester formation.

3.14.3.4. Combined influence of Temperature and methanol to oil molar ratio

Methanol to oil ratio and reaction temperature is another important parametric interaction which has noticeable effect on biodiesel yield (Figure 3.14.7d). Maximum yield of 93% was obtained temperature 60 (^{o}C) and methanol to oil ratio 9:1 at constant catalyst loading of 0.7 wt. % and reaction time of 120 min. However, a sudden drop in yield was seen, beyond the optimal molar ratio and reaction temperature. This decrease in output could be related to the change in reaction to the opposite direction (Changmai et al., 2021). It was reduced to 90% with high temperature of 150 ^{o}C and molar ratio of 9:1 as methanol starts boiling beyond 65 ^{o}C affecting its proper mixing with triglycerides and consequent low product formation (Run 11). 80% yield was achieved with higher temperature of 105 ^{o}C and molar ratio of 9:1 at Run 1. Low yield of 69% was obtained with lower molar ratio of 3:1 and temperature 105 ^{o}C at Run 16. It was further reduced to 64% at Run 18 with a higher molar ratio of 16:1. Results of ANOVA declared that combine effect of these parameters is not significant with p-value (0.0768) greater than 0.05. However, individual temperature was found to be significant with p-value of 0.0164 and molar ratio was not significant with a p-value of 0.6867.

3.14.3.5. Combined influence of Temperature and reaction time

The combined effect of temperature and reaction time of transesterification has been illustrated in Figure 3.14.7e. High yield of 93% was obtained at temperature 60 (^{o}C) and reaction time of 120 min at constant methanol to oil ratio 9:1 and catalyst loading of 0.7 wt. %. Percent yield of methyl ester was reduced to 80% with raise in temperature up to 150 ^{o}C and same

reaction time 120 at Run 26. Conversely, above the limit level (> 60 °C), reaction temperature triggers methanol gasification leading to reduction in content of FAMEs. The low yield of methyl ester was reduced to 85% with reaction time 60 min and temperature of 60 °C at Run 28. Yield was further reduced to 57% with temperature 60 °C and reaction time 120 min at Run 20. It is because sufficient time is required for proper mixing of triglycerides and methanol during transesterification to produce methyl ester. However, reaction time of 180 min with optimum temperature (60 °C) resulted in lowest yield of 58% which is comparatively lower than optimum yield (Run 9). The collective effect of reaction time and temperature on biodiesel yield was found significant in outcomes of ANOVA with p-value (0.0460) lesser than 0.05.

3.14.3.6. Combined influence of methanol to oil molar ratio and reaction time

The combined effect of methanol to oil ratio and reaction time on transesterification in the form of 3D plot has been depicted in Figure 3.14.7f. Maximum yield of 93% was obtained at methanol to oil ratio 9:1 and reaction time of 120 min at constant temperature 60 (°C) and catalyst loading of 0.7 wt. %. Minimum yield of 67% was obtained at molar ratio of 3:1 and time 60 min at Run 3. A lesser amount of methanol failed to convert more triglycerides into methyl esters and resulted in low yield. The yield was further reduced to 58% at molar ratio of 3:1 and higher time 180 min at Run 9. It has been observed that greater reaction time with unfavorable reaction conditions favors reversible reaction and minimum conversion of reactants into useful products (Nath et al., 2019). Higher molar ratio of 16:1 with low reaction time 60 min resulted in low yield of 65% at Run 24. Outcomes of ANOVA demonstrated this combined correlation significant with p-value < 0.05 (0.0493).

3.14.4. Characterization of Biodiesel

3.14.4.1 FTIR Analysis

Fourier-transform infrared spectroscopy is a powerful technique used to determine the functional groups present in biodiesel sample and confirm methyl ester formation in it. In our current investigation biodiesel of *Cupressus macrocarpa* was analyzed in the mid infra-red region of 500-4000 cm^{-1} covering the absorption bands characteristic of synthesized methyl ester

and *Cupressus macrocarpa* seed oil. FTIR spectrum of *Cupressus macrocarpa* seed oil and corresponding biodiesel has been illustrated in Figure 3.14.8 a and b.

Various stretches and bands corresponding to different functional groups were detected in the FTIR spectrum of *Cupressus macrocarpa* seed oil and biodiesel. Two main representative bands of methyl ester in IR region of 1743.43 cm^{-1} for carbonyl group (C=O) and 1464.5 cm^{-1} for methyl group (CH$_3$) were observed in the spectrum of *Cupressus macrocarpa*. One more important peak of biodiesel was seemed in IR region of 2853.29 cm^{-1} for C-H (sp^2) stretching and C-H (sp^3) at 2924.77 cm^{-1}.

Among all these peaks the area of the carbonyl group (C=O) is regarded as most sensitive to change in the chemical structure (Satya et al., 2020). Furthermore, the main variable IR region of the spectrum of synthesized methyl ester seed oil lied within ester control peak area around 1750-1705 cm^{-1}, 1350-1470 cm^{-1} and 1300-1160 cm^{-1}. Stretch peak for C-H$_2$ wagging frequency appeared at 1098.33 cm^{-1} in the IR spectrum of biodiesel. Deep Intense peak perceived for (C-O) at 1159.34 cm^{-1} which was detected in IR spectrum of methyl ester was found missing in the spectrum of *Cupressus macrocarpa* seed oil (Figure 3.14.8b).

Intense peak at 1057.74 cm^{-1} in the IR spectrum of *Cupressus macrocarpa* seed oil vanished in the spectrum of biodiesel. Hence, the conversion of triglycerides into fatty acid methyl esters during transesterification was confirmed by all these peaks of IR spectrum of seed oil and methyl ester.

3.14.4.2 NMR Spectroscopic Analysis

^{1}HNMR is an excellent powerful spectroscopic technique used for quantification of biodiesel. The application of NMR spectroscopy has been extensively used to monitor the process transesterification and determine blend levels of biodiesel. It is suitable technique to calculate total saturated and unsaturated fatty acid methyl esters in biodiesel sample at various stages of life cycle such as after transesterification, after storage, after purification and thermal treatment (Yu et al., 2021).^{1}HNMR spectrum of *Cupressus macrocarpa* biodiesel has been illustrated in Figure 3.14.9a. A characteristic peak of methoxy group (– OCH$_3$) in the ^{1}HNMR spectrum of CMBD was found at 3.654 ppm which confirmed biodiesel formation during

transesterification. An undesirable peak of methanol which is usually observed at 3.45 ppm in ^{1}HNMR spectrum was found absent in the spectrum of CMBD.

Peak for triplet α methylene proton (α-CH$_2$) was observed at 2.318 ppm whereas; peak of β-CH$_2$ (β-methylene) protons as a singlet was spotted at 1.251-1.397 ppm. Protons of β-methylene commonly express atoms of hydrogen positioned on carbon number 3 of aliphatic fatty chain. Peaks of terminal methyl protons were observed at 0.851-0.906 ppm in the spectrum. Peak of olefinic hydrogen (-CH=CH-) was detected at 5.277-5.394 ppm. The peak of allylic hydrogen (-CH$_2$) consisting of two hydrogen atoms per non conjugated group was located at 2.742-2.799 ppm. All these peaks in ^{1}HNMR spectrum of CMBD confirmed the presence of methyl esters and validated the process of transesterification. The total transformation of triglycerides into methyl esters was found to be 95 %.

Structural characteristics i.e. position of esters carbonyl (-COO-) and C-O group in synthesized biodiesel of *Cupressus macrocarpa* was explored with ^{13}CNMR spectrum as shown in Figure 3.14.9b. The distinguishing peak of methoxy carbon was spotted at 51.36 ppm in ^{13}CNMR spectrum. Signal for carbonyl group (-COOH) was found at 174.21 ppm. Peaks of unsaturation (-CH=CH-) in biodiesel positioned at 127.70-128.22 ppm representing inner nun-conjugated carbon whereas, chemical shifts at δ (ppm) 129.69-130.13 (-CH=CH-) signified outer carbon of nun-conjugated carbon. C-O group of methyl ester appeared at 76.64-77.48 ppm (-C-O). A long chain of ethylene carbon (-CH$_2$-)$_n$ appeared at 29.08-29.76 ppm. Besides, signal for aliphatic methylene (-CH$_2$-s) carbon was found at the region of 31.52-34.05 ppm.

3.14.4.3. GC/MS Analysis

Chemical composition of synthesized biodiesel of *Cupressus macrocarpa* seed oil was studied via Gas chromatography and Mass spectrometry analysis. It is the most widely used technique for identification of chemical structure and types of fatty acid methyl esters (FAME) in biodiesel sample (Raheem et al., 2020). Five distinct component methyl esters were observed in the chromatogram of biodiesel using library match software NO. NIST02 and were additionally confirmed by MS analysis (Figure 3.14.10). These five major methyl esters included both

saturated and unsaturated methyl esters. Saturated methyl esters included Dodecanoic acid, methyl ester (C12:0), Hexadecanoic acid methyl ester (C16:0) and Octadecanoic acid, methyl ester (C18: 1). unsaturated methyl ester comprised of 9, 12-Octadecadienoic acid methyl ester (C18:2) and 9-Octadecenoic acid methyl ester (C18:2). 9-Octadecenoic acid methyl ester obtained at retention time of 11.88 min was found as major component with highest abundance in chromatogram. The degree of unsaturation was found to be lesser which favors desirable physico-chemical properties in synthesized biodiesel. Higher saturated fatty acid methyl esters composition has tendency to enhance the cetane number of biodiesel (Esan et al., 2020). GC/MS analysis of *Cupressus macrocarpa* biodiesel disclosed that synthesized methyl ester is highly competent and can be recommended for wide scale production at industrial level.
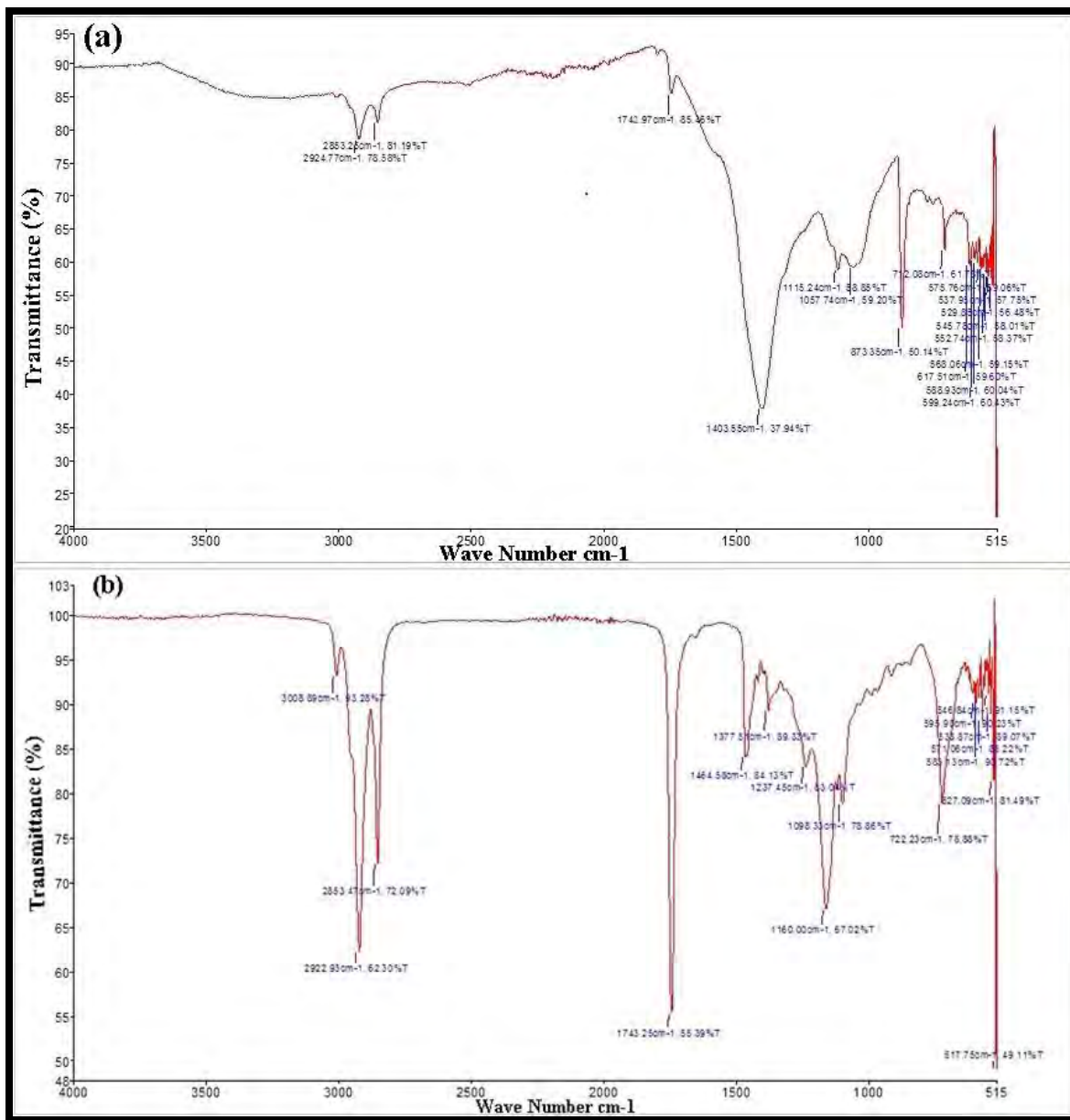
Figure 3.14.8 FTIR spectrum of **(a)** seed oil of *Cupressus macrocarpa* **(b)** *Cupressus macrocarpa* biodiesel
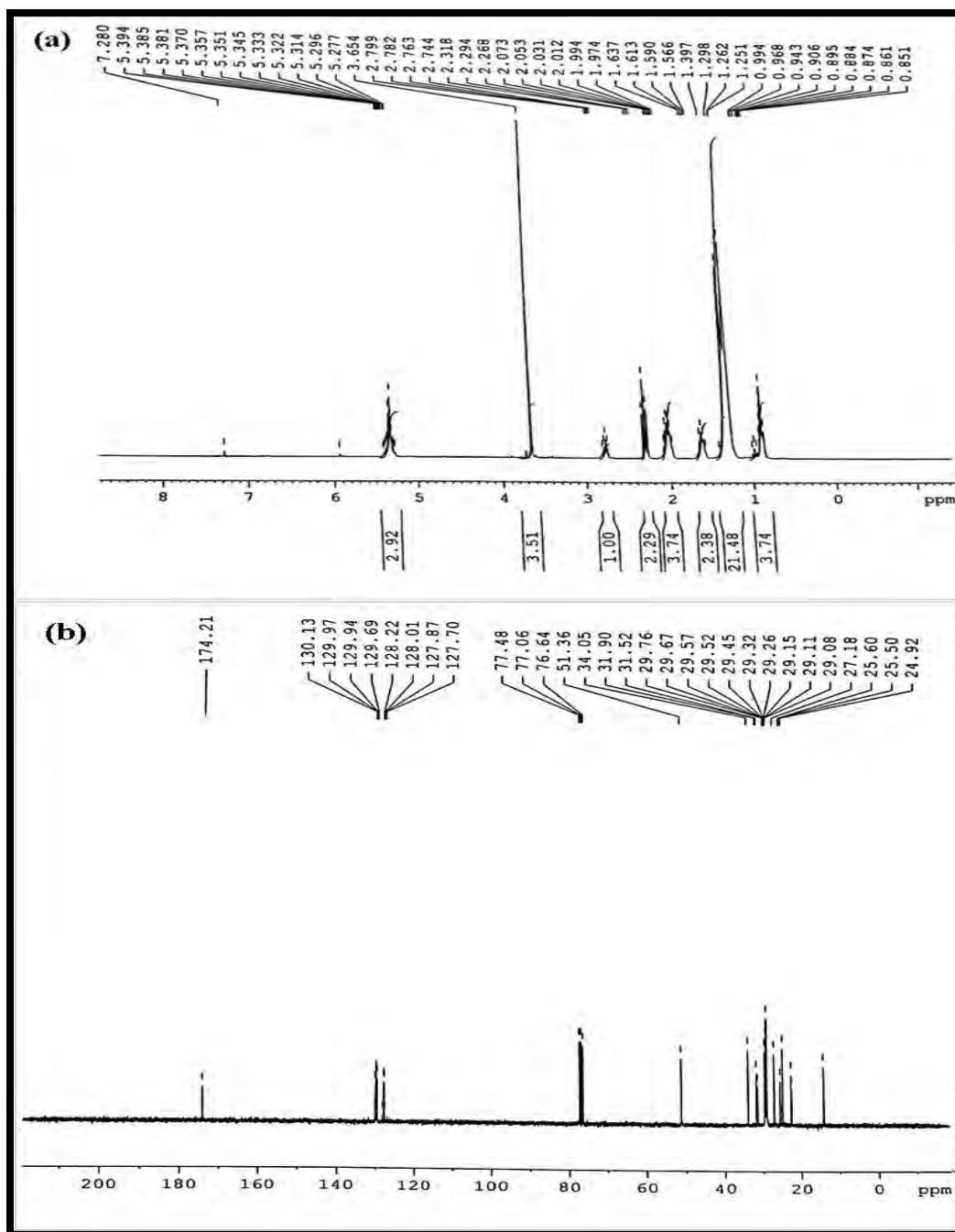
Figure 3.14.9 NMR spectrum of **(a)** ^{1}HNMR and **(b)** ^{13}CNMR of *Cupressus macrocarpa* biodiesel
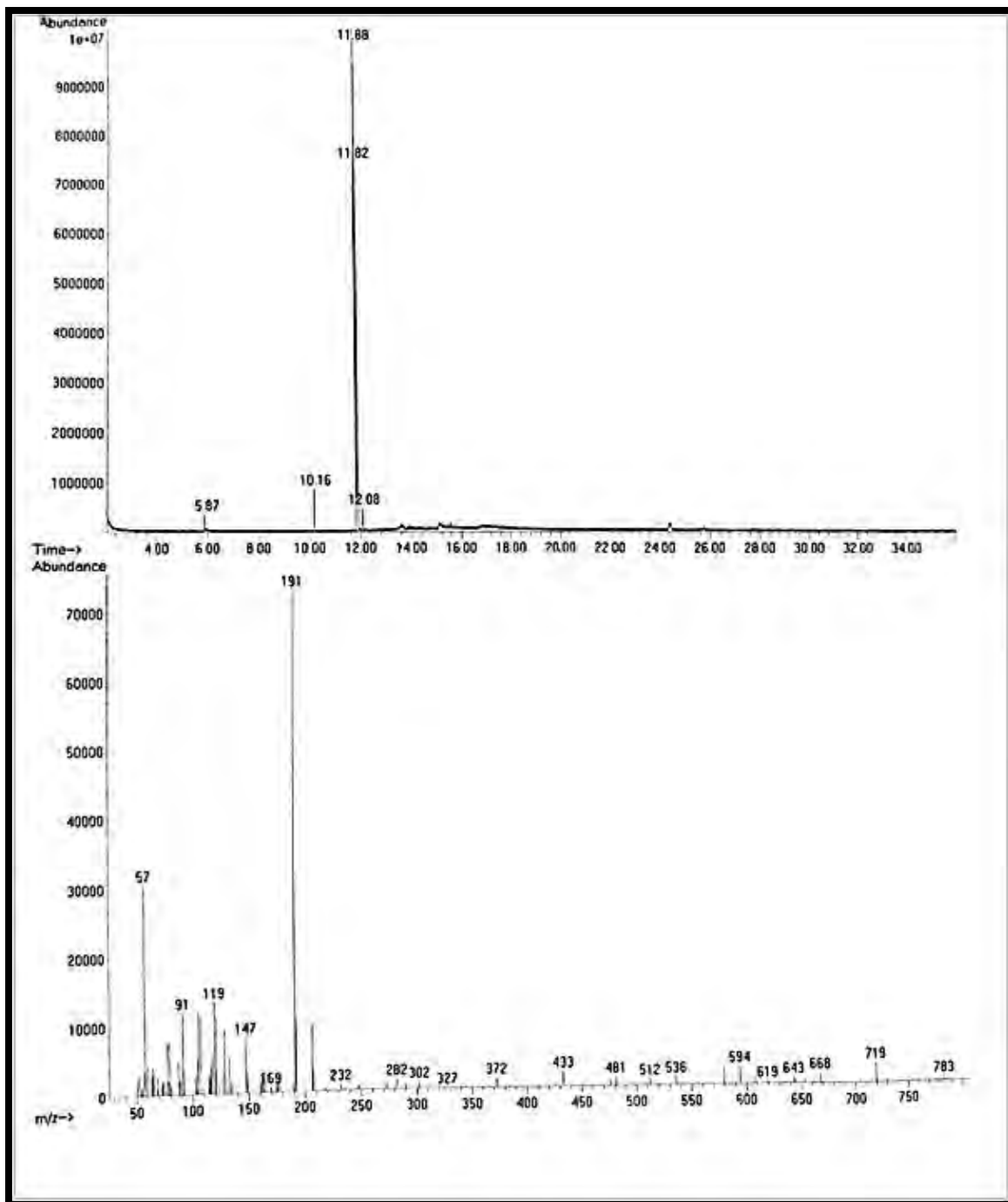
Figure 3.14.10 GC-MS spectrum of *Cupressus macrocarpa* biodiesel

3.14.5. Fuel properties of Biodiesel

Analysis of critical physico-chemical fuel properties of biodiesel such as flash point, viscosity, density, pour point, cloud point, acid value and sulphur content and their comparison with existing international standards of fuel is required prior to recommend it for industrial application. Fuel properties of methyl ester intensely depend upon fatty acid composition (chain length and number of double bonds) of the source oil.

Fuel properties of *Cupressus macrocarpa* biodiesel were investigated and compared with international standards of ASTM D-6571, EN 14214 and China GB/T 20828-2007 as depicted in Table 3.14.4. All these properties lay in the given limits of international standards. Biodiesel has a higher flash point than conventional fossil fuels. Higher flash points of liquid fuels have exhibited higher safety in transportation and storage. Flash point of biodiesel has direct correlation with residual alcohol content in synthesized biodiesel sample. Flash point of *Cupressus macrocarpa* biodiesel was 95 °C in the current investigation.

The acid number of biodiesel demonstrates the quantity of free fatty acids in the sample oil. The higher the value of acid number higher will be the amount of free fatty acids in it. It can be defined as the amount of potassium hydroxide required to neutralize acid moieties. High amount of free fatty acids influences biodiesel aging and affects its stability. Moreover, it leads to saponification reaction during transesterification. The acid value of synthesized biodiesel was 0.34 (mg KOH/gm).

Cold flow properties of biodiesel include pour point and cloud point. Pour point is a temperature at which a liquid fuel still maintains its fluidity whereas, cloud point is a temperature at which the cloud layer first appears on the surface of the fuel at a low temperature which is a sign of the onset of crystallization. Cold flow properties of fuels with high concentration of saturated fatty acids and longer chain are unsuitable and poor (Nestor et al., 2009). Saturated components of fuel crystalize at low temperature and cause precipitation issues like clogging in fuel lines. These properties mostly depend upon saturated esters and the effect of unsaturated esters is almost negligible (Lin et al., 2011). Cloud and pour point of *Cupressus macrocarpa* biodiesel was -7 °C and -8 °C respectively.

The resistance to flow of a certain liquid is known as kinematic viscosity. The required limit of kinematic viscosity in the international standards is between 3.5-5.0 mm^2/s. It has a great impact on fuel atomization and ultimately engine deposits formation upon injection into combustion chamber. Fuels with higher value of viscosity result in incomplete combustion and soot formation. Variation between the viscosity of seed oil and methyl ester can also be used to monitor transesterification (Dai et al., 2021). The degree of saturation and presence of long chain fatty acid methyl esters increases highly affects the viscosity of fuel. However, branching in the ester moiety has no affect on the viscosity of biofuel (Lunardi et al., 2021). The kinematic viscosity of synthesized *Cupressus macrocarpa* biodiesel in the current study was 4.21 (mm^2/s) which matched well with international standards and suitable for commercial application.

Density is one of the key properties of fuel which has a direct impact on engine performance. Other fuel characteristics like cetane number and heat value are under influence of the density (Gimbun et al., 2013). Density of biodiesel primarily depends upon its purity and composition of methyl esters present in it. It increases with increase in number of double bonds and decrease in chain length (Haq et al., 2019). Density of *Cupressus macrocarpa* biodiesel was 0.886 (mm^2/s) in the current investigation which lies under limits of international standards. Biodiesels have comparatively higher densities than petroleum-based diesel. Usually, biodiesel has low sulphur content as compared to petro-diesel thus, results in low or no sulphur dioxide gas. Minimizing sulphur content in petro-diesel is a challenging task for industries as it is a costly process. Sulphur compounds in the fuel are also responsible for formation of engine deposits emission during combustion process. Sulphur content of *Cupressus macrocarpa* biodiesel was 0.0009% which is almost negligible amount.

Table 3.14.4 - Comparison of fuel properties of *Cupressus macrocarpa* biodiesel with international standards**.**

Property	Methods	*Cupressus macrocarpa*		ASTM D-6751	EN-14214	China GB/T 20828-2007
		Mean	**St.Dev.**			
Color	Visual	2	-	2.0		
Acid number (mg KOH/g)	ASTM-D974	0.34	0.1	≤0.5	≤0.8	≤0.5
Flash Point (°C)	ASTM-D93	95	1.2	≥93	≥130	≥120
Pour Point (°C)	ASTM-D97	-8	0.4	-15-16	_	_
Viscosity (mm²/s at 40 °C.)	ASTM-D445	4.21	0.5	1.9-6.0	_	3.4-5.0
Density (kg/m³ at 40 °C)	ASTM-D1298	0.886	1.06	≤120	_	≤120
Sulphur content (wt.%)	ASTM-D4294	0.0009	1	≤0.05	≤0.05	≤0.20
Cloud point (°C)	ASTM-D2500	-7	1	-3.0-12	_	_

3.14.6. Catalyst Reusability

Investigation of reusability of a heterogeneous catalyst is one of the critical characteristics and talks about its economic viability and feasibility. Catalyst reusability is considerably affected by the method of transesterification, separation, purification and nature of the catalyst (Jayakumar et al., 2021). Green nano-particles of Fe_2O_3 were recovered at the end of the first cycle of transesterification by centrifugation, washed, oven dried and calcined. Fe_2O_3 exhibited maximum catalytic activity in first five runs of experimental trials and resulted in high yield of biodiesel from 93 to 85%. However, yield of methyl ester drops gradually after the fifth run. A low yield of 72% was observed in 7th cycle which was further reduced to 65 % in 8th cycle as shown in Figure 3.14.11. This decrease in yield with increase in number of cycles was attributed to leaching and poisoning of active sites of the Fe_2O_3 nano-particles by organic species present in the reacting mixture of transesterification. Poisoning of active sites of nano-particles results in shrinkage of whole surface area and pore volume. Therefore, reduction in availability of catalytic active sites declined in yield of methyl esters during transesterification. Nevertheless, loss in catalytic activity of nano-particles can be regained after repeating calcination step.
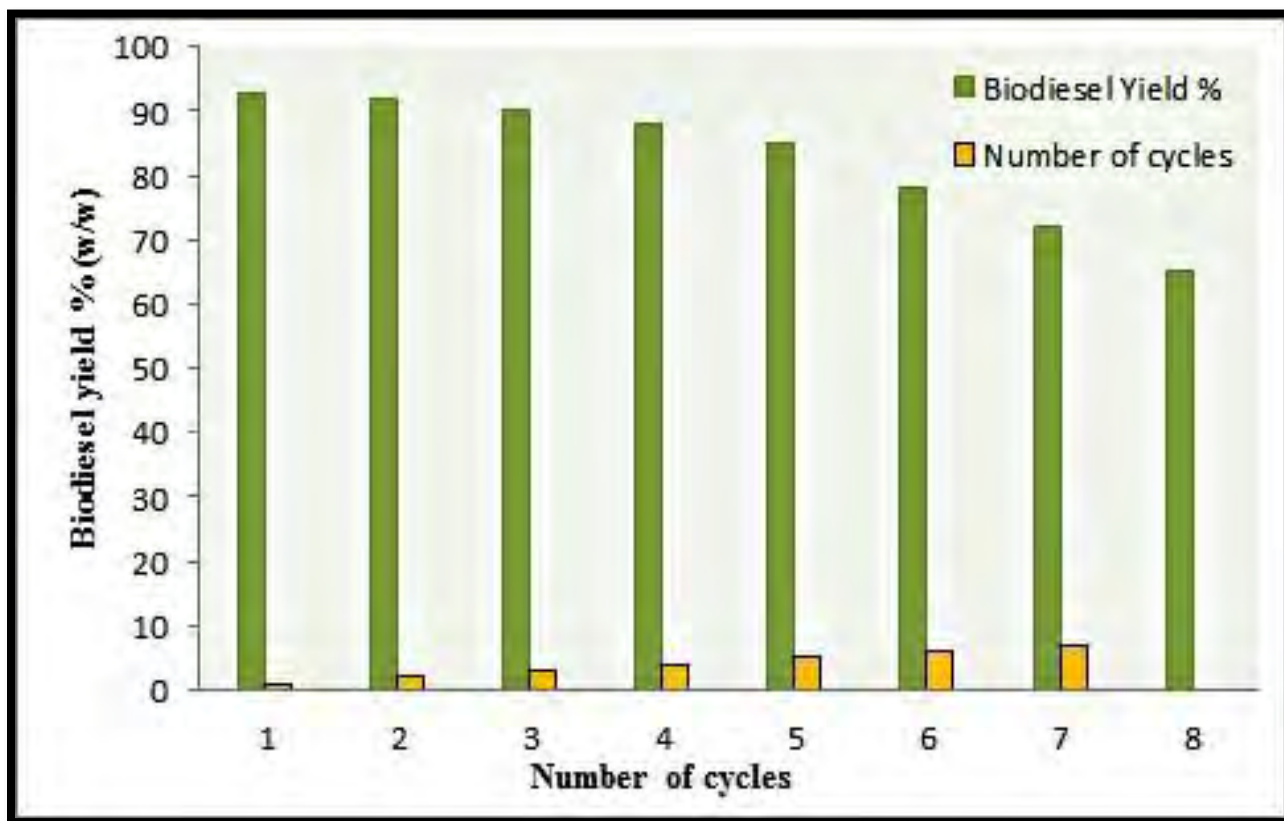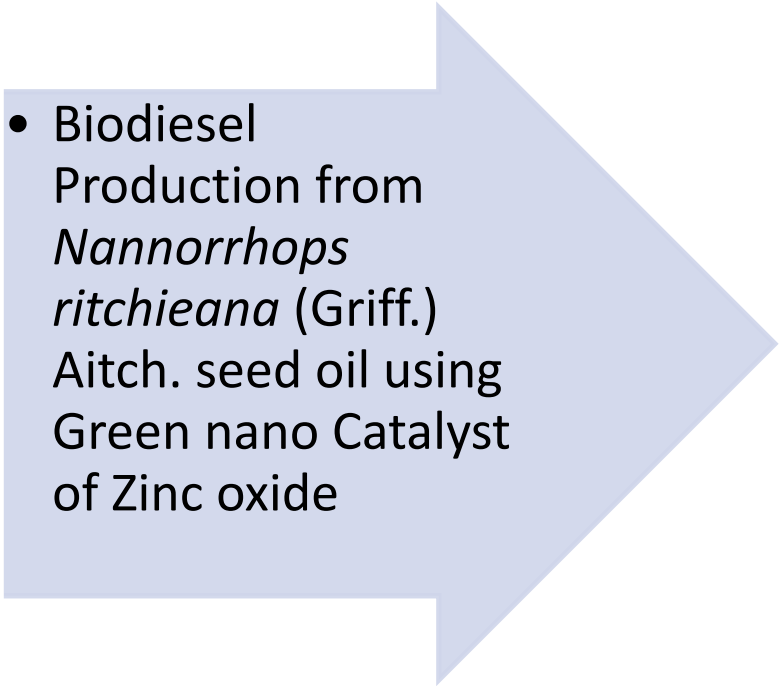
Figure 3.14.11 Reusibility of Iron oxide NPs in transesterification reaction

SECTION XV

- Biodiesel Production from *Nannorrhops ritchieana* (Griff.) Aitch. seed oil using Green nano Catalyst of Zinc oxide

Zinc oxide nanoparticles have excellent chemical, electrical, and thermal stabilities due to their energy band of 3.37 eV and bonding energy of 60 meV. (Watanabe, 2018). Moreover, the optical, electrical, and photocatalytic characteristics of zinc oxide nanoparticles (Kumar et al., 2014). In this study zinc oxide green nano catalyst is efficiently reduced by aqueous leaf extract of *Alternanthera pungens* for single step transesterification reaction.

3.15.1 Characterization of Zinc Oxide Nano Catalyst

3.15.1.1 X-Ray Diffraction (XRD) of ZnO

X-Ray Diffraction is one of the essential techniques used to detect elementary composition, size and crystalline structure of synthesized phyto-nanoparticles. XRD diffractogram of zinc oxide nano catalyst has been depicted in Figure 3.15.1. Diffracted Energy peaks recognized at 2θ values of 31.74 °, 35.40 °, 36.53, 47.54°, 56.55°, 62.85°, 67.93° and 69.03° which corresponded to the lattice plane 100, 002, 101, 012, 110, 013, 200, 112, 004 and 202 *hkl* respectively. Crystalline size of zinc oxide nanoparticles was determined using XRD pattern of deepest peak at 2θ value of 36.22° (highest peak 101).

The mean size of zinc oxide nanoparticles was 22 nm inferring that phyto-catalyst of zinc oxide are nanoparticles in nature. Results of ZnO obtained from X-Ray Diffraction and SEM are aligning with one another.

3.15.1.2 Scanning Electron Microscopy (SEM) of ZnO

Figure 3.15.2 demonstrates SEM micrograph of zinc oxide nanoparticles. SEM was used to study surface morphology (shape, structure and size) of nano particles. The topical view of the nano catalyst showed spherical and granular homogenous morphology with little agglomeration due to polarity and electrostatic attraction of nano-particles. Larger nano-particles were seen due to aggregation of small nano-particles in SEM micrograph. Our results are aligning with previously documented observations (Karthika et al., 2021).

3.15.1.3 Energy Diffraction X-ray (EDX) of ZnO

Elemental structure of zinc oxide nanoparticles was investigated with Energy diffraction (EDX). The EDX spectrum of ZnO is given in Figure 3.15.3. the essential phase of Zn and O

was confirmed from the spectrum with high purity. Mass percent of Zn and O was found 79.20% and 20.80% respectively. Moreover, another irrelevant peak was absent in the EDX spectrum which indicated that green nano-particles are free of impurities and have no extra element in it.

3.15.1.4 Fourier Transform Infrared Spectroscopy (FTIR)

FTIR spectrum of zinc oxide nanoparticles in the absorbance mode has been depicted in Figure 3.15.4. Two distinctive IR peaks were detected in the ZnO spectrum *i.e.* peak at 518.92 cm^{-1} and 523.86 cm^{-1} assigned to Zn-O stretching. FTIR spectrum of Oxides of metals generally has absorbance peaks in IR-region of 400-600 cm^{-1} (Kostić et al., 2016). Absence of other irrelevant peak revealed the pure nature of synthesized green nano-catalyst of zinc oxide.

3.15.1.5 Thermogravimetric analysis (TGA) of ZnO

Bulk decomposition properties of zinc oxide were studied with thermogravimetric analysis. Thermogram of ZnO nano-particles with corresponding derivative thermogram has been depicted in Figure 3.15.5 a and b. Decomposition of ZnO occurred in 3 major phases. Initially decomposition happened at temperature observed around 350-540 ∘C with a rapid reduction of 0.0366% in weight. Weight loss of approximately 0.0366% was observed in the bulk mass due to dehydration at the molecule surface.

The second phase of thermal deterioration (2.909%) was observed at temperature limit of 520 ∘C to 620 ∘C revealing quite higher thermal-stability of ZnO with efficient catalytic activity. Whereas, third stage of thermal decomposition was noticed at temperature limit of 700 ∘C-900 ∘C where additional conversion (1.225%) of green nano-particles occurred and progressively stirred forward towards thermal constancy. Endothermal peaks of ZnO are exhibited in the form of derivative curve (wt. %) shown in Fig. 6a.
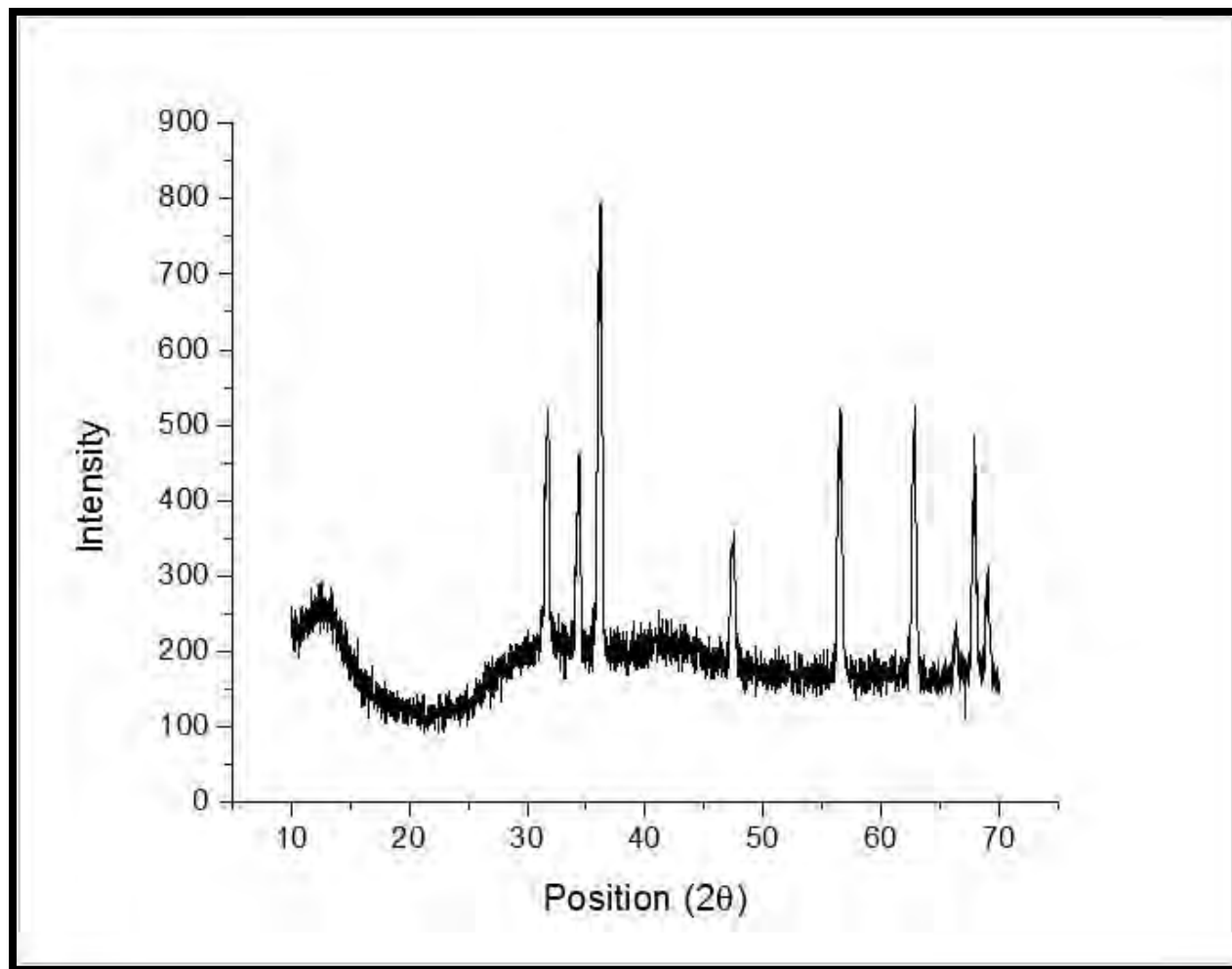
Figure 3.15.1 XRD pattern of zinc oxide nano catalyst
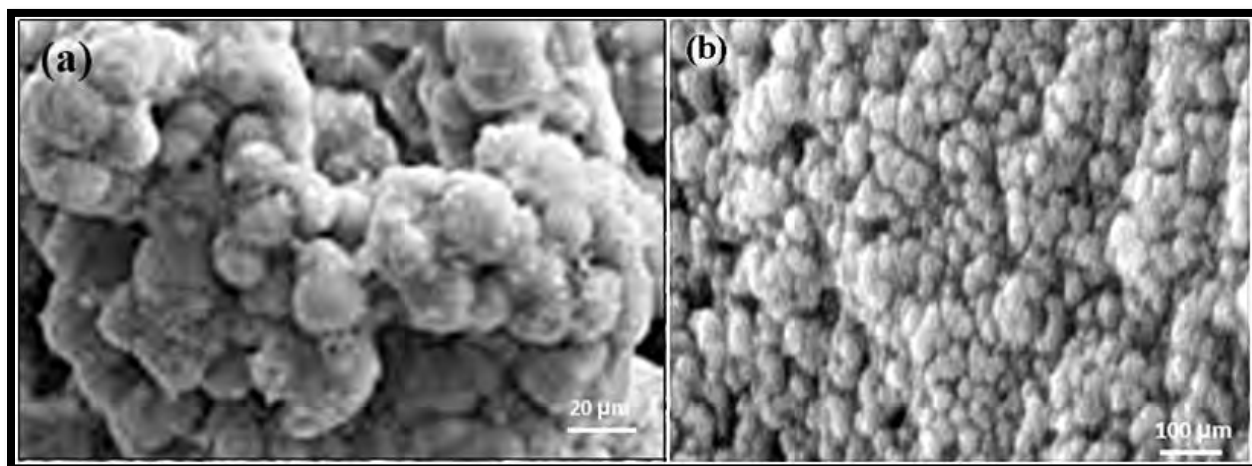
Figure 3.15.2 Scanning electron micrographs of zinc oxide nano catalyst
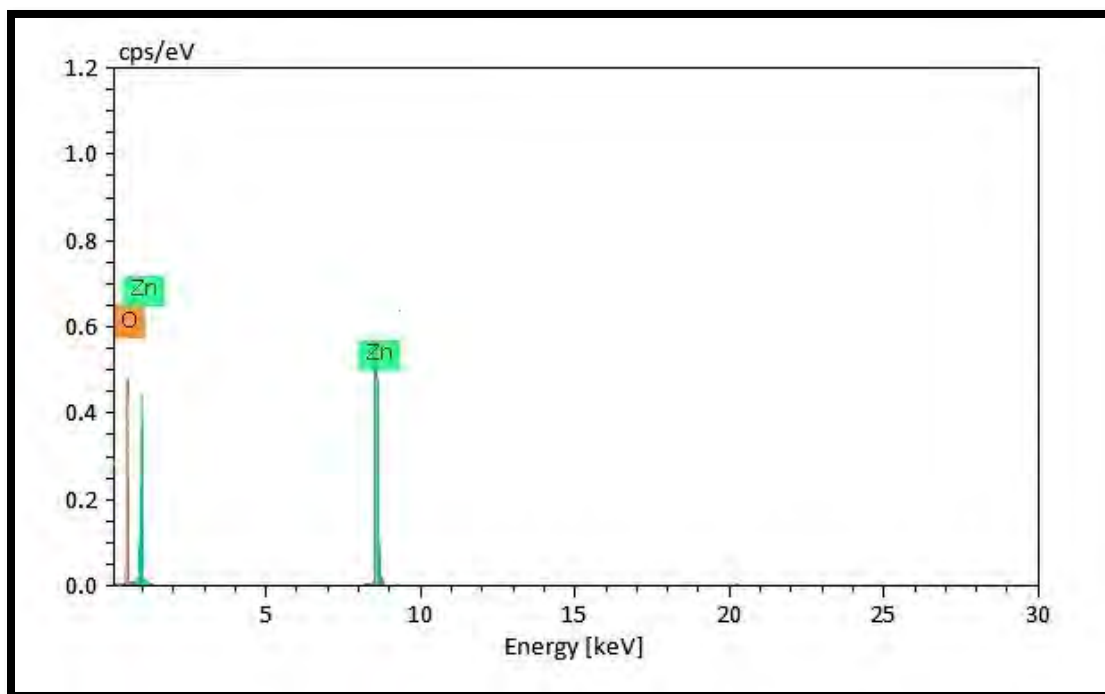
Figure 3.15.3 Energy diffraction X-Ray of zinc oxide nano catalyst
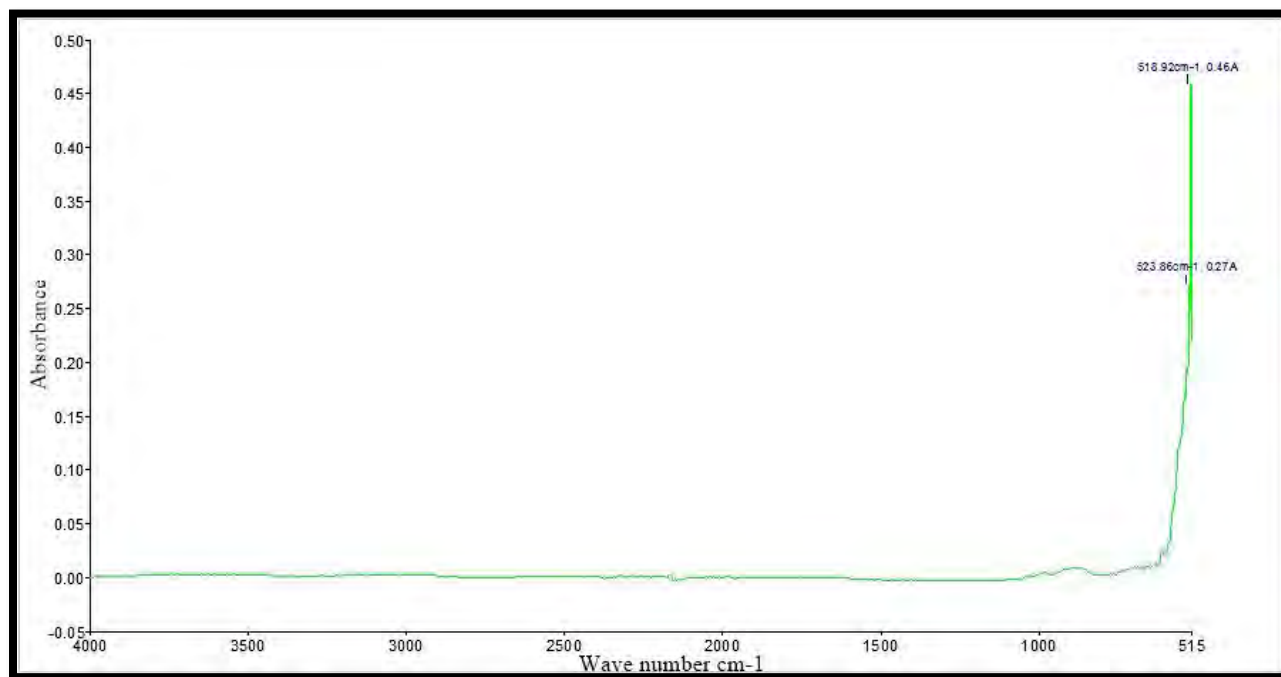
Figure 3.15.4 FTIR spectrum of zinc oxide nano catalyst
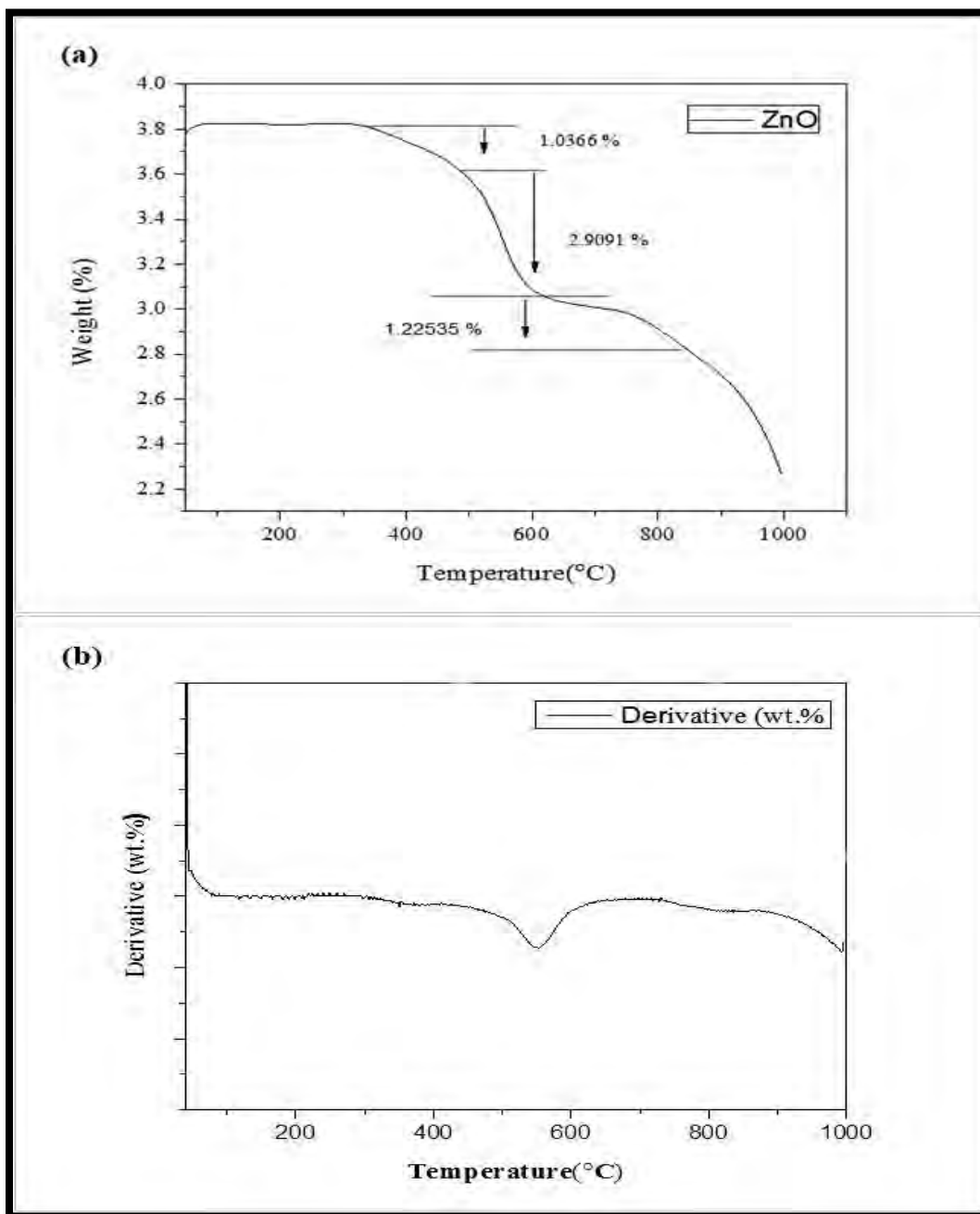
Figure 3.15.5 (a) TGA of zinc oxide nano catalyst (b) derivative thermogram of zinc oxide nano catalyst

3.15.2 Biodiesel synthesis *via* transesterification

In our present investigation, seed oil of *Nannorrhops ritchieana* was utilized for the green and sustainable production of methyl ester. *Nannorrhops ritchieana* grows wildly and does not need special are to grow. Previous literature study has documented that feedstock having higher oil content than 20% would be reflected best for methyl ester formation (Adewuyi, 2020). *Nannorrhops ritchieana* seed oil content was measured to be 25%. FFA concentration of seed oil of selected feedstock was found to be 0.32 (wt. %) which is significantly lower and immaculate for one step base-catalyze transesterification reaction. FFAs content higher than 3% is regarded as undesirable as it requires extra step of acid esterification (Mendonça et al., 2019). Therefore, *Nannorrhops ritchieana* seed oil can be efficiently used as a capable feedstock for biodiesel formation. Transesterification reaction of extracted oil was catalyzed by zinc oxide nano catalyst prepared through *Alternanthera pungens* aqueous leaf extract.

Transesterification reaction is significantly affected by reaction parameters. CCD was designed to investigate optimal conditions of transesterification is required to achieve highest FAME yield (Table 3.14.1 and Table 3.14.2). Figure 3.15.6 depicts a comparison of expected versus actual yield. Graphical illustration revealed that both predicted and actual values are spread close to the running line, showing that they have a good connection. Outcomes of ANOVA of the quadric model are presented in Table 3.14.3. Significant Quadric model was declared in our current study having a *p*-value of 0.0002 (<0.05). Additionally, lack of fit F-value of experimental model was declared not significant with a value of 0.3194 relative to the pure error. Predicted R² value of 0.7306 was found close to the Adjusted R² of 0.8606 and the variance between them was lesser than 0.2. The signal to noise ratio of the model was measured by Adequate Precision. A ratio greater than 4 is regarded as favorable. In the current experimental model Adequate Precision of 11.2676 demonstrated efficient experimental model. Polynomial equation (8) employed in the model is displayed below.

Biodiesel Yield (wt. %) = +82.99+1.44 *A-2.80 *B+4.09*C-1.28*D+3.05* AB-0.5798 *AC-2.95*AD-0.8632 *BC-0.8125* BD-3.19*CD-15.39*A²+8.52*B²-3.13* C²-4.82*D²   (21)

Table 3.15.1 Reaction parameters of transesterification with low and high values

Reaction parameters	–1	+1
Alcohol to oil ratio	3:1	12:1
Catalyst loading	0.18	1.48
Reaction time	55	180
Temperature	60	100

Table 3.15.2 Comprehensive experimental outcome of transesterification reaction of *Nannorrhops ritchieana* biodiesel

Run	A: D: Methanol to Oil molar Ratio	B: Catalyst loading (wt. %)	C: Reaction Time (min)	D: Temperature (◦C)	Yield (wt. %)
1	7:1	1.48	180	100	64
2	7:1	0.83	117.5	60	75
3	3:1	0.18	180	100	72
4	12:1	0.18	180	60	75
5	7:1	0.18	180	80	95
6	7:1	0.83	117.5	80	88
7	12:1	0.83	117.5	80	65
8	3:1	0.83	117.5	80	70
9	7:1	0.83	117.5	80	84
10	7:1	0.83	117.5	60	80
11	12:1	0.18	180	80	70
12	12:1	1.48	180	60	85
13	3:1	0.18	55	100	75
14	7:1	0.18	117.5	60	80
15	7:1	0.18	55	80	74

16	7:1	0.18	180	100	64
17	7:1	1.48	180	80	86
18	7:1	0.83	117.5	100	78
19	7:1	0.83	117.5	80	83
20	12:1	0.18	180	100	70
21	3:1	1.48	180	80	64
22	3:1	0.18	55	80	55
23	7:1	0.83	117.5	80	75
24	3:1	1.48	55	100	60
25	3:1	1.48	55	60	57
26	3:1	1.48	180	60	60
27	7:1	0.18	55	60	68
28	7:1	0.83	180	60	87
29	7:1	1.48	117.5	80	89
30	7:1	0.18	55	100	65

Table 3.15.3 Results of ANOVA for Response Surface Quadratic model

Source	Sum of Squares	Df	Mean Square	F-value	p-value	
Model	2719.09	14	194.22	6.62	0.0002	Significant
A-Alcohol to oil molar ratio	37.56	1	37.56	1.28	0.0358	
B-Catalyst loading	137.44	1	137.44	4.68	0.0470	
C-Reaction time	310.59	1	310.59	10.58	0.0054	
D-Temperature	31.42	1	31.42	1.07	0.0172	
AB	148.75	1	148.75	5.07	0.0398	
AC	5.39	1	5.39	0.1836	0.0414	
AD	139.96	1	139.96	4.77	0.0453	
BC	12.33	1	12.33	0.4199	0.0268	
BD	10.56	1	10.56	0.3599	0.0175	
CD	162.56	1	162.56	5.54	0.0327	
A²	691.81	1	691.81	23.57	0.0002	
B²	145.33	1	145.33	4.95	0.0418	
C²	24.10	1	24.10	0.8212	0.0792	
D²	91.35	1	91.35	3.11	0.0980	
Residual	440.28	15	29.35			
Lack of Fit	334.61	10	33.46	1.58	0.3194	not significant
Pure Error	105.67	5	21.13			
Cor Total	3159.37	29				

$R^2 = 0.8606$, Std. Dev = 5.42, C.V. % = 7.34, Adeq Precision = 11.2676
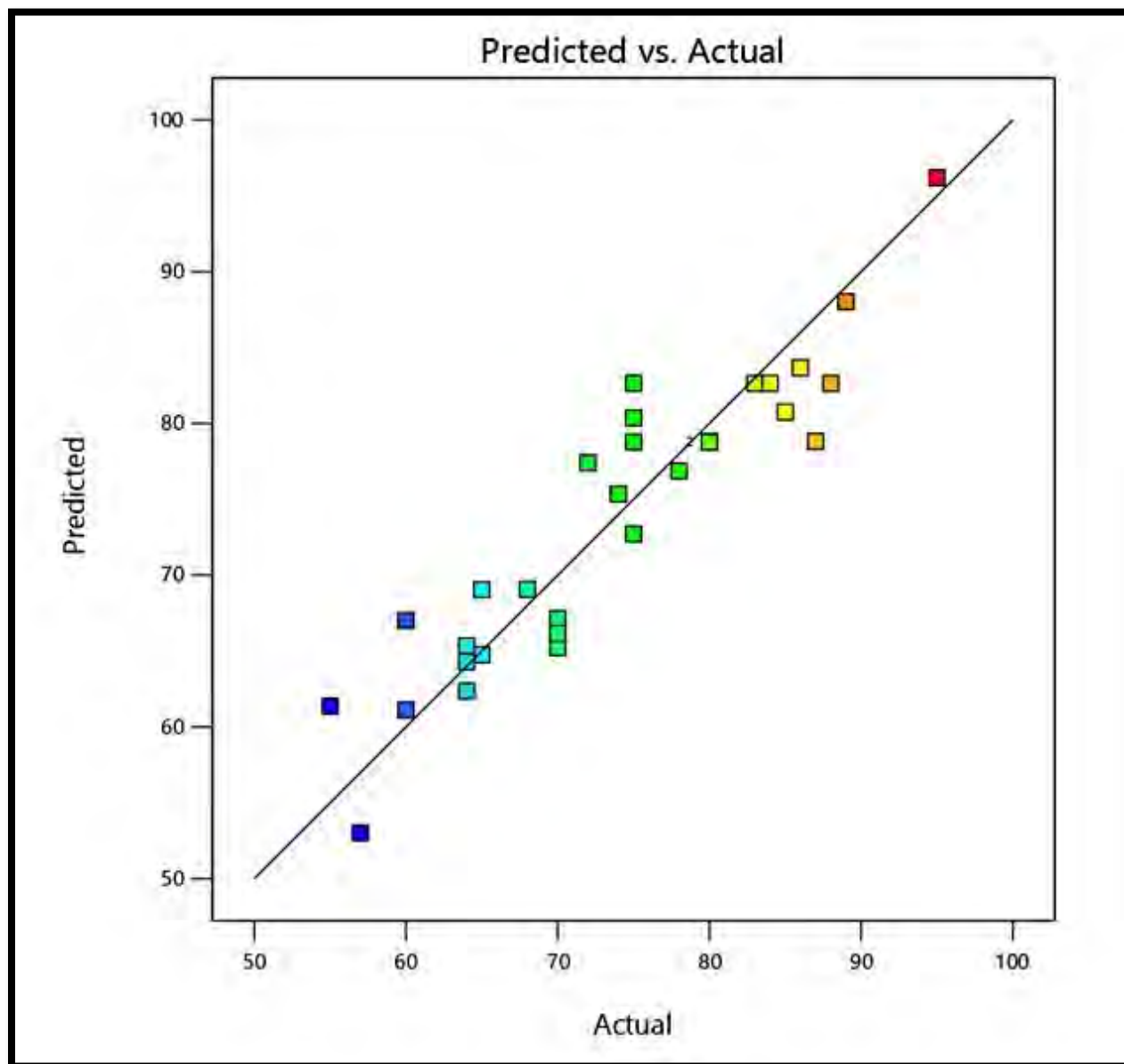
Figure 3.15.6 Evaluation of experimental and the predicted yield of biodiesel in the model
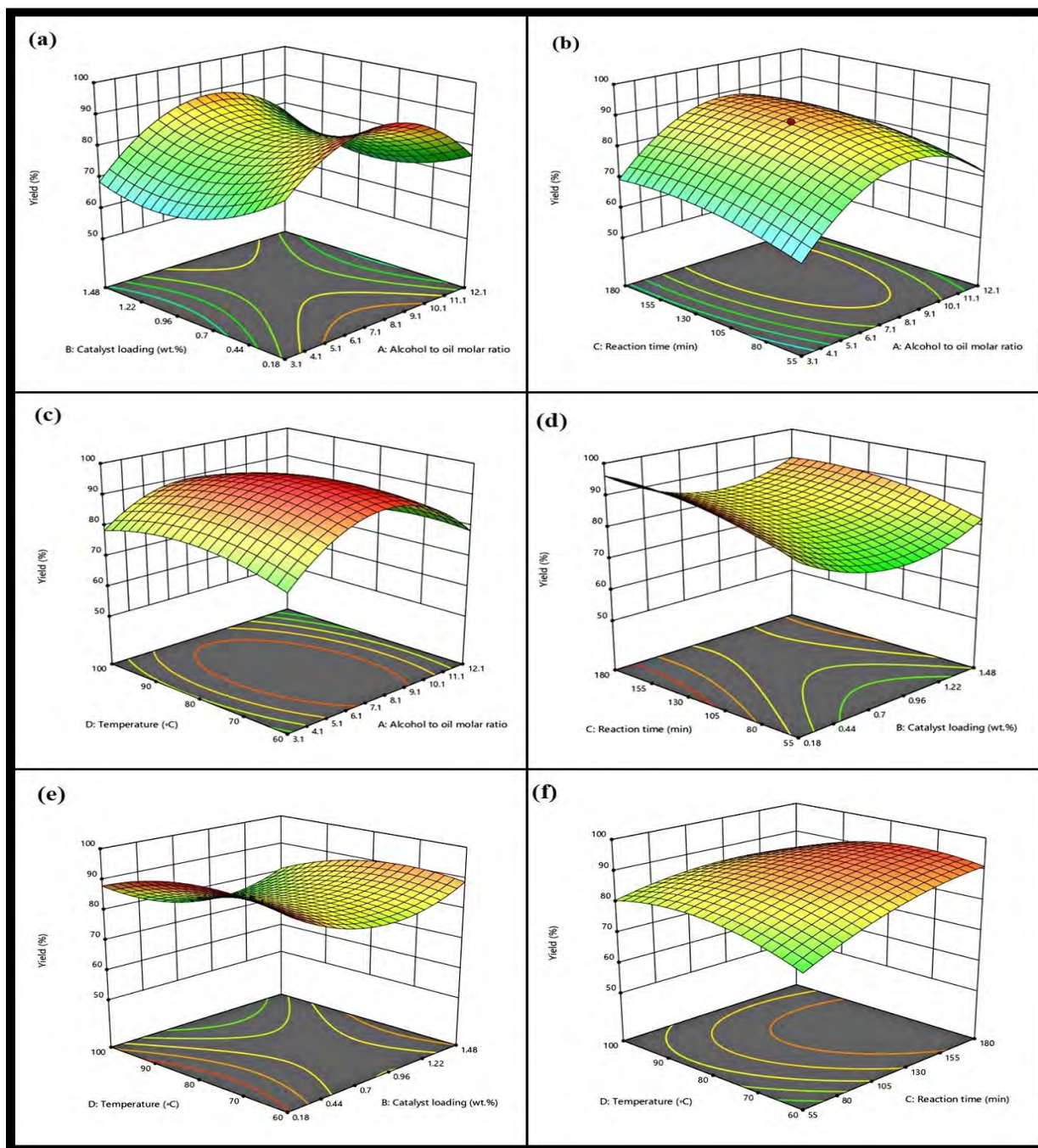
Figure 3.15.7 Impact of the reaction parameters of *Nannorrhops ritchieana* biodiesel.

3.15.3 Impact of reaction parameters on Transesterification

3.15.3.1 Combined influence of methanol to oil molar ratio and catalyst loading

Mutual interaction between Met:Oil and catalyst load substantially affect biodiesel yield during transesterification and are kept under consideration. For this purpose, various experimental trials were carried out in this study. Communal effect of Met:Oil and catalyst load on transesterification of *Nannorrhops ritchieana* seed oil is demonstrated in the frame of 3-D plot shown in Figure 3.15.7a. Highest FAME yield of 95% was achieved at catalyst load 0.18 (wt. %), Met:Oil of 7:1, time 180 (mins) and reaction temperature of 80 °C (Run 5). High catalyst load of 0.83 (wt. %) with same Met:Oil (7:1) resulted in low yield of 86% (Run 17). Similarly, higher Met:Oil of 12:1 with catalyst load of 0.18 ensued minimum yield of 70% at Run 11. The surplus amount of methanol causes thinning of catalyst concentration in the reacting mixture which favors reversible reaction of glycerolysis, easing reaction of glycerol with FAMEs where resynthesis of monoglycerides take place (Martins et al., 2015). The yield was furthermore cut to 64% at lesser Met:Oil of 3:1 and catalyst amount of 1.48 (wt. %) at Run 21. Mutual interaction of Met:Oil and catalyst load was found significant in ANOVA results with p-value 0.0398 (<0.05).

3.15.3.2 Combined influence of methanol to oil ratio and reaction time

Met:Oil and time is another important reaction parameter having immense impact on FAME yield. Figure 3.15.7b demonstrates the mutual interaction of Met:Oil and time. Highest yield of 95% was observed with reaction time (180 min) and Met:Oil of 7:1 keeping other parameters i.e. temperature (80 °C) and catalyst load (0.18 wt. %), (Run 5). Likewise previous interaction higher Met:Oil of 12:1 with reaction time of 180 min resulted in lower yield of 70% at Run 11. In contrast, lower time of 55 min and Met:Oil of 7:1 concluded in little high yield of 74% at (Run 15). Met:Oil of 3:1 and time of 55 min rendered yield up to 55 % at Run 22. It's most likely because there wasn't enough time or methanol for the reactants to thoroughly combine and reach state of equilibrium hence, ensued incomplete transformation of reactants into products (Aliyu etal., 2021). A significant correlation between Met:Oil and reaction time was observed in view of its *p*-value 0.0414.

3.15.3.3 Combined influence of methanol to oil molar ratio and temperature

Reciprocal interaction of Met:Oil and reaction temperature on transesterification has been exhibited in Figure 3.15.7c . FAME yield of 95% was achieved at run number 5 with reaction temperature of 80 ^{o}C and Met:Oil of 7:1 at constant catalyst load (0.18 wt. %) and time (180 min). Higher temperature of 100 ^{o}C and Met:Oil of 12:1 concluded in minimum yield of 70% at Run 20. The boiling point of methanol (65 ^{o}C) and saponification of glycerol were crucial limiting factors for biodiesel yield. Lower Met:Oil of 1:3 at temperature of 60 ^{o}C has ensured a yield of 87% (Run 28). Higher reaction temperature of 100 ^{o}C with Met:Oil of 7:1 further lowered yield up to 64% at Run 16. Hence, it was deduced from present investigation that mutual impact of Met:Oil and reaction temperature is laudable during transesterification. This mutual interaction was significant in view of its *p*-value < 0.05 (0.0453).

3.15.3.4 Combined influence of time and catalyst loading

The collective effect of time and catalyst load on transesterification in the frame of 3-D plot has been depicted in Figure 3.15.7d. highest FAME yield of 95% was achieved at catalyst loading of 0.18 wt. % and time (180 min) while keeping other two parameters reaction temperature of 80 ^{o}C and Met:Oil of 7:1 constant (Run 5). However, beyond optimal level reaction high catalyst loading of 1.48 (wt. %) with time of 117 min gave a yield of 89% at Run 29. Increase in nano-catalyst load up to 0.83 wt. % with medium time of 117 min rendered yield up to 88% (Run 6). The percentage yield was cut even more to 86% with same catalyst load and time of 180 min (Run 17). Shorter reaction time of 55 min with catalyst load of 0.18 wt. % was found insufficient and a yield of 74% was obtained at Run 15. In current investigation, collective impact of time and catalyst load was found significant in the results of ANOVA in view of its *p*-value (0.0268) < 0.05.

3.15.3.5 Combined influence of catalyst loading and reaction temperature

Mutual interaction of nano-catalyst load and temperature at constant time (180 min) and Met:Oil of 7:1 during transesterification is presented in Figure 3.15.7e. The highest FAME yield of 95% was achieved at catalyst loading of 0.18 wt. % and reaction temperature of 80 ^{o}C. The greatest interaction of oil with methanol is thought to be the cause in these reaction conditions

during transesterification (Din et al., 2019). Higher catalyst load of 1.48 wt. % along with elevated temperature of 100 °C rendered FAME yield up to 64% at Run 1. Optimum catalyst load of 0.18 wt. % and temperature 100 °C gave same low yield of FAME (64%) at Run 16. It is ascribed to low boiling point of methanol slowing down forward reaction. Catalyst load of 0.83 wt. % and temperature of 60 °C concluded in 87% yield of methyl ester at Run 28. Combine interaction of these parameters was significant in view of its *p*-value 0.0175.

3.15.3.6 Combined influence of time and temperature

Impact of mutual interaction of time and temperature on FAME yield at constant catalyst load (0.18 wt. %) and Met:Oil of 7:1 is exhibited in the frame of 3-D plot shown in Figure 3.15.7f. It can be seen from Run 5 that a maximum yield of 95% was attained at 180 min and 80 °C. FAME yield was compact to 80% with medium time 117 min and lower reaction temperature of 60 °C at Run 14. Additional decline in time duration up to 55 min with temperature 60 °C concluded in 68% yield at run 27. This investigation disclosed that rise in methyl ester yield with rise in reaction temperature and time is up to certain limit, afterward a substantial decline in percent yield happened which is probably because transesterification is endothermic. A higher reaction temperature of 100 °C and lower time of 55 min additionally lessened FAME yield and resulted in 65% yield at Run 30. Mutual interaction of time and temperature was found significant by having *p*-value of 0.0327.

3.15.4 Characterization of *Nannorrhops ritchieana* Biodiesel

3.15.4.1 FT-IR Analysis

FT-IR is a commonly applied technique to validate FAME formation in biodiesel sample which is further authenticated by NMR spectrum. FT-IR analysis was employed to investigate nature of functional groups pertaining synthesized methyl ester of *Nannorrhops ritchieana*. FTIR spectrum of *Nannorrhops ritchieana* seed oil and corresponding methyl ester is displayed in Figure 3.15.8 a and b respectively. Different stretches and bands were observed in FTIR spectrum of seed oil and methyl ester demonstrating various chemical groups. Among these, there are two main bands spotted at 1743.43 cm^{-1} for carbonyl group (C=O) and 1435.95 cm^{-1} for methyl group (CH$_3$). Another important representative peak of biodiesel appeared in IR region of

2853.266 cm^{-1} for C-H (sp^2) stretching and C-H (sp^3) at 2922.56 cm^{-1}. Area of the carbonyl group among all these peaks is considered sensitive to chemical change (Carde˜no et al., 2020). Furthermore, the largest variable IR region of seed oil and methyl ester was located about 1750-1705 cm^{-1}, 1350-1470 cm^{-1} and 1300-1170 cm^{-1}.

Stretch representing C-H$_2$ wagging-frequency appeared at 1098.84 cm^{-1} in the spectrum of methyl ester. Strong peak identified at 1159.34 cm^{-1} for (C-O) in spectrum of biodiesel wipe out in the spectrum of seed oil. Another deep peak at 1026.64 cm^{-1} in the IR spectrum of *Nannorrhops ritchieana* seed oil was gone in the FAME spectrum. Hence, all mentioned IR-peaks of IR spectrum of *Nannorrhops ritchieana* seed oil and methyl ester have proved the transformation of triglycerides into FAME.

3.15.4.2 NMR Spectroscopic Analysis

^{1}HNMR was applied to investigate percent yield of *Nannorrhops ritchieana* methyl ester and obtain quantitative data about chemical compounds present in the biodiesel. It is an analytical technique to approve synthesis of methyl ester from triglycerides during transesterification. Protons of synthesized esters and that of methylene group were considered to know about reaction product of transesterification. ^{1}HNMR spectrum of *Nannorrhops ritchieana* methyl ester is exhibited in Figure 3.15.9a. In ^{1}HNMR spectrum, distinctive methoxy group (–OCH$_3$) peak was observed at 3.659 ppm which inveterate the presence of FAMEs in the biodiesel. The unwanted free methanol peak at 3.45 ppm was absent. Moreover, peak representing triplet of α-CH$_2$ proton was spotted at 2.323 ppm. Deep peak protons of β-CH$_2$ (β-methylene) was observed at 1.265-1.305 ppm as singlet. In a sequence, proposed protons peaks of terminal methyl were detected at 0.898 and 0.909 ppm. Peak at 5.281-5.422 ppm was perceived for olefinic hydrogen (-CH=CH-). Peak of allylic hydrogen (-CH$_2$-) positioned at 2.748 ppm. The presence of mentioned peaks in ^{1}HNMR spectrum of NRBD confirmed the existence of FAME in it. Total conversion of reactants into FAME was found 94 %.

^{13}CNMR spectrum was used to study structural characteristics like carbonyl (-COO-) and C-O group position in methyl ester of *Nannorrhops ritchieana* (Figure 3.15.9b). Distinguishing peak of carbon of methoxy was detected at 51.40 ppm and signal for carbonyl group (-COOH) at 174.26 ppm. Peaks depicting the unsaturated position (-CH=CH-) in biodiesel were found at

127.88 (ppm) and chemical shifts at 129.95 (-CH=CH-). In contrast to the long chain of ethylene carbon $(-CH2)_n$ at 29.33 ppm, the C-O group in the methyl ester was present at 77.48 (-C-O). The signal for carbon present in aliphatic methylene (-CH2-s) was spotted at 34-27 ppm in spectrum the ^{13}CNMR.

3.15.4.3. GC/MS

Physical and chemical properties of biodiesel are intensely affected by variation in FAMEs composition present in it. Chemical composition and quality of synthesized methyl ester of *Nannorrhops ritchieana* was analyzed by GC/MS analysis. Seven distinct peaks were observed in the chromatograph of *Nannorrhops ritchieana* biodiesel predicted by library match software NO. NIST02 using retention times of FAMEs and were further validated by MS analysis as depicted in Figure 3.15.10. These seven peaks include both saturated and unsaturated fatty acids. FAMEs with unsaturated nature comprised of 5, 8-Octadecadienoic acid methyl ester (C18:2) and 9-Octadecenoic acid methyl ester (C18: 1) whereas, saturated fatty acids consisted of Decanoic acid, methyl ester (C10:0), Dodecanoic acid, methyl ester (C12:0), Hexadecanoic acid methyl ester (C16:0), Octadecanoic acid, methyl ester (C18:0) and 13-Docosenoic acid, methyl ester. 9-Octadecenoic acid methyl ester was found to be a major fatty acid with highest abundance. Lower levels of unsaturation were reported in the methyl ester sample., which is desirable because it results in smooth and consistent fuel combustion in diesel engines (Mares et al., 2021). GC/MS analysis of *Nannorrhops ritchieana* methyl ester revealed that utilized seed oil is highly efficient and appropriate for broad scale production of biodiesel.
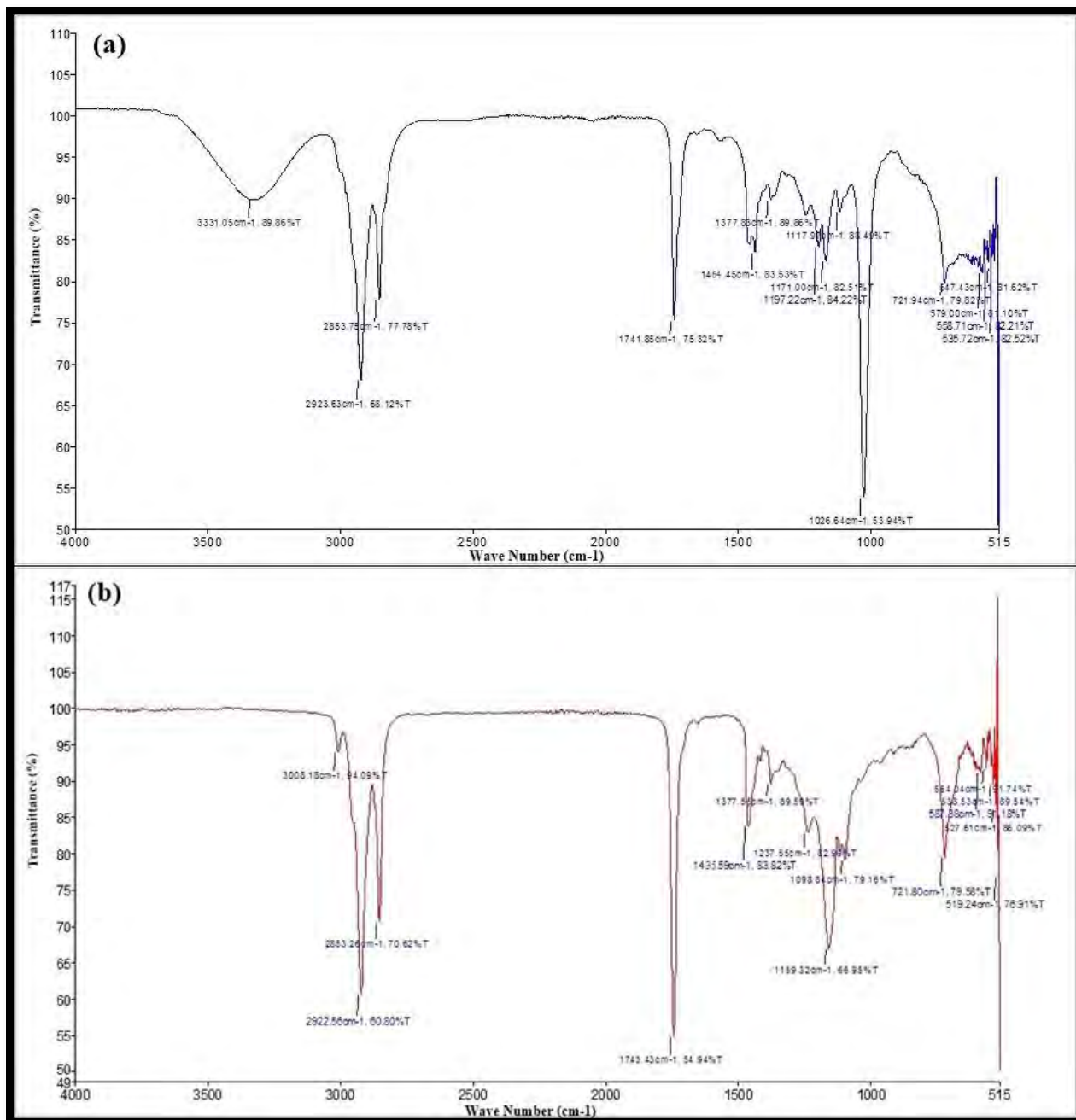
Figure 3.15.8 FTIR spectrum of **(a)** seed oil of *Nannorrhops ritchieana* **(b)** *Nannorrhops ritchieana* biodiesel
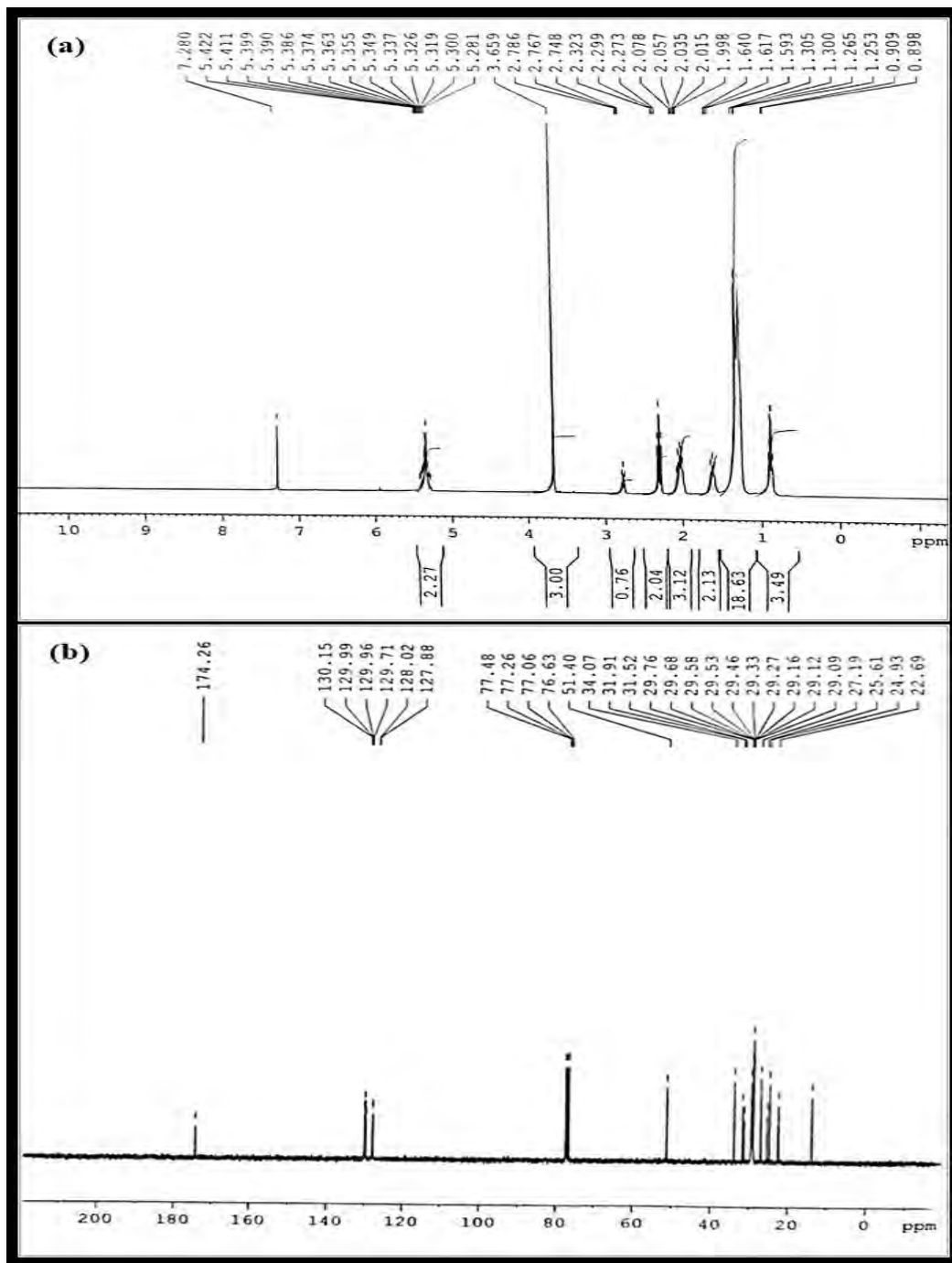
Figure 3.15.9 NMR spectrum of **(a)** ^{1}HNMR and **(b)** ^{13}CNMR of *Nannorrhops ritchieana*
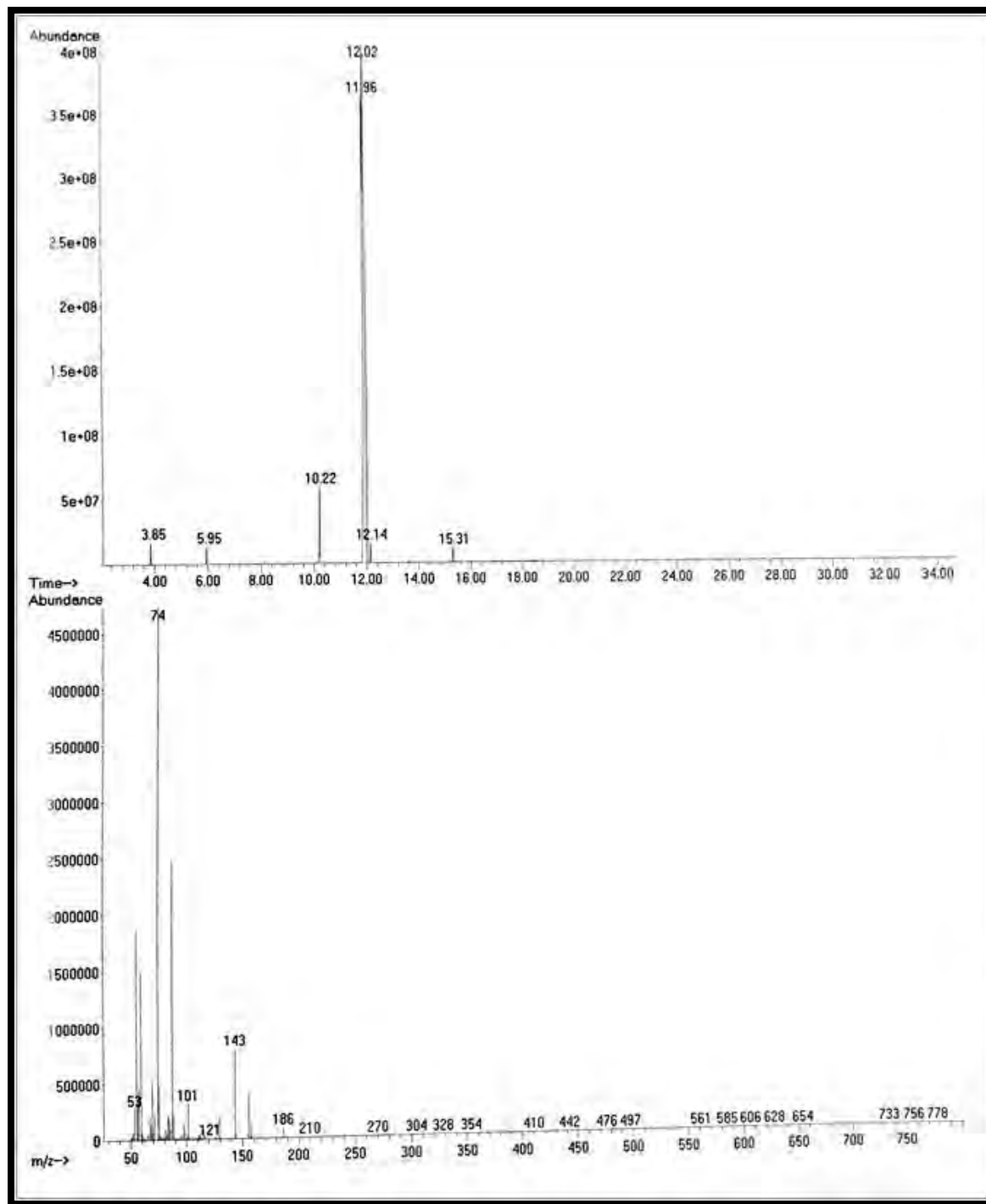
Figure 3.15.10 GC-MS spectrum of *Nannorrhops ritchieana* biodiesel

3.15.5. Fuel Properties of biodiesel

One of the most substantial criteria to examine is the fuel qualities of biodiesel which must lie under existing international standards of fuel. The composition of fatty acids in the source oil used in biodiesel production significantly affects its fuel properties and varies from feedstock to feedstock. Fuel properties of *Nannorrhops ritchieana* biodiesel were explored and matched with international standards of ASTM D-6571, EN 14214 and China GB/T 20828-2007 prior to practical implication. As shown in Table 3.15.4, all of these qualities were determined to be well matched with international standards.

Acid value is an important fuel property of biofuels which substantially affects fuel quality and engine efficiency. It is defined as the amount of potassium hydroxide needed to neutralized free fatty acids present in sample fuel liquid. Higher acid value of biodiesel creates troubles in fuel engine especially in rubber parts mainly in diesel engines from the past by causing corrosion. Acid value of *Nannorrhops ritchieana* methyl ester was determined via ASTM-D974 standard and was found to be 0.299 (mg KOH/gm) which circumcised within international limit.

Density of biodiesel directly affects engine efficiency, fuel spraying and movement of fuel inside pipelines and injector nozzles. Generally, biofuels have higher density than other diesel fuels. Higher fuel density is undesirable as it results in an increase in biodiesel viscosity and causing incomplete fuel combustion and exhaust pollutants emission (Changmai et al., 2021). Density of *Nannorrhops ritchieana* biodiesel was 0.912 (mm^2/s) which is in accordance with universal standards of fuel.

Viscosity is another important feature of methyl ester. Both higher and lower viscosity of fuel has an impact on fuel atomization and injector lubrication. Lower fuel viscosity results in leakage problems and provides lesser lubrication in fuel injection pumps corresponding to power loss for fuel engine. Similarly, higher viscosity fails to provide enough fuel in injection pump and results in loss in engine efficiency (Murguía-Ortiz et al., 2021). Kinematic viscosity of *Nannorrhops ritchieana* biodiesel was detected to be 6.45 (mm^2/s) which falls under specified range of ASTM D-6751 and European Union 14214 standard.

Flash point specifies the temperature point at which fuel ignites when kept at flame. Transportation of fuel and its storage are under immense influence of the corresponding flash point. Flash point with higher value is favorable as it minimizes risk of accidental fire [39]. Biodiesel has higher flash point as compared to conventional fossil fuels thus, has lower chance of risk during transportation. Flash point of *Nannorrhops ritchieana* methyl ester was found to be 93 ºC as shown in Table 3.15.4, higher enough than petro-diesel and can run smoothly in the sector of transport.

The pour and cloud point of biodiesel are parameters playing significant role in regulating operability of diesel engines at low temperatures in colder parts of the world. Pour point of biodiesel is under direct influence of saturated fatty acids and fluctuates with composition of fatty acid found in oil used in transesterification. Pour point of *Nannorrhops ritchieana* methyl ester was found to be -10 ºC which appears aligned to international standards. Likewise, cloud point specifies the temperature at which a fuel turns down to crystal phase. In our current study, cloud point was found -7 ºC as shown in Table 3.15.4 which is align to international standards. Sulphur content of *Nannorrhops ritchieana* methyl ester was determined by method of ASTM-D4294. A minimum sulphur content of 0.0012% was observed in synthesized methyl ester sample dropping in the scale of less than 1 ppm as compared to petro-diesel which has sulphur content in the range of 50 ppm. The presence of sulphur content less than 1 ppm is one of the great advantages of biodiesel over conventional petroleum-based fuel resulting in ecofriendly low sulphur dioxide gas emission (Ayhan and Ece 2020).

Table 3.15.4 Evaluation of fuel properties of *Nannorrhops ritchieana* (Griff.) biodiesel with international standards.

Fuel Property	Methods	*Nannorrhops ritchieana*		ASTM D-6751	EN-14214	China GB/T 20828-2007
		Mean	St.Dev.			
Color	Visual	1.5	-	2.0	-	-
Acid number (mg KOH/g)	ASTM-D974	0.299	0.1	≤0.5	≤0.8	≤0.5
Flash Point (°C)	ASTM-D93	93	1.2	≥93	≥130	≥120
Pour Point (°C)	ASTM-D97	-10	0.4	-15-16	_	_
Viscosity (mm²/s at 40 °C.)	ASTM-D445	6.45	0.5	1.9-6.0	_	3.4-5.0
Density (kg/m³ at 40 °C)	ASTM-D1298	0.912	1.06	≤120	_	≤120
Sulphur content (wt.%)	ASTM-D4294	0.0012	1	≤0.05	≤0.05	≤0.20
Cloud point (°C)	ASTM-D2500	-7	1	-3.0-12	_	_

3.15.6. Catalyst Reusability

It is very important to investigate reusability of a heterogeneous catalyst for detection of its economic viability and circularity in the biofuel sector. Reusability of a catalyst is significantly affected by the method of purification, separation and transesterification as well as nature of the catalyst itself (Maneerung et al., 2016). In this study, reusability of the synthesized Zinc oxide nano-particles was determined at optimal reaction parameters *i.e.* catalyst load (0.18 wt. %), reaction time (180 mins), reaction temperature (80 $^{\circ}$C), and Met:Oil of 7:1. Green nano catalyst of ZnO was recovered after first cycle of transesterification via centrifugation method and washed with alcohol in order to eliminate impurities of reaction mixture and dried in oven overnight at 60 $^{\circ}$C. Oven dried nano-catalyst was calcined for 3 h at 500 $^{\circ}$C and reused in forth coming cycles of transesterification.

High catalytic activity was observed in first three runs of experimental trials resulting in maximum yield of biodiesel from 95 to 86%. Nevertheless, drop in the yields of methyl ester was recorded after third run. Low yield of 77% was observed in 5th cycle which was lowered to 60 % in 6th cycle (Figure 3.15.11). It is chemically linked to leakage and intoxication due to organic components included in the transesterification-reacting mixture occupying the catalyst active sites. which shrink surface area of the catalyst. Hence, decrease in readiness of catalytic dynamic sites resulted declined in FAME yield. However, catalytic activity of the catalyst can be again revived after calcination.
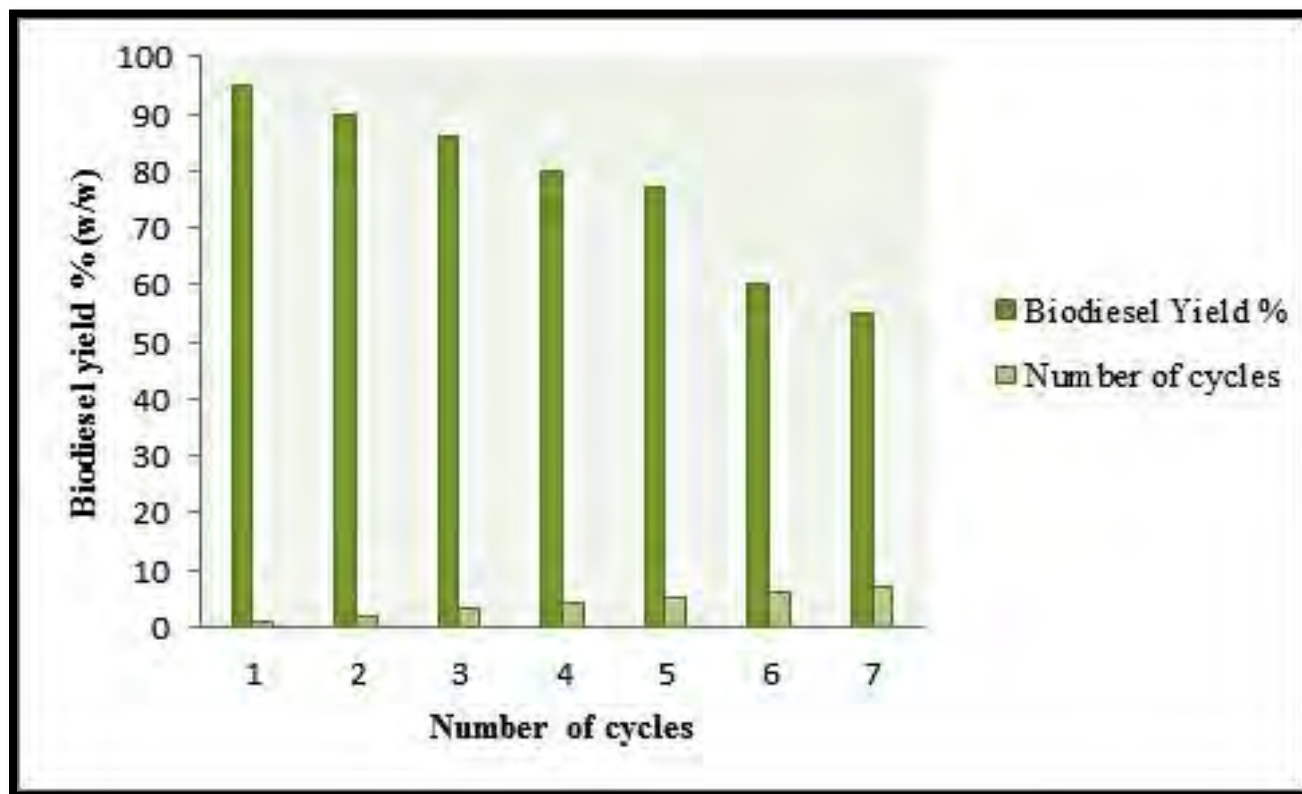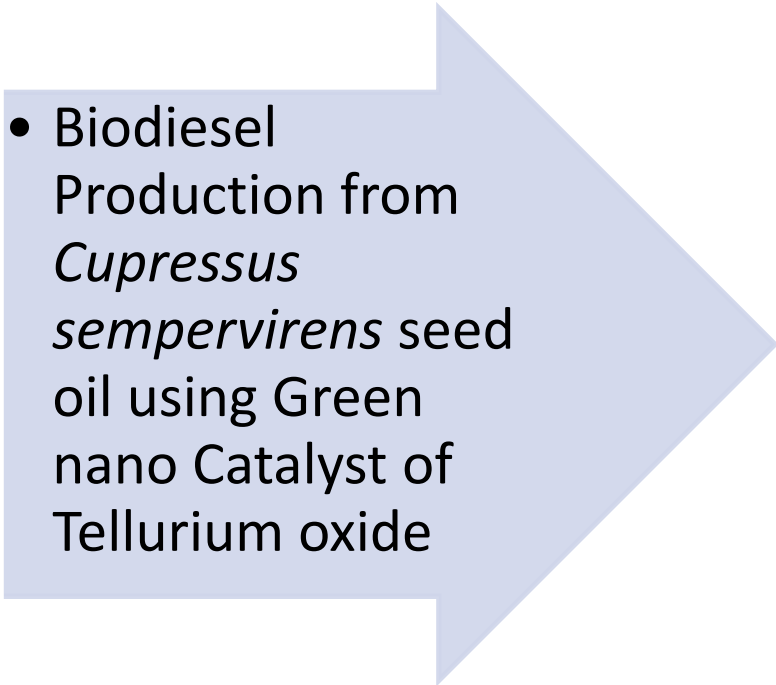
Figure 3.15.11 Reusibility of Zinc oxide NPs in transesterification

SECTION XVI

- Biodiesel Production from *Cupressus sempervirens* seed oil using Green nano Catalyst of Tellurium oxide

Tellurium nanoparticles (Te NPs) have attracted interest in both research and industry due to their superior biocompatibility, antibacterial, antioxidant, and anticancer activities, as well as their capacity to lower triglyceride and cholesterol levels (Elsoud et al., 2018). The biosynthesis of Tellurium oxide NPs in our current investigation was carried out using *Calendula arvensis* leaf extract.

3.16.1 Catalyst Characterization of tellurium oxide nanoparticles

3.16.1.1 X-Ray Diffraction (XRD) of TeO

Crystals purity and size of Tellurium oxide were verified using the X-Ray Diffraction method. Figure 3.16.1 shows an XRD diffractogram of tellurium oxide nanoparticles. Diffracted Energy peaks of the X-ray diffractogram showed the TeO nanoparticles to be pure crystalline, with 2θ values at 32.5 °, 35.2 °, 37.05 °, 44.11 °, 60.80 ° which corresponds to (220), (311), (400), (422) and (440) respectively. The crystalline size of tellurium oxide nanoparticles was determined using the XRD pattern of deepest peaks at 2θ value of 37.05∘ (highest peak 400).

About 45 nm crystalline size of Tellurium oxide nanoparticles revealed the nanoscale nature of the synthesized green nanoparticles. XRD pattern of TeO agreed with the findings of SEM.

3.16.1.2 Scanning Electron Microscopy (SEM) of TeO

Figure 3.16.2 shows a SEM image of tellurium oxide nanoparticles. Tellurium oxide nanoparticles (NPs) had a uniform morphology and looked to be face-centered cubic in shape. Cluster of particles is detected in SEM micrograph ascribed to polar and electro-static pull of nanoparticles towards each other.

3.16.1.3 Energy Diffraction X-ray (EDX) of TeO

Investigation of elemental composition of tellurium oxide nanoparticles was carried out via Energy diffraction X-Ray analysis. Figure 3.16.3 elucidates the EDX spectrum of TeO. The analysis of EDX confirmed the existence of both Tellurium at 0.13, 2.1, and 3.75 keV whereas, oxygen at 0.5 keV demonstrating high purity of synthesized particles. The mass percent of Te

and O was 83.10% and 16.90% respectively. Absence of other unnecessary peak in the EDX spectrum exposed that tellurium oxide nanoparticles have no impurities and extra elements.

3.16.1.4 Fourier Transform Infrared Spectroscopy (FTIR)

Tellurium oxide nanoparticles showed evidence of several functional groups by FTIR spectroscopic investigation. Figure 3.16.4 depicts the tellurium oxide nanoparticles' FTIR spectrum. Major absorption peaks at 1092.38 cm^{-1} and 609.42 cm^{-1} were visible in the TeO nanoparticles' FTIR spectra. the peak at 1092.38 cm^{-1} corresponds to the related vibration of the Te-O bond. Due to the existence of adsorbed water, the sharp peak at 609.42 cm^{-1} was assigned to the O-H group.

3.16.1.5 Thermogravimetric analysis (TGA) of TeO

Tellurium oxide nanoparticles heat stability and breakdown characteristics were investigated using thermogravimetric analysis (TGA). Thermogram of TeO is shown in Figure 3.16.5a, and the subsequent derivative curve (wt.%) with their endothermic peaks is shown in Figure 3.16.1b. Tellurium oxide nano catalyst encountered three separate primary phases of thermal breakdown. Initial catalyst deterioration, which accounted for 1.82% of the total mass, occurred between 150 ∘C and 420 ∘C due to desiccation and water loss from nanoparticle surfaces. Accordingly, this desiccation process proceeded in the following phase, which occurred at a temperature range of 430-530 ∘C and resulted in a loss of 0.16% in the total mass of TeO. A straight line was seen away from 200°C that lasted till 700 °C. At a temperature range of 531-680 ∘C, the third phase of disintegration was observed, during which 0.15% of the total mass of TeO was lost. The remarkable thermal stability of TeO in our current work was revealed by the TGA results.
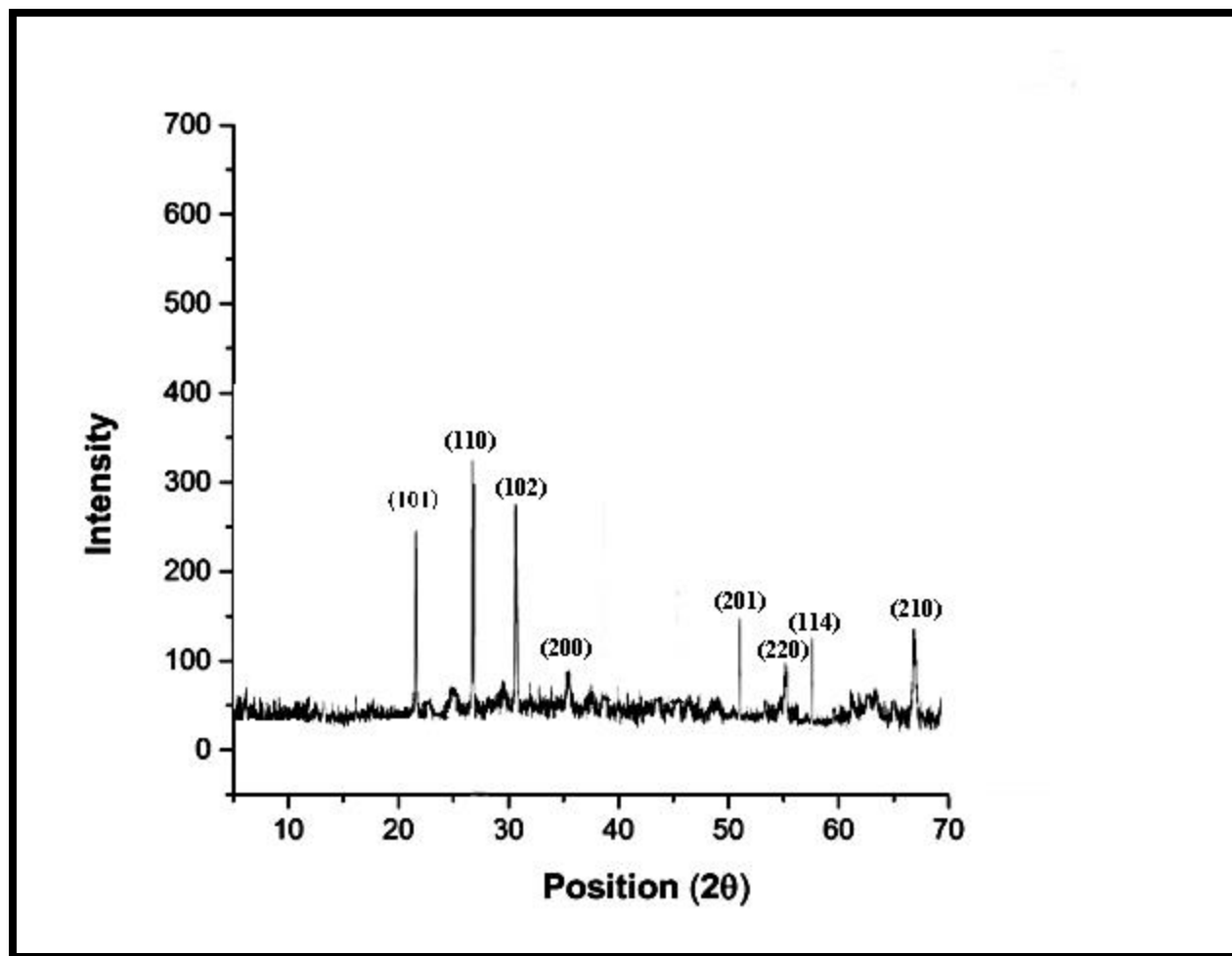
Figure 3.16.1 XRD pattern of tellurium oxide NPs
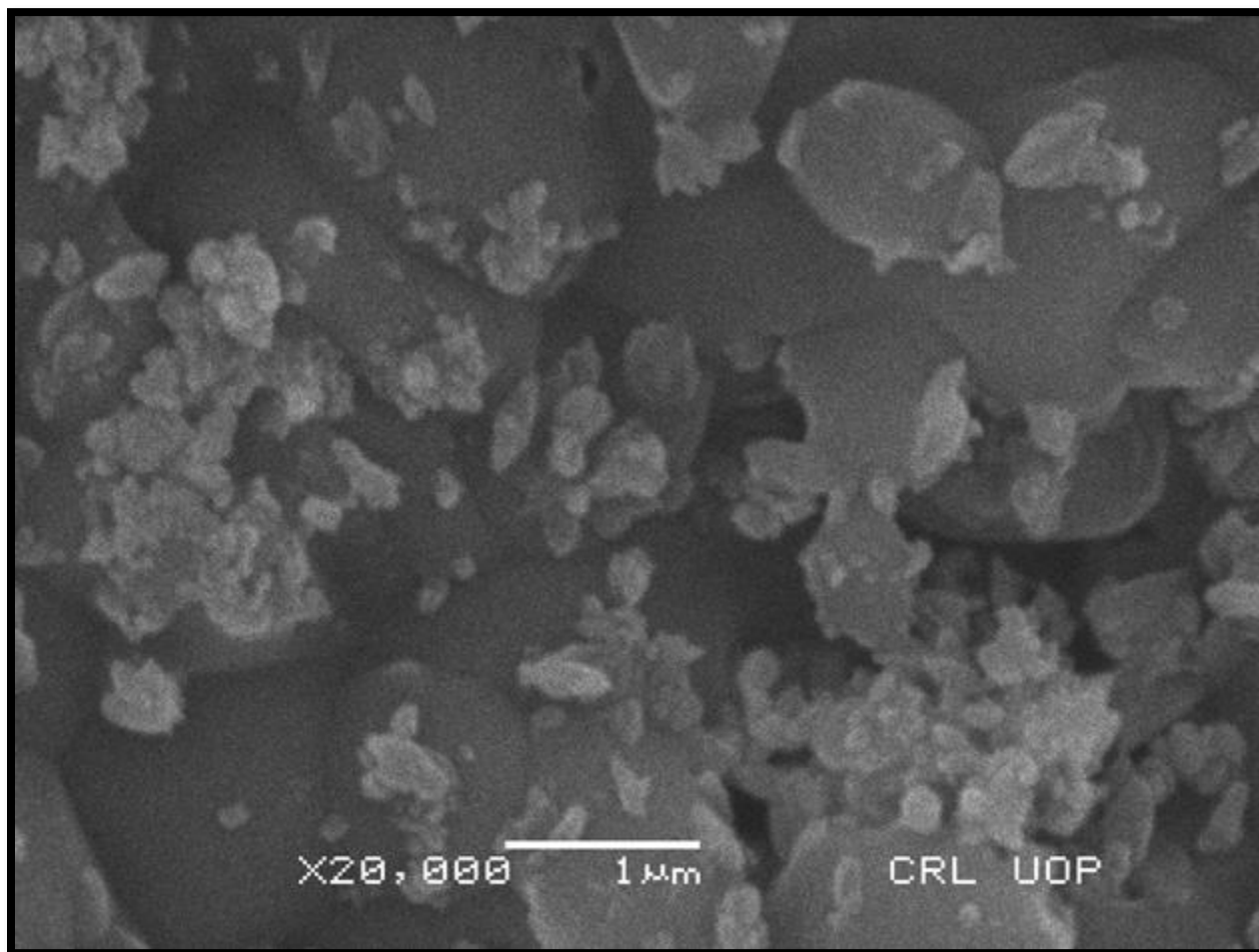
Figure 3.16.2 Scanning electron microscopy (SEM) of tellurium oxide NPs
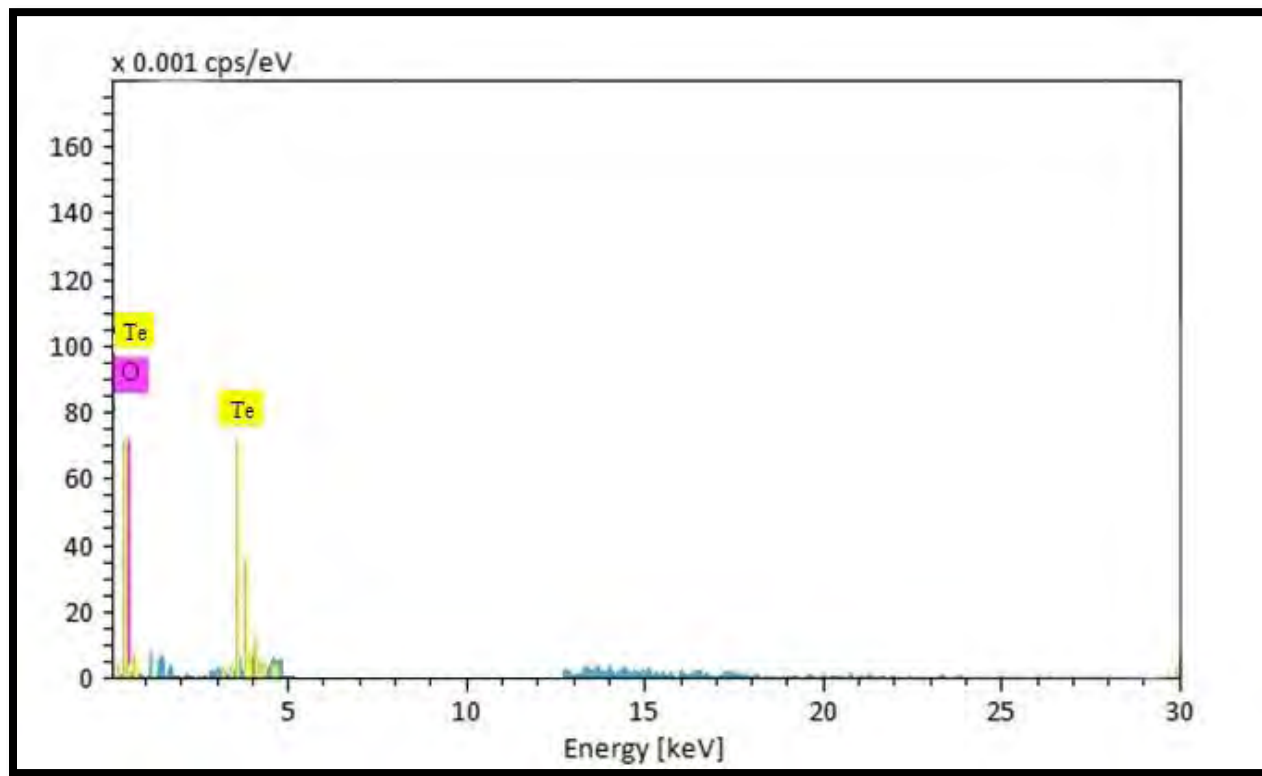
Figure 3.16.3 Energy diffraction X-Ray (EDX) of tellurium oxide NPs
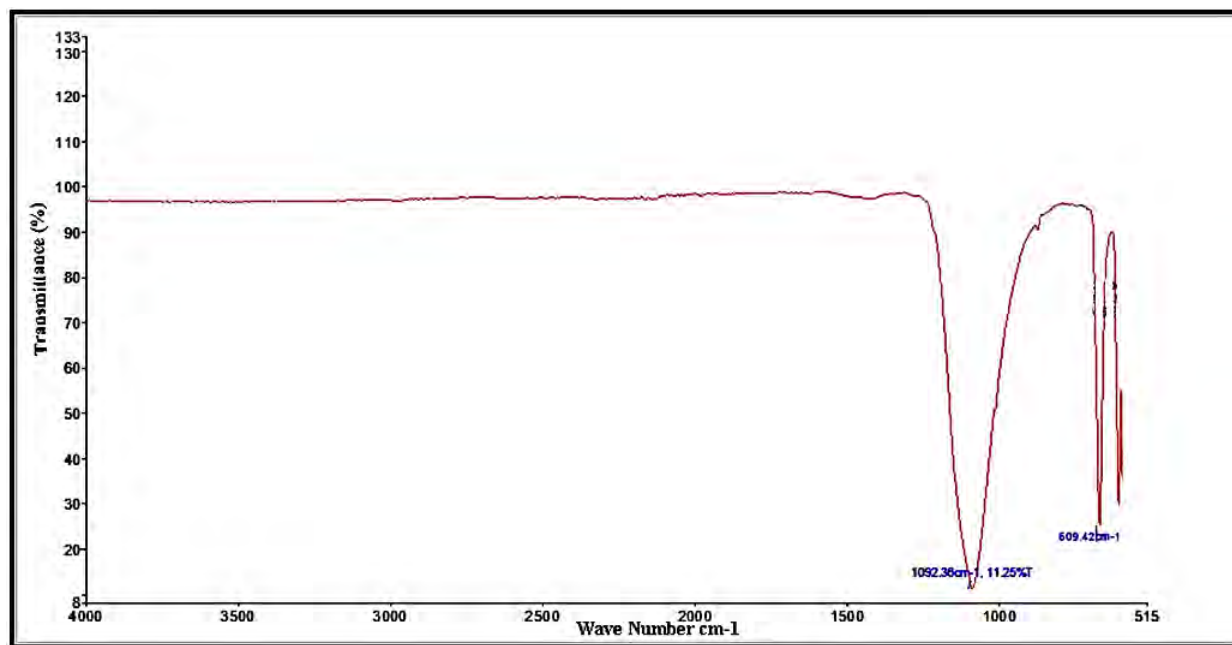
Figure 3.16.4 FTIR spectrum of tellurium oxide NPs
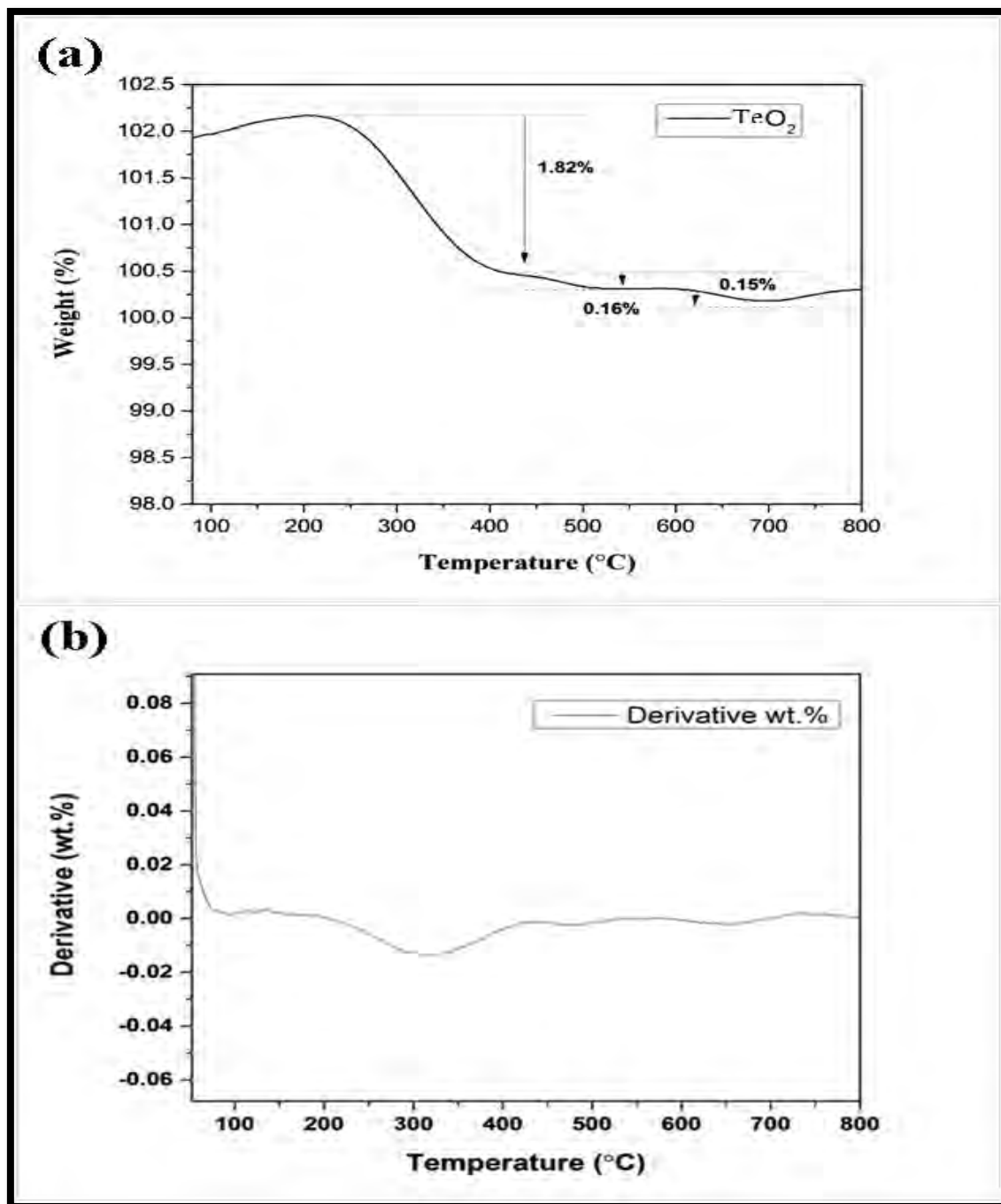
Figure 3.16.5 (a) TGA of tellurium oxide nanoparticles with (b) derivative thermogram

3.16.2 Biodiesel synthesis *via* transesterification

Cupressus sempervirens L. novel, non-edible seed oil was used to create sustainable biodiesel. According to earlier reports, only feedstock with an oil concentration of more than 20% will be taken into account for the manufacturing of biodiesel (Qiu et al., 2012). *Cupressus sempervirens* is recommended for large-scale biodiesel production due to its seed oil concentration of 29% (w/w), which is much higher than average. *Cupressus sempervirens* is also readily available in the wild, making it a highly promising source for the generation of renewable biodiesel. The amount of free fatty acids in seed oil before transesterification was estimated and found to be 0.42 (wt.%). The specification for much lower FFA content called for one stage transesterification. To partially transesterify triglycerides into fatty acid methyl esters, oil sources with greater than 3% FFA must undergo an additional stage of acid esterification (Adepoju et al., 2020). *Calendula arvensis* L aqueous leaf extract was used to make green nano-particles of TeO which were then employed to catalyze the transesterification of seed oil.

Reaction parameters have an impact on the transesterification reaction. As a result, it is necessary to analyze the best transesterification reaction conditions to achieve the highest yield of biodiesel. In the current study, a Central Composite Design (CCD) was created by DOE (Design of Experiment) using four independent transesterification variables with lower and higher values, namely the methanol to oil molar ratio of 2:1–14:1, the catalyst concentration of 0.36–0.88%, the reaction time of 60–180 min, and the temperature of 65–120 °C. (Table 3.16.1). The comparison of the transesterification yield's expected and actual yields is shown in Figure 3.16.6. The distribution of the anticipated and actual values is discovered to be close to the straight line, indicating a strong correlation between them. Table 3.16.3 presents the findings of a statistical analysis of variance (ANOVA) of the response surface quadric model. With a low *p*-value of 0.0015 (<0.05), the quadric model was judged to be significant. The F-value for the experimental model's lack of fit in relation to pure error was 5.22, which is not statistically significant. For the quadric model, a decent lack of fit value is one that is not statistically significant and has a chance of 24.53% being caused by noise. Temperature (C^2) was the most significant of the transesterification quadratic terms, with a p-value of 0.0086 (<0.05), followed by catalyst loading (B^2) and reaction time (A^2). The projected R^2 value was 0.7521, which is

closer to the corrected R^2 value of 0.8297 with a variance smaller than 0.2, based on the results provided in Table 4. The model's accuracy was confirmed to be adequate and to be greater than 4. The present experimental model's higher value of Adequate Precision showed how effectively the experimental model can be used to forecast biodiesel yield. The following is the polynomial equation (8) used in the quadric model.

Biodiesel Yield (wt. %) = +84.54+0.0000 *A-0.3941 *B-0.1320 C+3.80 *D-0.4375 *AB-0.9375 *AC-1.31 *AD-0.5625 *BC-1.18 *BD-2.94 *CD-5.23 *A²-5.69* B²-10.05 *C²-1.36 *D² (22)
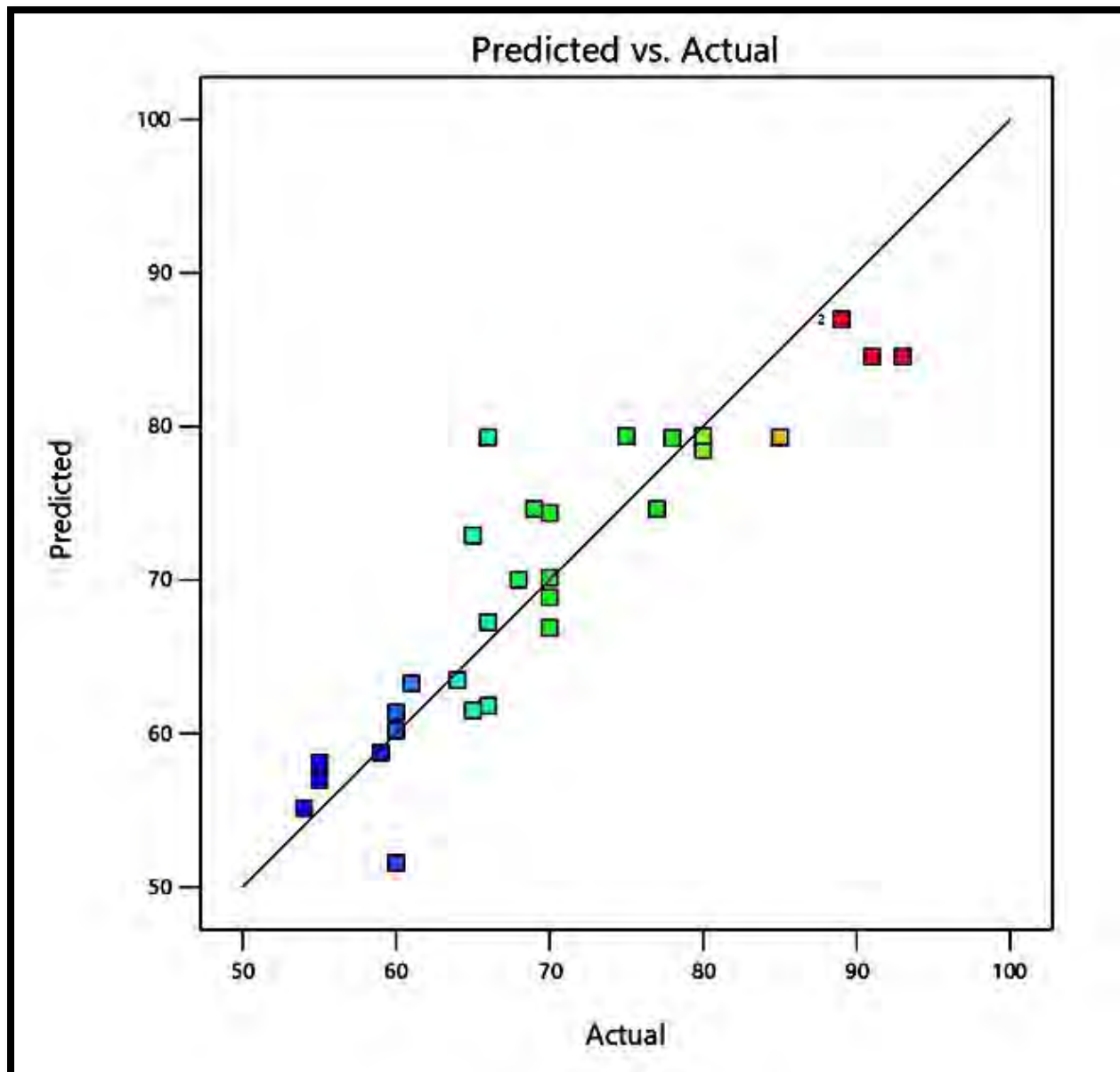
Figure 3.16.6 Comparison between the experimental and the predicted yield of biodiesel in model

Table 3.16.1- Experimental design by central composite design for transesterification reaction

Process parameters	−1	+1
Methanol to oil ratio	2:1	14:1
Catalyst loading (wt. %)	0.36	0. 88
Reaction time (min)	60	180
Temperature (∘C)	65	120

Table 3.16.2- Detailed experimental result for transesterification reaction of *Cupressus sempervirens* Biodiesel

	Factor 1	Factor 2	Factor 3	Factor 4	Response
Run	A: Alcohol to oil molar ratio	B: Catalyst loading wt.%	C: Temperature °C	D: Reaction time (min)	Yield wt.%
1	8.1	0.62	120	120	88
2	8.1	0.62	120	60	65
3	2.1	0.62	65	120	68
4	8.1	0.88	92.5	120	89
5	2.1	0.36	120	180	70
6	14.1	0.36	92.5	180	66
7	8.1	0.88	120	120	64
8	14.1	0.88	120	60	60
9	8.1	0.62	92.5	60	80
10	8.1	0.62	92.5	120	93
11	8.1	0.36	92.5	60	68
12	14.1	0.62	120	120	61
13	8.1	0.62	65	60	59
14	8:1	0.36	65	120	55

15	2.1	0.88	92.5	120	55
16	2.1	0.36	120	60	60
17	8.1	0.62	92.5	60	77
18	8.1	0.62	120	120	70
19	2.1	0.62	92.5	120	66
20	14.1	0.36	92.5	120	60
21	8.1	0.62	65	120	69
22	8.1	0.62	120	60	75
23	14.1	0.88	65	180	66
24	8.1	0.36	92.5	120	78
25	2.1	0.36	92.5	60	54
26	14.1	0.88	120	180	55
27	8.1	0.36	92.5	60	65
28	8.1	0.62	92.5	180	89
29	8.1	0.88	92.5	180	80
30	2.1	0.88	65	60	54

Table 3.16.3- ANOVA for Response Surface Quadratic model

Source	Sum of Squares	df	Mean Square	F Value	p-value	
Model	2985.71	14	213.26	5.22	0.0015	significant
A-Methanol to oil Ratio	0.0000	1	0.0000	0.0000	0.0254	
B-Catalyst Concentration	2.90	1	2.90	0.0709	0.0037	
C-Temperature	0.3255	1	0.3255	0.0080	0.0301	
D-Time	297.41	1	297.41	7.28	0.0165	
AB	3.06	1	3.06	0.0749	0.0680	
AC	14.06	1	14.06	0.3441	0.0262	
AD	27.56	1	27.56	0.6745	0.0243	
BC	5.06	1	5.06	0.1239	0.0298	
BD	23.25	1	23.25	0.5690	0.0423	
CD	138.06	1	138.06	3.38	0.0159	
A²	86.60	1	86.60	2.12	0.0461	
B²	106.15	1	106.15	2.60	0.0279	
C²	372.80	1	372.80	9.12	0.0086	
D²	7.58	1	7.58	0.1856	0.4727	
Residual	612.96	15	40.86			
Lack of Fit	566.46	11	51.50	4.43	0.0817	not significant
Pure Error	46.50	4	11.62			
Cor Total	3598.67	29				

$R^2 = 0.8297$, Std. Dev. = 4.39,   C.V. % = 8.09, Adeq Precision = 7.8311

3.16.3 Impact of reaction parameters on Transesterification

3.16.3.1 Combined influence of methanol to oil molar ratio and catalyst loading

The mutual effects of catalyst load and Met:Oil on biodiesel yield during transesterification are taken into account and have a significant impact. Numerous experimental experiments were conducted in this study with this goal in mind. The frame of the 3-D figure presented in Figure 3.16.7a illustrates the communal influence of Met:Oil and catalyst load on transesterification of *Cupressesus sempervirens* seed oil. At catalyst load of 0.62 (wt.%), Met:Oil of 8:1, duration of 120 (mins), and reaction temperature of 92.5 ∘C, the highest FAME yield of 93% was obtained (Run 10). Low yield of 86% was achieved with a high catalyst load of 0.88 (wt.%) and the same Met:Oil (8:1) ratio (Run 4). at Run 201, a higher Met:Oil ratio of 14:1 and a catalyst load of 0.36 wt.% led to a minimum yield of 60%. A surplus of methanol thins the catalyst concentration in the reacting mixture, favoring reversible glycerolysis and facilitating the reaction of glycerol with FAMEs, which leads to the resynthesis of monoglycerides (Balajii et al., 2020). Additionally, yield was reduced to 55% at Run 15 with a catalyst quantity of 0.88 (wt%) and a lower Met:Oil ratio of 2:1. With a *p*-value of 0.0254 (<0.05), the mutual interaction between catalyst load and Met:Oil was determined to be significant in the ANOVA findings.

3.16.3.2 Combined influence of methanol to oil ratio and reaction time

Another crucial reaction parameter with a significant impact on FAME output is Met:Oil. The mutual interplay of Met:Oil and time is seen in Figure 3.16.7b. With reaction time of 120 min and a Met:Oil ratio of 8:1, while maintaining other conditions such as temperature of 92.5 ∘C and catalyst load of 0.36 wt.%, the highest yield of 93% was observed (Run 10). Similar to the prior interaction, which had a greater Met:Oil ratio of 14:1 and a 180-minute reaction period, at Run 6 yield was reduced by 60%. Contrarily, a shorter period of 60 minutes and a lower Met:Oil ratio of 8:1 led to a little higher yield of 65% at (Run 27). At Run 25, a MET:Oil ratio 2:1 and a period of 60 minutes produced a yield of up to 55%. The most likely explanation is that the reactants were not given enough time or methanol to fully mix and establish an equilibrium state, leading to an incomplete transformation of the reactants into products (Adepoju, 2020). Given its *p*-value of 0.0243, a significant association between Met:Oil and response time was found.

3.16.3.3 Combined influence of methanol to oil molar ratio and temperature

Figure 3.16.7c shows the reciprocal interaction of Met:Oil and reaction temperature on transesterification. With a reaction temperature of 92.5 ◦C, a Met:Oil ratio of 8:1, and constant catalyst load (0.62 wt.%) and time 120 min run number 10 produced a 93% FAME yield. Using a Met:Oil ratio of 8:1 and a higher temperature of 120 oC resulted in a minimum yield of 70% at Run 18. The saponification of glycerol and the boiling point of methanol (65 ◦C) were significant yield-limiting issues for biodiesel. A lower Met:Oil ratio of 2:1 at 65 oC has secured an 68% yield (Run 3). At Run 12, a higher reaction temperature of 120 ◦C and a 14:1 Met:Oil ratio resulted in a yield reduction of up to 61%. As a result, it was concluded from the current experiment that the interaction between Met:Oil and reaction temperature is positive during transesterification. This mutual interaction's p-value of 0.05 indicated that it was significant (0.0262).

3.16.3.4 Combined influence of time and catalyst loading

Figure 3.16.7d shows the combined impact of time and catalyst load on transesterification within the context of a three-dimensional plot. While maintaining the other two parameters, reaction temperature of 92.5 ◦C and Met:Oil of 8:1, the greatest FAME production of 93% was obtained at catalyst loading of 0.62 wt.% and time (120 min) (Run 10). However, at Run 29, an above-optimal level reaction with a high catalyst loading of 0.88 (wt.%) and 180 min provided an 80% yield. With a medium time of 120 min and an increase in nano-catalyst load up to 0.63 wt.%, yield increased to 78%. (Run 24). With the same catalyst load and 60 min time period, the percentage yield was reduced even more to 77%. (Run 17). A yield of 68% was obtained at Run 11, and a shorter reaction time of 60 min with a catalyst load of 0.36 wt.% was determined to be insufficient. In the current study, the combined effect of time and catalyst load was determined to be significant in the ANOVA results due to its *p*-value (0.0423) <0.05.

3.16.3.5 Combined influence of catalyst loading and reaction temperature

The mutual interaction of the nanocatalyst load and temperature at constant 8:1 Met:Oil and time (120 min) is shown in Figure 3.16.7e,. A catalyst dosage of 0.62 weight percent and a

reaction temperature of 92.5 ∘C resulted in the highest FAME yield of 93% (Run 10). It is believed that the source of these reaction conditions during transesterification is the maximum contact of oil with methanol (Hadiyanto et al., 2016). FAME yield increased to 88% at Run 1 due to higher temperature of 120 oC and higher catalyst load of 0.62 wt.%. At Run 7, the lowest yield of FAME (64%) was produced with an catalyst load of 0.88 weight percent at 120 ∘C. The stalling of the forward reaction is attributed to the methanol's low boiling point. At Run 14, a catalyst load of 0.36 weight percent and a temperature of 65 ∘C resulted in an 55% yield of methyl ester. Given its *p*-value of 0.0298, the combined interaction of these parameters was significant.

3.16.3.6 Combined influence of time and temperature

Effects of time and temperature on FAME yield at constant catalyst load 0.62 wt.% and Met:Oil 8:1 in the frame of the three-dimensional has been displayed in Figure 3.16.7f. Run 5 demonstrates that at 120 minutes and 92.5 ∘C, a maximum yield of 93% was achieved. At Run 22, the FAME yield was condensed to 75% with a medium runtime of 60 min and a lower reaction temperature of 120 ∘C. At run 13, a further decrease in time length up to 60 min at 65 ∘C resulted in a 59% yield. This study showed that while methyl ester production increased with increased reaction temperature and duration up to a certain point, beyond that there was a significant fall in percent yield, which is likely due to the endothermic nature of transesterification. At Run 30, the FAME yield was reduced further by a lower reaction time of 60 min and a higher reaction temperature of 120 ∘C, yielding 65%. With a *p*-value of 0.0159, the mutual interaction between time and temperature was determined to be significant.
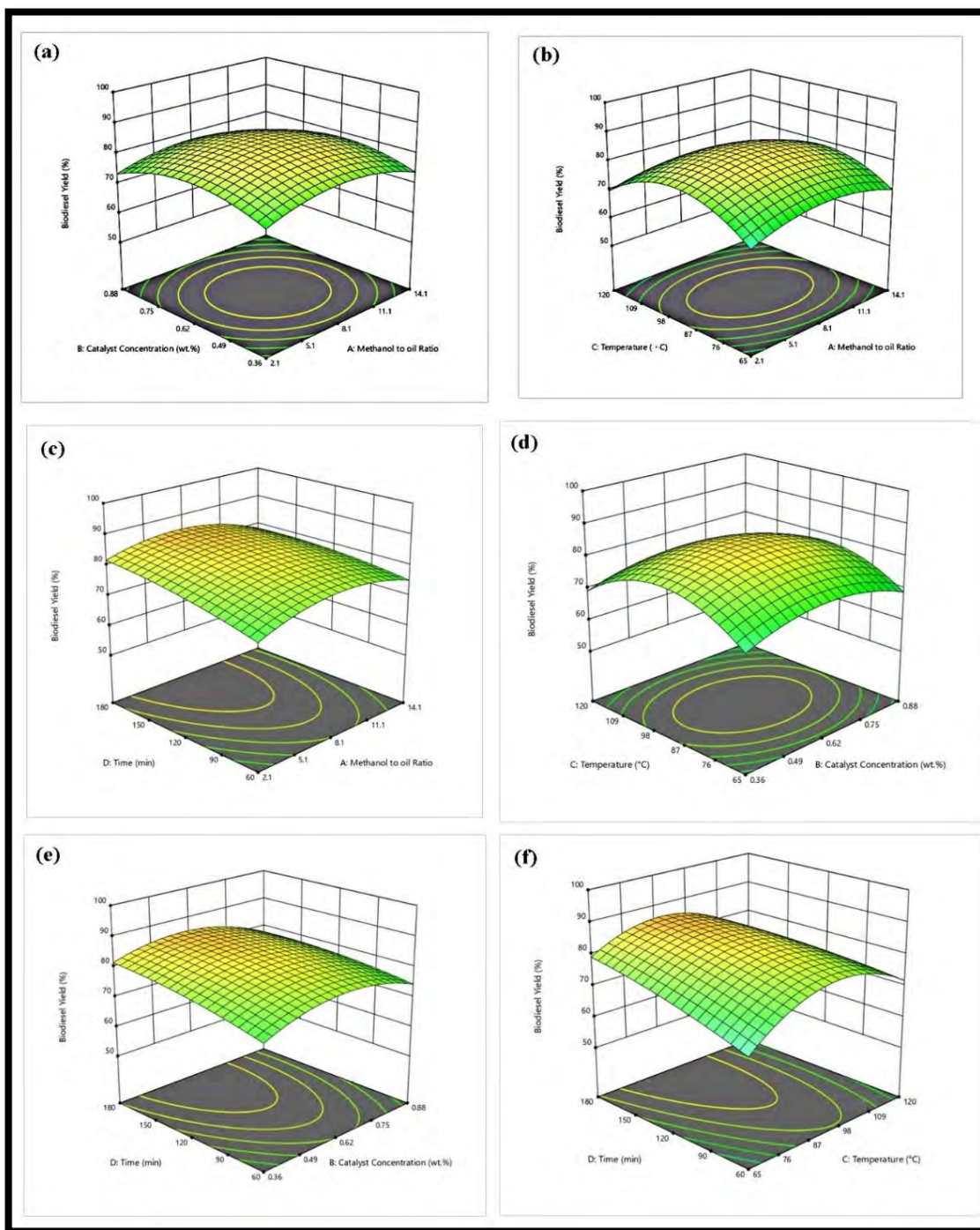
Figure 3.16.7 Influence of the reaction parameters of Transesterification on biodiesel

3.16.4 Characterization of *Cupressus sempervirens* Biodiesel

3.16.4.1 FT-IR Analysis

FT-IR analysis is frequently used to confirm FAME synthesis in biodiesel samples, which is subsequently confirmed by the NMR spectrum. The nature of the functional groups in the synthesized methyl ester of *Cupressus sempervirens* was investigated using FT-IR analysis. Figure 3.16.8 a and b, respectively, show the FTIR spectrum of *Cupressus sempervirens* seed oil and the corresponding methyl ester. The FTIR spectrum of seed oil and methyl ester showed distinct chemical groups through various stretches and bands. There are two prominent bands among them, located at 1464.20 cm^{-1} for the methyl group and 1743.54 cm^{-1} for the carbonyl group (C=O) (CH$_3$). In the IR range of 2853.30 cm^{-1} for C-H (sp^2) stretching and at 2922.74 cm^{-1} for C-H (sp^3), another significant representative peak of biodiesel was seen. The area of the carbonyl group among all of these peaks is thought to be chemically sensitive (Lin et al.., 2009). Additionally, the biggest variable IR regions of seed oil and methyl ester were found to be at distances of around 2200–3300 cm^{-1}, 1000–1800 cm^{-1}.

The stretch for C-H$_2$ wagging-frequency in the spectrum of methyl ester was seen at 1097.77 cm^{-1}. Strong peak found at 3317.80cm^{-1} for ($\equiv$ C-H) wipe out in the spectra of seed oil for biodiesel. The FAME spectra of the *Cupressus sempervirens* seed oil revealed the disappearance of another deep peak at 1022.77 cm^{-1} in the IR spectrum. Thus, the methyl ester and all the IR-peaks of the IR spectra of *Cupressus sempervirens* seed oil have demonstrated that triglycerides are converted to FAME.

3.16.4.2 NMR Spectroscopic Analysis

To evaluate the percentage yield of *Cupressus sempervirens* methyl ester and to gather quantitative information about the chemical constituents present in the biodiesel, ^{1}HNMR was used. Assuring the synthesis of methyl ester from triglycerides during transesterification is done analytically. The methylene group and the proton of produced esters were thought to be aware of the transesterification reaction product. Figure 3.16.9a shows the ^{1}HNMR spectrum of the methyl ester of *Cupressus sempervirens.* A significant methoxy group (- OCH$_3$) peak was seen in

the ^{1}HNMR spectrum at 3.675 ppm, indicating the existence of FAMEs in the biodiesel. There was no unwanted free methanol peak at 3.45 ppm. Additionally, a signal at 2.338 ppm that represented a triplet of -CH₂ proton was discovered. Deep peak protons of -CH₂ (-methylene) were seen as a singlet between 1.262 and 1.311 ppm. At 0.868 and 0.889 ppm, putative protons peaks of terminal methyl were found in a sequence. Olefinic hydrogen (-CH=CH-) was judged to peak at 5.294–5.370 ppm. At 2.759 ppm, the allylic hydrogen (-CH₂) peak is located. The presence of the aforementioned peaks in the ^{1}HNMR spectrum provided proof that FAME was present. the total conversion of reactants into FAME, was determined to be 93%.

The methyl ester of *Cupressus sempervirens* carbonyl (-COO-) and C-O group positions were studied using the ^{13}CNMR spectra (Figure 3.16.9b). The distinctive peak of methoxycarbon was found to be at 51.42 ppm, while the carbonyl group (-COOH) signal was found to be at 174.29 ppm. Chemical shifts and peaks indicating the unsaturated position (-CH=CH-) in biodiesel were discovered at 127.89 (ppm) and 129.73 ppm (-CH=CH-), respectively. The C-O group in the methyl ester was present at 77.48 ppm in contrast to the lengthy chain of ethylene carbon (-CH₂-)n at 29.33 ppm (-C-O). At 34-31 ppm in the ^{13}CNMR spectrum, the carbon signal for aliphatic methylene (-CH₂-s) was detected.

3.16.4.3. GC/MS

Variations in the composition of FAMEs contained in biodiesel have a significant impact on both its physical and chemical qualities. By using GC/MS analysis, the chemical make-up and purity of the synthesized methyl ester of *Cupressus sempervirens* were evaluated. As shown in Figure 3.16.10, seven unique peaks were detected in the chromatogram of *Cupressus sempervirens* biodiesel that were anticipated by the library match program NO. NIST02 utilizing the retention periods of FAMEs. Both saturated and unsaturated fatty acids are present in these seven peaks. Five FAMEs with an unsaturated nature make up the group. Saturated fatty acids included Octadecanoic acid, methyl ester (C18:0), Hexadecanoic acid, methyl ester (C16:0), while unsaturated FAMEs included 5, 8-Octadecadienoic acid methyl ester (C18:2), and 9-Octadecenoic acid, (2)-methyl-, methyl ester (C18:1). The primary fatty acid with the largest abundance was discovered to be 9-octadecenoic acid methyl ester. The methyl ester sample was found to have lower levels of unsaturation, which is desirable since it leads to more even and

reliable fuel combustion in diesel engines (Ajith et al., 2020). The methyl ester of *Cupressus sempervirens* shown by GC/MS analysis is highly effective and suitable for large-scale.
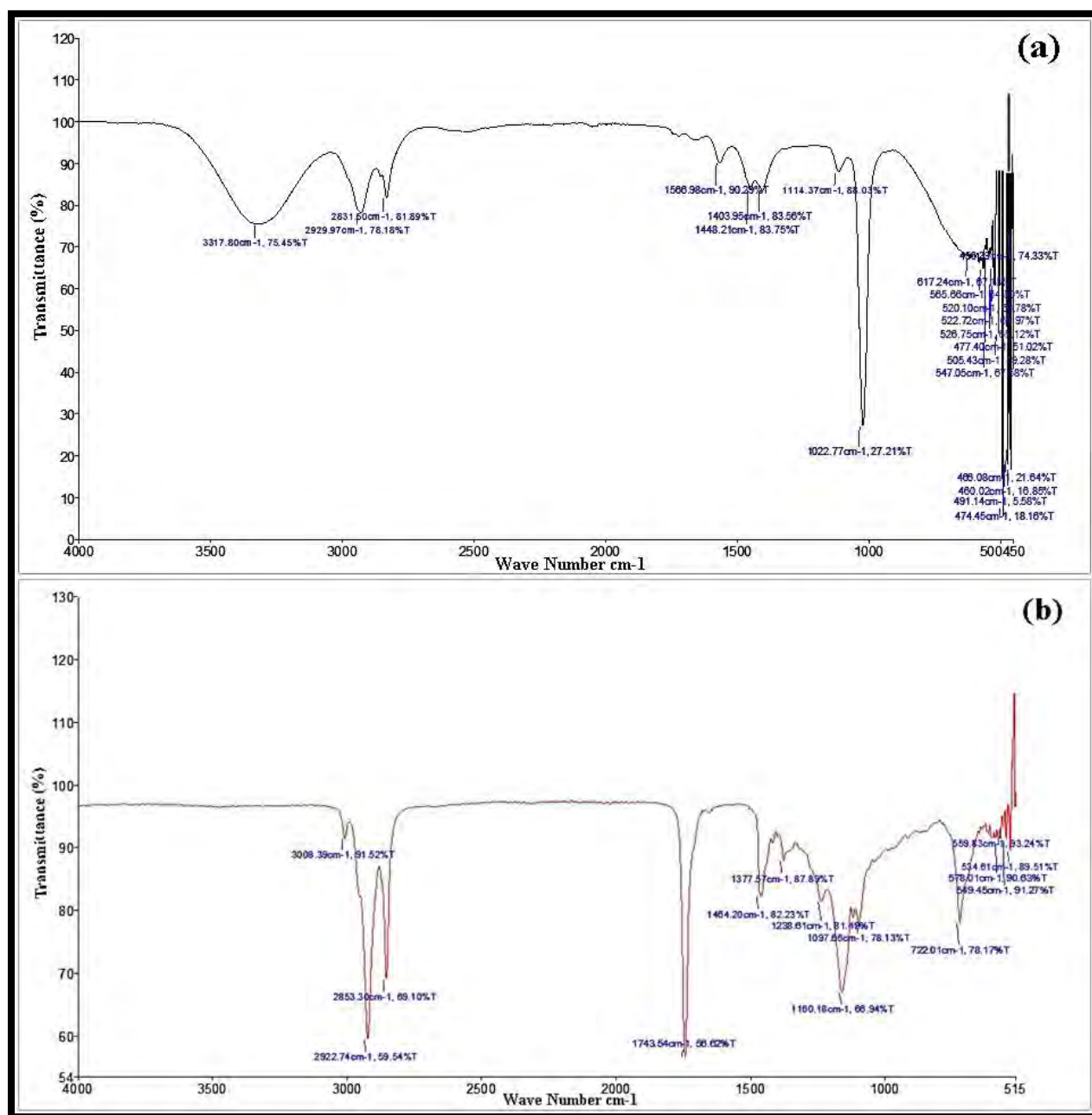
Figure 3.16.8 FTIR spectrum of *Cupressus sempervirens* **(a)** seed oil and **(b)** biodiesel
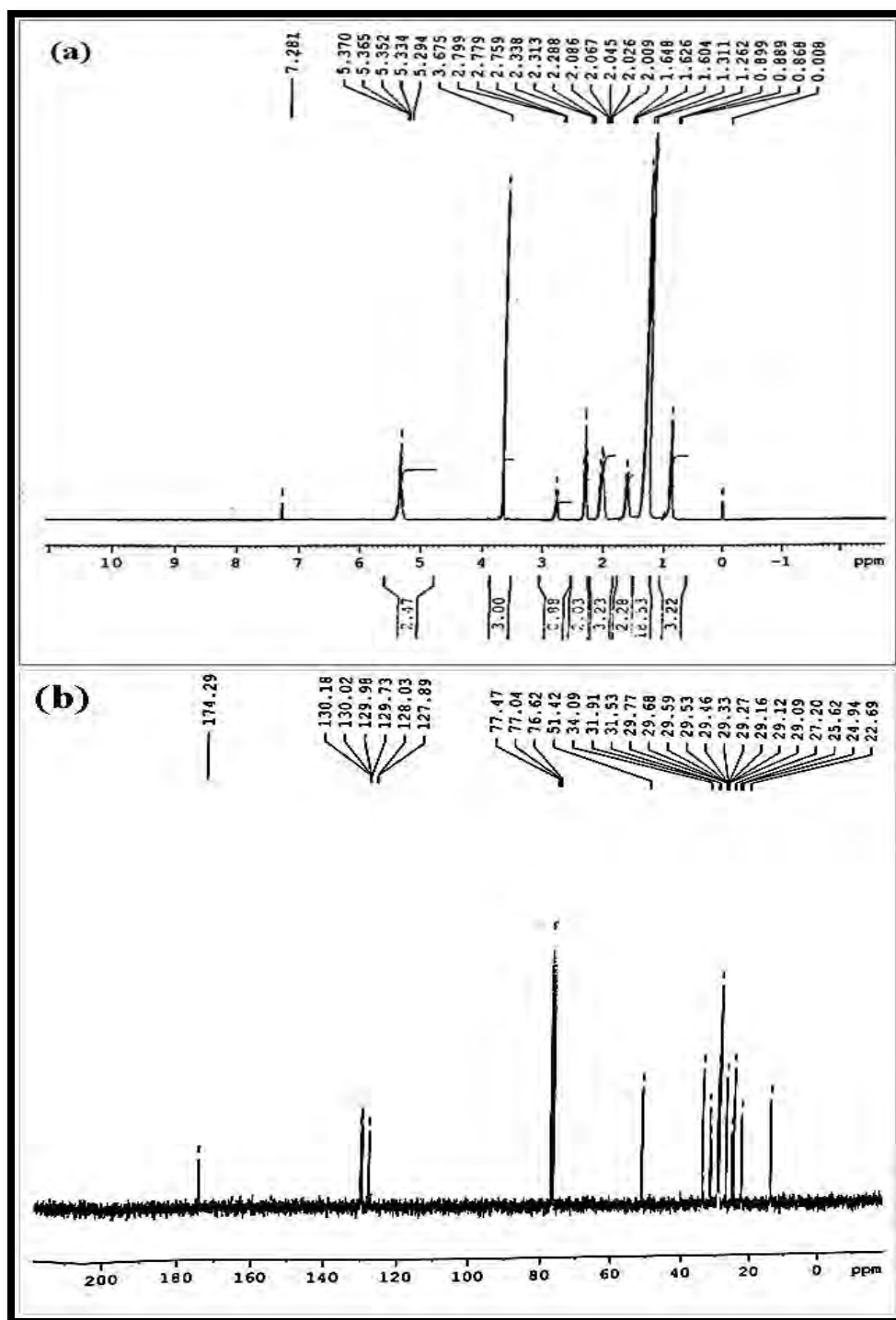
Figure 3.16.9 **(a)** ¹HNMR and **(b)** ¹³CNMR of *Cupressus sempervirens* biodiesel
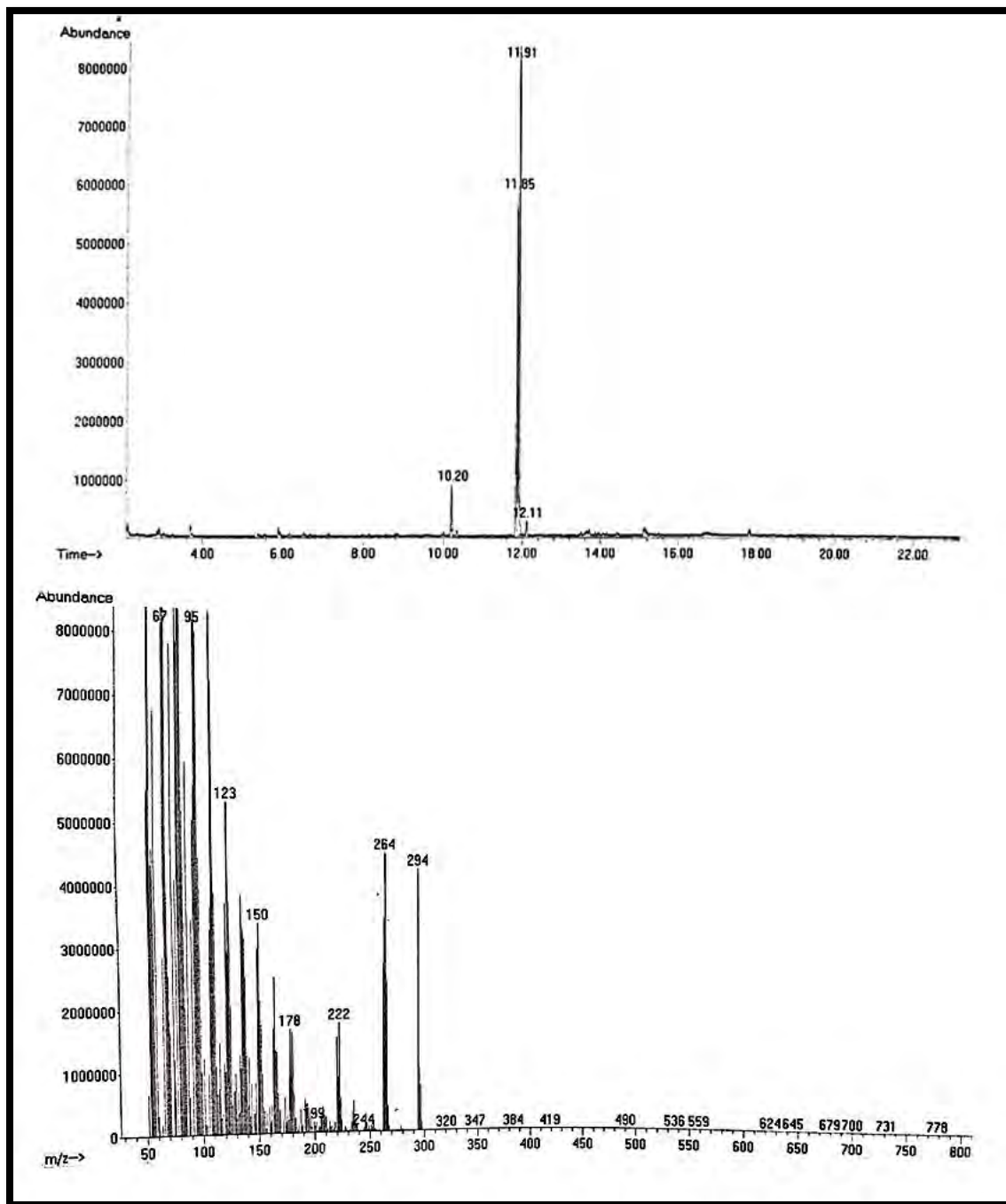
Figure 3.16.10 GC-MS spectrum of *Cupressus sempervirens* biodiesel

3.16.5. Fuel Properties of biodiesel

The fuel attributes of biodiesel, which must adhere to current international fuel regulations, are one of the most important factors to consider. The fatty acid makeup of the raw material used to make biodiesel has a big impact on how fuel-efficient it is and varies from feedstock to feedstock. Prior to practical application, the fuel qualities of *Cupressus sempervirens* biodiesel were investigated and compared with worldwide standards of ASTM D-6571, EN 14214, and China GB/T 20828-2007. All of these characteristics were found to be in line with international standards, as indicated in Table 3.16.4.

The acid value of biofuels is a significant fuel attribute that has a big impact on fuel quality and engine performance. The quantity of potassium hydroxide required to neutralize the free fatty acids found in a sample fuel liquid is what is meant by this term. Higher acid content in biodiesel causes problems in fuel engines, particularly in rubber parts, particularly in older diesel engines by producing corrosion. Utilizing the ASTM-D974 standard, the acid value of *Cupressus sempervirens* methyl ester was discovered to be 0.141 (mg KOH/gm), which was within the permitted international range.

Engine efficiency, fuel spraying, and fuel movement inside pipelines and injector nozzles are all directly impacted by biodiesel density. Biofuels often have a higher density than other types of diesel fuel. As a result of increased biodiesel viscosity, insufficient fuel combustion, and the emission of exhaust pollutants, higher fuel density is not desirable (Helmi et al., 2021). The density of *Cupressus sempervirens* biodiesel was 0.612 (mm^2/s), which is within the range of acceptable fuel density.

Another crucial characteristic of methyl ester is its viscosity. Fuel atomization and injector lubrication are impacted by both greater and lower fuel viscosities. Lower fuel viscosity causes leakage issues and offers less lubrication for fuel injection pumps, which reduces engine power. Like this, increased viscosity causes the injection pump to run out of gasoline and reduces engine performance (Khan et al., 2021). The biodiesel from *Cupressus sempervirens* was found to have a kinematic viscosity of 4.15 (mm^2/s), which is within the permitted range of the ASTM D-6751 and European Union 14214 standards.

The temperature at which fuel ignites while maintained at flame is known as the flash point. The equivalent flash point has a significant impact on fuel storage and transportation. Higher flash points are preferable as they reduce the risk of unintentional fire (Campli et al., 2021). Because biodiesel has a greater flash point than traditional fossil fuels, there is less risk during transportation. According to Table 4, the methyl ester of *Cupressus sempervirens* was discovered to have a flash point of 98 °C, which is higher than petro-diesel and suitable for use in the transportation industry.

The pour and cloud point of biodiesel are parameters playing a significant role in regulating operability of diesel engines at low temperatures in colder parts of the world. The pour point of biodiesel is under direct influence of saturated fatty acids and fluctuates with composition of fatty acid found in oil used in transesterification. The pour point of *Cupressus sempervirens* methyl ester was found to be -10 °C which appears aligned to international standards. Likewise, cloud point specifies the temperature at which a fuel turns down to crystal phase. In our current study, cloud point was found -8 °C as shown in Table 4 which is align to international standards. Using the ASTM-D4294 method, the methyl ester of *Cupressus sempervirens* sulfur content was determined. In contrast to petro-diesel, which has a sulphur concentration in the range of 50 ppm, a sample of synthesized methyl ester was found to have a minimum sulphur content of 0.0002% declining in the scale of less than 1 ppm. One of the major benefits of biodiesel over conventional petroleum-based fuel is the presence of sulphur content less than 1 ppm, which results in environmentally favorable low sulphur dioxide gas emission (Lamba et al., 2017).

Table 3.16.4 - Comparison of Fuel properties of previously reported biodiesel sources with that of *Cupressus sempervirens* biodiesel fuel properties**.**

Property	Methods	*Cupressus sempervirens*		ASTM D-6751	EN-14214	China GB/T 20828-2007
		Mean	St. Dev.			
Color	Visual	2	-	2.0		
Acid number (mg KOH/g)	ASTM-D974	0.141	0.1	≤0.5	≤0.8	≤0.5
Flash Point (°C)	ASTM-D93	98	1.2	≥93	≥130	≥120
Pour Point (°C)	ASTM-D97	-10	0.4	-15-16	_	_
Viscosity (mm²/s at 40 °C.)	ASTM-D445	4.15	0.5	1.9-6.0	_	3.4-5.0
Density (kg/m³ at 40 °C)	ASTM-D1298	0.612	1.06	≤120	_	≤120
Sulphur content (wt.%)	ASTM-D4294	0.0002	1	≤0.05	≤0.05	≤0.20
Cloud point (°C)	ASTM-D2500	-8	1	-3.0-12	_	_

3.16.6. Catalyst Reusability and recycling

To determine a nano-stability catalyst's and recyclability, it must be investigated as to whether it can be reused. Catalyst recyclability is necessary for the economically viable generation of biodiesel (LaGrow et al., 2019). Reusability of TeO nanoparticles was investigated under the ideal reaction circumstances (catalyst concentration of 0.62 weight percent, Met:Oil of 8:1, time of 120 min, and temperature of 92.5 ∘C). In the first few cycles, there was little change in the percentage production of biodiesel, and the transesterification catalytic activity of nanoparticles was successfully maintained. In the fifth cycle, the biodiesel output gradually dropped to 70%, and in the sixth cycle, it further dropped to 66%. It could be explained by a decrease in the green nanocatalyst's active sites brought on by the buildup of organic molecules on its surface (Figure 3.16.11). In the seventh cycle, the lowest yield of biodiesel, 60%, was obtained. Reusability of TeO nanoparticles in transesterification has the potential to lower the overall production's raw cost on a big scale.
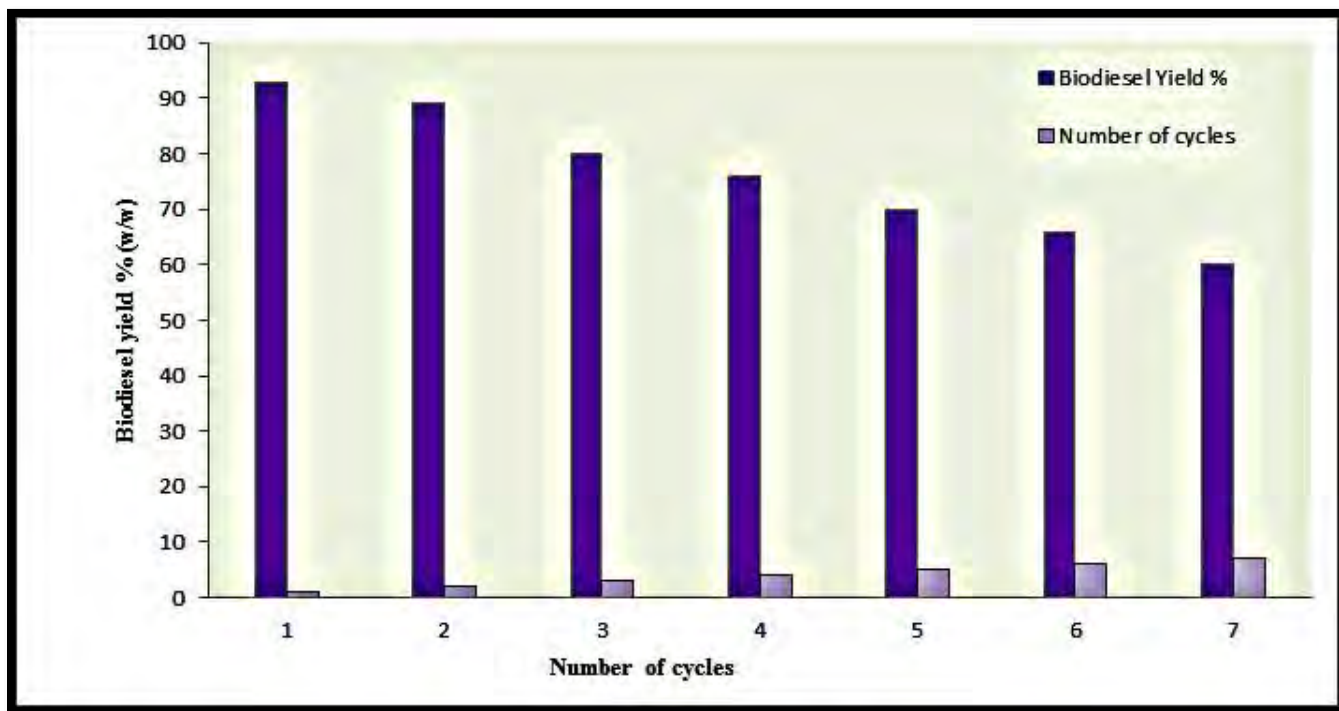
Figure 3.16.11 Reusibility of tellurium oxide NPs in transesterification reaction

4. Conclusion and Future Recommendations

Our current study inclusive investigated fifteen novel, non-edible seed oil feedstock as a source of green bioenergy regarding their micromophological characteristics *via* scanning electron microscopy (SEM). A comprehensive evaluation of selected oil seeds for their potential as green and renewable source of biodiesel to tackle issues raised by energy crises. Non-edible seed oil yielding oil plants can be cultured on waste or marginal land and have lower cultivation costs due to their ability to produce a large yield without requiring a lot of attention. These plants thrive well in arid and semi-arid environments and require less fertile ground and precipitation.

In this study, fifteen novel, highly potential non-edible, and novel feedstocks such as *Cestrum nocturnum* L, *Cichorium intybus* L, *Zanthoxylum armatum* DC, *Citrus medica* L, *Citrus paradisi* Macfad and *Citrus aurantium* L., *Cupressus sempervirens*, *Trachyspermum ammi* (L.), *Cupressus macrocarpa, Nannorrhops ritchieana* (Griff.) Aitch., *Cordia myxa* L., *Cordia dichotoma* G.Forst., *Chamaerops humilis* L., *Monotheca buxifolia*, and *Grewia asiatica* (L.) are used for biodiesel synthesis using a variety of green nanocatalysts.

Results of light microscopy of seeds revealed distinct variation in seed size (15.8 -1.8 mm in length and 9.4-1.1 in width), shape (round to Cuneiform) and color (from black to yellowish green). Non-edible seed oil content fall in range of 28-38% (w/w). Free fatty acid (FFA) content varied from 0.56-2.06 mg KOH/g. Ultra morphological investigation of seeds surfaces via SEM exhibited distinctive variation in surface sculpturing, cell arrangement, cell shape, periclinal wall shape, margins, protuberances and anticlinal wall shape. Seed surface sculpturing varied from reticulate, semitectate, wrinkled, rugose, papillate, perforate and striate. Periclinal wall arrangements confirmed variation from glabrous, raised, depressed, elevated, smooth, pentagonal, entire and ripple margins. Whereas anticlinal walls pattern demonstrated variation from angular, smooth, wavy, deep, dentate, entire, irregular, puzzled, elongated, curved and depressed. The obtained results ultimately concluded that Scanning electron microscopy could serve as an advanced tool representing hidden ultra-structural characters of seeds. It offers

significant knowledge to researchers and the local community for their accurate and genuine identification.

Fifteen different green nanocatalysts (Silver oxide, Copper oxide, Magnesium oxide, Antimony oxide, Lead oxide, Zirconium oxide, Niobium oxide, Calcium oxide, Indium Oxide, Nickel Oxide, Cobalt oxide, Manganese oxide, Iron oxide, Zinc oxide and Tellurium oxide) were synthesized with aqueous leaves extract of various plant species. The activity of these nanocatalysts were assessed during transesterification of seeds oils to methyl ester using optimized conditions with application of response surface methodology. Following comparative key findings using various green nanocatalysts on different seed oils were

- The optimum reaction conditions for *Zanthoxylum armatum* seed oil using Ag_2O nanocatalyst were 0.5 wt. % catalyst loading, and molar ratio 1:7, temperature 90 ℃ and reaction time 120 min giving a highest yield (95%) of methyl ester.

- the optimum reaction conditions of *Citrus medica* seed oil using CuO nanocatalyst were methanol to oil ratio 8:1, catalyst loading 0.18 wt.%, reaction time 120 min and temperature 85 ◦C giving a maximum yield of 93% of methyl ester.

- A highest yield of 95% of fatty acid methyl esters (FAMEs) from *Cichorium intybus* novel seed oil using MgO was obtained with optimal reaction conditions methanol to oil molar ratio 9:1, catalyst loading of 0.83 (wt. %), reaction time 180 (min) and temperature 85 °C.

- At optimum reaction conditions of 0.56 wt.% of the catalyst and molar ratio of 8:1, time of 180 min and temperature 95 ◦C the highest yield (94%) of methyl ester was produced from *Cestrum nocturnum* seed oil via green nano catalyst of Sb_2O_3.

- The highest yield of 93% of biodiesel from *Citrus paradisi* seed oil using PbO was noted to be attained at with the following reaction parameters: methanol to oil ratio of 7:1, catalyst loading of 0.32 (wt.%), reaction time of 105 min., and temperature of 80 ◦C.

- The optimum reaction conditions for *Grewia asiatica* seed oil using Nb_2O_5 nanocatalyst were catalyst loading of 0.32 (wt.%), a methanol to oil ratio of 9:1, reaction time 180 min, and a temperature of 60 ◦C giving the highest yield of 90% biodiesel.

- High yield of 95% of biodiesel was obtained from seed oil of *Monotheca buxifolia* using green nano-particles of calcium oxide at optimum reaction conditions such as methanol to oil molar ratio of 9:1, catalyst loading of 0.83 (wt.%), reaction time of 180 min and temperature of 85 $^{\circ}$C.

- Highest biodiesel yield of 95% was achieved was obtained from *Cordia myxa* seed oil using In_2O_3 nanocatalyst at optimum reaction conditions of methanol to oil ratio of 7:1, catalyst load 0.8 (wt.%), temperature 82.5 $\circ$C and time 180 min.

- The optimum reaction conditions for *Cordia dichotoma* seed oil using NiO nanocatalyst were molar ratio of 7:1, catalyst loading 0.16 (wt.%), reaction time 115 min and temperature 80 $\circ$C giving biodiesel yield of 94%.

- Maximum methyl ester yield of 92% was achieved from *Chamaerops humilis* seed oil using CoO nanocatalyst at optimal reaction conditions of molar ratio 6:1, catalyst loading of 0.54 (wt.%), temperature 60 $^{\circ}$C and reaction time 3 h.

- The optimum reaction conditions for *Trachyspermum ammi* seed oil using MnO_2 nanocatalyst were molar ratio of 8:1, catalyst loading 0.26 wt.% temperature 90 $^{\circ}$C, and time 120 min giving high yield of 94%.

- The maximum yield of 93% was obtained from *Cupressus macrocarpa* seed oil using Fe_2O_3 nanocatalyst at optimal reaction conditions of catalyst loading of 0.7 wt. %, temperature 60 ($^{\circ}$C), reaction time of 120 min and methanol to oil molar ratio 9:1.

- For *Nannorrhops ritchieana* seed oil using ZnO nanocatalyst the optimum reaction conditions were molar ratio of 7: 1, catalyst loading of 0.18 (wt.%), reaction temperature of 80 $^{\circ}$C and time of 180 minutes giving a highest yield of biodiesel (95%).

- Lastly, the optimum reaction conditions for *Cupressus sempervirens* seed oil using TeO nanocatalyst were catalyst load of 0.62 (wt.%), molar ratio of 8:1, reaction time of 120 (mins), and temperature of 92.5 $\circ$C giving the highest FAME yield of 93%.

The reusability of heterogeneous green nano-catalysts was investigated at optimal reaction conditions of transesterification. In the first five runs of the experimental trials, catalysts had their highest catalytic activity, which led to a high yield of biodiesel. However, after the sixth cycle, the methyl ester output gradually decreases. This drop in yield with an increase in cycles

was attributed to the organic species present in the transesterification reaction mixture leaching and poisoning the active sites of nanoparticles. Fuel properties of synthesized biodiesels were investigated and determined to be comparable to worldwide ASTM D-6571 EN 14214 and China GB/T 20828-2007 standards. It was finally concluded that waste biomass of non-edible seed oil seeds can be efficiently converted into value-added products like biodiesel and glycerol.

However, it is recommended to quantitatively demonstrate the viability of this technology, the technical difficulties, such as engine evaluation and economic feasibility, need be further researched. Economic research on biodiesel production is lacking. A bridge between laboratory investigations and practical application could be made with the use of such an analysis. In the future, after reusability testing, it is advised to examine catalyst active sites, its reaction mechanism, and catalytic characterization. Some strategies to reduce the cost include the use of integration process and utilization of waste or non-edible oils should also be investigated profoundly.

References

Abbasi, B. A., Iqbal, J., Khan, Z., Ahmad, R., Uddin, S., Shahbaz, A., ... & Mahmood, T. (2021). Phytofabrication of cobalt oxide nanoparticles from Rhamnus virgata leaves extract and investigation of different bioactivities. *Microscopy Research and Technique*, *84*(2), 192-201.

Abd Malek, M. N. F., Pushparaja, L., Hussin, N. M., Embong, N. H., Bhuyar, P., Rahim, M. H. A., & Maniam, G. P. (2021). Exploration of efficiency of nano calcium oxide (CaO) as catalyst for enhancement of biodiesel production. *Journal of microbiology, biotechnology and food sciences*, *11*(1), e3935-e3935.

Abd Manaf, I.S., Embong, N.H., Khazaai, S.N.M., Rahim, M.H.A., Yusoff, M.M., Lee, K.T. and Maniam, G.P., 2019. A review for key challenges of the development of biodiesel industry. *Energy Conversion and Management*, *185*, 508-517.

Abdullah, B., Muhammad, S. A. F. A. S., Shokravi, Z., Ismail, S., Kassim, K. A., Mahmood, A. N., & Aziz, M. M. A. (2019). Fourth generation biofuel: A review on risks and mitigation strategies. *Renewable and sustainable energy reviews*, *107*, 37-50.

Abukhadra, M. R., Salam, M. A., & Ibrahim, S. M. (2019). Insight into the catalytic conversion of palm oil into biodiesel using Na+/K+ trapped muscovite/phillipsite composite as a novel catalyst: Effect of ultrasonic irradiation and mechanism. *Renewable and Sustainable Energy Reviews*, *115*, 109346.

Adeniyi, O. M., Azimov, U., & Burluka, A. (2018). Algae biofuel: current status and future applications. *Renewable and sustainable energy reviews*, *90*, 316-335.

Adepoju, T. F., Olatunji, O. M., Ibeh, M. A., Salam, K. A., Olatunbosun, B. E., & Asuquo, A. J. (2020). *Heavea brasiliensis* (Rubber seed): An alternative source of renewable energy. *Scientific African*, *8*, e00339.

Adewale, P., Dumont, M. J., & Ngadi, M. (2015). Recent trends of biodiesel production from animal fat wastes and associated production techniques. *Renewable and Sustainable Energy Reviews*, *45*, 574-588.

Adewuyi, A. (2020). Challenges and prospects of renewable energy in Nigeria: A case of bioethanol and biodiesel production. *Energy Reports*, *6*, 77-88.

Ajith, B.S., Math, M.C., Patel GC, M. and Parappagoudar, M.B., 2022. Analysis and optimisation of transesterification parameters for high-yield Garcinia Gummi-Gutta biodiesel using RSM and TLBO. Australian Journal of Mechanical Engineering, 20(5), 1463-1478.

Ajith, M. P., Pardhiya, S., Prabhakar, A. K., & Rajamani, P. (2022). Ag@ CDs nanohybrid: Fabrication, design of a multi-mode chemosensory probe for selective Fe3+ detection and logic gate operation. *Chemosphere*, *303*, 135090.

Akubude, V. C., Nwaigwe, K. N., & Dintwa, E. (2019). Production of biodiesel from microalgae via nanocatalyzed transesterification process: A review. Materials Science for Energy *Technologies*, *2*(2), 216-225.

Akubude, V. C., Nwaigwe, K. N., & Dintwa, E. (2019). Production of biodiesel from microalgae via nanocatalyzed transesterification process: A review. Materials Science for Energy *Technologies*, *2*(2), 216-225.

Albuquerque, M. C. G., Machado, Y. L., Torres, A. E. B., Azevedo, D. C. S., Cavalcante Jr, C. L., Firmiano, L. R., & Parente Jr, E. J. S. (2009). Properties of biodiesel oils formulated using different biomass sources and their blends. *Renewable Energy*, *34*(3), 857-859.

Ali, C. H., Asif, A. H., Iqbal, T., Qureshi, A. S., Kazmi, M. A., Yasin, S., ... & Mu, B. Z. (2018). Improved transesterification of waste cooking oil into biodiesel using calcined goat bone as a catalyst. *Energy Sources, Part A: Recovery, Utilization, and Environmental Effects, 40*(9), 1076-1083.

Ali, J. S., Saleem, H., Mannan, A., Zengin, G., Mahomoodally, M. F., Locatelli, M., ... & Zia, M. (2020). Metabolic fingerprinting, antioxidant characterization, and enzyme-inhibitory response of Monotheca buxifolia (Falc.) A. DC. extracts. *BMC complementary medicine and therapies*, *20*(1), 1-13.

Aliyu, B. A., shafiu Nuhu, I., Igboro, S. B., & Alfa, A. U. (2021). Production of Biodiesel from Waste Vegetable Oil Using Chicken Eggshell Waste as Heterogeneous Catalyst. ATBU Journal of Science, Technology and Education, 9(2), 92-105.

Allami, H. A., Tabasizadeh, M., Rohani, A., Nayebzadeh, H., & Farzad, A. (2020). Effect of ultrasonic irradiation on the properties and performance of biodiesel produced from date seed oil used in the diesel engine. Ultrasonics sonochemistry, 60, 104672.

Alsaiari, M., Rozina, Ahmad, M., Zafar, M., Sultana, S., Rizk, M. A., Almohana, A. I., ... & Akhtar, M. S. (2022). Treatment of *Saussurea heteromalla* for biofuel synthesis using catalytic membrane reactor. Chemosphere, 305, 135335.

Ambat, I., Srivastava, V., & Sillanpää, M. (2018). Recent advancement in biodiesel production methodologies using various feedstock: A review. Renewable and sustainable energy reviews, 90, 356-369.

Ambat, I., Srivastava, V., Iftekhar, S., Haapaniemi, E., & Sillanpää, M. (2020). Effect of different co-solvents on biodiesel production from various low-cost feedstocks using Sr–Al double oxides. Renewable Energy, 146, 2158-2169.

Ameen, M., Ahmad, M., Zafar, M., Munir, M., Abbas, M. M., Sultana, S., ... & Kalam, M. A. (2022). Prospects of Catalysis for Process Sustainability of Eco-Green Biodiesel Synthesis via Transesterification: A State-Of-The-Art Review. Sustainability, 14(12), 7032.

Amesho, K. T., Lin, Y. C., Chen, C. E., Cheng, P. C., & Shangdiar, S. (2022). Kinetics studies of sustainable biodiesel synthesis from Jatropha curcas oil by exploiting bio-waste derived CaO-based heterogeneous catalyst via microwave heating system as a green chemistry technique. Fuel, 323, 123876.

Amirthavalli, V., Warrier, A.R. and Gurunathan, B., 2022. Various methods of biodiesel production and types of catalysts. Biofuels and Bioenergy, 111-132.

Anantharaman, A., Ramalakshmi, S., & George, M. (2016). Green synthesis of calcium oxide nanoparticles and its applications. Int. J. Eng. Res. Appl, 6(10), 27-31.

Ansori, A., & Mahfud, M. (2021). Ultrasound assisted interesterification for biodiesel production from palm oil and methyl acetate: Optimization using RSM. In Journal of Physics: Conference Series (Vol. 1747, No. 1, p. 012044). IOP Publishing.

Anwar, F., Rashid, U., Ashraf, M., & Nadeem, M. (2010). Okra (*Hibiscus esculentus*) seed oil for biodiesel production. Applied Energy, 87(3), 779-785.

Anwar, M., Rasul, M. G., Ashwath, N., & Nabi, M. N. (2019). The potential of utilising papaya seed oil and stone fruit kernel oil as non-edible feedstock for biodiesel production in Australia—A review. Energy Reports, 5, 280-297.

Arulmozhi, K. T., & Mythili, N. (2013). Studies on the chemical synthesis and characterization of lead oxide nanoparticles with different organic capping agents. AIP advances, 3(12), 122122.

Arumugam, A., & Ponnusami, V. J. R. E. (2019). Biodiesel production from *Calophyllum inophyllum* oil a potential non-edible feedstock: An overview. Renewable Energy, 131, 459-471.

Aryasomayajula Venkata Satya Lakshmi, S. B., Subramania Pillai, N., Khadhar Mohamed, M. S. B., & Narayanan, A. (2020). Biodiesel production from rubber seed oil using calcined eggshells impregnated with Al2O3 as heterogeneous catalyst: a comparative study of RSM and ANN optimization. Brazilian Journal of Chemical Engineering, 37(2), 351-368.

Aslan, V., & Eryilmaz, T. (2020). Polynomial regression method for optimization of biodiesel production from black mustard (*Brassica nigra* L.) seed oil using methanol, ethanol, NaOH, and KOH. Energy, 209, 118386.

Atabani, A. E., Silitonga, A. S., Ong, H. C., Mahlia, T. M. I., Masjuki, H. H., Badruddin, I. A., & Fayaz, H. (2013). Non-edible vegetable oils: a critical evaluation of oil extraction, fatty acid compositions, biodiesel production, characteristics, engine performance and emissions production. Renewable and sustainable energy reviews, 18, 211-245.

Avhad, M. R., & Marchetti, J. M. (2015). A review on recent advancement in catalytic materials for biodiesel production. Renewable and sustainable energy reviews, 50, 696-718.

Ayetor, G. K., Sunnu, A., & Parbey, J. (2015). Effect of biodiesel production parameters on viscosity and yield of methyl esters: *Jatropha curcas*, Elaeis guineensis and Cocos nucifera. Alexandria Engineering Journal, 54(4), 1285-1290.

Ayhan, V., & Ece, Y. M. (2020). New application to reduce NOx emissions of diesel engines: Electronically controlled direct water injection at compression stroke. Applied Energy, 260, 114328.

Ayoola, A. A., Hymore, F. K., Omonhinmin, C. A., Babalola, P. O., Fayomi, O. S. I., Olawole, O. C., ... & Babalola, A. (2020). Response surface methodology and artificial neural network analysis of crude palm kernel oil biodiesel production. Chemical Data Collections, 28, 100478.

Azarabadi, H., Eranki, P. L., & Landis, A. E. (2017). Life cycle impacts of commercial guayule rubber production estimated from batch-scale operation data. Int J Environ Sustain, 13(3), 15-30.

Bai, L., Tajikfar, A., Tamjidi, S., Foroutan, R., & Esmaeili, H. (2021). Synthesis of MnFe2O4@ graphene oxide catalyst for biodiesel production from waste edible oil. Renewable Energy, 170, 426-437.

Balajii, M., & Niju, S. (2020). Banana peduncle–A green and renelwable heterogeneous base catalyst for biodiesel production from *Ceiba pentandra* oil. Renewable Energy, 146, 2255-2269.

Banerjee, S., Rout, S., Banerjee, S., Atta, A., & Das, D. (2019). Fe_2O_3 nanocatalyst aided transesterification for biodiesel production from lipid-intact wet microalgal biomass: A biorefinery approach. Energy Conversion and Management, 195, 844-853.

Bano, S., Ganie, A. S., Sultana, S., Sabir, S., & Khan, M. Z. (2020). Fabrication and optimization of nanocatalyst for biodiesel production: an overview. Frontiers in Energy Research, 8, 579014.

Baskar, G., Gurugulladevi, A., Nishanthini, T., Aiswarya, R., & Tamilarasan, K. J. R. E. (2017). Optimization and kinetics of biodiesel production from Mahua oil using manganese doped zinc oxide nanocatalyst. Renewable energy, 103, 641-646.

Bateni, H., Karimi, K., Zamani, A., & Benakashani, F. (2014). Castor plant for biodiesel, biogas, and ethanol production with a biorefinery processing perspective. Applied Energy, 136, 14-22.

Biodiesel Synthesis, Optimization and Characterization from Novel Non-edible oil Seeds via High Performance Phyto-nano catalyst

506

Behera, B., Dey, B., & Balasubramanian, P. (2020). Algal biodiesel production with engineered biochar as a heterogeneous solid acid catalyst. Bioresource technology, 310, 123392.

Berman, P., Nizri, S., & Wiesman, Z. (2011). Castor oil biodiesel and its blends as alternative fuel. biomass and bioenergy, 35(7), 2861-2866.

Betiku, E., Akintunde, A. M., & Ojumu, T. V. (2016). Banana peels as a biobase catalyst for fatty acid methyl esters production using Napoleon's plume (*Bauhinia monandra*) seed oil: A process parameters optimization study. Energy, 103, 797-806.

Bhatia, S. K., Bhatia, R. K., Jeon, J. M., Pugazhendhi, A., Awasthi, M. K., Kumar, D., ... & Yang, Y. H. (2021). An overview on advancements in biobased transesterification methods for biodiesel production: Oil resources, extraction, biocatalysts, and process intensification technologies. Fuel, 285, 119117.

Biggs, R., Schlüter, M. and Schoon, M.L. eds., (2015). Principles for building resilience: sustaining ecosystem services in social-ecological systems.

Bindhu, M. R., Umadevi, M., Esmail, G. A., Al-Dhabi, N. A., & Arasu, M. V. (2020). Green synthesis and characterization of silver nanoparticles from *Moringa oleifera* flower and assessment of antimicrobial and sensing properties. Journal of Photochemistry and Photobiology B: Biology, 205, 111836.

Bohlouli, A., & Mahdavian, L. (2021). Catalysts used in biodiesel production: a review. Biofuels, 12(8), 885-898.

Bokhari, A., Chuah, L. F., Yusup, S., Klemeš, J. J., Akbar, M. M., & Kamil, R. N. M. (2016). Cleaner production of rubber seed oil methyl ester using a hydrodynamic cavitation: optimisation and parametric study. Journal of Cleaner Production, 136, 31-41.

Bokhari, J., & Khan, M. R. (2015). Evaluation of anti-asthmatic and antioxidant potential of *Boerhavia procumbens* in toluene diisocyanate (TDI) treated rats. Journal of ethnopharmacology, 172, 377-385.

Borah, M. J., Das, A., Das, V., Bhuyan, N., & Deka, D. (2019). Transesterification of waste cooking oil for biodiesel production catalyzed by Zn substituted waste egg shell derived CaO nanocatalyst. Fuel, 242, 345-354.

Borges, M. E., & Díaz, L. (2012). Recent developments on heterogeneous catalysts for biodiesel production by oil esterification and transesterification reactions: A review. Renewable and Sustainable Energy Reviews, 16(5), 2839-2849.

Calgaroto, C., Calgaroto, S., Mazutti, M. A., de Oliveira, D., Pergher, S., & De Oliveira, J. V. (2013). Production of biodiesel from soybean and *Jatropha Curcas* oils with KSF and amberlyst 15 catalysts in the presence of co-solvents. Sustainable Chemical Processes, 1(1), 1-6.

Campli, S., Acharya, M., Channapattana, S. V., Pawar, A. A., Gawali, S. V., & Hole, J. (2021). The effect of nickel oxide nano-additives in Azadirachta indica biodiesel-diesel blend on engine performance and emission characteristics by varying compression ratio. Environmental Progress & Sustainable Energy, 40(2), e13514.

Cardeño, F., Lapuerta, M., Rios, L., & Agudelo, J. R. (2020). Reconsideration of regulated contamination limits to improve filterability of biodiesel and blends with diesel fuels. Renewable Energy, 159, 1243-1251.

Caulk, R. A., & Tomac, I. (2017). Reuse of abandoned oil and gas wells for geothermal energy production. Renewable energy, 112, 388-397.

Chandra, H., Kumari, P., Bontempi, E., & Yadav, S. (2020). Medicinal plants: Treasure trove for green synthesis of metallic nanoparticles and their biomedical applications. Biocatalysis and Agricultural Biotechnology, 24, 101518.

Chang, M. Y., Chan, E. S., & Song, C. P. (2021). Biodiesel production catalysed by low-cost liquid enzyme Eversa® Transform 2.0: Effect of free fatty acid content on lipase methanol tolerance and kinetic model. Fuel, 283, 119266.

Changmai, B., Rano, R., Vanlalveni, C., & Rokhum, L. (2021). A novel *Citrus sinensis* peel ash coated magnetic nanoparticles as an easily recoverable solid catalyst for biodiesel production. Fuel, 286, 119447.

Changmai, B., Vanlalveni, C., Ingle, A. P., Bhagat, R., & Rokhum, L. (2020). Widely used catalysts in biodiesel production: a review. RSC advances, 10(68), 41625-41679.

Charoensaeng, A., Khaodhiar, S., Sabatini, D. A., & Arpornpong, N. (2018). Exhaust emissions of a diesel engine using ethanol-in-palm oil/diesel microemulsion-based biofuels. Environmental Engineering Research, 23(3), 242-249.

Chekin, F., Teodorescu, F., Coffinier, Y., Pan, G. H., Barras, A., Boukherroub, R., & Szunerits, S. (2016). MoS_2/reduced graphene oxide as active hybrid material for the electrochemical detection of folic acid in human serum. Biosensors and Bioelectronics, 85, 807-813.

Chengareddy, P., Arumugam, S., Pavan Kumar Reddy, P.H. and Madhan Mohan Reddy, P., 2021. A review on ultrasonicated transesterification process. Advances in Materials and Manufacturing Engineering: Select Proceedings of ICMME 2019, 579-585.

Cruz, G., Silva, A. V., Da Silva, J. B., de Nazare Caldeiras, R., & de Souza, M. E. (2020). Biofuels from oilseed fruits using different thermochemical processes: opportunities and challenges. Biofuels, Bioproducts and Biorefining, 14(3), 696-719.

Da Rós, P. C. M., e Silva, W. C., Grabauskas, D., Perez, V. H., & de Castro, H. F. (2014). Biodiesel from babassu oil: Characterization of the product obtained by enzymatic route accelerated by microwave irradiation. Industrial Crops and Products, 52, 313-320.

Dai, Y. M., Chen, K. T., Wang, Y. J., & Chen, C. C. (2014). Application of peanut husk ash as a low-cost solid catalyst for biodiesel production. International Journal of Chemical Engineering and Applications, 5(3), 276.

Dai, Y. M., Li, Y. Y., Lin, J. H., Kao, I. H., Lin, Y. J., & Chen, C. C. (2021). Applications of M2ZrO2 (M= Li, Na, K) composite as a catalyst for biodiesel production. Fuel, 286, 119392.

Davis, S. J., Lewis, N. S., Shaner, M., Aggarwal, S., Arent, D., Azevedo, I. L., ... & Caldeira, K. (2018). Net-zero emissions energy systems. Science 360: eaas9793.

Davoodbasha, M., Pugazhendhi, A., Kim, J. W., Lee, S. Y., & Nooruddin, T. (2021). Biodiesel production through transesterification of *Chlorella vulgaris*: Synthesis and characterization of CaO nanocatalyst. Fuel, 300, 121018.

Dawood, S., Ahmad, M., Ullah, K., Zafar, M., & Khan, K. (2018). Synthesis and characterization of methyl esters from non-edible plant species yellow oleander oil, using magnesium oxide (MgO) nano-catalyst. Materials Research Bulletin, 101, 371-379.

Dawood, S., Koyande, A. K., Ahmad, M., Mubashir, M., Asif, S., Klemeš, J. J., ... & Show, P. L. (2021). Synthesis of biodiesel from non-edible (Brachychiton populneus) oil in the presence of nickel oxide nanocatalyst: Parametric and optimisation studies. Chemosphere, 278, 130469..

de Barros, M. S. F., & dos Santos Calado, T. C. (2020). Plastic ingestion lead to reduced body condition and modified diet patterns in the rocky shore crab Pachygrapsus transversus (Gibbes, 1850)(Brachyura: Grapsidae). Marine Pollution Bulletin, 156, 111249.

de Jesus, S. S., Ferreira, G. F., Moreira, L. S., & Maciel Filho, R. (2020). Biodiesel production from microalgae by direct transesterification using green solvents. Renewable Energy, 160, 1283-1294.

Degfie, T. A., Mamo, T. T., & Mekonnen, Y. S. (2019). Optimized biodiesel production from waste cooking oil (WCO) using calcium oxide (CaO) nano-catalyst. Scientific reports, 9(1), 1-8.

Dehkordi, A. M., & Ghasemi, M. (2012). Transesterification of waste cooking oil to biodiesel using Ca and Zr mixed oxides as heterogeneous base catalysts. Fuel Processing Technology, 97, 45-51.

Demirbas, A. (2008). Biofuels sources, biofuel policy, biofuel economy and global biofuel projections. Energy conversion and management, 49(8), 2106-2116.

Demirbas, A. (2008). Biofuels sources, biofuel policy, biofuel economy and global biofuel projections. Energy conversion and management, 49(8), 2106-2116.

Dhake, K. P., Tambade, P. J., Qureshi, Z. S., Singhal, R. S., & Bhanage, B. M. (2011). HPMC-PVA film immobilized *Rhizopus oryzae* lipase as a biocatalyst for transesterification reaction. Acs Catalysis, 1(4), 316-322.

Dharmaraj, N., Prabu, P., Nagarajan, S., Kim, C. H., Park, J. H., & Kim, H. Y. (2006). Synthesis of nickel oxide nanoparticles using nickel acetate and poly (vinyl acetate) precursor. Materials Science and Engineering: B, 128(1-3), 111-114.

Diehl, B., & Randel, G. (2007). Analysis of biodiesel, diesel and gasoline by NMR spectroscopy–a quick and robust alternative to NIR and GC. Lipid Technology, 19(11), 258-260.

Din, M. I., Khalid, R., Hussain, Z., Hussain, T., Mujahid, A., Najeeb, J., & Izhar, F. (2020). Nanocatalytic assemblies for catalytic reduction of nitrophenols: a critical review. Critical reviews in analytical chemistry, 50(4), 322-338.

Doudin, K. I. (2021). Quantitative and qualitative analysis of biodiesel by NMR spectroscopic methods. Fuel, 284, 119114.

Elkelawy, M., Bastawissi, H. A. E., Esmaeil, K. K., Radwan, A. M., Panchal, H., Sadasivuni, K. K., ... & Walvekar, R. (2019). Experimental studies on the biodiesel production parameters optimization of sunflower and soybean oil mixture and DI engine combustion, performance, and emission analysis fueled with diesel/biodiesel blends. Fuel, 255, 115791.

Esan, A. O., Adeyemi, A. D., & Ganesan, S. (2020). A review on the recent application of dimethyl carbonate in sustainable biodiesel production. Journal of Cleaner Production, 257, 120561.

Ewis, D., Benamor, A., Ba-Abbad, M. M., Nasser, M., El-Naas, M., & Qiblawey, H. (2020). Removal of oil content from oil-water emulsions using iron oxide/bentonite nano adsorbents. Journal of Water Process Engineering, 38, 101583.

Falowo, O. A., Ojumu, T. V., Pereao, O., & Betiku, E. (2020). Sustainable biodiesel synthesis from honne-rubber-neem oil blend with a novel mesoporous base catalyst synthesized from a mixture of three agrowastes. Catalysts, 10(2), 190.

Fatah, M. A., Farag, H. A., & Ossman, M. E. (2012). Production of biodiesel from non-edible oil and effect of blending with diesel on fuel properties. Engineering Science and Technology, an International Journal, 2(4), 583-591.

Fedosov, S. N., Brask, J., & Xu, X. (2011). Analysis of biodiesel conversion using thin layer chromatography and nonlinear calibration curves. Journal of Chromatography A, 1218(19), 2785-2792.

Feyzi, M., & Shahbazi, Z. (2017). Preparation, kinetic and thermodynamic studies of Al–Sr nanocatalysts for biodiesel production. Journal of the Taiwan Institute of Chemical Engineers, 71, 145-155.

Foroutan, R., Mohammadi, R., & Ramavandi, B. (2021). Waste glass catalyst for biodiesel production from waste chicken fat: Optimization by RSM and ANNs and toxicity assessment. Fuel, 291, 120151.

Freitas, V. O. D., Matte, C. R., Poppe, J. K., Rodrigues, R. C., & Ayub, M. A. (2019). Ultrasound-assisted transesterification of soybean oil using combi-lipase biocatalysts. Brazilian Journal of Chemical Engineering, 36, 995-1005.

Galvan, D., de Aguiar, L. M., Rohwedder, J. J. R., Borsato, D., & Killner, M. H. M. (2020). Online monitoring of transesterification reaction by medium-resolution benchtop 1H NMR and NIR spectroscopy. Fuel Processing Technology, 208, 106511.

Gandhi, S. S., & Gogate, P. R. (2021). Intensified transesterification of castor oil using ultrasonic horn: response surface methodology (RSM) based optimization. International Journal of Green Energy, 18(14), 1523-1535.

Ganesan, D., Rajendran, A., & Thangavelu, V. (2009). An overview on the recent advances in the transesterification of vegetable oils for biodiesel production using chemical and biocatalysts. Reviews in Environmental Science and Bio/Technology, 8(4), 367-394.

Ganitha, S., Ganesan, S., & Ramesh, S. (2020). Modelling of biodiesel blend using optimised deep belief network: blending waste cooking oil methyl ester with tyre pyrolysis oil. IET Renewable Power Generation, 14(16), 3238-3251.

Gardy, J., Osatiashtiani, A., Céspedes, O., Hassanpour, A., Lai, X., Lee, A. F., ... & Rehan, M. (2018). A magnetically separable SO4/Fe-Al-TiO2 solid acid catalyst for biodiesel production from waste cooking oil. Applied Catalysis B: Environmental, 234, 268-278.

Geng, Y., & Doberstein, B. (2008). Developing the circular economy in China: Challenges and opportunities for achieving'leapfrog development'. The International Journal of Sustainable Development & World Ecology, 15(3), 231-239.

Ghadge, S. V., & Raheman, H. (2006). Process optimization for biodiesel production from mahua (Madhuca indica) oil using response surface methodology. Bioresource technology, 97(3), 379-384.

Ghanbariasad, A., Taghizadeh, S. M., Show, P. L., Nomanbhay, S., Berenjian, A., Ghasemi, Y., & Ebrahiminezhad, A. (2019). Controlled synthesis of iron oxyhydroxide (FeOOH) nanoparticles using secretory compounds from Chlorella vulgaris microalgae. Bioengineered, 10(1), 390-396.

Ghosh, A., Sarmah, N., Sundaram, S., & Mallick, T. K. (2019). Numerical studies of thermal comfort for semi-transparent building integrated photovoltaic (BIPV)-vacuum glazing system. Solar Energy, 190, 608-616.

Gimbun, J., Ali, S., Kanwal, C. C. S. C., Shah, L. A., Muhamad, N. H., Cheng, C. K., & Nurdin, S. (2013). Biodiesel production from rubber seed oil using activated cement clinker as catalyst. Procedia Engineering, 53, 13-19.

Gopalakrishnan, R., Loganathan, B., & Raghu, K. (2015). Green synthesis of Au–Ag bimetallic nanocomposites using Silybum marianum seed extract and their application as a catalyst. RSC Advances, 5(40), 31691-31699.

Gui, M. M., Lee, K. T., & Bhatia, S. (2008). Feasibility of edible oil vs. non-edible oil vs. waste edible oil as biodiesel feedstock. Energy, 33(11), 1646-1653.

Guldhe, A., Singh, B., Mutanda, T., Permaul, K., & Bux, F. (2015). Advances in synthesis of biodiesel via enzyme catalysis: Novel and sustainable approaches. Renewable and Sustainable Energy Reviews, 41, 1447-1464.

Gupta, A. R., & Rathod, V. K. (2018). Calcium diglyceroxide catalyzed biodiesel production from waste cooking oil in the presence of microwave: Optimization and kinetic studies. Renewable Energy, 121, 757-767.

Gupta, J., Agarwal, M., & Dalai, A. K. (2016). Optimization of biodiesel production from mixture of edible and nonedible vegetable oils. Biocatalysis and Agricultural Biotechnology, 8, 112-120.

Gurunathan, B., & Ravi, A. (2015). Biodiesel production from waste cooking oil using copper doped zinc oxide nanocomposite as heterogeneous catalyst. Bioresource technology, 188, 124-127.

Hadiyanto, H., Lestari, S. P., & Widayat, W. (2016). Preparation and characterization of Anadara Granosa shells and $CaCO_3$ as heterogeneous catalyst for biodiesel production. Bulletin of Chemical Reaction Engineering and Catalysis, 11(1), 21-26.

Hammouda, S. B., Zhao, F., Safaei, Z., Babu, I., Ramasamy, D. L., & Sillanpää, M. (2017). Reactivity of novel Ceria–Perovskite composites CeO2-LaMO₃ (MCu, Fe) in the catalytic wet peroxidative oxidation of the new emergent pollutant 'Bisphenol F': Characterization, kinetic and mechanism studies. Applied Catalysis B: Environmental, 218, 119-136.

Haq, Z. U., & Khan, S. M. (2019). The indispensable bond between Mazri Palm (Nannorrhops ritchiana) and the Indian Porcupine (*Hystrix indica*) leads them towards extinction!. Biodiversity and Conservation, 28(12), 3387-3388.

Hasan, R., Chong, C. C., Setiabudi, H. D., Jusoh, R., & Jalil, A. A. (2019). Process optimization of methylene blue adsorption onto eggshell–treated palm oil fuel ash. Environmental technology & innovation, 13, 62-73.

Hashmi, E. M., Jamal, Y., Maqbool, N., Shahzad, H. M. A., Imtiaz, B., & Khan, S. J. (2022). Production of biodiesel and water conservation through conversion of free fatty acids from a domestic wastewater drain. Energy Sources, Part A: Recovery, Utilization, and Environmental Effects, 44(3), 7031-7045.

Hasni, K., Ilham, Z., Dharma, S., & Varman, M. (2017). Optimization of biodiesel production from *Brucea javanica* seeds oil as novel non-edible feedstock using response surface methodology. Energy Conversion and Management, 149, 392-400.

Hayyan, A., Hashim, M. A., Hayyan, M., Mjalli, F. S., & AlNashef, I. M. (2014). A new processing route for cleaner production of biodiesel fuel using a choline chloride based deep eutectic solvent. Journal of Cleaner Production, 65, 246-251.

Hazrat, M. A., Rasul, M. G., Mofijur, M., Khan, M. M. K., Djavanroodi, F., Azad, A. K., ... & Silitonga, A. S. (2020). A mini review on the cold flow properties of biodiesel and its blends. Frontiers in Energy Research, 8, 598651.

Hebbar, H. H., Math, M. C., & Yatish, K. V. (2018). Optimization and kinetic study of CaO nano-particles catalyzed biodiesel production from *Bombax ceiba* oil. Energy, 143, 25-34.

Helmi, M., Tahvildari, K., Hemmati, A., & Safekordi, A. (2021). Phosphomolybdic acid/graphene oxide as novel green catalyst using for biodiesel production from waste cooking oil via electrolysis method: Optimization using with response surface methodology (RSM). Fuel, 287, 119528.

Helwani, Z., Ramli, M., Saputra, E., Bahruddin, B., Yolanda, D., Fatra, W., ... & Idroes, R. (2020). Impregnation of CaO from eggshell waste with magnetite as a solid catalyst (Fe3O4/CaO) for transesterification of palm oil off-grade. Catalysts, 10(2), 164.

Hoang, A. T., Ong, H. C., Fattah, I. R., Chong, C. T., Cheng, C. K., Sakthivel, R., & Ok, Y. S. (2021). Progress on the lignocellulosic biomass pyrolysis for biofuel production toward environmental sustainability. Fuel Processing Technology, 223, 106997.

Hosseini, S. H., Taghizadeh-Alisaraei, A., Ghobadian, B., & Abbaszadeh-Mayvan, A. (2020). Artificial neural network modeling of performance, emission, and vibration of a CI engine using alumina nano-catalyst added to diesel-biodiesel blends. Renewable energy, 149, 951-961.

Hu, S., Guan, Y., Wang, Y., & Han, H. (2011). Nano-magnetic catalyst KF/CaO–Fe3O4 for biodiesel production. Applied Energy, 88(8), 2685-2690.

Ingle, A. P., Chandel, A. K., Philippini, R., Martiniano, S. E., & da Silva, S. S. (2020). Advances in nanocatalysts mediated biodiesel production: a critical appraisal. Symmetry, 12(2), 256.

Ingle, A. P., Chandel, A. K., Philippini, R., Martiniano, S. E., & da Silva, S. S. (2020). Advances in nanocatalysts mediated biodiesel production: a critical appraisal. Symmetry, 12(2), 256.

Iravani, S., & Varma, R. S. (2020). Sustainable synthesis of cobalt and cobalt oxide nanoparticles and their catalytic and biomedical applications. Green Chemistry, 22(9), 2643-2661.

Istadi, I., Riyanto, T., Buchori, L., Anggoro, D. D., Gilbert, G., Meiranti, K. A., & Khofiyanida, E. (2020). Enhancing Brønsted and Lewis acid sites of the utilized spent RFCC catalyst waste for the continuous cracking process of palm oil to biofuels. Industrial & Engineering Chemistry Research, 59(20), 9459-9468.

Jacoby, J., Pasc, A., Carteret, C., Dupire, F., Stebe, M. J., Coupard, V., & Blin, J. L. (2013). Ordered mesoporous materials containing Mucor Miehei Lipase as biocatalyst for transesterification reaction. Process Biochemistry, 48(5-6), 831-837.

Jahirul, M. I., Rasul, M. G., Brown, R. J., Senadeera, W., Hosen, M. A., Haque, R., ... & Mahlia, T. M. I. (2021). Investigation of correlation between chemical composition and properties of biodiesel using principal component analysis (PCA) and artificial neural network (ANN). Renewable energy, 168, 632-646.

Joshi, M. C., Joshi, H. S., Rashid, M. K., & Gaur, S. (2011). A study of antimicrobial agent utilization and the resistance pattern of predominant microorganisms in the medical ward of a tertiary care centre in Uttar Pradesh, India. Pharmacology online, 1, 451-461.

Kafuku, G., & Mbarawa, M. (2010). Biodiesel production from *Croton megalocarpus* oil and its process optimization. Fuel, 89(9), 2556-2560.

Kafuku, G., Lam, M. K., Kansedo, J., Lee, K. T., & Mbarawa, M. (2010). Heterogeneous catalyzed biodiesel production from Moringa oleifera oil. Fuel Processing Technology, 91(11), 1525-1529.

Kannimuthu, K., Sangeetha, K., Sankar, S. S., Karmakar, A., Madhu, R., & Kundu, S. (2021). Investigation on nanostructured Cu-based electrocatalysts for improvising water splitting: a review. Inorganic Chemistry Frontiers, 8(1), 234-272.

Kansedo, J., Lee, K. T., & Bhatia, S. (2009). *Cerbera odollam* (sea mango) oil as a promising non-edible feedstock for biodiesel production. Fuel, 88(6), 1148-1150.

Kara, K., Ouanji, F., El Mahi, M., Lotfi, E. M., Kacimi, M., & Mahfoud, Z. (2019). Biodiesel synthesis from vegetable oil using eggshell waste as a heterogeneous catalyst. Biofuels.

Karimi, K., Tabatabaei, M., Sárvári Horváth, I., & Kumar, R. (2015). Recent trends in acetone, butanol, and ethanol (ABE) production. Biofuel Research Journal, 2(4), 301-308.

Karpagam, R., Rani, K., Ashokkumar, B., Moorthy, I. G., Dhakshinamoorthy, A., & Varalakshmi, P. (2020). Green energy from Coelastrella sp. M-60: Bio-nanoparticles mediated whole biomass transesterification for biodiesel production. Fuel, 279, 118490.

Kawashima, A., Matsubara, K., & Honda, K. (2009). Acceleration of catalytic activity of calcium oxide for biodiesel production. Bioresource Technology, 100(2), 696-700.

Khan, I. W., Naeem, A., Farooq, M., Ghazi, Z. A., & Saeed, T. (2021). Reusable Na-SiO2@ CeO2catalyst for efficient biodiesel production from non-edible wild olive oil as a new and potential feedstock. Energy Conversion and Management, 231, 113854.

Klein, S., Worch, E., & Knepper, T. P. (2015). Occurrence and spatial distribution of microplastics in river shore sediments of the Rhine-Main area in Germany. Environmental science & technology, 49(10), 6070-6076.

Knothe, G. (2001). Analytical methods used in the production and fuel quality assessment of biodiesel. Transactions of the ASAE, 44(2), 193.

Kostić, M. D., Veličković, A. V., Joković, N. M., Stamenković, O. S., & Veljković, V. B. (2016). Optimization and kinetic modeling of esterification of the oil obtained from waste plum stones as a pretreatment step in biodiesel production. Waste Management, 48, 619-629.

Kouzu, M., & Hidaka, J. S. (2012). Transesterification of vegetable oil into biodiesel catalyzed by CaO: a review. Fuel, 93, 1-12.

Kumar, D., Banerjee, A., & Singh, B. (2021). Biocatalysis in industrial biodiesel and bioethanol production. Green Sustainable Process for Chemical and Environmental Engineering and Science, 1-28.

Kumar, H., Sarma, A. K., & Kumar, P. (2020). A comprehensive review on preparation, characterization, and combustion characteristics of microemulsion based hybrid biofuels. Renewable and Sustainable Energy Reviews, 117, 109498.

Kumar, R., & Pal, P. (2021). Lipase immobilized graphene oxide biocatalyst assisted enzymatic transesterification of *Pongamia pinnata* (Karanja) oil and downstream enrichment of biodiesel by solar-driven direct contact membrane distillation followed by ultrafiltration. Fuel Processing Technology, 211, 106577.

Kumar, S., Aggrawal, M., Kumar, N., & Deswal, V. (2020). Optimisation and prediction of Karanja oil transesterification with domestic microwave by RSM and ANN. International Journal of Ambient Energy, 1-8.

Kumari, N., Aulakh, M. K., Sareen, S., Sharma, A., Sohal, H. S., Verma, M., ... & Mutreja, V. (2022). Greener Synthesis of Zirconium-Based Nanocatalyst for Transesterification. Topics in Catalysis, 1-10.

LaGrow, A. P., Besenhard, M. O., Hodzic, A., Sergides, A., Bogart, L. K., Gavriilidis, A., & Thanh, N. T. K. (2019). Unravelling the growth mechanism of the co-precipitation of iron oxide nanoparticles with the aid of synchrotron X-Ray diffraction in solution. Nanoscale, 11(14), 6620-6628.

Lamba, N., Gupta, K., Modak, J. M., & Madras, G. (2017). Biodiesel synthesis from *Calophyllum inophyllum* oil with different supercritical fluids. Bioresource technology, 241, 767-774.

Lawan, I., Zhou, W., Garba, Z. N., Zhang, M., Yuan, Z., & Chen, L. (2019). Critical insights into the effects of bio-based additives on biodiesels properties. Renewable and Sustainable Energy Reviews, 102, 83-95.

Lawan, I., Zhou, W., Garba, Z.N., Zhang, M., Yuan, Z. and Chen, L., 2019. Critical insights into the effects of bio-based additives on biodiesels properties. Renewable and Sustainable Energy Reviews, 102, 83-95.

Lee, H. V., Juan, J. C., & Taufiq-Yap, Y. H. (2015). Preparation and application of binary acid–base CaO–La$_2$O$_3$ catalyst for biodiesel production. Renewable Energy, 74, 124-132.

Lee, Y., Kim, S. B., Lee, T., Jang, M., Shin, A., Park, S. J., ... & Park, C. (2019). Efficient and simultaneous cleaner production of biodiesel and glycerol carbonate in solvent-free system via statistical optimization. Journal of Cleaner Production, 218, 985-992.

Li, J., Ren, X., Lv, H., Wang, Y., Li, Y., & Liu, B. (2020). Highly efficient hydrogen production from hydrolysis of ammonia borane over nanostructured Cu@ CuCoOx supported on graphene oxide. Journal of hazardous materials, 391, 122199.

Li, M., Zheng, Y., Chen, Y., & Zhu, X. (2014). Biodiesel production from waste cooking oil using a heterogeneous catalyst from pyrolyzed rice husk. Bioresource technology, 154, 345-348.

Li, Z., Ding, S., Chen, C., Qu, S., Du, L., Lu, J., & Ding, J. (2019). Recyclable Li/NaY zeolite as a heterogeneous alkaline catalyst for biodiesel production: Process optimization and kinetics study. Energy Conversion and Management, 192, 335-345.

Liang, X., Gong, G., Wu, H., & Yang, J. (2009). Highly efficient procedure for the synthesis of biodiesel from soybean oil using chloroaluminate ionic liquid as catalyst. Fuel, 88(4), 613-616.

Lin, L., Cunshan, Z., Vittayapadung, S., Xiangqian, S., & Mingdong, D. (2011). Opportunities and challenges for biodiesel fuel. Applied energy, 88(4), 1020-1031.

Lin, L., Ying, D., Chaitep, S., & Vittayapadung, S. (2009). Biodiesel production from crude rice bran oil and properties as fuel. Applied energy, 86(5), 681-688.

Liu, C., Zhang, L., Deng, J., Mu, Q., Dai, H., & He, H. (2008). Surfactant-aided hydrothermal synthesis and carbon dioxide adsorption behavior of three-dimensionally mesoporous calcium oxide single-crystallites with tri-, tetra-, and hexagonal morphologies. The Journal of Physical Chemistry C, 112(49), 19248-19256.

Lu, H., Yu, X., Yang, S., Yang, H., & Tu, S. T. (2016). MgO–Li2O catalysts templated by a PDMS–PEO comb-like copolymer for transesterification of vegetable oil to biodiesel. Fuel, 165, 215-223.

Lunardi, V. B., Gunawan, F., Soetaredjo, F. E., Santoso, S. P., Chen, C. H., Yuliana, M., ... & Ismadji, S. (2021). Efficient One-Step Conversion of a Low-Grade Vegetable Oil to

Biodiesel over a Zinc Carboxylate Metal–Organic Framework. ACS omega, 6(3), 1834-1845.

Ma, X., Liu, F., Helian, Y., Li, C., Wu, Z., Li, H., ... & Zhou, S. (2021). Current application of MOFs based heterogeneous catalysts in catalyzing transesterification/esterification for biodiesel production: A review. Energy Conversion and Management, 229, 113760.

Mahlia, T. M. I., Syazmi, Z. A. H. S., Mofijur, M., Abas, A. P., Bilad, M. R., Ong, H. C., & Silitonga, A. S. (2020). Patent landscape review on biodiesel production: Technology updates. Renewable and Sustainable Energy Reviews, 118, 109526.

Maina, J. W., Pozo-Gonzalo, C., Kong, L., Schütz, J., Hill, M., & Dumée, L. F. (2017). Metal organic framework based catalysts for CO 2 conversion. Materials Horizons, 4(3), 345-361.

Maina, S., Kachrimanidou, V., & Koutinas, A. (2017). A roadmap towards a circular and sustainable bioeconomy through waste valorization. Current Opinion in Green and Sustainable Chemistry, 8, 18-23.

Malani, R. S., Sardar, H., Malviya, Y., Goyal, A., & Moholkar, V. S. (2018). Ultrasound-intensified biodiesel production from mixed nonedible oil feedstock using heterogeneous acid catalyst supported on rubber de-oiled cake. Industrial & Engineering Chemistry Research, 57(44), 14926-14938.

Maneerung, T., Kawi, S., Dai, Y., & Wang, C. H. (2016). Sustainable biodiesel production via transesterification of waste cooking oil by using CaO catalysts prepared from chicken manure. Energy Conversion and Management, 123, 487-497.

Mares, E. K. L., Goncalves, M. A., da Luz, P. T. S., da Rocha Filho, G. N., Zamian, J. R., & da Conceição, L. R. V. (2021). Acai seed ash as a novel basic heterogeneous catalyst for biodiesel synthesis: Optimization of the biodiesel production process. Fuel, 299, 120887.

Martins, G. I., Secco, D., Tokura, L. K., Baricatti, R. A., Dolci, B. D., & Santos, R. F. (2015). Potential of tilapia oil and waste in biodiesel production. Renewable and Sustainable Energy Reviews, 42, 234-239.

Mata, T. M., Martins, A. A., & Caetano, N. S. (2010). Microalgae for biodiesel production and other applications: a review. Renewable and sustainable energy reviews, 14(1), 217-232.

Mathew, G. M., Raina, D., Narisetty, V., Kumar, V., Saran, S., Pugazhendi, A., ... & Binod, P. (2021). Recent advances in biodiesel production: Challenges and solutions. Science of The Total Environment, 794, 148751.

Mba, O. I., Dumont, M. J., & Ngadi, M. (2015). Palm oil: Processing, characterization and utilization in the food industry–A review. Food bioscience, 10, 26-41.

Medipally, S. R., Yusoff, F. M., Banerjee, S., & Shariff, M. (2015). Microalgae as sustainable renewable energy feedstock for biofuel production. BioMed research international, 2015.

Meghwal, P.R., Singh, A. and Singh, D., 2022. Underutilized Fruits and Vegetables in Hot Arid Regions of India: Status and Prospects: A Review. Agricultural Reviews, 43(1), 38-45.

Meher, L. C., Sagar, D. V., & Naik, S. N. (2006). Technical aspects of biodiesel production by transesterification—a review. Renewable and sustainable energy reviews, 10(3), 248-268.

Mendonça, I. M., Paes, O. A., Maia, P. J., Souza, M. P., Almeida, R. A., Silva, C. C., ... & de Freitas, F. A. (2019). New heterogeneous catalyst for biodiesel production from waste tucumã peels (*Astrocaryum aculeatum* Meyer): Parameters optimization study. Renewable Energy, 130, 103-110..

Meng, X., Yang, J., Xu, X., Zhang, L., Nie, Q., & Xian, M. (2009). Biodiesel production from oleaginous microorganisms. Renewable energy, 34(1), 1-5.

Milano, J., Ong, H. C., Masjuki, H. H., Silitonga, A. S., Chen, W. H., Kusumo, F., ... & Sebayang, A. H. (2018). Optimization of biodiesel production by microwave irradiation-assisted transesterification for waste cooking oil-*Calophyllum inophyllum* oil via response surface methodology. Energy conversion and management, 158, 400-415.

Mittal, V., Talapatra, K.N. and Ghosh, U.K., (2022). A comprehensive review on biodiesel production from microalgae through nanocatalytic transesterification process: lifecycle assessment and methodologies. International Nano Letters, 12(4), 351-378.

Mkhize, N. M., Sithole, B. B., & Ntunka, M. G. (2015). Heterogeneous acid-catalyzed biodiesel production from crude tall oil: a low-grade and less expensive feedstock. Journal of Wood Chemistry and Technology, 35(5), 374-385.

Mofijur, M., Siddiki, S. Y. A., Shuvho, M. B. A., Djavanroodi, F., Fattah, I. R., Ong, H. C., ... & Mahlia, T. M. I. (2021). Effect of nanocatalysts on the transesterification reaction of first, second and third generation biodiesel sources-A mini-review. Chemosphere, 270, 128642.

Mofijur, M., Siddiki, S. Y. A., Shuvho, M. B. A., Djavanroodi, F., Fattah, I. R., Ong, H. C., ... & Mahlia, T. M. I. (2021). Effect of nanocatalysts on the transesterification reaction of first, second and third generation biodiesel sources-A mini-review. Chemosphere, 270, 128642.

Moreira, K. S., Moura Junior, L. S., Monteiro, R. R., de Oliveira, A. L., Valle, C. P., Freire, T. M., ... & dos Santos, J. C. (2020). Optimization of the production of enzymatic biodiesel from residual babassu oil (Orbignya sp.) via RSM. Catalysts, 10(4), 414.

Muanruksa, P., & Kaewkannetra, P. (2020). Combination of fatty acids extraction and enzymatic esterification for biodiesel production using sludge palm oil as a low-cost substrate. Renewable Energy, 146, 901-906.

Mulvaney, D., Richards, R. M., Bazilian, M. D., Hensley, E., Clough, G., & Sridhar, S. (2021). Progress towards a circular economy in materials to decarbonize electricity and mobility. Renewable and Sustainable Energy Reviews, 137, 110604.

Murguía-Ortiz, D., Cordova, I., Manriquez, M. E., Ortiz-Islas, E., Cabrera-Sierra, R., Contreras, J. L., ... & Castro, L. V. (2021). Na-CaO/MgO dolomites used as heterogeneous catalysts in canola oil transesterification for biodiesel production. Materials Letters, 291, 129587.

Nath, B., Das, B., Kalita, P., & Basumatary, S. (2019). Waste to value addition: Utilization of waste Brassica nigra plant derived novel green heterogeneous base catalyst for effective synthesis of biodiesel. Journal of Cleaner Production, 239, 118112.

Navajas, A., Reyero, I., Jiménez-Barrera, E., Romero-Sarria, F., Llorca, J., & Gandía, L. M. (2020). Catalytic performance of bulk and Al2O3-supported molybdenum oxide for the production of biodiesel from oil with high free fatty acids content. Catalysts, 10(2), 158.

Naveenkumar, R., & Baskar, G. (2020). Optimization and techno-economic analysis of biodiesel production from *Calophyllum inophyllum* oil using heterogeneous nanocatalyst. Bioresource Technology, 315, 123852.

Nayebzadeh, H., Naderi, F., & Rahmanivahid, B. (2020). Assessment the synthesis conditions of separable magnetic spinel nanocatalyst for green fuel production: Optimization of transesterification reaction conditions using response surface methodology. Fuel, 271, 117595.

Nayebzadeh, H., Naderi, F., & Rahmanivahid, B. (2020). Assessment the synthesis conditions of separable magnetic spinel nanocatalyst for green fuel production: Optimization of transesterification reaction conditions using response surface methodology. Fuel, 271, 117595.

Nayebzadeh, H., Naderi, F., & Rahmanivahid, B. (2020). Assessment the synthesis conditions of separable magnetic spinel nanocatalyst for green fuel production: Optimization of transesterification reaction conditions using response surface methodology. Fuel, 271, 117595.

Nguyen, H. V., Ibanez, A., Salaün, M., Kodjikian, S., Trens, P., & Cattoën, X. (2021). Synthesis and properties of porous ester-silica nanoparticles. Microporous and Mesoporous Materials, 317, 110991.

Nisar, S., Hanif, M. A., Rashid, U., Hanif, A., Akhtar, M. N., & Ngamcharussrivichai, C. (2021). Trends in widely used catalysts for fatty acid methyl esters (Fame) production: A review. Catalysts, 11(9), 1085.

Njagi, E. C., Huang, H., Stafford, L., Genuino, H., Galindo, H. M., Collins, J. B., ... & Suib, S. L. (2011). Biosynthesis of iron and silver nanoparticles at room temperature using aqueous sorghum bran extracts. Langmuir, 27(1), 264-271.

Nomanbhay, S., Hussein, R., & Ong, M. Y. (2018). Sustainability of biodiesel production in Malaysia by production of bio-oil from crude glycerol using microwave pyrolysis: a review. Green Chemistry Letters and Reviews, 11(2), 135-157.

Obi, C., Ibezim-Ezeani, M. U., & Nwagbo, E. J. (2020). Production of biodiesel using novel C. lepodita oil in the presence of heterogeneous solid catalyst. Chem. Int, 6(2), 91-97.

Olutoye, M. A., Wong, S. W., Chin, L. H., Amani, H., Asif, M., & Hameed, B. H. (2016). Synthesis of fatty acid methyl esters via the transesterification of waste cooking oil by methanol with a barium-modified montmorillonite K10 catalyst. Renewable Energy, 86, 392-398.

Ong, H. C., Mofijur, M., Silitonga, A. S., Gumilang, D., Kusumo, F., & Mahlia, T. M. I. (2020). Physicochemical properties of biodiesel synthesised from grape seed, philippine tung, kesambi, and palm oils. Energies, 13(6), 1319.

Ong, M. Y., Nomanbhay, S., Kusumo, F., Raja Shahruzzaman, R. M. H., & Shamsuddin, A. H. (2021). Modeling and optimization of microwave-based bio-jet fuel from coconut oil: Investigation of response surface methodology (RSM) and artificial neural network methodology (ann). Energies, 14(2), 295.

Pali, H. S., Sharma, A., Kumar, N., & Singh, Y. (2021). Biodiesel yield and properties optimization from Kusum oil by RSM. Fuel, 291, 120218.

Panahi, F. H., Peighambardoust, S. J., Davaran, S., & Salehi, R. (2017). Development and characterization of PLA-mPEG copolymer containing iron nanoparticle-coated carbon nanotubes for controlled delivery of Docetaxel. Polymer, 117, 117-131.

Pandit, P. R., & Fulekar, M. H. (2017). Egg shell waste as heterogeneous nanocatalyst for biodiesel production: optimized by response surface methodology. Journal of environmental management, 198, 319-329..

Parameswaram, G., Srivani, A., Sumana, C., Rao, G. N., & Lingaiah, N. (2018). Selective Sransesterification of glycerol to glycerol carbonate over SrO-ZrO$_2$ base catalysts. Catalysis in Green Chemistry and Engineering, 1(1), 79-90.

Patchimpet, J., Zhang, Y., Simpson, B. K., Rui, X., Sangkharak, K., Eiad-ua, A., & Klomklao, S. (2021). Ultrasonic enhancement of lipase-catalyzed transesterification for biodiesel production from used cooking oil. Biomass Conversion and Biorefinery, 1-10.

Peng, B. X., Shu, Q., Wang, J. F., Wang, G. R., Wang, D. Z., & Han, M. H. (2008). Biodiesel production from waste oil feedstocks by solid acid catalysis. Process Safety and Environmental Protection, 86(6), 441-447.

Pinto, J. T., & Diemer, A. (2020). Supply chain integration strategies and circularity in the European steel industry. Resources, Conservation and Recycling, 153, 104517.

Pinzi, S., Leiva, D., López-García, I., Redel-Macías, M. D., & Dorado, M. P. (2014). Latest trends in feedstocks for biodiesel production. Biofuels, Bioproducts and Biorefining, 8(1), 126-143.

Pourkarimi, S., Hallajisani, A., Alizadehdakhel, A., & Nouralishahi, A. (2019). Biofuel production through micro-and macroalgae pyrolysis–A review of pyrolysis methods and process parameters. Journal of Analytical and Applied Pyrolysis, 142, 104599.

Qiu, F., Li, Y., Yang, D., Li, X., & Sun, P. (2011). Biodiesel production from mixed soybean oil and rapeseed oil. Applied Energy, 88(6), 2050-2055.

Quintero, A., Gonzalez, C. N., Sanchez, F., Usubillaga, A., & Rojas, L. (2001, July). Constituents and biological activity of *Citrus aurantium* amara L. essential oil. In International Conference on Medicinal and Aromatic Plants (Part II) 597 (pp. 115-117).

Raheem, I., Mohiddin, M. N. B., Tan, Y. H., Kansedo, J., Mubarak, N. M., Abdullah, M. O., & Ibrahim, M. L. (2020). A review on influence of reactor technologies and kinetic studies for biodiesel application. Journal of Industrial and Engineering Chemistry, 91, 54-68.

Rahimi, T., Kahrizi, D., Feyzi, M., Ahmadvandi, H. R., & Mostafaei, M. (2021). Catalytic performance of MgO/Fe2O3-SiO2 core-shell magnetic nanocatalyst for biodiesel production of Camelina sativa seed oil: Optimization by RSM-CCD method. Industrial Crops and Products, 159, 113065.

Rahimi, T., Kahrizi, D., Feyzi, M., Ahmadvandi, H. R., & Mostafaei, M. (2021). Catalytic performance of MgO/Fe2O3-SiO2 core-shell magnetic nanocatalyst for biodiesel production of Camelina sativa seed oil: Optimization by RSM-CCD method. Industrial Crops and Products, 159, 113065.

Rana, V. S., & Das, M. (2017). Fatty Acid and Non-Fatty Acid Components of the Seed Oil of *Celastrus paniculatus* willd. International journal of fruit science, 17(4), 407-414.

Rashid, U., Anwar, F., & Knothe, G. (2011). Biodiesel from Milo (*Thespesia populnea* L.) seed oil. biomass and bioenergy, 35(9), 4034-4039.

References

Rehan, M., Gardy, J., Demirbas, A., Rashid, U., Budzianowski, W. M., Pant, D., & Nizami, A. S. (2018). Waste to biodiesel: A preliminary assessment for Saudi Arabia. Bioresource technology, 250, 17-25.

Riayatsyah, T. M. I., Ong, H. C., Chong, W. T., Aditya, L., Hermansyah, H., & Mahlia, T. M. I. (2017). Life cycle cost and sensitivity analysis of Reutealis trisperma as non-edible feedstock for future biodiesel production. Energies, 10(7), 877.

Roy, T., Sahani, S., & Sharma, Y. C. (2020). Study on kinetics-thermodynamics and environmental parameter of biodiesel production from waste cooking oil and castor oil using potassium modified ceria oxide catalyst. Journal of Cleaner Production, 247, 119166.

Roy, T., Sahani, S., & Sharma, Y. C. (2020). Study on kinetics-thermodynamics and environmental parameter of biodiesel production from waste cooking oil and castor oil using potassium modified ceria oxide catalyst. Journal of Cleaner Production, 247, 119166.

Rozina, Ahmad, M., Zafar, M., & Ali, N. (2019). Biodiesel synthesis and physiochemical analysis of *Taraxacum officinale* FH Wigg seed oil. International Journal of Environmental Science and Technology, 16(8), 4103-4112.

Rozina, Ahmad, M., Zafar, M., Ali, N., & Lu, H. (2017). Biodiesel synthesis from *Saussurea heteromalla* (D. Don) Hand-Mazz integrating ethanol production using biorefinery approach. Energy, 141, 1810-1818.

Rozina, Asif, S., Ahmad, M., Zafar, M., & Ali, N. (2017). Prospects and potential of fatty acid methyl esters of some non-edible seed oils for use as biodiesel in Pakistan. Renewable and Sustainable Energy Reviews, 74, 687-702.

Sahafi, S. M., Ahmadibeni, A., Talebi, A. F., Goli, S. A. H., Aghbashlo, M., & Tabatabaei, M. (2018). Seed oils of *Sisymbrium irio* and *Sisymbrium sophia* as a potential non-edible feedstock for biodiesel production. Biofuels.

Sahani, S., Roy, T., & Sharma, Y. C. (2020). Studies on fast and green biodiesel production from an indigenous nonedible Indian feedstock using single phase strontium titanate catalyst. Energy Conversion and Management, 203, 112180.

Salaheldeen, M., Aroua, M. K., Mariod, A. A., Cheng, S. F., Abdelrahman, M. A., & Atabani, A. E. (2015). Physicochemical characterization and thermal behavior of biodiesel and biodiesel–diesel blends derived from crude Moringa peregrina seed oil. Energy Conversion and Management, 92, 535-542.

Salehian, P., & Karimi, K. (2013). Alkali pretreatment for improvement of biogas and ethanol production from different waste parts of pine tree. Industrial & Engineering Chemistry Research, 52(2), 972-978.

Saman, S., Balouch, A., Talpur, F. N., Memon, A. A., Mousavi, B. M., & Verpoort, F. (2021). Green synthesis of MgO nanocatalyst by using *Ziziphus mauritiana* leaves and seeds for biodiesel production. Applied Organometallic Chemistry, 35(5), e6199.

Sandhya, R., Velavan, R., & Ravichandran, J. (2020). Biodiesel production from waste cooking oil using copper doped zinc oxide nanocatalyst–process optimisation and economic analysis. International Journal of Oil, Gas and Coal Technology, 25(4), 488-497.

Saqib, S., Munis, M. F. H., Zaman, W., Ullah, F., Shah, S. N., Ayaz, A., ... & Bahadur, S. (2019). Synthesis, characterization and use of iron oxide nano particles for antibacterial activity. Microscopy research and technique, 82(4), 415-420.

Satya Lakshmi, S. B. A. V., Niju, S., Khadhar Mohamed, M. S. B., & Narayanan, A. (2020). Catalyst reusability and kinetic modeling of biodiesel produced from rubber seed oil. Energy Sources, Part A: Recovery, Utilization, and Environmental Effects, 1-16.

Sedghamiz, M. A., Raeissi, S., Attar, F., Salimi, M., & Mehrabi, K. (2019). In-situ transesterification of residual vegetable oil in spent bleaching clay with alkali catalysts using CCD-RSM design of experiment. Fuel, 237, 515-521.

Shaah, M. A. H., Hossain, M. S., Allafi, F. A. S., Alsaedi, A., Ismail, N., Ab Kadir, M. O., & Ahmad, M. I. (2021). A review on non-edible oil as a potential feedstock for biodiesel: physicochemical properties and production technologies. RSC advances, 11(40), 25018-25037.

Shaheen, A., Sultana, S., Lu, H., Ahmad, M., Asma, M., & Mahmood, T. (2018). Assessing the potential of different nano-composite (MgO, Al_2O_3-CaO and TiO2) for efficient conversion of *Silybum eburneum* seed oil to liquid biodiesel. Journal of Molecular Liquids, 249, 511-521.

Sharma, G., Soni, R., & Jasuja, N. D. (2017). Phytoassisted synthesis of magnesium oxide nanoparticles with *Swertia chirayaita*. Journal of Taibah University for Science, 11(3), 471-477.

Sharma, S., Saxena, V., Baranwal, A., Chandra, P., & Pandey, L. M. (2018). Engineered nanoporous materials mediated heterogeneous catalysts and their implications in biodiesel production. Materials Science for Energy Technologies, 1(1), 11-21.

Shenavaei Zare, T., Khoshsima, A., & ZareNezhad, B. (2020). Production of new surfactant-free microemulsion biofuels: phase behavior and nanostructure identification. Energy & Fuels, 34(4), 4643-4659.

Silitonga, A. S., Masjuki, H. H., Mahlia, T. M. I., Ong, H. C., Kusumo, F., Aditiya, H. B., & Ghazali, N. N. N. (2015). *Schleichera oleosa* L oil as feedstock for biodiesel production. Fuel, 156, 63-70.

Silitonga, A. S., Shamsuddin, A. H., Mahlia, T. M. I., Milano, J., Kusumo, F., Siswantoro, J., ... & Ong, H. C. (2020). Biodiesel synthesis from Ceiba pentandra oil by microwave irradiation-assisted transesterification: ELM modeling and optimization. Renewable Energy, 146, 1278-1291.

Silitonga, A. S., Shamsuddin, A. H., Mahlia, T. M. I., Milano, J., Kusumo, F., Siswantoro, J., ... & Ong, H. C. (2020). Biodiesel synthesis from *Ceiba pentandra* oil by microwave irradiation-assisted transesterification: ELM modeling and optimization. Renewable Energy, 146, 1278-1291.

Singh, C. S., Kumar, N., & Gautam, R. (2021). Supercritical transesterification route for biodiesel production: Effect of parameters on yield and future perspectives. Environmental Progress & Sustainable Energy, 40(6), e13685.

Singh, D., Sharma, D., Soni, S. L., Inda, C. S., Sharma, S., Sharma, P. K., & Jhalani, A. (2021). A comprehensive review of physicochemical properties, production process, performance

and emissions characteristics of 2nd generation biodiesel feedstock: Jatropha curcas. Fuel, 285, 119110.

Singh, K., Kumar, S. P., & Blümich, B. (2019). Monitoring the mechanism and kinetics of a transesterification reaction for the biodiesel production with low field 1H NMR spectroscopy. Fuel, 243, 192-201.

Sun, K., Lu, J., Ma, L., Han, Y., Fu, Z., & Ding, J. (2015). A comparative study on the catalytic performance of different types of zeolites for biodiesel production. Fuel, 158, 848-854.

Sundaramahalingam, M. A., Amrutha, C., Sivashanmugam, P., & Rajeshbanu, J. (2021). An encapsulated report on enzyme-assisted transesterification with an allusion to lipase. 3 Biotech, 11(11), 1-31.

Supriyanto, E., Sentanuhady, J., Dwiputra, A., Permana, A., & Muflikhun, M. A. (2021). The recent progress of natural sources and manufacturing process of biodiesel: a review. Sustainability, 13(10), 5599.

Suresh, M., Jawahar, C. P., & Richard, A. (2018). A review on biodiesel production, combustion, performance, and emission characteristics of non-edible oils in variable compression ratio diesel engine using biodiesel and its blends. Renewable and Sustainable Energy Reviews, 92, 38-49.

Székács, A. (2017). Environmental and ecological aspects in the overall assessment of bioeconomy. Journal of Agricultural and Environmental Ethics, 30(1), 153-170.

Tabatabaei, M., Aghbashlo, M., Dehhaghi, M., Panahi, H. K. S., Mollahosseini, A., Hosseini, M., & Soufiyan, M. M. (2019). Reactor technologies for biodiesel production and processing: A review. Progress in Energy and Combustion Science, 74, 239-303.

Tahir, M. H., Çakman, G., Goldfarb, J. L., Topcu, Y., Naqvi, S. R., & Ceylan, S. (2019). Demonstrating the suitability of canola residue biomass to biofuel conversion via pyrolysis through reaction kinetics, thermodynamics and evolved gas analyses. Bioresource technology, 279, 67-73.

Takase, M., Feng, W., Wang, W., Gu, X., Zhu, Y., Li, T., ... & Wu, X. (2014). Silybum marianum oil as a new potential non-edible feedstock for biodiesel: A comparison of its

production using conventional and ultrasonic assisted method. Fuel processing technology, 123, 19-26.

Takase, M., Pappoe, A. N. M., Afrifa, E. A., & Miyittah, M. (2018). High performance heterogeneous catalyst for biodiesel production from non-edible oil. Renewable Energy Focus, 25, 24-30.

Takase, M., Pappoe, A. N. M., Afrifa, E. A., & Miyittah, M. (2018). High performance heterogeneous catalyst for biodiesel production from non-edible oil. Renewable Energy Focus, 25, 24-30.

Tan, Y. H., Abdullah, M. O., Nolasco-Hipolito, C., & Zauzi, N. S. A. (2017). Application of RSM and Taguchi methods for optimizing the transesterification of waste cooking oil catalyzed by solid ostrich and chicken-eggshell derived CaO. Renewable Energy, 114, 437-447.

Tan, Y. H., Abdullah, M. O., Nolasco-Hipolito, C., & Zauzi, N. S. A. (2017). Application of RSM and Taguchi methods for optimizing the transesterification of waste cooking oil catalyzed by solid ostrich and chicken-eggshell derived CaO. Renewable Energy, 114, 437-447.

Tan, Z., Zhang, X., Kuang, Y., Du, H., Song, L., Han, X., & Liang, X. (2014). Optimized microemulsion production of biodiesel over lipase-catalyzed transesterification of soybean oil by response surface methodology. Green Processing and Synthesis, 3(6), 471-478.

Tang, Z. E., Lim, S., Pang, Y. L., Ong, H. C., & Lee, K. T. (2018). Synthesis of biomass as heterogeneous catalyst for application in biodiesel production: State of the art and fundamental review. Renewable and Sustainable Energy Reviews, 92, 235-253.

Taravus, S., Temur, H., & Yartasi, A. (2009). Alkali-catalyzed biodiesel production from mixtures of sunflower oil and beef tallow. Energy & Fuels, 23(8), 4112-4115.

Tavizón-Pozos, J. A., Chavez-Esquivel, G., Suárez-Toriello, V. A., Santolalla-Vargas, C. E., Luévano-Rivas, O. A., Valdés-Martínez, O. U., ... & Rodriguez, J. A. (2021). State of art of alkaline earth metal oxides catalysts used in the transesterification of oils for biodiesel production. Energies, 14(4), 1031.

Thangarasu, V., Siddharth, R., & Ramanathan, A. (2020). Modeling of process intensification of biodiesel production from Aegle Marmelos Correa seed oil using microreactor assisted with ultrasonic mixing. Ultrasonics Sonochemistry, 60, 104764.

Tobar, M., & Núñez, G. A. (2018). Supercritical transesterification of microalgae triglycerides for biodiesel production: effect of alcohol type and co-solvent. The Journal of Supercritical Fluids, 137, 50-56.

Torabi, A., Babaheydari, R. M., Akbari, G. H., & Mirabootalebi, S. O. (2020). Optimizing of micro-hardness of nanostructured Cu–Cr solid solution produced by mechanical alloying using ANN and genetic algorithm. SN Applied Sciences, 2(11), 1-9.

Velusamy, K., Devanand, J., Kumar, P. S., Soundarajan, K., Sivasubramanian, V., Sindhu, J., & Vo, D. V. N. (2021). A review on nano-catalysts and biochar-based catalysts for biofuel production. Fuel, 306, 121632.

Vidhu, V. K., & Philip, D. (2014). Spectroscopic, microscopic and catalytic properties of silver nanoparticles synthesized using Saraca indica flower. Spectrochimica Acta Part A: Molecular and Biomolecular Spectroscopy, 117, 102-108.

Vidhu, V. K., & Philip, D. (2014). Spectroscopic, microscopic and catalytic properties of silver nanoparticles synthesized using *Saraca indica* flower. Spectrochimica Acta Part A: Molecular and Biomolecular Spectroscopy, 117, 102-108.

Volli, V., & Purkait, M. K. (2015). Selective preparation of zeolite X and A from flyash and its use as catalyst for biodiesel production. Journal of hazardous materials, 297, 101-111.

Yadav, L. R., Pratibha, S., Manjunath, K., Shivanna, M., Ramakrishnappa, T., Dhananjaya, N., & Nagaraju, G. (2019). Green synthesis of AgZnO nanoparticles: Structural analysis, hydrogen generation, formylation and biodiesel applications. Journal of Science: Advanced Materials and Devices, 4(3), 425-431.

Yandri, E., Idroes, R., Setyobudi, R. H., Rudationo, C. B., Wahono, S. K., Mahaswa, R. K., ... & Susanto, H. (2021). Reducing Energy and Water Consumption in Textile Dyeing Industry with Cleaner Production by Inlet-Outlet Modification to Reuse Wastewater: Reducing Energy and Water Consumption in Textile Dyeing Industry. Proceedings of the Pakistan Academy of Sciences: A. Physical and Computational Sciences, 58(S), 49-58.

Yang, H., Hu, Y., Zhang, X., & Qiu, G. (2004). Mechanochemical synthesis of cobalt oxide nanoparticles. Materials Letters, 58(3-4), 387-389.

Yaqoob, H., Teoh, Y. H., Jamil, M. A., Rasheed, T., & Sher, F. (2020). An experimental investigation on tribological behaviour of tire-derived pyrolysis oil blended with biodiesel fuel. Sustainability, 12(23), 9975.

Yaşar, F. (2020). Comparision of fuel properties of biodiesel fuels produced from different oils to determine the most suitable feedstock type. Fuel, 264, 116817.

Yatish, K. V., Lalithamba, H. S., Suresh, R., & Latha, H. K. E. (2020). Ochrocarpus longifolius assisted green synthesis of CaTiO3 nanoparticle for biodiesel production and its kinetic study. Renewable Energy, 147, 310-321.

Yazdani, F., Akia, M., Khanbolouk, F., Hamze, H., & Arandiyan, H. (2021). Novel heterogeneous base nanocatalysts supported on a spray dried gamma alumina applying optimized production of biodiesel from waste cooking oil. Biofuels, 12(10), 1275-1281.

Yazdani, F., Akia, M., Khanbolouk, F., Hamze, H., & Arandiyan, H. (2021). Novel heterogeneous base nanocatalysts supported on a spray dried gamma alumina applying optimized production of biodiesel from waste cooking oil. Biofuels, 12(10), 1275-1281.

Yesilyurt, M. K., & Cesur, C. (2020). Biodiesel synthesis from Styrax officinalis L. seed oil as a novel and potential non-edible feedstock: a parametric optimization study through the Taguchi technique. Fuel, 265, 117025.

Yu, W., & Zhao, F. (2021). Prediction of critical properties of biodiesel fuels from FAMEs compositions using intelligent genetic algorithm-based back propagation neural network. Energy Sources, Part A: Recovery, Utilization, and Environmental Effects, 43(17), 2063-2076.

Yunusa, S. (2021). Effect of alumina support on cow bone based catalyst in one-step transesterification of neem seed oil. Applied Journal of Environmental Engineering Science, 7(2), 7-2.

Zaharin, M. S. M., Abdullah, N. R., Najafi, G., Sharudin, H., & Yusaf, T. (2017). Effects of physicochemical properties of biodiesel fuel blends with alcohol on diesel engine

performance and exhaust emissions: A review. Renewable and Sustainable energy reviews, 79, 475-493.

Zhang, Y., Niu, S., Han, K., Li, Y., & Lu, C. (2021). Synthesis of the SrO–CaO–Al$_2$O$_3$ trimetallic oxide catalyst for transesterification to produce biodiesel. Renewable Energy, 168, 981-990.

Zhao, C., Yang, L., Xing, S., Luo, W., Wang, Z., & Lv, P. (2018). Biodiesel production by a highly effective renewable catalyst from pyrolytic rice husk. Journal of cleaner production, 199, 772-780.

Zik, N. A. F. A., Sulaiman, S., & Jamal, P. (2020). Biodiesel production from waste cooking oil using calcium oxide/nanocrystal cellulose/polyvinyl alcohol catalyst in a packed bed reactor. Renewable Energy, 155, 267-277.

Zulqarnain, Ayoub, M., Yusoff, M.H.M., Nazir, M.H., Zahid, I., Ameen, M., Sher, F., Floresyona, D. and Budi Nursanto, E., 2021. A comprehensive review on oil extraction and biodiesel production technologies. Sustainability, 13(2), 788.

Published
Papaers

List of Publications

S.No	Title and Publication detail	Impact Factor
1.	Rozina, Ahmad, M. and Zafar, M., 2021. Conversion of waste seed oil of *Citrus aurantium* into methyl ester via green and recyclable nanoparticles of zirconium oxide in the context of circular bioeconomy approach. Waste Management, 136, pp.310-320.	8.816
2.	Rozina, Ahmad, M., Alruqi, M. and Zafar, M., 2022. Cleaner production of biodiesel from novel and non-edible seed oil of *Chamaerops humilis* using recyclable cobalt oxide nanoparticles: A contribution to resilient and sustainable world. *Journal of Cleaner Production*, *369*, p.133378	11.07
3.	Rozina, Ahmad M, Qureshi N, Zafar M, Ullah SA, Abidin SZ. Renewable energy production from novel and non-edible seed oil of *Cordia dichotoma* using nickel oxide nano catalyst. Fuel. 2023 Jan 15;332:126123.	8.035
4.	Rozina, Ahmad M, Elnaggar AY, Teong LK, Sultana S, Zafar M, Munir M, Hussein EE, Abidin SZ. Sustainable and eco-friendly synthesis of biodiesel from novel and non-edible seed oil of *Monotheca buxifolia* using green nano-catalyst of calcium oxide. Energy Conversion and Management. 2022 ;13:100142.	11.53
5.	Rozina, Alsaiari M, Ahmad M, Zafar M, Harraz FA, Algethami JS, Šljukić B, Santos DM, Akhtar MS. Transformation of waste seed biomass of Cordia myxa into valuable bioenergy through membrane bioreactor using green nanoparticles of indium oxide. Chemosphere. 2023 Feb 1;314:137604.	8.943
6.	Rozina, Ahmad, M., Asif, S., Klemeš, J.J., Mubashir, M., Bokhari, A., Sultana, S., Mukhtar, A., Zafar, M., Bazmi, A.A., Ullah, S. and Khan, M.S., 2022. Conversion of the toxic and hazardous *Zanthoxylum armatum* seed oil into methyl ester using green and recyclable silver oxide nanoparticles. Fuel, 310, p.122296.	8.035
7.	Rozina, Chia, S.R., Ahmad, M., Sultana, S., Zafar, M., Asif, S., Bokhari, A., Nomanbhay, S., Mubashir, M., Khoo, K.S. and Show, P.L., 2022. Green synthesis of biodiesel from *Citrus medica* seed oil using green nanoparticles of copper oxide. *Fuel*, *323*, p.124285.	8.035

8.	Rozina, , Ahmad, M., Zafar, M., Bokhari, A., Akhtar, M.S., Alshgari, R.A., Karami, A.M., Asif, S., Membrane reactor for production of biodiesel from nonedible seed oil of *Trachyspermum ammi* using heterogenous green nanocatalyst of manganese oxide, *Chemosphere* (2023), doi: https://doi.org/10.1016/j.chemosphere.2023.138078.	8.943
9.	Rozina, Mushtaq, Ahmad, Muhammad, Zafar, Zainab, Yousaf, Sher, Amanullah, Shazia, Sultana, Farhana, Bibi, 2021b. Identification of novel, non-edible oil seeds via scanning electron microscopy as potential feedstock for green synthesis of biodiesel. Microscopy Research and Technique 1–13.	2.893
10.	Rozina, Ahmad, M., Khan, A.M., Abbas, Q., Arfan, M., Mahmood, T., Zafar, M., Raza, J., Sultana, S., Akhtar, M.T. and Ameen, M., 2021. Implication of scanning electron microscopy as a tool for identification of novel, nonedible oil seeds for biodiesel production. Microscopy research and technique.	2.893
11.	Rozina, Ahmad M, Zafar M, Dawood S. Scanning electron microscopic identification of ten novel, non-edible oil seeds for bioenergy production. Microscopy Research and Technique. 2022 Sep;85(9):3245-55.	2.893
12.	Synthesis of Green and non-toxic Biodiesel from non-edible seed oil of *Cichorium intybus* using Recyclable Nanoparticles of MgO on February 11, 2023.	3.6

Conversion of waste seed oil of *Citrus aurantium* into methyl ester via green and recyclable nanoparticles of zirconium oxide in the context of circular bioeconomy approach

Rozina [*], Mushtaq Ahmad, Muhammad Zafar

Department of Plant Sciences, Quaid- i- Azam University, Islamabad 45320, Pakistan

ABSTRACT

In the current scenario of energy crises and depleting fossil fuels, there is need of sustainable and cheaper interventions with green technology to address these obstinate glitches. Biodiesel produced from waste, non-edible seed oils is a cleaner, green and alternate source of fuel for diesel engines which can possibly add to circular bioeconomy. In this study, *Citrus aurantium* a novel, nonedible and waste seed oil (38% w/w) producing feedstock was subjected to biodiesel synthesis using recyclable zirconium oxide nano particles synthesized with *Alternanthera pungens* aqueous leave extract. Maximum yield of 94% was obtained through optimized reaction parameters of methanol to oil molar ratio 6:1, reaction time 120 min, temperature 87.5 °C and catalyst loading of 0.5 wt% using Response Surface Methodology. Green nano particles of zirconium oxide were characterized via Scanning Electron Microscopy (SEM), X-Ray Diffraction (XRD) and Energy diffraction X-Ray (EDX) while; physiochemical characterization of synthesized biodiesel was carried through Fourier-transform infrared spectroscopy (FTIR), Gas Chromatography/Mass spectroscopy (GC/MS), and Nuclear magnetic resonance (NMR ^{1}H and ^{13}C). Fuel properties of methyl ester met international standards of ASTM D-6571, EN 14214 and China GB/T 20828-2007. It was concluded that biodiesel production from *Citrus aurantium* waste and non-edible seed oil can be efficiently employed for generation of renewable energy which would further provide assistance in transformation of linear economy to circular bioeconomy.

1. Introduction

Rapid growth in world's population has created challenges like high energy demand owing to extensive use of fossil fuels i.e. gas, oil and coal and resultant environmental pollution. All these chief sources of energy are cause of organic and inorganic air pollutants for instance gases like CO_x, SO_x, NO_x, CH_x (Hydrocarbons), ashes, tar droplets and soot. These pollutants are regular contributors to severe environmental glitches such as greenhouse effect and global warming (Ghani et al., 2020). Fossil fuels are non-renewable energy sources which are being exhausted with the passage of time at an exponential rate. These natural resources take thousands of years for them to get replenish (Meng et al., 2009). Therefore, fuel prices are increasing enormously, raising global inflation rate in return (Rashid et al., 2010).

The concept of circular economy and bioeconomy has been presented by European commission as system models in order to ensure inexpensive and resource efficient economy management. Circular

economy can be amalgamated with biofuel technology to produce renewable energy and save environment from unrestrained waste biomass disposal (Maina et al., 2017). Central principals of circular economy are recycling and reusing of materials which helps in harmonizing bioeconomy and are supposed to accelerate integrated approach of application of sustainable biomass resources. Bioeconomy depends upon conversion of recyclable carbon reservoirs from organic resources to a variety of products including bioenergy, fuel, bio-based chemicals, and polymers which lead towards circular economy (Székács, 2017). Circular economy emphasizes on sustainable utilization of natural resources and reducing dependency on non-renewable energy resources like fossil fuels. Progress in consumption of renewable energy resources such as bioethanol and biodiesel as substitute of conventional fossil fuels is a positive step towards circular economy. Hence, utilization of renewable energy resources for the production of bioenergy has been encouraged by the policy in European Commission in order to promote environmental and social sustainability (Alaswad et al., 2015).
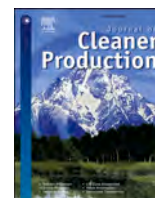
Cleaner production of biodiesel from novel and non-edible seed oil of *Chamaerops humilis* using recyclable cobalt oxide nanoparticles: A contribution to resilient and sustainable world

Rozina [a], Mushtaq Ahmad [a], Mansoor Alruqi [b,*], Muhammad Zafar [a]

[a] *Department of Plant Sciences, Quaid-i-Azam University Islamabad, 45320, Pakistan*
[b] *Department of Mechanical Engineering, College of Engineering, Shaqra University, Al Riyadh, 11911, Saudi Arabia*

ARTICLE INFO

ABSTRACT

Currently, global challenges of social, economic, and sustainable development entail energy and related services on a rising scale. The biofuel industry and engineering provide scientific solutions in the pursuit of eco-friendly and renewable energy sources and a circular economy. The present study engrossed in cleaner production of biodiesel from a novel feedstock of *Chamaerops humilis* with a high non-edible seed oil content of 30% (w/w). Cheaper and recyclable cobalt oxide nanoparticles were synthesized with leaf extract of *Galium boreale* to catalyzed transesterification. Characterization of cobalt oxide nanoparticles revealed their pure and nano nature with size of 40 nm. The highest methyl ester yield of 92% was achieved at optimal reaction conditions of methanol to oil ratio 6:1, catalyst loading of 0.54 (wt.%), temperature 60 °C and reaction time 3 h. Cobalt oxide nanoparticles were reusable up to five consecutive cycles. The 5, 8-octadecenoic acid was found as the leading fatty acid methyl ester in the sample of biodiesel. The fuel properties of biodiesel were in accord with international requirements. The minimum sulfur content of 0.0002% % indicated the clean and ecofriendly nature of biodiesel which is not only sustainable but economical too.

1. Introduction

United Nations proposed the Sustainable Development Goals (SDGs) to encourage sustainable development, adopt practices for cleaner production and tackle with serious challenging issues of the environment globally and locally. Numerous advanced technologies such as 'biofuel technology' and collaborative systems enable sustainable production and consumption to achieve these SDGs (Ameen et al., 2022). Biofuel technology mitigates the negative influences from the linear economic development and improves the quality of living standards by increasing resource efficiency (Maldonado-Guzmán et al., 2021). Biofuel technologies serve as cutting-edge for building a sustainable future by shifting linear economy to a circular economy and are crucial for implementing the SDGs (Ferasso et al., 2020).

There is a domineering need for a long-term sustainable investment mechanism and understanding circular economy as resilient and sustainable for promoting suitable biofuel technology to address environmental sustainability and renewable energy (Rozina et al., 2022a). The integration of the circularity, sustainability, and resilience domains

under a circular economy will lead to the holistic transformation of business, substituting inputs and improving the share of renewable and recyclable resources. Even though circular economy has achieved impetus in the scientific field, its theoretic structure and role in the sustainable development concept is still under debate (Schöggl et al., 2020).

Circular economy was introduced in response to linear and unsustainable production-consumption system (Kowalski and Makara, 2021). Moreover, resilience is considered as a criterion for sustainability hence, the transformation of systems menacing environmental resilience should be investigated (Fritsche et al., 2021). In this perspective, a framework was proposed by Biggs et al. (2015) to enhance the resilience of socio-ecological systems to live together with a natural system including biophysical restrictions.

A circular economy aims to reduce the level of waste to the least and accelerate society's transition to sustainable development. Both circular economy and the economy are tightly entwined in the areas of biomass, food waste, and biological products. Bioeconomy is designed to enable the transition from non-renewable resources like fossil fuels, to the use of renewable bioresources (Rozina et al., 2019). The use of bioresources
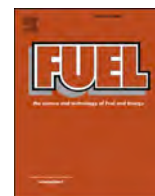

Renewable energy production from novel and non-edible seed oil of *Cordia dichotoma* using nickel oxide nano catalyst☆

Rozina [a],[*], Mushtaq Ahmad [a], Nasib Qureshi [b], Muhammad Zafar [a], Sher Aman Ullah [a], Sheikh Zain Ul Abidin [c]

[a] *Department of Plant Sciences, Quaid-i-Azam University, 45320 Islamabad, Pakistan*
[b] *United States Department of Agriculture, Agricultural Research Service, National Center for Agricultural Utilization Research, Bioenergy Research Unit, 1815 N University Street, Peoria, IL 61604, USA*
[c] *Institute of Biological Sciences, Gomal University, D.I Khan, Pakistan*

ARTICLE INFO

ABSTRACT

Renewable energy sources such as biodiesel have gained attention due to their pollution free and eco-friendly nature. The use of heterogenous nanocatalyst is preferred in biodiesel production to their ease of recovery and recyclability. In this study, biodiesel was produced from nonedible *Cordia dichotoma* seed oil using NiO nanocatalyst. NiO nanocatalyst was prepared with aqueous leaf extract of *Anagallis arvensis* L. Innovative techniques like X-ray Diffraction, Scanning Electron Microscopy, energy diffraction X-ray and thermogravimetric analysis were applied to analyse Nickel oxide nanoparticles. The maximum biodiesel yield of 94 % was calculated from methanol to oil molar ratio of 7:1, catalyst loading 0.16 (wt.%), reaction time 115 min and temperature 80 °C. Nuclear magnetic resonance confirmed the production of methyl ester (^{1}H NMR and ^{13}C NMR). The results of Gas Chromatography/Mass spectroscopy signified four distinctive peaks of methyl esters with 9-Octadecenoic acid methyl ester was identified as the major fatty acid methyl ester. Determined fuel properties of *Cordia dichotoma* methyl ester such as viscosity (8.24 mm^2/s), density (0.962 kg/m^3), flash point (99 °C) cloud point (−8 °C) and pour point (−10 °C) were comparable with international standards of ASTM D-6571, EN 14214 and China GB/T 20828-2007. Minimum sulfur content of 0.0001 % has elucidated the eco-friendly and clean nature of synthesized biodiesel of *Cordia dichotoma*.

1. Introduction

Depleting energy sources and rising prices of conventional fossil fuels have challenged the need of alternative energy sources such as biodiesel and bioethanol. Research in biofuel technology have proven critical momentum worldwide to discover a variety of alternative energy sources and explore their applicability [1]. Biodiesel is a clean and renewable fuel utilized in diesel engines constituted of lengthy chain of fatty acid monoalkyl ester derived from biomass sources. Biodiesel is biodegradable and non-hazardous to environment possessing properties comparable to Petro-diesel [2]. Utilization of petroleum-based fossil fuel in internal combustion engines produces large number of pollutants causing great destruction 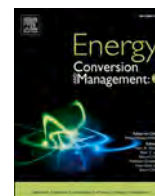to the environment. Biodiesels have low sulfur content, hence, have low emission capabilities and environmental pollution during combustion [3].

Biodiesel is synthesized from both vegetable oils and animal fats. More than 350 high potential oil yielding crops have been reported globally and higher than 95 % of biodiesel has been produced from edible seed oils like palm oil, soybean, and rape seed oil [4]. Vegetable oils vary in their physico-chemical properties. Hence, the fuel related properties of synthesized methyl ester rely on the type of feedstock used in transesterification. The use of edible oils in biodiesel production have created food versus fuel dilemmas and resultant shortages in the food supply [5]. Prices of vegetables oils have intensely risen in the past decade. In addition, biodiesel synthesis from edible oils has significantly influenced its economic viability. To overcome all these problems,

Sustainable and eco-friendly synthesis of biodiesel from novel and non-edible seed oil of *Monotheca buxifolia* using green nano-catalyst of calcium oxide

Rozina [a,b,*], Mushtaq Ahmad [a], Ashraf Y. Elnaggar [c], Lee Keat Teong [d], Shazia Sultana [a], Muhammad Zafar [a], Mamoona Munir [a], Enas E. Hussein [e], Sheikh Zain Ul Abidin [f]

[a] *Department of Plant Sciences, Quaid- i- Azam University, Islamabad 45320, Pakistan*
[b] *Department of Botany, Government Girls Degree College Zaida, Swabi, Pakistan*
[c] *Department of Food Nutrition Science (Previously Chemistry), College of Science, Taif University, P. O. Box 11099, Taif 21944, Saudi Arabia*
[d] *School of Chemical Engineering, University of Sains Malaysia*
[e] *National Water Research Center, P.O. Box 74, Shubra El-Kheima 13411, Egypt*
[f] *Institute of Biological Sciences, Gomal University, D.I Khan, Pakistan*

ARTICLE INFO

ABSTRACT

Presently, biodiesel offers a sustainable and renewable substitute for exhausting fossil fuels such as Petro-diesel. Large scale production of biodiesel could lead to positive outcomes in terms of environmental quality by reducing greenhouse gasses emission and Societal-Economic development. Hence, this research work focused on biodiesel synthesis from novel and non-edible seed oil of *Monotheca buxifolia* using green nano-particles of calcium oxide synthesized with aqueous leaves extract of *Boerhavia procumbens*. Advanced techniques like X-Ray Diffraction (XRD), Scanning Electron Microscopy (SEM), and Energy diffraction X-Ray (EDX) were used to characterize calcium oxide nano-particles. High yield of biodiesel (95%) was obtained at optimum reaction conditions such as methanol to oil molar ratio of 9:1, catalyst loading 0.83 (wt.%), reaction time 180 min and temperature 85 °C. Gas Chromatography/Mass spectroscopy (GC/MS) analysis of biodiesel revealed four distinct peaks of methyl esters. Results of Fourier-transform infrared spectroscopy (FTIR) and Nuclear magnetic resonance (NMR) confirmed the formation of methyl esters in biodiesel sample. Fuel properties of biodiesel such as density (0.821 kg/m^3), viscosity (5.35 mm^2/s), cloud point (-8 °C), pour point (-9 °C) and flash point (95 °C) were found equivalent to international ASTM D-6571, EN 14,214 and China GB/T 20828–2007 standards. It was finally concluded that *Monotheca buxifolia* is a highly potential, eco-friendly, and cheaper biomass feedstock for bio-diesel production.

Introduction

Fossil fuels are fundamental wellsprings of energy in transport and industrial sector. The rapid industrial growth and increasing human population has inflated the demand and price of petroleum-based fuels. It has also created severe environmental glitches like climate change, greenhouse gases emission and global warming. According to research survey, renewable energies are suitable and ecofriendly alternative to depleting fossil fuels [1]. Renewable fuels like bioethanol and biodiesel can play a significant role to overcome energy crises due to their sustainable, environment friendly and non-toxic nature [2].

Biodiesel is known as long chain fatty acid methyl esters produced

from biomass raw material like animal fats and vegetable oil [3]. Its economic importance and environment friendly nature have made it an alternate and potentially renewable fuel for diesel engines. Imperative issues associated with the biodiesel synthesis are the selection of a suitable feedstock, catalyst used, and techniques operated for biodiesel synthesis. Selection of a suitable feedstock plays a significant role in determining the cost of the fuel [4–6].

It is need of time to consider the societal appraisal of biofuels such as biodiesel. It is not only comparative to fossil fuels but there is also relation to an even shorter cycle of storing and using energy such as solar energy. Biofuels have three different types of products such as biogas, bioethanol and biodiesel in which bioethanol and biodiesel are used as transportation fuel. These are further divided into conventional and

Transformation of waste seed biomass of *Cordia myxa* into valuable bioenergy through membrane bioreactor using green nanoparticles of indium oxide

Rozina [a],[1], Mabkhoot Alsaiari [b],[c],[*],[1], Mushtaq Ahmad [a],[**], Muhammad Zafar [a], Farid A. Harraz [b],[d], Jari S. Algethami [b], Biljana Šljukić [e], Diogo M.F. Santos [e], Muhammad Saeed Akhtar [f],[***]

[a] *Department of Plant Sciences, Quaid-i-Azam University, Islamabad, 45320, Pakistan*
[b] *Promising Centre for Sensors and Electronic Devices (PCSED), Advanced Materials and Nano Research Centre, Najran University, Najran, 11001, Saudi Arabia*
[c] *Empty Quarter Research Unit, Department of Chemistry, College of Science and Art in Sharurah, Najran University, Sharurah, Saudi Arabia*
[d] *Nanomaterials and Nanotechnology Department, Central Metallurgical Research and Development Institute (CMRDI), P.O. Box: 87 Helwan, Cairo, 11421, Egypt*
[e] *Center of Physics and Engineering of Advanced Materials, Laboratory for Physics of Materials and Emerging Technologies, Chemical Engineering Department, Instituto Superior Técnico, Universidade de Lisboa, 1049–001, Lisbon, Portugal*
[f] *School of Chemical Engineering, Yeungnam University, Gyeongsan, 712-749, South Korea*

HIGHLIGHTS

- Waste seed oil of *Cordia myxa* as a novel and renewable energy source.
- Membrane technology as an effective tool for separation and purification.
- Synthesis of indium oxide nanoparticles to catalyze transesterification.
- Optimum yield of 95 wt % of methyl ester was obtained.
- All properties of methyl ester matched well with international standards.

GRAPHICAL ABSTRACT
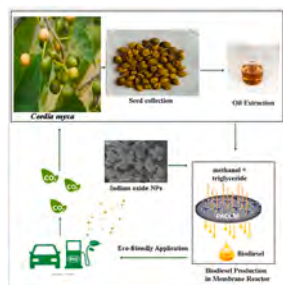
ARTICLE INFO

ABSTRACT

Depletion of non-renewable fuel has obliged researchers to seek out sustainable and environmentally friendly alternatives. Membranes have proven to be an effective technique in biofuel production for reaction, purification, and separation, with the ability to use both porous and non-porous membranes. It is demonstrated that a membrane-based sustainable and green production can result in a high degree of process intensification, whereas the recovery and repurposing of catalysts and alcohol are anticipated to increase the process economics. Therefore, in this study sustainable biodiesel was synthesized from inedible seed oil (37 wt%) of *Cordia myxa*

---

* Corresponding author. Promising Centre for Sensors and Electronic Devices (PCSED), Advanced Materials and Nano Research Centre, Najran University, Najran, 11001, Saudi Arabia.
** Corresponding author.
*** Corresponding author.
  E-mail addresses: mamalsaiari@nu.edu.sa (M. Alsaiari), mushtaq@qau.edu.pk (M. Ahmad), msakhtar@ynu.ac.kr (M.S. Akhtar).
[1] These are co-first authors contributed equally.
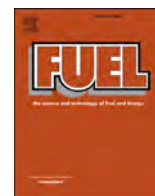
Full Length Article

Conversion of the toxic and hazardous *Zanthoxylum armatum* seed oil into methyl ester using green and recyclable silver oxide nanoparticles

Rozina [a], Mushtaq Ahmad [a], Saira Asif [b,c], Jiří Jaromír Klemeš [c], Muhammad Mubashir [d], Awais Bokhari [c,e,*], Shazia Sultana [a], Ahmad Mukhtar [f], Muhammad Zafar [a], Aqeel Ahmed Bazmi [e], Sami Ullah [g], Mohd Shariq Khan [h], Apurav Krishna Koyande [i], M. Mofijur [j,k], Pau-Loke Show [i,*]

[a] Department of Plant Sciences, Quaid-i-Azam University, 45320 Islamabad, Pakistan
[b] Faculty of Sciences, Department of Botany, PMAS Arid Agriculture University, Rawalpindi, Punjab 46300, Pakistan
[c] Sustainable Process Integration Laboratory, SPIL, NETME Centre, Faculty of Mechanical Engineering, Brno University of Technology, VUT Brno, Technická 2896/2, 616 00 Brno, Czech Republic
[d] Department of Petroleum Engineering, School of Engineering, Asia Pacific University of Technology and Innovation, 57000 Kuala Lumpur, Malaysia
[e] Chemical Engineering Department, COMSATS University Islamabad (CUI), Lahore Campus, Lahore, Punjab 54000, Pakistan
[f] Department of Chemical Engineering, NFC Institute of Engineering and Fertilizer Research Faisalabad, 38000, Pakistan
[g] Department of Chemistry, College of Science, King Khalid University, Abha, 61413, P. O. Box 9004, Saudi Arabia
[h] Department of Chemical Engineering, College of Engineering, Dhofar University, Salalah, Sultanate of Oman
[i] Department of Chemical and Environmental Engineering, Faculty Science and Engineering, University of Nottingham, Malaysia, 43500 Semenyih, Selangor Darul Ehsan, Malaysia
[j] Centre for Technology in Water and Wastewater, School of Civil and Environmental Engineering, University of Technology Sydney, Ultimo, NSW 2007, Australia
[k] Mechanical Engineering Department, Prince Mohammad Bin Fahd University, Al Khobar, 31952, Saudi Arabia

ARTICLE INFO

ABSTRACT

The cleaner and sustainable production of biodiesel from toxic and hazardous non-edible seed oils offer a remarkable opportunity to deal with energy crises and provide a renewable substitute to depleting fossil fuels. In the current study, the potential of the novel, toxic and non-edible seed oil of *Zanthoxylum armatum* was investigated for eco-friendly production of biodiesel catalysed by green nanoparticles of silver oxide. Silver oxide nanoparticles were synthesised with aqueous leaf extract of *Silybum marianum*. Heterogeneous green nanocatalysts were preferred due to their recyclable nature and easy recovery. The maximum yield of 95% of methyl ester was obtained at optimum reaction conditions of oil to methanol molar ratio 1:7, catalyst loading 0.5 (wt.%), reaction temperature 90 °C and reaction time 2 h. Characterisation of synthesised nanoparticles of silver oxide was carried out with X-Ray diffraction (XRD), scanning electron microscopy (SEM), and energy diffraction X-ray (EDX). Fourier-transform infrared spectroscopy (FTIR) and nuclear magnetic resonance (NMR) confirmed the formation of methyl esters. 5, 8-octadecenoic acid was found to be the major fatty acid methyl ester in the biodiesel sample. Fuel properties of biodiesel were investigated and found comparable to international standards of ASTM D-6571 and EN-14214. It was concluded from the current investigation that *Zanthoxylum armatum* is a potential biomass feedstock for the sustainable production of biodiesel using green nanoparticles of silver oxide.

Green synthesis of biodiesel from *Citrus medica* seed oil using green nanoparticles of copper oxide

Rozina [a], Shir Reen Chia [b,c], Mushtaq Ahmad [a,*], Shazia Sultana [a], Muhammad Zafar [a], Saira Asif [d,e], Awais Bokhari [e,f], Saifuddin Nomanbhay [c], Muhammad Mubashir [g], Kuan Shiong Khoo [h,*], Pau Loke Show [i,j,*]

[a] *Department of Plant Sciences, Quaid- i- Azam University, Islamabad 45320, Pakistan*
[b] *Department of Mechanical Engineering, College of Engineering, Universiti Tenaga Nasional (UNITEN), Jalan IKRAM-UNITEN, 43000 Kajang, Selangor, Malaysia*
[c] *AAIBE Chair of Renewable Energy, Institute of Sustainable Energy, Universiti Tenaga Nasional (UNITEN), Jalan IKRAM-UNITEN, 43000 Kajang, Selangor, Malaysia*
[d] *Faculty of Sciences, Department of Botany, PMAS Arid Agriculture University, Rawalpindi, Punjab 46300, Pakistan*
[e] *Sustainable Process Integration Laboratory, SPIL, NETME Centra, Faculty of Mechanical Engineering, Brno University of Technology, VUT Brno, Technická 2896/2, 616 00 Brno, Czech Republic*
[f] *Chemical Engineering Department, COMSATS University Islamabad (CUI), Lahore Campus, Lahore, Punjab 54000, Pakistan*
[g] *Department of Petroleum Engineering, School of Engineering, Asia Pacific University of Technology and Innovation, 57000 Kuala Lumpur, Malaysia*
[h] *Faculty of Applied Sciences, UCSI University, No. 1, Jalan Menara Gading, UCSI Heights, 56000 Cheras Kuala Lumpur, Malaysia*
[i] *Zhejiang Provincial Key Laboratory for Subtropical Water Environment and Marine Biological Resources Protection, Wenzhou University, Wenzhou 325035, China*
[j] *Department of Chemical and Environmental Engineering, Faculty of Science and Engineering, University of Nottingham Malaysia, Jalan Broga, 43500 Semenyih, Selangor Darul Ehsan, Malaysia*

ARTICLE INFO

ABSTRACT

Currently, increasing energy demand due to overpopulation has provoked an urge for renewable energy sources like biodiesel. Biodiesel production from non-edible seed oils provides striking solution to the problems associated with the energy crisis. In this study, the potential of *Citrus medica* as a novel and non-edible seed oil (33% w/w) producing feedstock was investigated for biodiesel production using green and recyclable nanoparticles (NPs) of copper oxide synthesized with aqueous leaf extract of *Portulaca oleracea*. Green NPs of copper oxide were characterized by advanced techniques like X-Ray Diffraction (XRD), Scanning Electron Microscopy (SEM), and Energy Diffraction X-Ray (EDX). A maximum yield of 93% of methyl ester was achieved at the optimum reaction condition of methanol to oil ratio 8:1, catalyst loading 0.18 wt%, reaction time 120 min and temperature 85 °C. Both Fourier-transform infrared spectroscopy (FTIR) and nuclear magnetic resonance of biodiesel confirmed the presence of methyl ester in the synthesized biodiesel sample. Five distinct peaks of methyl esters were identified in biodiesel by gas chromatography-mass spectrometry (GC–MS) analysis. Fuel properties of methyl esters were investigated and found analogous to the international standards. The results indicated that *Citrus medica* is a potential, environmentally friendly biomass feedstock for renewable production of biodiesel using green NPs of copper oxide as catalyst.

1. Introduction

Rapid increment in urbanization, overconsumption of fossil fuel and

resultant greenhouse gas (GHG) emission has diverted researcher's interest towards the investigation of other renewable and eco-friendly energy sources [1,2]. The demand for fossil fuels worldwide has

---

Journal Pre-proof

Membrane reactor for production of biodiesel from nonedible seed oil of *Trachyspermum ammi* using heterogenous green nanocatalyst of manganese oxide

Rozina, Mushtaq Ahmad, Muhammad Zafar, Awais Bokhari, Muhammad Saeed Akhtar, Razan A. Alshgari, Abdulnasser Mahmoud Karami, Saira Asif

Please cite this article as: Rozina, , Ahmad, M., Zafar, M., Bokhari, A., Akhtar, M.S., Alshgari, R.A., Karami, A.M., Asif, S., Membrane reactor for production of biodiesel from nonedible seed oil of *Trachyspermum ammi* using heterogenous green nanocatalyst of manganese oxide, *Chemosphere* (2023), doi: https://doi.org/10.1016/j.chemosphere.2023.138078.

This is a PDF file of an article that has undergone enhancements after acceptance, such as the addition of a cover page and metadata, and formatting for readability, but it is not yet the definitive version of record. This version will undergo additional copyediting, typesetting and review before it is published in its final form, but we are providing this version to give early visibility of the article. Please note that, during the production process, errors may be discovered which could affect the content, and all legal disclaimers that apply to the journal pertain.

RESEARCH ARTICLE

Identification of novel, non-edible oil seeds via scanning electron microscopy as potential feedstock for green synthesis of biodiesel

Rozina[1] | Mushtaq Ahmad[1] | Muhammad Zafar[1] | Zainab Yousaf[1] |
Sher Aman Ullah[1] | Shazia Sultana[1] | Farhana Bibi[2]

[1]Department of Plant Sciences, Quaid-i-Azam University, Islamabad, Pakistan

[2]Department of Microbiology, Quaid-i-Azam University, Islamabad, Pakistan

Correspondence
Rozina, Department of Plant Sciences, Quaid-i-Azam University, Islamabad 45320, Pakistan.
Email: rozinaroshni@yahoo.com

Review Editor: Mingying Yang

Abstract

In the present era, environmental glitches associated with extensive emission of greenhouse gases (GHG) and energy crises caused by exhausting fossil fuel reservoirs has diverted researcher's interest toward alternative and renewable energy sources. Biodiesel is a renewable, biodegradable, and sustainable alternative to petro-diesel. Biodiesel synthesized from non-edible seed oils is preferred due its cost effectiveness and eco-friendly nature. Hence, our present study focused on investigation and identification of micromorphological characters of six novel, non-edible seed oil feedstock for biodiesel production via scanning electron microscopy (SEM). Results of light microscopy of seeds revealed distinct variation in seed size (15.8–1.8 mm in length and 9.4–1.1 in width), shape (round to Cuneiform), and color (from black to yellowish green). Non-edible seed oil content fall in range of 28–38% (wt/wt). Free fatty acid (FFA) content varied from 0.56 to 2.06 mg KOH/g. Multivariate analysis was performed to investigate correlation between three significant variables of seed oil yielding feedstock such as potential for biodiesel synthesis, oil content, and FFA content via principal component analysis. Ultra morphological investigation of seeds surfaces via SEM exhibited distinctive variation in surface sculpturing, cell arrangement, cell shape, periclinal wall shape, margins, protuberances, and anticlinal wall shape. Seed surface sculpturing varied from reticulate, semitectate, wrinkled, rugose, papillate, perforate, and striate. Periclinal wall arrangements confirmed variation from glabrous, raised, depressed, elevated, smooth, pentagonal, entire, and ripple margins. Whereas, anticlinal walls pattern demonstrated variation from angular, smooth, wavy, deep, dentate, entire, irregular, puzzled, elongated, curved, and depressed. Finally, it was concluded from obtained results that SEM could be a possible useful tool in disclosing veiled micromorphological characters of non-edible oil yielding seeds, which provides useful information to researchers for their correct, authentic identification, and classification in modern synthetic system.

KEYWORDS
bioenergy, identification, micro-morphology, non-edible oil yielding seeds, scanning electron microscopy

RESEARCH ARTICLE

MICROSCOPY
RESEARCH & TECHNIQUE WILEY

Implication of scanning electron microscopy as a tool for identification of novel, nonedible oil seeds for biodiesel production

Rozina[1,2] | Mushtaq Ahmad[1] | Amir Muhammad Khan[3,4] | Qamar Abbas[5] | Muhammad Arfan[6] | Tariq Mahmood[7] | Muhammad Zafar[1] | Jamil Raza[1] | Shazia Sultana[1] | Maryam Tanveer Akhtar[8] | Maria Ameen[1]

[1]Department of Plant Sciences, Quaid-i-Azam University, Islamabad, Pakistan

[2]Department of Botany, Government Girls Degree College Zaida, Swabi, KP, Pakistan

[3]Department of Botany, University of Mianwali, Mianwali, Pakistan

[4]Department of Botany, University of Sargodha, Sargodha, Pakistan

[5]Department of Biological Sciences, Karakoram International University, Gilgit, Pakistan

[6]Department of Botany, University of Education Lahore, Vehari Campus, Vehari, Pakistan

[7]Department of Forestry, College of Agriculture, University of Sargodha, Sargodha, Pakistan

[8]Department of Environmental Sciences, International Islamic University, Islamabad, Pakistan

Correspondence
Rozina, Department of Botany, Government Girls Degree College Zaida, Swabi, KP, Pakistan
Email: rozinaroshni@yahoo.com

Review Editor: Alberto Diaspro

Abstract

Biodiesel is a promising, bio-based, renewable, nontoxic, environment friendly, and alternative fuel for petroleum derived fuels which helps to reduce dependency on conventional fossil fuels. In this study, six novel, nonedible seed oil producing feed-stock were explored for their potential for sustainable production of biodiesel. It is very important to correctly identify oil yielding plant species. Scanning electron microscopy (SEM) was used as reliable tool for authentic identification of oil yielding seeds. Macromorphological characters of seeds were studied with light microscopy (LM). Outcomes of LM of seeds exposed distinctive variation in seed size from 16.3 to 3.2 mm in length and 12.4 to 0.9 mm in width, shape varied from oval to triangular, and color from black to light brown. Oil content of nonedible seed ranged from 25 to 30% (w/w). Free fatty acid content of seed oil varied from 0.32 to 2.5 mg KOH/g. Moreover, ultra structural study of seeds via SEM showed variation in surface sculpturing, cell arrangement, cell shape, periclinal wall shape, margins, protuberances, and anticlinal wall shape. Surface sculpturing varied from rugged, reticulate, varrucose, papillate, and striate. Periclinal wall arrangements confirmed variation from rough, wavy, raised, depressed, smooth, and elevated whereas, anticlinal walls pattern showed variation from profuse undulating, smooth, raised, grooved, deep, curved, and depressed. It was concluded that SEM could be a latent and advanced technique in unveiling hidden micromorphological characters of nonedible oil yielding seeds which delivers valuable information to researchers and indigenous people for precise and authentic identification and recognition.

RESEARCH ARTICLE

Scanning electron microscopic identification of ten novel, non-edible oil seeds for bioenergy production

Rozina[1] | Mushtaq Ahmad[1] | Muhammad Zafar[1] | Sumreen Dawood[2]

[1]Department of Plant Sciences, Quaid-i-Azam University Islamabad, Islamabad, Pakistan

[2]Department of Botany, Rawalpindi Women University, Rawalpindi, Pakistan

Correspondence
Rozina, Department of Plant Sciences, Quaid-i-Azam University Islamabad, Islamabad 45320, Pakistan.
Email: rozinaroshni@yahoo.com

Review Editor: Chuanbin Mao

Abstract

Biodiesel is a sustainable, inexpensive, and alternative energy source produced from vegetable oils and animal fats. Precise and authentic identification of oil yielding plant species is very crucial. Therefore, scanning electron microscopy (SEM) was employed in our current investigation to study micromorphological characteristics of ten novel oil yielding seeds for their reliable identification. Macromorphological characters of sample seeds were explored by light microscopy. Seed size varied from 16 to 6.2 mm in length and 18.4–4.5 mm in width. Seed shape varied from ovoid to cordial and color from beige to brown. Seed oil content ranged from 25% to 45% (w/w). Whereas free fatty acid (FFA) content of seed oil varied from 0.42 to 3.4 mg KOH/g. Biodiesel potential of *Chamaerops humilis* was found to be highest (98%) in all. Besides, ultra-structural observation of seeds demonstrated variation in surface sculpturing which varied from rugous, reticulate, perforate, striate, and webby. Periclinal wall arrangements varied from rough, ridged, depressed, thick and curved whereas, anticlinal walls pattern showed variation from wavy, smooth, raised, deep and depressed. It was ultimately concluded that Scanning electron microscopy could serve as an advanced tool representing hidden ultra-structural characters of seeds. It offers significant knowledge to researchers and local community for their accurate and genuine identification.

Research Highlights

- Non-edible oil yielding seeds as promising source of bioenergy.
- Scanning electron microscopy (SEM) as reliable tool for identification.
- Variation in Micromorphological characters among selected seeds.
- Classification of non-edible oil yielding plants via micromorphological characters.

KEYWORDS
biodiesel, identification, micro-morphology, non-edible oil yielding seeds, scanning electron microscopy

1 | INTRODUCTION

Currently, biofuels are receiving intense attention as a viable and sustainable alternative energy source. Biofuel has advantages like long-term viability, lower sulfur content, and ready-to-use characteristics that do not necessitate engine modifications (Ashfaq et al., 2019). The wide access to biomass sources for clean energy generation serves as an alternative to exhausting fossil fuel reservoirs (Rozina Ahmad et al., 2019). Biofuels are environmentally friendly energy sources which are renewable and biodegradable. The most common biofuels are ethanol, biodiesel, and methane (Ahmad et al., 2020; Vardy et al., 2017). Biodiesel is defined as a blend of fatty acid methyl esters (FAMEs) and is one of the most promising alternative energy sources. It has attained a market of 2.8 billion gallons in just over a decade.

Synthesis of green and non-toxic biodiesel from non-edible seed oil of *Cichorium intybus* using recyclable nanoparticles of MgO

Rozina [a,b,*], Mushtaq Ahmad [a], Muhammad Zafar [a]

[a] *Department of Plant Sciences, Quaid - i - Azam University Islamabad, 45320, Pakistan*
[b] *Government Girls Degree College Zaida, Swabi, Higher Education Department KP, Pakistan*

A B S T R A C T

Our current investigation aimed to explore *Cichorium intybus* as a novel and nonedible seed oil (34% w/w) producing plant species for green and sustainable production of biodiesel to contribute an alternative substitute to depleting fossil fuel reservoirs. Transesterification of *Cichorium intybus* seed oil was catalyzed by green nanoparticles of MgO synthesized with *Parthenium hysterophorus* leaf extract. The highest yield of 95% of fatty acid methyl esters (FAMEs) was achieved with optimal reaction conditions of methanol to oil molar ratio 9:1, catalyst loading of 0.83 (wt%), time 180 (min) and temperature 85 °C at constant stirring. Physiochemical characterization of the catalyst was carried out which revealed pure and nano nature of synthesized nano-catalyst. MgO nanoparticles exhibited maximum reusability up to the 6th reaction. Fourier-transform infrared spectroscopy (FT-IR) and Nuclear magnetic resonance (NMR ^{1}H and ^{13}C) validated methyl ester formation in the sample of biodiesel. Findings of Gas Chromatography/Mass spectroscopy signified four distinct peaks of methyl esters with 9-Octadecenoic acid methyl ester found as representative fatty acid methyl ester. Fuel properties of methyl ester were found equivalent to ASTM D-6571 and EN 14214 standards. This investigation has disclosed that green nanoparticles of MgO are highly efficient in biodiesel production from *Cichorium intybus* seed oil during transesterification reaction.

1. Introduction

Increasing energy demand with rise in global population is one of the key glitches of today. It has been currently estimated that world's population will upsurge about 9.6 billion by 2050 and non-fossil fuels like biofuel will account for major global energy demand in early 2040 s onward [1]. World's primary energy demand was assessed to be around 14,278 tons of oil with 2890 Mteo utilized in transport section by 2020 urging the exploration of renewable energy sources [2]. As the emission of greenhouse gases have vital effect on environment and human health, therefore, the consideration towards alternative and renewable energy sources has been amplified among researchers and industrialists. Moreover, exhausting fossil fuel reservoirs urge struggles for renewable and more reliable energy resources. There is a variety of promising renewable energy resources like wind energy, solar energy, hydrothermal energy, and biofuel energy ensuring energy security and restrained impacts of climate change [3]. Biofuels are playing a significant role in decreasing greenhouse gases emission. Carbon emission from fuel energy is estimated to be reduced by 10% in 2050 due to utilization of biofuels [4].

Fatty acid methyl esters, in particular, are referred to as "biodiesel". Biodiesel is an auspicious, renewable, biodegradable, non-toxic, non-explosive, environmentally friendly and reliable source of energy which can possibly substitute conventional and depleting petro-diesel [5,6]. Physiochemical properties of methyl ester are equivalent to that of conventional petro-diesel, making it commercially usable and reliable. Transesterification is the most extensively used method for biodiesel synthesis in which triglycerides react with methanol in the existence of a particular catalyst resulting in the production of methyl ester and glycerol. Based on type of sources, biofuels have been classified into four different generations. Biofuels of first generation are obtained from sources which are edible in nature, second generation biofuels are those which are synthesized from non-edible seed oils, third generation include biofuels from algal sources, whereas fourth generation biofuels are produced from genetically modified algae [7].

Both edible and non-edible feedstock of oil can be used for methyl ester formation. However, non-edible feedstock is preferred over edible feedstock to avoid risk of food *versus* fuel competition as world's population is increasing every day and more people will be needed to feed in